

**UNCLASSIFIED**

**AD NUMBER**

**AD872161**

**LIMITATION CHANGES**

**TO:**

**Approved for public release; distribution is unlimited.**

**FROM:**

**Distribution authorized to U.S. Gov't. agencies and their contractors;  
Administrative/Operational Use; FEB 1970. Other requests shall be referred to Army Aviation Materiel Labs., Fotr Eustis, VA.**

**AUTHORITY**

**USAAMRDC ltr 20 Mar 1973**

**THIS PAGE IS UNCLASSIFIED**

AD872161

AB

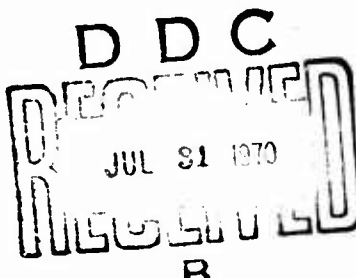
USAALABS TECHNICAL REPORT 69-76  
FLUID MECHANICS ANALYSIS OF  
HIGH-PRESSURE-RATIO CENTRIFUGAL COMPRESSOR DATA

AD No. —  
ECS FILE COPY

By

Robert C. Dean, Jr.  
David D. Wright  
Peter W. Runstadler, Jr.

February 1970



U. S. ARMY AVIATION MATERIEL LABORATORIES  
FORT EUSTIS, VIRGINIA

CONTRACT DAAJ02-68-C-0073  
CREARE INCORPORATED  
HANOVER, NEW HAMPSHIRE

This document is subject to special  
export controls and each transmission  
to foreign governments or foreign  
nationals may be made only with  
prior approval of U.S. Army Aviation  
Materiel Laboratories, Fort Eustis,  
Virginia 23604



587

### DISCLAIMERS

The findings in this report are not to be construed as an official Department of the Army position unless so designated by other authorized documents.

When Government drawings, specifications, or other data are used for any purpose other than in connection with a definitely related Government procurement operation, the United States Government thereby incurs no responsibility nor any obligation whatsoever; and the fact that the Government may have formulated, furnished, or in any way supplied the said drawings, specifications, or other data is not to be regarded by implication or otherwise as in any manner licensing the holder or any other person or corporation, or conveying any rights or permission, to manufacture, use, or sell any patented invention that may in any way be related thereto.

### DISPOSITION INSTRUCTIONS

Destroy this report when no longer needed. Do not return it to the originator.

ACCESSION for	WHITE SECTION <input type="checkbox"/>
GFSI	BUFF SECTION <input checked="" type="checkbox"/>
GDC	<input type="checkbox"/>
U/A REQUESTED	<input type="checkbox"/>
DISPOSITION	.....
SEARCHING AVAILABILITY CODES	
QST.	AVAIL. AND OF SPECIAL
21	



DEPARTMENT OF THE ARMY  
U S ARMY AVIATION MATERIEL LABORATORIES  
FORT EUSTIS, VIRGINIA 23604

The object of this contractual effort was to obtain maximum benefit from centrifugal compressor data acquired under a previous contract, improving fluid dynamic flow models and performance prediction capabilities. This program was also to define potential performance improvement items and critical research required to improve design criteria.

This report was prepared by Create Incorporated under the terms of Contract DAAJ02-68-C-0073. It presents the evaluation and analysis of the previously acquired data and the results of comparisons of these data with compressor performance predicted by existing flow models and design methods. New flow models and design methods are discussed, and recommendations for needed research are presented.

While the conclusions indicate that the initial performance targets of the subject high-pressure-ratio centrifugal compressor can be met or exceeded by recommended application of aerodynamic principles, it must be borne in mind that it is easier to make recommendations in retrospect than to meet ambitious predictions in prospect, and it should be made clear that no degradation of the previous work is intended.

This report has been reviewed by technical personnel of this command, and the conclusions and recommendations contained herein are concurred in by this command.

TASK 1G162203D14413  
Contract DAAJ02-68-C-0073  
USAAVLABS TECHNICAL REPORT 69-76  
February 1970

FLUID MECHANICS ANALYSIS OF  
HIGH-PRESSURE-RATIO CENTRIFUGAL COMPRESSOR DATA

Final Report

by

Robert C. Dean, Jr.  
David D. Wright  
Peter W. Runstadler, Jr.

D D C  
RECORDED  
JUL 31 1970  
RECORDED  
B

Prepared by

Creare Incorporated  
Hanover, New Hampshire

for

U. S. ARMY AVIATION MATERIEL LABORATORIES  
FORT EUSTIS, VIRGINIA

This document is subject to special export controls, and each transmittal to foreign governments or foreign nationals may be made only with prior approval of U. S. Army Aviation Materiel Laboratories, Fort Eustis, Virginia 23604.

## SUMMARY

The results of a review and distillation of the fluid dynamic information gained during the Boeing-AVLABS program to develop superior high-pressure-ratio compressors for small gas turbine service are reported. The objectives were to critically test the design flow models proposed by Welliver and Acurio (1967) of Boeing, to improve these models where feasible, and then to redesign the compressor with concrete guidelines for reaching the U. S. Army Aviation Materiel Laboratories (USAAVLABS) target of pressure ratio 10 and 80% total to static stage efficiency at 2 lbm/sec flow.

This report presents an extensive review of the Boeing data and a testing of the Boeing flow models. The models are improved to a certain extent. Basic weaknesses in the scientific foundations are delineated. A research program to strengthen the foundations is presented in brief.

The redesign effort produced very encouraging results. By raising the specific speed, by adopting a tandem row transonic inducer, and by using an improved diffuser, a stage efficiency between 80% and 85% is predicted with confidence.

The results of this study are expected to enable the attainment of the USAAVLABS target without great difficulty in the next round of exploratory development

#### FOREWORD

We wish to acknowledge the contributions, support, and constructive criticism of people who have significantly aided this work.

A. D. Welliver of the Commercial Airplane Division, The Boeing Company, served as a consultant on this program. His critical, often outspoken reviews of our findings and conclusions were essential to success. He provided a direct link to the Boeing-AVLABS effort, which he directed. Most importantly, his conditioned feel for the truth about turbomachinery and the practicality of new concepts has kept us closer to the right way than we would have gone alone.

Various centrifugal compressor experts have reviewed parts of this work and offered helpful comments. We appreciate those efforts, particularly of Colin Rodgers of Solar and David Kenny of Pratt and Whitney.

Behind all of our knowledge lies a long research effort. The development of whatever expertise we have in centrifugal compressor fluid mechanics has been sponsored by numerous industrial organizations over the past fifteen years. To them we owe a basic debt of gratitude.

Finally, we especially want to recognize and praise the support of this somewhat uncommon program by the United States Army Aviation Materiel Laboratories. Particularly the patient guidance of Robert Langworthy and Henry Morrow has been stimulating and essential. Their knowledge and appreciation of the information to be gained from this work was in large part responsible for these results.

The effort reported herein was authorized by DA Task LG162203D14413.

## TABLE OF CONTENTS

	<u>Page</u>
SUMMARY . . . . .	iii
FOREWORD . . . . .	iv
LIST OF ILLUSTRATIONS . . . . .	x
LIST OF TABLES . . . . .	xxiii
LIST OF SYMBOLS . . . . .	xxv
1.0 INTRODUCTION . . . . .	1
2.0 OBJECTIVES . . . . .	2
3.0 DATA EMPLOYED FROM THE BOEING-USAAVLABS PROGRAM. . . . .	4
3.1 Workhorse Geometry & Instrumentation. . .	6
3.2 RF-2 Geometry & Instrumentation . . . . .	16
3.3 Workhorse Stage Data. . . . .	33
3.4 RF-2 Stage Data . . . . .	57
4.0 ANALYSIS OF THE INFORMATION CONTENT OF THE DATA . . . . .	120
4.1 Impeller Internal Flow Data . . . . .	121
4.2 Significance of Impeller Tip Measure- ments . . . . .	126
4.2.1 Introduction . . . . .	126
4.2.2 Input Information. . . . .	130
4.2.3 True Mixing Loss . . . . .	134
4.2.4 Instrument Indications . . . . .	143
4.2.5 Comparison of "Instrument- Indicated" Flow Properties and "True" Properties. . . . .	151
4.2.6 Utilization of Impeller Tip Measurements . . . . .	157

	<u>Page</u>
4.2.7 Comparison of Results. . . . .	164
4.2.8 Significance of Errors Produced by Instrument Indications. . . . .	165
4.3 Diffuser Data . . . . .	167
4.3.1 Selection of Data. . . . .	167
4.3.2 Uncertainty Analysis . . . . .	169
<b>5.0 TESTS OF EXISTING FLOW MODELS FOR DESIGN PREDICTIONS. . . . .</b>	<b>179</b>
5.1 Test of Inducer Leading Edge Model. . . . .	182
5.1.1 Inlet Vector Diagrams. . . . .	183
5.1.2 Inlet Blockage Factors . . . . .	183
5.1.3 Flow Incidence Angles. . . . .	183
5.1.4 Supercritical Flow . . . . .	185
5.1.5 Reynolds Number Effects. . . . .	186
5.1.6 Conclusion . . . . .	188
5.2 Inducer Flow Distribution . . . . .	190
5.2.1 Selection of Data. . . . .	192
5.2.2 Evidence That Workhorse Separates on the Hub . . . . .	192
5.2.3 RF-2 Inducer Flow. . . . .	196
5.3 Impeller Separation Point Prediction Model . . . . .	211
5.3.1 Impeller Separation Predictions. .	212
5.4 Impeller Separated Flow . . . . .	220
5.4.1 Calculation of Wake Pressure . . .	220
5.4.2 Results of Wake Pressure Comparison . . . . .	223
5.4.3 Conclusions. . . . .	226
5.5 Tests of Flow Models for Impeller Secondary Effects . . . . .	228
5.5.1 Cover Friction . . . . .	228
5.5.2 Rear Disc Friction . . . . .	231
5.5.3 Leakage over Blades. . . . .	232
5.5.4 Impeller Internal Shear Mixing and Passage Friction . . . . .	232
5.5.5 Secondary Flow . . . . .	235
5.6 Test of Impeller Discharge Flow Pattern Model . . . . .	237
5.7 Test of Impeller Discharge Mixing Model .	244
5.7.1 Influence of the Unknown Factors .	247
5.7.2 Test of the Mixing Loss Theory . .	251

	<u>Page</u>
5.8 Test of the Flow Models for the Vaneless and Semivaneless Space . . . . .	253
5.8.1 Test of Flow Model for Predicting Diffuser Throat Blockage . . . . .	254
5.8.1.1 Possible Causes of Discrepancy . . . . .	263
5.8.1.2 Summary . . . . .	272
5.8.2 Diffuser Entry Model . . . . .	273
5.9 Comparison of Creare-USAAVLABS Channel Diffuser Data With Boeing-USAAVLABS Diffuser Data . . . . .	289
5.9.1 Uncertainty. . . . .	289
5.9.2 Data Reduction . . . . .	289
5.9.3 Comparison . . . . .	292
5.9.4 Summary of Tests of Channel Diffuser Models. . . . .	297
5.10 Summary Assessment of Adequacy of Existing Models . . . . .	299
 6.0 DEVELOPMENT OF NEW FLOW MODELS . . . . .	302
6.1 Inducer Flow. . . . .	303
6.1.1 Transonic Airfoil Theory . . . . .	307
6.1.2 Adaptation of Transonic Airfoil Theory to Inducer Flow . . . . .	322
6.1.3 Comments . . . . .	327
6.1.4 Conclusions. . . . .	327
6.2 Inducer Pressure Distribution . . . . .	329
6.3 Impeller Separation . . . . .	331
6.4 Impeller Separated Flow and Discharge Pattern . . . . .	334
6.5 Improved Models for Secondary Effects . .	336
6.5.1 Cover Friction Losses and Influ- ence on Internal Flow. . . . .	336
6.5.2 Rear Disc Friction . . . . .	336
6.5.3 Impeller Blade Tip Leakage . . . . .	338
6.5.4 Internal Shear & Passage Friction.	339
6.5.5 Secondary Flow . . . . .	340
6.5.6 Summary. . . . .	341
6.6 Impeller Discharge Mixing . . . . .	344
6.7 Impeller-Diffuser Interaction . . . . .	347

	<u>Page</u>
6.7.1 Nature of Diffuser Backflow Into Impeller. . . . .	350
6.7.2 Estimate of Backflow Work Input. .	356
6.8 Diffuser Entry Flow . . . . .	362
6.8.1 General Description of Flow. . . .	362
6.8.1.1 Flow in Absence of Side- wall Effects. . . . .	362
6.8.1.2 Sidewall Boundary Layer Effects . . . . .	367
6.8.1.3 Shock Wave - Sidewall Boundary Layer Inter- action. . . . .	370
6.8.2 The Development of a Boundary Layer Analysis for the Diffuser Entry. . . . .	370
6.8.3 Qualitative Design Rules . . . . .	378
6.8.4 Practical Prediction of Blockage .	384
6.9 Diffuser Design Methods . . . . .	391
6.9.1 Diffuser Passage Design. . . . .	391
6.9.2 Secondary Effects. . . . .	401
6.9.3 Surge Prediction Model . . . . .	403
6.9.4 Choke Prediction . . . . .	409
7.0 STAGE REDESIGN . . . . .	411
7.1 Inducer and Impeller Geometry to Separation. . . . .	412
7.2 Impeller Geometry After Separation . .	431
7.3 Impeller Tip-Diffuser Entry . . . . .	433
7.3.1 Impeller Discharge Mixing Losses .	434
7.3.2 Diffuser Entry Region. . . . .	436
7.4 Vane Diffuser Geometry. . . . .	446
7.4.1 Optimization of the Cascade Diffuser . . . . .	449
7.4.2 Deswirl. . . . .	453
7.5 Stage Characteristics . . . . .	456
8.0 RESEARCH NEEDED. . . . .	463
8.1 Inducer . . . . .	464
8.1.1 The Subsonic Inducer . . . . .	464
8.1.2 Separation Prediction & Control. .	466

	<u>Page</u>
8.1.3 Transonic Inducer. . . . .	466
8.1.4 Coupling Between Transonic & Subsonic Inducers. . . . .	466
8.1.5 Inducer Exploratory Development. .	467
8.2 Impeller. . . . .	468
8.3 Impeller Tip/Diffuser Entry . . . . .	472
8.4 Diffusers . . . . .	476
8.5 Instrumentation . . . . .	477
8.6 Miscellaneous . . . . .	478
 9.0 CONCLUSIONS. . . . .	479
 10.0 RECOMMENDATIONS. . . . .	481
 11.0 LITERATURE CITED . . . . .	483
 APPENDICES	
I. Yaw Probe - Error Caused by Velocity Gradient. . . . .	490
II. Impeller Discharge Mixing -- Sudden Expansion Analysis. . . . .	493
III. Impeller Internal Separated Flow Model.	501
IV. Preparation of Diffuser Isobaric Plots.	511
V. Sample Uncertainty Calculation for Welliver and Acurio Channel Diffuser Data. . . . .	515
VI. Data Reductions for Section 4.3 . . . .	520
VII. Definition of $p_T_{rel}$ . . . . .	527
 DISTRIBUTION . . . . .	529

## LIST OF ILLUSTRATIONS

<u>Figure</u>	<u>Page</u>
1 Coordinate System . . . . .	xxvi
2 Station Convention and Stage Terminology . . .	xxvii
3 Vane-Island Diffuser Geometry . . . . .	xxviii
4 Impeller Geometry . . . . .	7
5 Diffuser Backplate Instrumentation as Viewed From Compressor Inlet . . . . .	11
6 Cover Static Pressure Taps. Workhorse . . . .	12
7 Impeller Tip Probes. Workhorse . . . . .	13
8 Railroad Track Traversing Stagnation Pressure Probe. Workhorse . . . . .	14
9 Locations of Impeller Tip Probes at Typical Setting. Workhorse . . . . .	15
10 Impeller Geometry at Zero RPM. RF-2 . . . .	17
11 Geometric Relations. RF-2 . . . . .	19
12 Cover Static Pressure Taps. RF-2 . . . . .	22
13 VI-3 and VI-4 Diffuser Geometry. RF-2 . . . .	23
14 V2 and V2-2 Diffuser Geometry. RF-2 . . . .	25
15 Circumferential Cover Static Pressure Tap Locations. RF-2 . . . . .	27
16 Diffuser Backplate Instrumentation as Viewed from Compressor Inlet. RF-2 . . . . .	28
17 Locations of Impeller Tip Probes at a Typical Setting . . . . .	30

<u>Figure</u>		<u>Page</u>
18	Impeller Tip Probes. RF-2. . . . .	31
19	Diffuser Throat Stagnation Pressure Rakes . .	32
20	Cover Static Pressure. Workhorse . . . . .	36
21	Cover Static Pressure. Workhorse . . . . .	37
22	Impeller Tip Stagnation Pressure. Workhorse .	38
23	Impeller Tip Stagnation Pressure. Workhorse .	39
24	Impeller Tip Flow Angle. Workhorse . . . . .	40
25	Impeller Tip Stagnation Temperature. Workhorse	41
26	DI-1 Diffuser Static Pressure Tap Locations and Numbers. Workhorse . . . . .	43
27	Static Pressure Field. Workhorse . . . . .	45
28	Static Pressure Field. Workhorse . . . . .	46
29	Static Pressure Field. Workhorse . . . . .	47
30	Stagnation Pressure Traverse Data From Railroad Track Probe. Workhorse . . . . .	48
31	Stagnation Pressure Traverse Data From Railroad Track Probe. Workhorse . . . . .	49
32	Schlieren Photographs of DI-1. Workhorse . . .	50
33	Oil Slick Trace, 30,000 RPM. Workhorse, DI-1, Line 5 . . . . .	51
34	Oil Slick Trace, 38,400 RPM. Workhorse, DI-1, Line 7 . . . . .	52
35	Collector Temperature Rise Versus Mass Flow. Workhorse . . . . .	53

<u>Figure</u>		<u>Page</u>
36	Collector Static Pressure Ratio Versus Mass Flow. Workhorse . . . . .	54
37	Collector Static Pressure Ratio Versus Mass Flow. Workhorse . . . . .	55
38	Diffuser Traverse with Total Probe at Station 1 - DI-1, Conditions Unknown. Workhorse . . . . .	56
39	Cover Static Pressure. RF-2 . . . . .	61
40	Cover and Hub Static Pressure. RF-2. . . . .	62
41	Cover Static Pressure. RF-2 . . . . .	63
42	Impeller Tip Stagnation Pressure. RF-2. . . .	64
43	Impeller Tip Stagnation Pressure. RF-2 . . . .	65
44	Impeller Tip Stagnation Pressure. RF-2 . . . .	66
45	Impeller Tip Stagnation Pressure. RF-2 . . . .	67
46	Impeller Tip Stagnation Pressure. RF-2 . . . .	68
47	Impeller Tip Flow Angle. RF-2 . . . . .	69
48	Impeller Tip Stagnation Temperature. RF-2 . .	70
49	V1-3 Diffuser Static Pressure Taps. RF-2. . .	71
50	Diffuser Static Pressures. RF-2. . . . .	73
51	Diffuser Static Pressures. RF-2. . . . .	74
52	Diffuser Static Pressures. RF-2. . . . .	75
53	Diffuser Static Pressures. RF-2. . . . .	76
54	Diffuser Static Pressures. RF-2. . . . .	77

<u>Figure</u>		<u>Page</u>
55	Diffuser Static Pressures. RF-2. . . . .	78
56	Diffuser Throat Stagnation Pressure. RF-2. . .	79
57	Diffuser Throat Stagnation Pressure. RF-2. . .	80
58	Collector Temperature Rise Versus Mass Flow. RF-2. .	81
59	Collector Static Pressure Ratio Versus Mass Flow. RF-2. . . . . . . . . . . . . . . . . . .	82
60	Cover Static Pressure. RF-2 . . . . . . . . .	83
61	Cover Static Pressure. RF-2. . . . . . . . .	84
62	Cover Static Pressure. RF-2. . . . . . . . .	85
63	V1-4 Diffuser Static Pressure Taps. RF-2 . . .	87
64	Diffuser Static Pressure. RF-2 . . . . . . .	89
65	Diffuser Static Pressure. RF-2 . . . . . . .	90
66	Diffuser Static Pressure. RF-2 . . . . . . .	91
67	Diffuser Throat Stagnation Pressure. RF-2 . .	92
68	Diffuser Throat Stagnation Pressure. RF-2 . .	93
69	Collector Temperature Rise Versus Mass Flow. RF-2 .	94
70	Collector Static Pressure Ratio Versus Mass Flow. RF-2 . . . . . . . . . . . . . . . . . . .	95
71	Cover and Hub Static Pressure. RF-2. . . . .	96
72	Impeller Tip Stagnation Pressure. RF-2 . . . .	97
73	Impeller Tip Stagnation Pressure. RF-2 . . . .	98
74	V2 Diffuser Static Pressure Taps. RF-2 . . . .	99

<u>Figure</u>		<u>Page</u>
75	Diffuser Static Pressures. RF-2 . . . . .	101
76	Diffuser Static Pressures. RF-2 . . . . .	102
77	Diffuser Static Pressures. RF-2 . . . . .	103
78	Diffuser Throat Stagnation Pressure. RF-2 . . .	104
79	Diffuser Throat Stagnation Pressure. RF-2 . . .	105
80	Collector Temperature Rise Versus Mass Flow RF-2 .	106
81	Collector Static Pressure Ratio Versus Mass Flow. RF-2. . . . . . . . . . . . . . . . . . .	107
82	Cover and Hub Static Pressure. RF-2 . . . . .	108
83	Impeller Tip Stagnation Pressure. RF-2. . . . .	109
84	Impeller Tip Stagnation Pressure. RF-2. . . . .	110
85	V2-2 Diffuser Static Pressure Taps. . . . .	111
86	Diffuser Static Pressures. RF-2 . . . . .	113
87	Diffuser Static Pressures. RF-2 . . . . .	114
88	Diffuser Static Pressures. RF-2 . . . . .	115
89	Diffuser Throat Stagnation Pressure. RF-2 . . .	116
90	Diffuser Throat Stagnation Pressure. RF-2 . . .	117
91	Collector Temperature Rise Versus Mass Flow RF-2 .	118
92	Collector Static Pressure Ratio Versus Mass Flow. RF-2 . . . . . . . . . . . . . . . . . . .	119
93	Tangential Variation of Cover Pressure. . . . .	123

<u>Figure</u>	<u>Page</u>
94 Cover Static Pressure (Station 15) Verses Mass Flow . . . . .	125
95 Workhouse Impeller Discharge Loss Calculations . . . . .	127
96 RF-2 Impeller Discharge Loss Calculations . .	128
97 Schematic of Impeller Outflow Geometry . . . .	133
98 Separation Line Geometry . . . . .	135
99 Development of the Wake . . . . .	136
100 Assumed $p_{O_2}$ Distribution . . . . .	137
101 Assumed $T_{O_2}$ Distribution . . . . .	138
102 Assumed $C_{r_2}$ Distribution . . . . .	139
103 Assumed $C_{e_2}$ Distribution . . . . .	140
104 Calculated $p_2$ Distribution . . . . .	141
105 Steady Flow Yaw Angle Sensitivity of Cobra- Type Yaw Probes . . . . .	148
106 Comparison of "True" and "Instrument Indicated" Impeller Discharge Profiles . . . . .	154
107 Axial Flow Angle Distribution. Comparison of "True" and "Instrument Indicated" Values . . .	156
108 Boeing's Flowmeter Setup in Workhorse and RF-2 . . . . .	172
109 Pressure Tap Errors . . . . .	174
110 Static Pressure Errors as a Function of Mach Number . . . . .	175
111 Definition of Inducer Incidence Angle . . . .	182

<u>Figure</u>	<u>Page</u>
112 The Influence of Impeller Relative Diffusion on Compressor Stage Efficiency, Showing RF-2 Performance . . . . .	191
113 Workhorse Cover Static Pressure Verses Meridional Distance From Leading Edge . . . . .	194
114 Potential Solution, Blade-Surface Velocities, Workhorse ( $W_1 = 1086$ ) . . . . . rms	195
115 Comparison of Typical Impeller Discharge Profiles for Workhorse and RF-2 . . . . .	197
116 Impeller Cover Pressure Data, Results of Potential Solutions and Separated Impeller Theory . . . . .	199
117 Cover Tap Data Showing Construction of Mean Curve . . . . .	202
118 A Comparison of Cover Data and Potential Solutions by Welliver and Acurio (1967, 67-45) and by Winslow (1968) . . . . .	205
119 Aerodynamic Blockage in Inducer Required to Bring Isentropic Potential Solution (2% Blockage Already) into Agreement With Measured Cover Pressure at Design Point (Potential Solution 2.0 lb m/sec; data 2.0 lb m/sec) . .	207
120 Dependence of Tip Pressure upon Separation Pressure . . . . .	209
121 Boundary Layer Calculation With Potential Solution . . . . .	213
122 Cover Pressure Prediction of Relative Mach Number With Three Assumed Overvelocities . .	214
123 Boundary Layer Calculations Using Measured Pressure in the Inducer . . . . .	216

<u>Figure</u>		<u>Page</u>
124	Boundary Layer Calculations Using Measured Pressure in the Inducer . . . . .	217
125	Boundary Layer Calculations Using Measured Pressure in the Inducer . . . . .	218
126	Model for Jet Pressure Variation . . . . .	221
127	RF-2 Blade Loading at the Cover From the Potential Solution . . . . .	224
128	Calculated Relative Mach Number of Jet at Various Radii and with Various Tip Mean Slip Factor Assumptions - Based on Measured Cover Pressure Data. . . . .	225
129	Wiesner's (1967) Slip Factor Correlation Showing Scatter of Slip and Deviation Data Verses Correlation Factor . . . . .	239
130	Vaneless and Semivaneless Space Loss in Excess of Impeller Discharge Mixing Loss, $P_o^* - P_{o_4}$ . . . . .	248
131	Mixed-out Radius Ratio, $R^*$ , Verses Impeller Tip Swirl Parameter $\lambda_2 = (C_o/C_r)$ and Wake Width $E_2$ . . . . .	250
132	Impeller Discharge Mixing (Extrapolated From Figure 131) . . . . .	250
133	Isobaric Plot for Test 3366 . . . . .	255
134	Isobaric Plot for Test 3369 . . . . .	257
135	Boundary Layer Calculation for Test 3354, Line 7 . . . . .	260
136	Boundary Layer Calculation for Test 3366, Line 5 . . . . .	261
137	Boundary Layer Calculation for Test 3369, Line 5 . . . . .	262

<u>Figure</u>	<u>Page</u>
138 Throat Blockage Comparison . . . . .	264
139 Schematic of Impeller Jet and Wake Moving Through the Diffuser . . . . .	269
140 Penetration of Wake Fluid into Jet Fluid -- Schematic of Changing Interface Form . . . .	271
141 Schematic of Vortex Roll-up on Interfaces; Between Jet and Wake . . . . .	271
142 Comparison of Pressure Recovery for Compre- sor Channel With Two-Dimensional Diffuser Data-Workhorse . . . . .	274
143 Diffuser Throat Centerline Stagnation Pressure Deduced by $p_x - p_y$ Method- Workhorse . . . . .	276
144 Static-Pressure Variation in Diffuser - RF-2	279
145 Static-Pressure Variation in Diffuser - RF-2	280
146 Static-Pressure Variation in Diffuser - RF-2	281
147 Static-Pressure Variation in Diffuser - RF-2	282
148 Comparison of Boeing-AVLABS Channel Diffuser Data From Compressors With Creare-AVLABS Straight-Channel Diffuser Data. Pressure Recovery C Verses Throat Blockage $B_4$ and Mach Number $M_4$ . . . . .	293
149 Comparison of Boeing-AVLABS Channel Diffuser Data From Compressors With Creare-AVLABS Straight-Channel Diffuser Data. Pressure Recovery C Verses Throat Blockage $B_4$ and Mach Number $M_4$ . . . . .	294

<u>Figure</u>	<u>Page</u>
150 Comparison of Boeing-AVLABS Channel Diffuser Data From Compressors With Creare-AVLABS Straight-Channel Diffuser Data. Pressure Recovery C Verses Throat Blockage $B_4$ and Mach Number $M_4$ . . . . .	295
151 Development of the Flow Past an Airfoil as the Stream Mach Number Increases to Unity . . . . .	308
152 Surface Pressure Classifications for Supercritical Approach Mach Numbers . . . . .	310
153 Schematic Representation of Expansion and Compression Waves Within Supersonic Region on "Peaky"-Type Airfoils . . . . .	311
154 "Roof Top" Pressure Distribution in the Supersonic Region on an Airfoil at Supercritical Approach Mach Numbers. Airfoil: NPL 491 . . . . .	313
155 Change in "Separation Effects" Boundary With Alteration in Leading Edge Radius and Parameter K. . . . .	316
156 Transonic Airfoil Correlation by Sinnott and Osborne (1961) . . . . .	319
157 Shock Location and Evaluation of Static Pressure Distribution on Transonic Airfoil . . . . .	320
158 Empirical Shock Pressure Ratio Relation Derived by Sinnott and Osborne (1961) . . . . .	321
159 Velocity Contours Around Centrifugal Compressor Inducer Leading Edge. Positive Incidence.	325
160 Velocity Contours Around Centrifugal Compressor Inducer Leading Edge. Negative Incidence.	325
161 Static Pressures at $R = 1.03$ . RF-2. . . . .	348

<u>Figure</u>	<u>Page</u>
162 Limiting Wall Streamline Traces From Faulder's (1954) Diffuser . . . . .	352
.163 Limiting Wall Streamline Traces From Faulder's (1954) Diffuser . . . . .	353
164 Schematic of Backflow Pattern in Rotor Space .	355
165 Interaction of Tip Leakage and Blade (Wall) Motion in an Axial Cascade . . . . .	357
166 Isobarics Measured in Workhorse Diffuser (Numbers on Contours are p) . . . . .	364
167 Diffuser Sidewall Separation Measured by Johnston (1954) in Faulder's (1954) Vaned Diffuser . . . . .	368
168 Diffuser Entry Shock Pattern . . . . .	371
169 Coordinate System . . . . .	375
170 Vane Leading Edge Shape Concept to Accommodate Streamline Orientation . . . . .	385
171 Variation of Channel Diffuser Recovery With $B_4$ and $AS_4$ (Runstadler 1969). . . . .	390
172 Cascade and Vane-Island Diffusers. . . . .	392
173 Straight-Channel Diffuser Performance (Runstadler 1969). . . . .	394
174 Straight-Channel Diffuser Performance (Runstadler 1969). . . . .	395
175 Straight-Channel Diffuser Performance (Runstadler 1969). . . . .	396
176 Variation of Blockage With Diffuser Throat Depth for Constant $A_4$ and $\delta^*$ . . . . .	398

<u>Figure</u>	<u>Page</u>
177 Variation of Maximum Recovery With Blockage. . . . .	399
178 Schematic of Channel Diffuser Recovery Characteristics. . . . .	405
179 Channel Diffuser Pressure Recovery Versus Mass Flow. . . . .	406
180 Balje's Correlation of Efficiency Versus Specific Speed . . . . .	414
181 Variation of Inducer Tip Relative Mach Number With Specific Speed and Pressure Ratio. . . . .	415
182 The Influence of Inducer Tip Mach Number on Stage Efficiency (Single-Row Inducers) . . . . .	417
183 Variation of Impeller Friction Work With Inlet Preswirl Angle (for Morris and Kenny's Impeller). . . . .	418
184 State-of-the-Art Centrifugal Compressor Diffuser Performance and Projected Ultimate (from Dean 1968) . . . . .	419
185 Tandem Inducer Concept . . . . .	421
186 Transonic Inducer Vector Diagram . . . . .	424
187 Meridional Plan of Redesigned Stage . . . . .	427
188 Diffuser Entry Axial Expansion . . . . .	437
189 Comparison of Meridional and Streamline-Wise Views of Depth Expansion and Perturbation of Hub Wall Static Pressure Due to Wall Curvature. . . . .	439
190 Streamline Trajectory Changes Due to Diffuser Entry Axial Expansion. . . . .	440

<u>Figure</u>	<u>Page</u>
191 Mach Number Schedule of Various Axial Expansions . . . . .	441
192 Sidewall Boundary Layer Displacement Thickness Growth for Various Axial Expansions ( $\theta_i$ = initial momentum thickness assumed at $R = 1$ ). . . . .	443
193 Sidewall Boundary Layer Momentum Thickness Growth for Various Axial Expansions ( $\theta_i$ = initial value assumed at $R = 1$ ). . . . .	444
194 Boundary Layer Growth on Curved and Straight Sidewall . . . . .	445
195 Pressure Loading in Straight-Channel Cascade Diffuser . . . . .	448
196 Cascade Diffuser, First-Row Vanes. . . . .	454
197 State-of-the-Art Centrifugal Compressor Performance and Predicted Ultimate (from Dean 1968) . . . . .	474
198 Yaw Probe Geometry . . . . .	490
199 Control Volume Geometry. . . . .	495
200 Wake Static Pressure Ratio Versus Radius . . .	507
201 Pressures at Separation. . . . .	508
202 T-s Diagram for an Arbitrary Process Between Stagnation States 1 and 2. . . . .	527

LIST OF TABLES

<u>Table</u>		<u>Page</u>
I	Workhorse Impeller Geometry at Zero RPM . . . . .	8
II	Diffuser Geometry . . . . .	9
III	RF-2 Impeller Geometry at Zero Rpm . . . . .	21
IV	Summary of Workhorse Data . . . . .	34
V	Summary of RF-2 Data. . . . .	59
VI	Comparison of "True" and "Instrument Indicated" Reduced Data . . . . .	159
VII	Angle of Incidence as Calculated From Measured Static Pressures and Referenced to Mean Camber Line of Inducer Blade . . . . .	184
VIII	Inducer Blade Shape Kappa Factor (K). . . . .	187
IX	Test of Simple Mixing Calculation . . . . .	242
X	Comparison of Diffuser Data Reduction Schemes . . . . .	283
XI	Uncertainty in Creare-AVLABS Data . . . . .	290
XII	Diffuser Blockage Comparison. . . . .	388
XIII	Transonic Inducer . . . . .	422
XIV	Subsonic Inducer. . . . .	429
XV	Impeller Characteristics. . . . .	433
XVI	Increase in Stage Efficiency Due to Impeller Improvements (Compared to RF-2) . .	434
XVII	Impeller Tip Properties . . . . .	435

<u>Table</u>		<u>Page</u>
XVIII	Two-Row Cascade Diffuser Parameters . . .	455
XIX	Stage Characteristics . . . . .	457
XX	Summary of Losses (Decrease of Stage Efficiency in Points. . . . .	462

LIST OF SYMBOLS \*

A flow area (normal to mean velocity vector,  
specifically defined)

a acceleration

a speed of sound

AS channel diffuser throat aspect ratio (b/W)

B boundary layer blockage:

$$B = 1 - \frac{A_{\text{effective}}}{A_{\text{geometrical}}}$$

b meridional depth of passage (normal to mean  
meridional velocity component)

BF blockage factor:

$$BF = \frac{A_{\text{effective}}}{A_{\text{geometrical}}}$$

C absolute velocity (relative to a Newtonian frame,  
e.g., compressor casing)

c<sub>f</sub> wall friction coefficient:

$$c_f = \frac{T}{\rho w^2 / 2g_0}$$

where w is measured relative to subject wall

c<sub>p</sub> pressure recovery coefficient:

$$c_p = \frac{p_{\text{exit}} - p_{\text{ref}}}{(p_0 - p)_{\text{ref}}}$$

where measuring and reference states and  
stations must be specifically defined

c<sub>p</sub> specific heat at constant pressure

\* See Figures 1, 2, and 3 for visualization of the symbols.

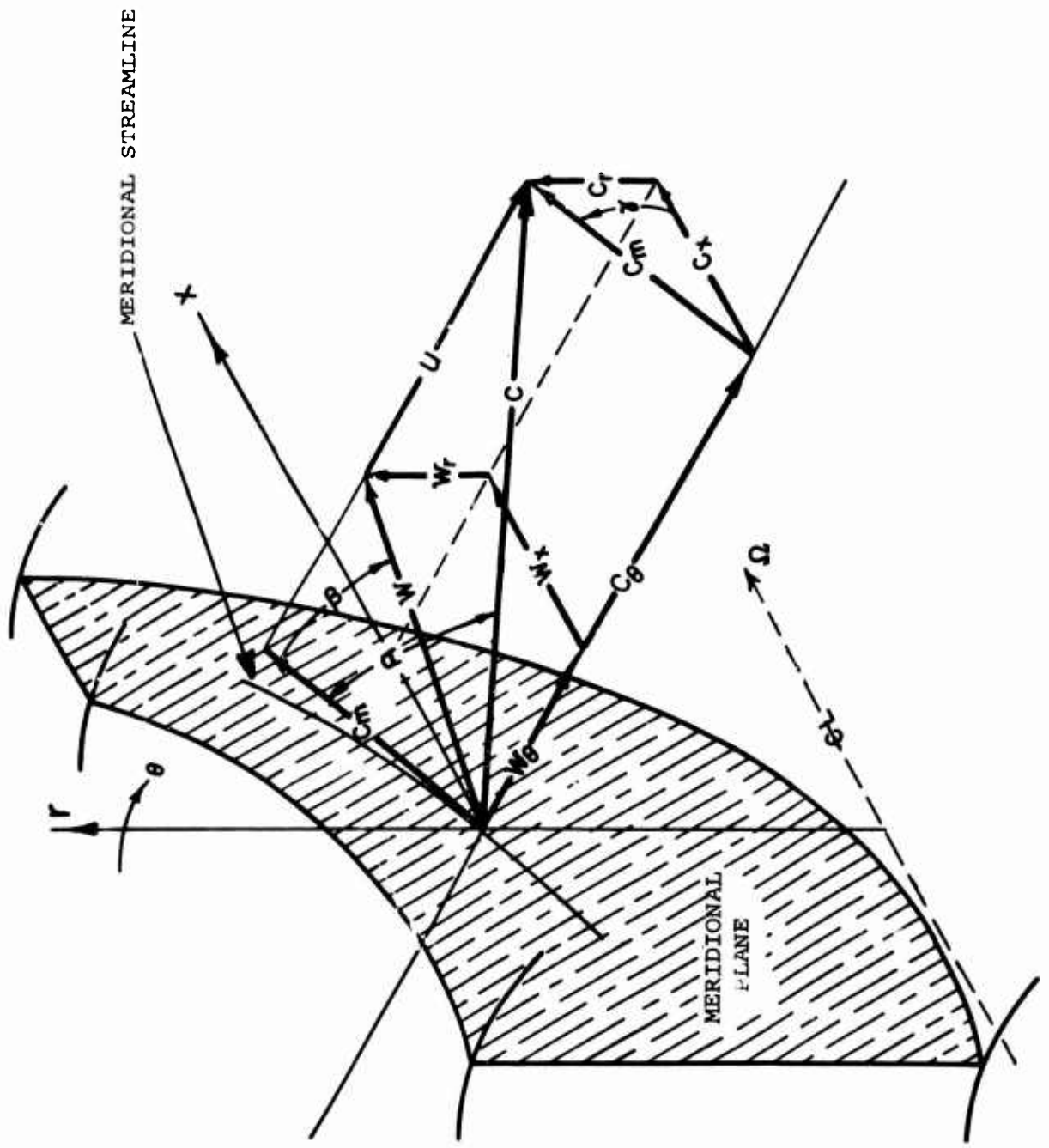


Figure 1. Coordinate System.

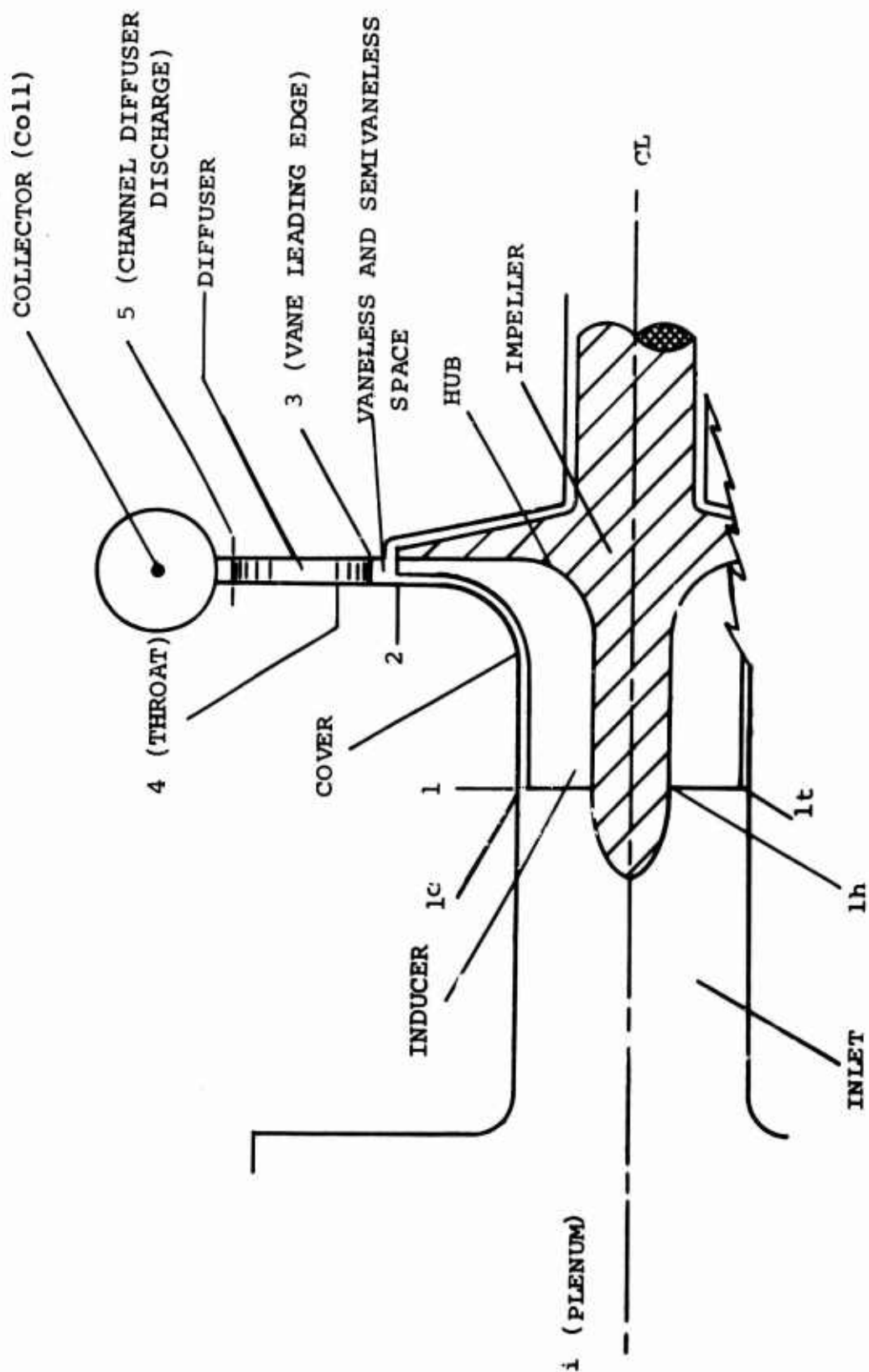
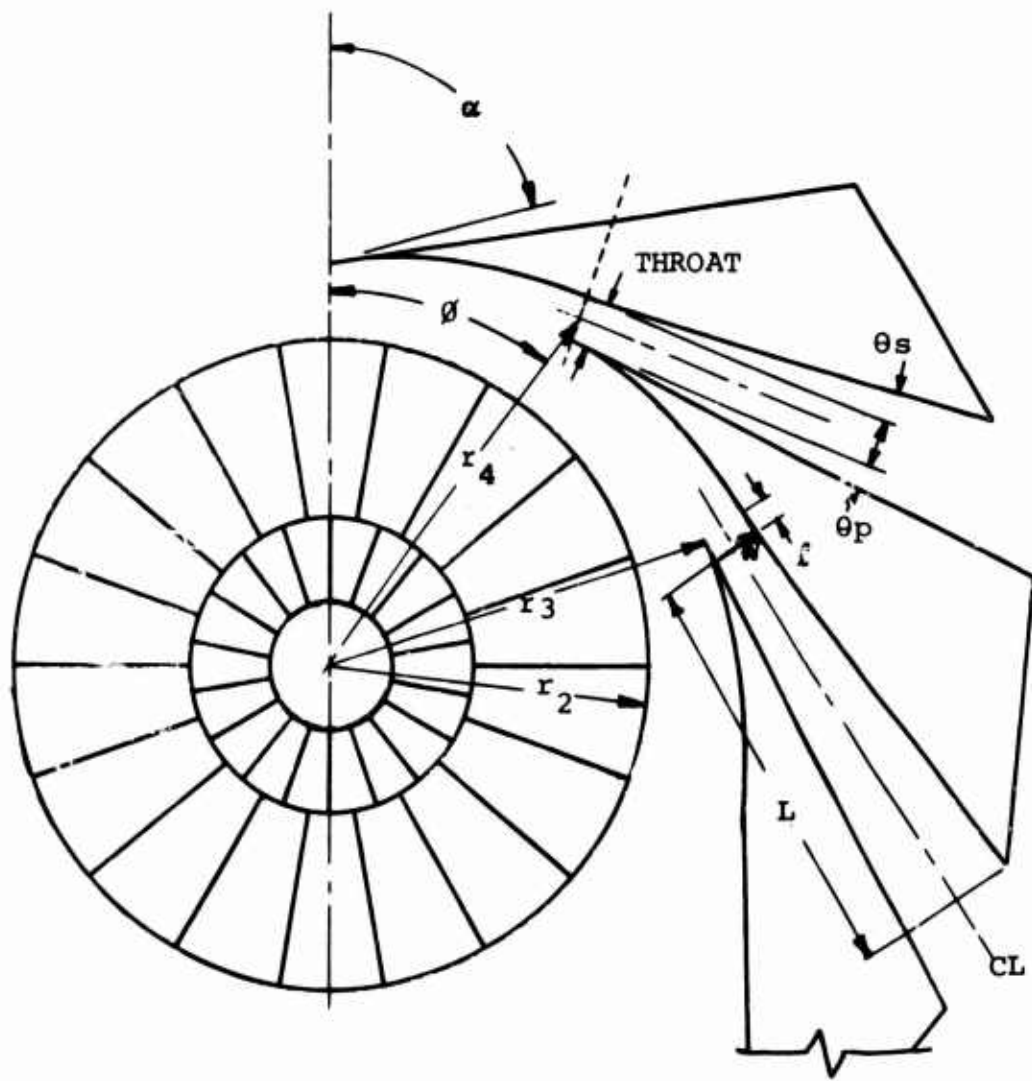


Figure 2. Station Convention and Stage Terminology.



WHERE  $\alpha$  = DIFFUSER ANGLE - FROM RADIAL TO "CENTER LINE" DIRECTION  
 $\theta$  = DIFFUSER VANE SPACING (ANGULAR)  
 $\theta_s$  = SUCTION SURFACE DIVERGENCE ANGLE  
 $\theta_p$  = PRESSURE SURFACE DIVERGENCE ANGLE  
 $w$  = THROAT WIDTH  
 $L$  = DIFFUSER LENGTH (OF BOUNDED REGION)  
 $r_2$  = IMPELLER TIP RADIUS  
 $r_3$  = DIFFUSER VANE LEADING EDGE RADIUS  
 $r_4$  = DIFFUSER THROAT RADIUS  
 $l$  = LENGTH OF CONSTANT AREA SECTION AHEAD OF THE THROAT

Figure 3. Vane-Island Diffuser Geometry.

DR diffusion ratio:

$$DR = w_1/w_{sep}$$

E energy

F force

g<sub>o</sub> proportionality constant in Newton's Second Law,

$$F = Ma/g_o$$

H boundary layer shape factor =  $\delta^*/\theta$

H<sub>i</sub> boundary layer shape factor for incompressible flow  
before transformation to compressible flow

h static enthalpy/unit mass

h<sub>o</sub> stagnation enthalpy/unit mass

h<sub>T</sub> total enthalpy/unit mass (in a coordinate system  
rotating in Newtonian space in absence of electricity,  
magnetism, gravity, and capillarity):

$$h_T = h + \frac{w^2 - u^2}{2g_o J}$$

i incidence angle of flow onto blades

J constant = 778 ft-lb<sub>f</sub>/BTU

k ratio of specific heats

L diffuser center line length (from throat to exit plane)

l length of channel diffuser throat, see Figure 3

M Mach number

M mass

m distance along specified meridional trajectory  
(often streamline or potential solution)

m mass flow rate

N shaft speed

$N_s$  specific speed:

$$N_s = \frac{N\sqrt{Q_i}}{(\Delta h_o)^{3/4}}$$

where  $N$  = rpm,  $Q_i$  = inlet flow =  $m/\rho_{o_i}$  in  $\text{ft}^3/\text{sec.}$

$\Delta h_o$  = stage enthalpy rise in  $\text{ft-lb}_f/\text{lbf}$

p static pressure

$p_o$  stagnation pressure

pr pressure ratio:

$$pr = p_{coll}/p_{o_i}$$

$p_T$  total pressure; a rotating coordinate property defined by:

$$\frac{p_T}{p_{o_i}} = \left(\frac{T_T}{T_{o_i}}\right)^{\frac{k}{k-1}}$$

q dynamic pressure:

$$q = \frac{1}{2g_o} \rho C^2$$

Q heat

R radius ratio,  $r/r_2$

R gas constant

R recovery factor:

$$R = \frac{p_o}{p_{o_{ref}}}$$

xxx

$^{\circ}R$  degrees Rankine  
 $r$  radius from impeller center line  
 $r$  radial coordinate (see Figure 1)  
 $S$  distance between impeller blades:  
$$S = 2\pi r/Z$$
  
 $s$  distance along streamline  
 $s$  entropy/unit mass  
 $T$  static temperature  
 $T_o$  stagnation temperature  
 $T_T$  total temperature (defined by  $h_T$  and  $c_p$  for a perfect gas)  
 $t$  blade thickness (in direction specified)  
 $u$  impeller (metal) velocity  
 $w$  diffuser throat width (in principal plane of divergence)  
 $w$  relative velocity (in coordinate system rotating steadily in Newtonian space)  
 $w_x$  shaft work per unit mass of fluid  
 $w_{x_i}$  work input to impeller per unit mass of fluid  
 $x$  axial coordinate (see Figure 1)  
 $Z$  number of blades  
 $\alpha$  absolute flow angle (see Figure 1)  
 $\beta$  relative flow angle (see Figure 1)

$\gamma$  pitch angle in meridional plane (see Figure 1)

$\delta^*$  boundary layer displacement thickness

$e$  ratio of wake/passage widths

$\eta$  efficiency:

$$\eta = \frac{h_{o_s} - h_{o_i}}{w_x}$$

(measuring stations must be specifically defined)

$\theta$  boundary layer momentum thickness

$\theta$  tangential angular coordinate (see Figure 1)

$2\theta$  diffuser divergence angle

$\theta_s$  or  $\theta_p$  divergence angle of suction or pressure surface of channel diffuser, see Figure 3.

$\lambda$  swirl parameter:

$$\lambda = c_\theta / c_r$$

$\mu_i$  work input coefficient:

$$\mu_i = \frac{w_x}{u^2 / g_o}$$

$\xi$  vorticity

$\pi Mi$  impeller tip Mach number:

$$\pi Mi = u_2 / a_{o_i}$$

$\rho$  density

$\rho_o$  stagnation density

$\sigma$  slip factor:

$$\sigma = \frac{C_\theta}{C_{\theta_{ref}}}$$

where  $C_{\theta_{ref}}$  = ideal tangential velocity imparted to fluid by impeller blade; for inclined blades must be specifically defined in terms of  $m$ ,  $\rho$ ,  $\beta_{blade}$ , etc.; for radial discharge blades ( $\beta_{blade} = 0$ ),  $C_{\theta_{ref}} = u_2$ .

$\tau$  fluid shear stress

$\tau$  torque

$\psi$  yaw angle (between velocity vector and null direction of flow angle measuring probe)

$\Omega$  impeller angular velocity

#### Subscripts

1, 2, 3, -- stations in the stage (see Figure 2)

blade blade property

CL center line

c cover

coll collector station (receiving volume after diffuser)

crit critical value (must be specifically defined)

d diffuser

eff effective

geom geometrical

h hub

i	inlet or impeller
j	jet
le	leading edge
o	stagnation
p	pressure surface of blade
r	radial component (see Figure 1)
ref	reference state or station (must be specifically defined)
rel	relative to impeller coordinates
s	indicates that process follows an isentropic path
s	suction surface
s	suction surface of blade
sep	flow separation value
surf	surface property
T	total (see definitions of $h_T$ , $T_T$ , and $p_T$ )
t	tip or throat
w	wake
x	upstream of shock (e.g., $M_x$ ) or axial component (see Figure 1) <sup>X</sup>
y	downstream of shock (e.g., $M_y$ )
$\theta$	tangential component (see Figure 1)

### Superscripts

- \* mixed out state (must be specifically defined)
- \*\* identifies diffuser entry core loss in excess of impeller discharge mixing
- ' time-varying property
- ^ instrument-indicated property
- ~ mass-flow-averaged property
- time-averaged property
- = area-averaged property
- vector quantity

### Miscellaneous

ln natural logarithm

log base 10 logarithm

exp  $\exp a \equiv e^a$

e base of the natural logarithms ( $e = 2.71828\dots$ )

f( ) function of ( )

$\tan^{-1}$  ( ) inverse operator:

$$\alpha = \tan^{-1} \lambda \quad \text{means} \quad \tan \alpha = \lambda$$

$\Delta$  incremental (but finite) change

$d$  incremental (but infinitesimal) change, total derivative

$\partial$  incremental (but infinitesimal) change, partial derivative

STANDARD UNITS

Except as noted, all quantities herein have the following units:

C, W, u	fps
c <sub>p</sub>	BTU/lbm - °R
F	lbf (pounds force)
g <sub>o</sub>	(1bm/lbf) ft/sec <sup>2</sup>
M	1bm (pounds mass)
m	lbm/sec
N	rpm
p, p <sub>o</sub> , p <sub>T</sub>	psia
q	psi
R	53.35 ft-lbf/lbm - °R
r, L, w, δ*, etc.	inches
s	BTU/lbm - °R
T, T <sub>o</sub> , T <sub>T</sub>	degrees Rankine (°R)
time	sec
w <sub>x</sub> , Q, h, h <sub>o</sub> , E, etc.	BTU/lbm
p	lbm/ft <sup>3</sup>
τ	torque, ft-lbf
τ	shear stress, psi
Ω	radians/sec
α, β, γ, ψ, etc.	degrees

## 1.0 INTRODUCTION

The exploratory development of high-pressure-ratio centrifugal stages carried out by the Turbine Division of The Boeing Company under U. S. Army Aviation Materiel Laboratories (USAAVLABS) sponsorship (Contract DA 44-177-AMC-173(T)) produced a very large amount of detailed data on internal flow. It also generated a number of new and improved fluid dynamic models for use in design. Due to the scope of that program, it was not possible to test the models fully nor to thoroughly diagnose all of the data collected. Therefore, USAAVLABS empowered Creare Incorporated (a consultant to the Boeing-AVLABS program) to make a thorough study of the data and flow models, with the objective of improving these models where needed and redesigning the stage so that the original objective of pressure ratio 10 and 80% efficiency could be achieved. This report presents the results of that effort.

Section 3 contains all data selected for study and describes the instrumentation probes used to obtain the data. This is followed by a critical examination of the possible and probable errors in the data, Section 4.

The rest of the report deals with testing design flow models against the data and improving these flow models where required. A redesign study and a recommended research program conclude the work.

## 2.0 OBJECTIVES

The objectives of this program were:

### 2.1 DATA REVIEW

Review all Government-furnished impeller, diffuser, and overall compressor stage data previously collected under Contract DA 44-177-AMC-173(T), and determine which data are consistent from a basic fluid dynamic point of view. Any data found to be fluid dynamically inconsistent under this review shall be so labeled and excluded from further examination.

### 2.2 FLUID DYNAMIC EVALUATION

Perform a fluid dynamic evaluation of the data using the best fluid dynamic techniques currently available. The results of this evaluation shall include, but not necessarily be limited to, information obtained relative to:

- (1) The amount of impeller diffusion actually obtained.
- (2) The location of the flow separation point in the impeller.
- (3) The fluid and flow properties at the impeller discharge.
- (4) Mixing losses.
- (5) The proportion of impeller discharge area that is jet flow in terms of flow area and the quantity of fluid leaving the impeller.
- (6) Diffuser-impeller coupling.
- (7) Impeller performance, diffuser performance, and stage performance.

### 2.3 FLOW MODEL DEVELOPMENT AND EVALUATION

Compare the results of the fluid dynamic evaluation performed pursuant to Paragraph 2.2 above, with the results predicted by currently available flow models. The results of this comparison should include but not necessarily be limited to:

- (1) Fluid dynamics of impeller, diffuser, and stage.
- (2) Impeller diffusion.
- (3) Location of the separation point in the impeller.
- (4) Mixing losses.
- (5) Diffuser-impeller coupling.
- (6) Fluid and flow properties at impeller discharge.
- (7) Compressor range and surge point.
- (8) Sensitivity of overall compressor performance to changes in either impeller or diffuser.

#### **2.4 RECOMMENDATIONS FOR IMPROVEMENT**

Make recommendations relative to the design of a small, high-pressure-ratio centrifugal compressor (corrected weight rate of air flow approximately 2 lb/sec at 10:1 pressure ratio) based on the results of the work performed under Paragraphs 2.1 and 2.2 above. These recommendations shall take the form of:

- (1) Design improvements with predictions of the gains to be realized from these improvements and the certainty of those gains.
- (2) Critical research needed to improve the design criteria of centrifugal compressors.
- (3) Presentation of flow models as improved as a result of this study.

### 3.0 DATA EMPLOYED FROM THE BOEING-USAAVLABS PROGRAM

Boeing tested three radial compressor designs and two mixed flow designs. In addition, various diffuser systems were used with some of the basic compressor configurations. We have selected two stages for analysis; they are designated Workhorse and RF-2 stages. Some of the other configurations tested used vaneless diffusers which were badly stalled due to the high impeller exit swirl. All but Workhorse and RF-2 offer very limited and uncertain data.

The Workhorse stage was developed from a previous compressor with a 6:1 pressure ratio; to achieve the 10:1 overall pressure ratio target, the wheel diameter was extended to 9.2 in. This stage was built primarily to test diffuser configurations in the development of the high-pressure-ratio centrifugal compressor stage. It was to be representative of a typical centrifugal impeller but was not intended to have particularly high performance. As it turned out, the Workhorse stage had higher performance than any of the other stages tested in the first phase of the compressor research program as reported in Welliver and Acurio (1967, 67-30). Several diffuser configurations were tested with this stage, but we have been able to find only one complete set of data which includes impeller measurements and diffuser throat stagnation pressure measurements.

The instrumentation used with the Workhorse stage is explained in Section 3.1. The data for the Workhorse stage are in Section 3.3.

The RF-2 stage was then built as a culmination of the efforts of the previous research. This stage had a higher overall pressure ratio than Workhorse at a higher efficiency and a slightly lower mass flow. Boeing tested 16 different diffuser configurations with the RF-2; we have included data from only 4 of these because these 4 cases are the only ones offering a full set of impeller and diffuser measurements.

The instrumentation locations for RF-2 are described in Section 3.2, while the data are presented in Section 3.4.

Most of the measurements have been corrected to standard reference conditions by Boeing. These corrections consist of defining two factors: a pressure ratio correction factor and a temperature ratio correction factor. These factors are merely the ratios of the properties actually measured in the inlet duct (stagnation temperature and pressure) to the standard values of 520° R and 14.7 psi (29.92 in. Hg). The data have then been corrected in the following way: all pressures and temperatures are divided by the respective correction factors, and the mass flow has been multiplied by the square root of the temperature correction factor and divided by the pressure correction factor. The rotative speed is divided by the square root of the temperature correction factor.

All of the data for RF-2 and most of the data for Workhorse have been corrected in this manner. Uncorrected data are marked; if the pressure correction factors are available, they are indicated on the figure.

The references to "line number" designate (qualitatively) different mass flows. Line three is near surge, line seven is near choke, and line five is about mid-range. The usage shifted slightly from Workhorse to RF-2, and no quantitative importance should be attached to it -- only the qualitative meaning suggested above.

### 3.1 WORKHORSE GEOMETRY AND INSTRUMENTATION

The aerodynamic design of the Workhorse impeller is given in Figure 4 and Table I for 0 rpm. At 50,000 rpm, Boeing estimates the radial deflection of the impeller tip to be 0.020 inch. There were 23 impeller blades and 17 inlet guide vanes.

Data are reported for inlet guide vane settings of 0° and 17° (prewhirl in direction of impeller rotation). The guide vane flow deflection angles were not measured, but were deduced from Carter's rule. There was a total pressure loss across the inlet guide vanes even when they were set in the 0° position (0.967 stagnation pressure ratio deduced from the change in choking flow on removal of the guide vanes). Some of the data has been corrected for this loss. This is marked where it has been done.

The diffuser configuration for Workhorse used here is called the DI-1. Its geometry is tabulated in Table II.

The inlet duct for Workhorse was bell-shaped. Stagnation temperature and pressure profiles were measured there for deducing inlet conditions. In front of the bell-mouthed inlet was a short duct connecting the compressor to the flowmeter plenum chamber. (See Figure 108)

There are many details of construction of the Workhorse compressor which may be of interest. Those not recorded here can be found in Welliver and Acurio (1967, 67-30).

The design conditions for Workhorse were 2.43 lbm/sec, 50,000 rpm, overall pressure ratio 10:1, and total to static efficiency of 80%. The highest reported total to static efficiency for the Workhorse stage was 70.3% at pressure ratio 8.9:1 and 2.37 lbm/sec. The highest efficiency using the DI-1 diffuser configuration was 69.6% at pressure ratio 8.6:1 and 2.2 lbm/sec.

Summary of the data incorporated in this study appears on page 21. In order to get one complete set of data we have included data from many different tests. The individual tests are clearly designated.

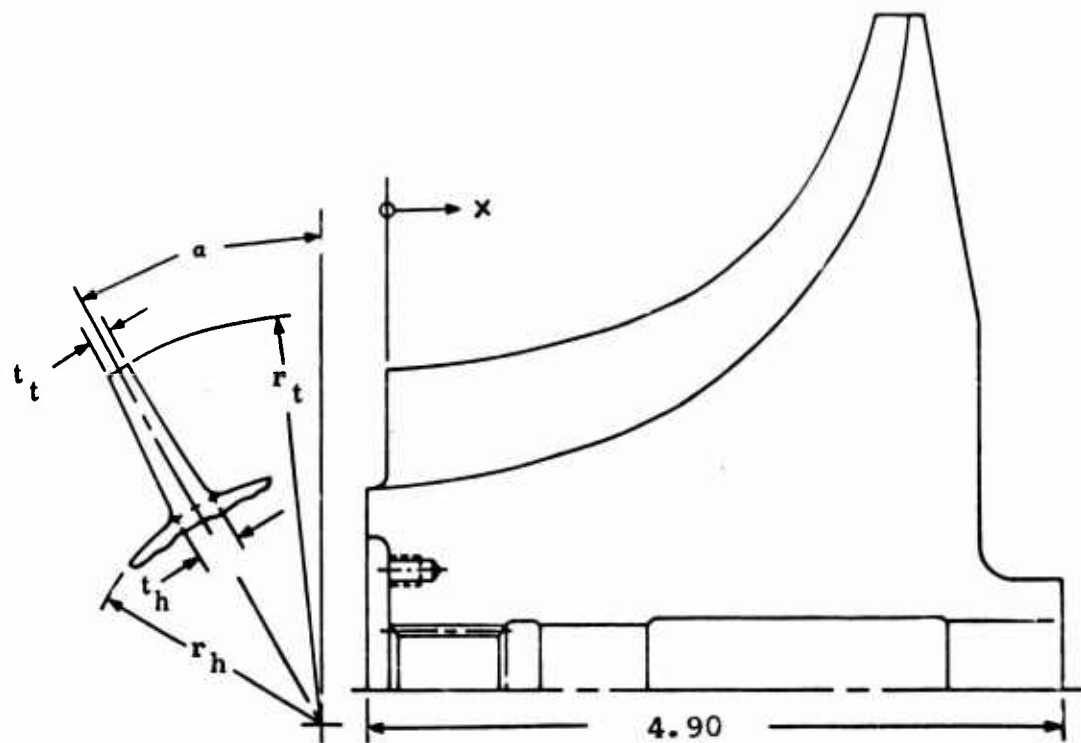


Figure 4 . Impeller Geometry.  
Workhorse

TABLE I. WORKHORSE IMPELLER GEOMETRY AT ZERO RPM

Axial Distance	Blade Turning Angle $\alpha$	Hub Radius $r_h$	Tip Radius $r_t$	Hub Thickness $t_h$	Tip Thickness $t_t$
0	0	1.400	2.210	0.000	0.000
.03	-	1.402	2.212	0.034	0.034
.13	-	1.412	2.220	0.066	0.063
.23	-	1.425	2.230	0.088	0.081
0.341	10.05	1.440	2.240	0.100	0.080
0.682	18.90	1.490	2.280	0.112	0.081
1.023	26.30	1.565	2.340	0.103	0.072
1.360	32.05	1.660	2.415	0.095	0.065
1.690	36.20	1.775	2.520	0.090	0.060
2.010	33.95	1.930	2.660	0.086	0.057
2.300	40.60	2.110	2.825	0.085	0.057
2.560	41.40	2.320	3.025	0.084	0.056
2.780	41.70	2.530	3.240	0.086	0.058
2.970	41.80	2.735	3.470	0.099	0.061
3.110	41.80	2.930	3.675	0.094	0.064
3.200	41.80	3.070	3.860	0.101	0.069
3.350	41.80	3.340	4.220	0.090	0.055
3.450*	-	3.600 *	4.600	-	-
3.500	41.80	3.680	4.600	0.077	0.040
3.600	41.80	4.020	4.600	0.068	0.045
3.700	41.81	4.600	4.600	-	0.050

\* Scaled from Boeing Drawing 45-3934.

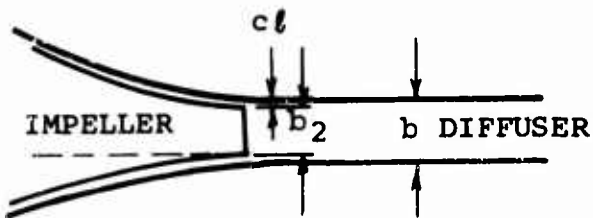


TABLE II. DIFFUSER GEOMETRY

Variable <sup>a</sup>	Diffuser Configuration				
	D1-1	V1-3	V1-4	V2	V2-2
L	5.58 <sup>b</sup>	6.14 <sup>b</sup>	6.14 <sup>b</sup>	5.91 <sup>b</sup>	5.91 <sup>b</sup>
W	0.559 <sup>b</sup> +.006-.007	0.444 +.002,-.003	0.475 +.001,-.003	0.426 +.001,-.003	0.546 +.005
$\ell$	0.5	0.125	0.125	0.125	0.125
$\alpha$	75 25° <sup>d</sup>	75.3° <sup>d</sup>	75.3° <sup>d</sup>	75.3° <sup>d</sup>	75.3° <sup>d</sup>
$R_3$	1.06	1.06	1.06	1.05	1.06
$b_4$	0.250 <sup>d</sup>	0.183	0.183	0.203	0.158
$A_4$ (total)	1.118	0.813	0.869	0.865	0.862
$\theta$	45°	36°	36°	36°	36°
$2\theta$	10° <sup>c</sup>	10° <sup>c,e</sup>	10° <sup>c,e</sup>	10°	10°
L/W	10	13.8	12.9	13.9	10.8
$AS=b_4/W$	0.447	0.413	0.385	0.476	0.289
$b_2 + c\ell$	0.250	0.180	0.180	0.180	0.135
Clearance ( $c\ell$ )	0.020 <sup>d</sup>	0.016	0.016	0.015	0.009
$b_4/(b_2 + c\ell)$	0.992	0.934	0.934	1.041	1.0972

a) See Figure 3 for definition of parameters  
 b) Scaled from drawings  
 c) Unsymmetrical divergence -- The 10° angle is all in the pressure surface  
 d) Estimate, unable to confirm, but reasonably certain  
 e) These diffusers have 0.375 section of 5° divergence downstream of throat

The static pressure tap (0.020 in. diameter) locations on the cover are shown in Figure 6. Data from tap 8A, which is located at an axial distance of 0.14 inch from the inducer leading edge, have been lost; it appears from other considerations that this data would be vital to diagnosis. The cover static pressure reported are the averages of three circumferentially spaced pressure taps at tap location 8 and two taps at tap locations 9 - 11. The nominal cover clearance was 0.020.

Figure 5 is a view of the diffuser backplate as viewed from the compressor inlet and shows the locations of the various impeller probes as well as the cover pressure tap line. The impeller tip probes are shown in Figures 7, 8, and 9 with their dimensions. Some of these dimensions have been estimated from photographs and sketches made by Boeing and are so marked.

Total pressure in the vaneless space, diffuser entry, and through the diffuser was recorded on a traversing total pressure probe called the "railroad track" probe. The geometric details of this probe are shown in Figure 8. The path which the "railroad track" probe traverses in relation to the other instruments is shown in Figure 5.

All impeller tip probes were set at the flow angle indicated by the yaw probe. The traversing stagnation temperature probe and the stagnation pressure tube between the yaw tubes were set at the yaw-probe-measured flow angle at each axial position. The yaw probe was calibrated using radial flow through a dummy (bladeless) impeller. All probes were tested in a Mach 1.3 wind tunnel for angle response and, with the obvious exception of the yaw probe, all had reasonably flat response for a  $\pm 10^\circ$  angle variation. The test calibration curves for the specific probes used could not be positively identified and thus are not included.

Station I is a reference point in the channel diffuser where the area ratio is 2.0. Some performance measurements were made there. In addition, a total tube traverse was made across the channel. The result of this traverse is shown in Figure 38.

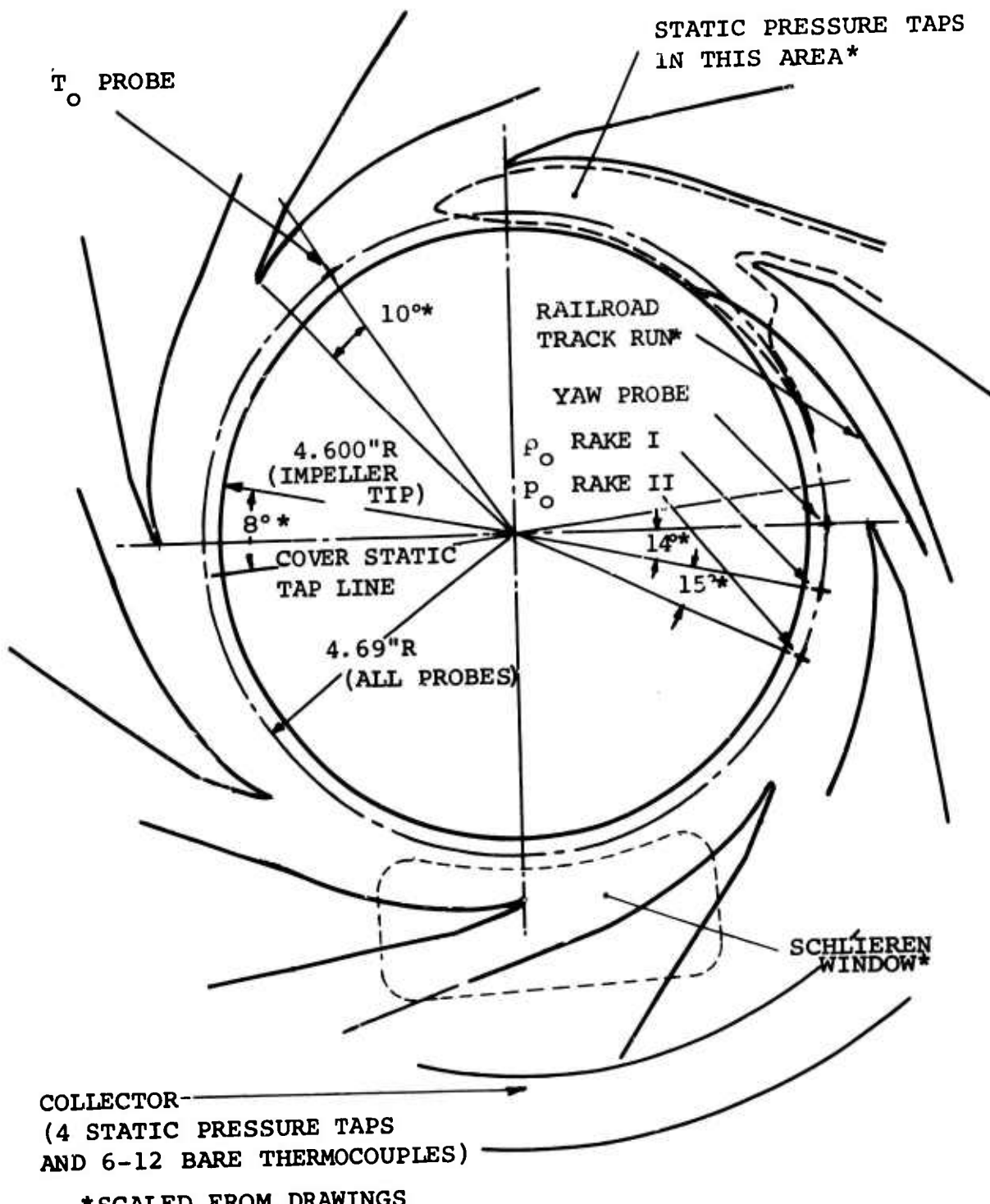
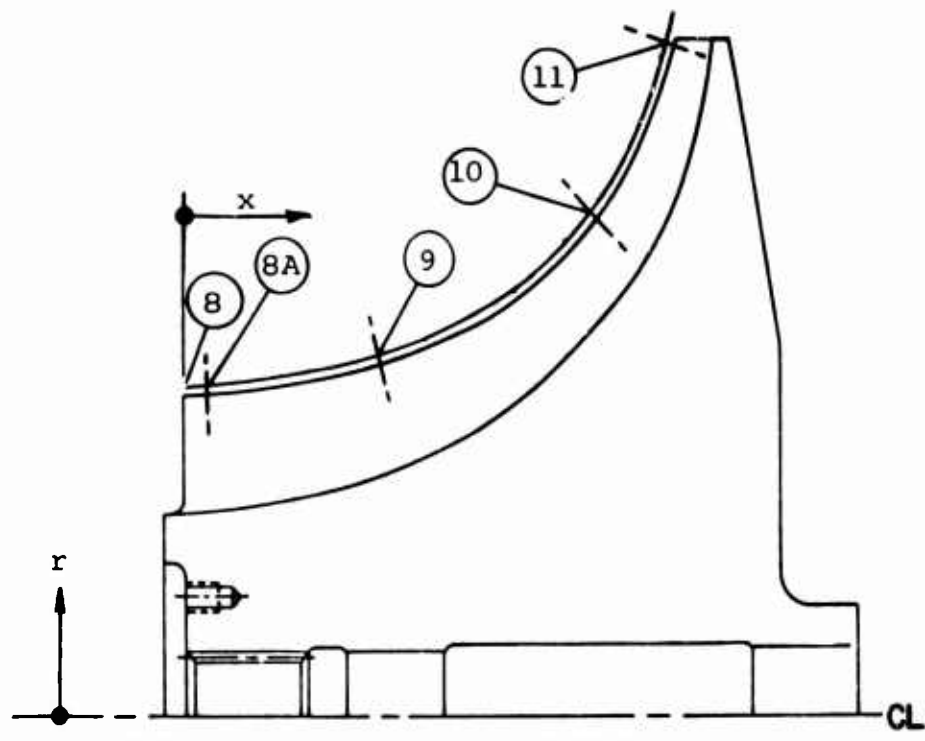


Figure 5 . Diffuser Backplate Instrumentation  
 as Viewed From Compressor Inlet.  
 Workhorse

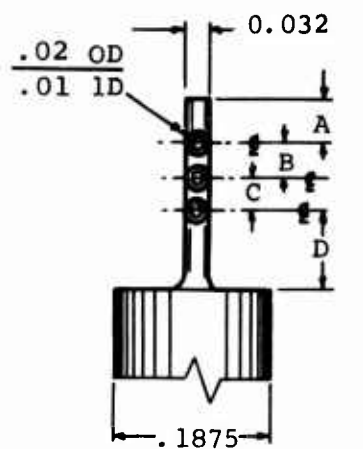


Tap No.	x	r*
8	0	2.235
8A	.14	2.245
9	1.44	2.375
10	2.84	3.33
11	3.40	4.4

\* Dimension to cover tap

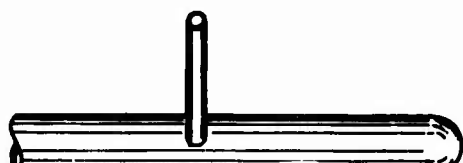
Note: The reference station for the tap locations was scaled from Boeing Drawing 45-3934.

Figure 6 . Cover Static Pressure Taps.  
Workhorse

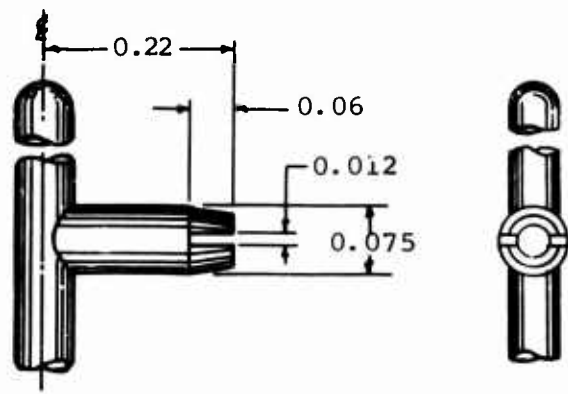
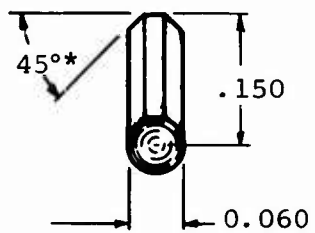


	RAKE I	RAKE II
A	0.050	0.025
B	0.040	0.095
C	0.040	0.095
D	0.080	0.025

TOTAL PRESSURE RAKES



YAW PROBE



SLOTTED SHIELD STAGNATION  
TEMPERATURE PROBE

\*Scaled From Photograph

Figure 7. Impeller Tip Probes.  
Workhorse

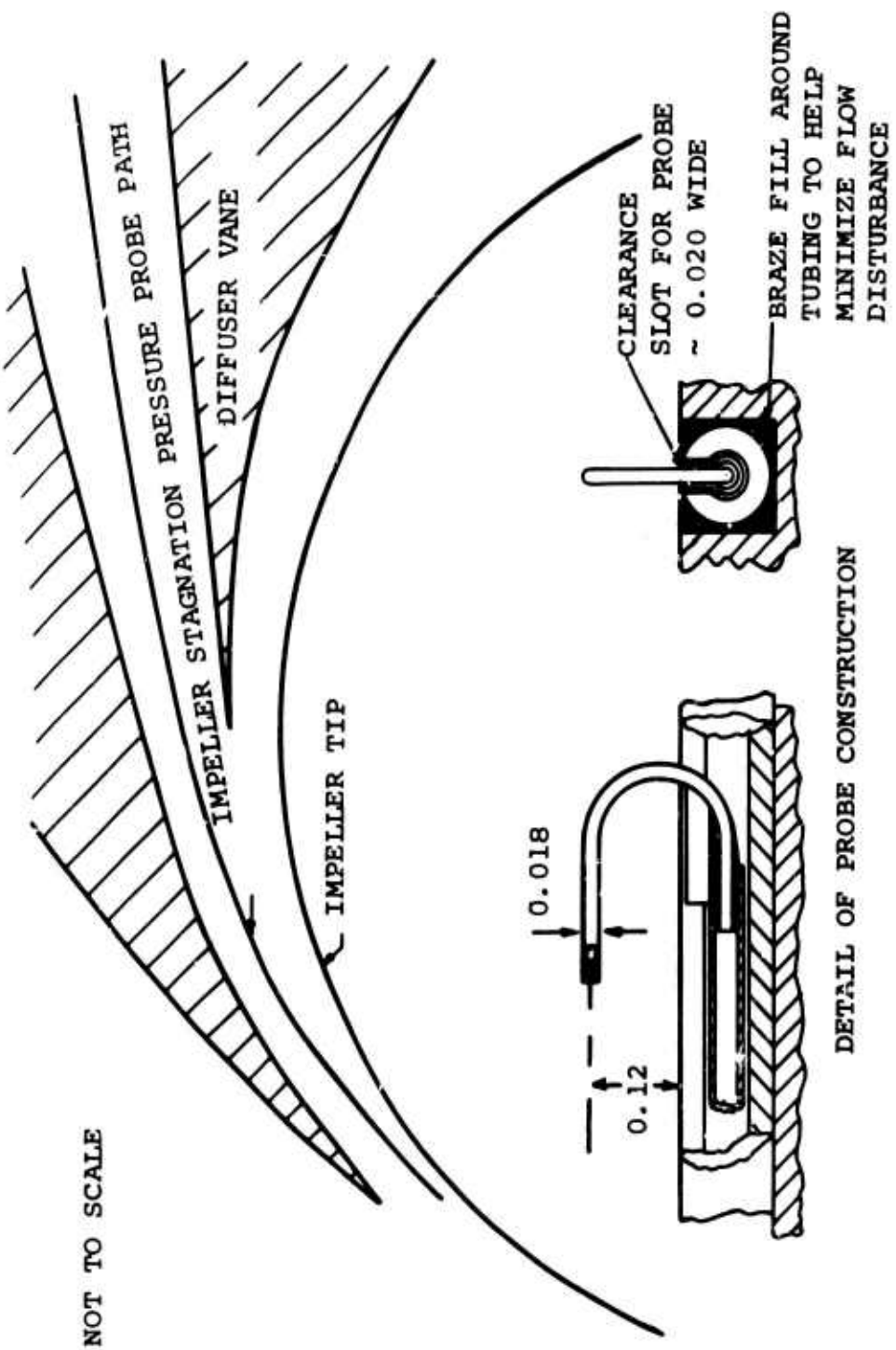
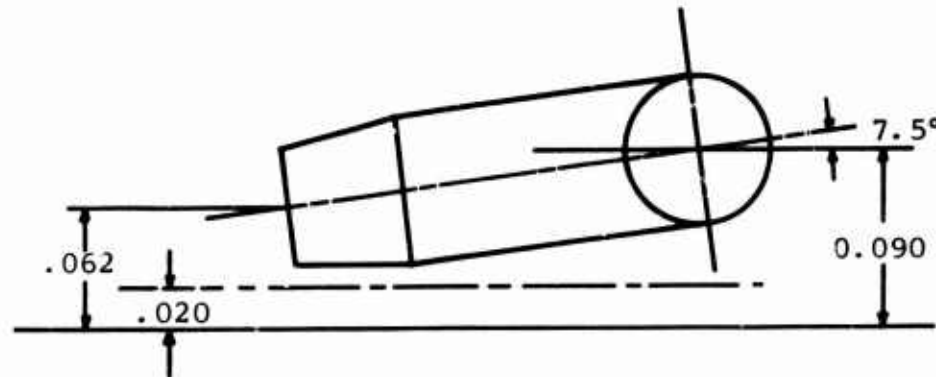
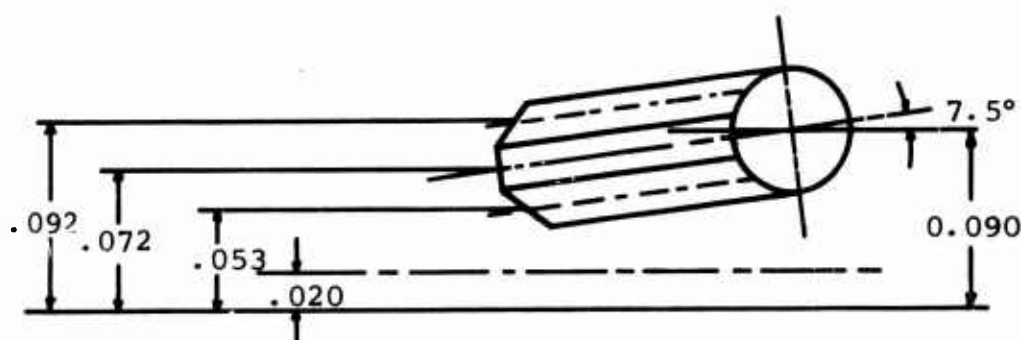


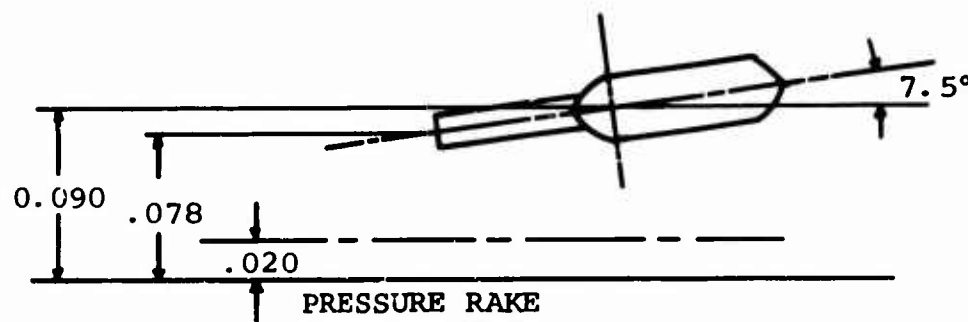
Figure 8 . Railroad Track Traversing Stagnation Pressure Probe.  
Workhorse



SLOTTED SHIELD STAGNATION TEMPERATURE PROBE



YAW PROBE



PRESSURE RAKE

— IMPELLER AT 0 RPM  
- - - IMPELLER TIP AT 50,000 RPM

Figure 9 . Locations of Impeller Tip Probes  
at Typical Setting.  
Workhorse

### 3.2 RF-2 GEOMETRY AND INSTRUMENTATION

A meridional view of the RF-2 impeller and geometric coordinates of the impeller are shown in Figures 10 and 11 and Table III. The geometry shown is for zero rpm. Boeing estimates the radial expansion of the impeller to be 0.02 inch at the tip at 50,000 rpm. There were no guide vanes ahead of this impeller. The inlet duct arrangement is shown in Figure 12.

Data from four diffuser configurations in the RF-2 stage have been reported. The four configurations were named by Boeing: V1-3, V1-4, V2, and V2-2. The geometry of these diffusers is indicated in Figures 13 and 14 and is tabulated in Table II.

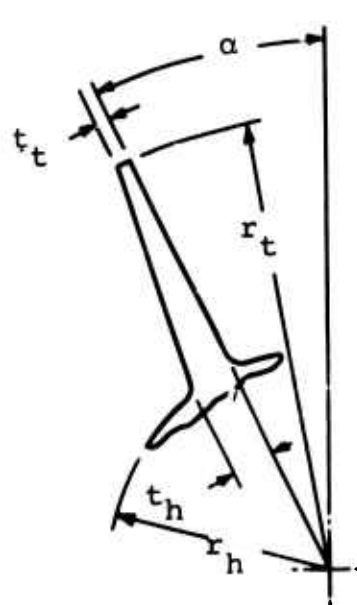
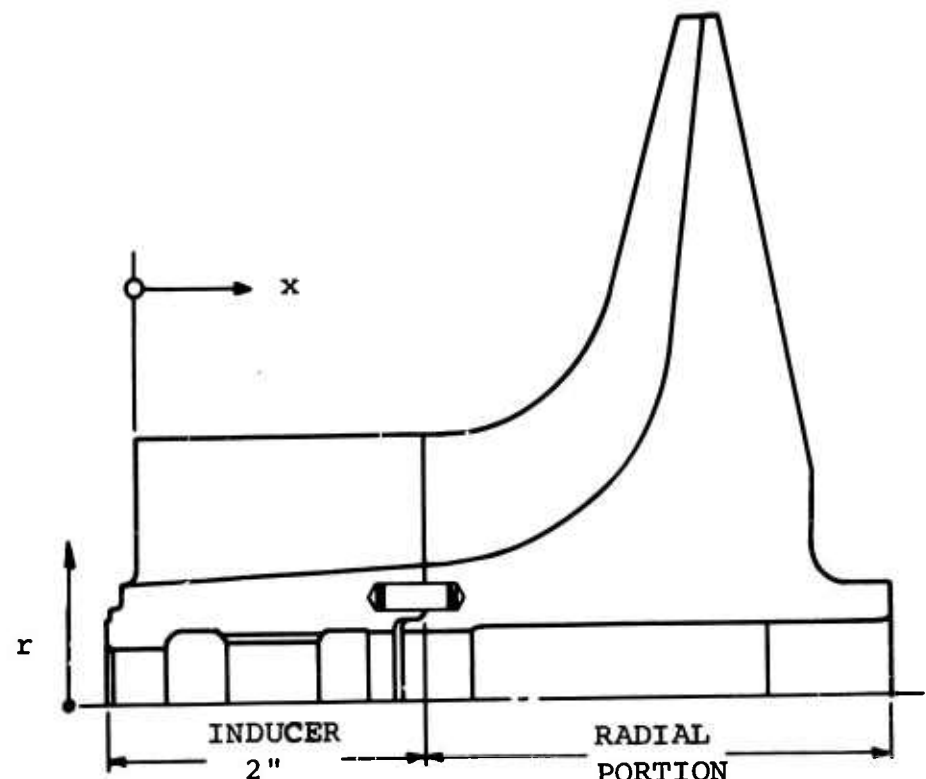
As with Workhorse, there are many interesting mechanical details to this compressor which we have not reported because they are not pertinent to the aerodynamic evaluation. These other details for the interested reader can be found in Welliver and Acurio (1967, 67-47).

The design conditions for the RF-2 were 2.0 lbm/sec, 50,000 rpm, 10:1 pressure ratio and 80% total-to-static efficiency. The highest reported efficiency was 72.6% at 9:1 pressure ratio, 1.9 lbm/sec.

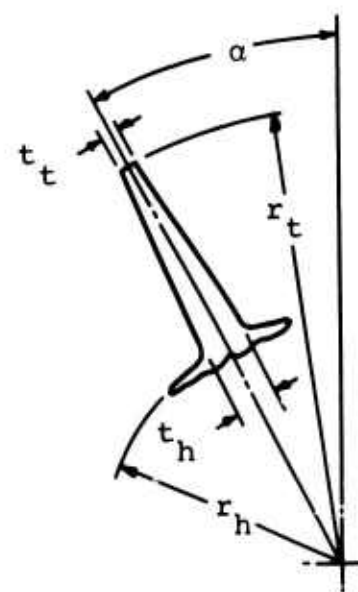
The data for each of the configurations are grouped according to the actual test for which they were taken as shown on page 59. The data grouped under each configuration are for the same geometry although they had to be abstracted from a large number of different tests.

The static pressure tap locations on the cover are shown in Figure 12. The circumferential spacing of these taps is shown in Figure 15. The static pressure recorded are the averages of these three circumferentially spaced taps. The geometry of the static pressure taps is also indicated schematically.

Figure 16 shows a view of the diffuser backplate as viewed from the compressor inlet. The collector used for RF-2 testing is the same collector which was used for Workhorse and thus has the same static pressure taps and thermocouple locations. The impeller tip probes which



INDUCER BLADING  
(NOT SYMMETRICAL)



IMPELLER BLADING  
(SYMMETRICAL)

Figure 10. Impeller Geometry at Zero RPM.  
RF-2

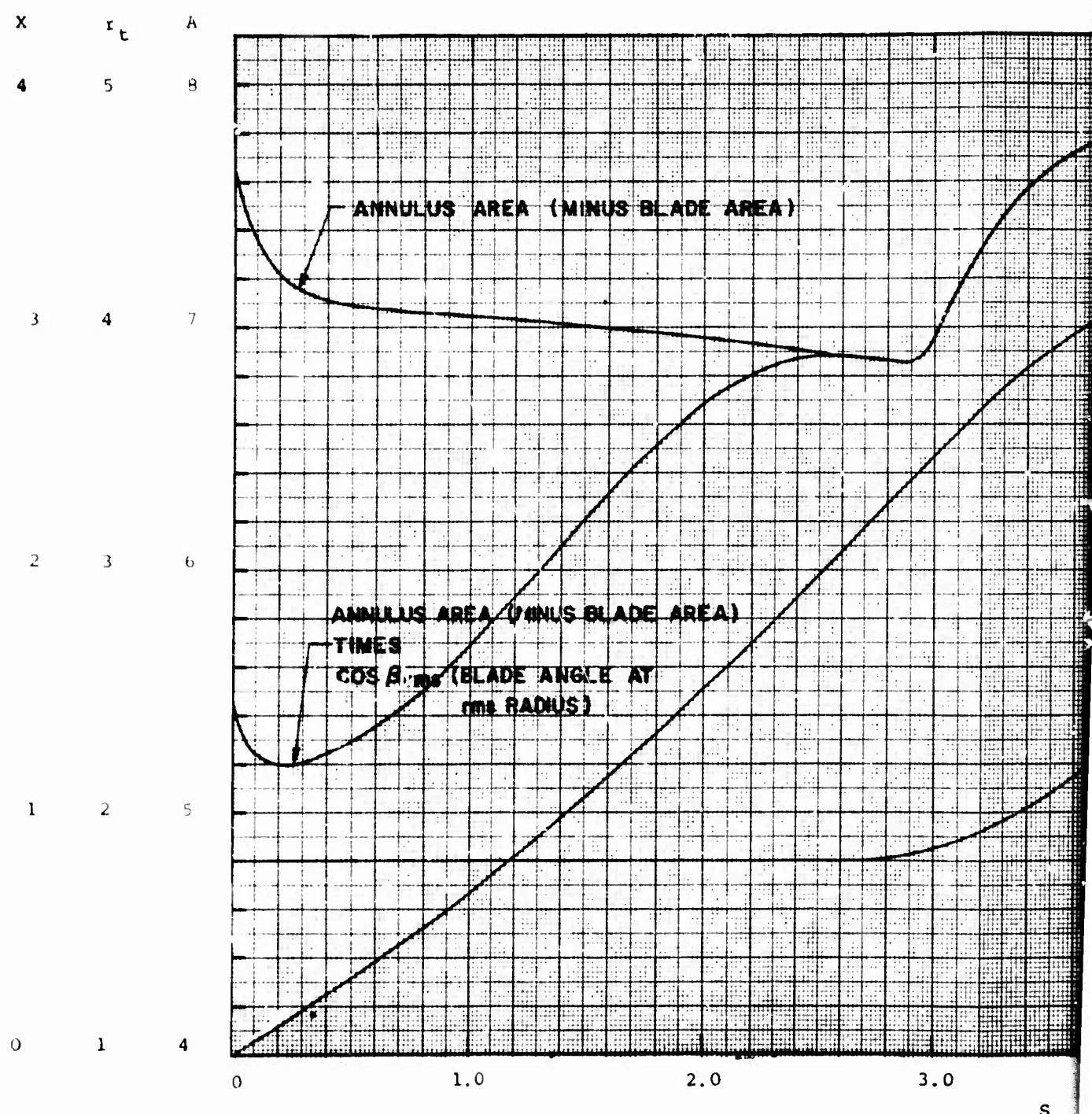
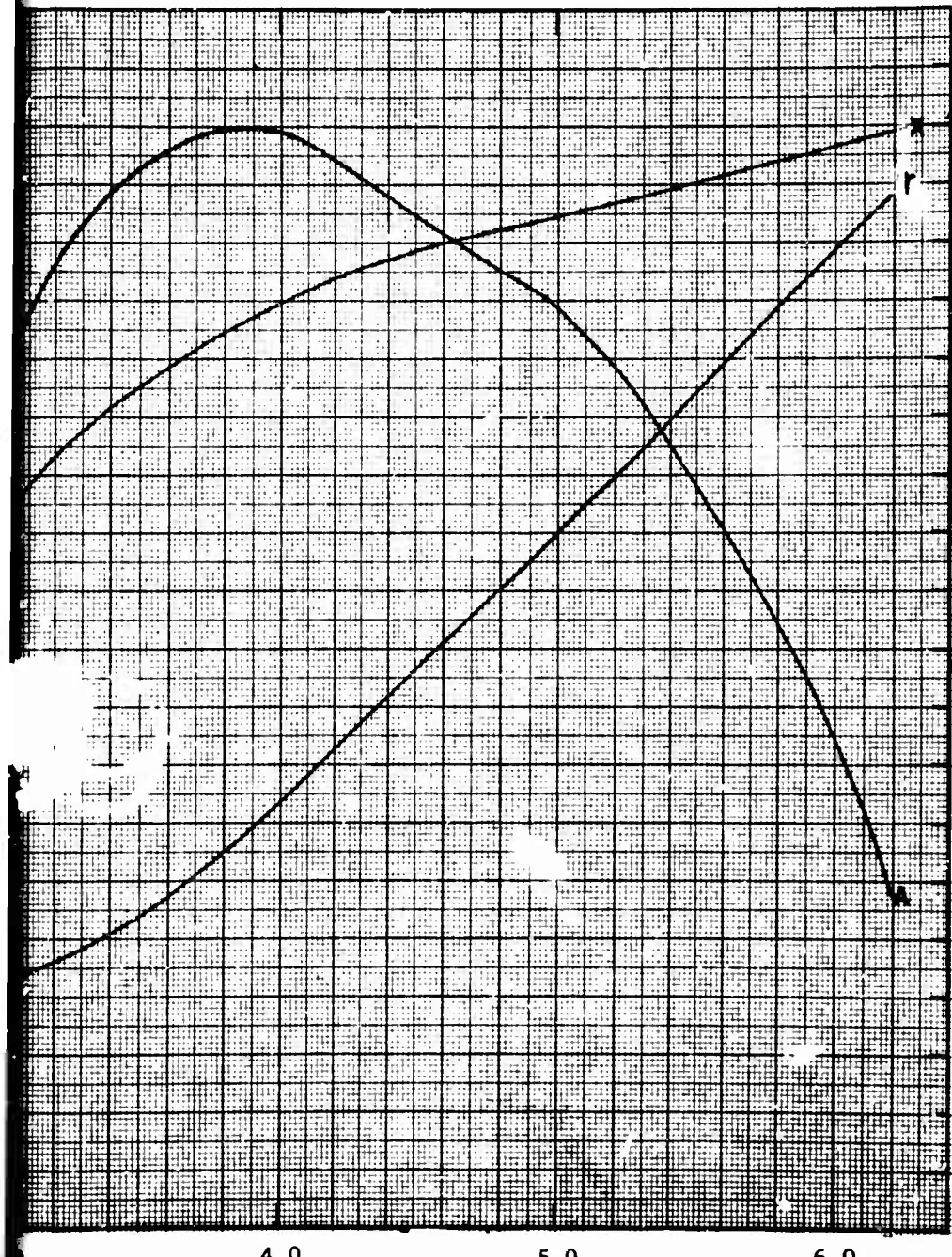


Figure 11. Geometric Relations.  
RF-2



s

TABLE III. RF-2 IMPELLER GEOMETRY AT ZERO RPM

Axial Distance <i>x</i>	Blade Turning Angle	Hub Radius <i>r<sub>h</sub></i>	Tip Radius <i>r<sub>t</sub></i>	Hub* Thickness <i>t<sub>h</sub></i>	Tip* Thickness <i>t<sub>t</sub></i>
0	0	0.813	1.80	0	0
0.01	-	0.813	1.80	0.023	0.032
0.02	-	0.814	1.80	0.027	0.036
0.03	-	0.814	1.80	0.031	0.038
0.04	-	0.815	1.80	0.034	0.04
0.06	-	0.815	1.80	0.040	0.043
0.08	-	0.817	1.80	0.046	0.044
0.10	-	0.818	1.80	0.050	0.044
0.12	4.78***	0.819	1.80	0.054	0.044
0.15	-	0.821	1.80	0.057	0.043
0.3	11.60	0.829	1.80	0.062	0.042
0.500	18.59	0.839	1.80	0.061	0.041
0.700	24.87	0.850	1.80	0.060	0.039
0.900	30.32	0.860	1.80	0.059	0.037
1.100	34.88	0.871	1.80	0.058	0.035
1.300	38.53	0.881	1.80	0.057	0.033
1.500	41.27	0.892	1.80	0.056	0.032
1.700	43.10	0.902	1.80	0.055	0.031
1.900	44.03	0.913	1.80	0.055	0.030
2.000	44.15	0.918	1.80	0.055	0.030
2.430	44.80	0.958	1.839	0.055	0.030
2.860	44.80	1.108	2.051	0.055	0.030
3.290	44.80	1.431	2.711	0.055	0.030
3.720	44.80	2.313	4.316	0.055	0.030
3.785**	44.80	-	4.573	0.055	0.030
3.965**	44.80	4.573	-	0.055	0.030

\* Blade thicknesses measured normal to *x* -- after handworking of the blades

\*\* Estimated graphically (tip of impeller)

\*\*\* Not corrected for handworking

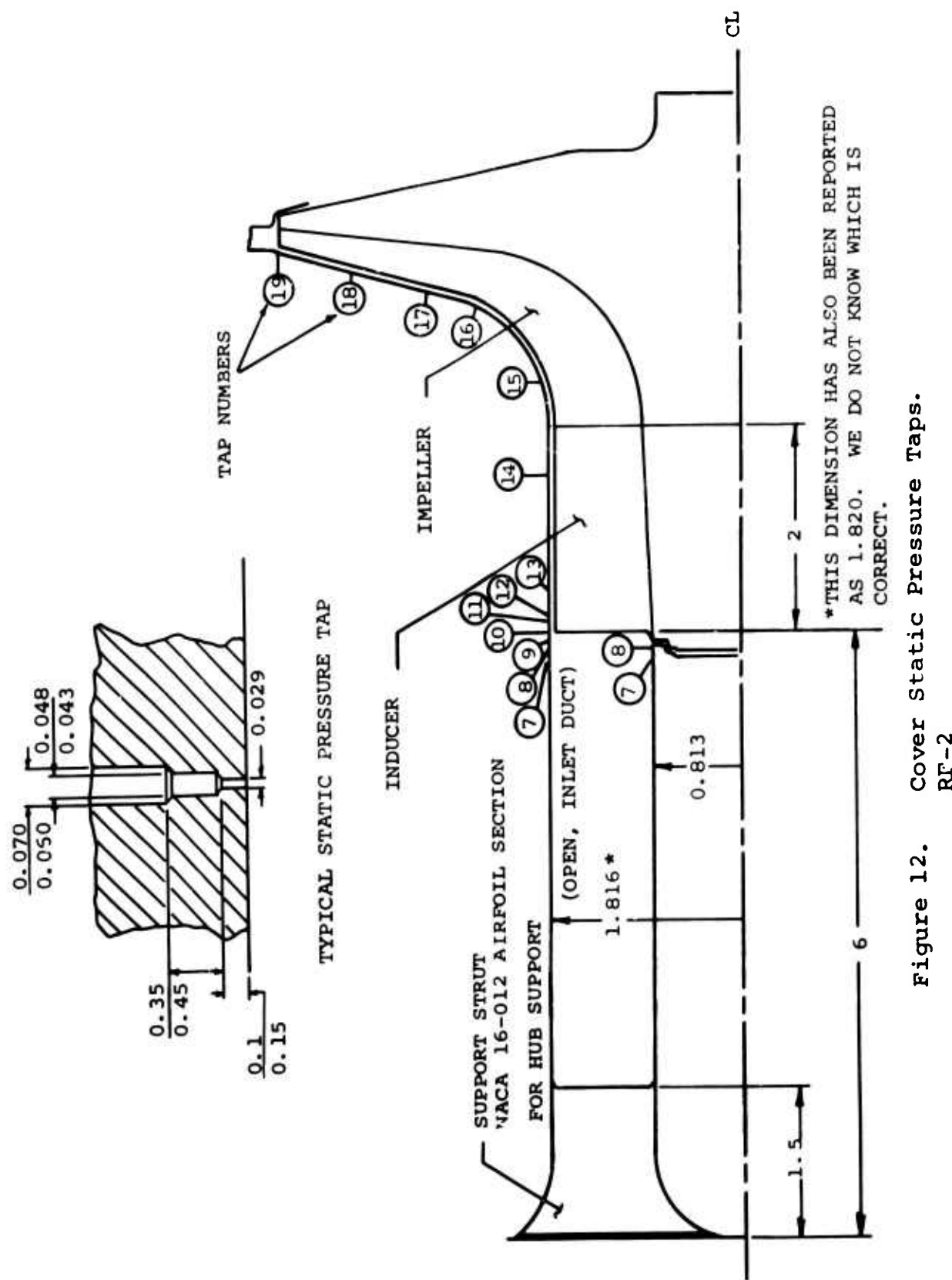


Figure 12. Cover Static Pressure Taps.  
RF-2

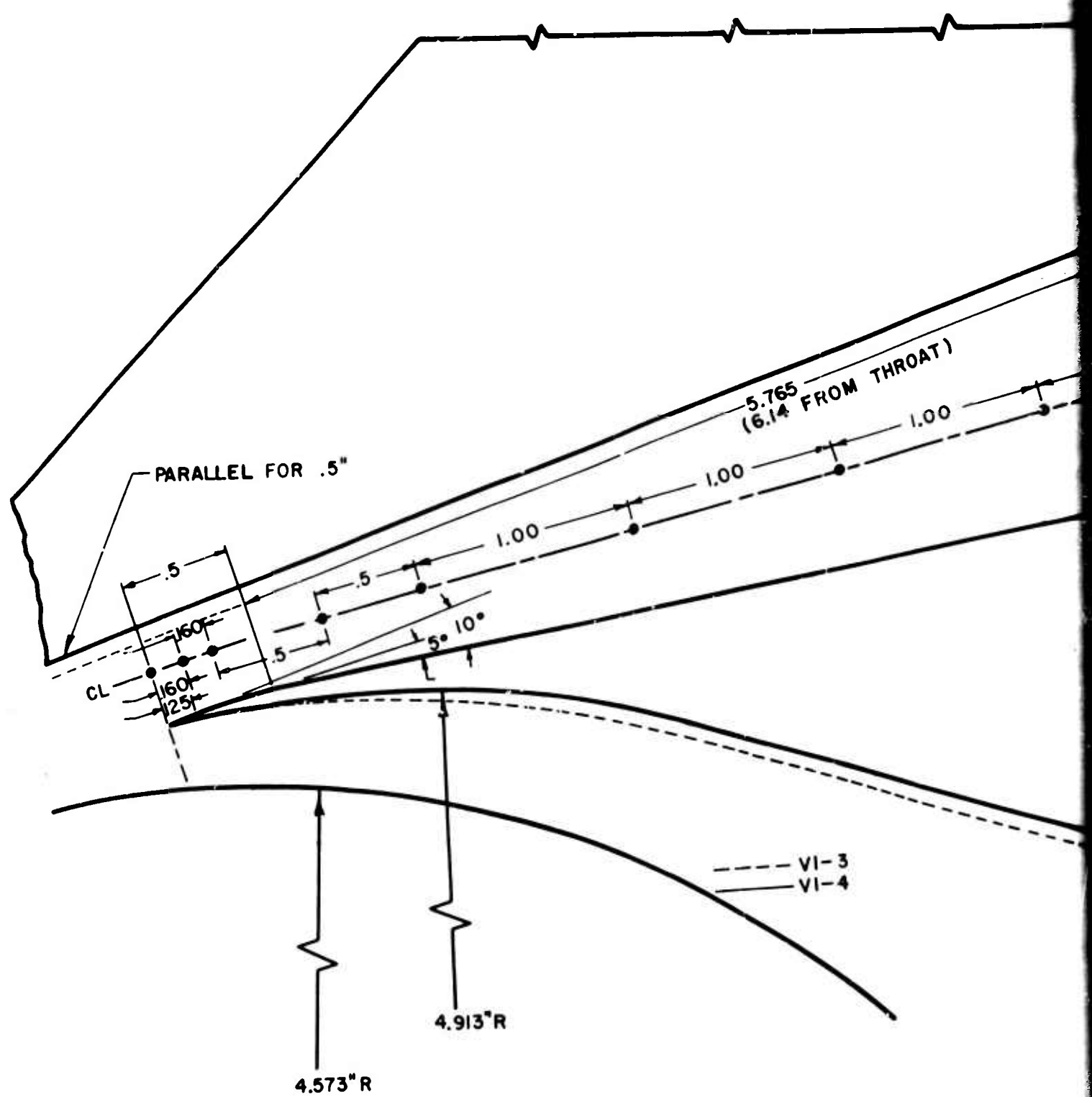
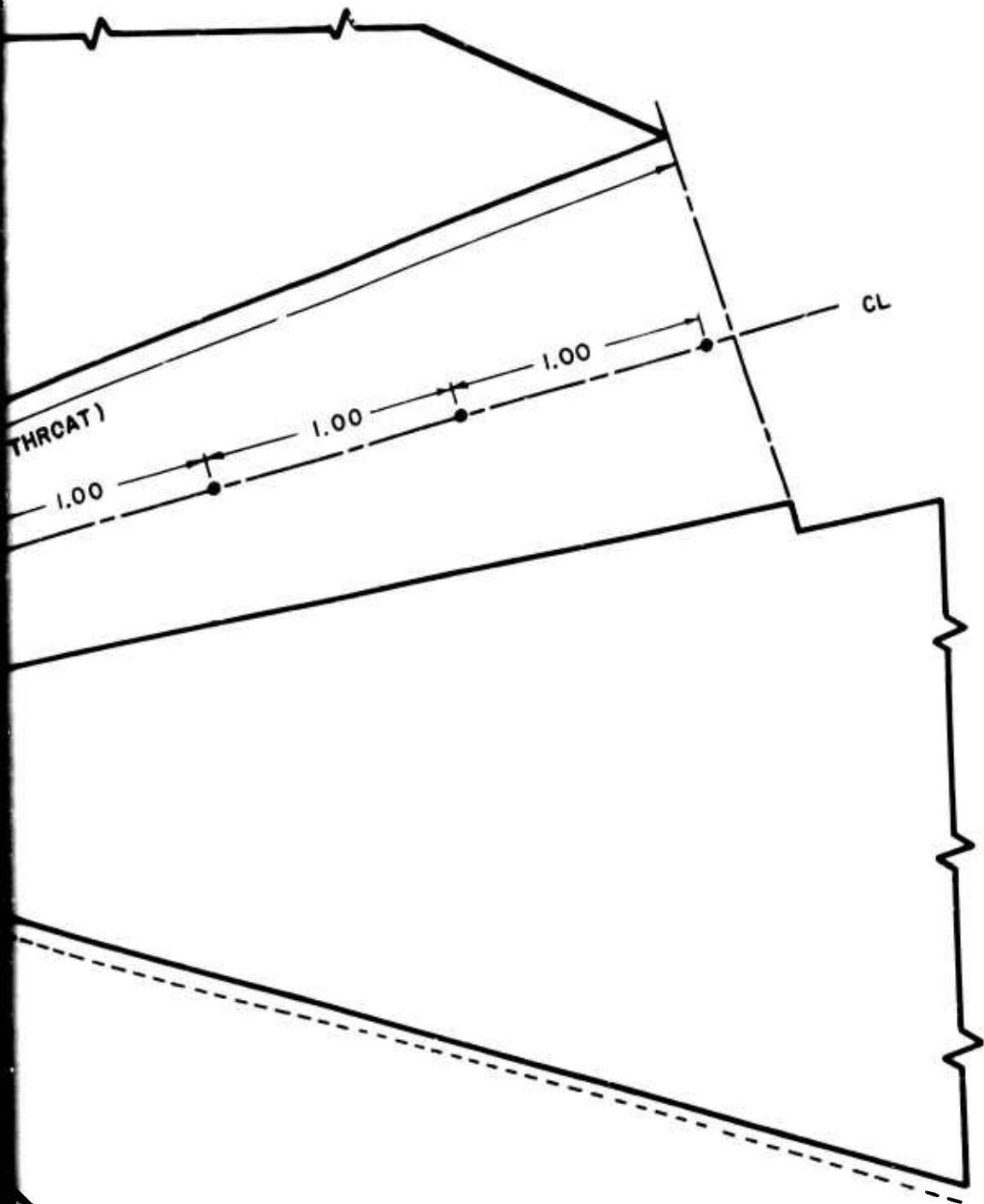


Figure 13. V1-3 and V1-4 Diffuser Geometry.  
RF-2



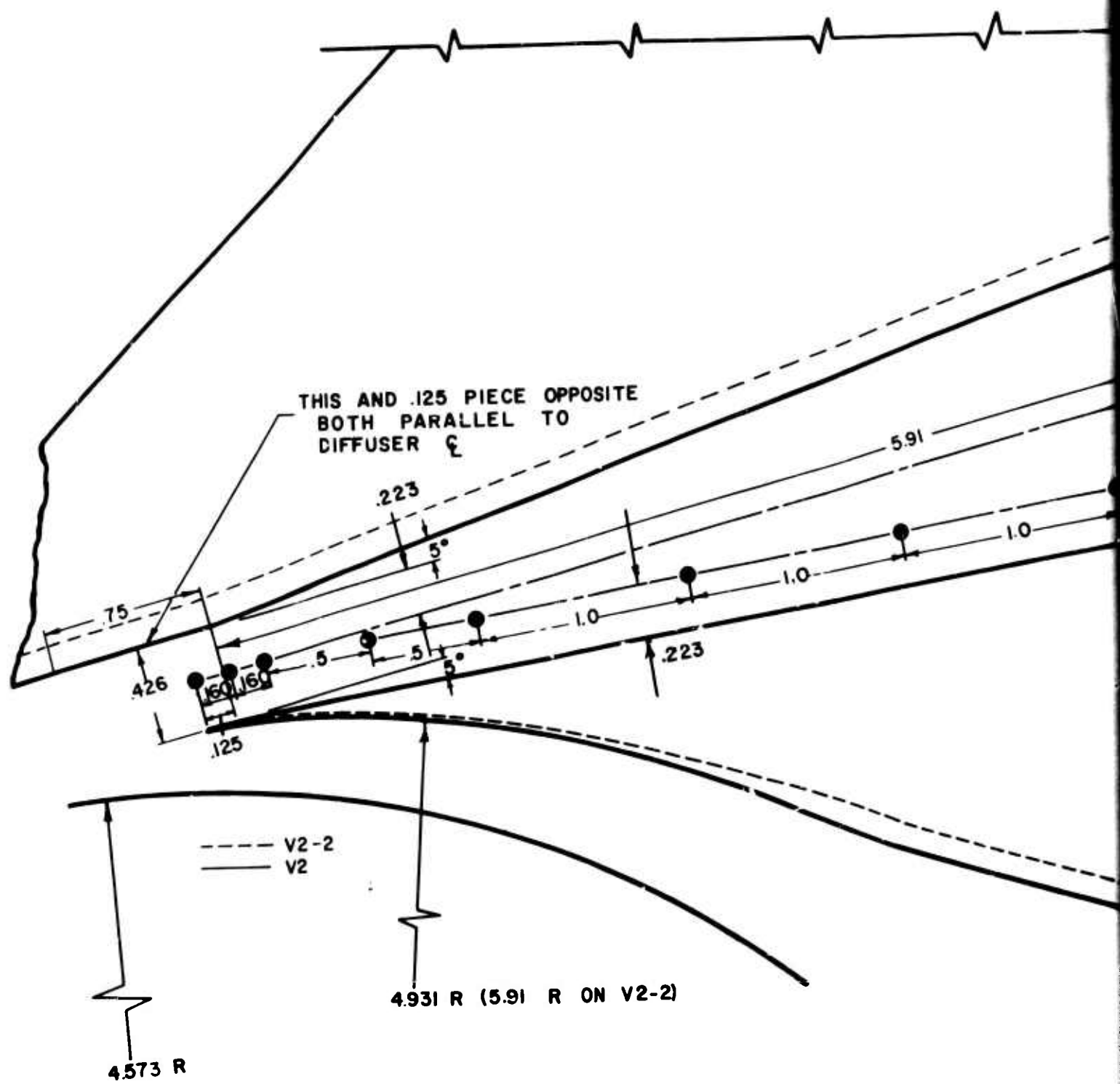
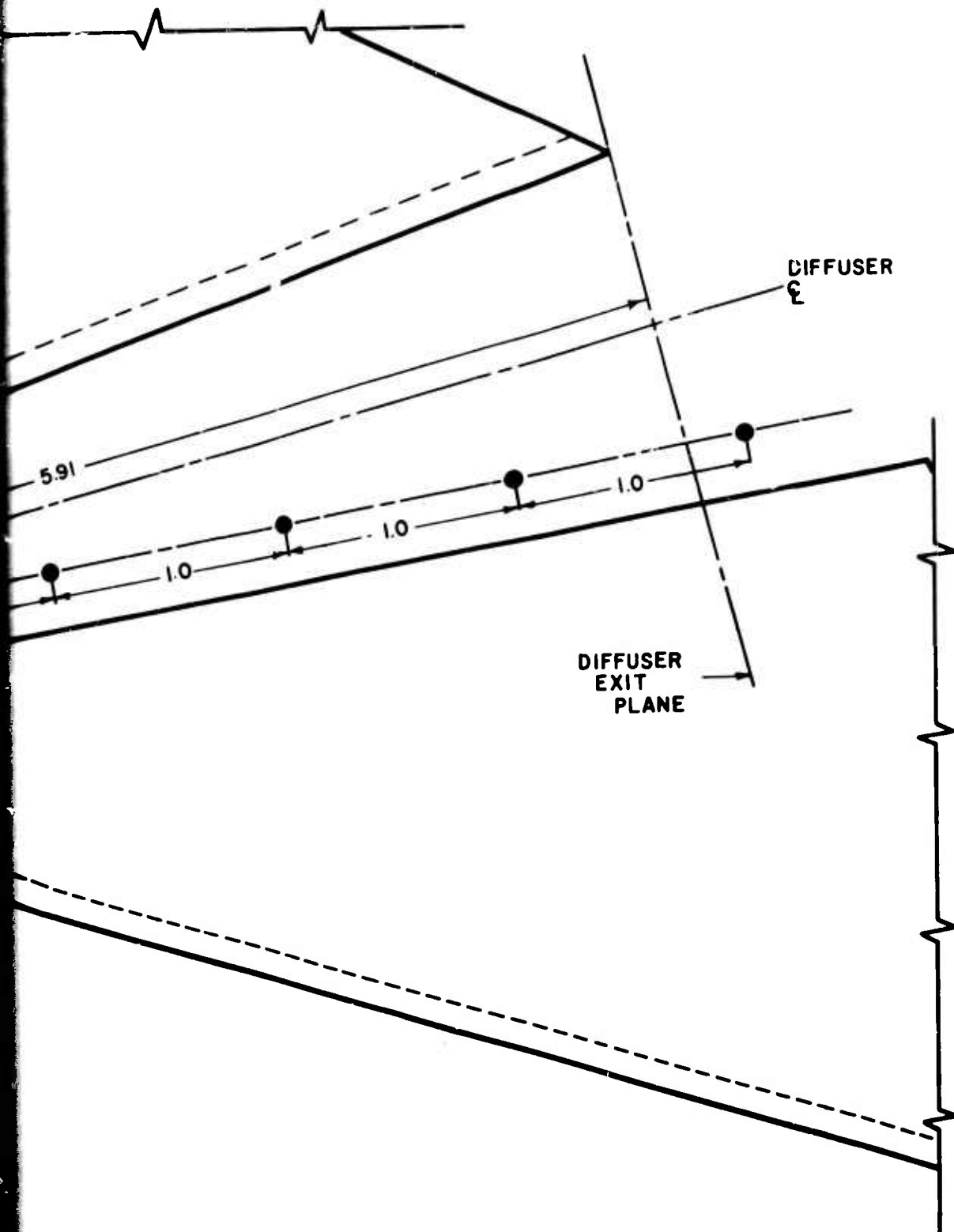
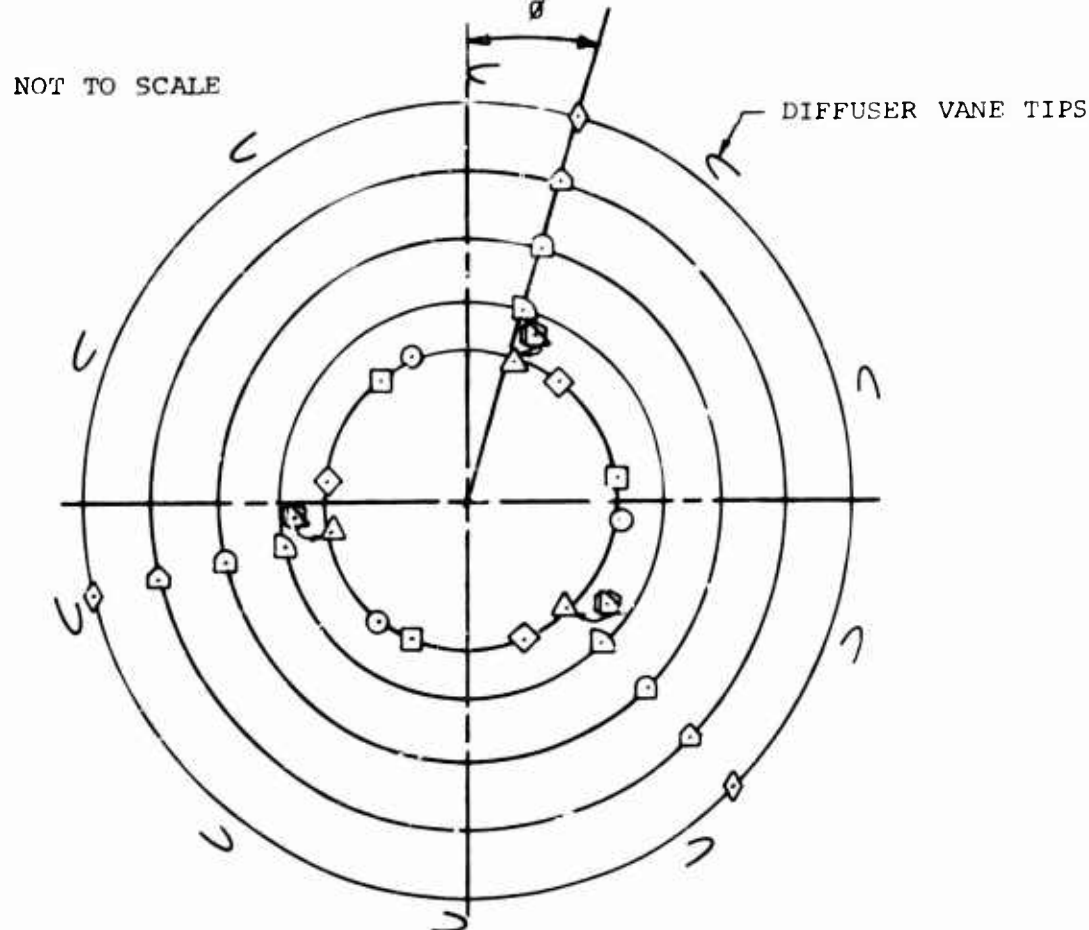


Figure 14. V2 and V2-2 Diffuser Geometry.  
RF-2





TAP NO.	$r$	$x$	$\theta^*$
7	1.816	0.813 - 0.35	-
8	1.816	0.813 - 0.20	-
9	1.816	- 0.10	-
10	1.816	0	18
11	1.816	0.10	38
12	1.816	0.20	83
13	1.816	0.45	98
14	1.816	1.50	16.5
15	1.816	2.32	16.5
16	2.25	3.02	16.5
17	3.00	-	16.5
18	3.80	-	16.5
19	4.54	-	16.5

\* $\theta$  IS THE ANGLE TO THE FIRST OF THE THREE STATIC PRESSURE TAP ROWS

Figure 15. Circumferential Cover Static Pressure Tap Locations.  
RF-2

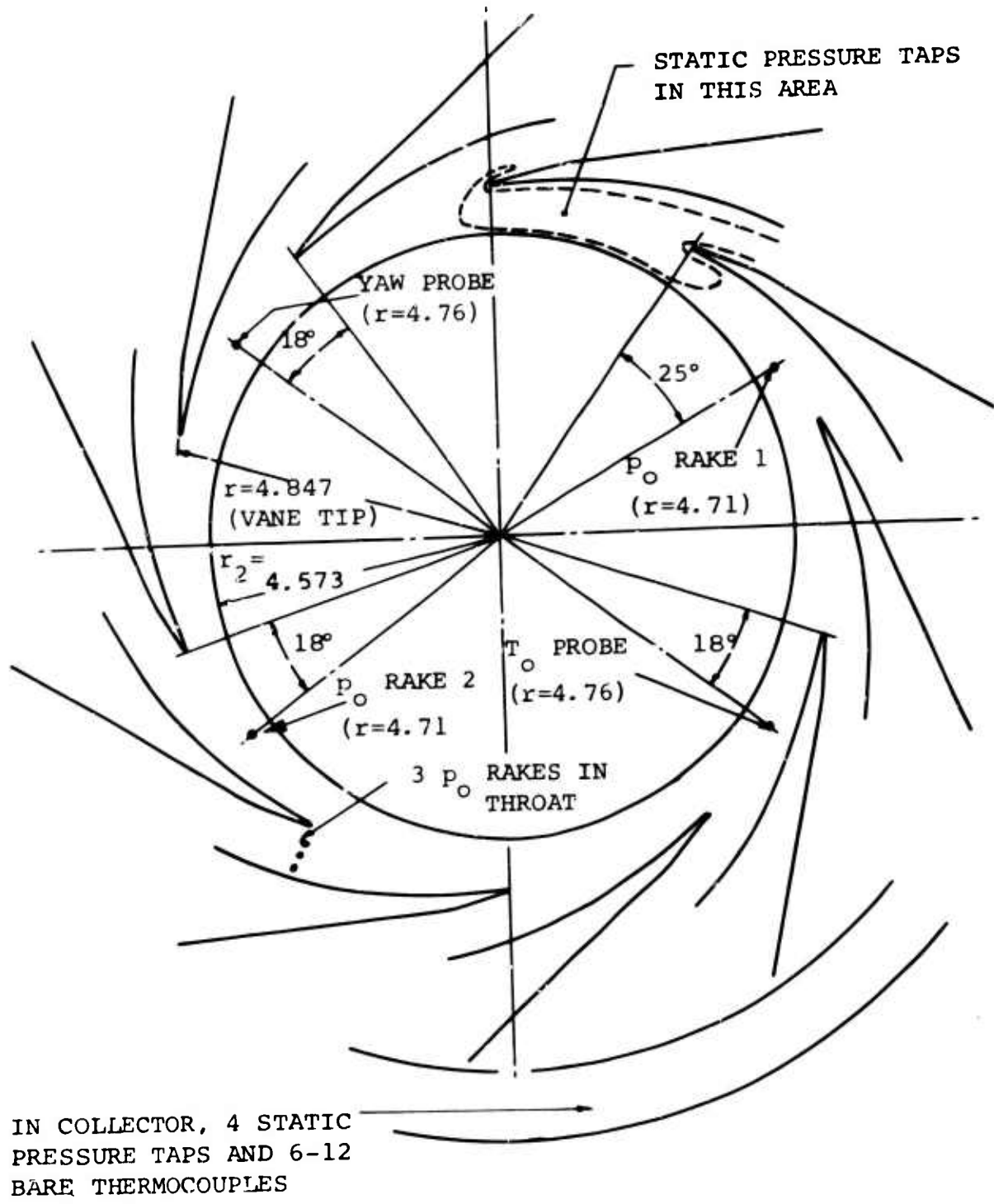


Figure 16. Diffuser Backplate Instrumentation  
as Viewed From Compressor Inlet.  
RF-2

were used are shown in Figures 17 and 18. As for the Workhorse, some of the probe dimensions have had to be scaled from sketches, drawings, and photographs; these dimensions are so marked.

In addition to the static pressure taps in the diffuser entry region (shown schematically in Figure 17 and in more detail in Figures 26, 49, 63, and 85), there were three total pressure rakes in the diffuser throat, providing nine point measurements. The throat rakes are shown in Figure 19.

The stage pressure ratio is determined from static pressure in the collector and from the average inlet stagnation pressure, which was determined by a three-point traverse at each of three circumferential stations in the inlet duct using a Kiel probe. This total pressure was then (probably) area averaged to determine the inlet stagnation pressure. None of the individual data from these Kiel probes was presented, however.

The static pressures in the diffuser were recorded digitally on tape and then reduced later. The overall pressure ratio, cover and inlet duct static pressures, and the temperature rise were recorded manually.

The only significant differences between the instrumentation used on RF-2 and on Workhorse are that RF-2 used a smaller total temperature probe than Workhorse and did not use the traversing "railroad track" total pressure probe. Also, schlieren photographs and oil trace patterns were not obtained for the RF-2. The rest of the data are recorded in essentially the same way.

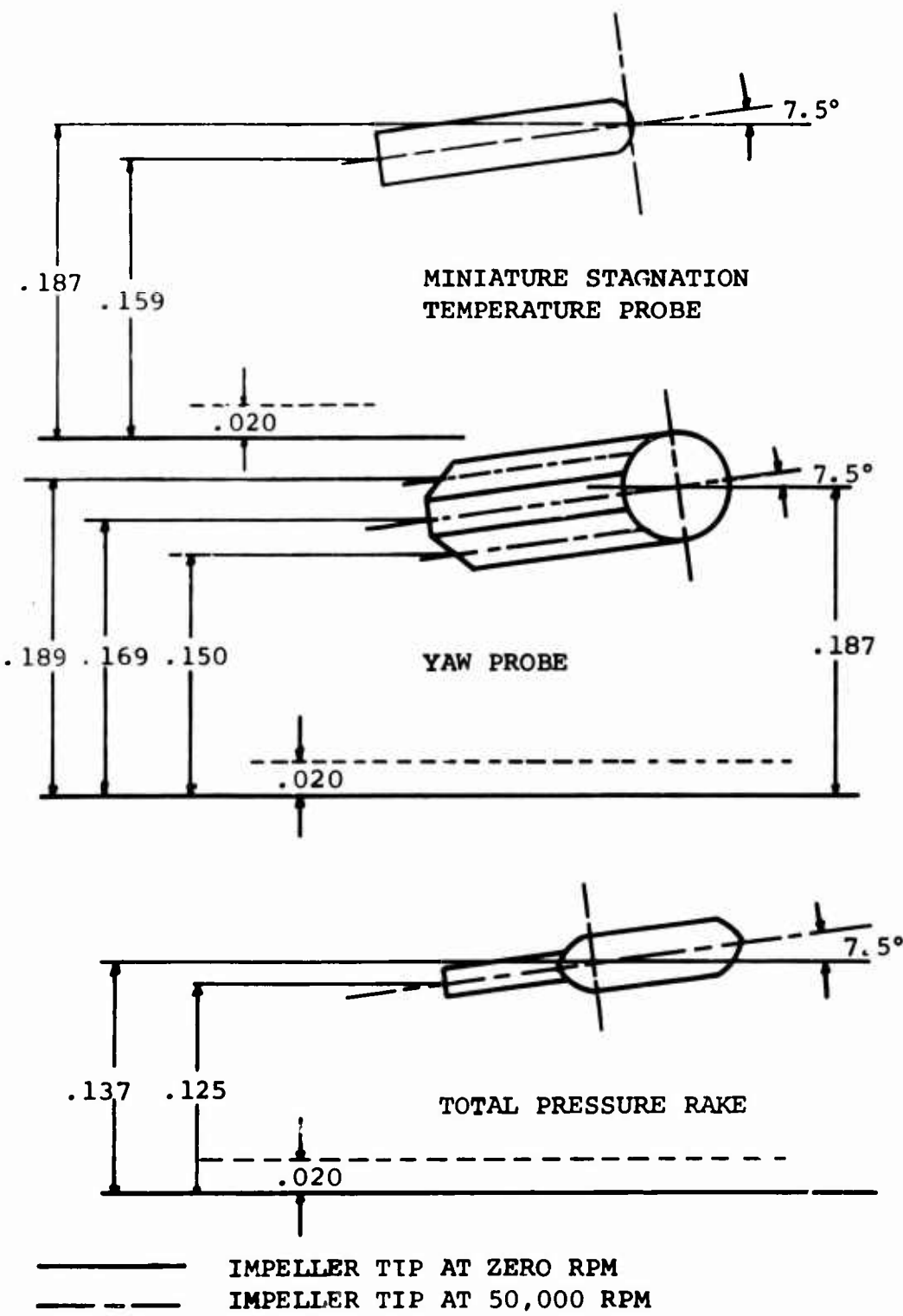
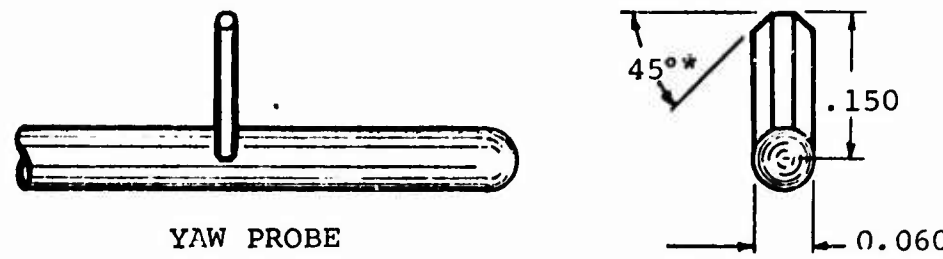
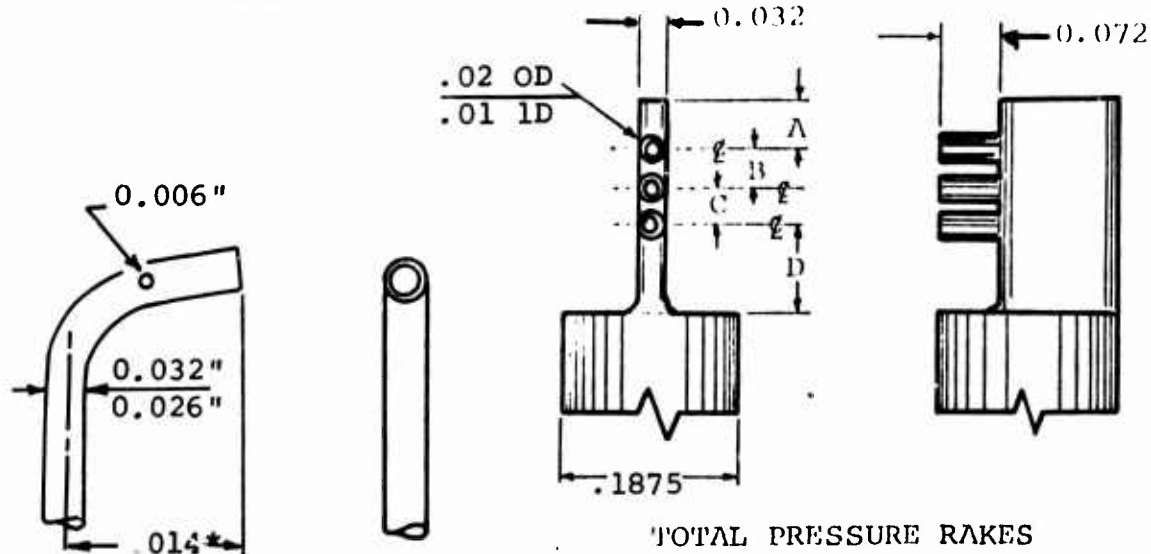


Figure 17. Locations of Impeller Tip Probes at a Typical Setting.  
RF-2



\*SCALED FROM SKETCH OR PHOTOGRAPH

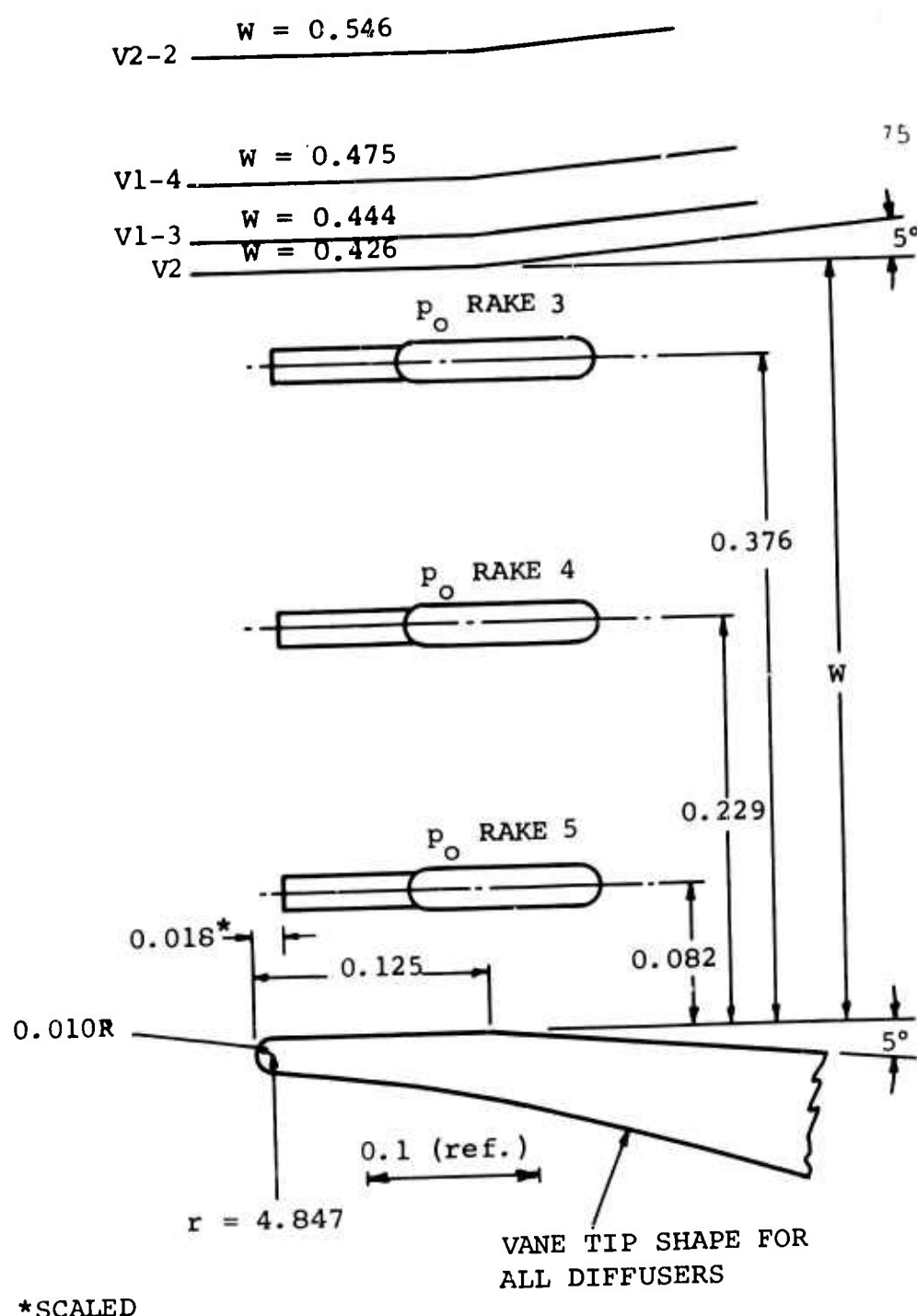


MINIATURE STAGNATION  
TEMPERATURE PROBE

RAKE	1	2,3,4,5	2,4*
A	0.025	0.030	0.025
B	0.065	0.040	0.040
C	0.065	0.040	0.040
D	0.025	0.050	0.060

\*FOR TEST 3369A AND 3369B ONLY

Figure 18. Impeller Tip Probes.  
RF-2



\* SCALED

Figure 19. Diffuser Throat Stagnation Pressure Rakes.

### 3.3 WORKHORSE STAGE DATA

All the data used in this study from the Workhorse stage are presented in Figures 20 through 38.

Table IV summarizes the data used.

TABLE IV. SUMMARY OF WORKHORSE DATA

- NOTES: 1) All entries are "Boeing-Corrected" Data from Welliver and Acurio (1967) (67-30).  
 2) Only design speed (50,000 rpm) data included.  
 3) None of the data are corrected to account for inlet guide vane losses.  
 4) Aerodynamic instrumentation probes and their locations are shown in Figures 5 to 9.

Measurement	Remarks	Figure No.					
		3306A <sup>d</sup>	3306B	3306F	3339 <sup>c</sup>	3317	3350
$p_c = f(m)^a$	Data from five taps	20	21	-	-	-	-
$p_{o_2}^a = f(x)$	Three probes at impeller exit	22	23	-	-	-	-
$d^a = f(x)$	Yaw probe, $\pm 1^\circ$ at impeller exit	24	24	-	-	-	-
$T_{o_2}^a = f(x)$	At impeller exit	25	25	-	-	-	-
$p^a = f(r, \theta)$	"Diffuser" static pressure field	-	-	27	28	29	-
$p_o^a = f(r, \theta)$	Traversing stagnation pressure probe identified as "railroad track" probe	30	31	-	-	-	-
Schlieren	Covers most of diffuser entry region for one channel	-	-	-	-	32	-

TABLE IV. - Continued

Measurement	Remarks	Figure No.					
		3306A <sup>d</sup>	3306B	3306F	3339 <sup>c</sup>	3317	3350
Oil slick wall traces	30,000 rpm and 38,400 rpm only	-	-	-	-	-	33,34
$T_{coll}^{a,b}$	Reported as $T_{coll} - T_{O_i}$	35	35	-	-	-	-
$p_{coll}^{a,b}$	Reported as pressure ratio	36	37	-	-	-	-
(a)	Low response rate instrumentation -- only one-dimensional resolution						
(b)	Gas velocity in the collector was reported to be low enough so that $p_{coll} \approx p_{O_{coll}}$ , and $T_{coll} \approx T_{O_{coll}}$						
(c)	Inlet guide vanes were removed for this test						
(d)	Boeing test numbers						

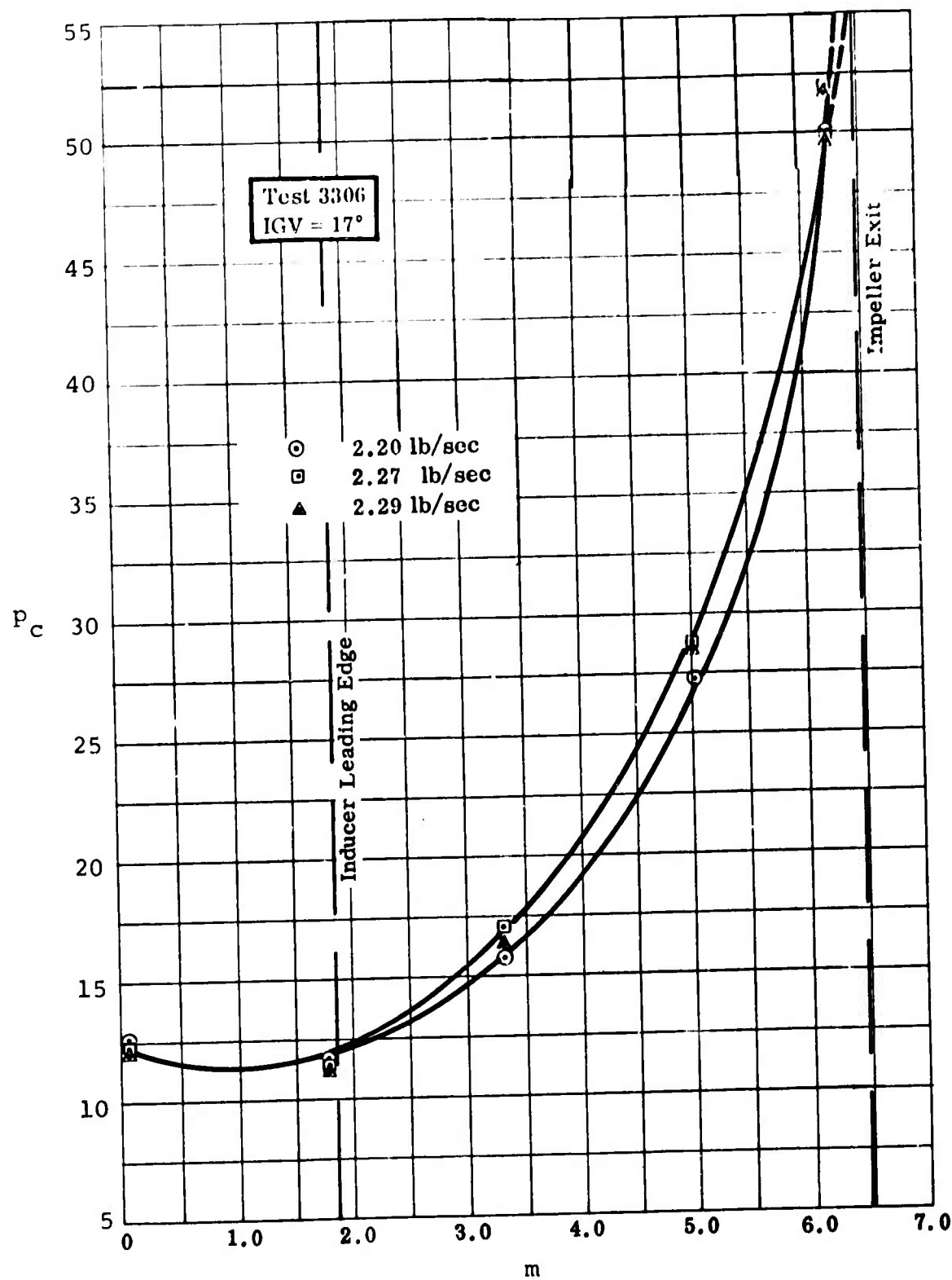


Figure 20. Cover Static Pressure.  
Workhorse.

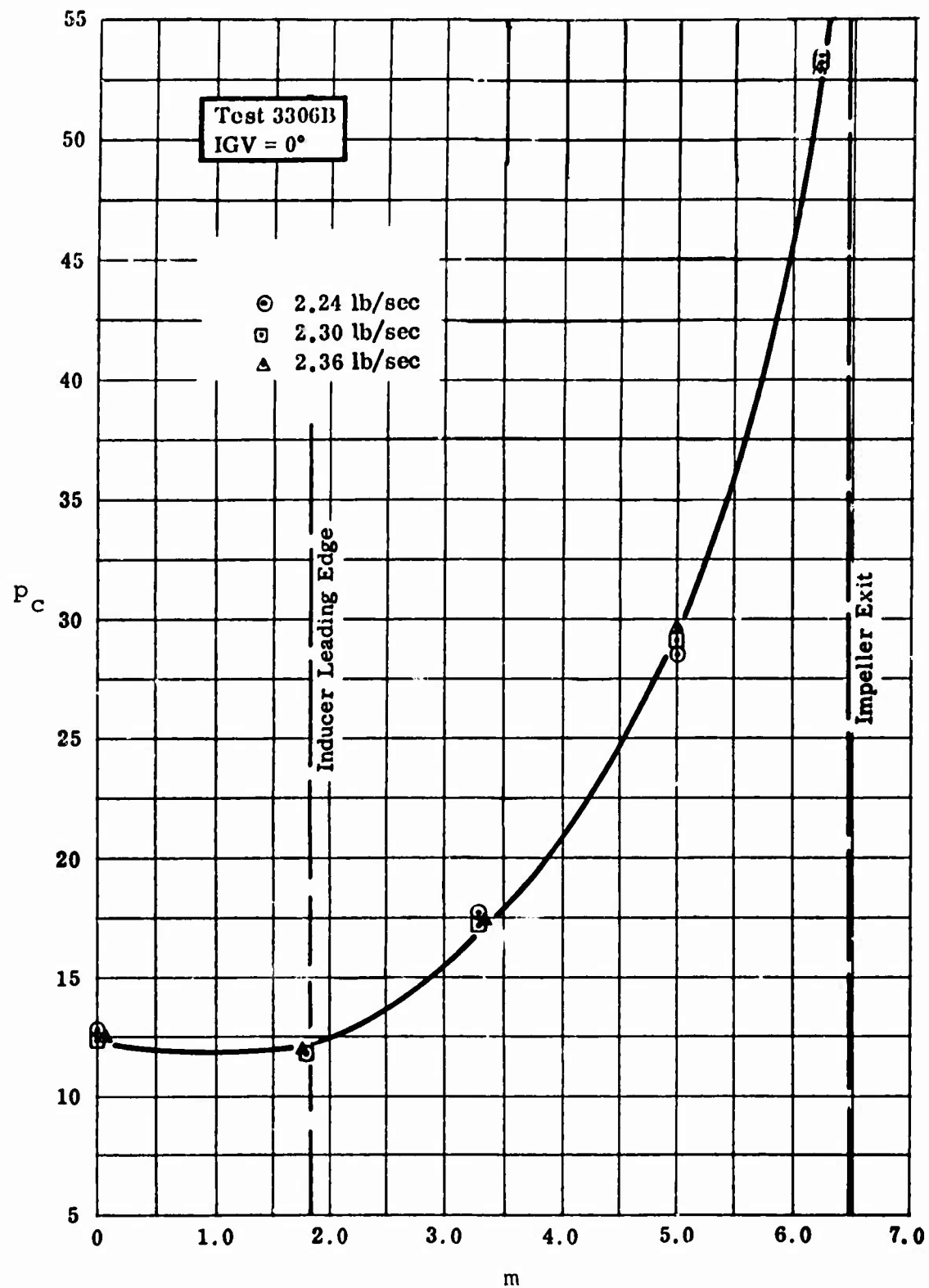


Figure 21. Cover Static Pressure.  
Workhorse

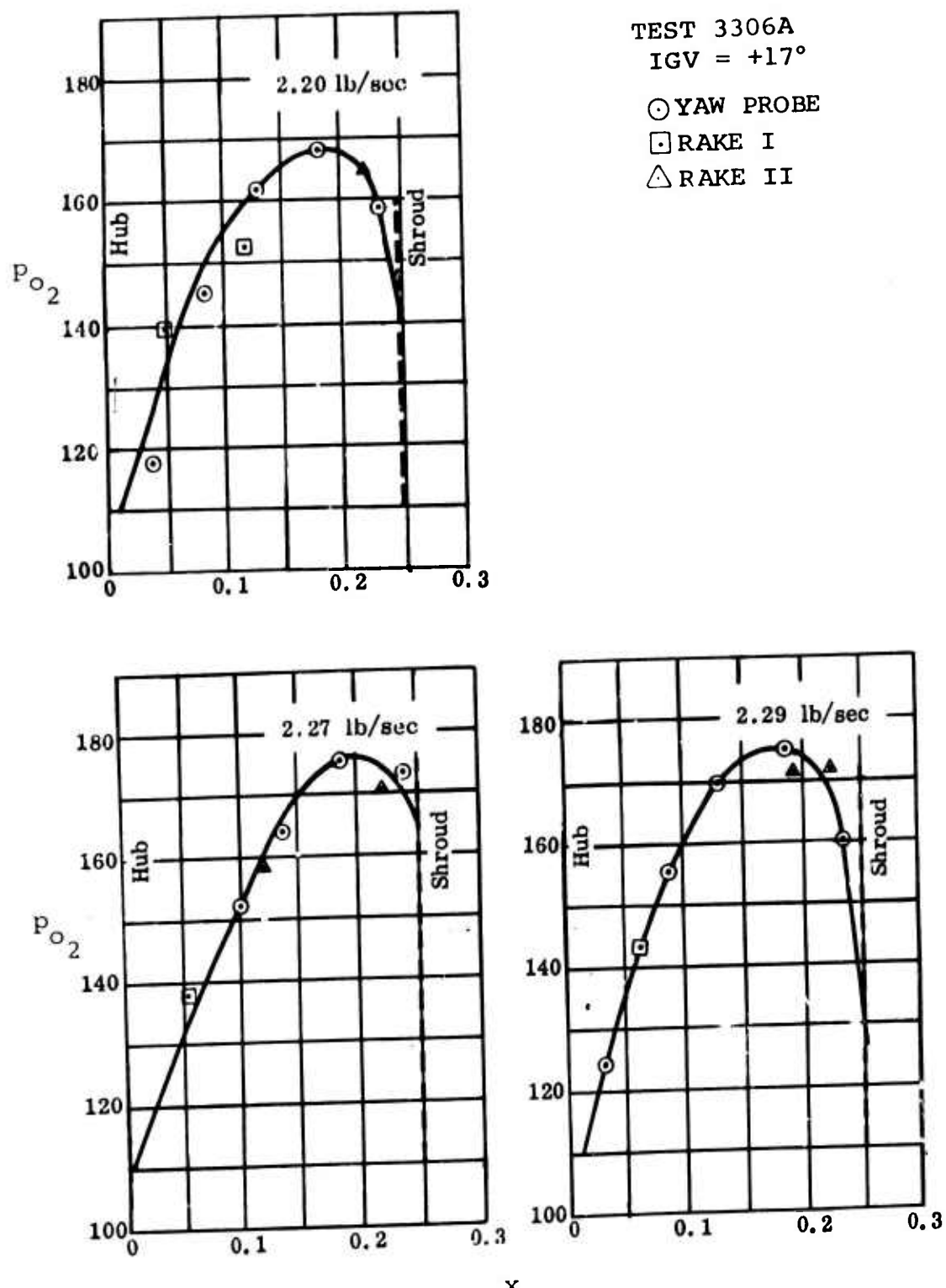


Figure 22. Impeller Tip Stagnation Pressure.  
Workhorse

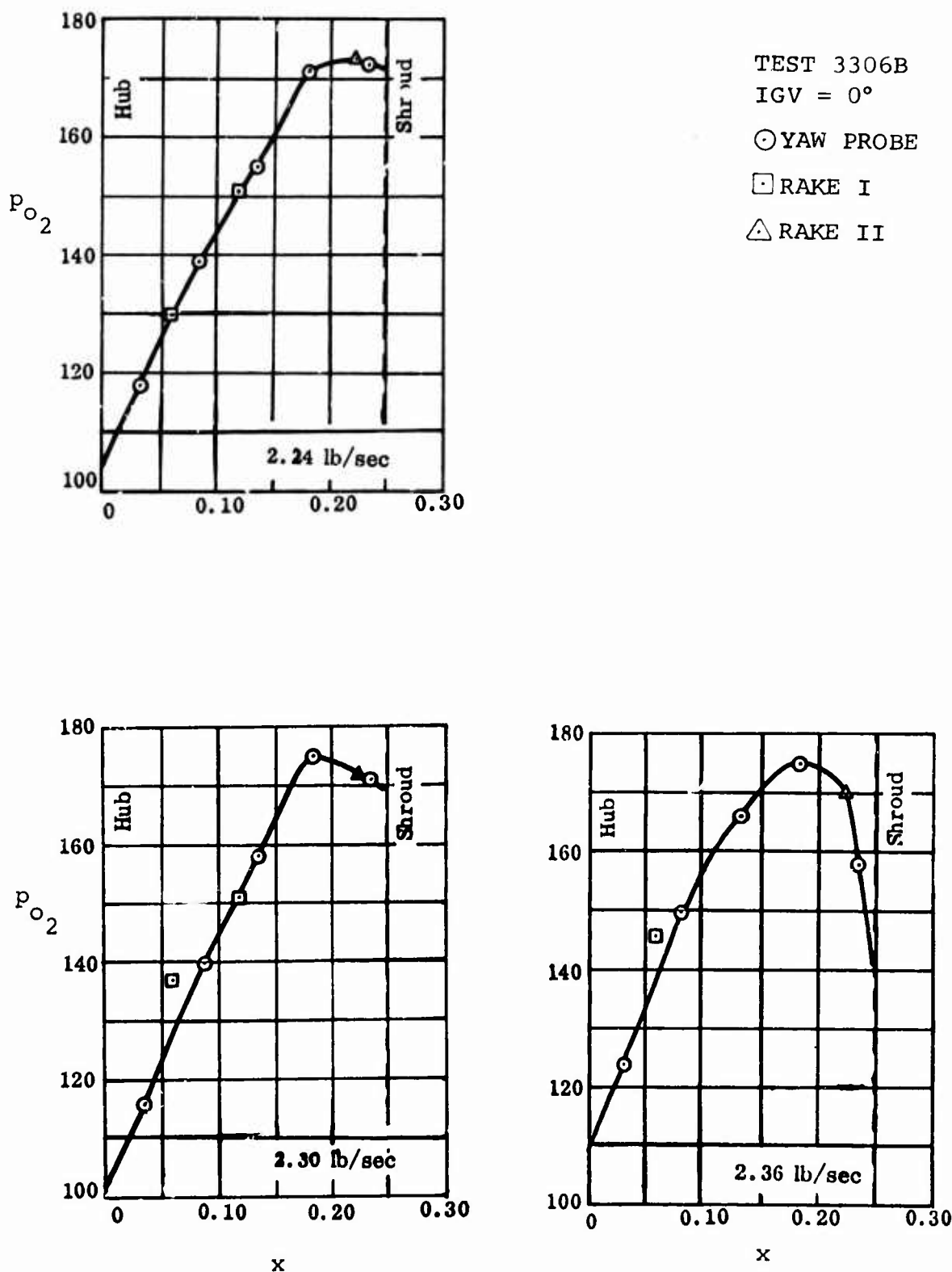


Figure 23. Impeller Tip Stagnation Pressure.  
Workhorse

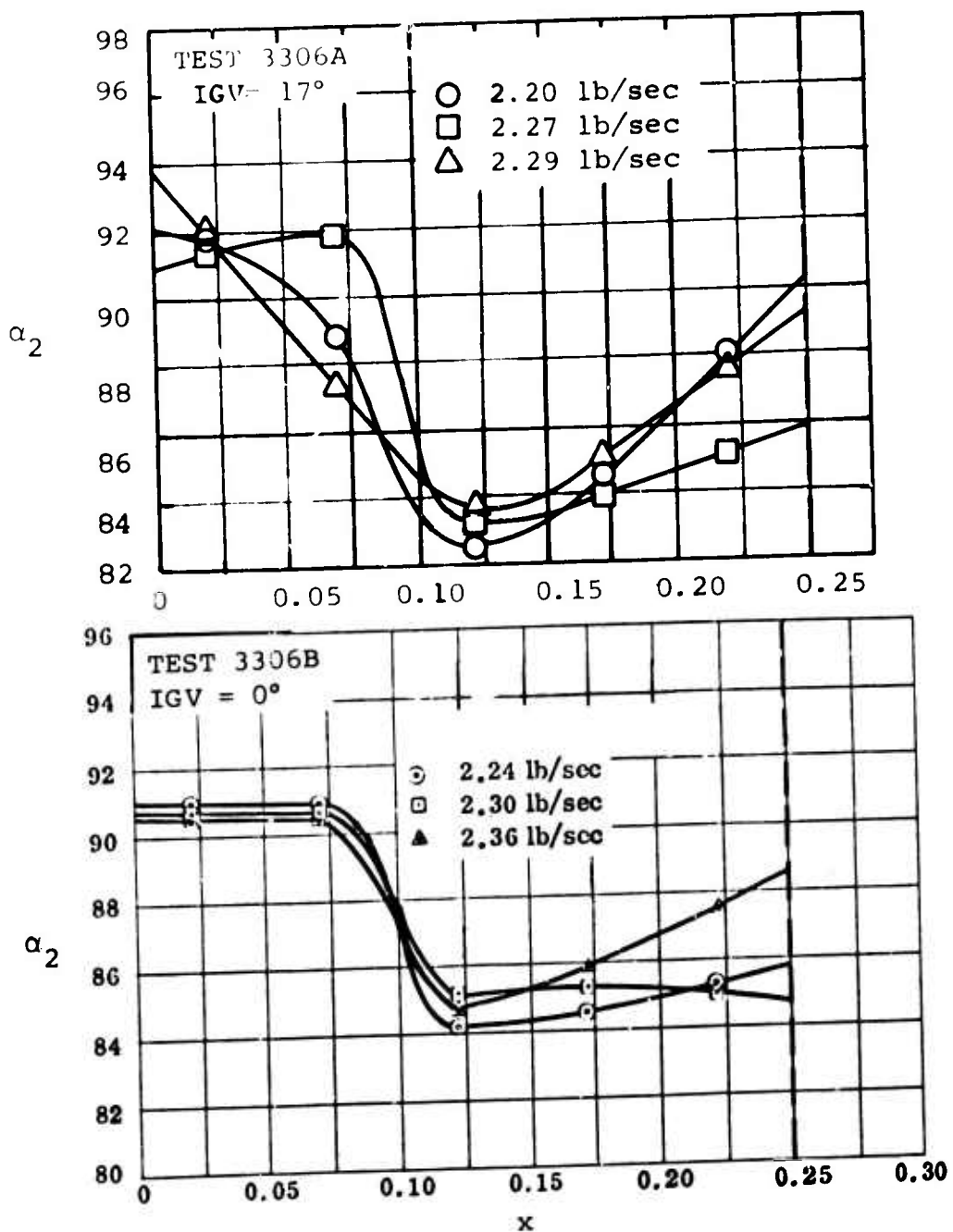


Figure 24. Impeller Tip Flow Angle.  
Workhorse

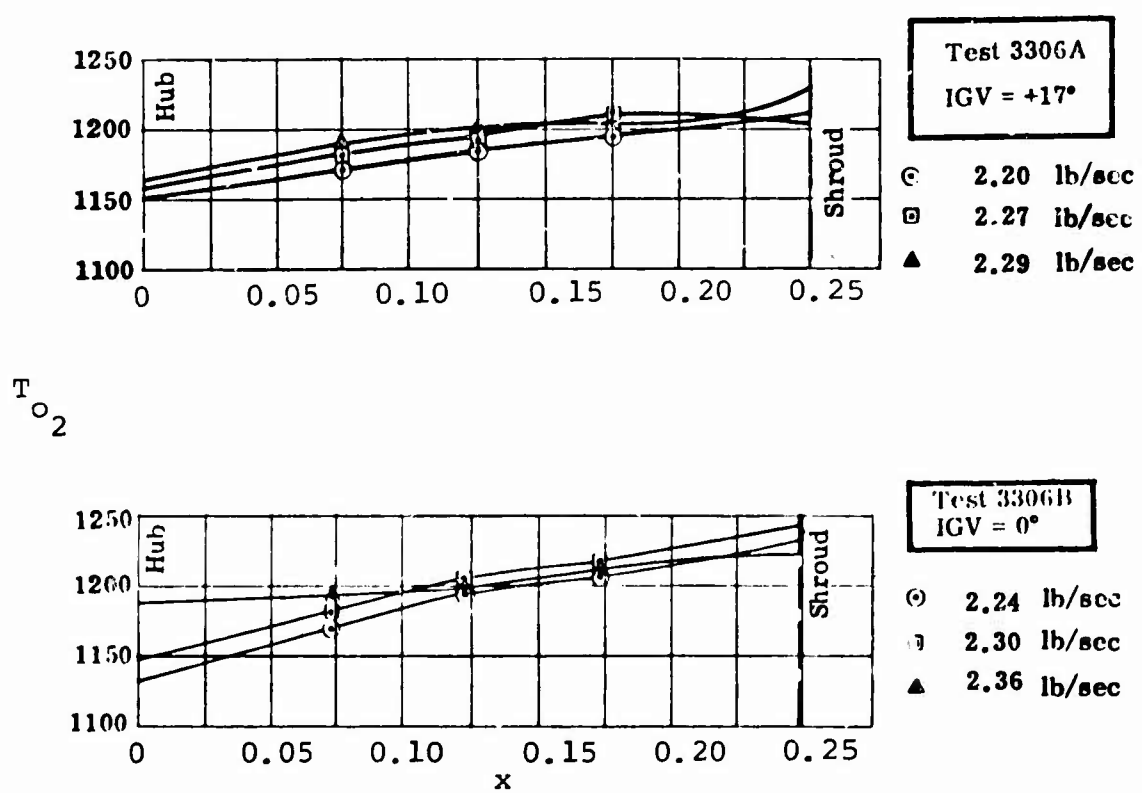


Figure 25. Impeller Tip Stagnation Temperature.  
Workhorse

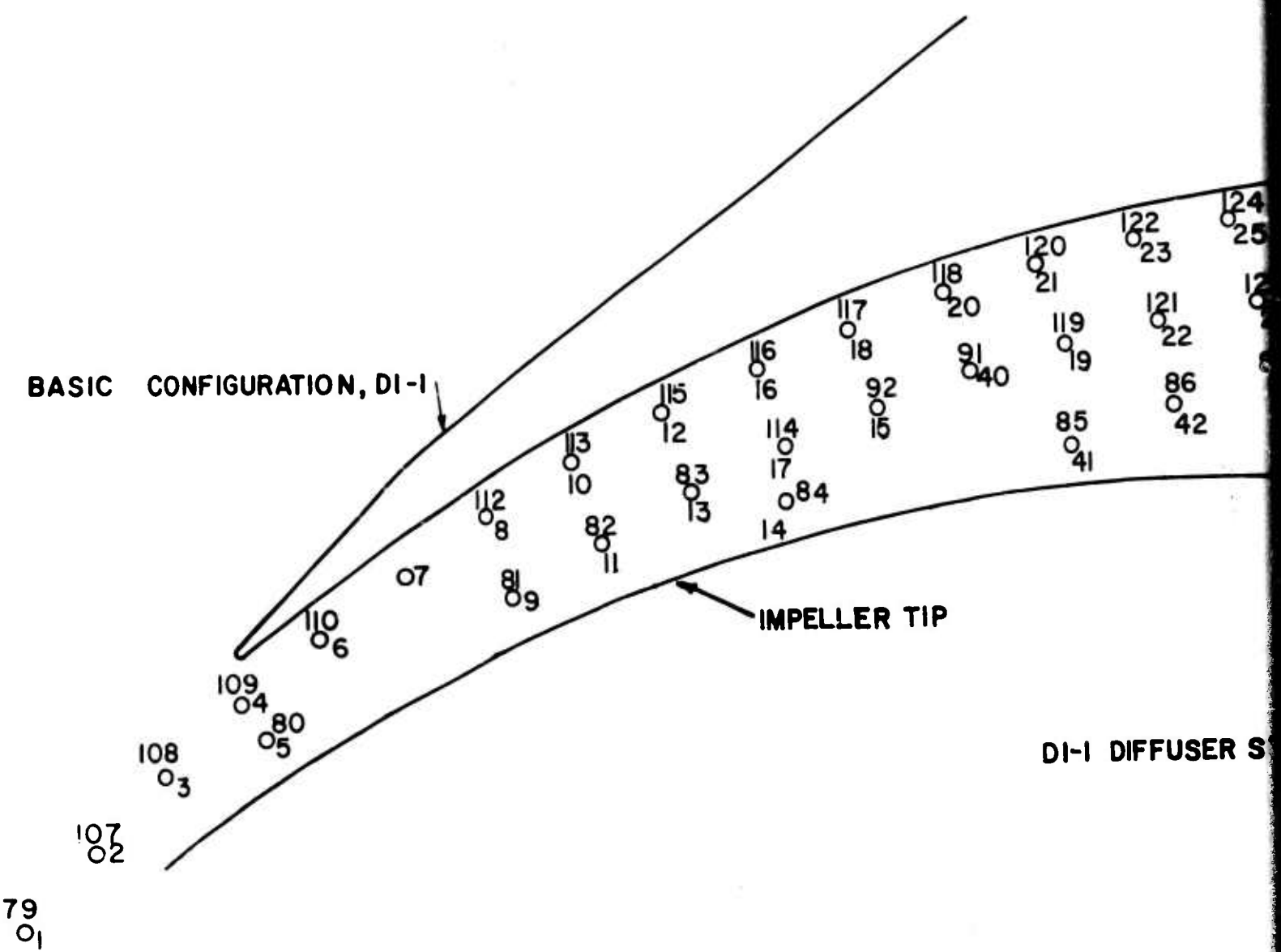
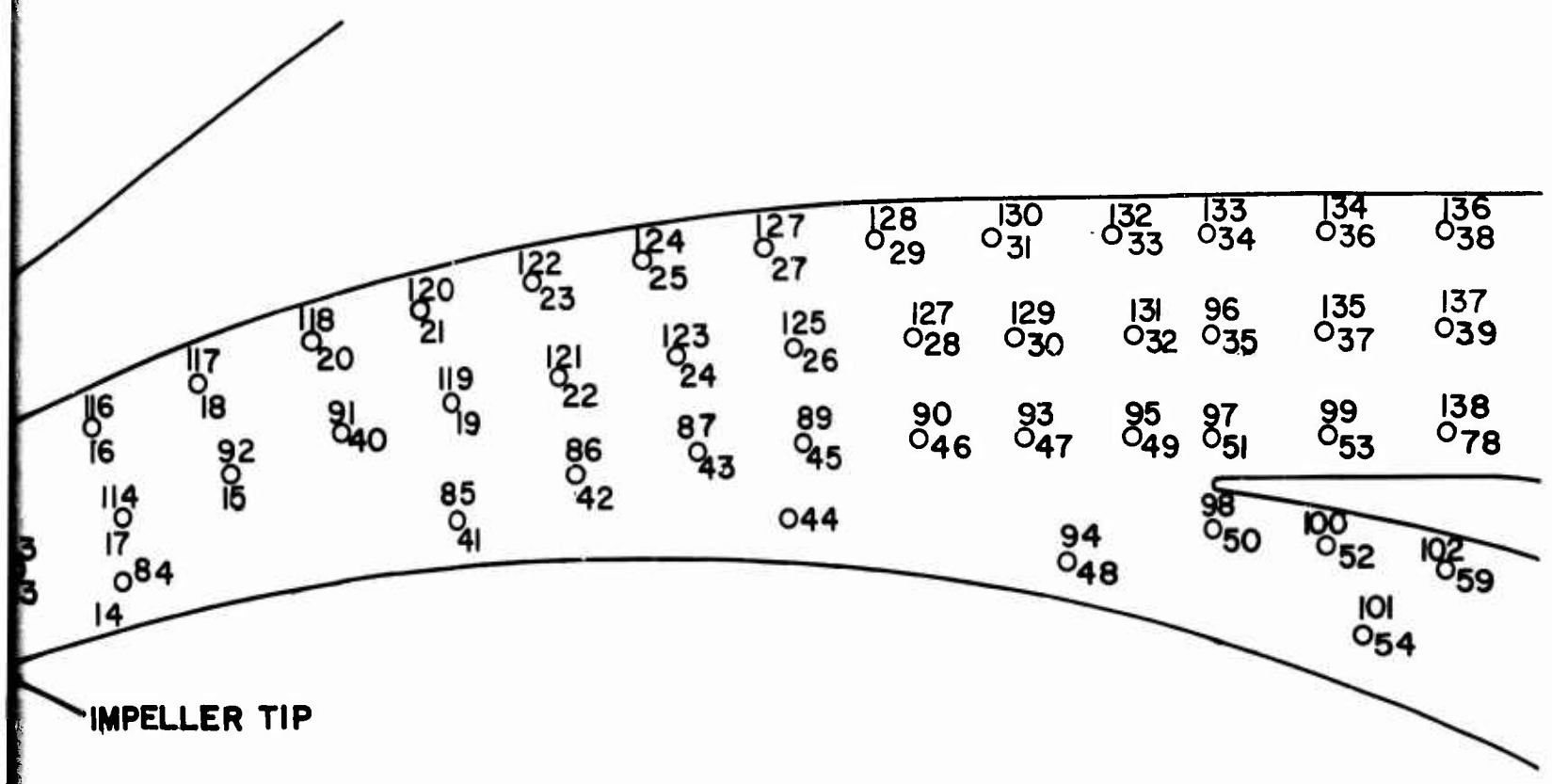
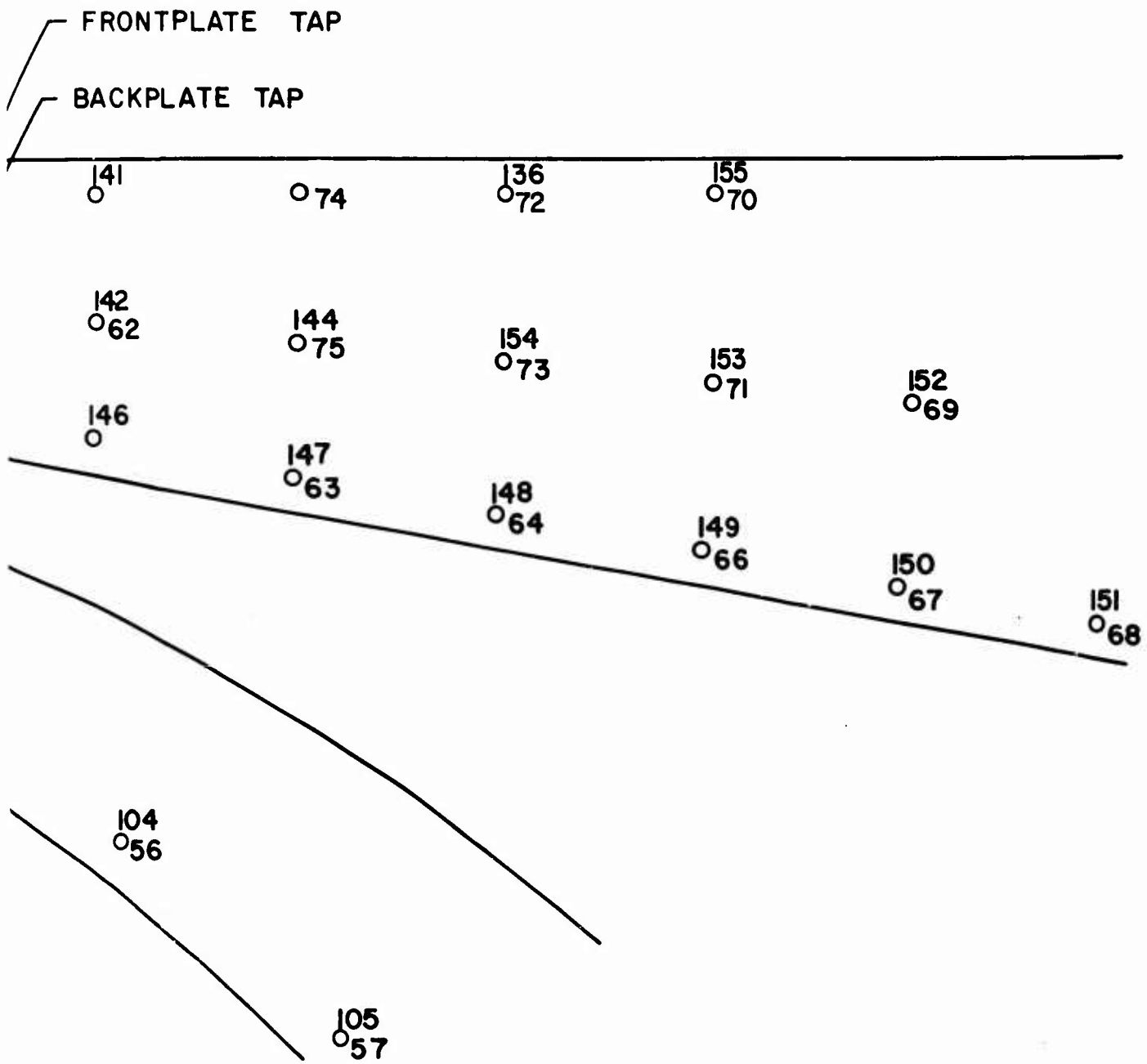


Figure 26 . DI-1 Diffuser Static Pressure Tap Locations and Numbers.  
Workhorse





C

DI 1 PRESSURE SURVEY													
TEST NO. 3306 F				SPEED = 50000 RPM				AIR FLOW = 2.36					
IGV = 0		THROAT AREA = 1.118		RADIUS RATIO = 1.06									
LINE NO. 5		$\delta = 1.000$ (PRESSURE CORRECTION FACTOR)											
ALL PRESSURES ARE IN PSIA													
TAP NO.	STATIC PRESSURE	TAP NO.	STATIC PRESSURE	TAP NO.	STATIC PRESSURE	TAP NO.	STATIC PRESSURE	TAP NO.	STATIC PRESSURE	TAP NO.	STATIC PRESSURE		
1	64.1	2	65.7	3	65.1	4	70.0	5	69.0	6	69.7		
7	65.6	8	69.3	9	62.0	10	67.1	11	64.5	12	70.3		
13	64.9	14	63.0	15	66.6	16	71.7	17	64.9	18	70.5		
19	69.8	20	74.4	21	74.2	22	71.6	23	75.2	24	71.6		
25	77.5	26	71.1	27	77.1	28	71.4	29	77.9	30	68.2		
31	75.5	32	64.6	33	68.9	34	65.7	35	74.2	36	69.9		
37	63.0	38	76.9	39	73.2	40	68.2	41	63.2	42	64.7		
43	67.2	44	63.8	45	68.4	46	67.0	47	65.7	48	61.2		
49	60.4	50	78.6	51	82.5	52	60.2	53	71.7	54	58.4		
55	63.9	56	70.0	57	58.2	58	61.7	59	63.8	60	93.5		
62	106.2	63	112.6	64	115.5	65	94.4	66	117.2	67	118.3		
68	119.1	69	118.4	70	117.7	71	117.3	72	115.9	73	114.2		
74	112.7	75	112.5	77	95.4	78	71.4	79	63.3	80	62.9		
81	62.3	82	53.7	83	63.9	84	23.1	85	0.0	87	68.0		
88	21.4	89	0.0	90	69.1	91	69.2	92	64.8	93	69.1		
94	58.2	95	65.9	96	75.1	97	86.1	98	79.2	99	74.1		
100	70.9	101	66.0	102	69.8	103	63.0	104	67.7	105	55.9		
106	62.2	107	64.5	108	65.0	109	34.4	110	70.9	112	68.3		
113	21.9	114	34.9	115	73.7	116	75.0	117	74.5	118	77.4		
119	71.1	120	76.0	121	73.6	122	79.8	123	75.6	124	81.0		
125	75.2	126	80.0	127	76.2	128	78.7	129	71.8	130	76.0		
132	73.7	133	67.5	134	72.9	135	66.3	136	76.8	137	72.0		
139	94.8	140	94.4	141	107.2	142	107.9	144	113.5	146	106.9		
147	112.7	148	115.3	149	117.1	150	118.3	151	119.0	152	119.1		
153	118.2	154	116.5	155	118.1	156	116.5	157	120.2	158	120.8		
159	120.8	160	120.9										

Figure 27. Static Pressure Field.  
Workhorse

D1-1\* PRESSURE SURVEY

TEST NO. 3339

SPEED = 5000 RPM

AIR FLOW = 2.45

IGV = REMOVED

THRCAT AREA = 1.118

RADIUS RATIO = 1.06

LINE NO. 3

$\delta = 0.989$  (PRESSURE CORRECTION FACTOR)

ALL PRESSURES ARE IN PSIA

TAP NO.	STATIC PRESSURE										
2	67.1	3	66.6	4	91.9	5	82.4	6	54.5	7	63.8
8	69.9	9	66.3	10	71.1	11	65.4	13	66.8	15	67.5
17	61.3	19	68.9	20	72.3	21	73.3	24	73.8	25	80.1
27	80.9	28	74.5	29	81.1	31	78.8	32	66.0	33	68.9
34	83.4	35	94.8	35	86.0	36	80.6	37	81.8	38	81.0
39	79.1	40	66.9	41	61.4	42	65.6	43	68.3	44	69.1
45	71.8	46	69.5	47	68.2	48	62.9	49	70.9	50	84.8
51	92.6	52	61.3	53	82.1	54	58.2	55	65.2	56	64.9
57	63.2	58	63.9	59	63.1	60	94.8	62	109.9	63	116.5
64	119.8	65	97.6	66	121.4	68	117.6	69	122.9	70	121.8
71	121.9	72	119.7	73	119.8	74	116.3	75	116.6	77	97.8
78	77.9	84	67.9	115	0.0	118	75.0	122	54.5	127	75.0
156	0.0	157	124.6	158	125.3	159	125.4	160	125.4		

Figure 28 . Static Pressure Field,  
Workhorse

DI-1 PRESSURE SURVEY					
TEST NO. 3317		SPEED = 50000 RPM		AIR FLOW = 2.37	
IGV = 0		THROAT AREA = 1.118		RADIUS RATIO = 1.06	
LINE NO. 5		$\delta = 0.995$ (PRESSURE CORRECTION FACTOR)			
ALL PRESSURES ARE IN PSIA					
TAP STATIC NO. PRESSURE	TAP STATIC NO. PRESSURE	TAP STATIC NO. PRESSURE	TAP STATIC NO. PRESSURE	TAP STATIC NO. PRESSURE	TAP STATIC NO. PRESSURE
1 64.4	2 64.7	3 63.9	4 71.9	5 70.3	6 61.1
7 67.7	8 68.1	9 68.7	10 70.3	11 66.1	12 70.1
13 65.1	15 66.6	16 72.0	17 59.0	19 68.9	20 72.2
21 74.4	22 70.7	23 75.8	24 70.8	25 77.6	27 74.9
28 73.3	29 77.3	30 70.0	31 76.2	32 66.0	33 70.0
34 69.8	35 77.2	36 79.2	37 80.2	38 76.1	39 74.1
40 66.5	41 62.3	42 64.3	43 66.1	44 67.4	45 68.3
46 68.1	47 65.8	48 61.4	49 64.1	50 22.4	51 84.3
52 66.7	53 80.2	54 62.8	55 60.5	56 62.4	57 64.1
58 62.7	59 66.7	60 75.0	62 92.7	63 100.8	64 105.4
65 76.9	66 108.4	67 110.3	68 111.5	69 109.8	70 108.7
71 107.8	72 105.8	73 105.0	74 101.7	75 101.1	77 73.1
78 72.9	79 63.1	80 65.5	81 64.4	83 63.6	86 64.4
87 66.9	90 68.6	91 68.4	92 64.7	93 69.3	95 66.8
96 78.6	97 87.3	98 78.1	99 83.7	100 70.9	102 70.1
104 60.9	105 62.7	106 62.9	107 63.0	108 63.7	110 69.2
112 69.6	115 72.9	116 74.9	117 73.0	118 71.9	118 75.7
119 70.1	120 75.5	121 72.7	122 78.6	123 74.8	124 79.0
125 73.4	127 76.2	128 78.6	129 72.6	131 70.4	132 74.4
134 79.2	135 82.0	136 78.0	138 76.4	139 69.7	140 0.0
142 95.3	148 102.0	146 92.8	147 101.3	148 105.3	149 108.3
150 110.3	151 111.5	152 110.6	153 109.0	154 106.3	155 109.1
156 106.3	157 113.0	158 113.6	159 113.7	160 113.7	

Figure 29. Static Pressure Field.  
Workhorse

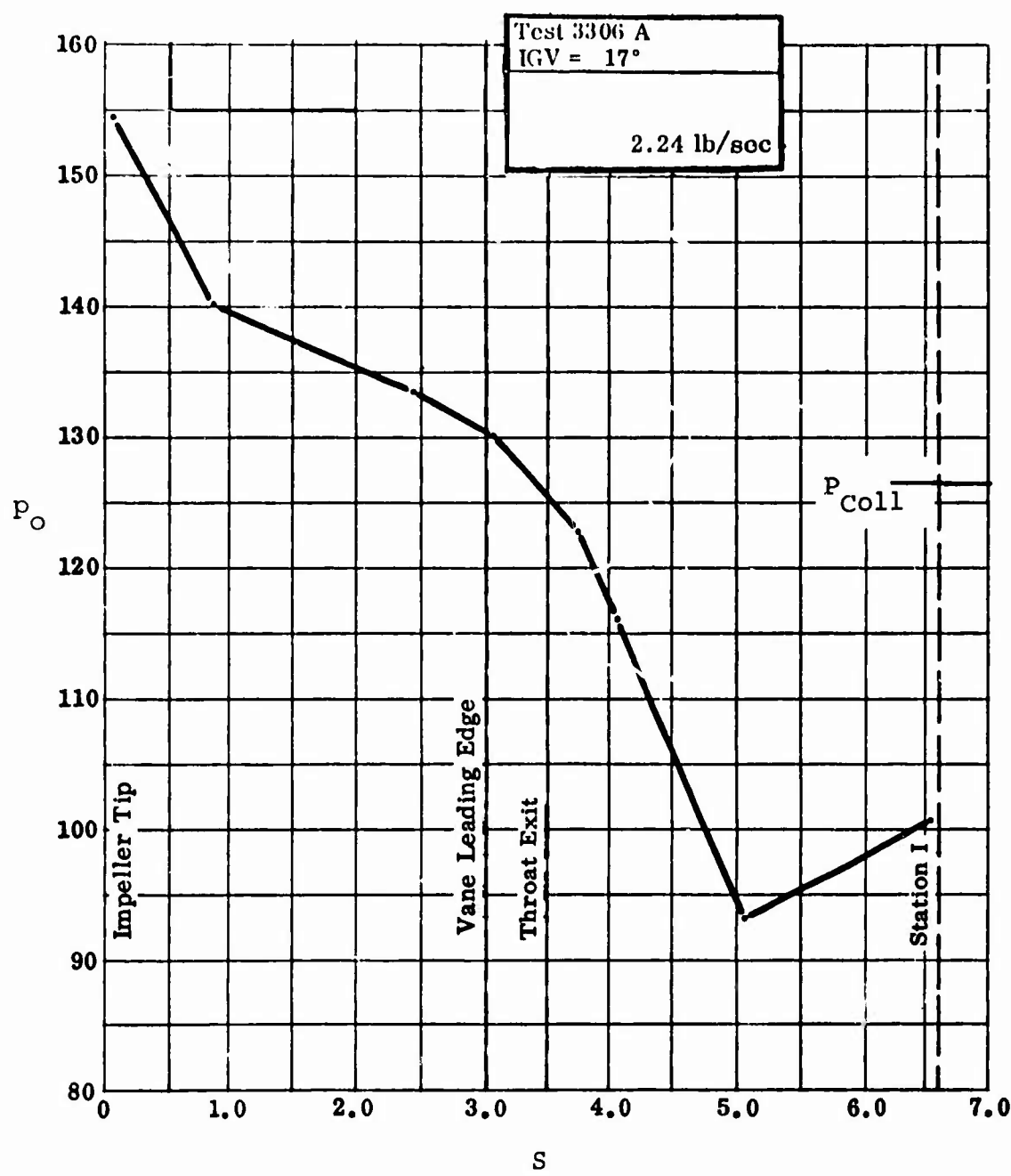


Figure 30. Stagnation Pressure Traverse From Railroad Track Probe.  
Workhorse

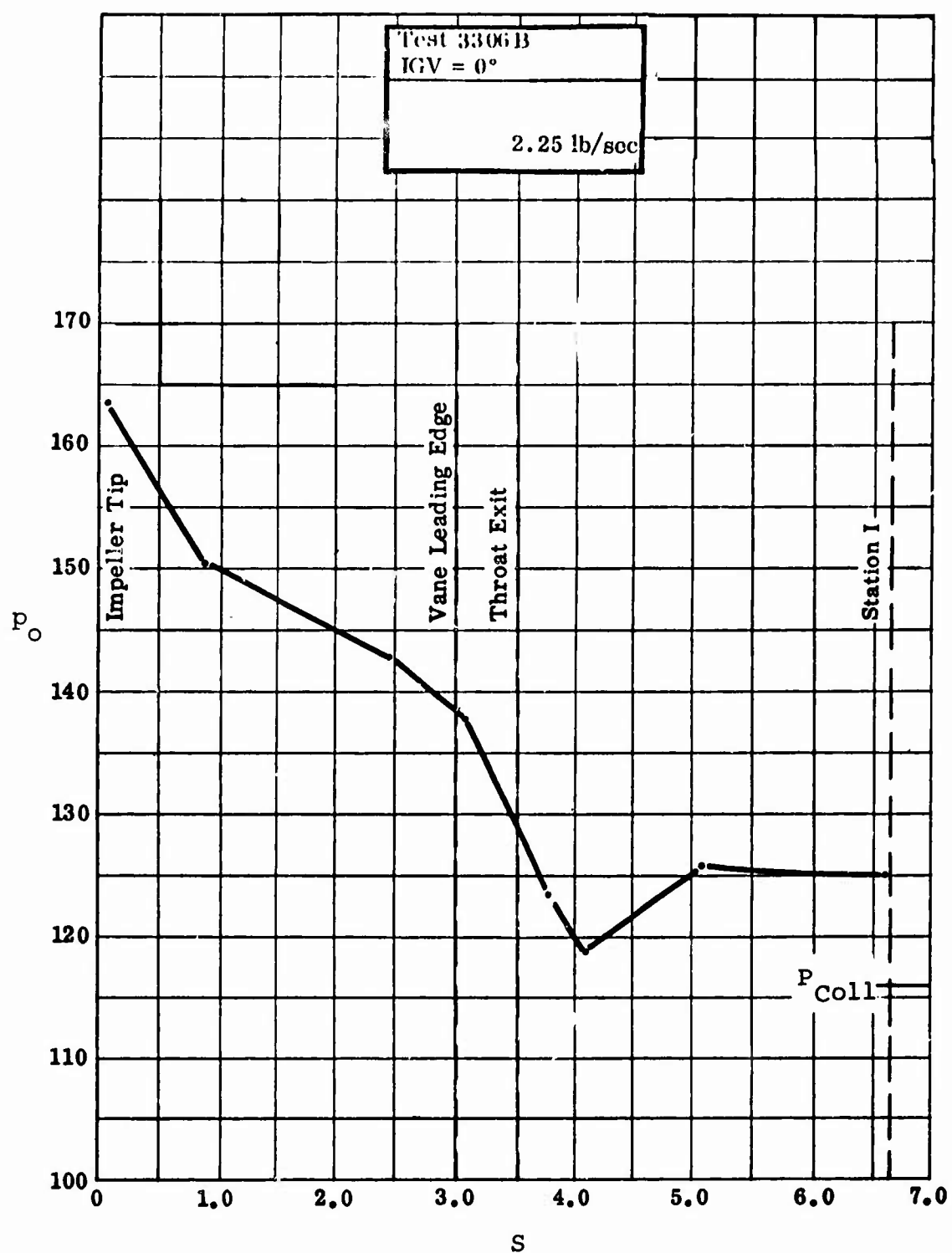


Figure 31. Stagnation Pressure Traverse From Railroad Track Probe.  
Workhorse

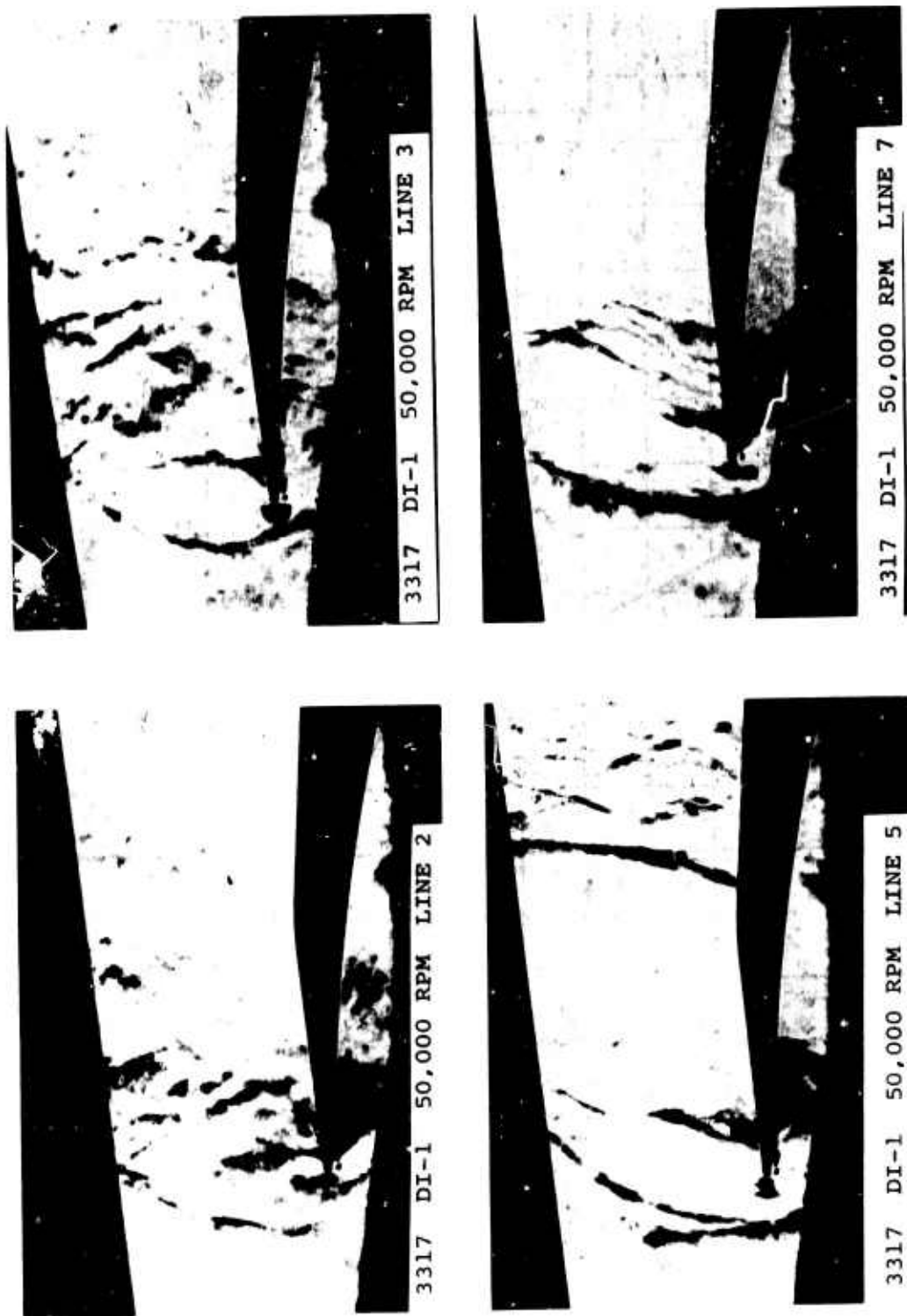


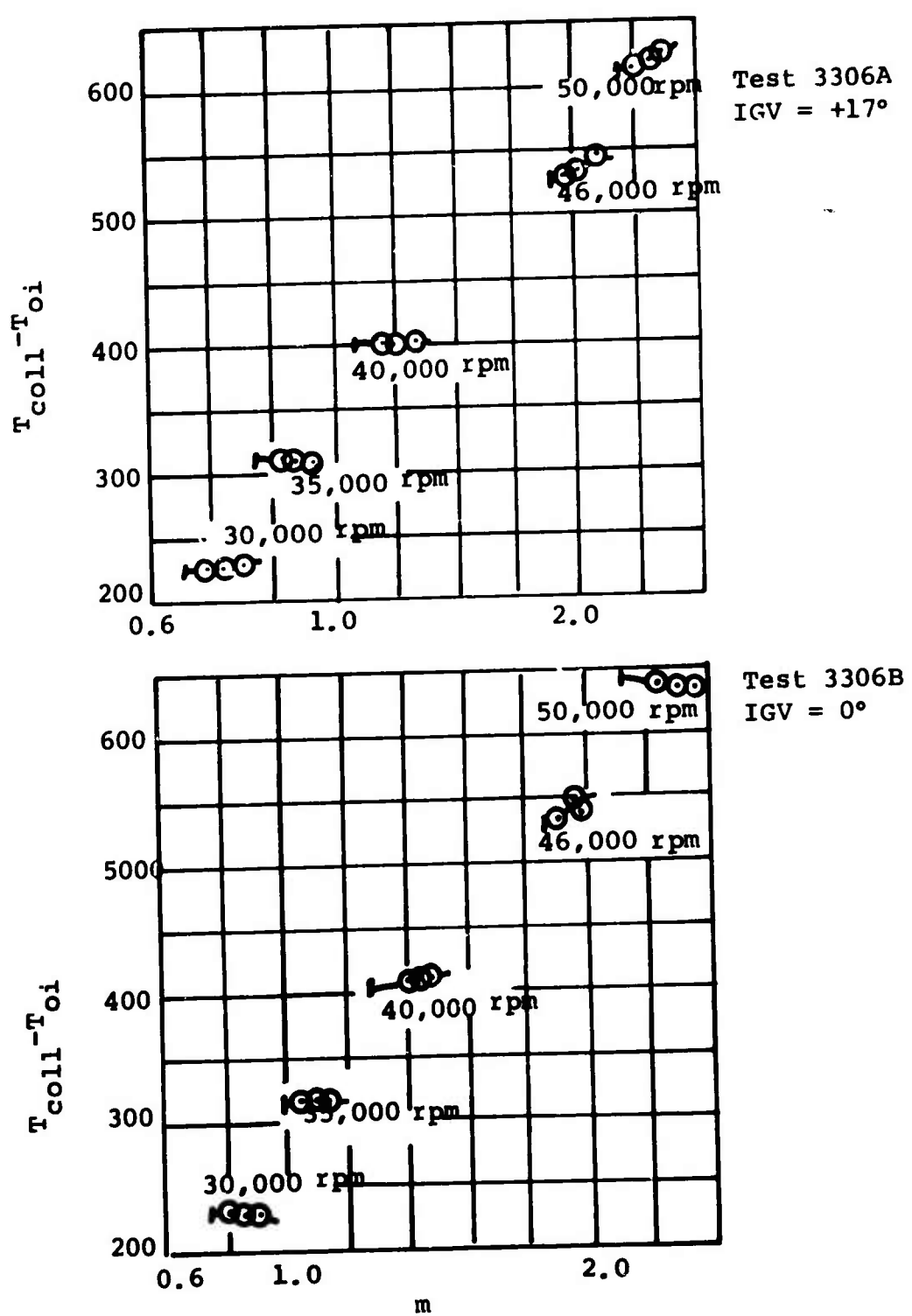
Figure 32 . Schlieren Photograph of DI-1.  
Workhorse



Figure 33. Oil Slick Traces, 30,000 RPM.  
Workhorse, DI-1, Line 5.



Figure 34. Oil Slick Trace, 38,400 RPM.  
Workhorse, DI-1, Line 7.



**Figure 35.** Collector Temperature Rise Versus Mass Flow.  
Workhorse

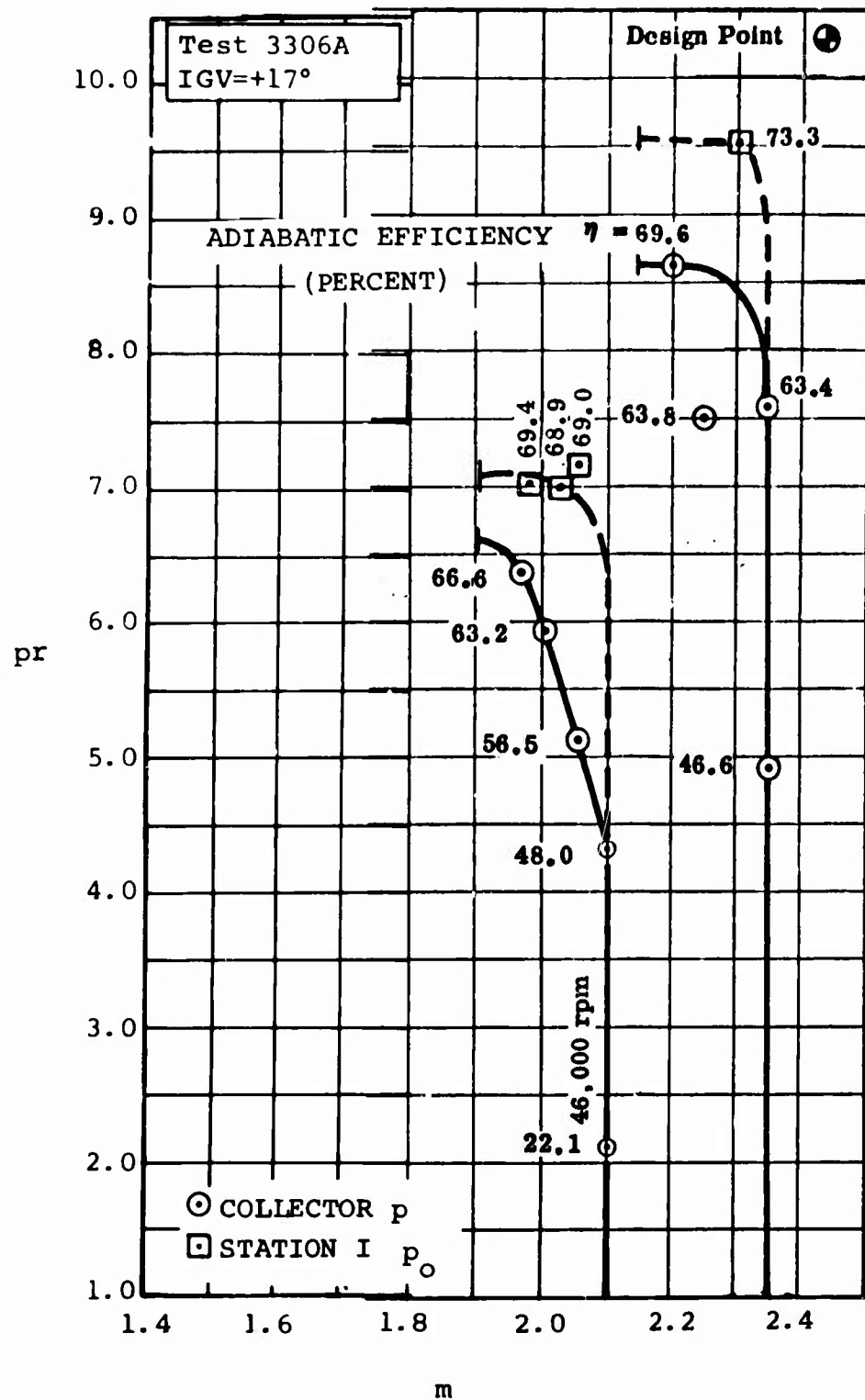
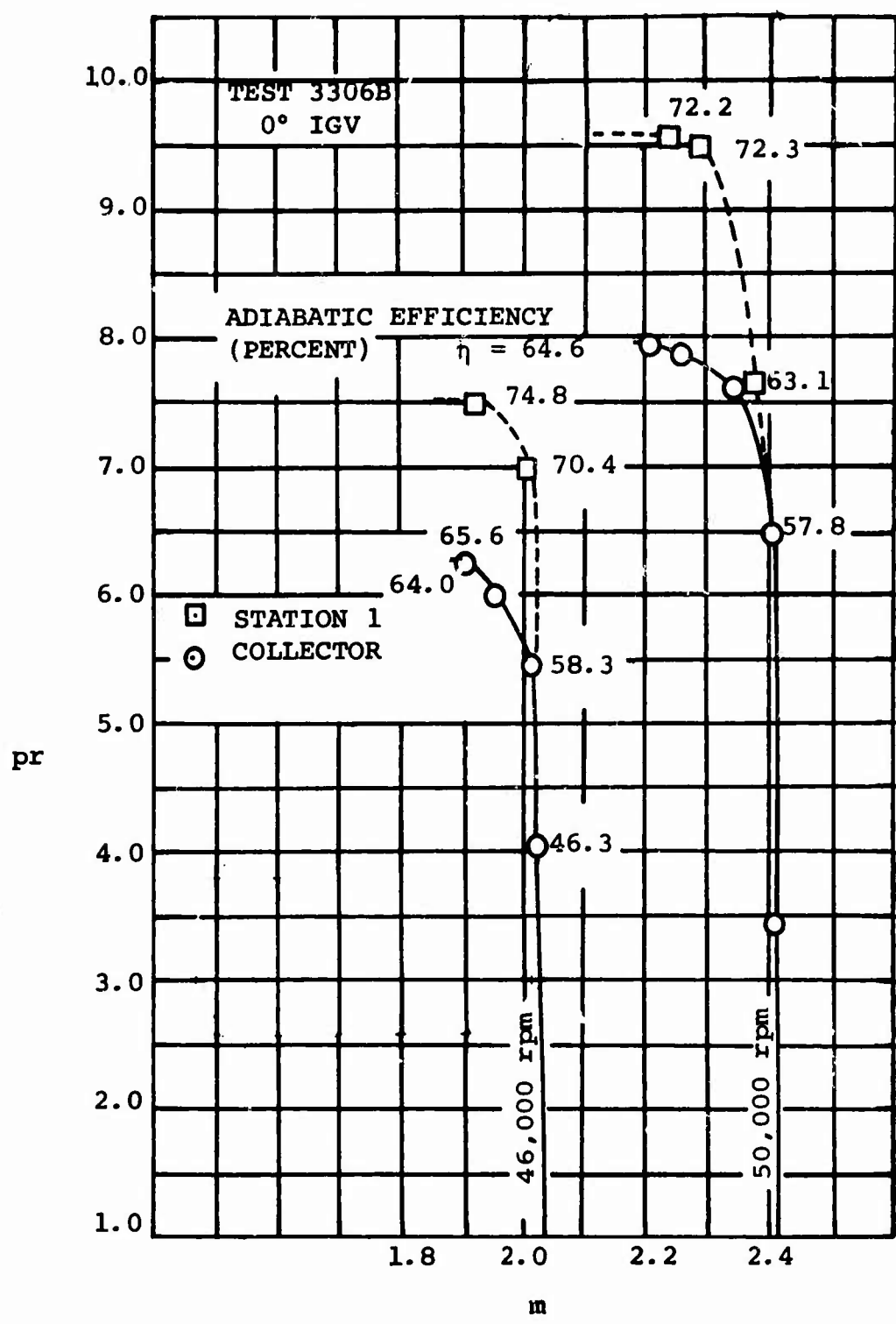


Figure 36. Collector Static Pressure Ratio Versus Mass Flow.  
Workhorse



**Figure 37.** Collector Static Pressure Ratio Versus Mass Flow.  
**Workhorse**

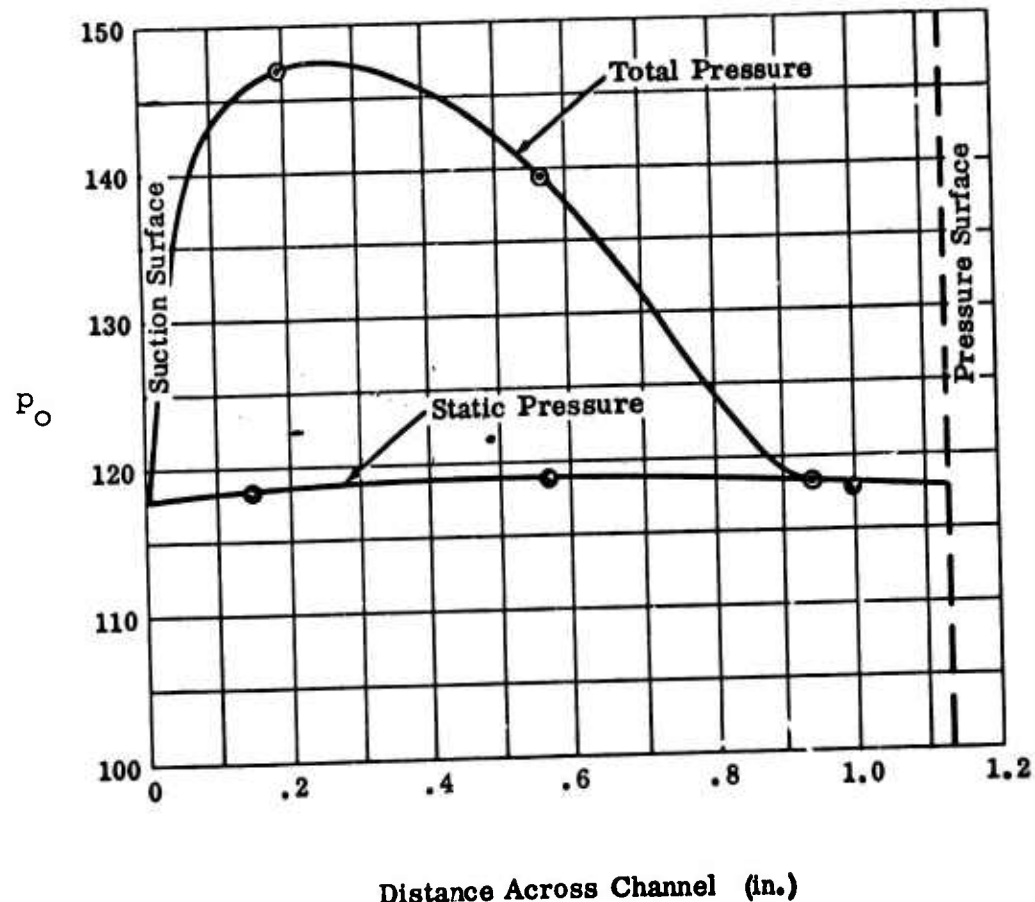
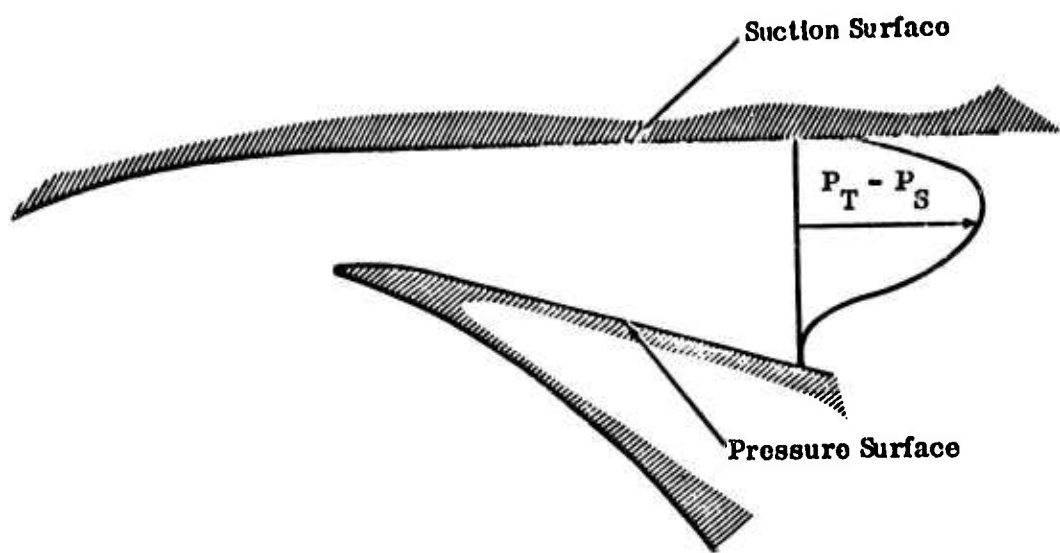


Figure 38. Diffuser Traverse With Total Probe at Station 1 - DI-1, Conditions Unknown.  
Workhorse

### 3.4 RF-2 STAGE DATA

All the data used in this study from the RF-2 stage are presented in Figures 39 through 92.

Table V summarizes the data used.

TABLE V. SUMMARY OF RF-2 DATA

Notes: 1) All entries are "Boeing corrected" data from Welliver and Acurio (1967) (67-47)  
 2) All data at  $\Omega = 50,000$  rpm  
 3) Only directly measured data included  
 4) For details of instrumentation see Figures 11 to 19

Measurement	Remarks	3352C <sup>b</sup>	3353
1. $p_c^e = f(m)$	average from three meridional locations	39	40
2. $p_h^e = f(m)$	average from three meridional planes upstream of impeller	-	
3. $p_{O_2}^e = f(x)$	impact tube pressure rake	-	42
4. $a_2^e = f(x)$	cobra yaw probe	-	47
5. $T_{O_2}^e = f(x)$	"miniature" $T_o$ probe	-	48
6. $p^e = f(r, \theta)$	cover and hub wall throughout diffuser	50-52	-
7. $p_{O_4}^e = f(x)$	fixed rakes at 3 positions (in diffuser throat only one inserted at a time)	-	-
8. $T_{coll}^{c,e}$	average of several probes <sup>d</sup>	58	-
9. $p_{coll}^{c,e}$	average of several taps <sup>d</sup>	59	59
a) Boeing's designation for this diffuser system.			c) Gas enough
b) Boeing test number			

VI-3 <sup>a</sup> Configuration Figure Number						VI-4 <sup>a</sup> Configuration Figure Number				
3352C <sup>b</sup>	3353	3353A	3353C	3353D	3353E	3353F	3354 <sup>b</sup>	3354A	3354B	3366 <sup>b</sup>
39	40	-	41	-	-	-	60-62	-	-	-
-	-	-	-	-	-	-	-	-	-	-
-	42	-	43-46	-	-	-	-	-	-	-
-	47	-	-	-	-	-	-	-	-	-
-	48	-	-	-	-	-	-	-	-	-
50-52	-	-	-	53-55	-	-	64-66	-	-	75-77
-	-	-	-	56,57	56,57	56,57	-	67,68	67,68	-
58	-	-	-	58	-	-	69	-	-	80
59	59	59	59	59	-	-	70	-	-	81

c) Gas velocity in the collector was reported to be low enough so that  $p_{coll} \approx p_{O_{coll}}$ ,  $T_{coll} \approx T_{O_{coll}}$

d

e

V2 <sup>a</sup> Configuration Figure Number					V2-2 <sup>a</sup> Configuration Figure Number			
3366A	3366B	3366C	3366D	3366E	3369 <sup>b</sup>	3369A	3369B	3370A
-	-	71	-	-	-	-	-	82
-	-	71	-	-	-	-	-	82
72, 73	-	-	-	72, 73	-	83, 84	-	83, 84
-	-	-	-	-	-	-	-	-
-	-	-	-	-	-	-	-	-
-	-	-	-	-	86-88	-	-	-
-	78, 79	78, 79	78, 79	-	89, 90	-	-	-
-	80	-	-	-	91	-	91	-
-	-	-	-	-	92	-	-	-

- ) Exact number not known, but probably 4 pressure taps and  
6-12 thermocouples  
)) Low response rate instrumentation

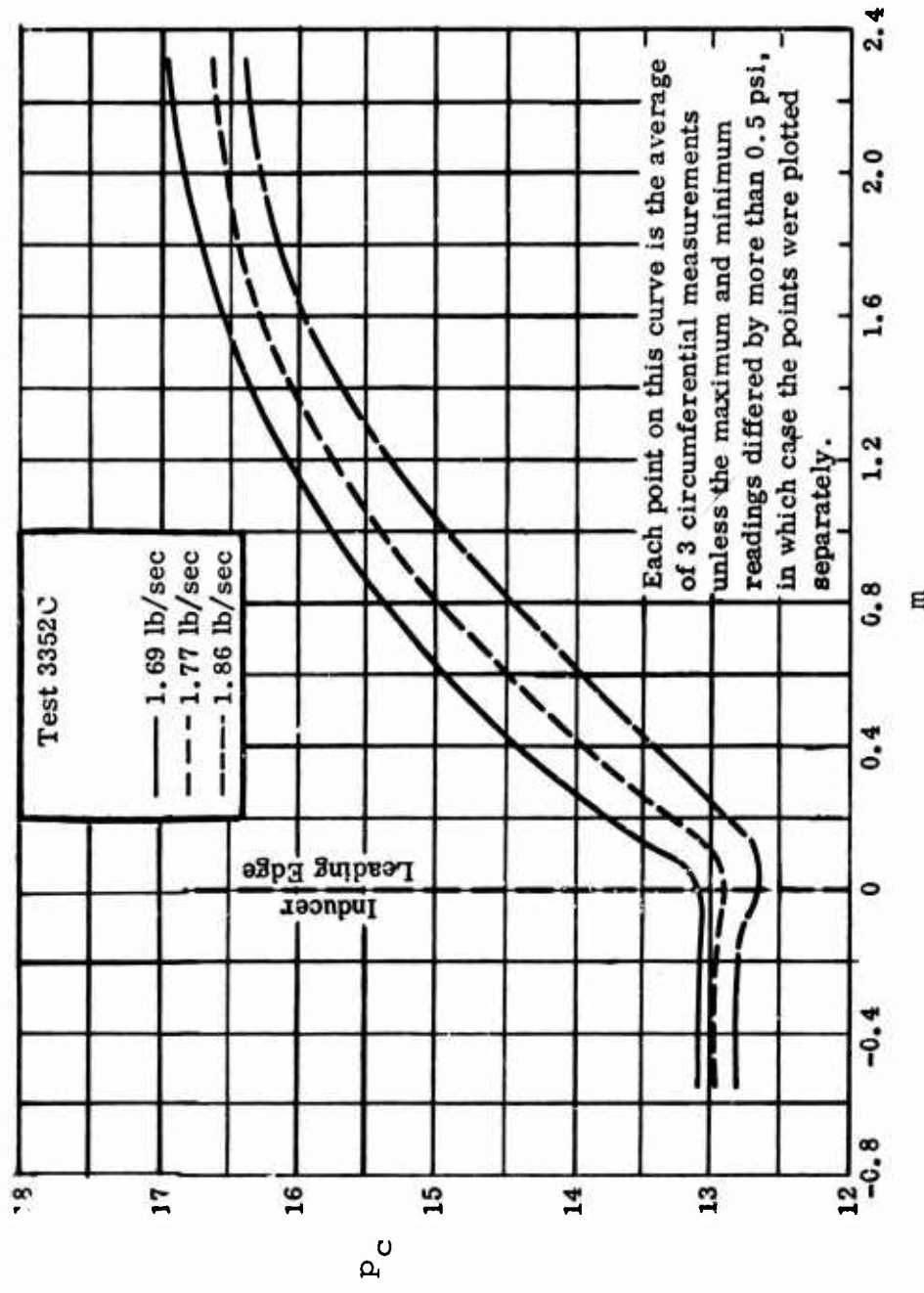


Figure 39. Cover Static Pressure.  
RF-2

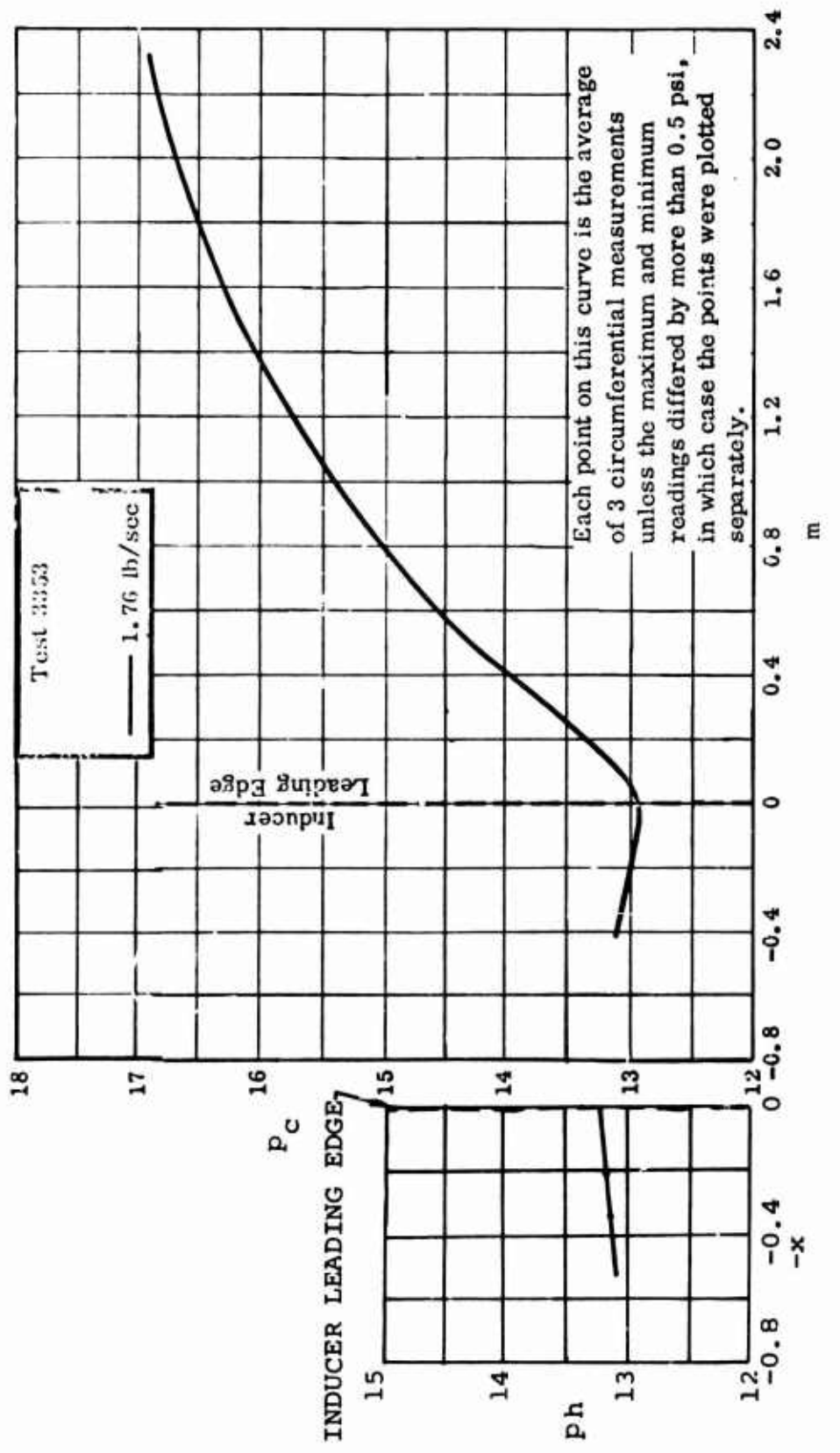


Figure 40. Cover and Hub Static Pressure.  
RF-2

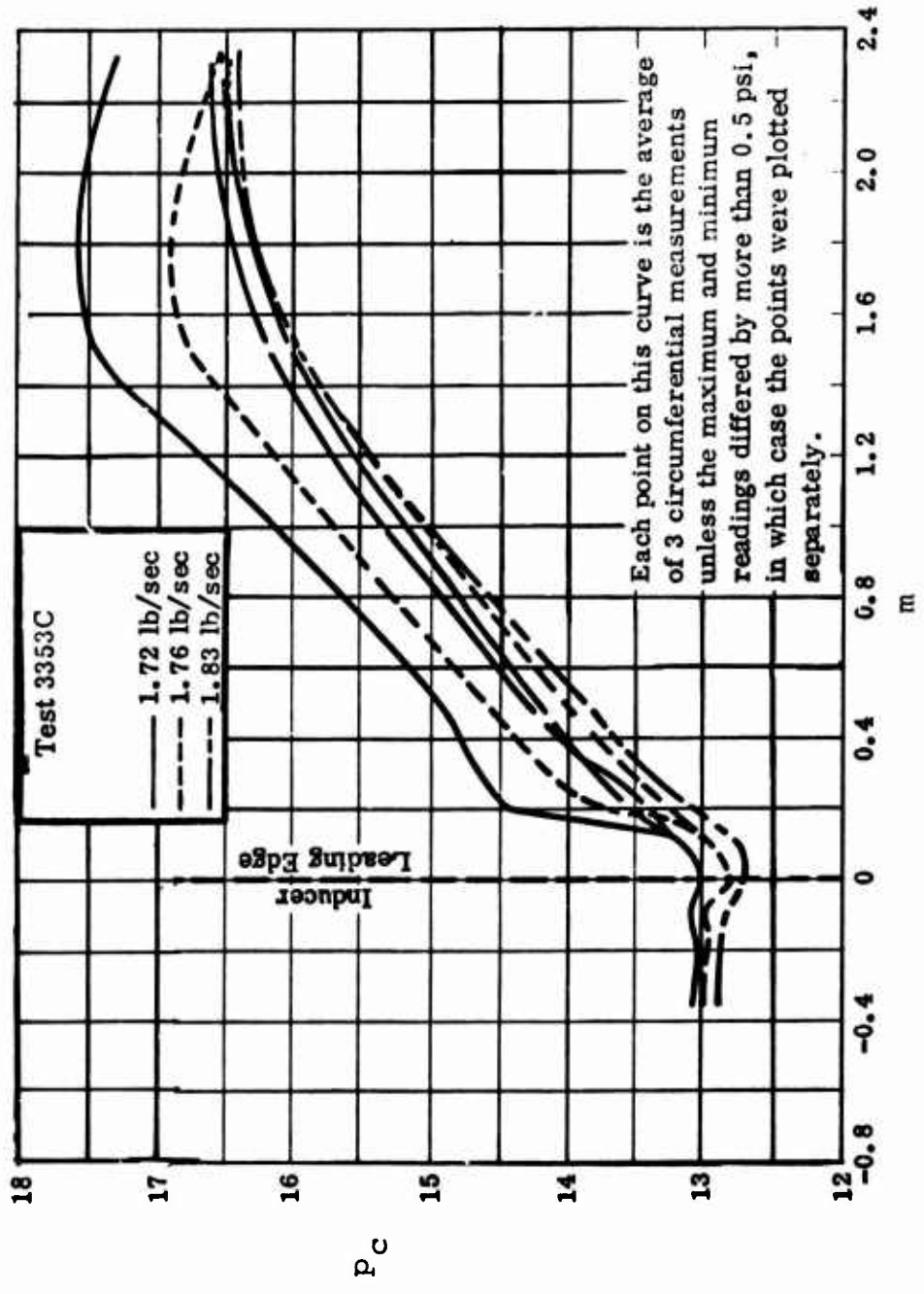


Figure 41. Cover Static Pressure.  
RF-2

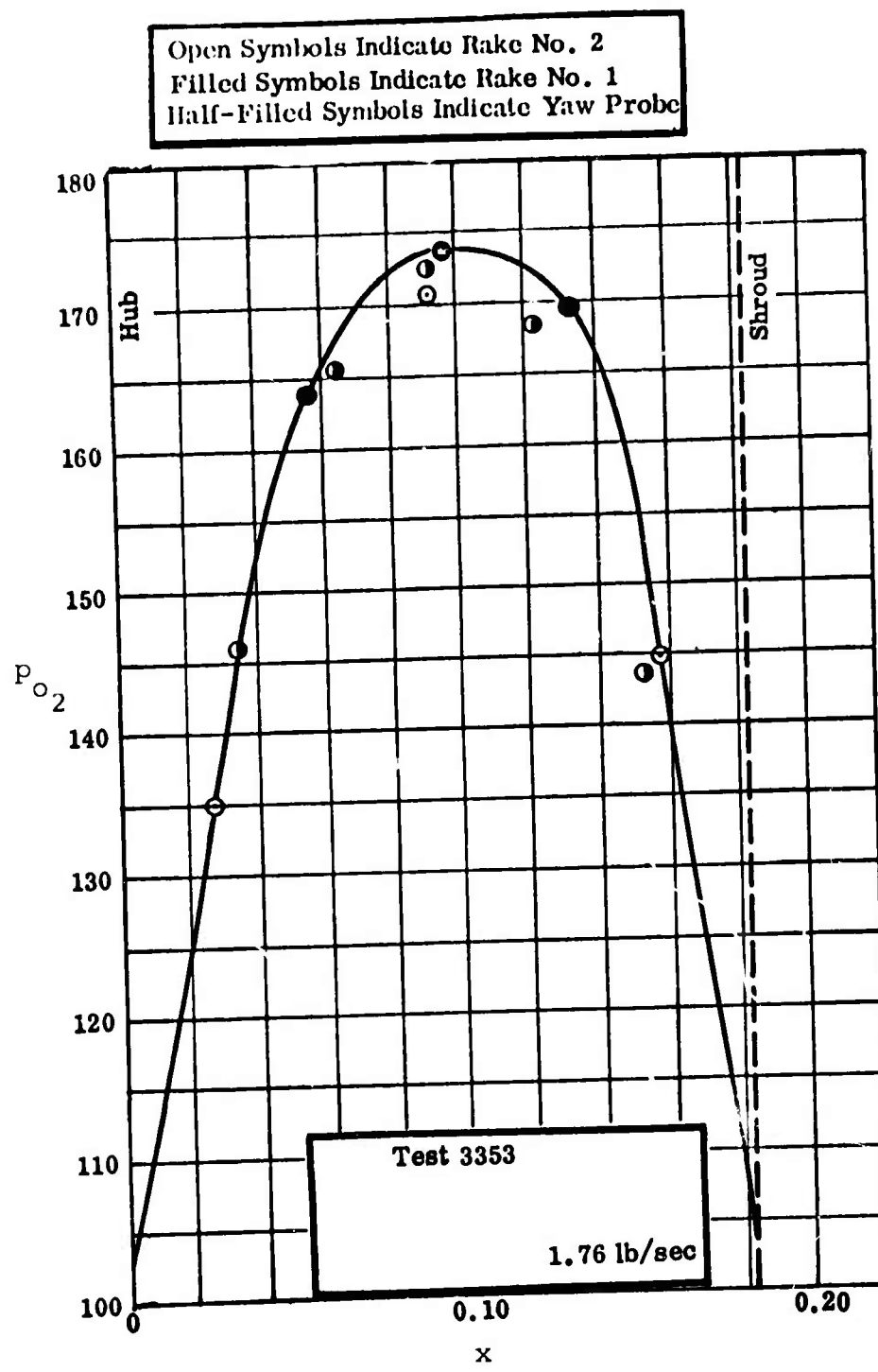


Figure 42. Impeller Tip Stagnation Pressure.  
RF-2

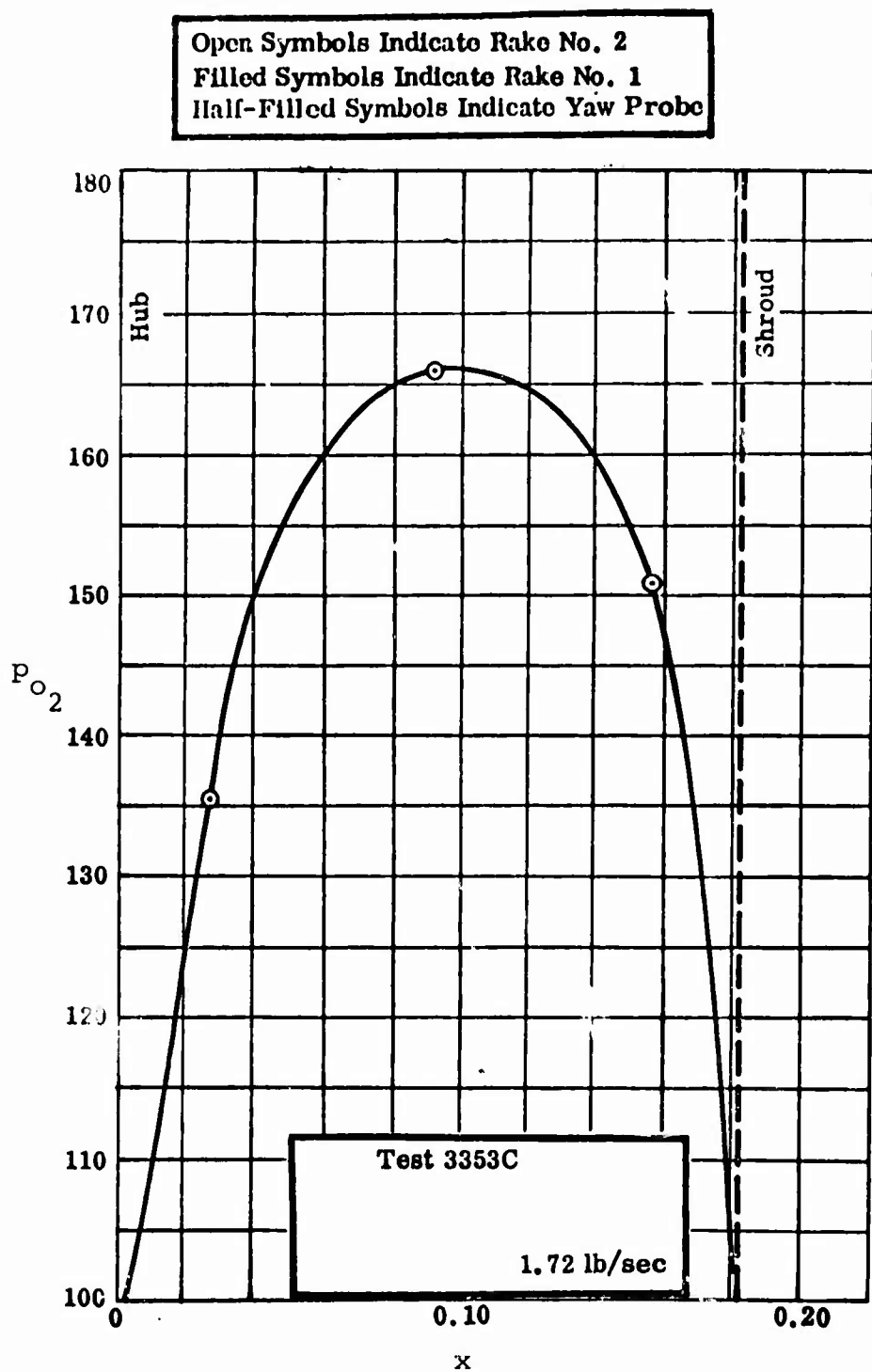


Figure 43. Impeller Tip Stagnation Pressure.  
RF-2

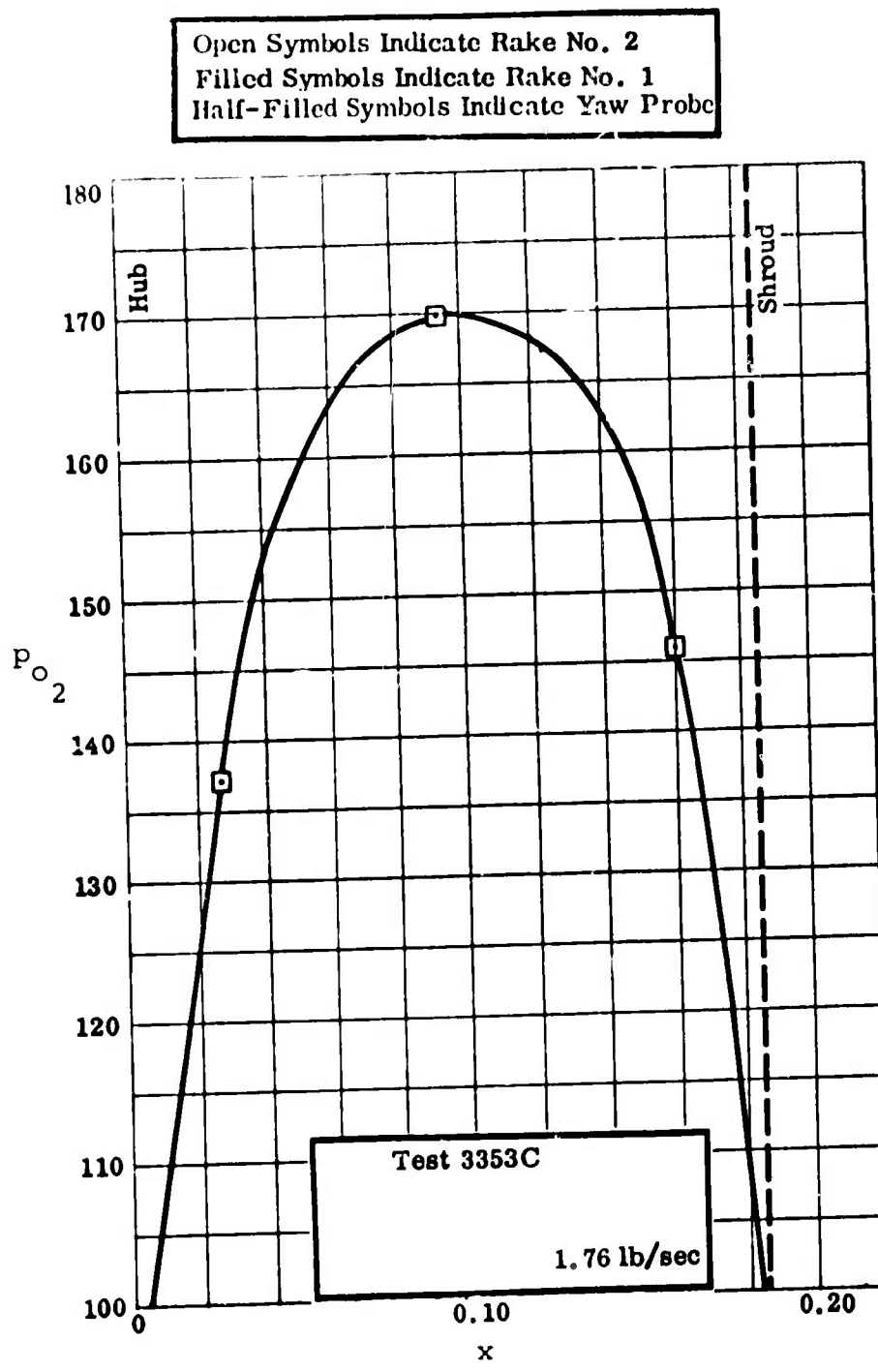


Figure 44. Impeller Tip Stagnation Pressure.  
RF-2

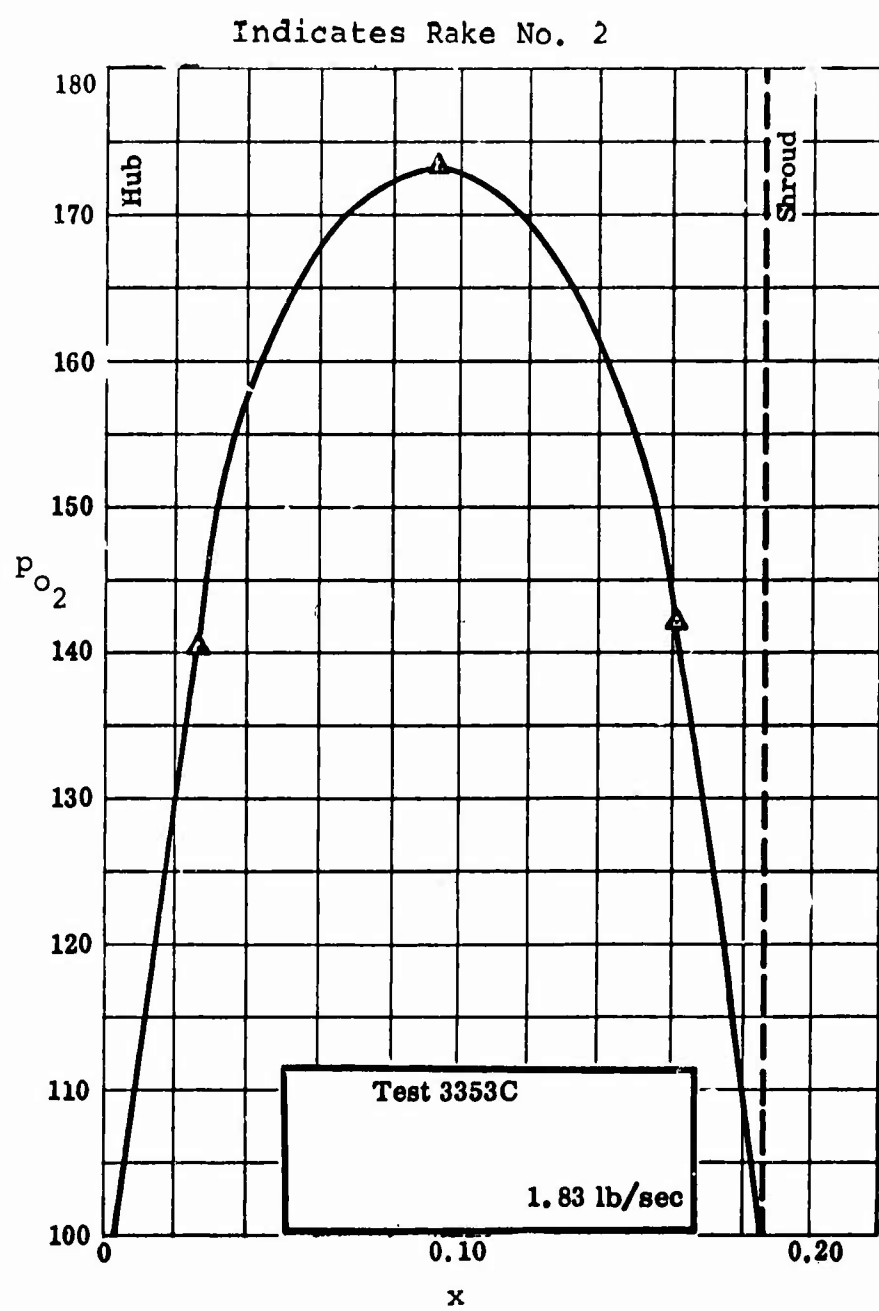


Figure 45. Impeller Tip Stagnation Pressure.  
RF-2

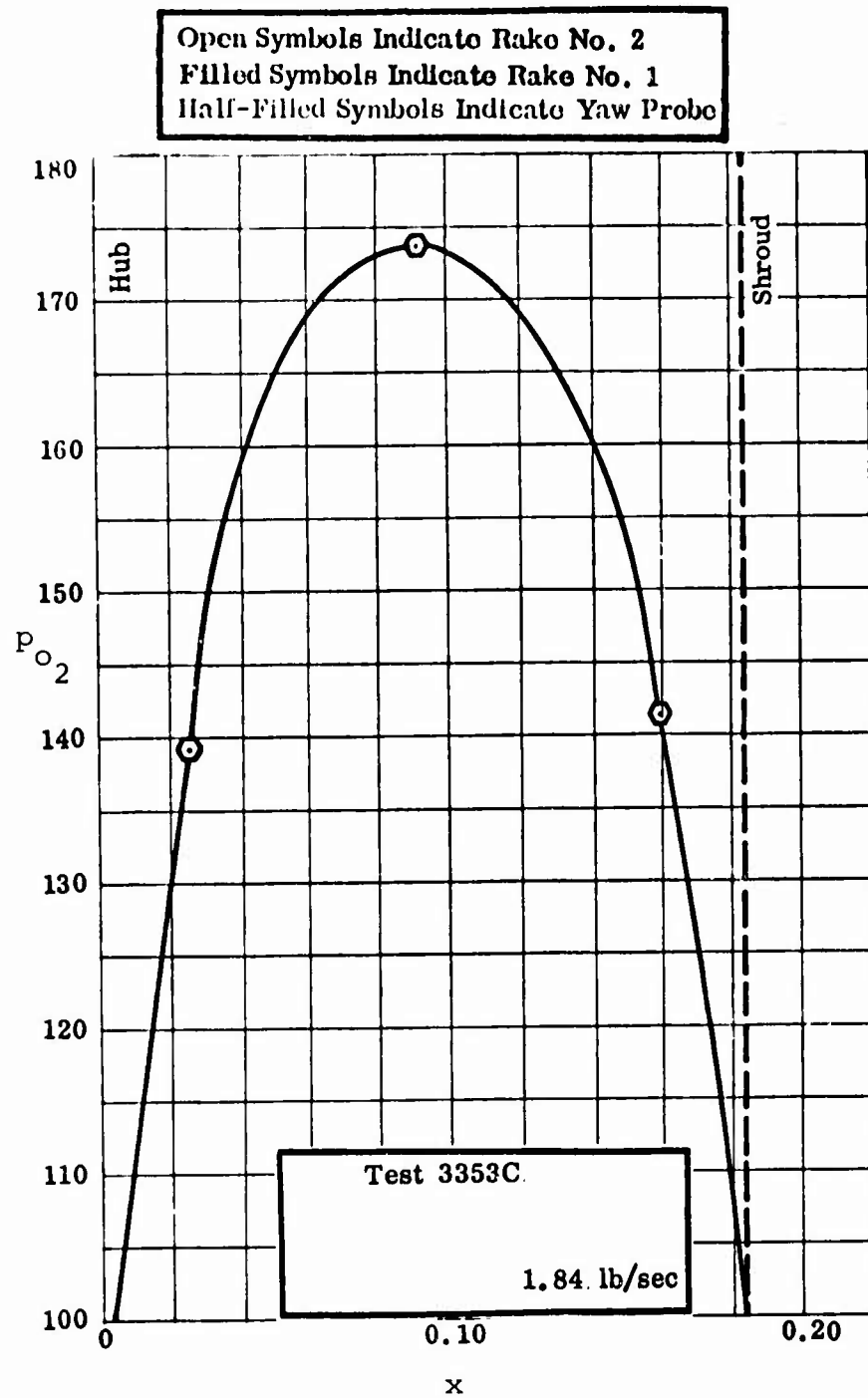


Figure 46. Impeller Tip Stagnation Pressure.  
RF-2

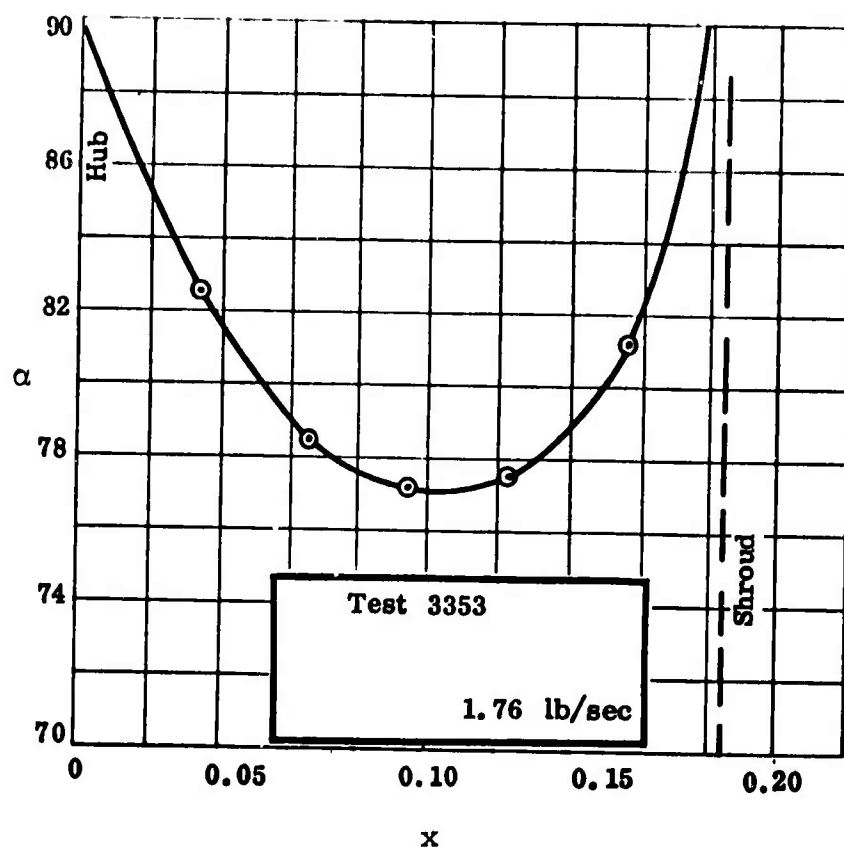
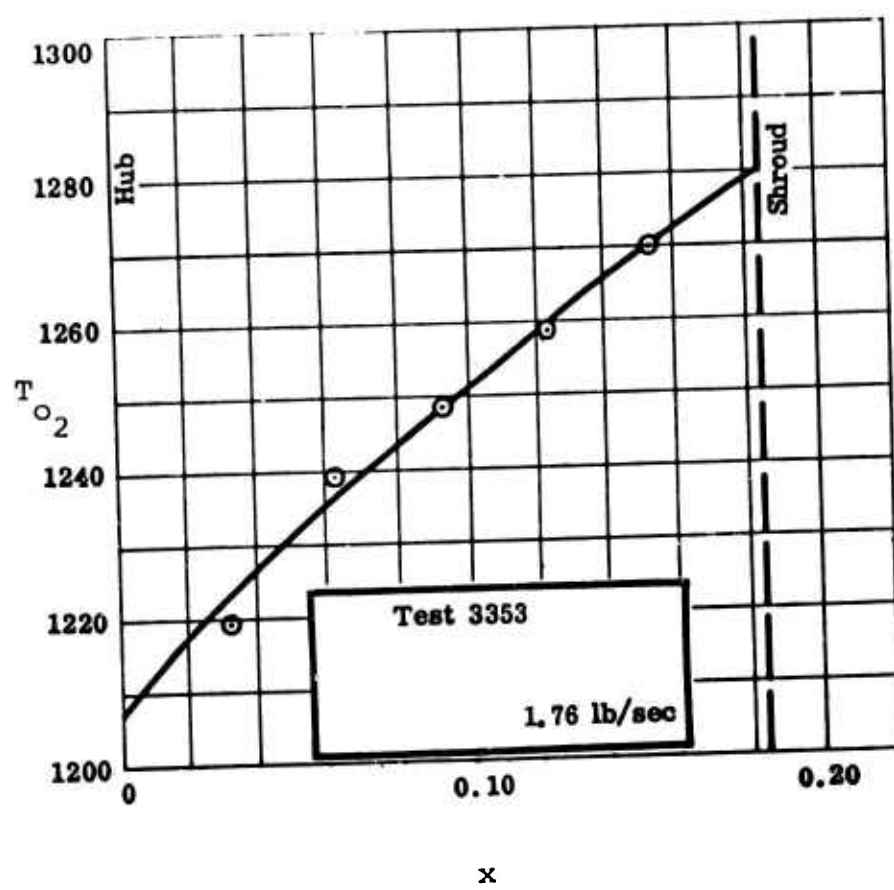
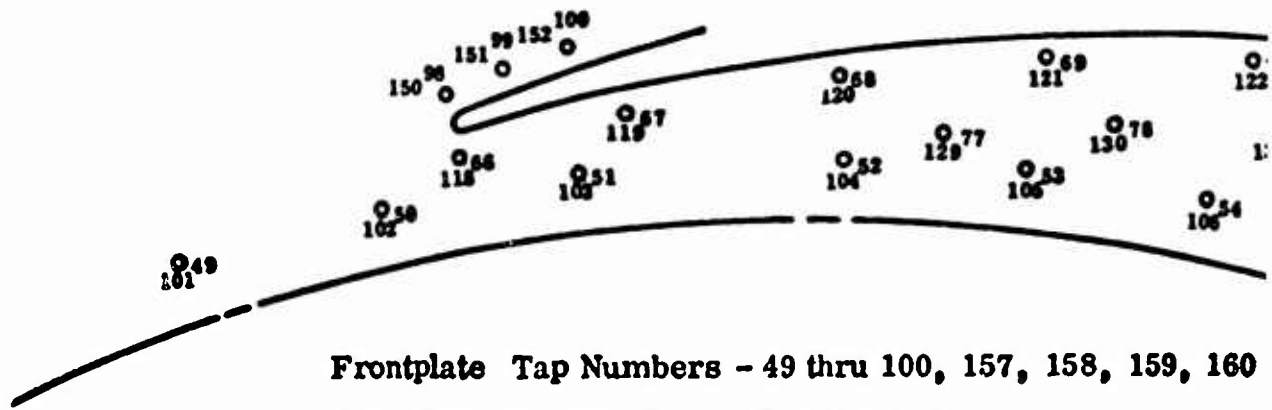


Figure 47. Impeller Tip Flow Angle.  
RF-2



NOTE: SCALE IS CORRECT

Figure 48. Impeller Tip Stagnation Temperature.  
RF-2

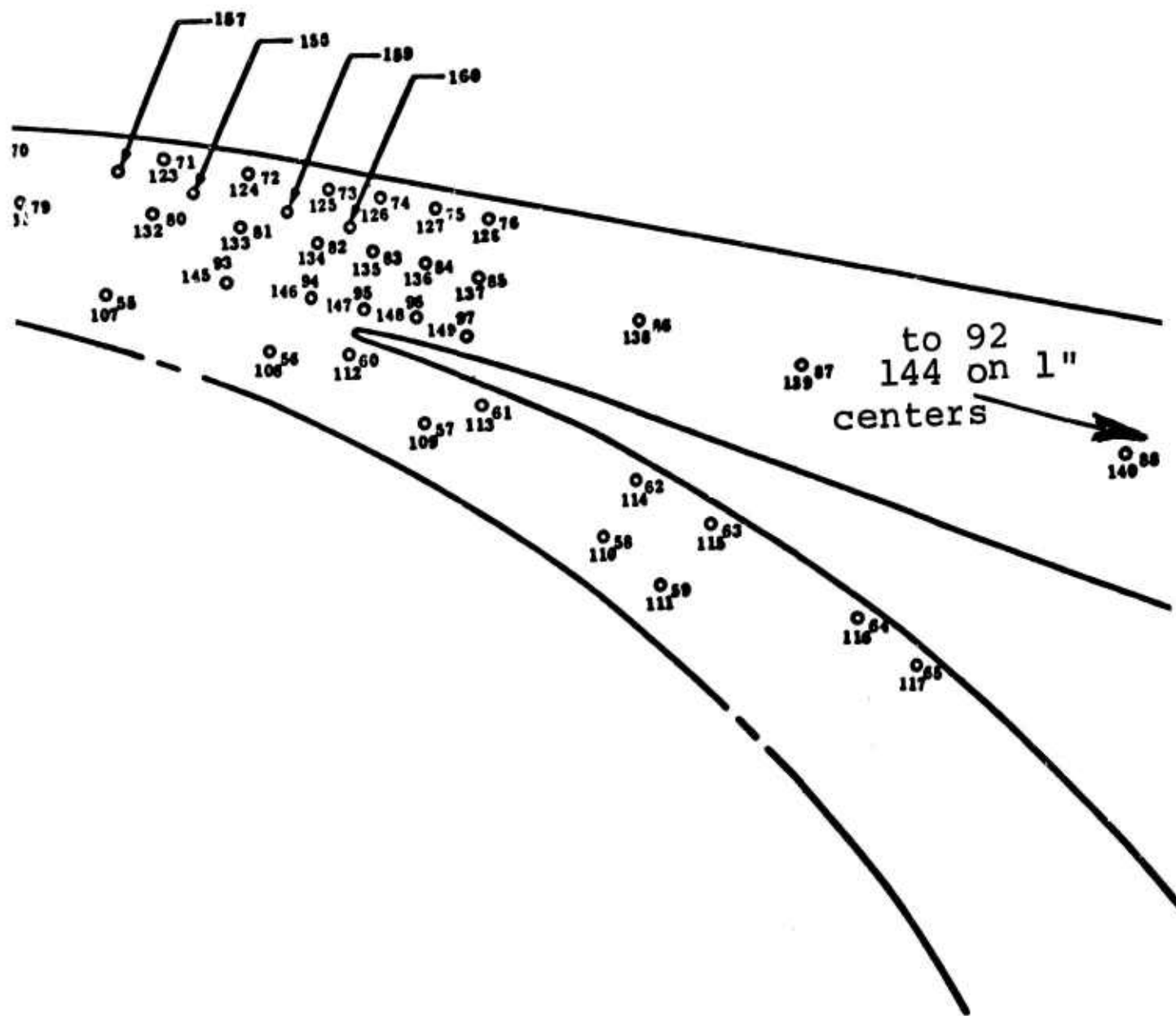


**Frontplate Tap Numbers - 49 thru 100, 151, 152, 157, 158, 159, 160**

**Rearplate Tap Numbers - 101 thru 152**

- |             |                          |
|-------------|--------------------------|
| <b>V1</b>   | (Thickness = 0.230 inch) |
| <b>V1-1</b> | (Thickness = 0.200 inch) |
| <b>V1-2</b> | (Thickness = 0.190 inch) |
| <b>V1-3</b> | (Thickness = 0.193 inch) |

**Figure 49. V1-3 Diffuser Static Pressure Taps.  
RF-2**



<u>Tap No.</u>	<u>Static Pressure</u>						
49	70.8	76	106.9	103	56.0	130	71.4
50	79.2	77	74.9	104	73.4	131	75.7
51	54.2	78	72.2	105	69.9	132	75.4
52	74.2	79	76.6	106	69.0	133	71.9
53	70.3	80	77.5	107	70.8	134	90.6
54	69.6	81	74.5	108	75.9	135	97.8
55	71.1	82	91.3	109	57.4	136	101.6
56	77.3	83	99.2	110	73.9	137	103.7
57	55.5	84	102.3	111	73.0	138	116.4
58	75.1	85	104.9	112	85.5	139	112.8
59	73.6	86	117.0	113	64.5	140	83.8
60	89.6	87	124.5	114	78.4	141	131.6
61	64.9	88	130.6	115	80.0	142	131.6
62	80.4	89	132.4	116	76.4	143	132.5
63	80.5	90	133.0	117	77.9	144	132.7
64	77.5	91	133.3	118	88.6	145	69.4
65	77.2	92	133.4	119	63.8	146	88.6
66	90.2	93	71.5	120	79.6	147	103.6
67	62.8	94	90.0	121	77.2	148	98.3
68	80.5	95	104.4	122	79.9	149	103.1
69	78.2	96	100.6	123	81.3	150	104.2
70	80.6	97	104.3	124	72.3	151	101.4
71	82.3	98	104.4	125	91.7	152	104.9
72	75.8	99	101.8	126	98.2	157	
73	92.5	100	105.9	127	102.8	158	
74	99.0	101	70.2	128	105.9	159	
75	103.5	102	78.1	129	73.8	160	

CONFIGURATION V1-3  
THROAT SIZE -  $A_T = 0.813 \text{ in}^2$   
 $\frac{A_T}{A_{ot}} = 0.813$   
 $b = 0.183$

TEST 3352C  
LINE 3  
1.69 lb/sec

Figure 50. Diffuser Static Pressures.  
RF-2

<u>Tap No.</u>	<u>Static Pressure</u>						
49	71.1	76	93.5	103	67.2	130	72.4
50	67.1	77	73.0	104	71.3	131	74.8
51	67.0	78	73.3	105	70.3	132	74.8
52	70.9	79	76.0	106	70.0	133	73.2
53	70.0	80	77.6	107	70.3	134	66.6
54	69.7	81	76.2	108	66.9	135	84.2
55	70.0	82	67.5	109	70.0	136	84.2
56	66.7	83	86.8	110	71.0	137	89.9
57	68.9	84	85.3	111	71.8	138	108.9
58	71.1	85	91.9	112	86.3	139	107.6
59	71.5	86	109.7	113	73.0	140	80.7
60	86.6	87	118.6	114	74.8	141	125.0
61	74.4	88	124.4	115	78.8	142	125.2
62	78.0	89	125.9	116	77.4	143	126.0
63	80.1	90	126.5	117	78.7	144	126.2
64	79.0	91	126.8	118	88.1	145	70.9
65	78.2	92	127.0	119	72.4	146	66.6
66	86.9	93	72.9	120	76.6	147	90.3
67	72.0	94	67.4	121	77.3	148	80.1
68	78.3	95	93.1	122	79.5	149	90.4
69	78.7	96	82.0	123	81.4	150	90.6
70	80.8	97	92.0	124	72.9	151	83.0
71	82.6	98	92.6	125	68.2	152	92.8
72	77.2	99	82.8	126	84.6	157	
73	69.0	100	94.1	127	86.8	158	
74	85.8	101	71.3	128	92.3	159	
75	87.5	102	67.5	129	72.3	160	

CONFIGURATION V1-3  
THROAT SIZE -  $A_T = 0.813 \text{ in}^2$   
 $\frac{ot}{b} = 0.183$

TEST 3352C  
LINE 5  
1.77 lb/sec

Figure 51. Diffuser Static Pressures.  
RF-2

<u>Tap No.</u>	<u>Static Pressure</u>						
49	70.4	76	92.5	103	67.1	130	71.6
50	66.3	77	72.3	104	70.6	131	74.0
51	66.2	78	72.6	105	69.6	132	74.0
52	70.1	79	75.2	106	69.3	133	72.5
53	69.3	80	76.8	107	69.5	134	65.8
54	69.0	81	75.4	108	66.1	135	83.2
55	69.2	82	66.8	109	69.1	136	83.3
56	65.9	83	85.8	110	70.2	137	88.9
57	68.1	84	84.5	111	71.0	138	107.8
58	70.3	85	90.9	112	85.4	139	106.5
59	70.8	86	108.6	113	72.2	140	79.9
60	85.7	87	117.3	114	74.0	141	123.9
61	73.6	88	123.0	115	78.0	142	123.9
62	77.2	89	124.5	116	76.6	143	123.8
63	79.3	90	125.1	117	77.8	144	125.0
64	78.1	91	125.4	118	87.2	145	70.1
65	77.4	92	125.6	119	71.6	146	65.8
66	86.0	93	72.2	120	75.8	147	89.4
67	71.3	94	66.6	121	76.5	148	79.2
68	77.5	95	92.1	122	78.6	149	89.5
69	77.9	96	81.2	123	80.5	150	89.6
70	80.0	97	91.0	124	72.2	151	82.2
71	81.8	98	91.6	125	67.5	152	91.8
72	76.4	99	81.9	126	83.6	157	
73	68.2	100	93.1	127	85.9	158	
74	84.9	101	70.6	128	91.3	159	
75	86.5	102	66.8	129	71.6	160	

CONFIGURATION V1-3  
 THROAT SIZE -  $A_T^{ot} = 0.813 \text{ in}^2$   
 $b = 0.183$

TEST 3352C  
 LINE 7  
 $1.85 \text{ lb/sec}$

Figure 52. Diffuser Static Pressures.  
 RF-2

<u>Tap No.</u>	<u>Static Pressure</u>						
49	70.0	76	107.5	103	55.4	130	72.5
50	80.7	77	75.0	104	73.3	131	76.8
51	52.9	78	72.5	105	70.0	132	75.2
52	74.5	79	77.0	106	70.1	133	73.9
53	70.8	80	76.2	107	69.6	134	92.3
54	70.8	81	74.3	108	77.7	135	98.5
55	69.9	82	92.1	109	56.5	136	103.5
56	79.8	83	99.8	110	74.3	137	105.0
57	54.0	84	103.4	111	72.9	138	117.5
58	75.6	85	105.7	112	84.3	139	124.7
59	73.5	86	117.4	113	64.3	140	130.5
60	89.7	87	124.5	114	79.2	141	132.2
61	63.8	88	130.4	115	80.8	142	133.0
62	80.9	89	128.5	116	77.1	143	133.2
63	80.4	90	132.5	117	79.6	144	133.4
64	77.5	91	133.1	118	88.9	145	71.0
65	79.1	92	133.3	119	63.9	146	89.8
66	90.1	93	71.5	120	80.4	147	105.0
67	61.9	94	90.7	121	78.4	148	101.7
68	80.5	95	104.8	122	81.3	149	104.6
69	78.6	96	101.8	123	80.9	150	105.6
70	81.5	97	105.2	124	73.6	151	103.0
71	81.1	98	104.7	125	93.5	152	106.4
72	75.8	99	102.7	126	99.6	157	---
73	93.5	100	106.5	127	104.6	158	---
74	99.7	101	69.5	128	107.2	159	---
75	104.5	102	79.1	129	74.6	160	90.3

CONFIGURATION V1-3  
 THROAT SIZE -  $A_T^{ot} = 0.813 \text{ in}^2$   
 $b = 0.183$

TEST 3353D  
 LINE 3  
 $1.66 \text{ lb/sec}$

Figure 53. Diffuser Static Pressures.  
 RF-2

<u>Tap No.</u>	<u>Static Pressure</u>						
49	72.5	76	103.7	103	59.6	130	72.9
50	69.7	77	76.8	104	71.3	131	75.8
51	59.0	78	73.1	105	70.9	132	77.1
52	71.5	79	76.2	106	69.3	133	74.8
53	71.1	80	78.2	107	71.2	134	86.9
54	69.5	81	75.3	108	67.9	135	94.4
55	71.5	82	87.0	109	61.4	136	98.0
56	68.1	83	95.5	110	72.4	137	100.6
57	60.5	84	98.0	111	74.0	138	115.0
58	72.9	85	101.2	112	86.7	139	122.9
59	74.3	86	114.9	113	67.7	140	129.1
60	89.2	87	122.9	114	77.3	141	130.6
61	68.3	88	129.0	115	81.8	142	131.4
62	79.2	89	127.0	116	77.6	143	131.5
63	81.7	90	131.3	117	78.4	144	131.8
64	78.0	91	131.5	118	89.4	145	71.9
65	78.0	92	131.6	119	67.0	146	85.2
66	89.7	93	72.2	120	77.9	147	100.3
67	65.9	94	85.9	121	78.9	148	95.8
68	79.2	95	101.2	122	80.2	149	100.2
69	79.2	96	95.8	123	82.8	150	101.0
70	80.4	97	100.8	124	73.5	151	97.7
71	83.0	98	131.6	125	87.3	152	102.2
72	76.3	99	97.3	126	95.2	157	---
73	87.4	100	102.4	127	99.6	158	---
74	95.3	101	72.1	128	103.4	159	---
75	99.4	102	70.4	129	76.3	160	90.2

CONFIGURATION V1-3  
THROAT SIZE -  $A_T = 0.813 \text{ in}^2$   
 $b_{ot} = 0.183$

TEST 3353D  
Line 5  
1.75 lb/sec

Figure 54. Diffuser Static Pressures.  
RF-2

<u>Tap No.</u>	<u>Static Pressure</u>						
49	71.3	76	79.6	103	66.2	130	73.1
50	66.5	77	75.1	104	69.6	131	74.9
51	66.5	78	73.3	105	71.5	132	75.9
52	69.3	79	75.3	106	69.5	133	74.9
53	71.4	80	77.3	107	69.8	134	66.0
54	69.4	81	75.6	108	66.1	135	81.4
55	69.6	82	66.4	109	69.2	136	78.8
56	66.0	83	83.6	110	70.7	137	86.6
57	68.4	84	71.8	111	71.1	138	107.2
58	70.7	85	87.9	112	84.4	139	116.1
59	70.9	86	107.1	113	73.0	140	121.9
60	85.5	87	116.2	114	75.1	141	123.4
61	73.5	88	122.0	115	78.9	142	124.1
62	77.7	89	120.0	116	78.2	143	124.4
63	79.4	90	124.0	117	78.9	144	124.6
64	78.9	91	124.3	118	86.9	145	72.0
65	78.5	92	124.5	119	71.5	146	65.4
66	85.9	93	72.3	120	75.3	147	88.7
67	70.4	94	65.6	121	79.6	148	76.8
68	76.3	95	90.5	122	79.8	149	87.4
69	80.2	96	77.4	123	81.8	150	89.3
70	80.4	97	88.4	124	73.6	151	77.2
71	82.2	98	90.3	125	67.9	152	89.6
72	76.5	99	76.5	126	81.0	157	---
73	68.1	100	90.1	127	82.3	158	---
74	71.8	101	61.3	128	89.1	159	---
75	82.2	102	66.8	129	75.0	160	90.6

CONFIGURATION V1-3  
THROAT SIZE -  $A_T = 0.813 \text{ in}^2$   
 $\frac{A_T}{A_{ot}} = 0.183$

TEST 3353D  
LINE 7  
1.83 lb/sec

Figure 55. Diffuser Static Pressures.  
RF-2

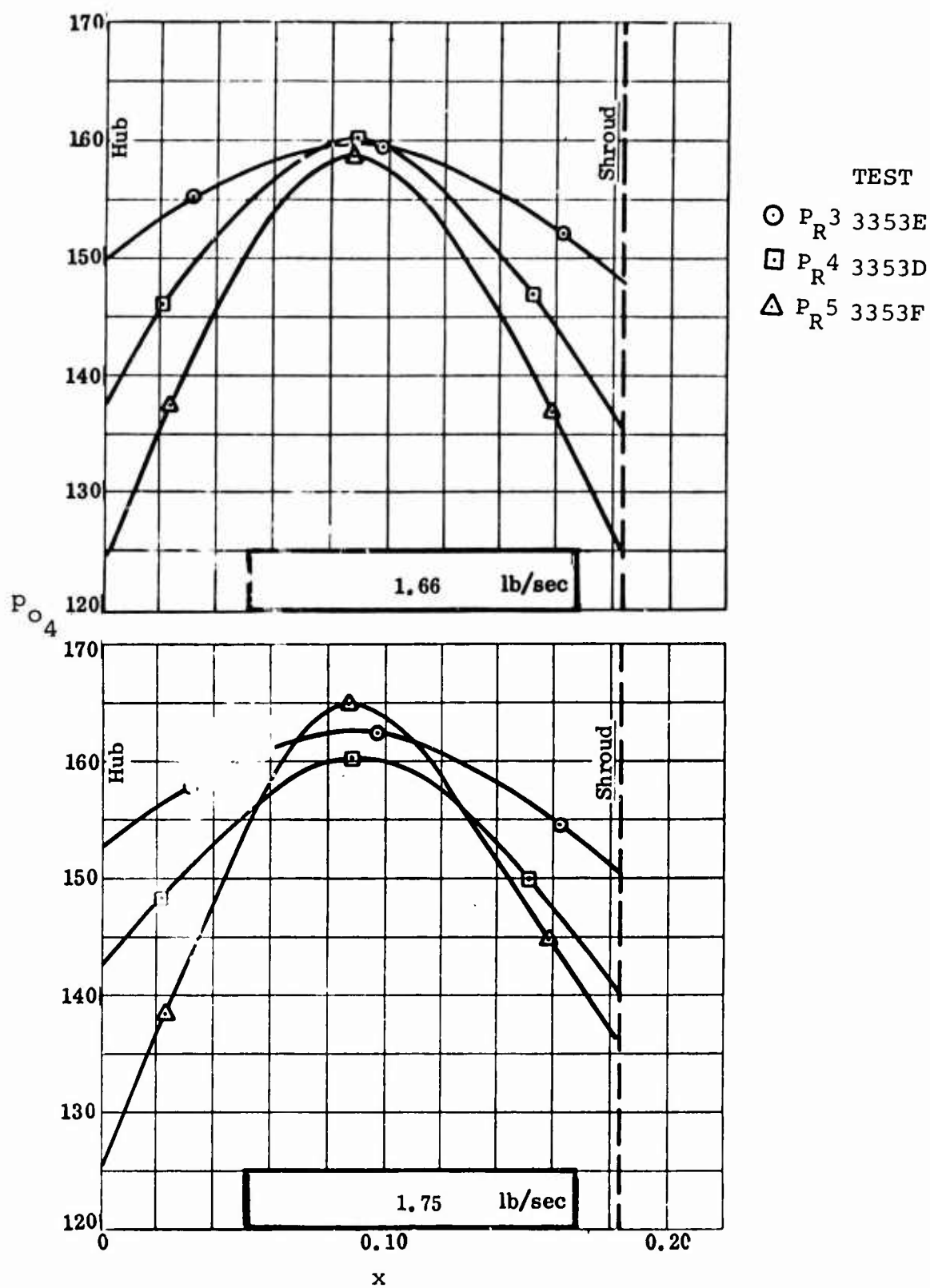


Figure 56. Diffuser Throat Stagnation Pressure.  
RF-2

TEST

○  $P_R^3$  3353E

□  $P_R^4$  3353D

△  $P_R^5$  3353F

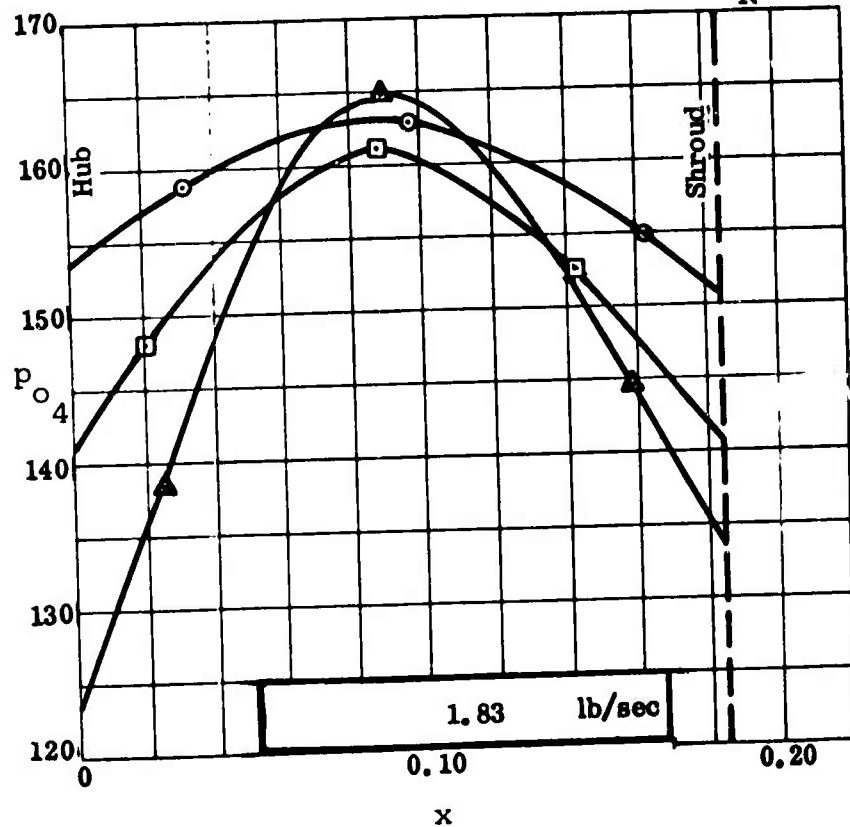


Figure 57. Diffuser Throat Stagnation Pressure.  
RF-2

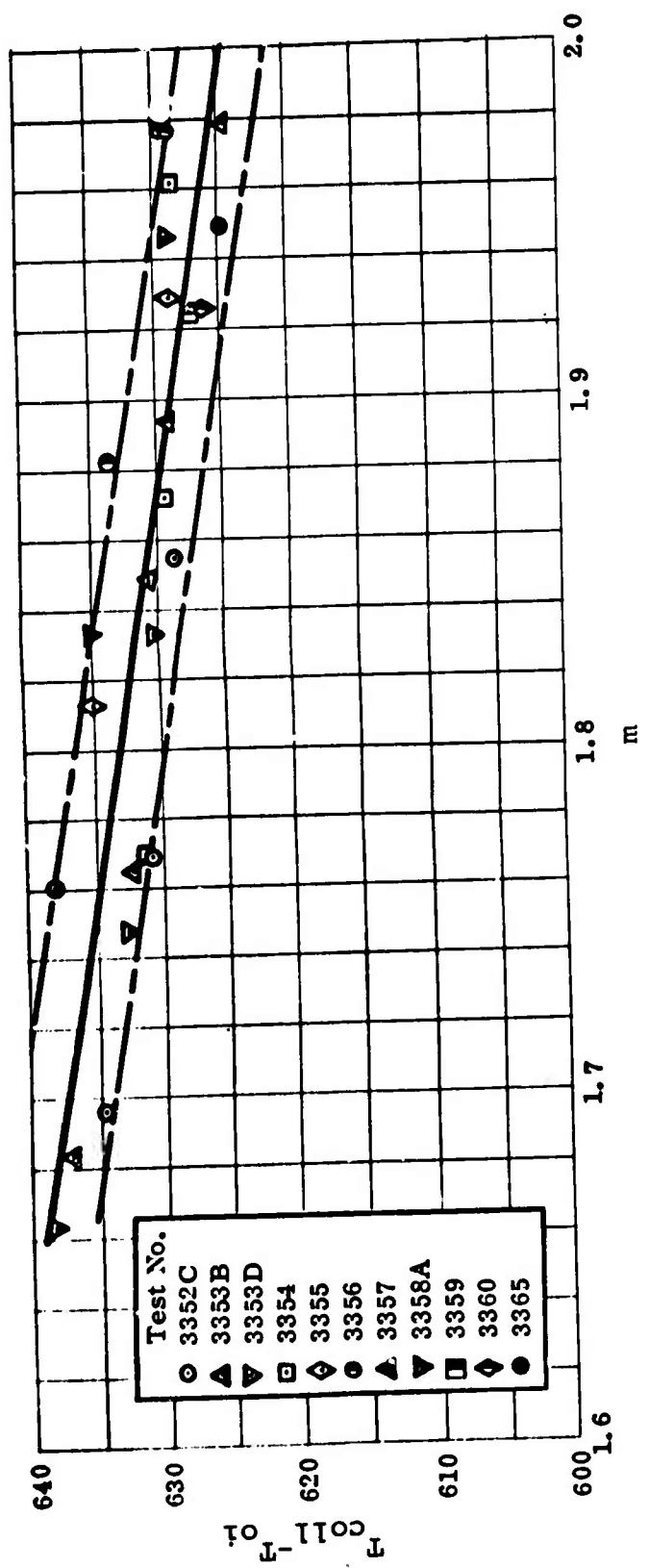


Figure 58. Collector Temperature Rise Versus Mass Flow.  
RF-2

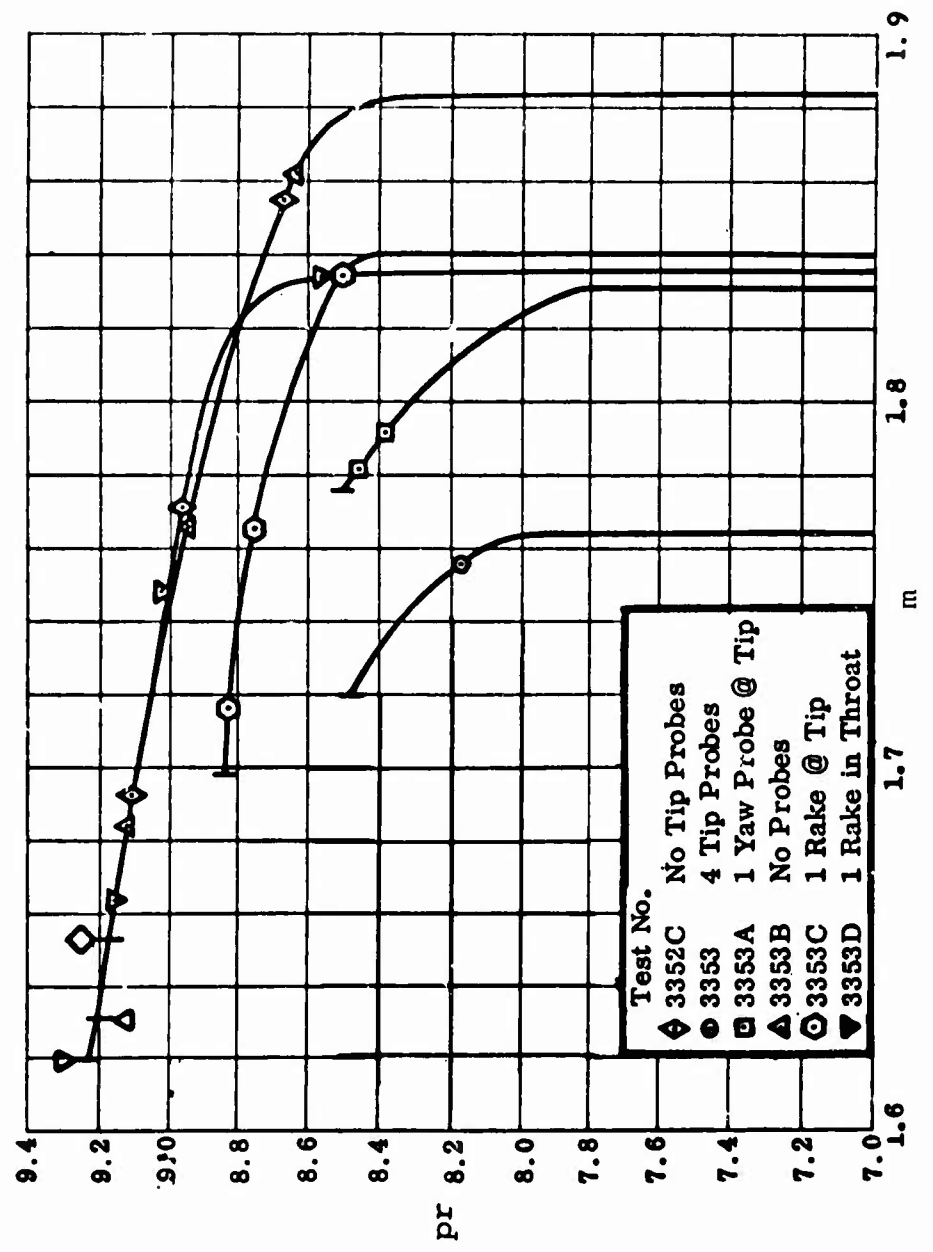


Figure 59. Collector Static Pressure Ratio Versus  
Mass Flow.  
RF-2

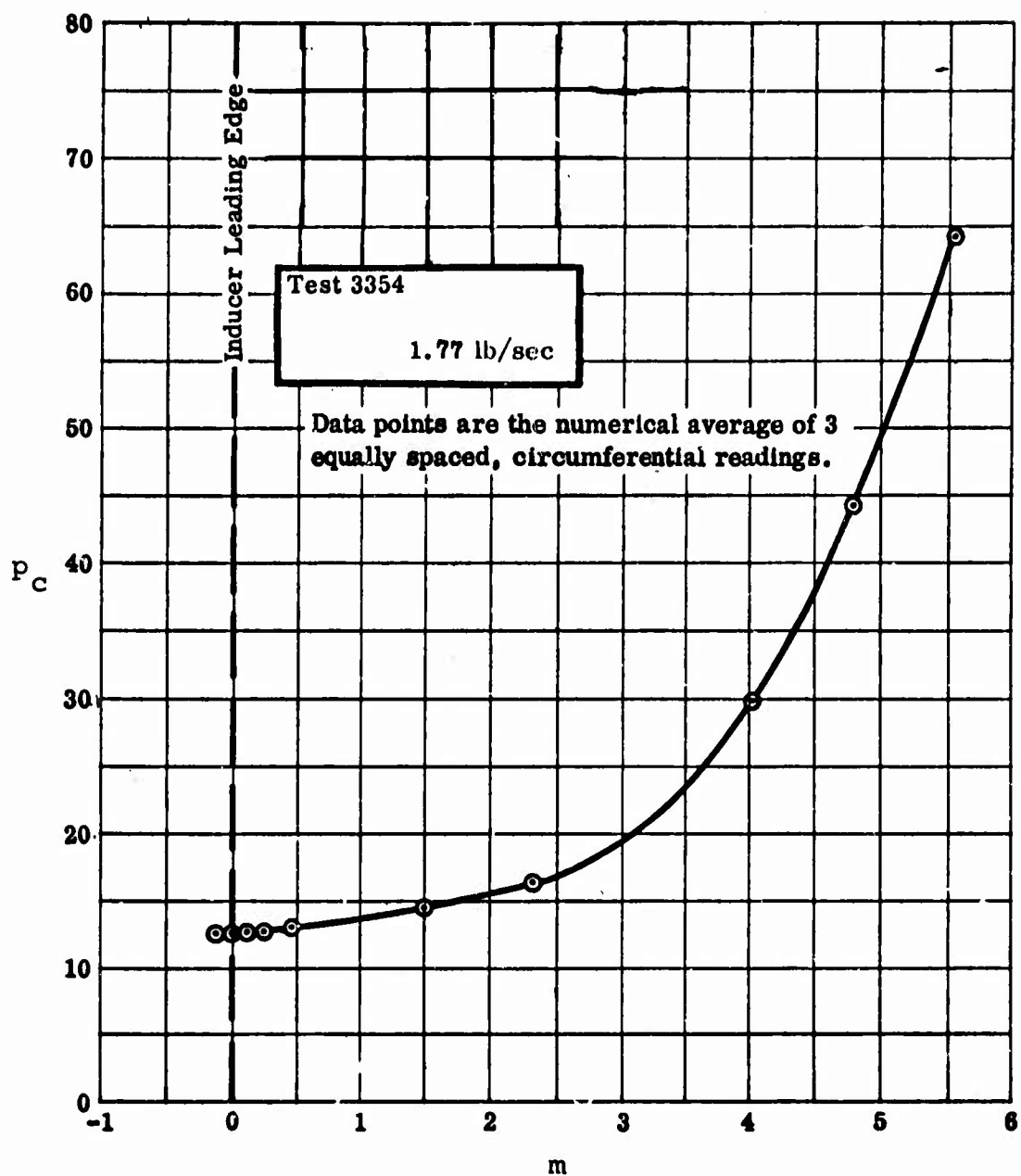


Figure 60. Cover Static Pressure.  
RF-2

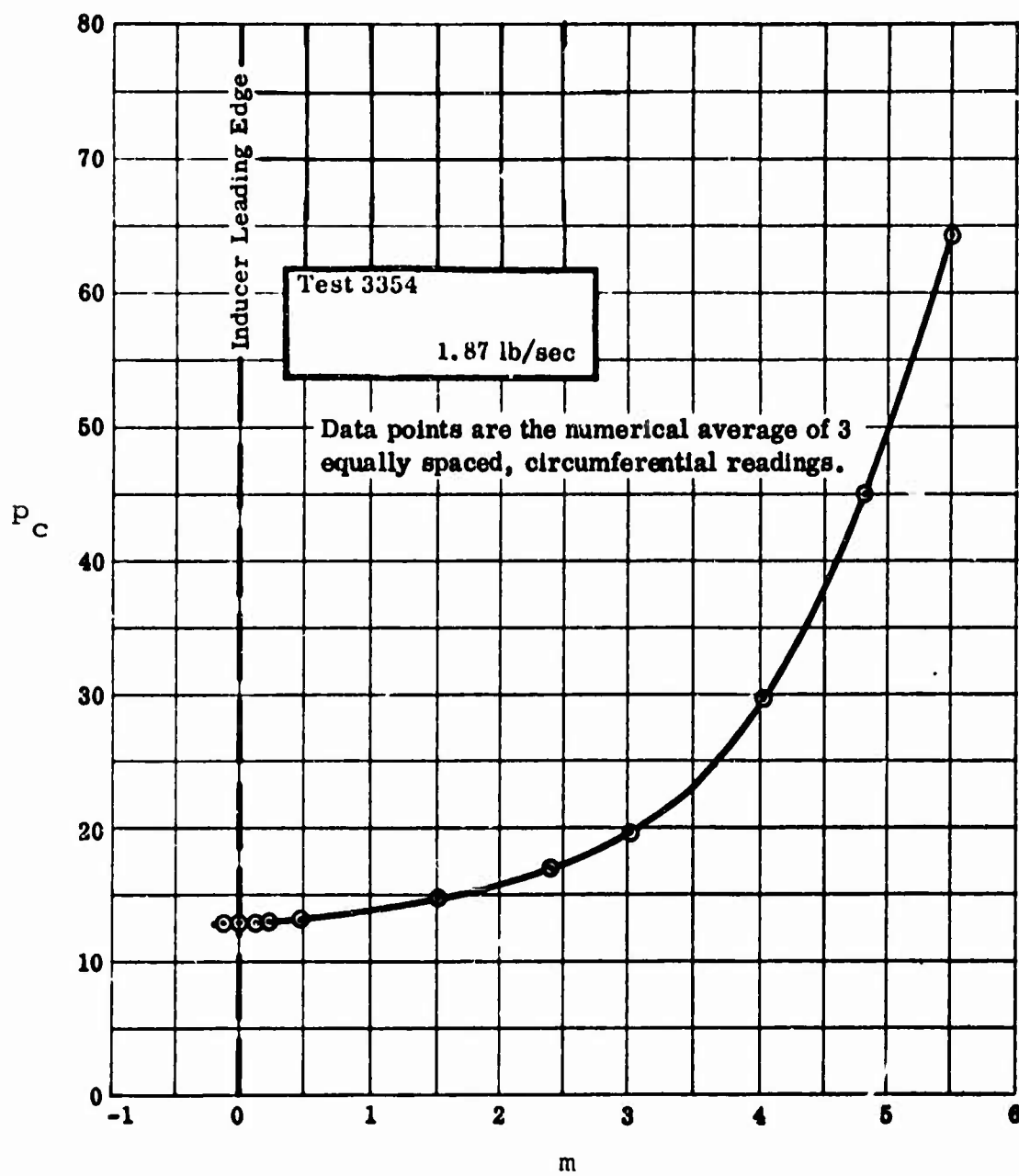


Figure 61. Cover Static Pressure.  
RF-2

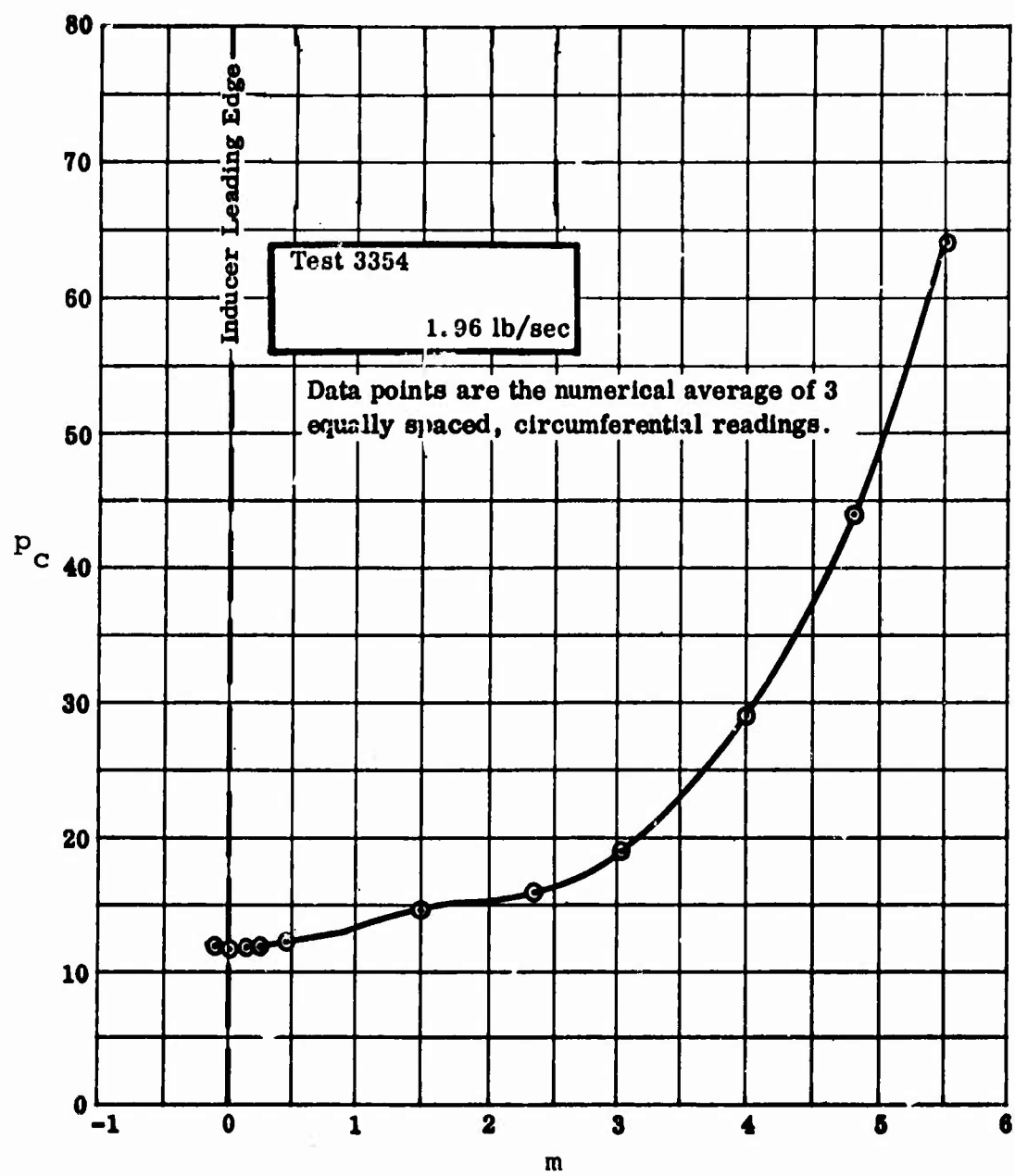
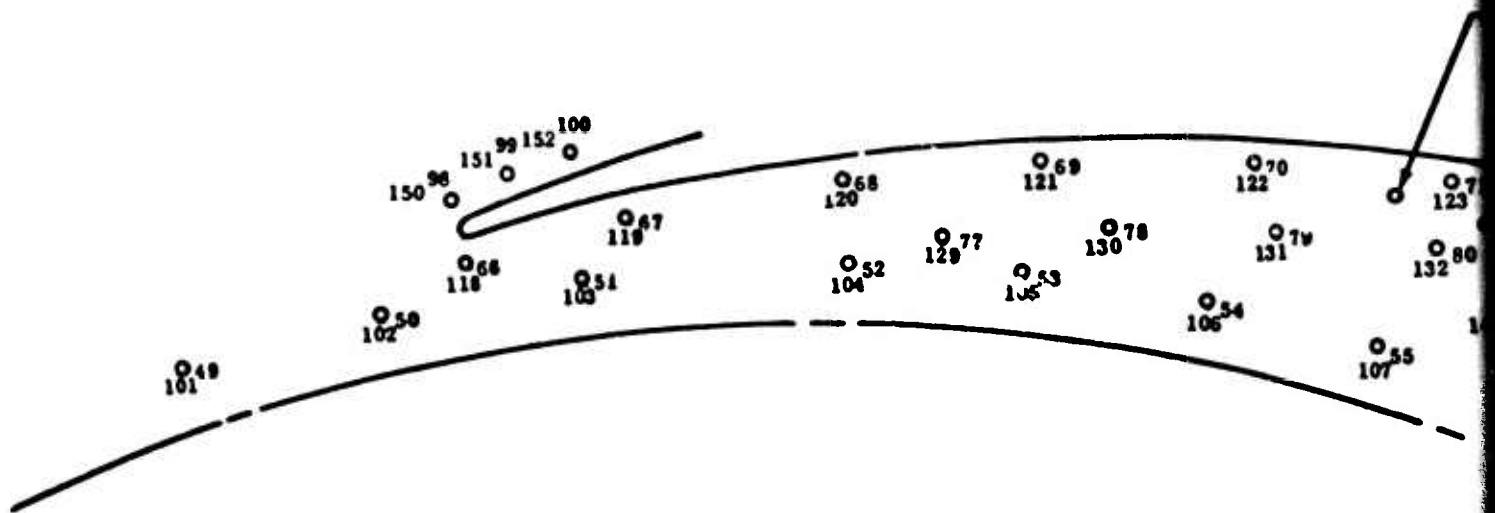


Figure 62. Cover Static Pressure.  
RF-2

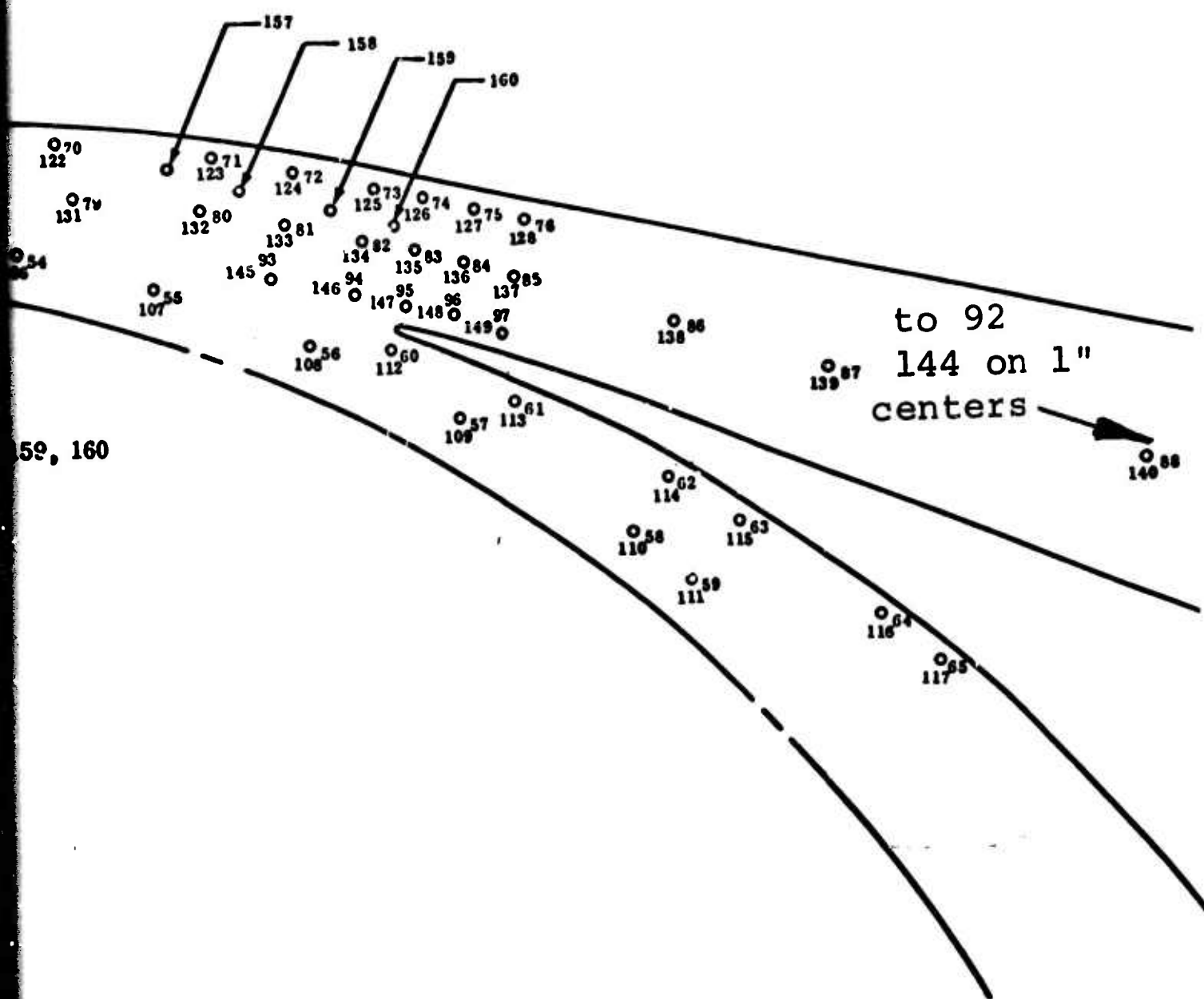


Frontplate Tap Numbers - 49 thru 100, 157, 158, 159, 160

Rearplate Tap Numbers - 101 thru 152

V1-4

Figure 63. V1-4 Diffuser Static Pressure Taps.  
RF-2



1

<u>Tap No.</u>	<u>Static Pressure</u>						
49	68.2	76	106.6	103	54.4	130	70.2
50	81.9	77	72.8	104	71.7	131	75.3
51	52.7	78	70.4	105	68.4	132	74.3
52	72.4	79	75.5	106	67.4	133	78.4
53	68.0	80	74.6	107	68.3	134	92.4
54	67.9	81	79.1	108	79.4	135	99.7
55	68.3	82	92.6	109	54.0	136	102.8
56	80.9	83	99.6	110	73.1	137	104.7
57	49.4	84	102.8	111	71.6	138	116.
58	74.0	85	104.9	112	86.2	139	123.1
59	72.2	86	116.0	113	62.8	140	129.4
60	88.9	87	123.1	114	78.7	141	131.4
61	62.4	88	129.4	115	78.7	142	132.0
62	79.7	89	131.4	116	74.7	143	132.5
63	68.6	90	132.2	117	76.7	144	132.7
64	75.0	91	132.5	118	88.8	145	74.6
65	76.3	92	132.6	119	63.0	146	90.5
66	89.6	93	75.2	120	78.6	147	104.3
67	61.2	94	91.0	121	75.7	148	101.4
68	78.9	95	105.0	122	79.0	149	104.0
69	75.8	96	101.5	123	79.1	150	105.5
70	78.9	97	104.5	124	81.7	151	103.3
71	79.3	98	105.6	125	94.1	152	106.1
72	83.4	99	103.0	126	98.4	157	---
73	93.9	100	106.5	127	103.6	158	---
74	99.3	101	68.4	128	106.5	159	---
75	103.1	102	80.9	129	72.9	160	90.0

CONFIGURATION V1-4  
THROAT SIZE -  $A_T = 0.869 \text{ in}^2$   
 $b_{ot} = 0.183$

TEST 3354  
LINE 3  
1.77 lb/sec

Figure 64. Diffuser Static Pressure.  
RF-2

<u>Tap No.</u>	<u>Static Pressure</u>						
49	69.2	76	102.0	103	58.4	130	70.1
50	75.6	77	72.7	104	69.7	131	72.5
51	57.8	78	70.3	105	68.6	132	75.5
52	69.7	79	72.7	106	66.5	133	75.2
53	67.7	80	76.0	107	69.6	134	88.2
54	66.4	81	75.8	108	73.8	135	95.3
55	69.4	82	88.6	109	57.6	136	97.6
56	74.6	83	95.5	110	71.3	137	100.3
57	50.2	84	97.8	111	71.8	138	113.2
58	71.5	85	100.6	112	87.4	139	121.1
59	71.7	86	113.2	113	64.9	140	127.6
60	87.4	87	121.2	114	76.4	141	129.5
61	65.9	88	127.7	115	78.6	142	130.1
62	77.7	89	129.6	116	74.5	143	130.7
63	78.8	90	130.3	117	75.3	144	130.8
64	75.1	91	130.6	118	89.7	145	71.6
65	75.1	92	130.7	119	65.9	146	86.7
66	88.2	93	71.8	120	76.1	147	99.7
67	65.0	94	87.1	121	75.2	148	95.3
68	76.8	95	101.3	122	76.2	149	99.8
69	75.7	96	95.3	123	80.2	150	100.2
70	76.2	97	100.3	124	77.8	151	97.3
71	80.5	98	101.3	125	39.4	152	101.6
72	80.0	99	96.7	126	93.8	157	---
73	89.4	100	102.1	127	98.9	158	---
74	95.0	101	69.6	128	102.0	159	---
75	98.3	102	75.9	129	73.0	160	90.0

CONFIGURATION V1-4  
 THROAT SIZE -  $A_T = 0.869 \text{ in}^2$   
 $\frac{\text{ot}}{b} = 0.183$

TEST 3354  
 LINE 5  
 $1.87 \text{ lb/sec}$

Figure 65. Diffuser Static Pressure.  
 RF-2

<b>Tap No.</b>	<b>Static Pressure</b>						
49	68.1	76	93.0	103	65.8	130	70.9
50	66.7	77	70.6	104	76.7	131	72.4
51	65.1	78	70.8	105	68.7	132	74.4
52	67.3	79	72.4	106	67.3	133	74.9
53	67.5	80	74.7	107	67.9	134	75.2
54	66.7	81	75.6	108	67.0	135	87.1
55	67.4	82	75.2	109	64.6	136	86.7
56	67.0	83	87.7	110	68.8	137	91.0
57	56.8	84	87.1	111	70.1	138	108.1
58	68.8	85	91.6	112	88.9	139	117.0
59	69.9	86	108.3	113	70.5	140	123.5
60	85.4	87	117.2	114	74.1	141	125.2
61	71.0	88	123.6	115	76.8	142	125.6
62	75.7	89	125.3	116	75.0	143	126.4
63	77.5	90	126.0	117	75.8	144	126.5
64	75.8	91	126.4	118	90.3	145	71.4
65	75.9	92	126.5	119	71.8	146	74.6
66	86.0	93	71.5	120	73.2	147	92.1
67	70.5	94	75.4	121	75.5	148	83.0
68	74.3	95	93.9	122	76.8	149	90.5
69	76.3	96	83.1	123	79.0	150	91.9
70	76.9	97	91.0	124	77.2	151	83.3
71	79.4	98	93.0	125	74.0	152	92.5
72	79.7	99	82.4	126	85.3	157	---
73	74.4	100	93.0	127	88.8	158	---
74	87.0	101	68.9	128	93.1	159	---
75	88.1	102	67.1	129	71.3	160	90.1

CONFIGURATION V1-4  
 THROAT SIZE -  $A_T^{ot} = 0.869 \text{ in}^2$   
 $b = 0.183$ 
TEST 3354  
LINE 7  
1.96 lb/sec

Figure 66. Diffuser Static Pressure.  
RF-2

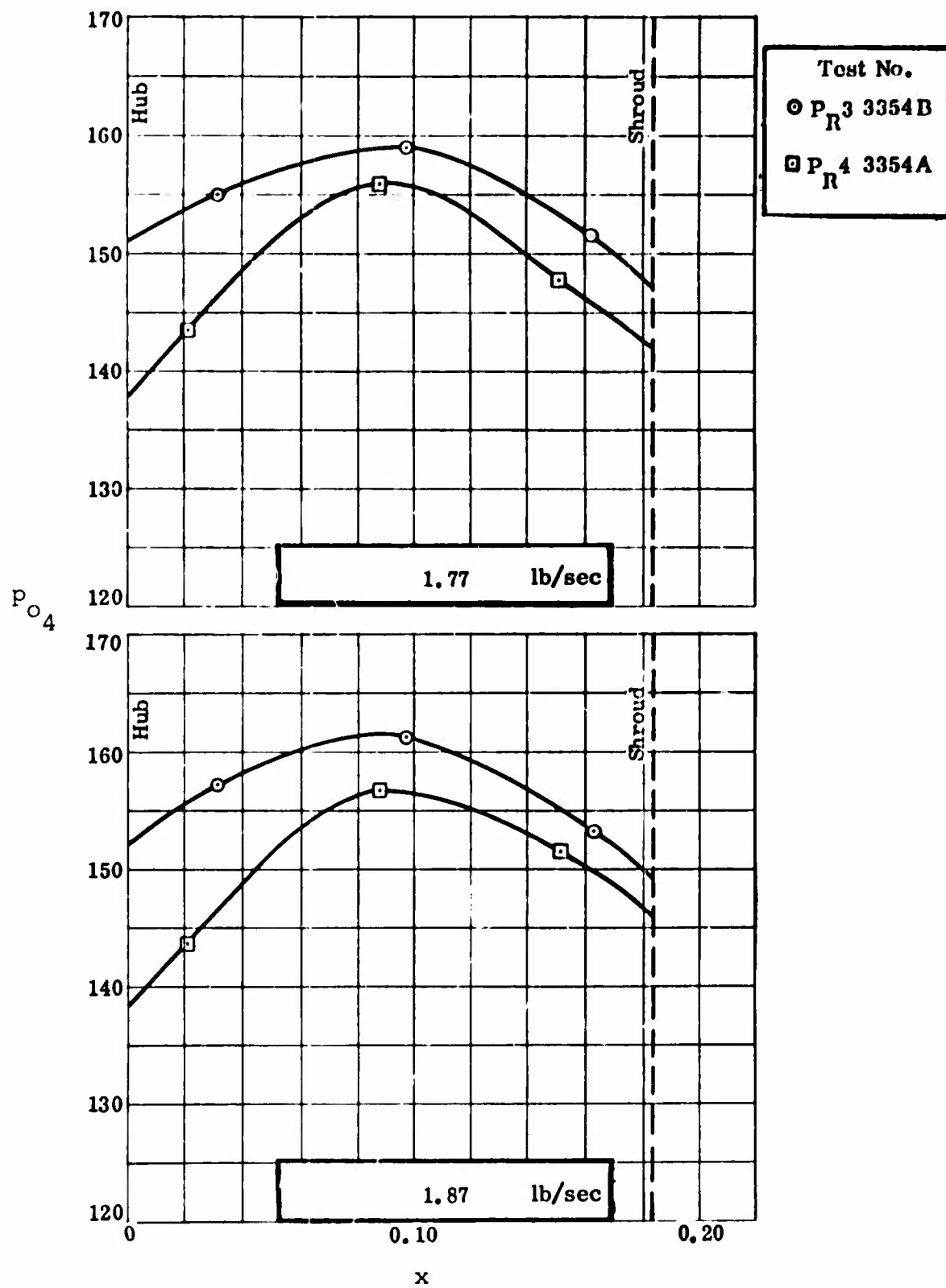


Figure 67. Diffuser Throat Stagnation Pressure.  
RF--2

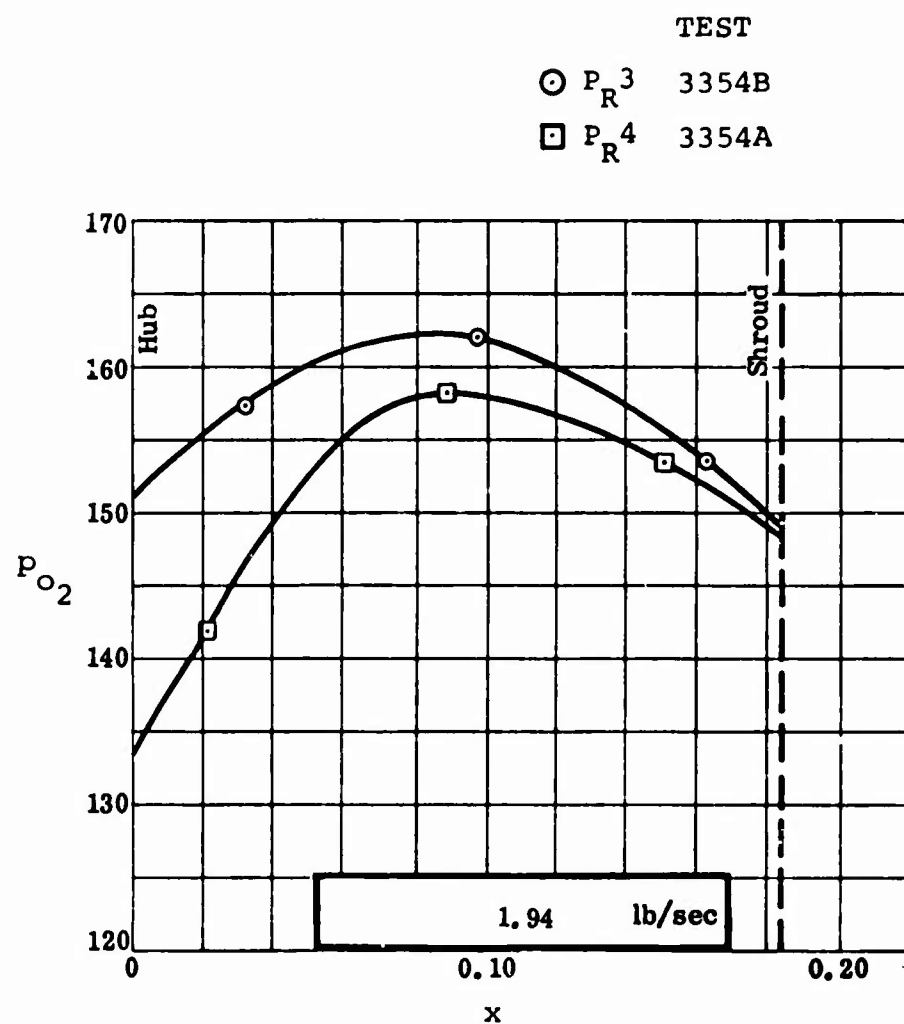


Figure 68. Diffuser Throat Stagnation Pressure.  
RF-2

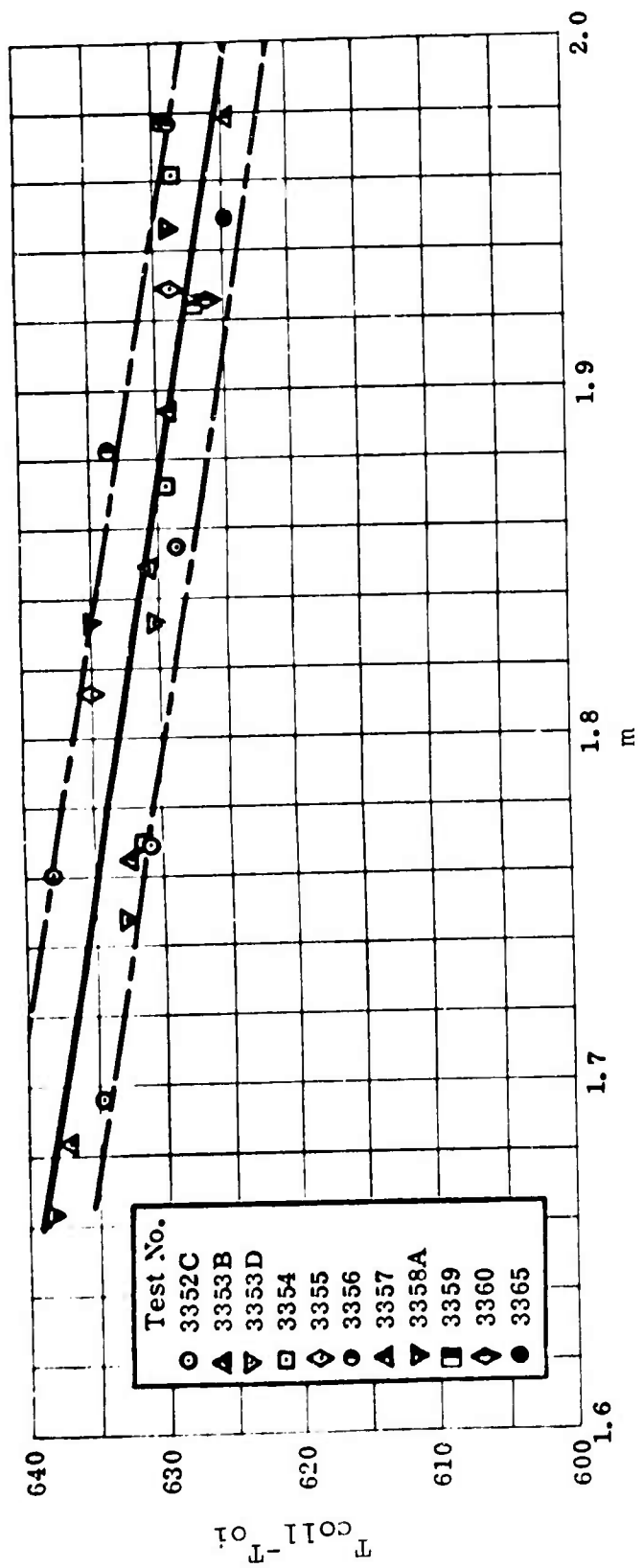


Figure 69. Collector Temperature Rise versus  
Mass Flow.  
RF-2

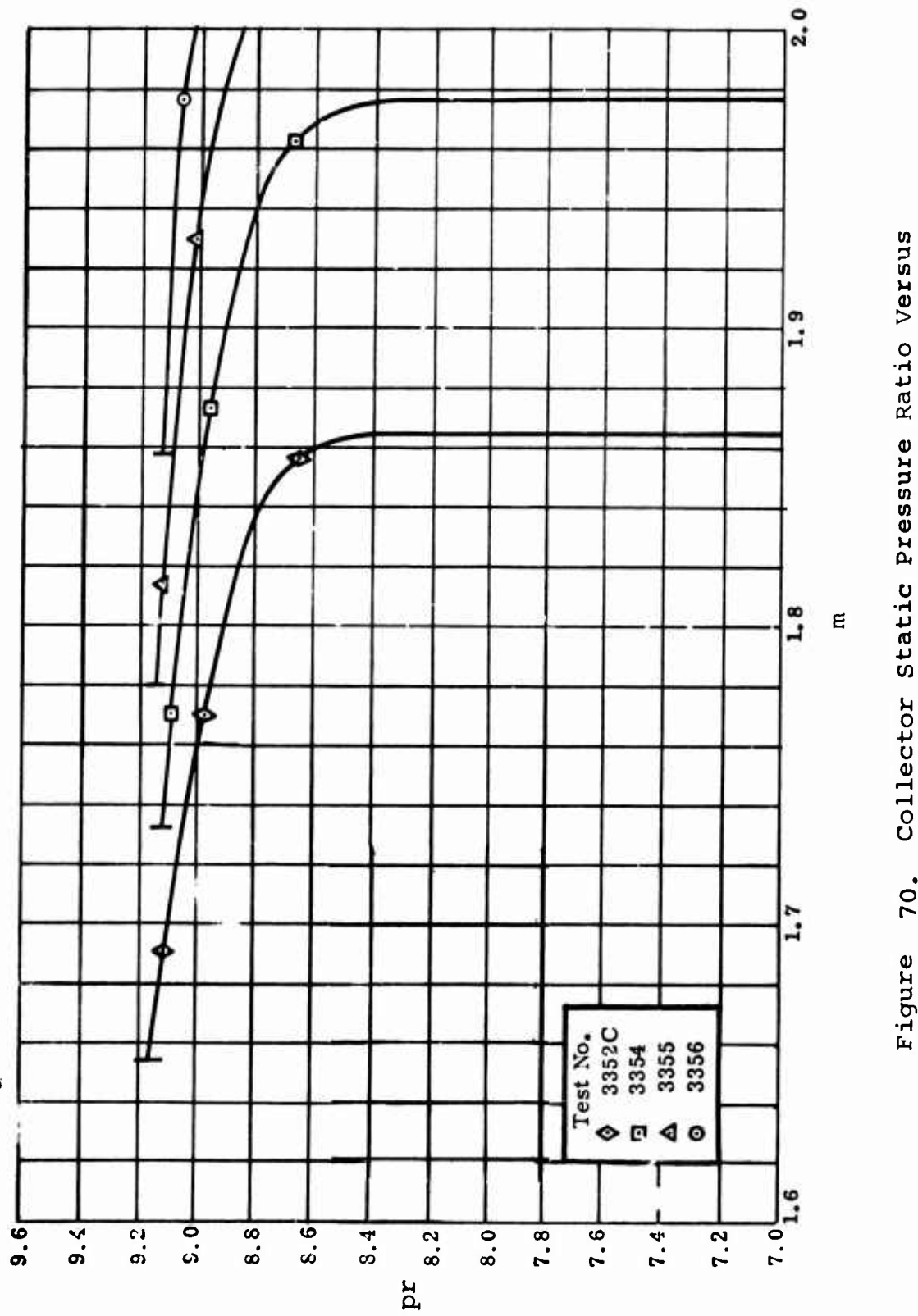


Figure 70. Collector Static Pressure Ratio Versus  
Mass Flow.  
RF-2

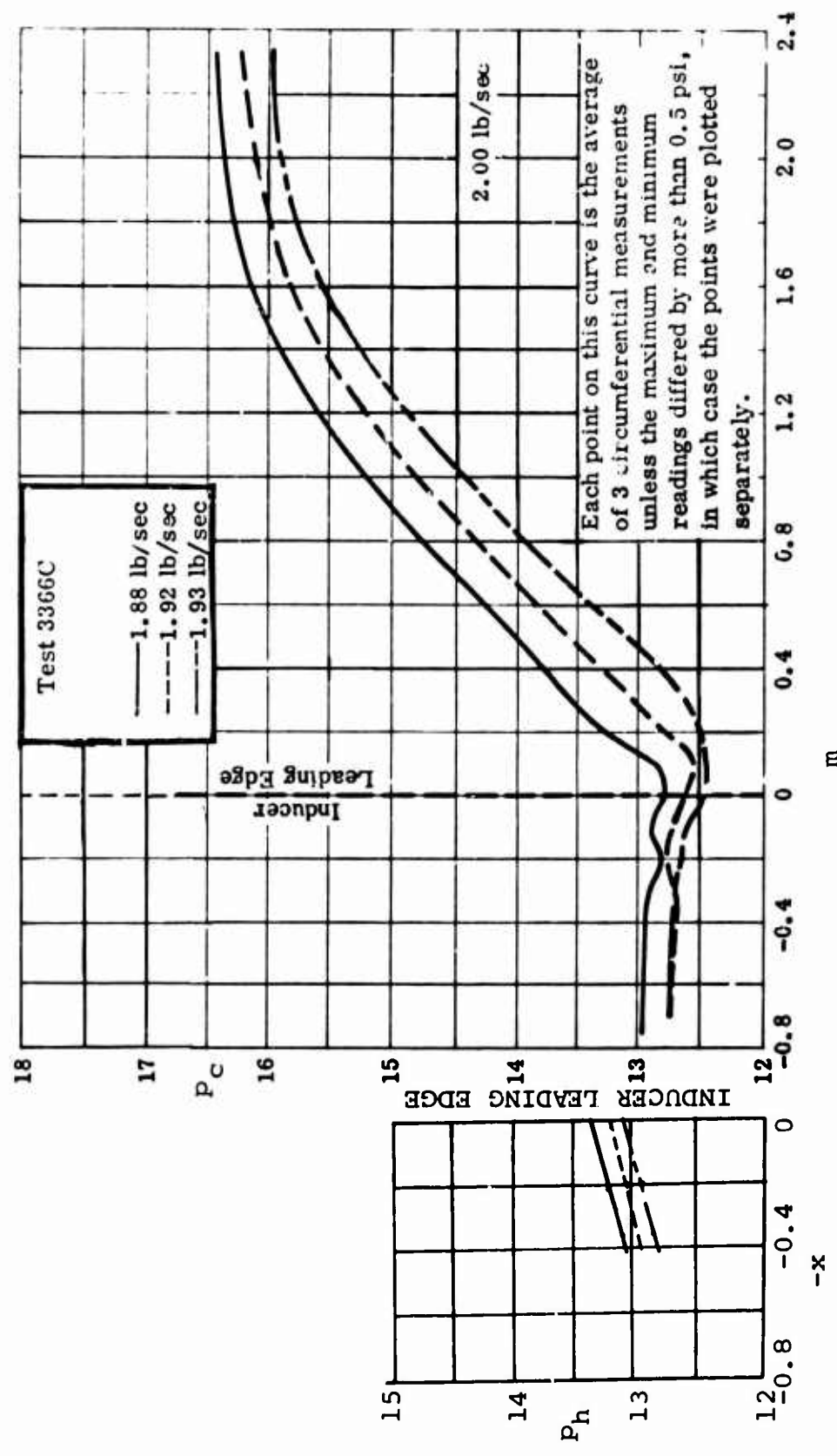


Figure 71. Cover and Hub Static Pressure.  
RF-2

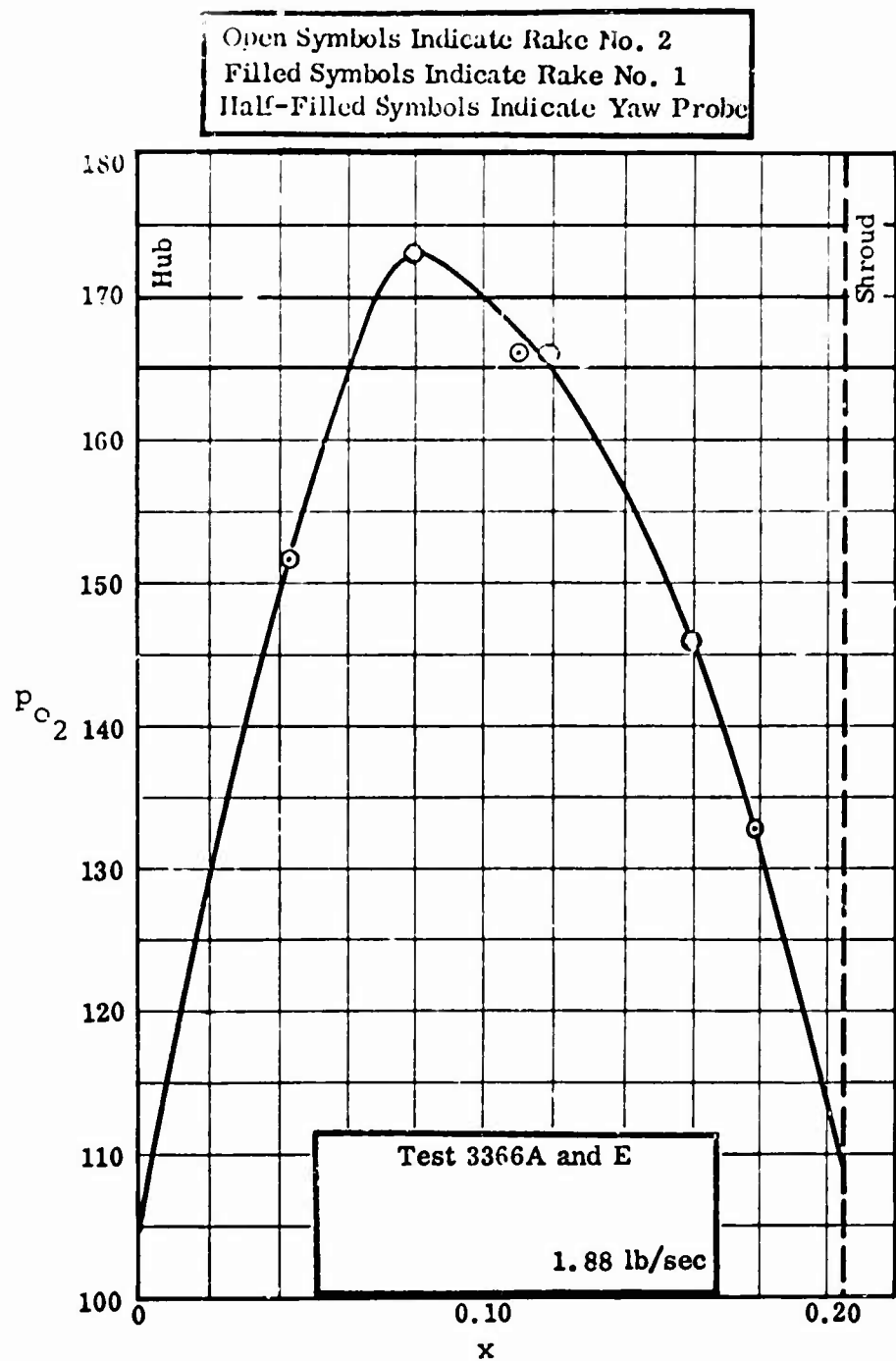


Figure 72. Impeller Tip Stagnation Pressure.  
RF-2

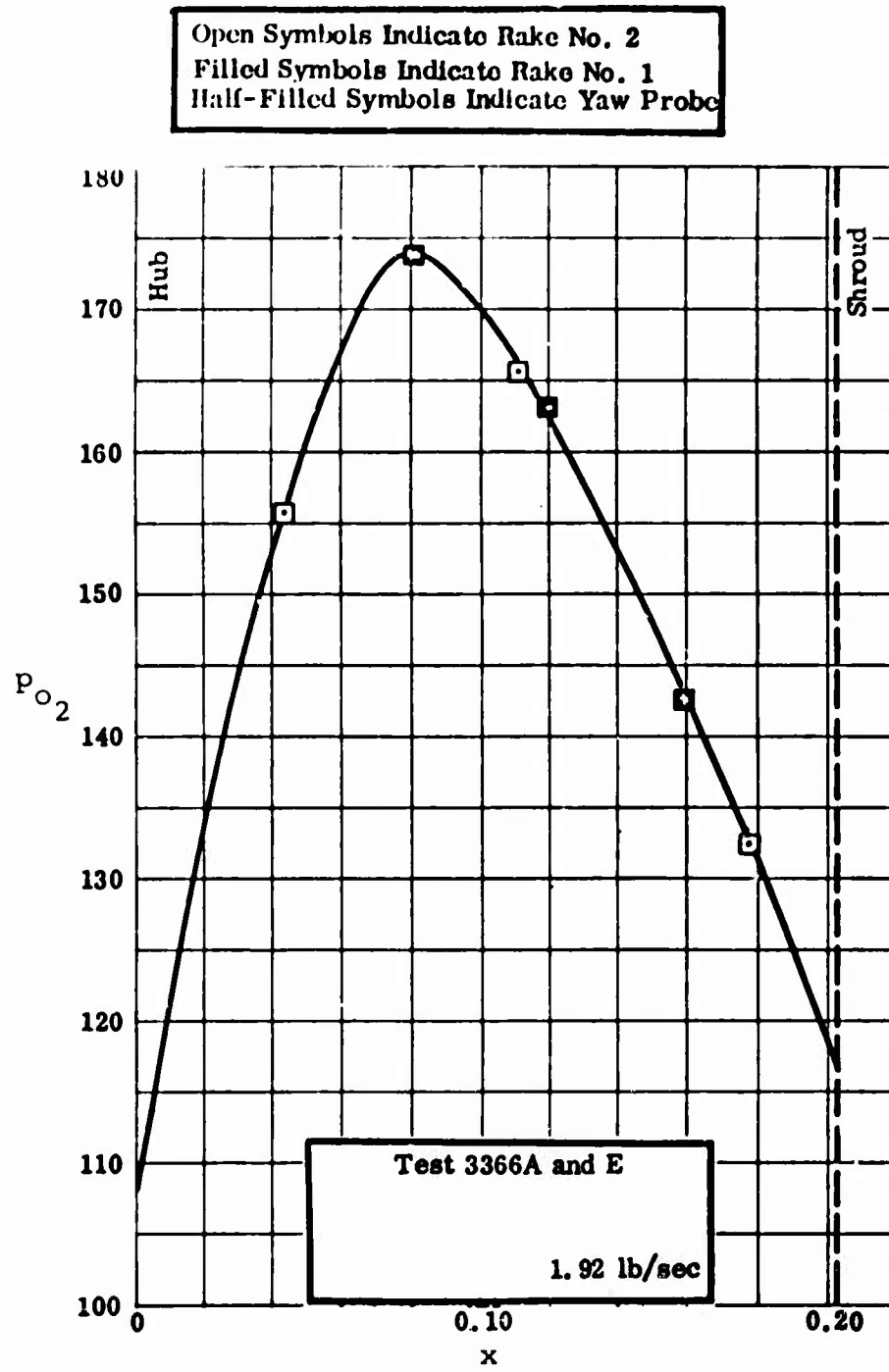
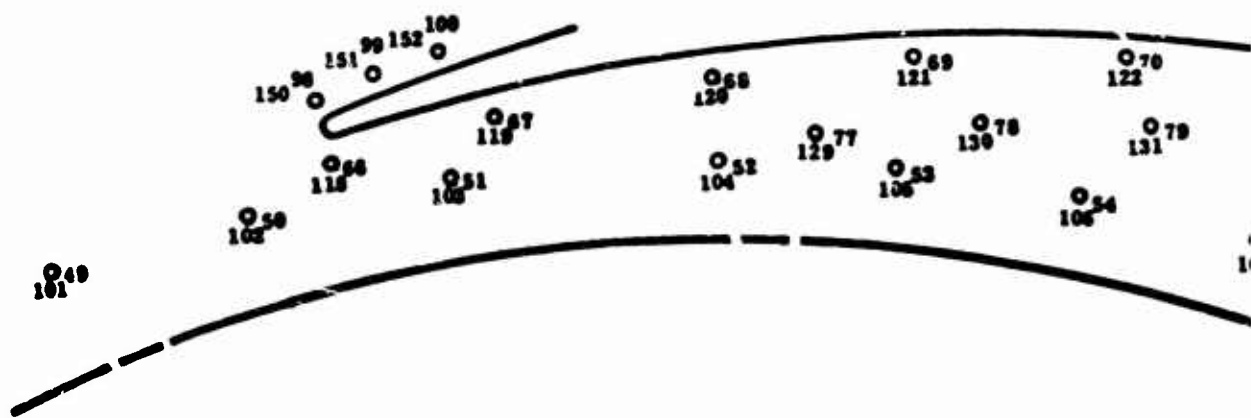


Figure 73. Impeller Tip Stagnation Pressure.

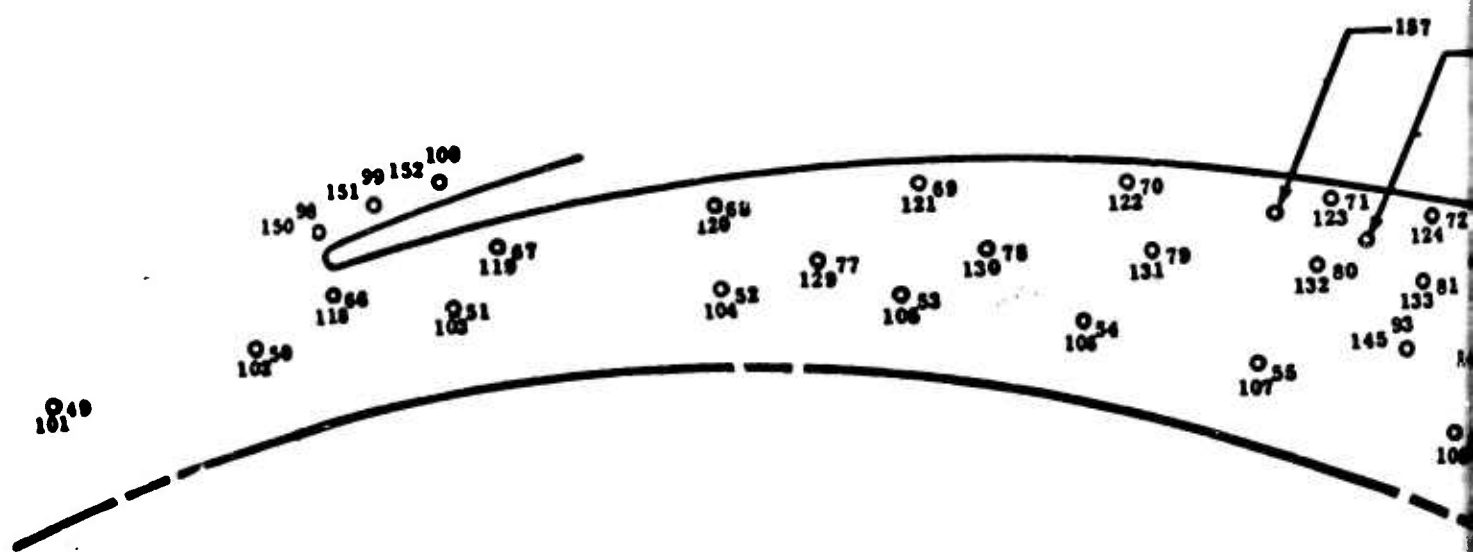


**Frontplate Tap Numbers - 19 thru 100, 157, 158, 159, 160**

**Rearplate Tap Numbers - 101 thru 152**

V2

**Figure 74. V2 Diffuser Static Pressure Taps.  
RF-2**

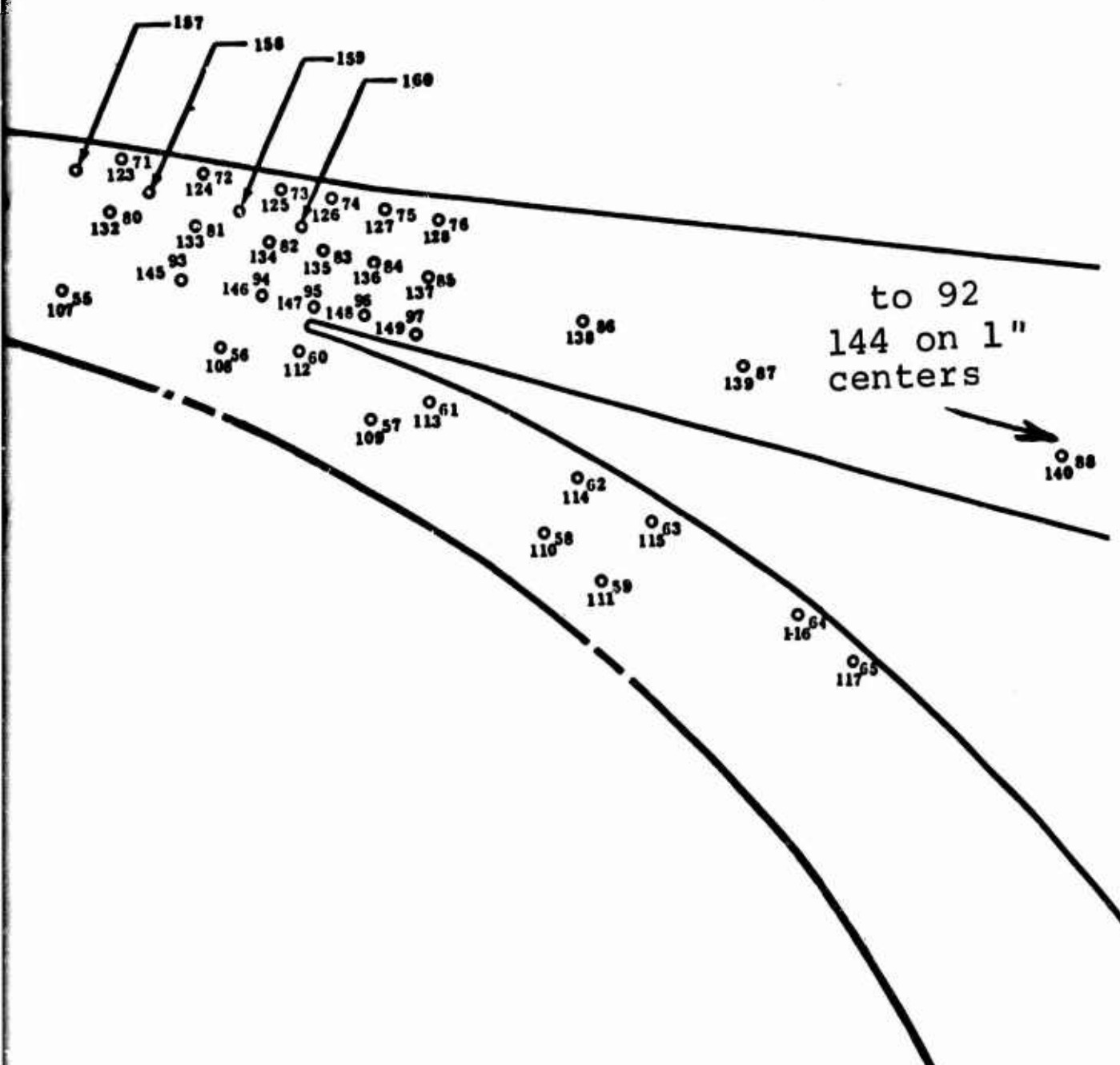


**Frontplate Tap Numbers - 49 thru 100, 157, 158, 159, 160**

**Rearplate Tap Numbers - 101 thru 152**

V2

**Figure 74. V2 Diffuser Static Pressure Taps.  
RF-2**



to 92  
144 on 1"  
centers

<u>Tap No.</u>	<u>Static Pressure</u>						
49	70.2	76	108.3	103	54.0	130	71.8
50	75.5	77	74.0	104	73.1	131	75.4
51	51.9	78	71.4	105	69.6	132	76.9
52	73.0	79	75.8	106	68.4	133	73.9
53	69.3	80	76.6	107	70.4	134	92.0
54	68.4	81	73.1	108	76.0	135	98.4
55	69.6	82	90.6	109	54.1	136	102.5
56	51.8	83	97.7	110	73.2	137	107.7
57	73.2	84	101.7	111	72.8	138	120.3
58	76.6	85	107.4	112	87.8	139	126.2
59	72.7	86	120.0	113	61.4	140	131.9
60	91.6	87	126.1	114	78.9	141	
61	60.8	88	131.9	115	80.4	142	
62	79.3	89	133.7	116	77.4	143	134.8
63	80.0	90	134.5	117	79.8	144	135.1
64	77.3	91	134.9	118	88.4	145	70.7
65	78.7	92	135.0	119	63.4	146	89.4
66	89.6	93	70.8	120	79.7	147	103.8
67	62.8	94	90.2	121	77.9	148	101.7
68	79.1	95	103.9	122	80.2	149	108.1
69	77.1	96	101.6	123	82.3	150	103.7
70	79.5	97	108.1	124	75.0	151	103.0
71	81.7	98	103.3	125	91.0	152	108.8
72	74.0	99	102.1	126	97.7	157	79.0
73	90.6	100	109.2	127	101.4	158	77.6
74	97.2	101	70.4	128	108.4	159	74.1
75	100.6	102	75.6	129	74.0	160	94.4

CONFIGURATION V2  
 THROAT SIZE  $A_T = 0.865 \text{ in.}^2$   
 $a_{ot} = 0.203$

TEST 3366  
 LINE 3  
 $1.80 \text{ lb/sec}$

Figure 75. Diffuser Static Pressures.  
 RF-2

<u>Tap No.</u>	<u>Static Pressure</u>						
49	70.0	76	104.9	103	56.1	130	71.4
50	65.3	77	73.4	104	71.7	131	74.0
51	57.2	78	71.0	105	69.3	132	76.7
52	70.7	79	74.3	106	67.9	133	74.2
53	68.3	80	76.8	107	70.5	134	87.3
54	67.2	81	73.9	108	68.0	135	94.2
55	68.9	82	86.6	109	55.8	136	97.8
56	56.5	83	93.9	110	72.3	137	104.1
57	71.2	84	97.2	111	74.4	138	118.0
58	67.9	85	103.9	112	88.7	139	124.1
59	71.2	86	117.8	113	63.8	140	129.9
60	89.7	87	124.1	114	77.5	141	
61	63.8	88	129.9	115	79.7	142	
62	78.6	89	131.7	116	77.0	143	132.7
63	79.9	90	132.5	117	78.9	144	132.9
64	77.2	91	132.8	118	88.7	145	71.1
65	78.0	92	132.8	119	65.6	146	85.1
66	87.4	93	71.2	120	77.9	147	98.9
67	66.1	94	86.4	121	77.0	148	97.2
68	77.9	95	101.1	122	79.0	149	104.7
69	76.7	96	97.1	123	82.4	150	98.4
70	78.5	97	105.0	124	75.3	151	98.2
71	81.8	98	99.9	125	85.3	152	105.2
72	74.5	99	97.1	126	93.8	157	78.8
73	85.0	100	105.8	127	96.8	158	78.3
74	93.2	101	70.9	128	105.2	159	67.2
75	95.8	102	65.9	129	73.7	160	90.9

CONFIGURATION V2  
THROAT SIZE -  $A_{T_{ot}} = 0.865 \text{ in.}^2$   
 $b = 0.203$

TEST 3366  
LINE 5  
1.88 lb/sec

Figure 76. Diffuser Static Pressures.  
RF-2

<u>Tap No.</u>	<u>Static Pressure</u>						
49	69.1	76	93.5	103	71.9	130	64.2
50	62.1	77	71.9	104	74.1	131	69.3
51	63.0	78	70.9	105	76.4	132	69.3
52	68.0	79	74.0	106	74.8	133	68.4
53	68.0	80	76.3	107	66.3	134	69.6
54	67.2	81	74.3	108	85.8	135	65.9
55	67.7	82	63.5	109	76.4	136	62.7
56	61.4	83	85.9	110	94.1	137	70.1
57	68.9	84	74.5	111	111.8	138	70.4
58	64.3	85	93.8	112	119.6	139	89.2
59	69.0	86	111.7	113	126.5	140	69.4
60	86.5	87	119.6	114		141	75.7
61	69.4	88	126.3	115		142	78.1
62	76.8	89	128.2	116	129.3	143	77.4
63	78.4	90	128.9	117	129.5	144	79.5
64	77.5	91	129.2	118	71.5	145	88.5
65	78.5	92	129.2	119	66.4	146	71.5
66	83.9	93	71.2	120	90.3	147	75.3
67	71.4	94	64.5	121	78.6	148	77.2
68	75.2	95	94.9	122	94.8	149	79.5
69	77.0	96	77.1	123	88.7	150	82.0
70	79.0	97	95.1	124	83.7	151	76.1
71	81.5	98	92.2	125	96.2	152	65.8
72	75.0	99	81.1	126	78.1	157	84.2
73	64.9	100	96.9	127	78.5	158	76.4
74	83.3	101	70.7	128	67.4	159	94.2
75	75.8	102	63.5	129	75.2	160	73.0

CONFIGURATION V2  
THROAT SIZE -  $A_{T_{ot}} = 0.865 \text{ in}^2$   
 $b = 0.203$

TEST 3366  
LINE 7  
1.95 lb/sec

Figure 77. Diffuser Static Pressures.  
RF-2

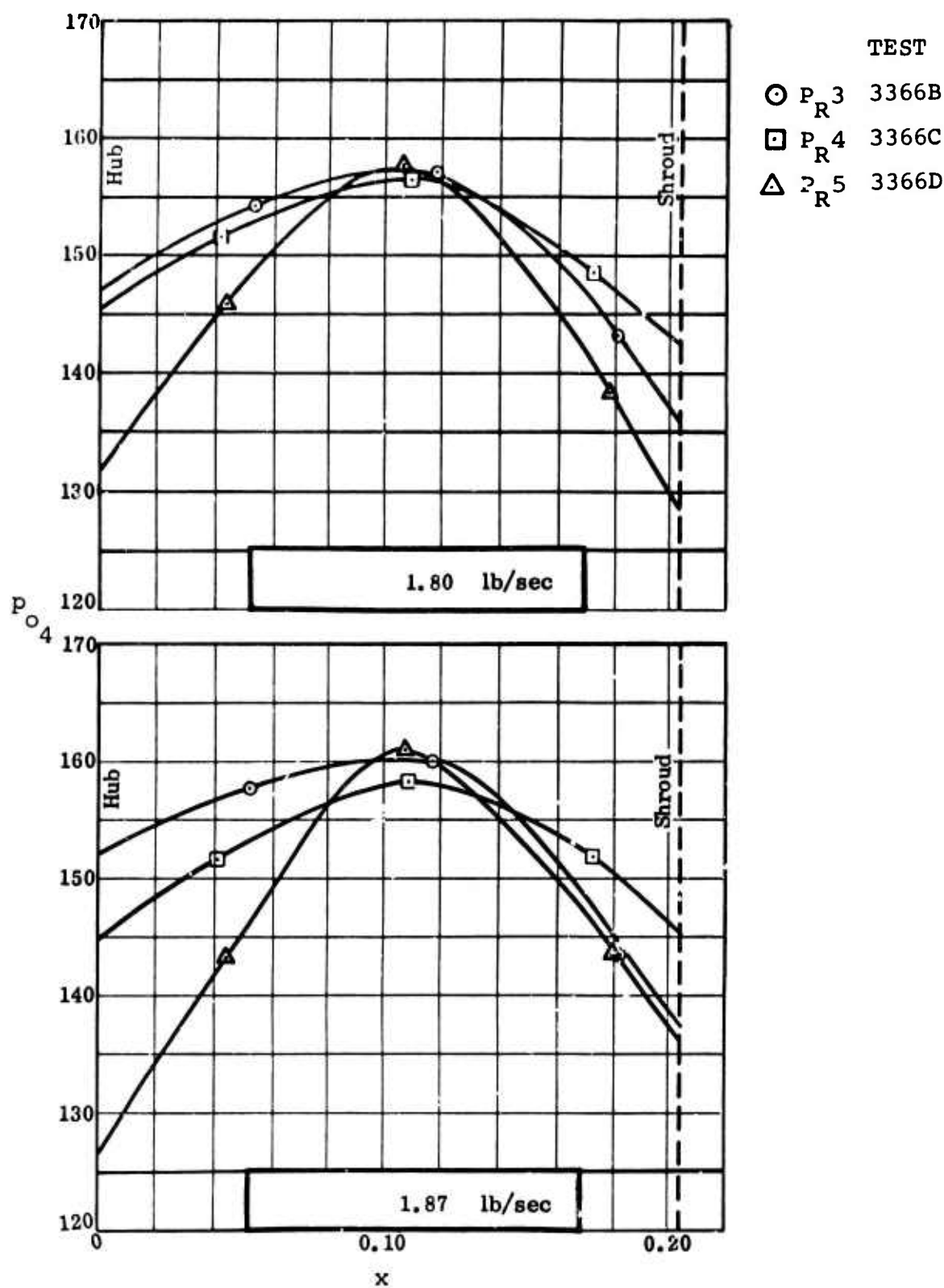


Figure 78. Diffuser Throat Stagnation Pressure.  
RF-2

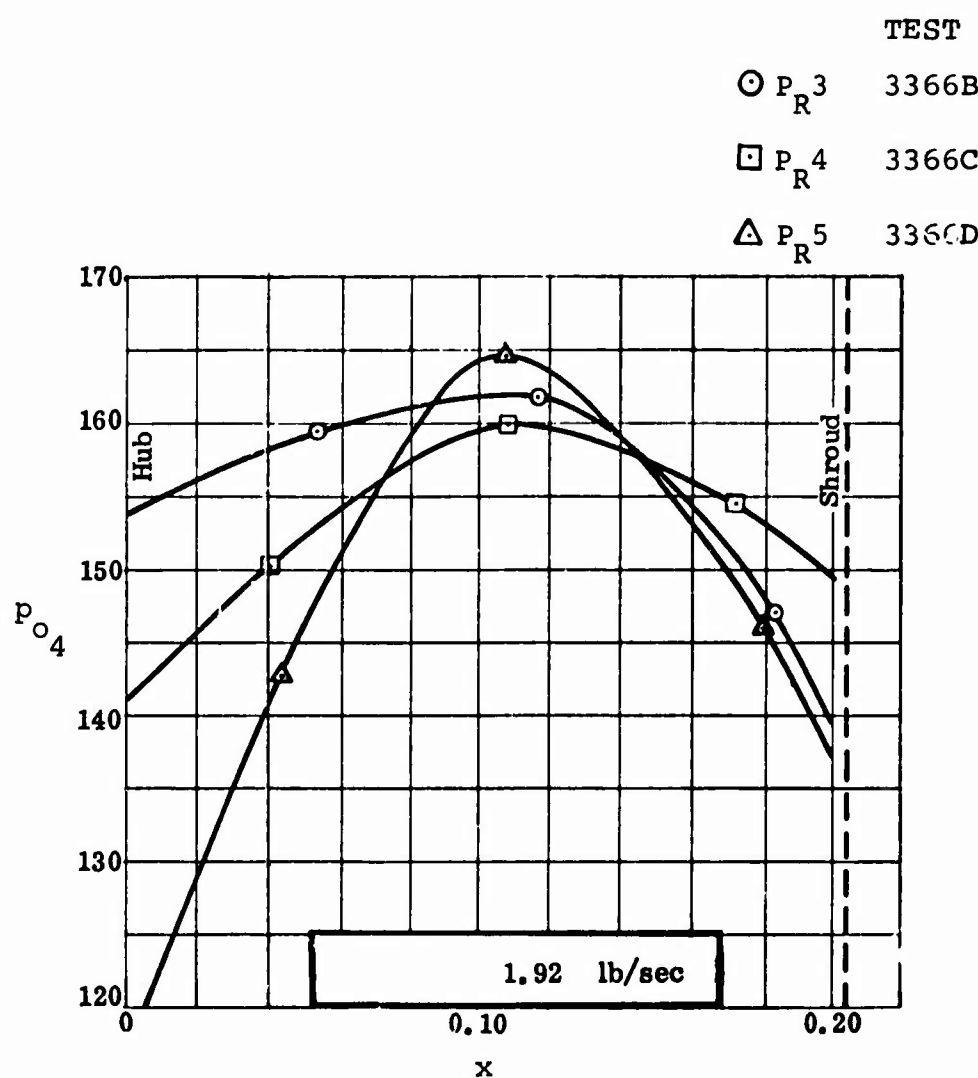


Figure 79. Diffuser Throat Stagnation Pressure.  
RF-2

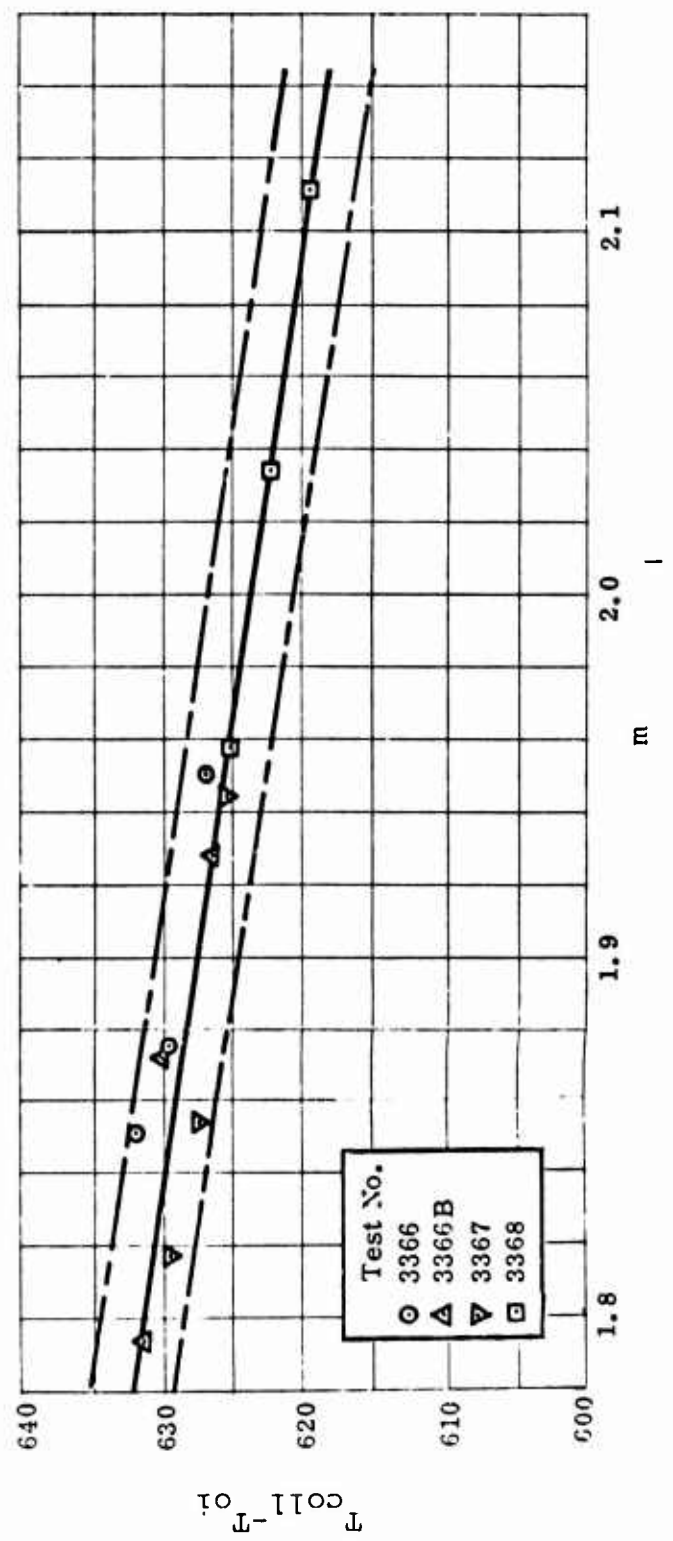


Figure 80. Collector Temperature Rise Versus Mass Flow.  
RF-2

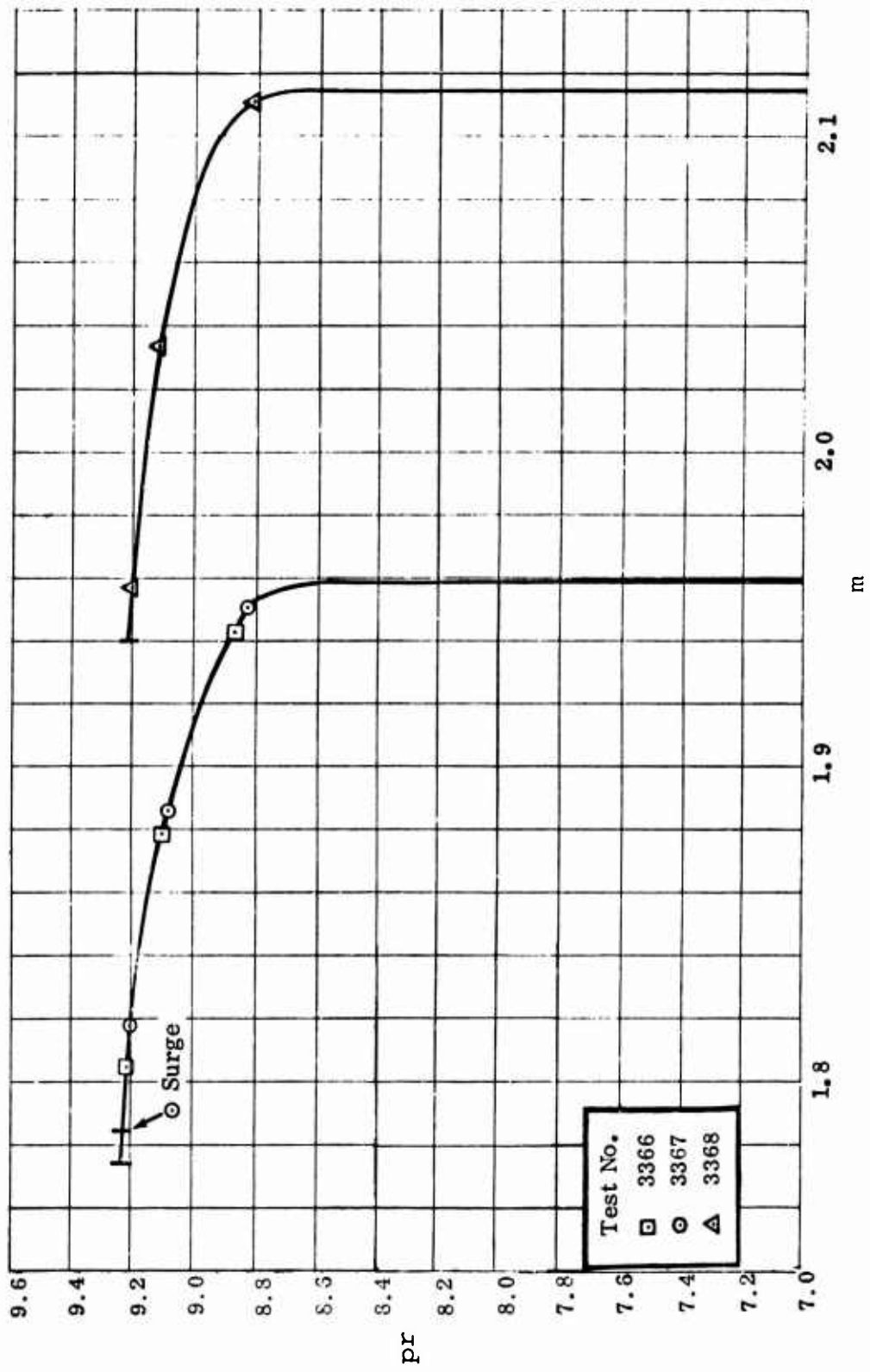


Figure 81. Collector Static Pressure Ratio Versus Mass Flow.  
RF-2

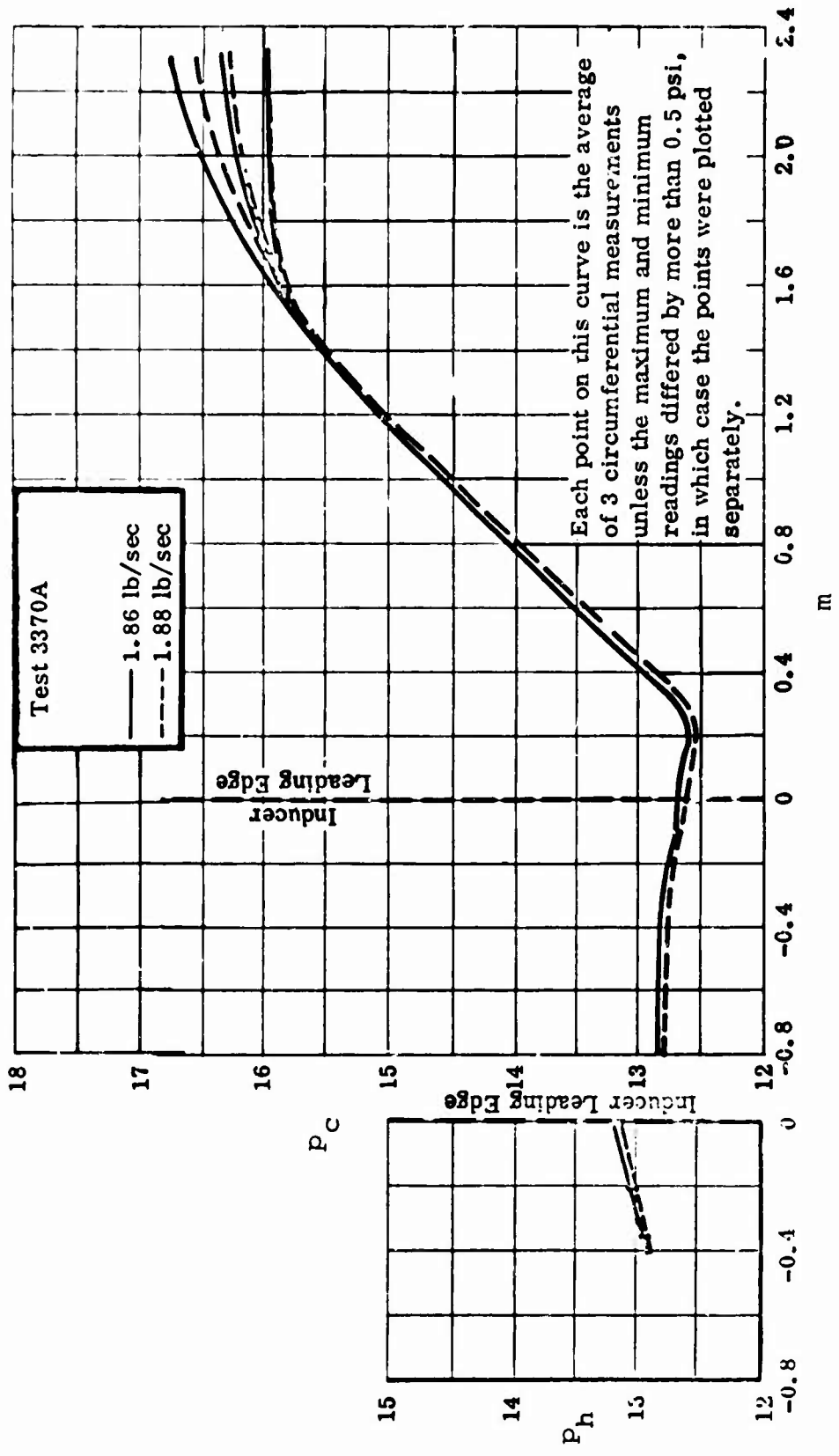


Figure 82. Cover and Hub Static Pressure.  
RF-2

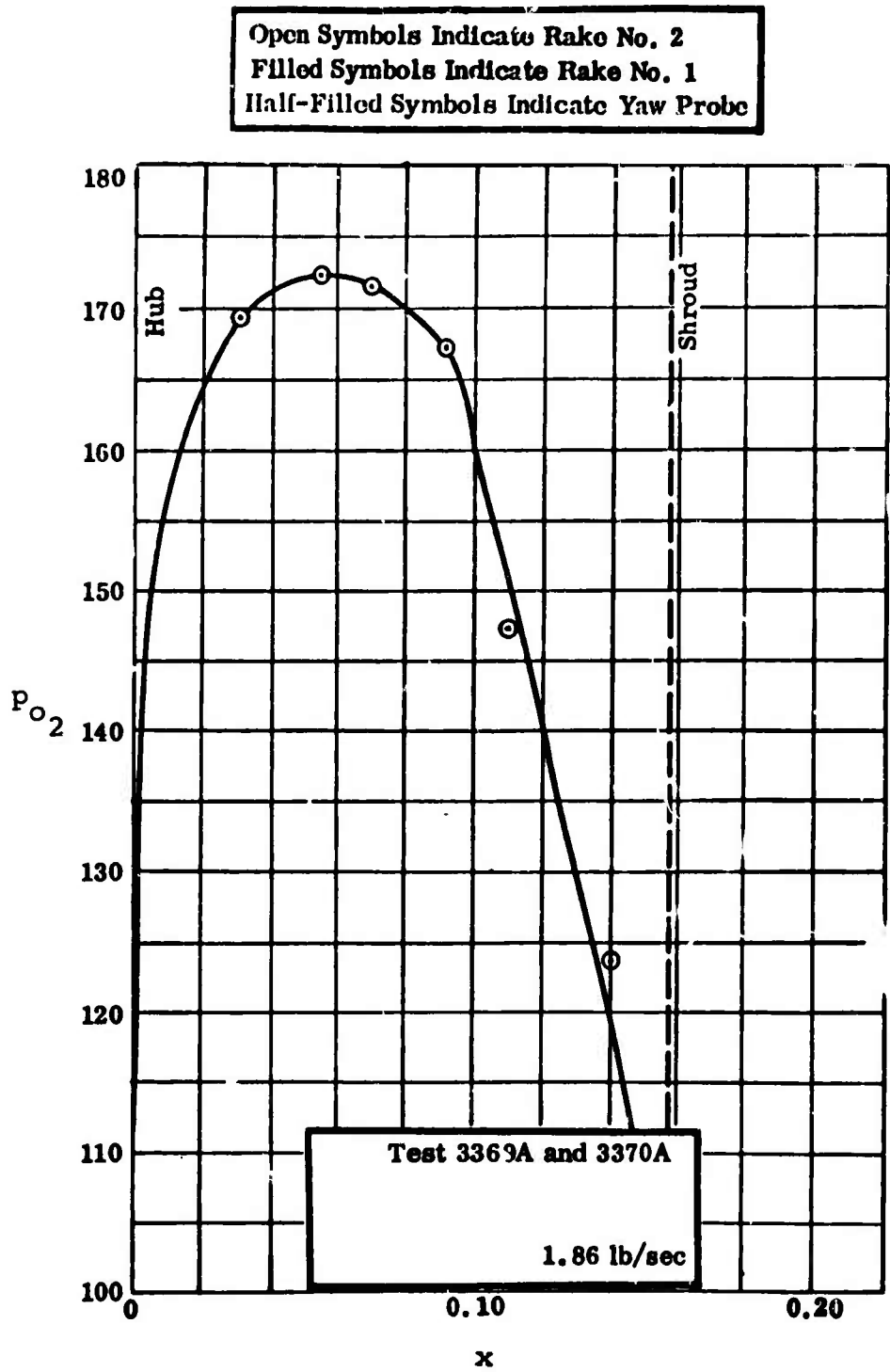


Figure 83. Impeller Tip Stagnation Pressure.  
RF-2

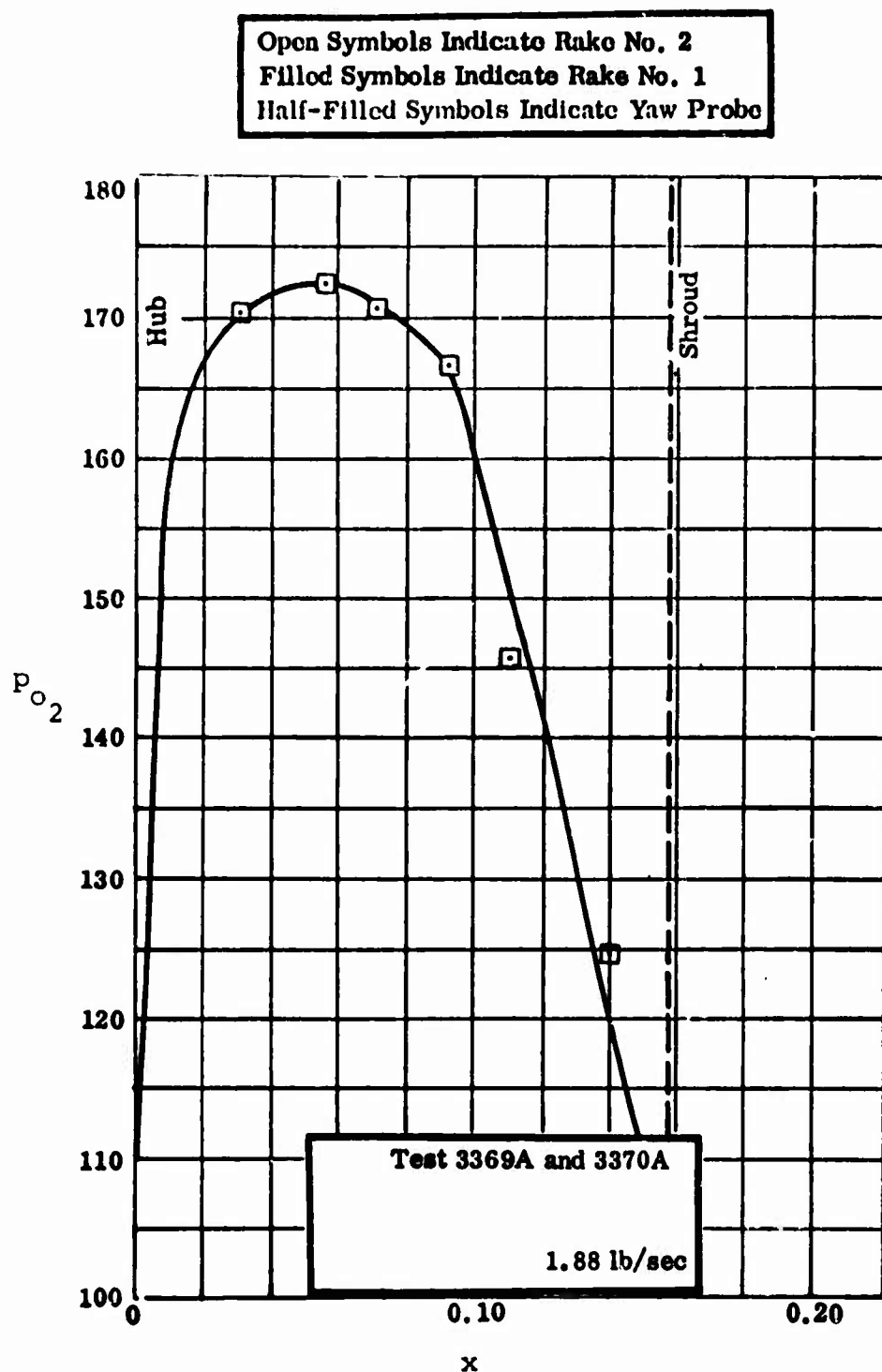
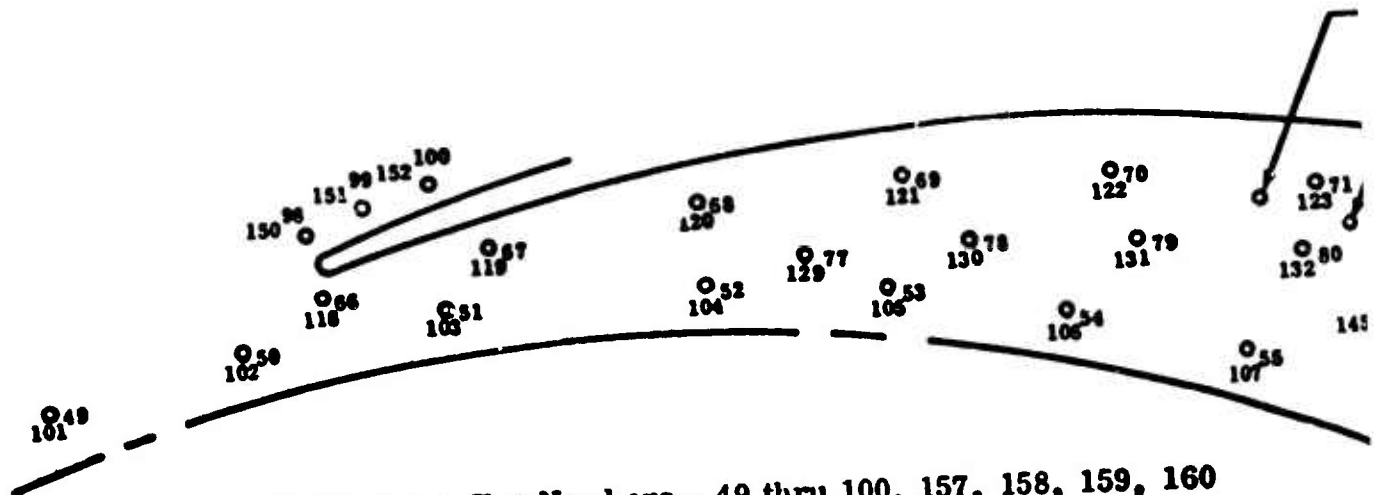


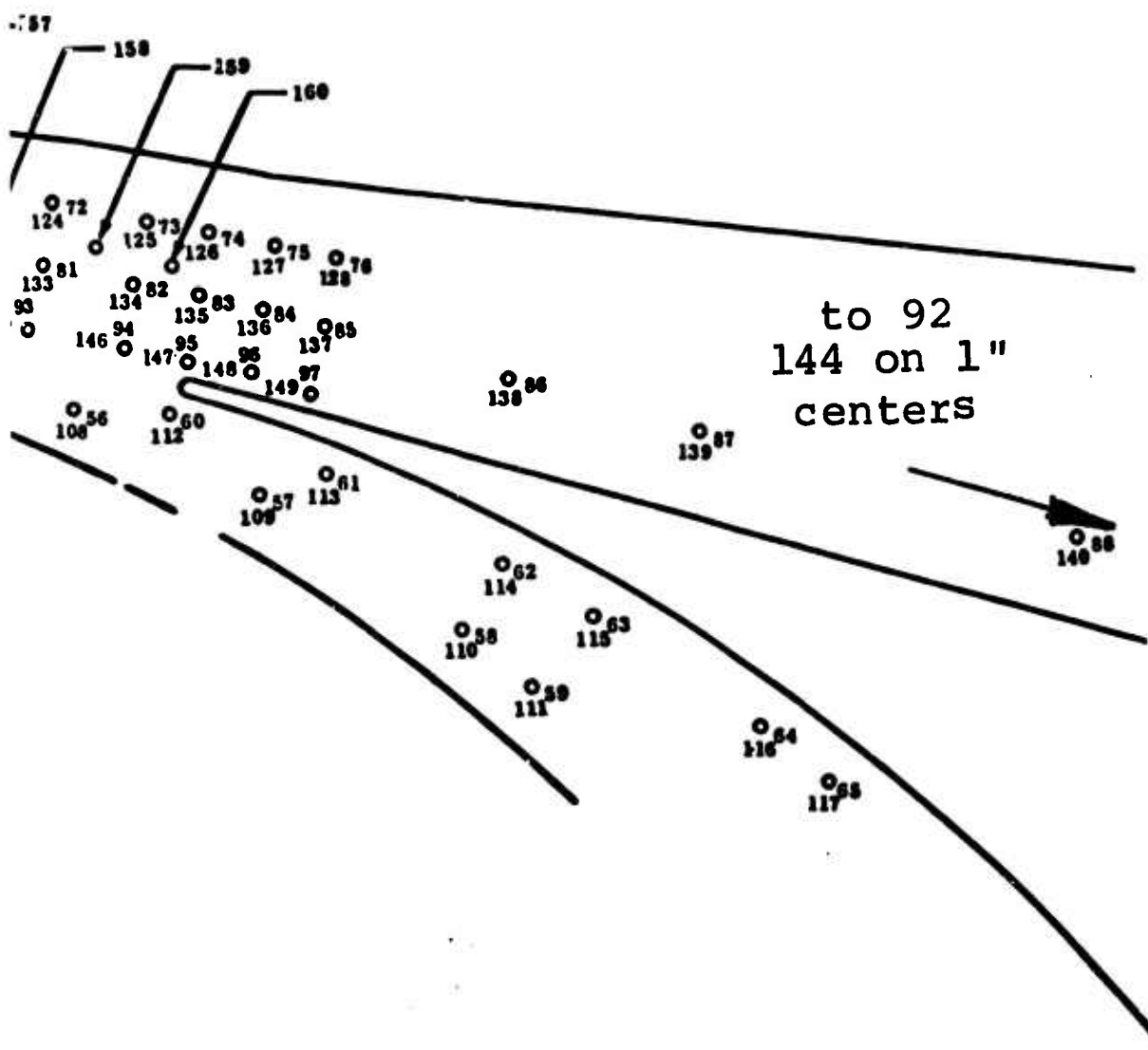
Figure 84. Impeller Tip Stagnation Pressure.  
RF-2



Frontplate Tap Numbers - 49 thru 100, 157, 158, 159, 160  
 Rearplate Tap Numbers - 101 thru 152

V2-2

Figure 85. V2-2 Diffuser Static Pressure Taps.



to 92  
144 on 1"  
centers

<u>Tap No.</u>	<u>Static Pressure</u>						
49	66.4	76	101.3	103	60.7	130	69.6
50	76.6	77	69.7	104	68.9	131	70.0
51	59.3	78	68.6	105	68.3	132	73.4
52	67.5	79	69.5	106	65.8	133	79.9
53	66.9	80	74.4	107	66.8	134	89.5
54	64.5	81	80.1	108	77.4	135	92.6
55	65.4	82	88.9	109	63.9	136	95.3
56	76.9	83	93.0	110	68.8	137	100.8
57	61.4	84	95.0	111	70.3	138	113.4
58	67.6	85	101.0	112	92.4	139	120.1
59	68.9	86	113.6	113	69.5	140	126.6
60	85.0	87	119.9	114	72.8	141	
61	69.4	88	126.5	115	76.3	142	
62	73.8	89	129.3	116	73.1	143	131.7
63	76.8	90	130.9	117	73.0	144	132.3
64	73.5	91	131.7	118	93.1	145	76.6
65	72.5	92	132.2	119	64.5	146	87.6
66	84.2	93	75.2	120	73.5	147	99.6
67	68.4	94	86.6	121	74.3	148	93.7
68	73.4	95	99.7	122	73.4	149	101.8
69	74.5	96	93.4	123	78.8	150	98.9
70	73.7	97	101.0	124	85.0	151	96.3
71	78.9	98	99.4	125	90.6	152	103.3
72	84.2	99	95.0	126	92.2	157	74.4
73	90.2	100	103.4	127	95.5	158	79.5
74	92.0	101	67.4	128	101.6	159	85.6
75	94.9	102	77.9	129	70.5	160	91.0

CONFIGURATION V2-2  
 THROAT SIZE -  $A_T = 0.862 \text{ in.}^2$   
 $A_{tot} = 0.158$

TEST 3369  
 LINE 3  
 $1.86 \text{ lb/sec}$

Figure 86. Diffuser Static Pressures.  
 RF-2

<u>Tap No.</u>	<u>Static Pressure</u>						
49	66.3	76	99.7	103	63.2	130	69.9
50	75.7	77	68.9	104	68.5	131	70.2
51	61.6	78	68.9	105	68.3	132	73.3
52	67.1	79	69.7	106	66.4	133	78.9
53	66.9	80	73.0	107	66.2	134	88.3
54	65.0	81	79.1	108	76.2	135	90.6
55	64.7	82	87.7	109	66.7	136	92.7
56	76.0	83	91.1	110	68.5	137	98.9
57	63.9	84	92.6	111	69.5	138	112.4
58	67.2	85	99.3	112	92.5	139	119.4
59	68.2	86	112.8	113	71.1	140	126.2
60	84.9	87	119.4	114	72.4	141	
61	70.9	88	126.2	115	75.4	142	
62	73.4	89	129.1	116	73.4	143	131.3
63	76.1	90	130.6	117	73.3	144	131.9
64	73.9	91	131.4	118	93.0	145	75.9
65	72.9	92	131.9	119	66.0	146	86.4
66	84.0	93	74.4	120	72.9	147	98.5
67	69.9	94	85.5	121	74.3	148	91.4
68	72.8	95	98.1	122	73.7	149	99.9
69	74.5	96	91.1	123	77.5	150	97.6
70	74.2	97	99.4	124	83.8	151	94.4
71	77.8	98	97.9	125	89.0	152	101.9
72	83.2	99	93.1	126	90.1	157	73.6
73	88.8	100	102.2	127	93.0	158	78.4
74	90.0	101	67.3	128	99.8	159	84.5
75	92.6	102	77.0	129	69.6	160	89.5

CONFIGURATION V2-2  
 THROAT SIZE -  $A_T^{ot} = 0.862 \text{ in.}^2$   
 $b = 0.158$

TEST 3369  
 LINE 5  
 $1.89 \text{ lb/sec}$

Figure 87. Diffuser Static Pressures.  
 RF-2

<u>Tap No.</u>	<u>Static Pressure</u>						
49	65.4	76	94.1	103	70.7	130	69.9
50	72.6	77	67.8	104	67.9	131	70.6
51	67.7	78	68.8	105	67.3	132	71.6
52	66.4	79	70.0	106	66.7	133	76.2
53	65.9	80	71.1	107	65.5	134	85.4
54	65.1	81	76.3	108	73.4	135	85.9
55	63.9	82	84.4	109	70.9	136	82.0
56	73.7	83	86.0	110	67.8	137	93.6
57	67.4	84	81.2	111	68.1	138	108.9
58	66.4	85	93.8	112	92.2	139	116.5
59	66.8	86	109.1	113	72.6	140	123.7
60	84.0	87	116.4	114	72.1	141	
61	72.4	88	123.6	115	74.0	142	
62	72.9	89	126.6	116	73.6	143	129.0
63	74.4	90	128.2	117	73.8	144	129.5
64	73.9	91	129.0	118	92.2	145	73.3
65	73.3	92	129.4	119	68.1	146	83.7
66	83.1	93	71.7	120	72.5	147	96.3
67	71.9	94	82.7	121	73.9	148	81.8
68	72.2	95	94.9	122	74.4	149	94.9
69	74.0	96	81.0	123	75.6	150	94.3
70	74.7	97	94.2	124	81.2	151	87.9
71	75.7	98	93.3	125	85.5	152	97.7
72	80.3	99	86.3	126	84.5	157	72.6
73	85.1	100	97.7	127	82.9	158	75.2
74	84.1	101	66.5	128	94.4	159	81.3
75	82.1	102	73.6	129	68.6	160	85.4

CONFIGURATION V2-2  
THROAT SIZE -  $A_T = 0.862 \text{ in.}^2$   
 $\frac{A_{ot}}{A_T} = b = 0.158$

TEST 3369  
LINE 7  
1.92 lb/sec

Figure 88. Diffuser Static Pressures.  
RF-2

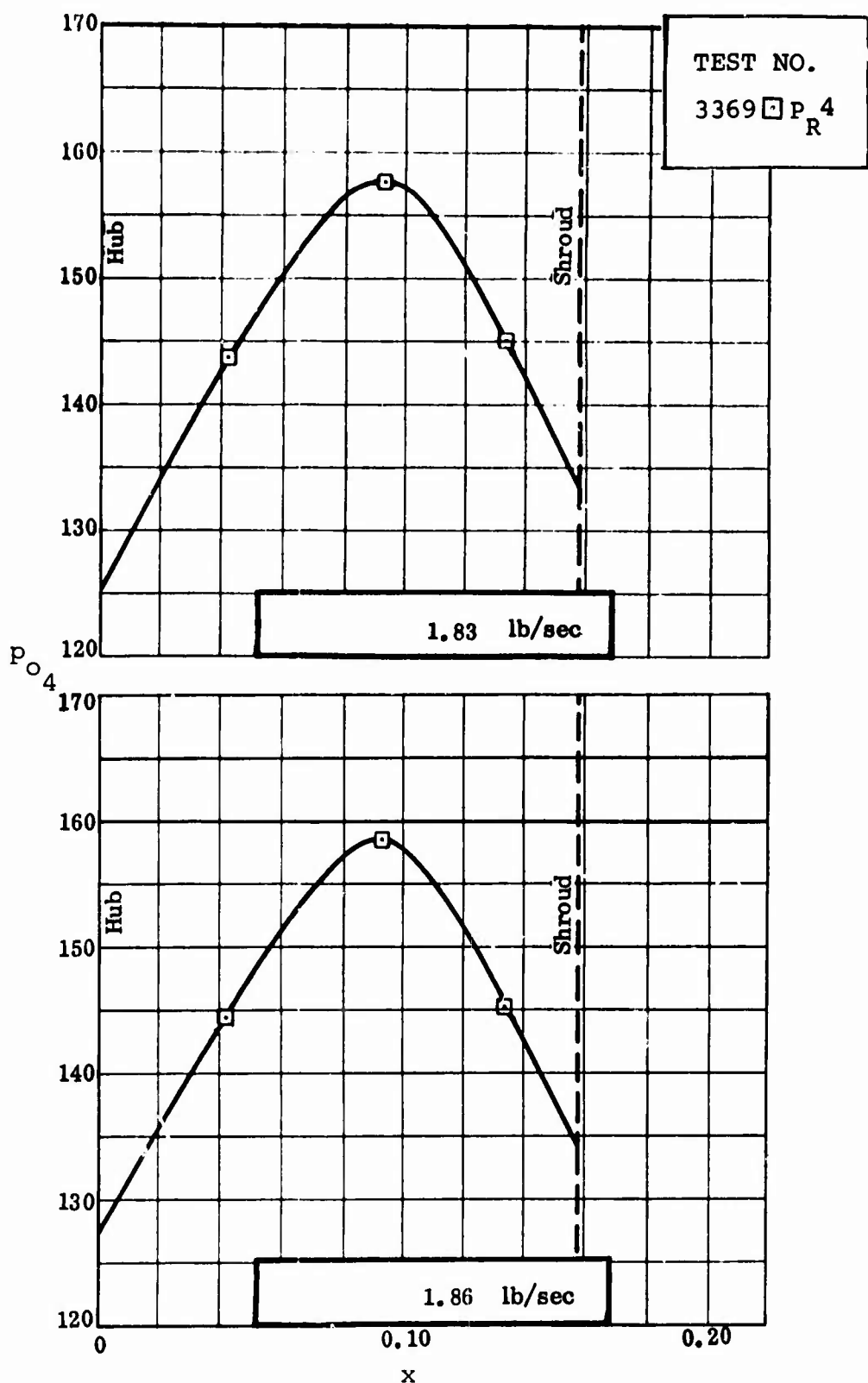


Figure 89. Diffuser Throat Stagnation Pressure.  
RF-2

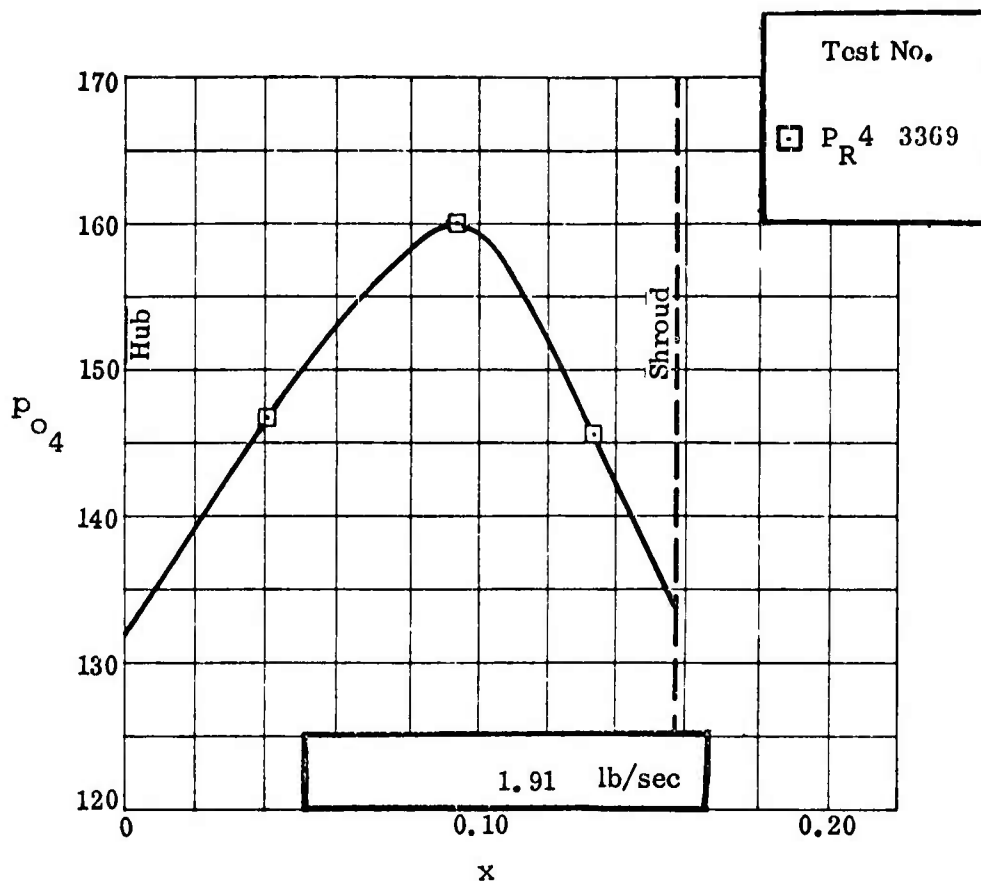


Figure 90. Diffuser Throat Stagnation Pressure.  
RF-2

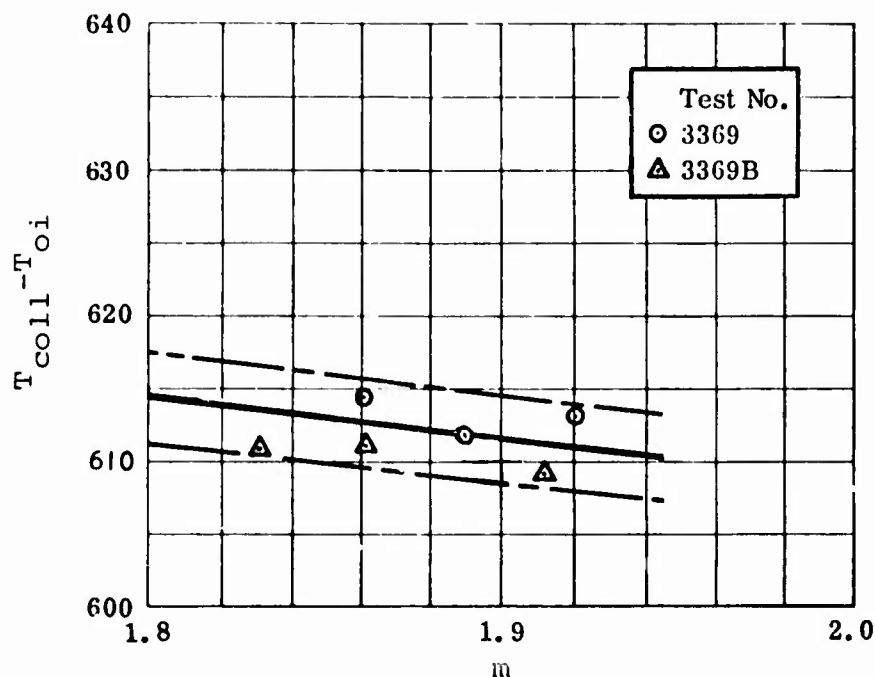


Figure 91. Collector Temperature Rise Versus Mass Flow.  
RF-2

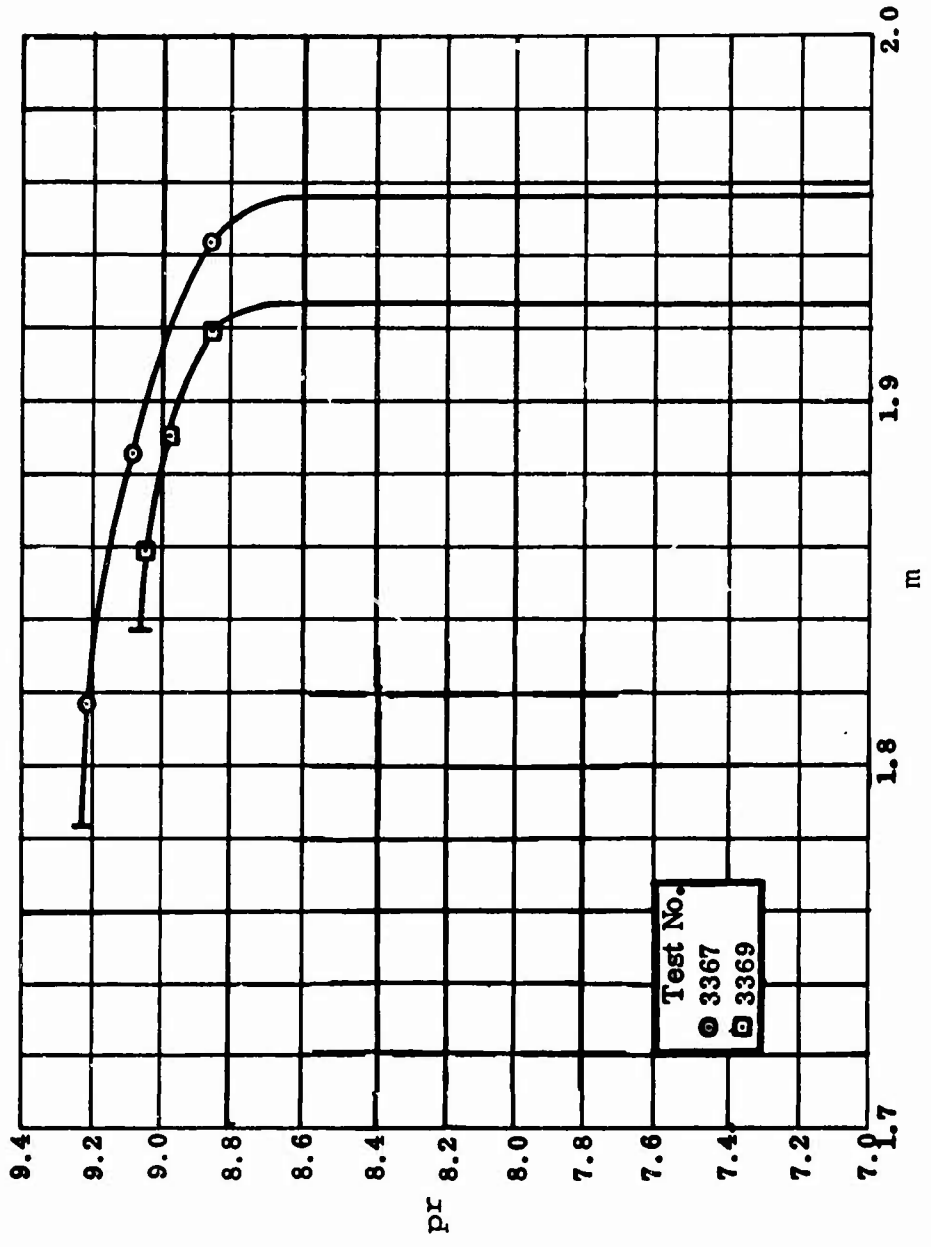


Figure 92. Collector Static pressure Ratio Versus Mass Flow.  
RF-2

#### 4.0 ANALYSIS OF THE INFORMATION CONTENT OF THE DATA

Before proceeding to use the input data for diagnosis of the detailed processes of the Boeing-AVLABS compressors, it is important to clarify just how useful the information may be. In this Section, we attempt to estimate how the measurements made relate to fluid dynamically and thermodynamically significant quantities of the compressor's processes. An estimate is made, when the data are employed, of the uncertainty in the derived results.

#### 4.1 IMPELLER INTERNAL FLOW DATA

Other than inlet stagnation conditions and mass flow, the only data available from which to deduce the internal flow of the impeller come from the cover static pressure taps.

For Workhorse, some cover static pressure distributions were measured, but unfortunately our analysis (Section 5.2) shows quite positively that the Workhorse impeller separated in the inducer on the hub. Of course, cover static pressure measurements at the tip produced poor resolution of a hub stall. Therefore, we can do little with the details of the cover pressure distributions measured for Workhorse.

For RF-2, the separation quite plainly occurred in the usual place at the impeller blade tips. Therefore, the cover pressure distribution contains significant information which we have used extensively in Section 5. Our purpose here is to evaluate how significant the Boeing-AVLABS RF-2 impeller data are in fact.

##### 4.1.1 Uncertainty

The usual types of uncertainties beset the cover static pressure measurements. That is, there is a considerable uncertainty as to what the indications of these pressure taps mean. Even if the tap indications are corrected for tap geometry errors and if the taps are assumed to time-average the varying pressure at their orifices caused by the loaded blades moving by, a major uncertainty is introduced when an attempt is made to relate the time-average indications to meaningful fluid dynamic and thermodynamic properties of the flow. This is the same problem encountered more drastically at the impeller tip, where the flow distortion is known to be large but is unknown in detail. Fortunately, in the rest of the impeller, the distortion problem does not have such a critical impact on interpreting the data for the flow pattern, especially in the inducer, and can be better estimated from other information.

We have assumed herein that the cover static pressure taps time-average the fluctuating pressure at their orifices. Further, we have assumed that the static pressure varies

linearly across the flow between the blades, where the blades are unseparated, and across the jet beyond the separation point.

In order to estimate the jet width for the purposes of transforming the pressure-tap time-average indication to wake pressure, we have assumed that the jet width is given by the two-dimensional separated flow model. Fortunately, because the Boeing-AVLABS impellers were heavily separated, and therefore the jets were narrow relative to the pitch between the blades, a highly accurate estimate of the jet width is not vital to the accuracy of the data reduction.

With these assumptions of the nature of the flow pattern between the blades, it is possible to relate the pressure tap indications to the mean pressure, wake pressure, and suction surface pressures of the impeller tip flow pattern. The variation of the change of pressure across the through flow was calculated from the usual angular momentum considerations embodied in the "rapid approximate methods" for making blade loading calculations.

The principal uncertainty in the cover static pressure data arises from circumferential variation in static pressure at diffuser blade pitch. There is no doubt from the measurements that the static pressure field of the diffuser penetrates through the impeller all the way to the inlet. The variations measured in the inducer are as large as 1-1/2 psi peak to peak, as shown in Figure 93. At the tip of the impeller, they are much larger, amounting to as much as 25 psi peak to peak.

The consequences of the impeller turning through the stationary pressure pattern of the diffuser are not at all certain. Of course, the presence of the diffuser pattern results in an unsteady relative flow in the impeller; the relative fluctuations caused are not at all insignificant since they amount to as much as 25% of the relative dynamic pressure. Just what this oscillation means to the relative flow is not at all plain, and we have not attempted further analysis of it. What is most important to deduce is what sort of average of the circumferential static pressure pattern is meaningful to the impeller processes.

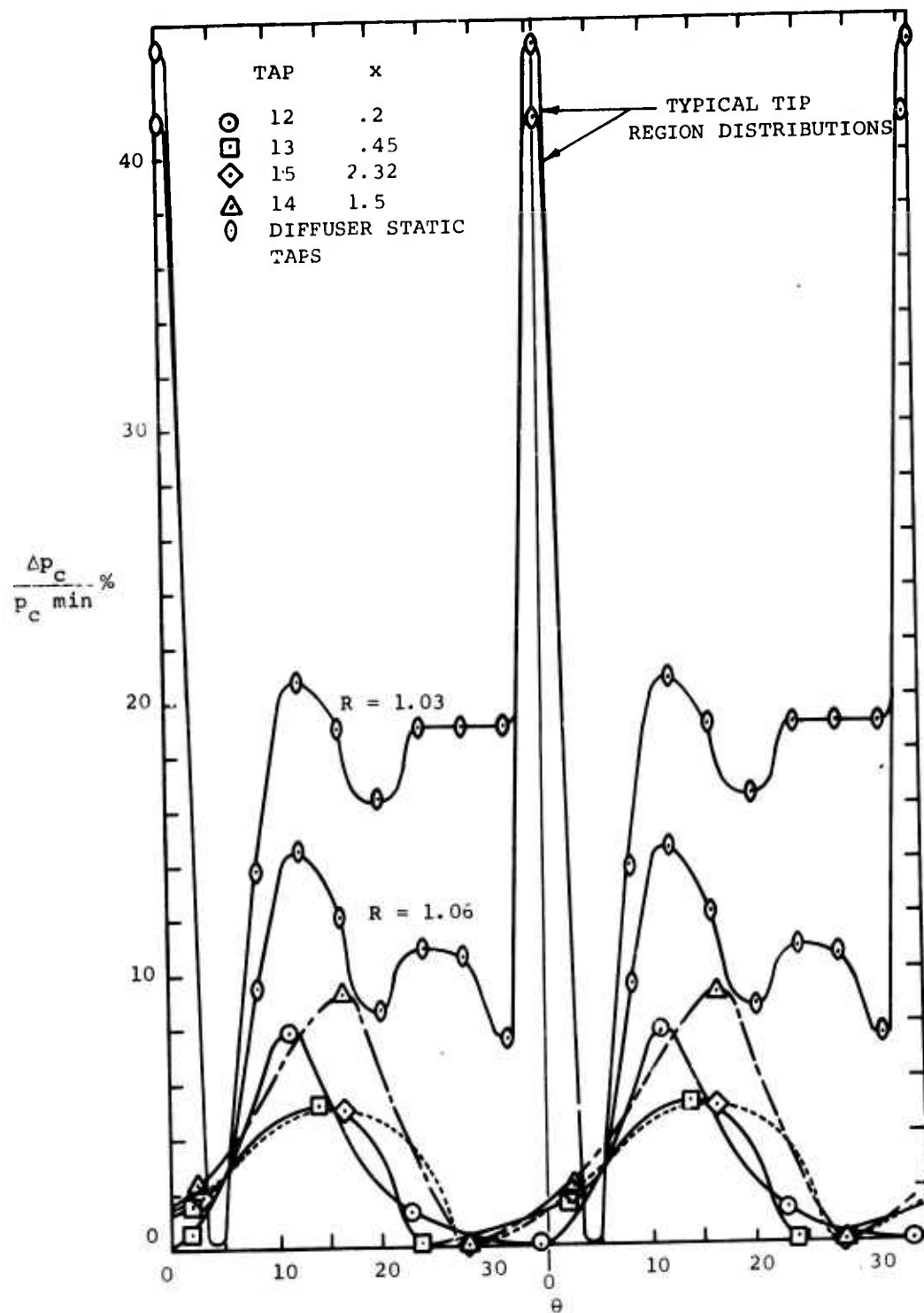


Figure 93. Tangential Variation of Cover Pressure.  
RF-2

The circumferential oscillation of as much as 1-1/2 psi peak to peak in the inducer caused concern. As will be shown in Section 5, an increase in pressure recovery in the inducer of only 0.8 psi would yield a 3-point gain in stage efficiency. During the diagnosis of inducer behavior, the 3/4-psi difference shown in Figure 93 between the peak and average values is a sizable fraction of the pressure recovery in the inducer. Should one use peak or mean pressure as significant for boundary layer calculations and computing recovery?

Our studies in Section 5.4 of the impeller data suggest that the cover static pressure tap readings are fluid dynamically and thermodynamically significant when interpreted as time averages of the fluctuating pressure at the tap orifice and then linearly averaged around the circumference. The scheme for averaging the data from a single tap is illustrated in Figure 94.

The main reason for our confidence is that all the evidence seems to fit together well. However, it must continuously be remembered that we probably know the significant pressure distribution at the inducer tip to only  $\pm 1$  psi; this uncertainty band of inducer diffusion ratio is equivalent to  $\pm 4$  points in stage efficiency.

Additional disturbance of the static pressure tap readings caused by the passage of blading under the taps, hence turbulence by them due to tip leakage, etc., leads to some uncertainty, no doubt. However, we estimate that these effects produce a much smaller uncertainty than the limited sampling made by Boeing of the spatial circumferential pressure distribution on the cover.

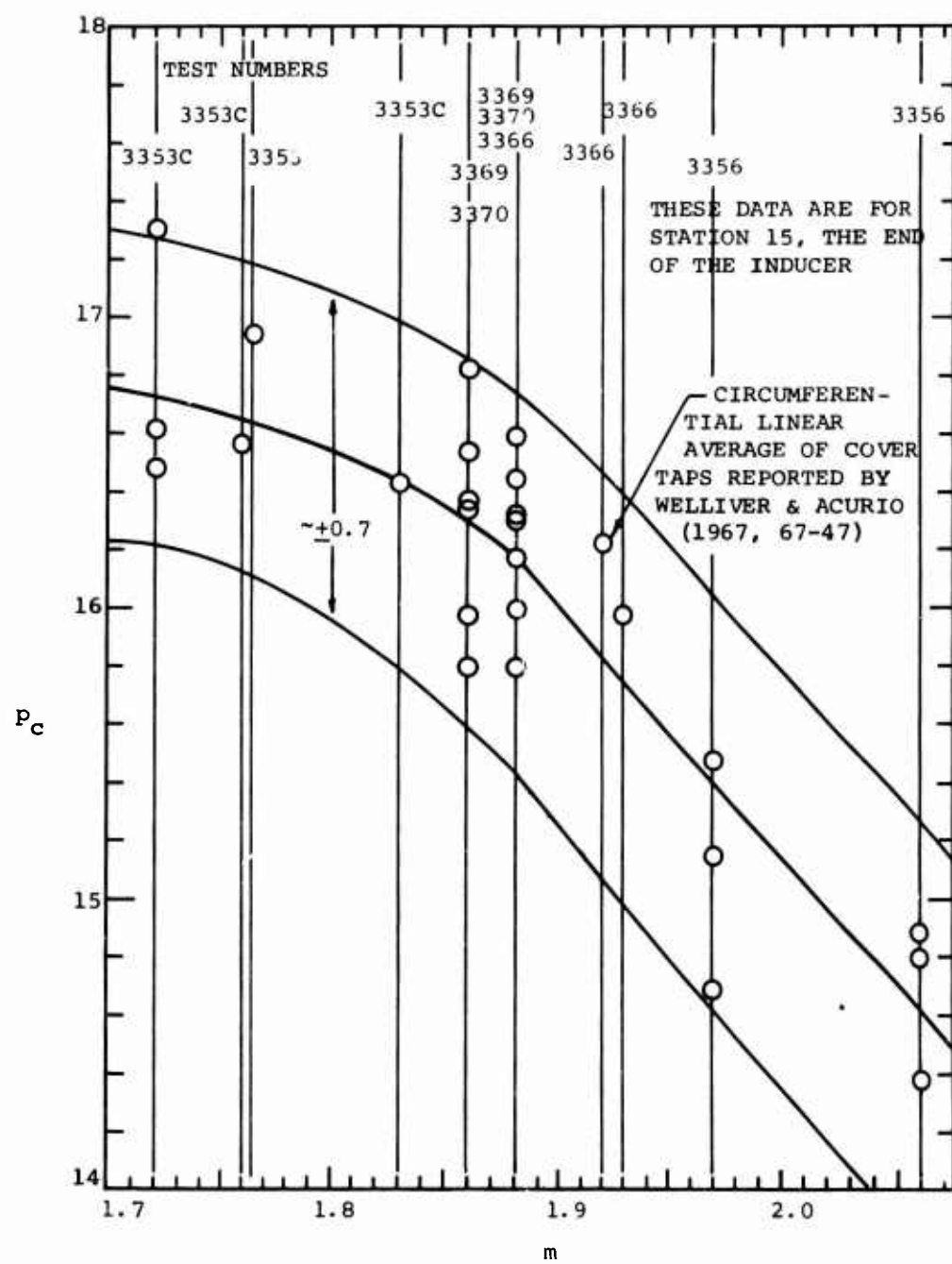


Figure 94. Cover Static Pressure (Station 15) Versus Mass Flow.  
RF-2

## 4.2 SIGNIFICANCE OF IMPELLER TIP MEASUREMENTS

### 4.2.1 Introduction

One of the major purposes of this examination of the Boeing-AVLABS data has been to test the quality of the prediction models available. Should these prove lacking, better prediction models were to be developed. Newly developed analyses should strongly highlight the important flow mechanisms with a detailed, quantitative understanding of their nature so that design means for a major improvement in stage performance can be found.

It is impossible to test the quality of the prediction models without asking, what information is contained in the indications of the aerodynamic probes employed in the Boeing-AVLABS program? Because we know that probes do not necessarily indicate fluid-dynamically and thermodynamically significant averages, there may be considerable information lost. Indeed, the indications of probes may not allow a sufficiently precise calculation of even the average fluid state at a given station in the machine. If this be so, then their indications cannot be employed as a significant test of the prediction models.

One serious data interpretation anomaly persisted through the Boeing-AVLABS program. That is, the impeller discharge mixing loss model seems to fall short by approximately a factor of 2 from predicting the magnitude of the stagnation pressure loss between the impeller tip and the diffuser throat. The existing situation in this regard is displayed in Figures 95 and 96.

No means had been found whereby the input variables could be adjusted satisfactorily to conform both to the magnitude of the total pressure loss observed (between the impeller tip probes and the diffuser throat probes) and to the impeller discharge static pressure indicated by wall taps.

One possible explanation of this situation is that a loss mechanism exists, near the tip of the impeller, which is at least as powerful as the impeller discharge mixing loss mechanism hypothesized in the theory of Dean and Senoo.

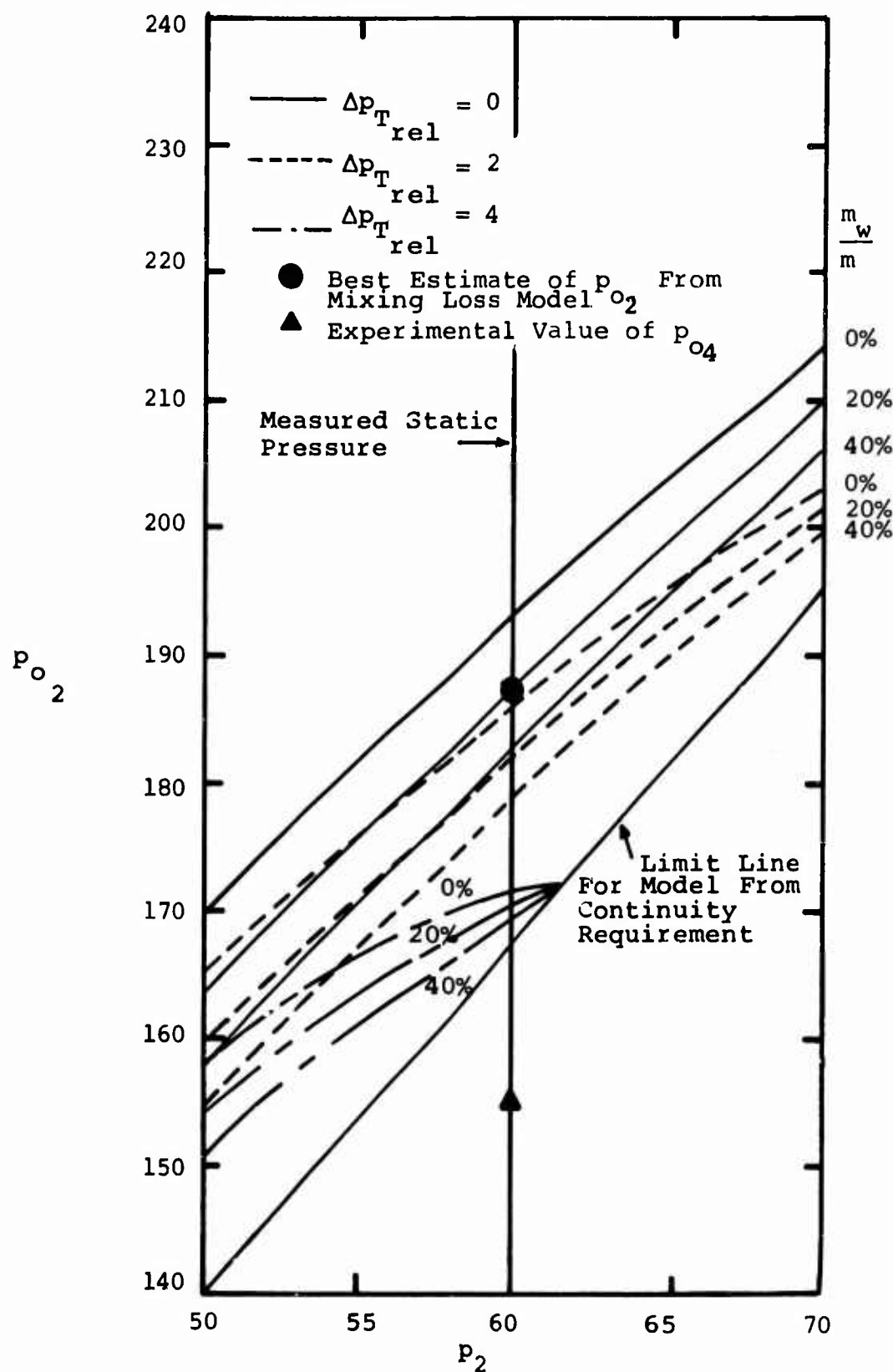


Figure 95. Workhorse Impeller Discharge Loss Calculations.

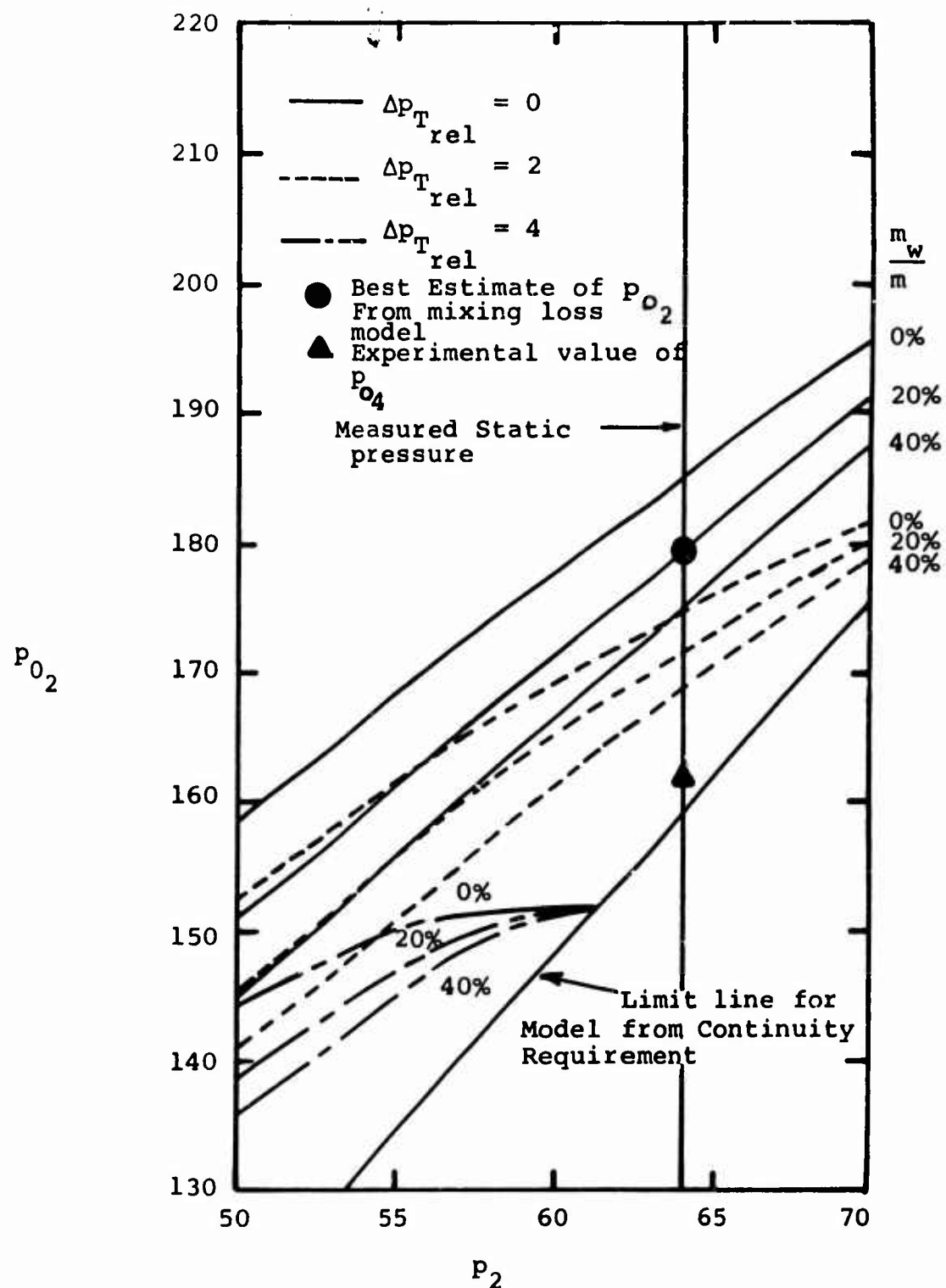


Figure 96. RF-2 Impeller Discharge Loss Calculations.

For instance, there may be major backflows on the hub and/or on the cover which mix with the fluid discharging from the impeller, causing an artificially high indicated slip factor,  $\sigma$ . Oil slick traces on the schlieren windows of the Workhorse stages, as well as other evidence discussed in Section 6.7, indicate that such backflows are present and that they may be of large magnitude.\* Further, it is likely that a backflow occurring in impeller space is modulated by the passage of the impeller past the diffuser vanes. The backflow situation thus is doubly unsteady; unsteady both in rotor and diffuser space. Therefore the low response instrumentation employed in the Boeing-AVLABS program could not reveal by any means the true nature of the backflow nor would the oil slick traces. If indeed the Boeing-deduced  $\sigma$  is too high by 0.04 - 0.06, the "missing" loss could be explained; too high a value of  $p_{j2}^o$  would be used from the

start. Compare, for example, Figures 23 and 83 with Figures 95 and 96.

Before we resort to an explanation of the missing 50% of the loss on the above basis or on the basis of suspicious loss mechanisms involving complex, three-dimensional, unsteady flow patterns, it is wise to ask, Do the indications of the probes used give meaningful quantities which, when injected into the two-dimensional discharge mixing loss model provide a fair measure of the impeller discharge mixing losses? Or, in other words, Do impeller tip instruments of the usual sort allow a meaningful separation of losses between impeller and diffuser? The purpose of this section is to answer these questions in as realistic a fashion as possible.

The strategy is to use realistic three-dimensional impeller discharge flow patterns, steady in impeller space, derived from low-speed measurements and visualization studies of centrifugal compressors and pumps. With realistic flow patterns, we can then determine what the meaning of instrument indications is relative to fluid dynamically and thermodynamically significant properties of the flow and to the predictions of the mixing loss model.

---

\* The oil trace patterns in Figures 33 and 34 show the backflows even though they are for lower rotative speed.

#### 4.2.2 Input Information

Nowhere in the centrifugal compressor open literature have we ever found any reliable and competent detailed measurements of the discharge flow pattern from a centrifugal impeller.

The principal reason for this lack is that the flow is in almost every case separated, three-dimensional, and often unsteady. Therefore, high-response-rate and high-resolution instrumentation is absolutely essential to making meaningful measurements.

Further, because it is vital to deduce the relative flow pattern, while it is by far easier to measure the absolute pattern, an unsatisfactory transformation must be made between absolute and relative coordinates. For instance, significant changes in relative velocity, magnitude, and direction can lead to changes in absolute velocity direction but only to negligible changes in absolute velocity magnitude. So both the magnitude and the associated angle of the absolute outflow must be measured in time and space. Because the relative flow is often unsteady, the angle and magnitude measurements must be made simultaneously. These demands require a high order of instrumentation science and technique, which has rarely been applied to this problem.

In this vacuum of good measurements, we must turn to other evidence. Various investigators have made visualization studies of flow in centrifugal machinery. Of course, almost all of this work has been done at very low speeds, but experience teaches that the general messages derived at low speed are applicable qualitatively to high-speed machines. Also, studies of many sets of conventional internal data for high-speed machines help to sort out the possible from the impossible. Finally, the application of fundamental dynamics and thermodynamics gives a fair idea of the nature of the flow even though the problem is so complex as to be analytically intractable.

From these various sources, we have derived over the years a qualitative picture of the flow pattern leaving a centrifugal impeller; the picture has held up reliably

against all the data we have studied in detail. However, it is impossible to use this picture in a quantitative way for establishment of the exact flow conditions at the tip of a particular impeller.

In the work below, where we shall examine the indications of conventional instruments installed at the impeller tip, it is not critical that we have an exactly representative flow pattern for the Workhorse or RF-2 impellers. Rather, what we need is something sufficiently typical so that the estimates made of the significance of the instrument indications are not misleading. While we cannot prove the matter, we are of the firm opinion that the diagnosis of instrument indications made herein is a reliable assessment of the situation.

From the impeller analysis, the measured static pressure at the impeller tip, the mass flow rate, the impeller geometry, and the inlet stagnation conditions, we can deduce the relative Mach number of the through flow at the impeller tip, the area of the separated wake region (i.e. blockage), constrained only by the necessity for assuming an internal impeller relative total pressure loss for the through flow and a mass flow fraction for the wake.

As will be shown in Section 5.4 the Boeing-AVLABS data demonstrate practically nil relative total pressure loss for the through flow.

We have no accurate way to assess the mass flow through the wake region at discharge, although our experience suggests that the magnitude is about 20% of the total flow for the Boeing-AVLABS type of impeller. Also, examination of Figure 96 shows that a large alteration in the assumed mass flow fraction for the wake does not greatly change the impeller discharge mixing loss nor the mixed-out properties of the flow.

We shall assume below, as a result of these considerations, that there is no relative total pressure loss in the through flow jet and a 20% mass flow fraction in the wake.

With this information, we still lack means to set the relative outflow angle of the through flow. We also have

not yet established the geometrical shape of the jet and wake regions.

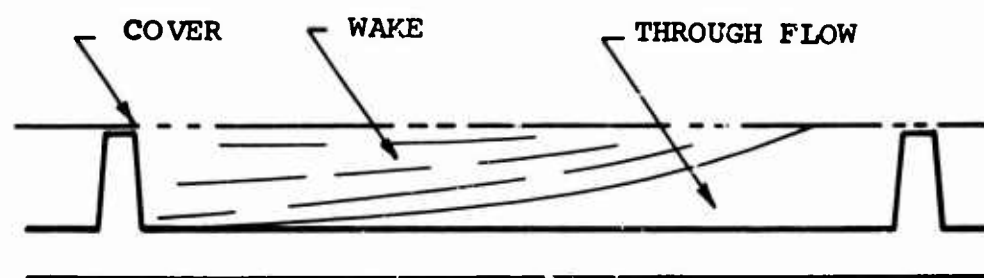
The relative flow angle could be set if we had information available on the slip factor. We do have some data from the Boeing-AVLABS program on what is supposed to be the mass-flow-average slip factor for Workhorse and RF-2. These numbers are 0.93 and 0.88 respectively. We shall argue in Section 6.7 for RF-2 that the Boeing-deduced slip factor is too high and should be more on the order of 0.84. This value was used here to set up a typical discharge flow pattern.

Even with a mass-flow-averaged value, we do not know per se how the slip factor is distributed over the discharged flow. Because the relative velocity is low in the wake as shown by various investigators, by hot-wire measurements, and by relative static pressure distribution measurements, the wake slip factor must be very close to 1.0; it will be assumed to be such. In the through flow jet, the width of the jet in the  $r-\theta$  plane will vary from cover to hub and so should the slip factor. Lacking a better model, we will use one of the classical potential flow models for the deviation between the flow and the blading. Stanitz's and Busemann's versions are typical candidates (see Wiesner, 1966).

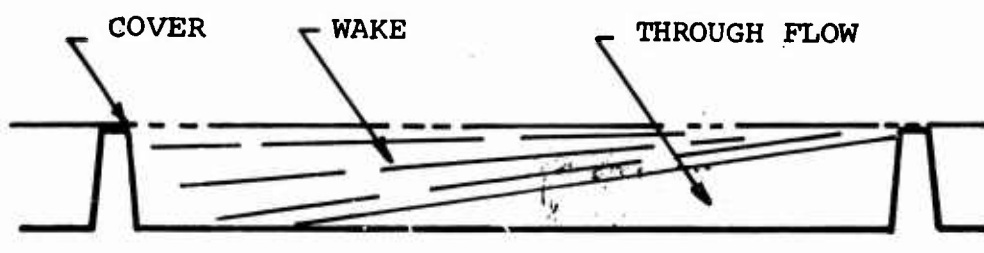
In employing these models, the conventional flow width parameter (the distance between the blades) is replaced by the local  $r-\theta$  plane width of the through-flow jet. The slip factor varies from cover to hub, decreasing toward the hub because the through flow is wider there than on the cover.

If the Stanitz or Busemann equations are used without modification, the slip factors derived prove to be too high when integrated and compared to values deduced from the Boeing-AVLABS data. Therefore, the form of the Stanitz relationship for slip factor was preserved, but values were reduced by an integration constant which gave a mass-flow-averaged value that satisfied the Boeing-AVLABS data.

For the geometry of the outflow, we have less certain grounds. However, visualization studies have shown that the through-flow jet tends to be skewed in the manner shown in Figure 97.



FROM FLOW VISUALIZATION STUDIES



ASSUMED FOR COMPUTATION

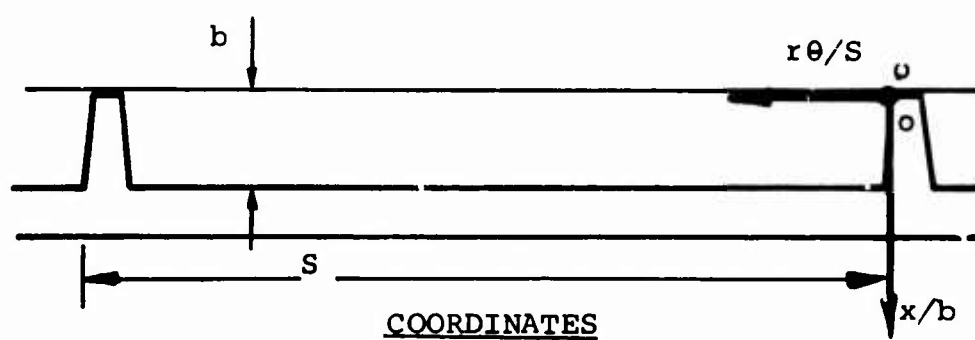


Figure 97. Schematic of Impeller Outflow Pattern.

This skewing is caused by the through-flow stream separating from the cover and running up the hub side. The phenomenon is identical to separation in a pipe bend. However, in a rotating impeller, the Coriolis forces will eventually drive the separated flow back onto the pressure surface, which is the only place where it is stable. So the separation in the impeller tends to be skewed as illustrated in Figure 98, and the separated through-flow stream tends to twist as illustrated in Figure 99.

The reason that the slip factors are lower for this flow pattern than would be predicted by the straight application of the classical slip factor theories is that relatively strong secondary flows occur in the passage as the through-flow stream adjusts under the impulse of Coriolis forces back onto the pressure surface. These lead to relative flows as illustrated in Figure 99, which on the hub obviously increase the relative tangential velocity in the negative direction and lower the slip factor.

Again, we emphasize that the purpose in choosing this flow pattern was not to predict the flow out of the Boeing-AVLABS impellers but rather to adopt a reasonably authentic relative flow pattern which can be used to evaluate the inherent errors of the Boeing-AVLABS measurements made near the impeller tip.

Because Workhorse and RF-2 impellers had rather sharp bends to radial, we estimate that the through-flow jet is quite skewed at the impeller tip. Therefore, we have adopted the model shown in Figure 97.

The square envelope curves shown in Figures 100 to 103 were drawn from the above criteria. The curves were then smoothed by hand to attempt to simulate more reasonable boundary conditions for the flow variables. The static pressure was then calculated and is plotted in Figure 104.

#### 4.2.3 True Mixing Loss

One of the most important objectives of measurements near the impeller tip is to separate losses attributable to the impeller from those caused by the diffuser. Impeller

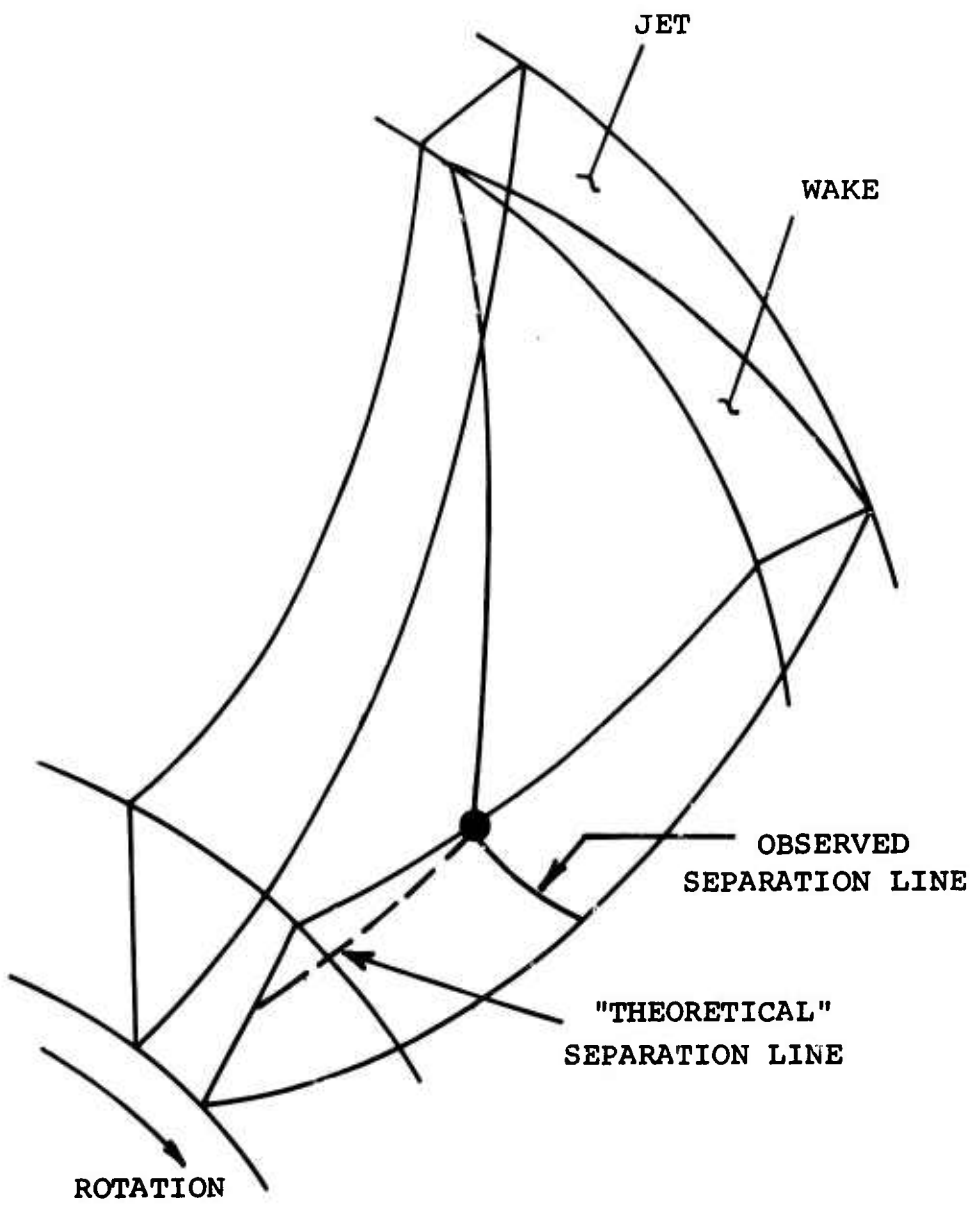


Figure 98. Separation Line Geometry.

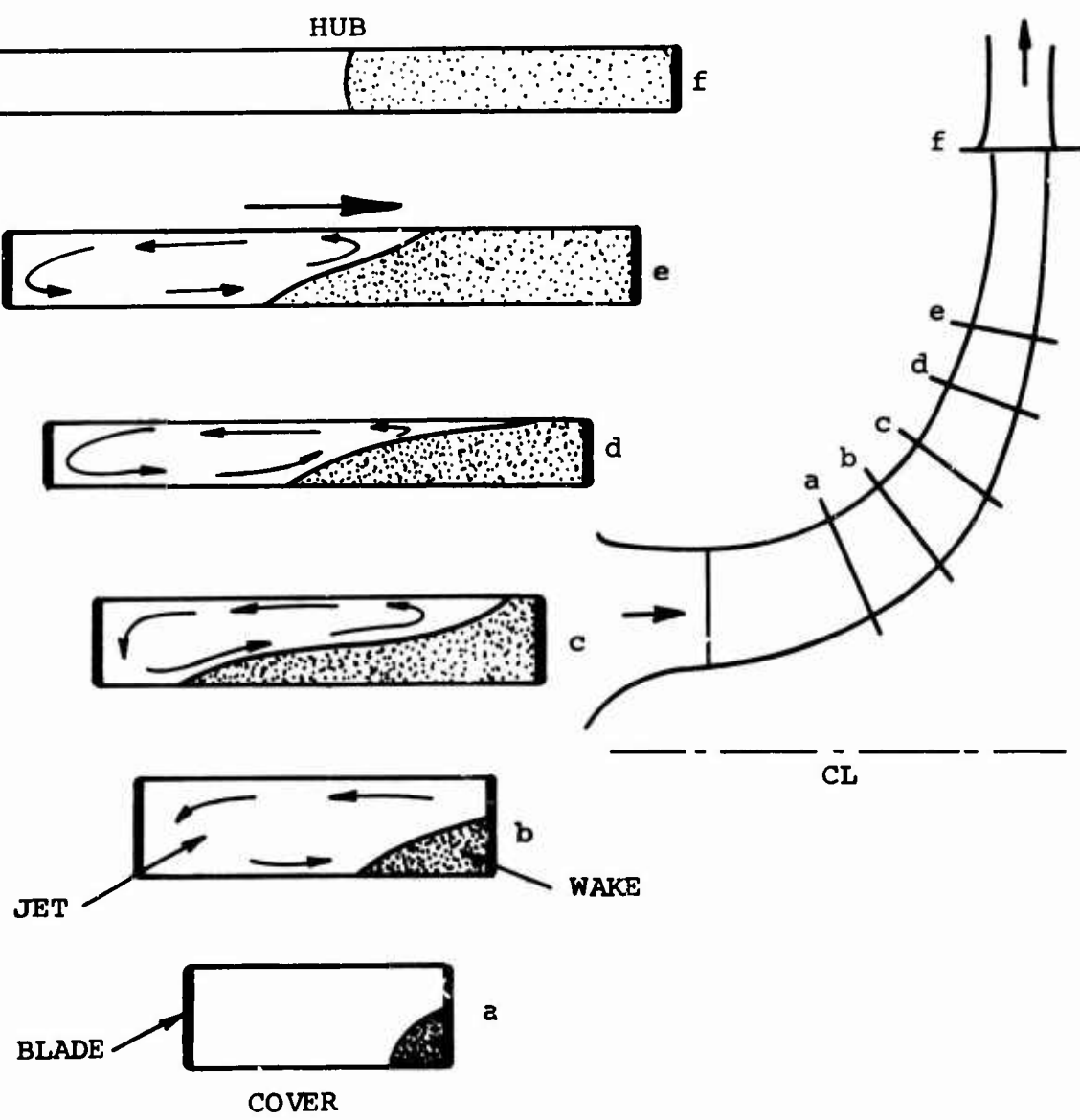


Figure 99. Development of the Wake.

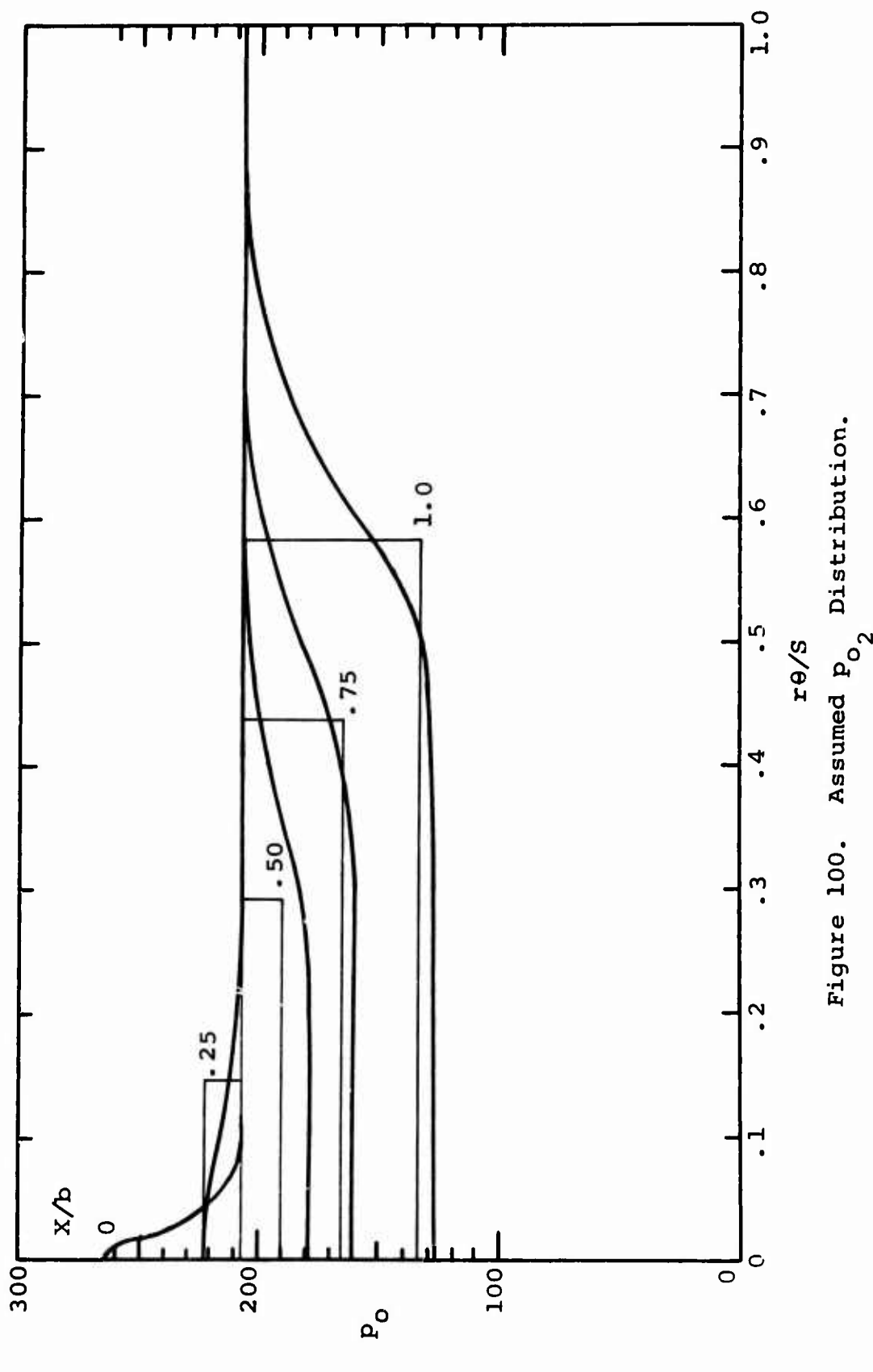


Figure 100. Assumed  $p_{O_2}$  Distribution.

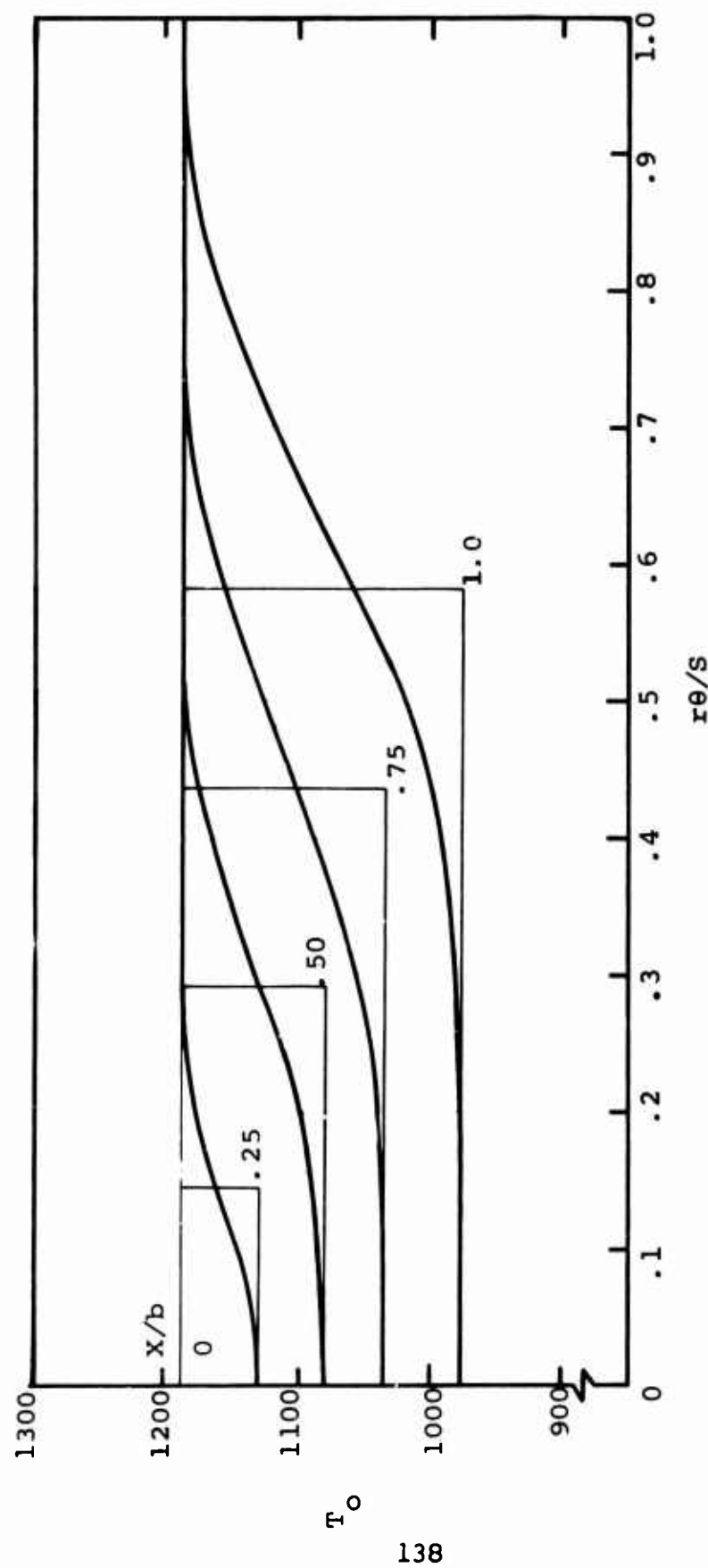


Figure 101. Assumed  $T_{o_2}$  Distribution.

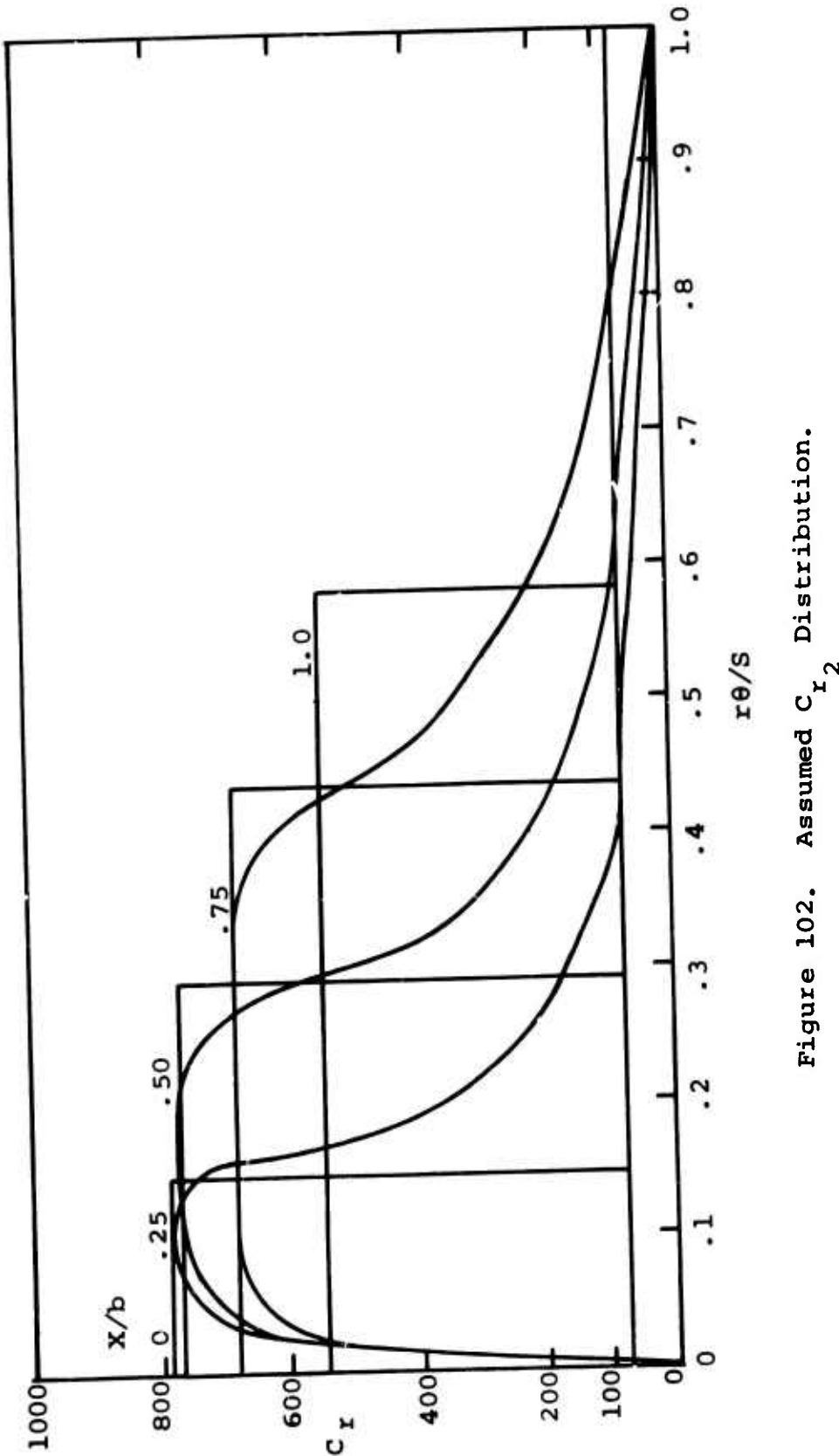


Figure 102. Assumed  $C_{r_2}$  Distribution.

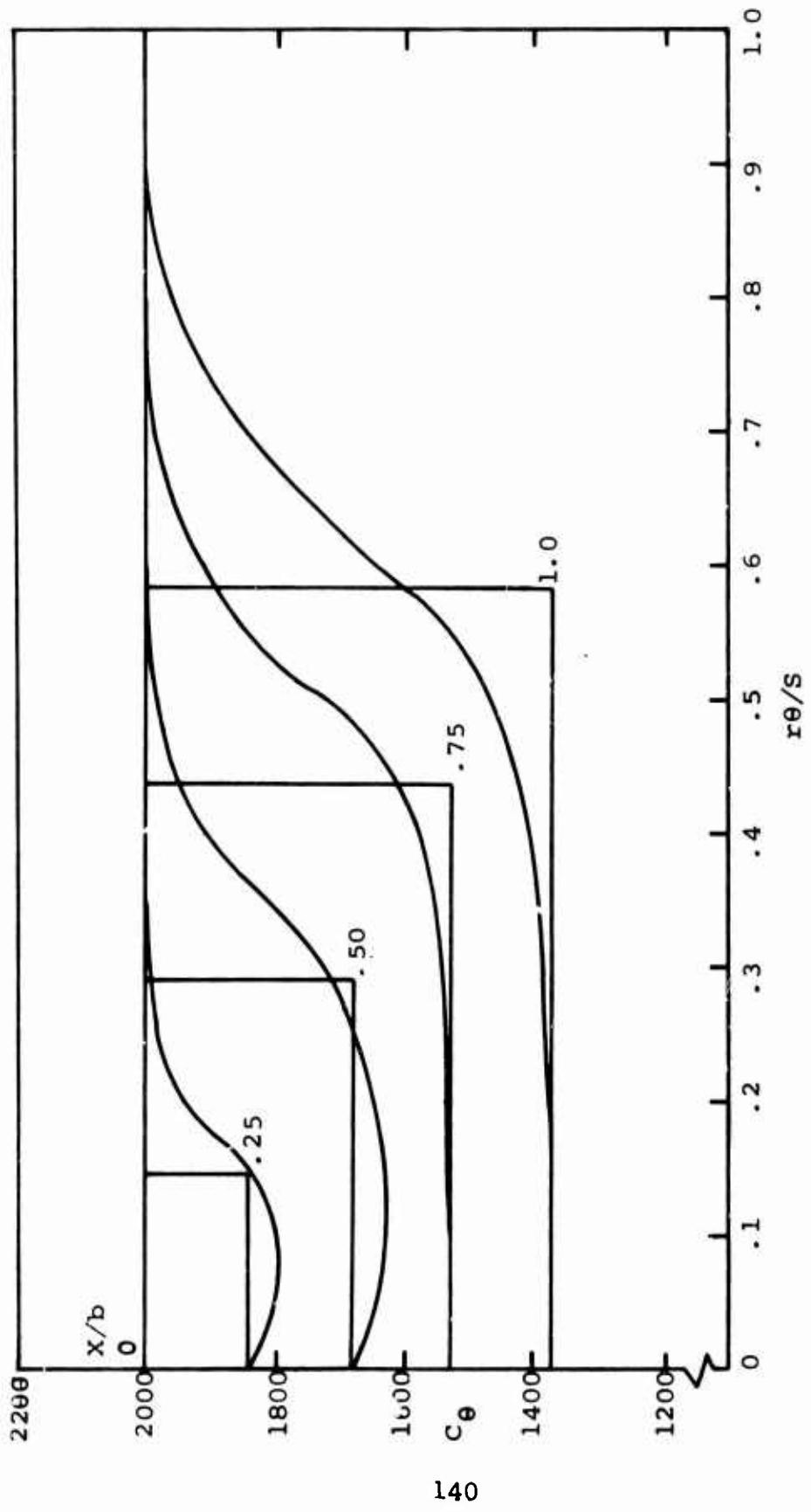


Figure 103. Assumed  $C_{\theta_2}$  Distribution.

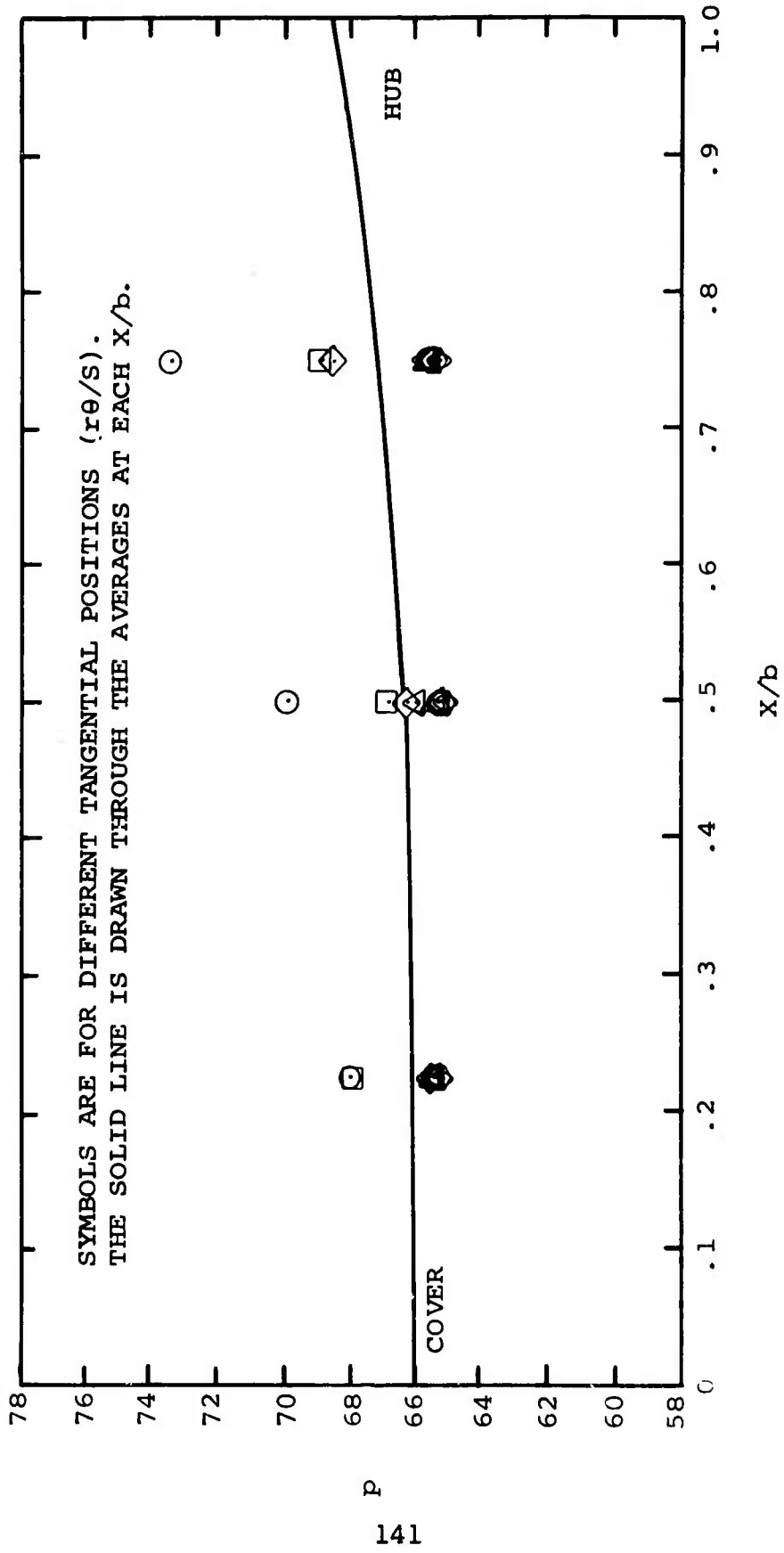


Figure 104. Calculated  $p_2$  Distribution.

discharge mixing loss can be a large fraction of the total loss engendered by the impeller. This loss is often calculated by the theory of Dean and Senoo (1960) as simplified by Johnston and Dean (1965) and modified for compressible flow and a three-dimensional discharge pattern (see Appendix II). In order to use the theory, it is necessary to evaluate various flux integrals at impeller discharge.

Conventionally, the flux integrals are calculated from the indications of probes inserted near the impeller tip such as the stagnation temperature rakes installed at approximately  $R = 1.03$  in the Boeing-AVLABS tests. Also, static pressure data from the sidewalls and yaw angle traverses may be employed. Because the instruments have a low response rate, they produce some sort of an "average" of the tangential variations at their particular  $x$  location.

For instance, if there were a complete stall on the cover, stagnation pressure and temperature and wall static indications could be relatively unaffected. The only evidence of the stall would be found in angle measurements; we shall show shortly that these are the most suspect of all the instrument indications. So it could be easy for mass flow to be indicated near the cover in the integrations of the conventional data, where in fact there would be none. For these reasons, considerable suspicion surrounds the thermodynamic and fluid-dynamic meaning of instrument indications at the impeller tip and the various sorts of averages that must be calculated from them in order to separate losses and determine fluid dynamic work input.

In order to assess the seriousness of this situation, the flow pattern, Figures 100 to 104, was injected directly into the mixing loss calculation in order to produce a "true" mixing loss. Then, various (mathematical) instruments were tracked through this pattern in order to deduce their indications. The indicated readings were then used in the conventional fashion to form the flux integrals and an "indicated" mixing loss was computed. Finally, the "instrument indicated" and "true" losses were compared. We discovered that there is a major difference between the "true" and "instrument indicated" values.

### Procedure for Calculating "True" Mixing Loss

The flow properties shown in Figures 100-104 were integrated according to the demands of the Dean-Senoo mixing loss theory presented in Appendix II. For that, integrals of radial and tangential momentum flux, stagnation pressure (entropy), and stagnation enthalpy flux, along with the static pressure area integral for force, were made by computerized finite difference double integrations.

The result is summarized in Table VI and compared to the "instrument indicated" mixing loss and mixed out flow properties.

#### 4.2.4 Instrument Indications

Because no detailed time and spatial distributions of flow properties at the tip of the impeller are available for the Boeing-AVLABS compressors (or for any other high-speed machines), it is impossible to determine from actual data what the meaning is of instrument indications.

Various workers have considered this question in the past; the matter has been explored to a certain extent for turbines and axial compressors; for example, Wong and Stewart (1955), Hubbard (1963), Stein (1960). Dussourd (1962) considered pressure measurements and their meaning for centrifugal impeller inducers. In certain cases the studies have considered how instrument indications relate to flow properties meaningful to turbomachines. But usually the interest in the investigation is concentrated more on how a given probe responds at a point to the unsteady flow. For instance, Delio et al (1949) and Johnson (1955) dwell on the response of pneumatic probe systems in unsteady flow fields. Moffat and Dean (1967) studied the response of total temperature probes installed in the tip of centrifugal impellers.

These works give us a fairly reliable means for calculating the indications of various conventional instruments providing that we have prior knowledge of the detailed flow pattern. However, if the nature of the flow pattern is unknown in advance, it is impossible to deduce the flow pattern from the averages produced by the instruments, even if the full

physical theory of the instrument response is known. This fact is fundamental; essential information on the nature of the flow pattern is inherently lost in the averaging process and can never be recovered!

It turns out for calculations such as the impeller discharge mixing loss that the detailed nature of the distortion is of great importance because the required integrals of fluxes are not linear. For example, the tangential momentum flux is given by the integral

$$\iint \rho C_r C_\theta r d\theta dx$$

By multiplying together "average" values at a given axial position of  $\rho$ ,  $C_r$  and  $C_\theta$ , one does not produce a meaningful average of  $(\rho C_r C_\theta)$ . The same is true for all the other flux integrals. Only by having the detailed three-dimensional distribution relative to the impeller of these properties can the flux integrals be made properly when the flow is steady relative to the impeller.

A further complication is that the flow relative to the impeller is likely to be unsteady, so that the flux integrals must be triple, i.e., made in time as well as in space. Therefore, to do the calculation correctly, the three-dimensional spatial and time distributions of the subject properties must be available. Without these, it is impossible to calculate the mixing loss accurately from the theory and, of course, it is impossible to test the theory against the "observed" losses.

One of the principal purposes of this program is to ascertain the viability of the various prediction models now available for centrifugal stages. From what has been said above, it is obvious that this cannot be done in a definitive way with the data we have from the Boeing-AVLABS program. But, we can estimate the magnitude of the error inherent in attempting to test the theory. Of particular concern here is the impeller discharge mixing loss theory.

In order to get an estimate of the inherent error involved, "instrument indicated" flow properties were needed as input

to the mixing loss theory. Using the detailed flow distributions shown in Figures 100-104, the instrument indications given by the types of probes used by Boeing were calculated; then these were put into the mixing loss theory, and the "loss" calculated. This "instrument indicated" loss is compared in Table VI to the "true" loss calculated from the full double integration of the flux quantities from the full three-dimensional distribution of Figures 100-104.

In this process, we are ignoring the impeller relative unsteadiness of the flow pattern because we have no reliable information on that. It is possible that the errors calculated could be significantly larger if the time variance of the flow pattern were incorporated also. However, it is likely that spatial distortion is responsible for the bulk of the actual error, so what we shall do below will give fair measure, it is believed, of the inherent error using experimental observations to deduce the level of the impeller discharge mixing losses.

In the centrifugal stage, the flow is more distorted at the impeller discharge than anywhere else. Therefore, we expect inherent errors produced by using low response rate instrument indications to be smaller in other parts of the machine. Nevertheless, as indicated in Section 6.7 the uncertainty caused by unsteady flow in the diffuser channel entry is also estimated to be significant.

#### Response of Instruments

We are concerned in the Boeing-AVLABS data with wall static taps, simple and Kiel-type stagnation pressure probes, pneumatic cobra-type yaw meters, and stagnation temperature probes. The types of instruments used by Boeing are shown in Figures 7 and 18. The response of these instruments to unsteady conditions at their sensing orifice will now be discussed.

#### Wall Static Taps

Welliver and Acurio (1967) consider the response of pneumatic instruments and conclude that they tend to indicate according to their form:

- Form (1) A time average of the static pressure at the instruments' sensing orifice when a long, constant-diameter tube is connected to the tap.
- Form (2) An rms average when the sensing orifice is sharp and expands immediately into an enlarged chamber.

We have further consulted available theory and experiments and concur with Welliver and Acurio.

Because Boeing's wall static taps were Form (1), we will assume that they time-average the fluctuating static pressure at their sensing orifice (subject to the fixed errors - see Section 4.3).

#### Stagnation Pressure Probes

The construction of the Boeing stagnation pressure probes was Form (1) for both the simple-tube type and the Kiel type. Because the actual angle fluctuations in the compressor were relatively small and stagnation pressure readings remain within a  $\pm 1\%$  error over a range of at least  $\pm 15^\circ$  of flow incidence, in a steady flow, we will assume that the flow angle fluctuations did not affect the averaging process. Therefore, stagnation pressure probes of both types will be assumed to time-average the fluctuating stagnation pressure at their sensing orifice.

If the flow is supersonic, the time-average stagnation pressure will correspond to the one-dimensional normal shock value ( $p_{oy}$ ) downstream from the probe's bow shock, which is assumed to have an upstream Mach number ( $M_x$ ) equal to the free stream Mach number at the point where the tip of the probe lies.

Because the Mach numbers involved below will not exceed about 1.4 and the stagnation pressure loss across the shock is only 4%, no significant error is introduced by correcting for the shock loss after the averages are made rather than before. This may be done because the flow Mach number at the tip of the stagnation probe does not vary much. Correction for the influence of fluctuating conditions on the shock is insignificant.

### Yaw Probe

The "cobra"-type yaw probes used by Boeing are shown in Figures 7 and 18. A stagnation pressure tube is held between two yaw tubes cut off at a 45° angle\* to the tube axis.

To our knowledge no data are available on the dynamic response of cobra-type yaw probes.

It is reasonable to assume that the angle indicating orifices on each side of the yaw probe time-averaged the fluctuating pressures at their sensing orifices. This implies that the pressure difference indicated between the yaw tubes is the time-average of the instantaneous pressure difference between the two yaw orifices. However, it is necessary to determine how the instantaneous pressure difference varies with the flow incidence angle onto the probe.\*\*

First, we shall assume that the probe is insensitive to pitch angle variation perpendicular to the plane of the yaw probes. (Such probes are quite insensitive to pitch in steady flow.) Secondly, we must develop some relationship between the yaw angle (in the plane of the tube) and the instantaneous pressure difference. No information is available on this subject, to our knowledge. Therefore, we have assumed that the instantaneous pressure difference varies with incidence angle in unsteady flow exactly as it does in steady flow. Figure 105 is a steady-flow plot for the Boeing-type yaw probe of the pressure difference vs. yaw angle. A straight line of slope K has been fitted over the range of interest.

In the Boeing work, the probe was nulled; that is, the probe was rotated in the flow until the indicated pressure difference on slow response readout gear was zero (see Welliver and Acurio, Volume I of 67-30).

\* This angle is not given by Welliver and Acurio; it was measured from their illustrations.

\*\* The yaw angle error due to radial gradients of properties is negligible, as shown in Appendix I.

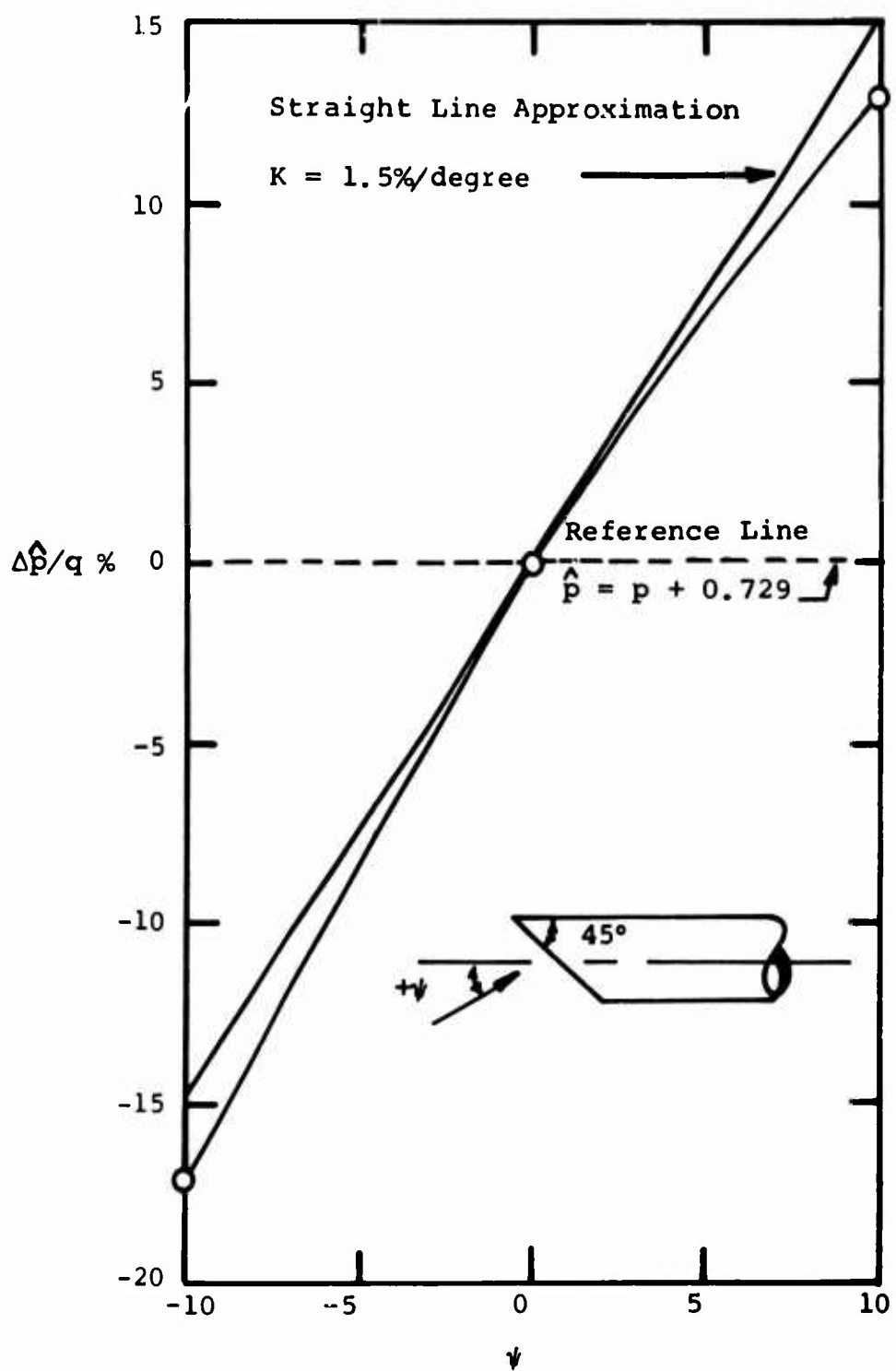


Figure 105. Steady-Flow Yaw Angle Sensitivity of Cobra-Type Yaw Probes.

The instantaneous pressure difference at the tip of the probe may be written:

$$\Delta p \approx 2Kq\psi$$

where the factor of 2 accounts for the fact that a yaw probe uses 2 yaw tubes.

The time average will be

$$\bar{\Delta p} = \frac{1}{t} \int_0^t 2Kq\psi dt \approx 2K(\bar{q}\psi) = K \frac{(\rho C^2 \psi)}{g_o}$$

At higher Mach numbers,  $q$  should be replaced by  $(p_o - p)$  and the effects of shocks on the probe taken into account in determining  $K$ . However, the general relationship above should remain unchanged by these effects, although the magnitude of the errors will be affected somewhat.

When the probe-indicated pressure differential goes to zero,

$$\hat{\Delta p} = 0$$

then the probe is said to be nulled.\*

Since the probe time averages the flow it sees,

$$\hat{\Delta p} = \bar{\Delta p}$$

then

$$\overline{(\rho C^2 \psi)} = 0$$

\* A bar over quantities ( $\bar{f}$ ) identifies a time average; ( $\hat{f}$ ) identifies the probe indication on slow-response readout equipment. This may or may not be equal to time, spatial, or mass-flow averages.

Note that the time-average yaw angle ( $\bar{\gamma}$ ) is not necessarily zero when the probe is nulled. There will be an error in the indicated angle of the time-average flow direction because the yaw probe is also sensitive to density and velocity fluctuations. As a result we can expect that the angles measured by Boeing contain a systematic error (i.e.,  $\hat{\alpha} \neq \bar{\alpha}$ ).

The size of this error will be calculated for the flow pattern of Figures 100-104.

#### Total Temperature

Moffat has studied the response of the Boeing-AVLABS total temperature probe and offers a theory in Welliver and Acurio (1967), Volume II of 67-30. For the calculations here, we shall assume that

- (1)  $h$  (heat transfer coefficient) = constant
- (2) angle effects are negligible (probe set at  $\bar{\alpha}$ )

Using Equation 194 from the reference,

$$T_j = T_o - (1-A) C^2 / 2g_o J c_p$$

and the Energy Balance Equation

$$1/t \int_0^t h(T_j - T) dt = 0 \text{ (no net energy flux)}$$

Letting the period be one blade passage, and  $t = \theta/\theta_b$  blades, then

$$0 = \int_0^1 h(T_j - T) d(\theta/\theta_b)$$

From the above equation it is apparent that the junction is sometimes hotter and sometimes cooler than the air around it. Since  $h$  is constant, and for these frequencies,  $T_j$  is constant (within  $\pm 0.5^\circ R$ ),  $T_j$  will be the mean temperature of the surrounding fluid.

$$T_j = \text{the junction temperature} = \bar{T}_o - \frac{(1-A)}{2g_o J c_p} \bar{C}^2$$

The probe reading is corrected during ordinary data reduction for the effect of A, viz:

$$\hat{T}_o = T_j + \frac{(1-A)}{2g_o J c_p} (\hat{C})^2$$

Substituting the expression just derived for junction temperature,

$$\hat{T}_o = [\bar{T}_o - \frac{(1-A)}{2g_o J c_p} \bar{C}^2] + \frac{(1-A)}{2g_o J c_p} (\hat{C})^2$$

so:

$$\hat{T}_o = \bar{T}_o - \frac{(1-A)}{2g_o J c_p} [(\bar{C}^2) - (\hat{C})^2]$$

$A \approx 0.928$  (p. 277, Welliver and Acurio (1967, Volume II))

For the Boeing-AVLABS compressors, our computations have shown that  $\bar{C}^2 - \hat{C}^2$  is small enough that  $\hat{T}_o = T_o$  within  $2\text{--}3^\circ$  R. Thus for all practical purposes, the stagnation temperature probes perform a spatial (time) average of the stagnation temperature of the flow.

#### 4.2.5 Comparison of "Instrument-Indicated" Flow Properties and "True" Properties

Following the procedures of Section 4.2.4 and using the instrument characteristics and response assumed therein, we will now present the results of the instrument response error analysis.

##### Wall Static Pressure on Hub and Shroud

A relative distribution of static pressure is given in Figure 104. The pressure variations are small because a

uniform  $p_2$  base was the starting point in generating the three-dimensional pattern. A static pressure tap was assumed to track through the points on the walls and to time average. No account was taken of the 1/2 to 1% of dynamic pressure fixed error which should be produced by the Boeing wall static taps.

The results are:

$$\text{time average cover static pressure } p_s = 66.0 \text{ psia}$$
$$\text{time average hub static pressure } p_h = 68.5 \text{ psia}$$

The static pressure at the tip of the impeller proves to be an extremely critical piece of data (e.g., see Figures 95 and 96). The mean pressure at the impeller tip indicated by the Boeing wall taps (a linear average of hub and shroud pressure) is 67.25 psia. This number is normally injected into the mixing loss analysis in order to calculate the relative velocity of the through flow. A change in static pressure of 1 psi, under RF-2 conditions, will alter the relative velocity calculated by about 3% to 4%. The deviation between the "instrument indicated" static pressure for this case and that of the "true" static pressure is about 0.7 psi, so we can expect an error in calculating the relative velocity from the "instrument indicated" static pressure of as much as 3% locally.

#### Stagnation Pressure

The impeller discharge stagnation pressure is a vital characteristic of the stage. The "instrument indicated" distribution of stagnation pressure is normally mass-flow-averaged based on "instrument indicated" velocities, densities, and flow angles to yield an "instrument indicated" mass-flow-averaged stagnation pressure. This value is then employed to calculate impeller efficiency and as a base point upon which to swing the downstream stagnation pressure measurements in the diffuser in order to calculate diffuser losses.

In the data reduction procedure commonly used, there are several serious systematic errors which may be introduced through the nature of instrument response characteristics

and particularly because of the distorted three-dimensional flow pattern leaving the impeller. We plan here to explore the magnitude of these errors using the three-dimensional flow distribution in Figures 100-104.

The  $p_o^2$  distributions of Figure 100 were linearly (time) averaged in accordance with assumed stagnation pressure probe response (Section 4.2.4). The "instrument indicated" axial distribution of stagnation pressure,  $p_o$ , in Figure 106 resulted. Entered there also is the "true" stagnation pressure mass-flow-averaged in the tangential direction. For this particular case, the difference between the "instrument indicated" and the "true" stagnation pressure profiles is not large.

Note that the stagnation pressure is high in the low outflow (i.e., wake) regions of the impeller discharge because the work input there is considerably larger than it is for the through flow. So while there is a substantial entropy increase in the low outflow regions, the added work input holds the stagnation pressure up. In the high outflow region, the work input (slip factor) is considerably lower; so while the efficiency of the compression process in those regions is much higher than it is for the wake region, the stagnation pressure comes out about the same.

#### Flow Angle

Following Boeing's procedure, the mathematical probe is nulled so that  $(\rho C^2 \psi) = 0$ . Under these conditions, the flow will have an instantaneous incidence angle onto the probe given by

$$\psi = \hat{\alpha} - \alpha$$

where

$\alpha$  = true instantaneous flow angle

$\hat{\alpha}$  = instrument indicated angle on slow-response readout equipment

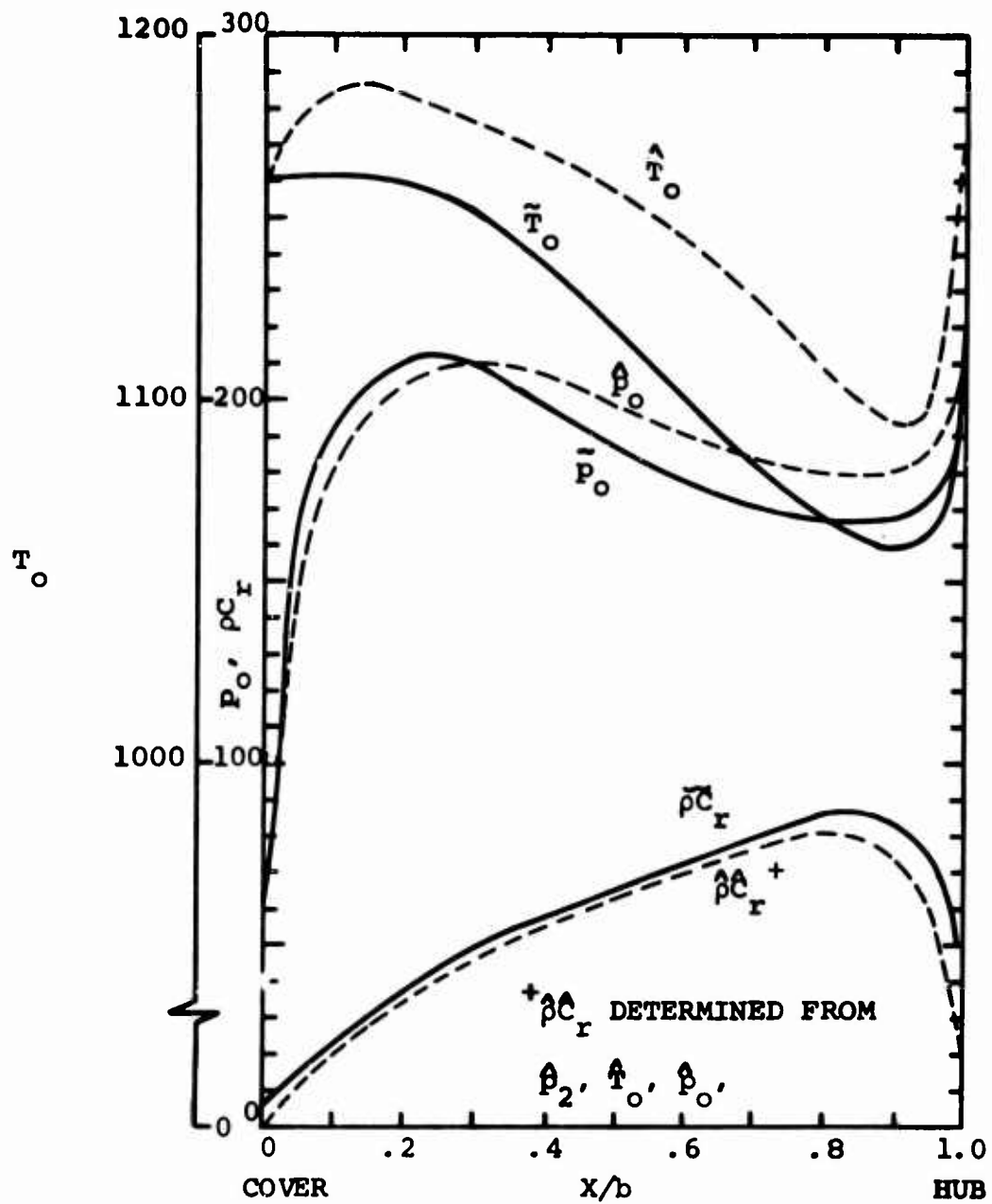


Figure 106. Comparison of "True" and "Instrument Indicated" Impeller Discharge Profiles.

When the probe is nulled,

$$\overline{\rho C^2}(\alpha - \hat{\alpha}) = 0 - \overline{\rho C^2 \alpha} - \overline{\hat{\alpha} \rho C^2}$$

so the indicated flow angle will be

$$\hat{\alpha} = \frac{\overline{\rho C^2 \alpha}}{\overline{\rho C^2}}$$

This is a sort of "dynamic-pressure-averaged" angle.

The error analysis procedure was to compute  $\hat{\alpha}$  for each of the three axial locations of the data in Figures 100-104. These "instrument indicated" angles were compared to the "true" angle distribution. Figure 107 compares the "true" and "instrument indicated" axial angle profiles.

No meaningful overall angle value can be calculated from  $\hat{\alpha}$ ; rather, we calculate a "true" average angle from the "true" mass-flow-average tangential velocity and the "true" bulk mean radial velocity (Table VI).

#### Total Temperature

The theory of total temperature probe response expounded in Section 4.2.4 has been used to calculate the stagnation temperature indicated by the probe. This analysis has shown that the probe reads the time-average stagnation temperature of the flow at its location within a maximum error of 3° Fahrenheit. Therefore, we can assume:

$$\hat{T}_o = \bar{T}_o$$

Of course we have not included uncertainties in instrument readout, calibration, etc., and have assumed that the probe data have been corrected for the recovery factor effect of parameter A.

While the probe gives an accurate time average, the reading is not thermodynamically significant. Rather, the mass-flow-averaged stagnation temperature is needed. The

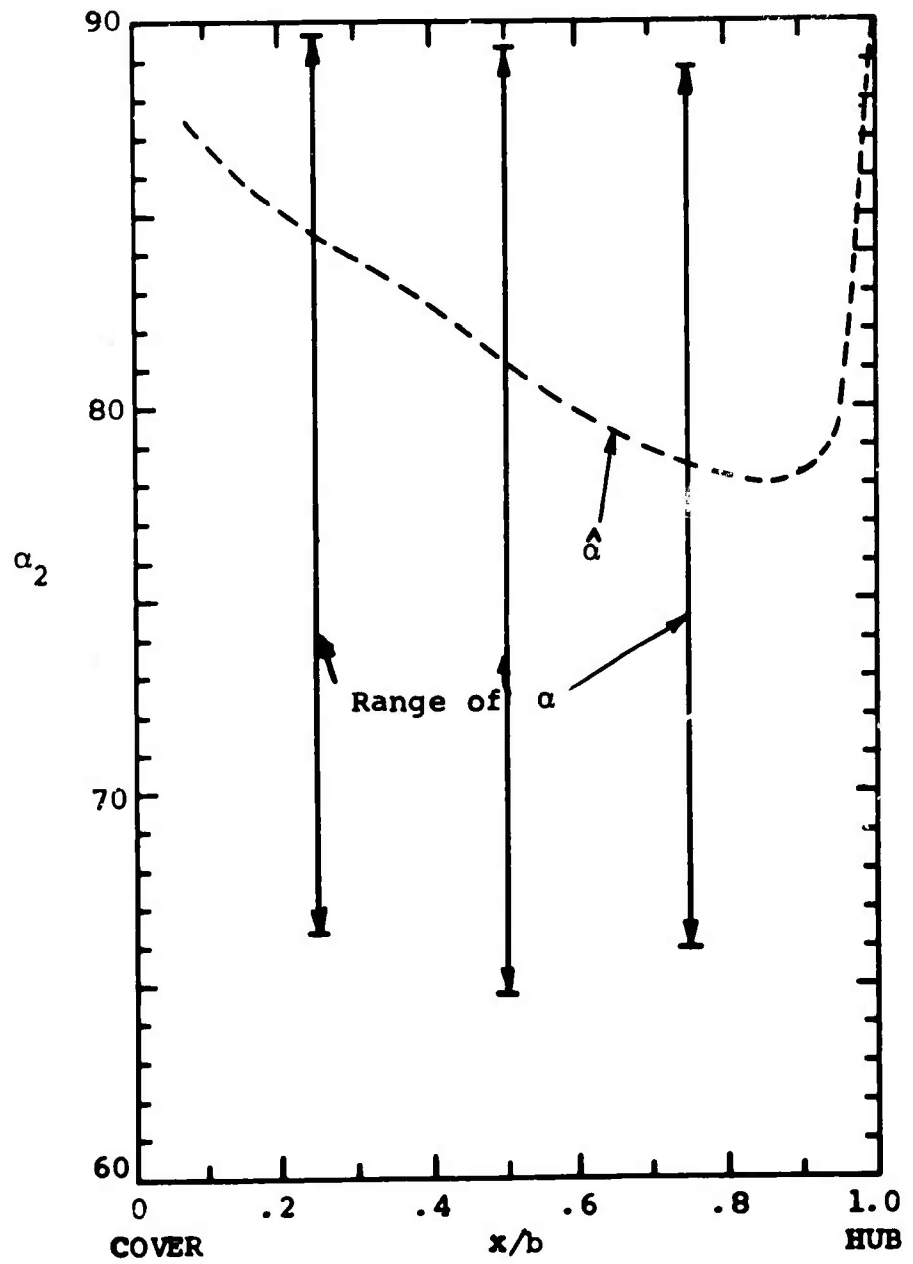


**Figure 107. Axial Flow Angle Distribution Comparison of "True" and "Instrument Indicated" Values.**

tangentially mass-flow-averaged "true" stagnation temperature  $\hat{T}_o(x)$  is given by

$$\hat{T}_o(x) = \frac{\int \rho C_r T_o d(r\theta)}{\int \rho C_r d(r\theta)}$$

In Figure 106 the probe "indicated" stagnation temperature and the tangentially mass-flow-averaged "true" values are compared. Note that maximum local errors of 45° F are estimated across much of the passage.

The error in the "instrument indicated" stagnation temperature  $\hat{T}_o$  is produced here largely because the probes spend most of the time in the wake.

Near the hub, the stagnation temperature error is not nearly so large, for, as can be seen in Figures 100 to 103, the flow is tangentially rather uniform on that side of the passage without the large wake region of the shroud.

The instrument indicated flow properties and the useful output quantities derived from them are presented in Figures 106 and 107 and Table VI.

#### 4.2.6 Utilization of Impeller Tip Measurements

Now that we have "instrument indicated" measurements for the tip of the impeller, the next question is what do we do with them? There are a number of schemes which can be employed to deduce output quantities such as impeller discharge mixed-out properties, impeller efficiency, work input, etc. If the data reduction method selected gives fluid dynamically and thermodynamically misleading indications of the "average" impeller discharge state, then losses cannot be appropriately divided between impeller and diffuser. This type of error, which apparently is fairly common in the art, deflects the developer's attention from the culprit.

In order to get a feeling for the magnitude of this problem, we have taken the "instrument indicated" profile distributions in Figure 106 and 107 and have used them as if these were outputs from tip probes. Six different

methods have been used for reducing the data; the results of these are compared to "true" values integrated from the three-dimensional distributions at impeller tip. The average "true" values are fluid dynamically and thermodynamically significant and therefore can be regarded as standards for comparison.

#### Calculation of "Instrument Indicated" Tip Properties

From the profiles of Figures 106 and 107, we must deduce "tip" values representing the flow state at the exit of the impeller. There are many different ways in which this can be done; for instance, measured data are often "mass-flow-averaged". But to do that, "instrument indicated" profiles must be used to calculate density and radial velocity. Since the "instrument indicated" properties are uncertain, then the deduced distribution of  $\rho C_r$  is uncertain too.

Another way is to assume a uniform mass flow equal to the value of  $\rho C_r$  given by the known mass flow. Then we can linearly average the profiles in Figures 106 and 107 from cover to hub. We have chosen to use that method as one of those studied here.

The cover to hub linear averages of the "instrument indicated" properties are tabulated in Column 1 of Table VI. The instrument indicated angle shown was area averaged over the entire discharge flow pattern using the local dynamic pressure as a weighting factor. It is very difficult to decide what is a meaningful way of averaging the angle data; this way is as good as any. In any event, we did not use the angle data in any of the data reduction schemes.

#### Data Reduction Schemes

Three common means of reducing the data are employed here for comparative purposes. The actual calculations made are contained in Appendix VI.

##### Method Number 1

This approach is widely used in the rt. A tip blockage factor, say, 0.8, is assumed arbitrarily, based on

TABLE V

Property	Instrument Indicated Value	Reduction 1	Reduction 2	Reduction 3	Reduction 4
$\bar{\rho}C_r$	62.17	62.17 <sup>b</sup>	62.17 <sup>b</sup>	62.17 <sup>b</sup>	62.17 <sup>b</sup>
$T_{coll}$	1106.1	1106.1 <sup>b</sup>	1106.1 <sup>b</sup>	1106.1 <sup>b</sup>	1106.1 <sup>b</sup>
$\bar{p}_2$	67.25 <sup>c</sup>	67.25 <sup>b</sup>	67.25 <sup>b</sup>	67.25 <sup>b</sup>	67.25 <sup>b</sup>
$T_{O_2}$	1150 <sup>d</sup>	1106.1	1106.4	1106.1	1106.1
$\tilde{p}_{O_2}$	196 <sup>d</sup>	196 <sup>b</sup>	195.4 <sup>b</sup>	211.4	202.8
$\bar{\alpha}$	81.5 <sup>e</sup>	79.3	- <sup>a</sup>	- <sup>a</sup>	- <sup>a</sup>
$\epsilon_2$	-	.2	.519	.632	.698
$\tilde{C}_{\theta_2}$	-	1842	1772	1778	1782
$\sigma$	-	.921	.886	.889	.891
$C_r^*$	-	278	265	261.9	269.4
$C_\theta^*$	-	1842	1772	1778	1782
$T_o^*$	-	1106.1	1106.4	1106.1	1106.1
$p^*$	-	68.2	71.6	73.7	71.6
$\alpha^*$	-	81.4	81.5	81.6	81.4
$p_o^*$	-	196(-)	193.2	195	190.1
$\tilde{p}_{O_2} - p_o^*$	-	~0	2.2	16.4	12.7

a) Not meaningful quantity  
 b) Input to calculate mixing losses  
 c) Linear average of hub and cover  
 d) Linear values  
 e) Dynamic values

I. COMPARISON OF "TRUE" AND "INSTRUMENT  
INDICATED" REDUCED DATA

Reduction 5a	Reduction 5b	"True" Value	Remarks
62.17 <sup>b</sup>	62.17 <sup>b</sup>	62.17	Overall Measurements
1106.1 <sup>b</sup>	1106.1 <sup>b</sup>	1106.1	Overall Measurements
67.25 <sup>b</sup>	67.25 <sup>b</sup>	66.5	Impeller Tip Measurements
1077.1	1077.1	1106.1	Impeller Tip Measurements
197	188.5	183.3	Impeller Tip Measurements
- <sup>a</sup>	- <sup>a</sup>	- <sup>a</sup>	Impeller Tip Measurements
.624	.684	- <sup>a</sup>	Deduced Quantities
1703.5	1703.5	1703.5	Deduced Quantities
.852 <sup>b</sup>	.852 <sup>b</sup>	.852	Deduced Quantities
261.5	269.4	281.5	Results After Mixing
1703.5	1703.5	1703.5	Results After Mixing
1077.1	1077.1	1106.1	Results After Mixing
73.5	71.3	70.35	Results After Mixing
81.3	81	80.6	Results After Mixing
182.7	177.5	171	Results After Mixing
14.3	11	12.3	Results After Mixing

average of profile in Figure 106  
pressure average over range of true  
in Figure 107

"experience". Then "instrument indicated" values are lifted from Table VI for

$$\hat{p}_2 = 67.25$$

$$\hat{p}_{O_2} = 196$$

The collector temperature gives

$$\hat{T}_{O_2} = 1106.1 \text{ (from the "true" } T_{O_2})$$

and the metered mass flow divided by impeller tip flow area gives

$$\bar{\rho C_r} = 62.17$$

From this input information, the following is calculated

$$\bar{T}_2 = 816$$

$$\bar{C}_2 = 1874$$

$$\bar{\rho}_2 = 0.223$$

$$\bar{C}_r = 349$$

$$\bar{C}_\theta = 1842$$

This information is sufficient to enter the mixing loss calculation which gives the mixed-out values shown in the column headed "Reduction 1" in Table VI .

#### Boeing Method: Number 2

This is the procedure used by Welliver and Acurio. It assumes that the axial "instrument indicated" profiles of  $\hat{p}_{O_2}$  and  $\hat{T}_{O_2}$  are correct except that there is a systematic

error in the  $\hat{T}_o$  profile caused by erroneous tangential averaging by  $C_2$  the temperature probes. The stagnation temperature profile is lowered, without changing its shape, until the "indicated" mass flow average of it matches the temperature measured in the collector. An iterative process is required to do this.

The average tip static pressure is injected which gives the "indicated" axial distributions of properties:

$x/b$	$\hat{T}_o$	$\hat{C}_\theta$	$\hat{\rho}C_r$
0.25	1136	1863.7	120.5
0.50	1112	1791.1	125
0.75	1076	1682	140.5

The "mass flow average"  $\hat{T}_o$  comes out from this distribution to be 1106.4, which is close enough to the collector temperature of 1106.1 given by the "true" mass flow average in the last column of Table VI. The mass-flow-average tangential velocity is not taken from the profile in the table above but, rather, is calculated from the stage temperature rise, while the mass flow per unit area  $\hat{\rho}C_r$  is derived from the mass flow rather than from the profile above, because the "indicated" profile gives about twice the actual value when averaged. However, the mass-flow-averaged stagnation pressure is calculated from the profile. We then have representative values:

$$\hat{C}_\theta = 1772$$

$$\hat{\rho}C_r = 195.4$$

$$\bar{\rho}C_r = 62.17$$

The mixing model may then be entered with the added assumption of no flow in the wake. The relative total pressure of the jet follows from the input data and is not assumed.

The calculations detailed in Appendix VI yield the mixed-out properties listed in Column 2 of Table VI.

Tip Static Pressure/Collector Temperature Method:  
Number 3

In the absence of any impeller tip probes, the only tip information at hand would be the impeller tip static pressure. Since this is one of the most reliable and indicative measurements, it is interesting to see what is deduced by using it in combination with collector temperature and mass flow.

We assume that the mass-flow-average stagnation temperature at the tip of the impeller is equal to the temperature in the collector and that the mass flow in the wake from the impeller is equal to zero. Into the calculations are injected:

$$\bar{p}_2 = 67.25 \text{ (the linear average of the "instrument indicated" values on cover and hub)}$$

$$\bar{T}_{o_2} = 1106.1 \text{ (the "true" mass flow average from the last column of Table XXIV)}$$

$$\rho C_r = 62.17 \text{ (derived from the measured mass flow and impeller tip flow area)}$$

With this information the mixed out flow properties listed in the column headed "Reduction No. 3" in Table VI result.

Tip Static Pressure/Collector Temperature: Number 4

This scheme is identical to Method 3 except that  $m_w/m = 0.20$  is assumed. This wake flow estimate is widely used herein.

Tip Static Pressure/Slip Factor Method: Number 5

Because the collector temperature reflects added, nonuseful work done by the impeller against friction and backflow, its use overestimates the through-flow slip factor as discussed in Section 6.7. To emphasize the effect on prediction of impeller discharge conditions, the "true" mass-flow-averaged slip factor from Table VI is used instead of the collector temperature. In Method 5a,  $m_w/m = 0$ ; in Method 5b,  $m_w/m = 0.20$ .

#### 4.2.7 Comparison of Results

Table VI shows that there are quite significant differences among the different data reduction schemes and between all of them and the "true" values which are fluid-dynamically and thermodynamically significant.

The first method, No. 1, because it uses collector temperature, overstates the impeller discharge tangential velocity and therefore gives an erroneously high slip factor. Commensurately, it overstates the tip mass-flow-averaged stagnation pressure. Further, because of the arbitrary assumption of a very small wake (20%), it predicts essentially no impeller discharge mixing loss. The weakness of this method is recourse to arbitrary tip "blockage" factors and use of collector temperature. The mixed-out properties predicted are inaccurate, the discharge mixing loss is badly underestimated, and the impeller's efficiency is very much overestimated. Since our best estimate of the tip "blockage factor" for RF-2 and Workhorse impellers is 0.25 in contrast to the commonly used value of 0.8, the difficulties with this method are emphasized.

The first four data reduction schemes greatly overestimate the mixed-out stagnation pressure because they rely upon the collector temperature which does not correspond to the temperature rise corresponding to the through-flow mass-flow-averaged tangential velocity  $C_{\theta}$ . That is basically responsible for the high value of tangential velocity and slip factor. The first reduction scheme utilizes the linear average of stagnation pressure at the tip of the impeller, which is considerably higher than the "true" mass flow average. The second and third reduction schemes fall into difficulty by assigning all of the work input determined from collector temperature to the through-flow jet and thereby derive too high a value for jet stagnation pressure through ignoring high-stagnation temperature fluid passing through the wake region. When 20% of the wake mass flow is assumed in Reduction Method 4, this difficulty is avoided; the loss predicted then is close to the "true" value but, because  $T_{coll}$  is still used,  $p_{o_2}$  and  $p_{o_2}^*$  are about 20 psi high.

When  $T_{coll}$  is abandoned and the "true"  $C_\theta$  (or  $\sigma_2$ ) is injected, then both the loss and  $p_o^*$  are closer to the "true" values.

#### 4.2.8 Significance of the Errors Produced by Instrument Indications

As may be seen plainly in Table VI, serious errors in mixed-out flow properties, particularly in slip factor (i.e., tangential velocity) and mixed-out stagnation pressure, are encountered. None of the five common reduction schemes is completely adequate; the first three, which are widely used in the art, produce quite significant errors that amount to more than an atmosphere overestimation of the impeller discharge stagnation pressure and as much as 7 points excess slip factor. Even the method giving answers closest to the "true" values predicts  $p_o^*$  6.5 psi high.

The principal lesson of this exercise is to illustrate the inherent errors which are likely to be incorporated in the impeller tip "instrument indicated" properties measured in the Boeing-AVLABS program. The moral is that one must treat such information with considerable skepticism when it is suspected that the flow leaving the impeller is highly distorted.

In order to reduce the inherent errors contained in probing information, it is best to locate the probes well beyond the impeller discharge mixing zone. Therefore, in the Boeing-AVLABS data, the diffuser throat stagnation pressure measurements should be regarded as much more indicative of the true impeller discharge stagnation pressure after mixing rather than the measurements at  $R = 1.03$ . Of course, by locating impeller diagnostic probes remote from the impeller tip, the uncertainty of injecting loss processes from the diffuser entry region is introduced. This matter is discussed at some length in Section 6.7.

When backflow from the diffuser occurs, the collector temperature includes the extra work on the backflow. Then collector temperature becomes a poor measure of the impeller's work on the through flow, as may be seen plainly

in Table VI. Welliver and Acurio (1967) emphasized that the temperature rise they measured was considerably higher than the slip factors they deduced, even though those were much too high in themselves. What Welliver and Acurio did not emphasize was the impact of this error upon impeller loss predictions.

An obvious recommendation arising out of this study is that much more sophisticated flow diagnosis measurements are essential in future research. Conventional instruments now used at the tip of impellers give misleading, even meaningless data in some cases. No further attempt should be made to better understand flow patterns, losses, boundary layer blockage, and so forth, without resort to high-response instrumentation and four-dimensional measurements. This need will greatly complicate centrifugal compressor research and require the most sophisticated modern data handling methods in order to be successful. However, it is our firm recommendation from this work and our experience that the move to a much higher level of measurement sophistication is absolutely essential. Otherwise, the fundamental flow processes responsible for current centrifugal compressor performance lying considerably below ultimate performance will not be discovered.

The answer to the original question concerning the whereabouts of the "missing loss" in Figures 95 and 96 appears to be that Boeing was misled by the indicated data and data reduction scheme into overestimating mass-flow-average slip factors for their impellers. Actually, as shown, for example, in Figures 22, 23, 42, and 83, the  $p_o$  distributions, if taken at face value, produce a slip factor around 0.82 - 0.84 if a high impeller efficiency is assumed (discounting backflow and cover and disc friction) and if the measurements at  $R = 1.03$  are interpreted as impeller tip values. These assumptions appear to be reasonable. Further, as Table VI claims, the  $p_o$  probes should give  $p_o$  high, by not more than 15 psi.  
 $\sigma_2$

If we lower the  $p_o$  Boeing-AVLARS data, an even lower  $\sigma_2$  would be indicated.

We conclude from this study that the "missing loss" is

hidden in a high indicated slip factor for the Boeing-AVLABS data.

#### 4.3 DIFFUSER DATA

Welliver and Acurio (1967, 67-30 and 67-47) compared the pressure recovery performance of the channel diffusers of the Workhorse and RF-2 stages against the laboratory diffuser data of Runstadler (1967). Fair agreement was obtained. Since that time, a larger collection of straight channel diffuser data of much better quality has been secured by Creare under AVLabs Contract DAAJ02-67-C-0106, Runstadler (1969). In Section 5.9, a critical comparison will be made of diffuser performance in the actual compressors and in the laboratory rig. For that end, an assessment of the inherent uncertainty in the diffuser measurements is essential. An uncertainty analysis of the Boeing-AVLabs diffuser data is developed below. The size of the uncertainty bands does not encourage close checking of diffuser performance.

##### 4.3.1 Selection of Data

A careful search through the Workhorse and RF-2 data revealed that the only runs for which adequate information was available for diffuser analysis are RF-2 tests:

- (1) 3354 and 3354A
- (2) 3366 and 3366C
- (3) 3369 and 3369B
- (4) 3352C and 3353D

The first test of each of the test pairs selected provided static pressure and total temperature measurements. The second gave total pressure on the center line (approximately) of the diffuser throat.

The data determining the performance of a given diffuser must be taken from two runs, because this is the way the measurements were performed. There is a snag in the scheme, however, because the mass flow was kept at (roughly) the same value for the two runs. This should not have been done; compensation is needed for the fact that one total

pressure probe inserted into one throat drives the choke flow of the machine down by about 7%\* -- almost the change which would occur if one passage were completely shut.

None of the data from the Workhorse tests is adequate for diffuser analysis. Stagnation pressure measurements in the diffuser throat taken with the "railroad track" probe are very suspicious, because they show a lower pressure in the diffuser throat than was measured in the collector. See Figures 30 and 31. Note also that  $p_o$  falls and then rises again -- an impossible situation unless massive heat transfer occurred, e. g., 100° R temperature change at a flow rate of 2 lbm/sec in a 1.5-inch length. Also, compare Figures 22 and 23 and Figures 30 and 31 at  $S = 0.85$  (approximate location of pressure rakes, Figure 9). This comparison shows a major difference in indicated stagnation pressure.

From these considerations we concluded that the railroad track probe does not measure stagnation pressure accurately. The error does not seem to be related to yaw angle considerations because the railroad track probe was nominally aligned with the flow, and impact tubes are fairly insensitive to yaw angle over about a  $\pm 15^\circ$  range. It appears that one or three things is occurring:

- (1) The probe is Mach no. sensitive due to burrs or other causes.
- (2) The 0.020-inch-wide slot that the railroad track runs in creates a major flow disturbance, although the disturbance may be confined to the region in front of one diffuser channel.
- (3) The probe itself creates a major flow perturbation.

We favor the second explanation because the jet from the separated impeller would cross the slot at about a  $10^\circ$  angle and some local transitory separation would not be at all surprising.

---

\* See Figure 59

If the third possibility were true, it is likely that all of the other probes would produce similar effects. The fact that the yaw probe and the other two pressure rakes give measurements which seem to fit together well (see Figures 22 and 23) suggests that this does not happen.

Due to this difficulty, none of the Workhorse data available is employed here for diffuser analysis.

The reason for selecting the cited runs from the RF-2 data is that they all have stagnation pressure measurements in the diffuser throat. This data may not include the best diffusers, but it is likely that the runs selected are representative since none of the other tests show significantly higher overall performance.

#### 4.3.2 Uncertainty Analysis

The uncertainties in the quantities calculated from the diffuser measurements were analyzed following the methods suggested in Dean et al (1953). The uncertainties in calculated quantities are found in terms of the uncertainties in the primary measurements. This computation is reasonably intricate and has been relegated to Appendix V. Only a brief description of the process is given here.

The root mean square of the uncertainties in the primary measurements, each weighed by a suitable influence coefficient, is defined as the uncertainty in the derived quantity. The reason for this definition instead of a linear average is clearly illustrated by an example.

Suppose there is a derived quantity which is a difference of two large primary measurements, each of which has the same percentage uncertainty. For instance, a differential pressure measurement made by subtracting the readings of two identical gauges. A linear uncertainty evaluation scheme would show zero uncertainty. But this would be true only if both measurements were wrong by the same amount in the same direction at the same time. This is not likely. Kline and McClintock (1953) show that if the error distributions are near "normal", the root mean square averaged uncertainty is the most accurate reflection of the true uncertainty.

These uncertainties are all evaluated at 20:1 odds. In terms of the computed results, this means that 19 out of 20 data points should fall within the uncertainty band. For small sample experiments (such as these), the statistical meaning of the uncertainty is not as clear, but it is interpreted as the "measurement confidence interval".

From the equations derived in Appendix V, the uncertainties in  $C_p$ , B, and m can be evaluated once the primary measurement uncertainties are known. The most difficult part of such an analysis is estimating reasonable uncertainties for the primary measured quantities.

The evaluation of the primary measurement uncertainties is done in two stages. First, the uncertainties in the instruments are evaluated. Second, the reading errors associated with the instruments and the nature of the flow which is being measured are calculated from correlations. These are then combined to give an uncertainty level for each primary measurement.

It is important to understand the difference between repeatability and precision in physical measurements. It is entirely possible to have results from an experiment which are repeatable to 1/10 of a percent but whose precision is not better than 10% (e.g., a barometer which had a solution of mercury and copper instead of pure mercury would probably be very repeatable but would not be very precise). There are two kinds of errors we have been discussing above: fixed errors and random errors. Random errors will usually show up as scatter in the data and are due to equipment unsteadiness and operator mistakes. Fixed errors usually do not show up until an independent investigation of the same phenomenon produces different results. We are attempting here to evaluate both kinds of errors to make sure that conclusions drawn from these studies are warranted and meaningful.

#### Uncertainties in Primary Measuring Equipment

##### Pressure

Pressure measurements made by Boeing's Dymec system are

accurate to within 0.25% of the full-scale reading of the transducer, Winslow (1968). For typical measurements of static pressure, collector pressure, and total pressure, this amounts to  $\pm 0.5$  psi.

#### Mass Flow

The mass flow is claimed to be precise to  $\pm 0.5\%$ . This is extreme accuracy for a gas-flow-rate measuring device. It is doubtful whether this kind of accuracy is possible with the flowmeter setup used by Boeing. A description of the flowmeter used for both the Workhorse and RF-2 stages is found on Page 293 of Welliver and Acurio (1967, 67-30). Figure 108 is a sketch of this apparatus with comments that indicate that the flowmeter was not arranged satisfactorily for high-precision metering.

The differential pressure across the metering nozzle was measured on a 0-to-16-inch water manometer which has a resolution of  $\pm 0.01$  inch of water. With this particular gauge\*, however, results more precise than  $\pm 0.10$  inch of water cannot be obtained unless a special manometer fluid is used. This is due to thermal and capillary errors; see page 80 of Dean et al (1953). This manometer error is random due to the nonuniform "wetting" characteristics of water caused by infinitesimal amounts of impurities.

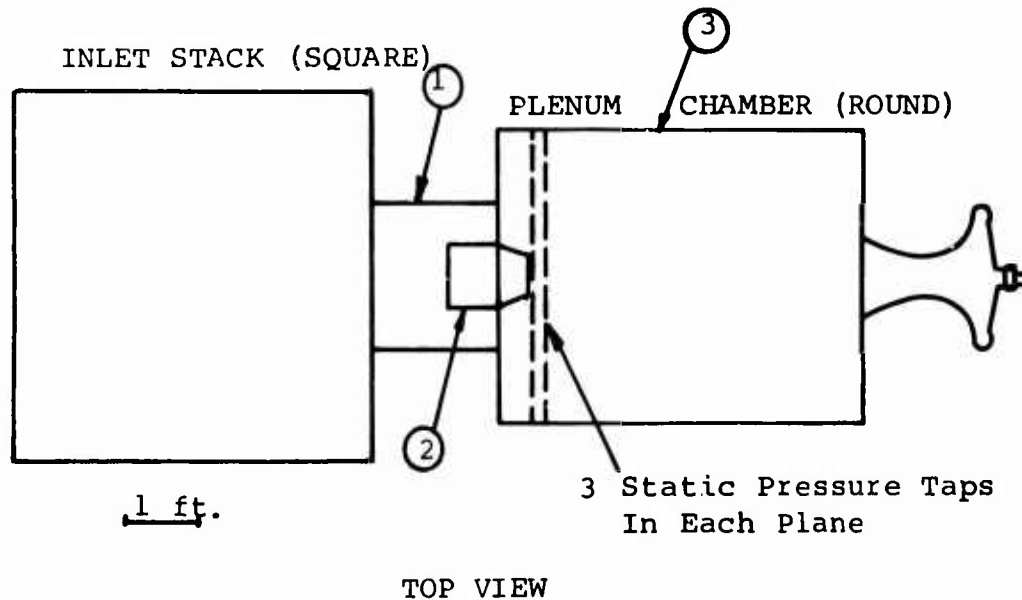
The total capillary effect for this manometer is  $\pm 0.2$  inch. If 0.1 inch were added to each reading, the measurement uncertainty would be  $\pm 0.1$  inch of water.

The minimum uncertainty in calculated mass flow introduced from this source alone is  $\pm 0.3\%$  (when  $\Delta p = 16$  inches H<sub>2</sub>O), while the probable uncertainty (it is not likely that all mass flow registered a differential pressure this high) from this source is greater than the  $\pm 0.5\%$  accuracy claimed. A more likely (but still conservative) figure of  $\pm 1\%$  will be used for the flowmeter uncertainty.

#### Temperature

The temperature measurements have been taken with thermocouples as part of the Dymec system and are probably accurate to  $\pm 5^\circ$  R, Winslow (1968).

\* Meriam 40HA10 or 40HB10 gauge.



TOP VIEW

- NOTES:
- 1 The 2-ft. inlet is too short to be effective in straightening the flow.
  - 2 The square edges of the section ahead of the nozzle may produce an unsteady inlet flow. The acceleration from this section (7 inch diameter) to the nozzle throat (5.46 inch diameter) is too small to insure a smooth flow.
  - 3 The plenum chamber is too short (60 inch) and has no special provision to make the flow uniform.

Figure 108. Boeing's Flowmeter Setup for Workhorse and RF-2.

### Geometric

There are a large number of possible geometric error sources. The measured tolerances on diffuser throat dimensions are given in Table II, as this appears to be the most critical set of dimensions from an aerodynamic standpoint.

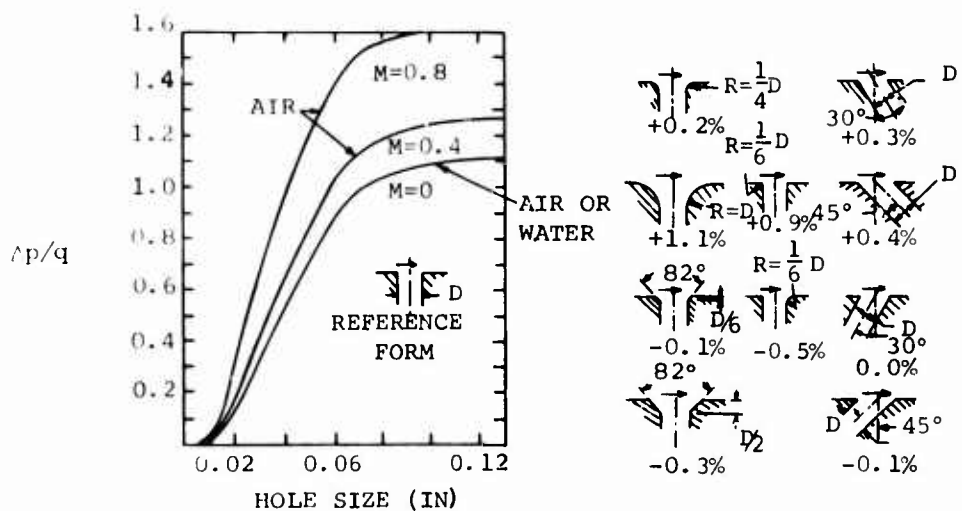
The deflection of the impeller tip at 50,000 rpm was estimated to be 0.020 from stress calculations. This amounts to a 0.44% higher tip speed than would be expected and a 0.8 psi increase in tip static pressure.

The above observations cite the probable uncertainties introduced by the primary measurement equipment. As will be shown below, most of these uncertainties are small compared to the uncertainties caused by unsteadiness and lack of complete information about the flow.

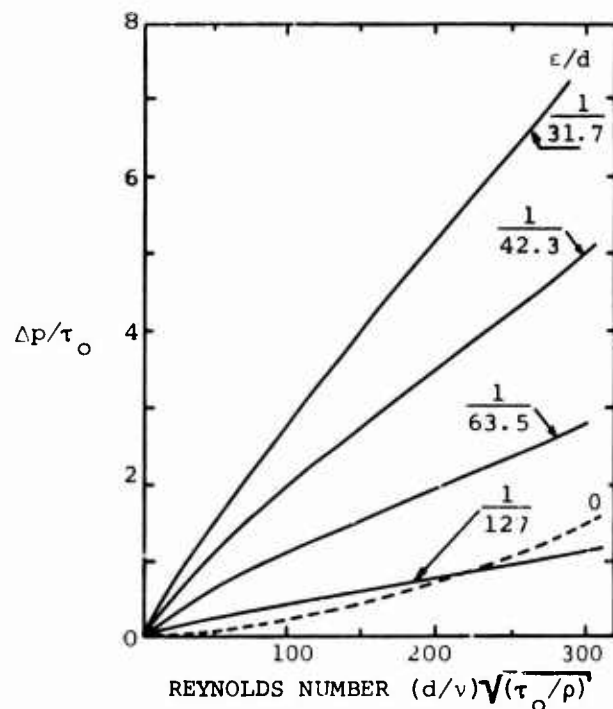
### Flow Uncertainties: Throat Static Pressure

The diffuser static pressure distributions show a considerable uncertainty, caused by finite tap spacing, about the minimum static pressure in the throat. A conservative estimate for this additional uncertainty is  $\pm 2$  psi; we feel that the actual uncertainty at 20:1 odds is considerably greater due to friction, shock, and flow curvature effects in the constant-area throat. In Section 5.8.2, the proper estimation of throat pressure and the impact of errors in deducing throat pressure are considered at length.

Pressure taps in high-speed airflow have an inherent error. They read a higher pressure than actually exists. Rayle (1949) and Shaw (1959) describe the results of detailed investigations of these phenomena. Rayle experimented with compressible and incompressible flow. Shaw investigated only incompressible flow, but he included the effect of small burrs left on the holes by imperfect drilling. Figure 109 shows the results of both investigations, and Figure 110 gives an extrapolation of Rayle's results to Mach 1.



RAYLE'S RESULTS SHOWING VARIATIONS OF TAP ERROR WITH HOLE SIZE, MACH NUMBER, AND HOLE GEOMETRY



SHAW'S RESULTS SHOWING THE EFFECT OF BURRS AND REYNOLDS NUMBER  
 $\epsilon/d$  IS THE BURR HEIGHT/HOLE DIAMETER

Figure 109. Pressure Tap Errors.

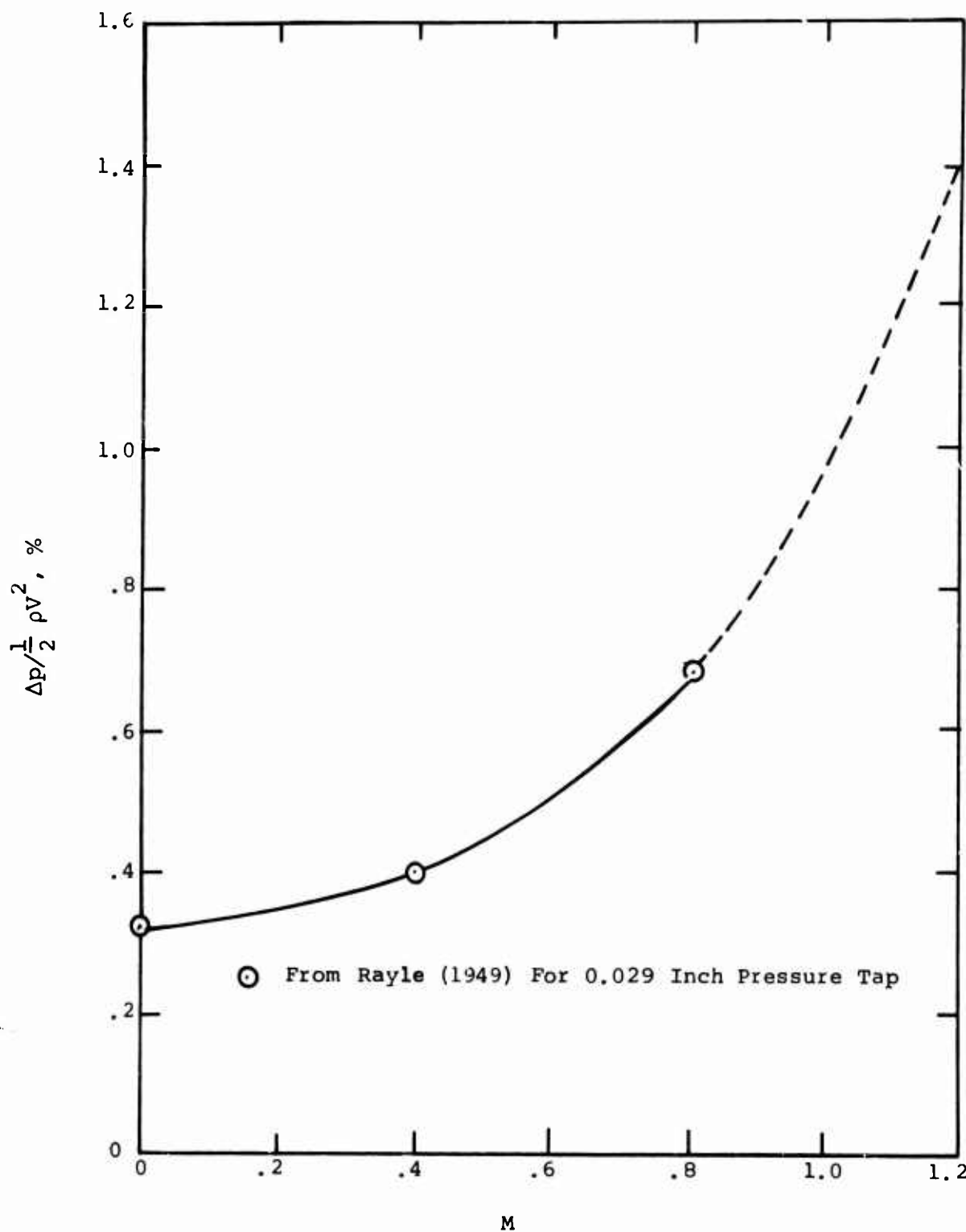


Figure 110. Static Pressure Errors as a Function of Mach Number.

Shaw's results suggest that unless the taps were very carefully deburred, another large error could result. For the 0.029-inch static taps used by Boeing, a 0.001-inch burr would cause six times the error of a smooth tap. This result is for incompressible flow and probably is not as large for compressible flow.

Overall errors of 1% to 2% of the dynamic head are expected, based on Rayle's results. This amounts to about a 0.5 - 2 psi error, which would be considerably greater if there were even tiny burrs.

#### Throat Area

Table II shows the measured variation of the throat width  $w_4$ . In addition, an uncertainty of about  $\pm 0.002$  inch is assumed for the diffuser throat depth  $b_4$  due to machining tolerances and to warpage at high temperatures.

#### Stagnation Temperature at the Throat

The uncertainty of stagnation temperature measurements stands out\* but these measurements are not highly critical to diffuser performance uncertainty. These measurements are used at the throat in order to deduce the blockage.

The average measured total temperature at the impeller tip is about 100° above the collector temperature. We shall assume that the throat total temperature is equal to the collector temperature, so the throat total temperature may be uncertain by about  $\pm 40^\circ$ . Fortunately, the temperature uncertainty has a very small effect on the diffuser performance uncertainty, so the value we use is probably not too critical. We have used  $\pm 10^\circ$  representing the limit of heat transfer, thermocouple error, etc.

#### Throat Stagnation Pressure

The uncertainties in the measurements of the stagnation

---

\* Compare Figures 48 and 58.

pressure rakes in the diffuser throat are difficult to assess. The flow is unsteady. The magnitude of the unsteadiness is unknown; the mixing theory of Dean and Senoo (1960) suggests that unsteady jet-wake mixing effects should be small in the throat -- a 1-psi fluctuation presumably is large at this radius ratio. How large other unsteady flow effects are is unknown, but we shall assume that unsteady effects can be neglected.

It was observed that the choking mass flow was reduced 7% by the insertion of one probe in one throat of one of the ten parallel channel diffusers (see Figure 59). This means that the measured channel does not pass anywhere near its share of the flow. It is clear that the total pressure probe causes a significant flow perturbation. We have assigned an uncertainty of  $\pm$  5 psi to the stagnation pressure measurements, although we would not be willing to bet 20:1 odds that the actual throat stagnation pressure is within 5 psi of the measured value.

#### Static Pressure in the Collector

This has been assumed to have an uncertainty level equal to that of the pressure transducer equipment ( $\pm$  0.5 psi).

#### Overall Uncertainty of Compressor Diffuser Performance Results

If we put all these numbers into the uncertainty calculation for a typical case (Test 3354, Line 7), we arrive at the following figures for the primary measurement uncertainties:

$$\frac{\Delta p_4}{p_4} = \pm 0.034$$

$$\frac{\Delta p_{o4}}{p_{o4}} = \pm 0.032$$

$$\frac{\Delta A_4}{A_4} = \pm 0.0126$$

$$\frac{\Delta T_{O_4}}{T_{O_4}} = \pm 0.009$$

$$\frac{\Delta m}{m} = \pm 0.01$$

$$\frac{\Delta p_{coll}}{p_{coll}} = \pm 0.004$$

This yields the uncertainty in the derived quantities:

$$\frac{\Delta m_T}{m_T} = \pm 3.6\%$$

$$\frac{\Delta C_p}{C_p} = \pm 8\%$$

$$\frac{\Delta B}{B} = \pm 40\%$$

The reason for doing uncertainty calculations is to appreciate the magnitude of possible errors in experimental data. No experimental data are completely free from errors. These data were taken well, but there are no exceptions to the previous statement. It is unfortunate that no dynamic instrumentation was installed in the diffuser (nor near the impeller, for that matter) to record unsteadiness levels. Also, a better definition of the static pressure field in the throat region would have been very informative.

The uncertainties estimated here are used in Section 5.9 during the critical study of the diffuser and its flow models.

## 5.0 TESTS OF EXISTING FLOW MODELS FOR DESIGN PREDICTIONS

A major objective of this program is to critically examine existing methods for analyzing the fluid dynamics of high pressure ratio centrifugal compressors. These analytical tools are essential for accurate design and development. In design, valid models are absolutely necessary for optimization of the very complex situation described by many variables which must be chosen to specify a stage. Without good analytical tools, the probability of even approaching an optimum design is remote, particularly for this class of machine, behind which there is little empirical experience upon which to rest. For development, good analytical tools are just as necessary for diagnosis which must precede cure.

The perfection of analytical tools is doubly important for the centrifugal compressor, as contrasted to the axial, for example, because the complex flow situation at the impeller tip/diffuser entry has yet defied sufficient experimental diagnosis in high-speed machines. We should always rely upon the best analytical models available for diagnosis of test data; otherwise, as was exemplified in Section 4.2, our deductions may likely be myths.

Analytical tools in common use today for developing centrifugal compressors range from prosaic correlations to elaborate analyses. Neither is the best tool which can be devised. The flow problem in a centrifugal compressor is so complex that prosaic correlations are of little use unless an extensive line of closely related machines is being built. For the one-of-a-kind high-pressure-ratio centrifugal compressor of today, these correlations are at best only suggestive.

Similarly, at the other end of the spectrum, the elaborate analysis fails too. This is because many of the critical flow phenomena in centrifugal compressors, such as secondary flow in the impeller and on the diffuser sidewalls are intractable with even the most erudite modern fluid dynamic theories.

Plainly, a compromise between correlations and elaborate theory is demanded. Over many years we have consistently attempted to construct working theories for the centrifugal

compressor which recognize the critical fluid dynamic phenomena and which use adequate analytical methods. Today it seems obvious that many centrifugal compressors are separated early in the impeller and thus require a separated flow analysis for much of the radial extent of the impeller. Yet, centrifugal compressor design is being carried out today by supposedly accomplished designers without recognition of this fact. Similarly, only recently have most designers recognized that a significant part of the stage loss is often found in impeller discharge mixing caused by unusually large wakes or passage blockage exiting from a separated impeller. We have constructed models which can handle these situations and have been using them for a long time. These models were used extensively by Welliver and Acurio in the diagnosis of their data and in their design of the RF-2 stage. At the same time, we assisted them in building new and better models for the inducer and for the supersonic diffuser.

In this program, a primary objective has been to subject this structure of flow models to further critical testing against the Boeing-AVLABS data. While considerable model testing was done during the Boeing-AVLABS program, the scope of that program precluded adequate model evaluation. Further, the evaluations that were made left some serious anomalies which are highlighted by Welliver and Acurio (1967, 67-47).

In this section, we shall complete the testing of the prediction model structure against the Boeing-AVLABS data. Unfortunately, as we have discussed in Section 4, the Boeing-AVLABS data are too uncertain to critically test all aspects of the models. Nevertheless, important deductions can be made.

Nothing in the scope of this program has precluded the incorporation and testing of flow models other than those preferred by Creare. Of course, many of the analytical tools in current use are proprietary and not available to us. However, we have systematically incorporated the best we can find from the works of others in the long construction of our prediction methods. From what evidence we can discern, there are few prediction schemes with more potential in use today. Of course, many aspects of the fluid dynamics of the centrifugal compressor remain obscure, as has been

displayed by Dean (1968). Much room for controversy still exists over proper interpretation and modeling of the flows. Therefore, we do not regard our analytical modeling system as "true" or "absolute". But, in lieu of other evidence, we do assert that it is about as competent a structure as can be erected today. For this reason, we have made little attempt in this program at a catholic review and testing of centrifugal compressor design analysis methods.

Below, the analytical models will be briefly explained with the equations sufficiently developed for the purpose of testing the validity of the models. We have not attempted to make this a reference work that lays down easily-used recipes for flow analysis.

### 5.1 TEST OF INDUCER LEADING EDGE MODEL

Design methods for the inducer entry flow are very meager. Present design procedures usually treat the inducer region on a quasi one-dimensional basis. The approach axial velocity and the inducer wheel speed are resolved into a relative approach velocity onto the inducer blading and this is used with "experience" to prescribe the incidence onto the inducer blading. The mean camber line of the inducer blading and the inducer blade thickness schedule are defined to obtain the required blade surface velocities.

Boeing's potential flow analysis treats the inducer flow on a quasi one-dimensional basis to evaluate the meridional streamline pattern as determined by radial variations in blade blockage, turning schedule, hub and cover profiles, and downstream impeller geometry. The blade surface velocities determined by the criterion of irrotational absolute flow assuming the flow follows the blading, Stanitz (1953) have been used.

Welliver and Acurio (1967) used this solution in the design of the Boeing-AVLABS impeller. They designed for about  $+1^\circ$  incidence with respect to the vane pressure surface as indicated in Figure 111, using the blocked flow area to calculate the approach axial velocity. If the unblocked flow area is used instead, then  $+3^\circ$  to  $+5^\circ$  incidence was recommended.

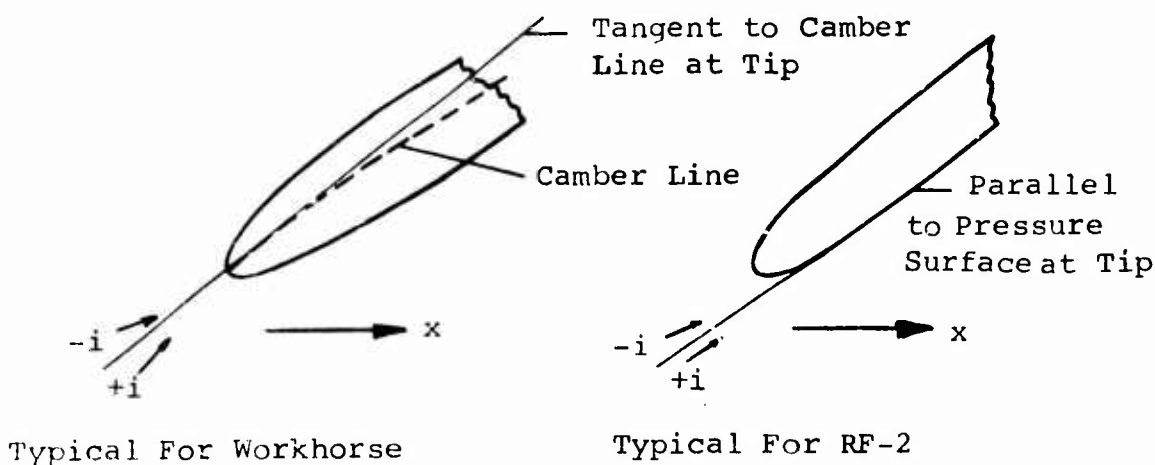


Figure 111. Definition of Inducer Incidence Angle.

Welliver and Acurio report inlet vector diagrams, inlet blockage factor as a function of airflow, and inducer incidence as a function of mass flow and impeller speed.

### 5.1.1 Inlet Vector Diagrams

The incidence values in 67-47 for the RF-2 impeller are reported as being calculated for the unblocked flow area. The inlet vector diagrams have been calculated using the measured mass flow rates and using the impeller potential flow solution to estimate the inlet axial velocity distribution. The potential flow solution shows a radial redistribution of velocity at the inducer leading edge, resulting from blade thickness effects and the upstream influence of the downstream flow through the impeller. The radial redistribution reported is about 8 ft/sec/in. The data on the hub and cover indicate that the actual redistribution is on the order of 70 ft/sec/in. Reasons for this disparity are discussed in section 5.2.

### 5.1.2 Inlet Blockage Factors

The inlet blockage factors reported in Figure 159 of 67-47 were calculated from the measured static pressures upstream of the inducer. These values represent blockage at the impeller inlet produced by boundary layer growth in the bell-mouth and inlet preceding the inducer. The values are very close to unity, with most grouped around an inlet blockage factor of 0.98. This corresponds to the boundary layer blockage to be expected (i.e., approximately 0.03). The values for Tests 3366A and 3356A, which show a larger scatter around the mean value, are probably due to the uncertainty in measuring the mass flow rate in these tests.

### 5.1.3 Flow Incidence Angles

Flow incidence angles deduced from the measured static pressures on hub and cover ahead of the inducer, assuming a "smeared out" inlet blockage are tabulated in Table VII. The values of incidence are measured to the mean camber line, see Figure 111. At the RMS radius, they range from 1.5 to 2° higher than the Boeing-AVLABS numbers. The incidence based on static pressures and a "smeared out"

TABLE VII. ANGLE OF INCIDENCE AS CALCULATED  
FROM MEASURED STATIC PRESSURES AND  
REFERENCED TO MEAN CAMBER LINE OF  
INDUCER BLADE

Run	N	m	i (Hub)	i (RMS)	i (Tip)
3352C	50,000	1.75	+2.6	+4.9	+5.1
3353C	50,000	1.72	+2.8	+5.1	+5.3
3353C	50,000	1.76	+2.1	+4.4	+4.8
3353C	50,000	1.83	+1.2	+3.1	+4.0
3356A	50,000	1.97	-1.2	+1.1	+1.6
3356A	50,000	2.06	-2.8	-0.5	+0.1
3366A	50,000	1.88	+1.6	+3.9	+4.1
3366A	50,000	1.92	+0.4	+2.6	+3.1
3366A	50,000	1.93	-0.3	+2.0	+2.5

inlet blockage produce an almost constant angle of incidence across the flow passage.

In axial compressor design, blade incidence is calculated on the basis of the "unblocked" approach flow, and the blade angle is set at an incidence of  $+3^\circ$  to  $+5^\circ$  to compensate for blade blockage. If anything, the values of incidence given in Table VII are slightly lower than common design practice since a positive incidence of  $+3^\circ$  to  $+5^\circ$  is obtained only at the lowest flow rate.

#### 5.1.4 Supercritical Flow

The inlet Mach number relative to the inducer blade tip varies on these tests from a low of 0.817 (Run 3353C,  $m = 1.72 \text{ lbm/sec}$ ) to 0.875 (Run 3356A,  $m = 2.06 \text{ lbm/sec}$ ). It can be expected that the inducer blades are operating in the supercritical transonic flow regime. The local supersonic velocities can be expected to have a strong influence on the flow over the pressure and suction surfaces of the inducer blades near the tip as discussed by Dean (1968) and considered further in Section 6.1.

Of primary importance are the local normal shocks terminating the imbedded supersonic flows on both the suction and pressure surfaces. At present the only analytical recourse is to attempt use of available knowledge from transonic wing technology to qualitatively evaluate the influence of the shape of the inducer blading near the leading edge. In the supercritical regime, a normal shock will terminate the supersonic expansion region. It is desirable to limit the strength of this shock in order to protect the boundary layers on the suction or pressure surface. As discussed in Section 6.1, "peaky" type blade profiles appear to be desirable to produce an isentropic recompression on the suction surface and so reduce the Mach number preceding the terminal shock. This should minimize the tendency for local boundary layer separation.

A compilation of empirical wing technology data such as given by Pearcey (1961) has formulated the nose shape parameter K discussed by Welliver and Acurio (1967) which

qualitatively describes the transonic behavior of isolated airfoils. They postulate that, at least on the suction surface, the same qualitative ideas regarding transonic flow behavior should apply.

Welliver and Acurio showed that the Workhorse impeller, which had better performance than other impellers previously tested, had a low value of the transonic parameter K (at least relative to the other inducers tested). Table VIII presents a listing of these values of the transonic parameter for the Workhorse and RF-2 impellers as given by Shorr, Welliver and Winslow (1969).

Now the actual value of the parameter K depends upon the choice of the "airfoil" chord and details of the nose geometry. Welliver and Acurio assumed a 1-in. chord length. As long as consistency is maintained when the various impellers are compared, it appears reasonable to make a qualitative comparison of the details of the nose shape on this basis.

One concern in placing much emphasis upon the transonic parameter K, as given in Table VIII, is the fact that the physical size of the inducer blading is extremely small. Blade thicknesses are on the order of .020 to .030 inch. The miniature dimensions make the finishing of the blade to a precise shape prescribed by wing technology extremely difficult. The RF-2 inducer had 18 blades, so we may expect to find a large variation in blade profile from blade to blade. Whether the actual "hardware" blading actually had the leading edge shape required to obtain good transonic behavior is debatable.

Despite these practical complications, the values of K listed in Table VIII imply that the RF-2 inducer should have had leading edge geometry that would avoid severe shock/boundary layer interaction effects.

#### 5.1.5 Reynolds Number Effects

Length Reynolds numbers encountered on inducer blade leading edge surfaces are quite low. For the RF-2 geometry, the length Reynolds number on the inducer tip suction surface does not reach a value of  $3 \times 10^5$  until

TABLE VIII. INDUCER BLADE SHAPE KAPPA  
FACTOR (K)

Impeller	RMS Radius	Tip Radius
RF-2	0.056	0.097
Workhorse	0.044	0.095

approximately a streamwise distance of 0.5 in. The shocks which form in the supersonic regions around the nose probably fell upon a laminar boundary layer. Since the pressure rise that separates a laminar boundary layer is extremely small, any such shocks will most likely separate the laminar boundary layer.

If the shocks fall far enough back on the inducer blading (in terms of the boundary layer thickness Reynolds number), they will induce separation and transition of the laminar boundary layer, with a probable reattachment of a turbulent boundary layer immediately downstream of the boundary layer-shock interaction point. However, as one goes closer to the hub on the inducer blading surfaces, the unit streamwise Reynolds number decreases. This makes even more severe the consequences of laminar boundary layer growth and possible separation of the inducer flow. It may well be that the presence of laminar boundary layers on the leading surfaces of the inducer precludes attaching any real importance to the details of the inducer blading nose profiles. The presence of virtually any shocks will separate the laminar boundary layer found along the first 0.5 to 1.0 in. of the inducer blading. It would appear that little can be done to prevent this laminar separation from occurring. This is particularly so if the nose shape cannot be configured to put the terminating normal shock far back on the surface of the inducer blading.

It may be possible, by careful design of the inducer leading edge profile, and by specification of the incidence onto the blading, to delay the velocity peak on the suction surface until the boundary layer has achieved a sufficiently high Reynolds number to undergo transition before flow diffusion or shocks cause separation. These points are considered in more detail in Section 6.1.

#### 5.1.6 Conclusion

With the Boeing-AVLABS data, we find the critical testing of the Welliver and Acurio inducer leading-edge flow model adopted from transonic wing technology to be impossible. Furthermore, we are not convinced that the subtle nose shapes wanted were actually generated on the blading. Dimensional changes of  $\pm 0.002$  in. could greatly alter the

critical K parameter. To hope to hold such accuracy in production by hand-finishing is beyond reason. But most disarming is the low Reynolds numbers of these blades compared to the wings for which the technology was developed. Wing thicknesses and surface lengths are 80 to 100 times greater. In the small centrifugal inducer, the leading edge shocks will fall most likely on laminar boundary layers in contrast to the wing. At best, a laminar bubble should be the result; at worst, complete and unrecoverable separation. Research is vital to resolve this critical region. If the Welliver and Acuilo hypothesis is fallacious, another approach is essential, for the designer must have a working inducer design tool.

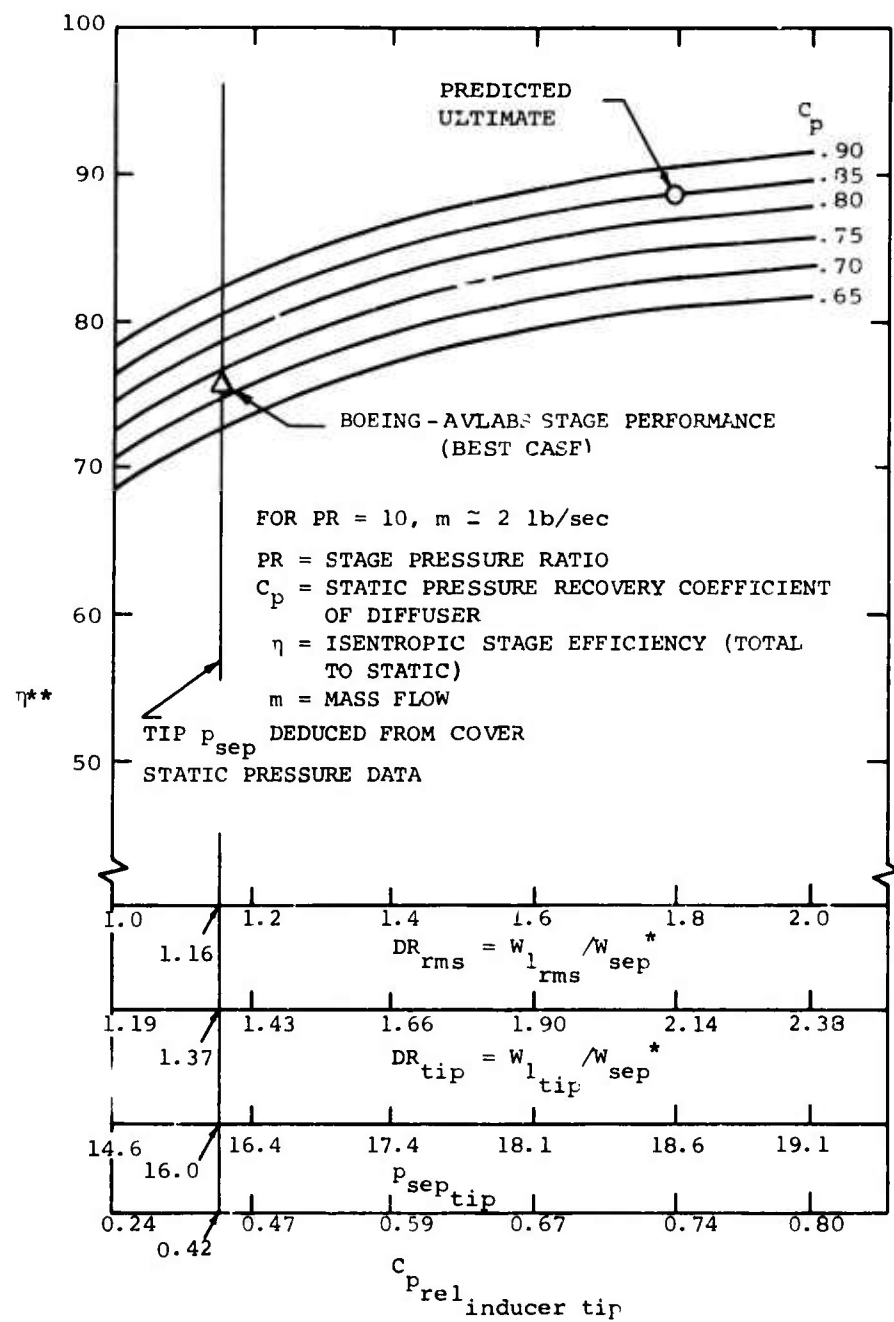
## 5.2 INDUCER FLOW DISTRIBUTION

The principal function of the so-called inducer portion of a centrifugal impeller is to cause an increase in the relative flow area, which is supposed to slow down the relative flow and accomplish relative diffusion. A reduction in the relative flow velocity is most essential, for stage efficiency proves to be strongly sensitive to the impeller's internal diffusion.

Centrifugal compressor workers do not seem to appreciate this fact universally. For the Boeing-AVLABS pressure ratio 10 compressors, approximately 1 psi gained in the inducer yields a 4-point improvement in stage efficiency! Similarly, impeller tip discharge pressure increases about four times the increase in static pressure at the impeller separation point. In other words, if 1 psi more relative diffusion can be gained, the tip pressure increases about 4 psi. Yet this is only part of the explanation of why the stage efficiency increases so dramatically with internal diffusion; the rest evolves from the reduction in impeller discharge mixing loss, as further diffusion of the relative stream causes a smaller wake at impeller tip. Figure 112 graphically portrays the relationship between inducer diffusion and stage efficiency.

Granting that internal diffusion is essential for high performance, how can maximum recovery be assured? To do that requires either extensive empirical development of the inducer or competent analytical models. Our objective here is to test the adequacy of the models we have for predicting inducer diffusion.

Behind the entry region, the potential flow analyses typified by the work of Stanitz et al should be applicable. The flow is not yet separated and should be in most cases "channel-like"; that is, the mean flow at any radius follows the camber line of the blading, and the flow is essentially two-dimensional. We will attempt to test the competence of this sort of model, as exemplified by the Boeing potential flow analysis program for centrifugal impellers. The methods



\* UNBLOCKED AT 1  
 \*\* NOT ACCOUNTING FOR DISK AND COVER FRICTION ( $\approx$  TWO POINTS DECREASE)

Figure 112. The Influence of Impeller Relative Diffusion on Compressor Stage Efficiency, Showing RF-2 Performance.

of these programs are not displayed herein; see Welliver and Acurio (1967, 67-30).

Because the relative Mach numbers are often close to 1 near the throat of the inducer, so small area changes make large Mach number changes; and because the boundary layers are growing thick on their approach to separation toward the end of the inducer, accurate prediction of boundary layer blockage is required. Here the analytical tools are not so good, primarily because the boundary layer grows from the leading edge through the complex entry region discussed in Section 5.1. Our success at describing accurately the boundary layers in the remainder of the inducer hinges critically on our competence in the entry region. This matter is examined in depth in Section 5.3.

#### 5.2.1 Selection of Data

The only evidence available for the inducer portion of the impeller must be derived from cover static pressure measurements coupled with mass flow, inlet stagnation properties, and impeller geometry. Cover data were taken for the Workhorse and RF-2. Unfortunately, the Workhorse inducer yields little useful information for the present purpose because it separated on the hub. Had we static pressure distributions on the hub, we could make meaningful tests of the analytical tools. The cover static pressures are too far removed from the critical events on the hub to make any useful assessment from them.

Before proceeding to examine the RF-2 inducer data in detail, we will present the evidence that the Workhorse separated on the hub.

#### 5.2.2 Evidence That Workhorse Separates on the Hub

The principal evidence is:

- (1) The cover static pressure falls considerably below the potential solutions right from the inducer inlet.
- (2) The inducer static pressure rise is considerably less than that predicted by the potential solutions.
- (3) The potential solution shows the hub loading to be excessive; boundary layer calculations indicate early separation.

- (4) The impeller exit profiles show a thick region of degenerate fluid on the hub, suggesting hub separation.

Figure 113 presents Workhorse cover static pressure distributions in the inducer region. Two potential solutions for different mass flows are displayed. Both of these curves are considerably higher in pressure than the measured values. For the RF-2 impeller, we shall ascertain below that Boeing underestimated the aerodynamic boundary layer blockage in the inducer. But for Workhorse, changing this blockage in the calculations within reasonable limits will not suffice to bring the potential solutions into line with the cover measurements. Even at the lowest mass flow tested, the Workhorse inducer cover data have the same shape as the curve in Figure 113. Therefore, we are confident that the low pressure measured in the inducer for Workhorse is occasioned by separation, not blockage.

Figure 114 displays the calculated blade surface velocities for the Workhorse from the potential solution. These extend only for about the first 3/4 inch into the impeller, but it is evident from an examination of the velocity distribution along the hub suction surface (next to bottom curve) that this surface is heavily loaded. A series of boundary layer calculations was run, using this velocity distribution. For every assumption of inducer entry overvelocity ratio from 1.0 to 1.5, the boundary layer separated quickly from the hub. At very high overvelocity ratios, separation was indicated at the tip also. But for overvelocities of 1.2 or less, the tip suction surface streamline remained unseparated.

From this evidence it is clear that the hub of the Workhorse inducer is critical and did separate early, severely compromising the inducer's diffusion accomplishments.

The above evidence is strongly based on the potential solutions. If the potential solutions are erroneous, the evidence would not have any necessary validity. Fortunately there is additional evidence found at the impeller exit. First, the static pressure at the impeller tip was considerably below the design predictions of Boeing. It was also 4 to 5 psi below the impeller tip pressure

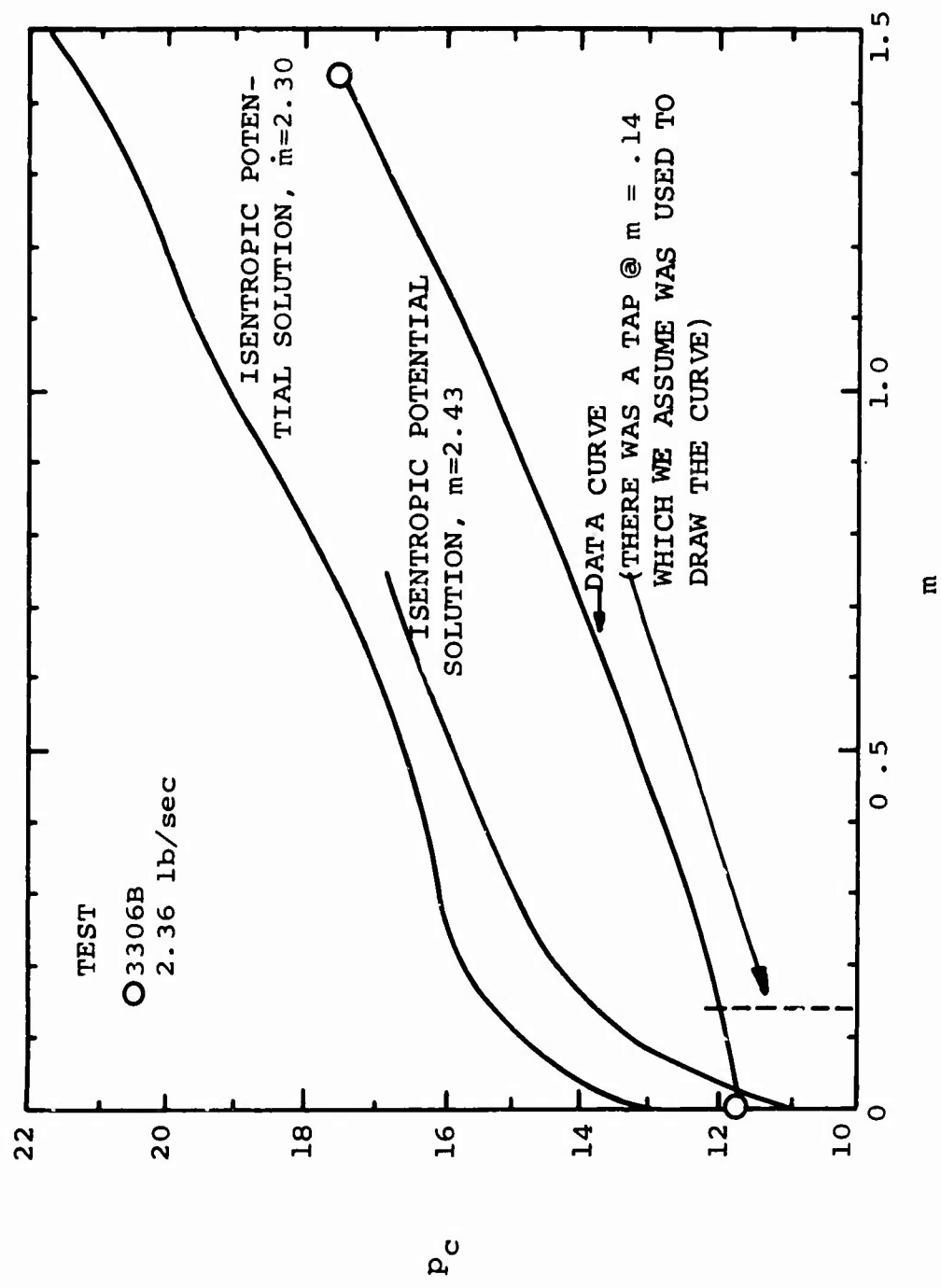
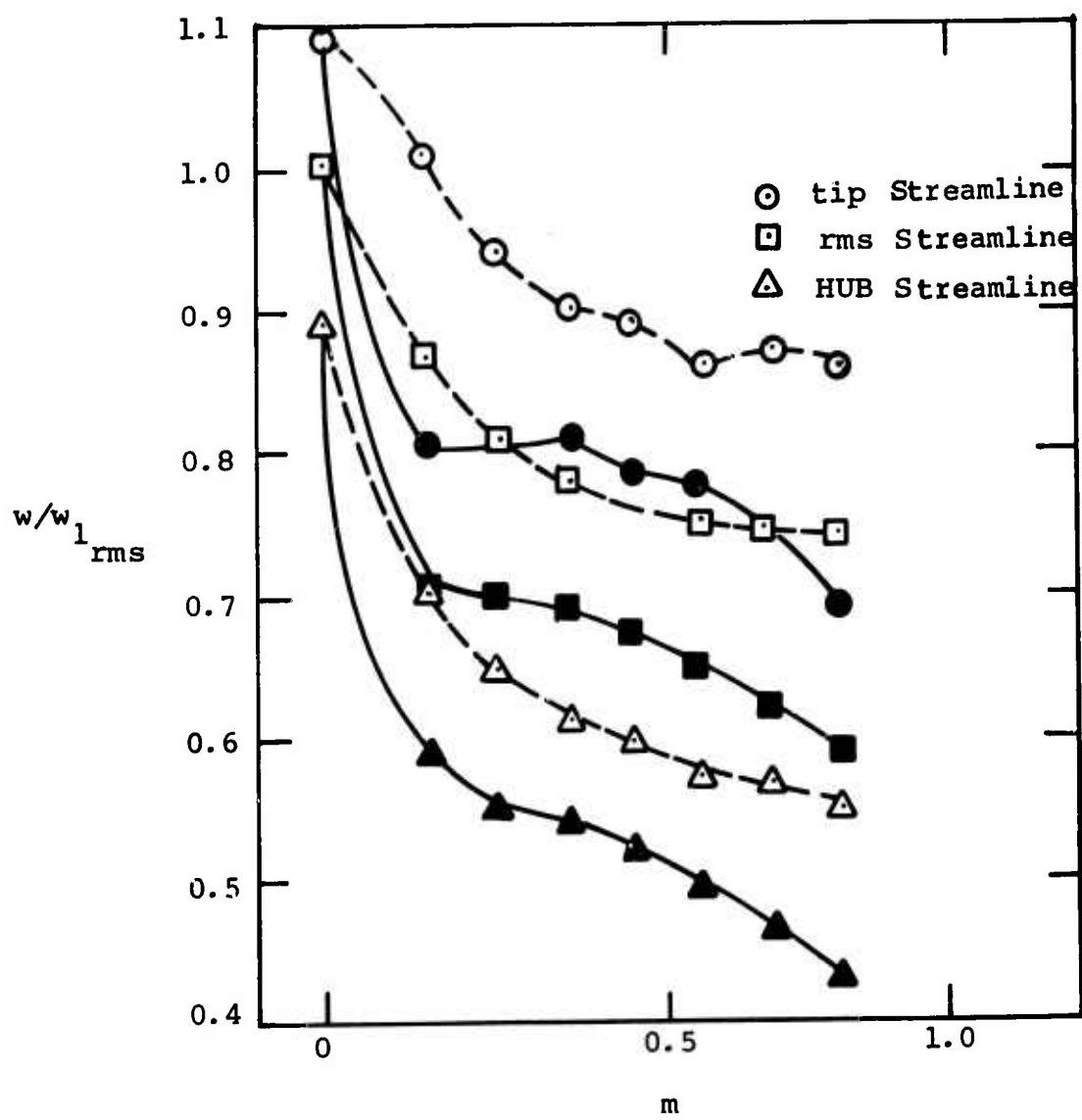


Figure 113. Workhorse Cover Static Pressure versus Meridional Distance From Leading Edge.



NOTE: SOLID SYMBOLS ARE ON PRESSURE SURFACE.  
OPEN SYMBOLS ARE ON SUCTION SURFACE.

Figure 114. Potential Solution, Blade-Surface  
Velocities, Workhorse ( $w_{1 \text{ rms}} = 1086$ ).

achieved by RF-2, despite almost identical tip speeds. The substandard tip static pressure of Workhorse suggests poor relative diffusion and an early inducer separation.

More evidence can be found in the distribution of flow properties at the tip of Workhorse, especially when compared to similar measurements at the tip of RF-2. In examining these profiles, the lessons of Section 4.2 must not be forgotten. However, there is such a distinct change in profile shape between Workhorse and RF-2 that the message comes through the noise of the probe measurements.

In Figure 115, typical tip profiles for Workhorse and RF-2 are compared. Note the distinct evidence of a low flow region on the hub of Workhorse. There we would not expect to see nearly as much flow deficiency as on the cover because the separated stream should tend to run up the hub under the impulse of the bend to radial. For Workhorse, a strong flow deficiency at the hub means that something drastic occurred upstream on that surface.

### 5.2.3 RF-2 Inducer Flow

Static pressure data from the cover of the RF-2 inducer has been analyzed in considerable detail. The data, which may be found in Section 3, are plotted in Figure 116, along with results from the analytical models.

The static pressures indicated on the cover were not corrected by the methods described in Section 4 for tap errors. Figure 116 indicates the uncorrected pressures. The corrections were applied in the analysis, however.

The measured static pressure varies considerably with mass flow at some cover locations. This is particularly true in the high relative Mach number region near the inducer throat, where small flow changes produce large Mach number and static pressure changes. However, near the leading edge of the inducer, the change is quite small.

The impeller tip static pressure hardly changes at all (0.3 psi) over the full flow range of the RF-2 stage. This

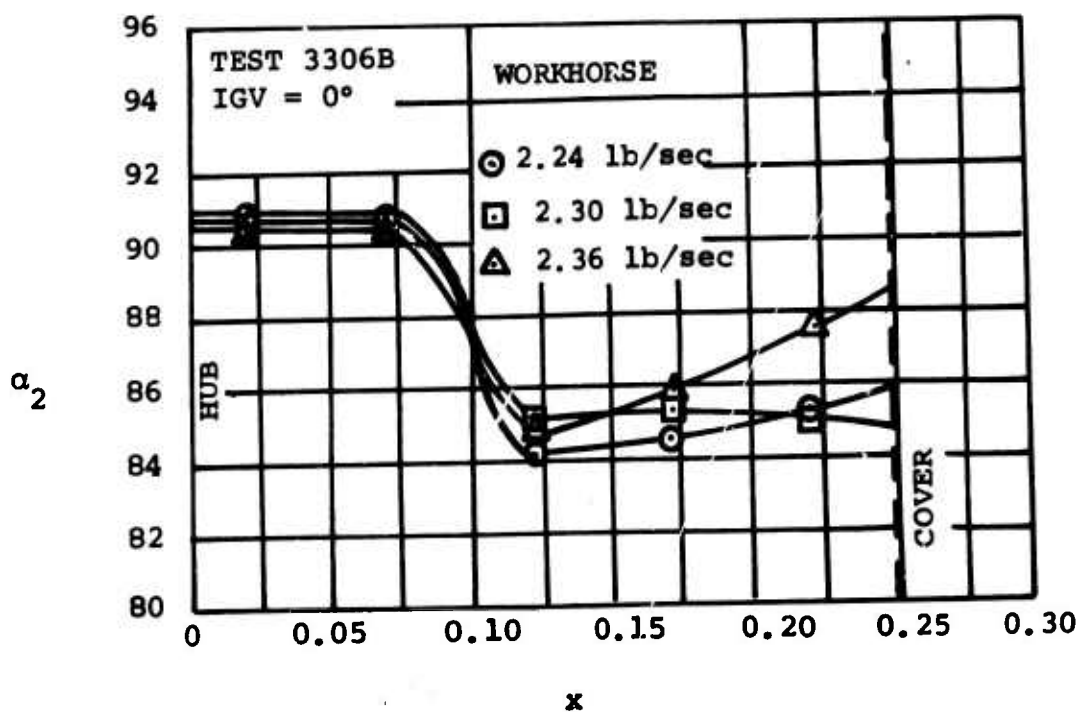
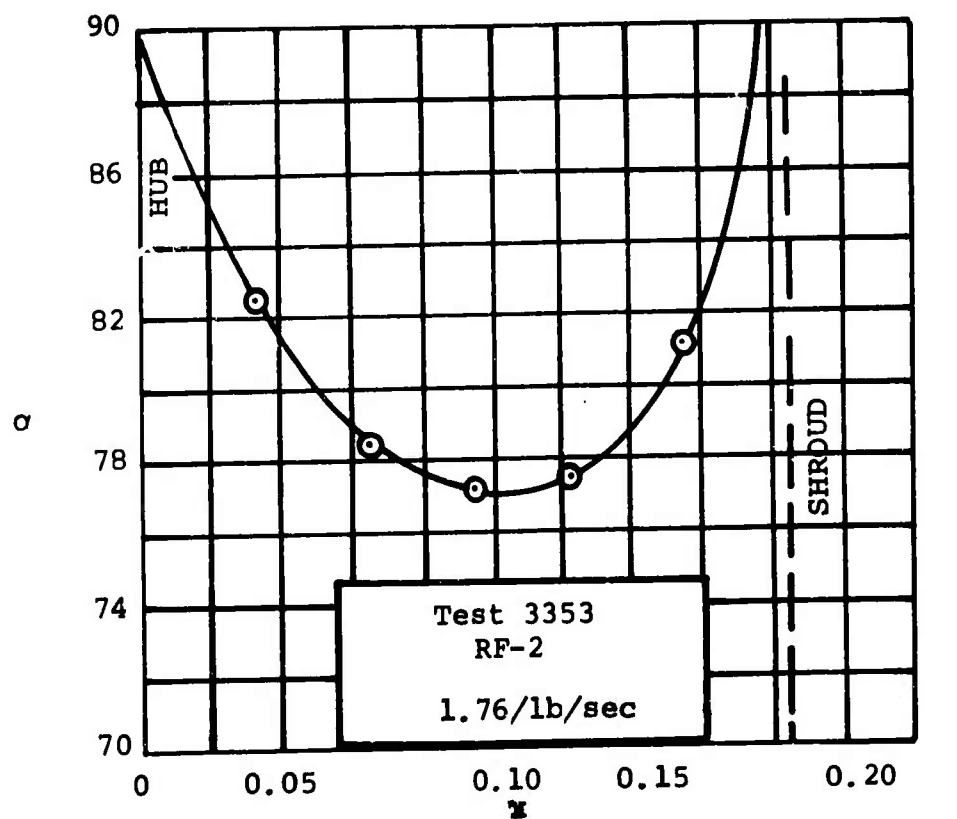


Figure 115. Comparison of Typical Impeller Discharge Property Profiles for Workhorse and RF-2.

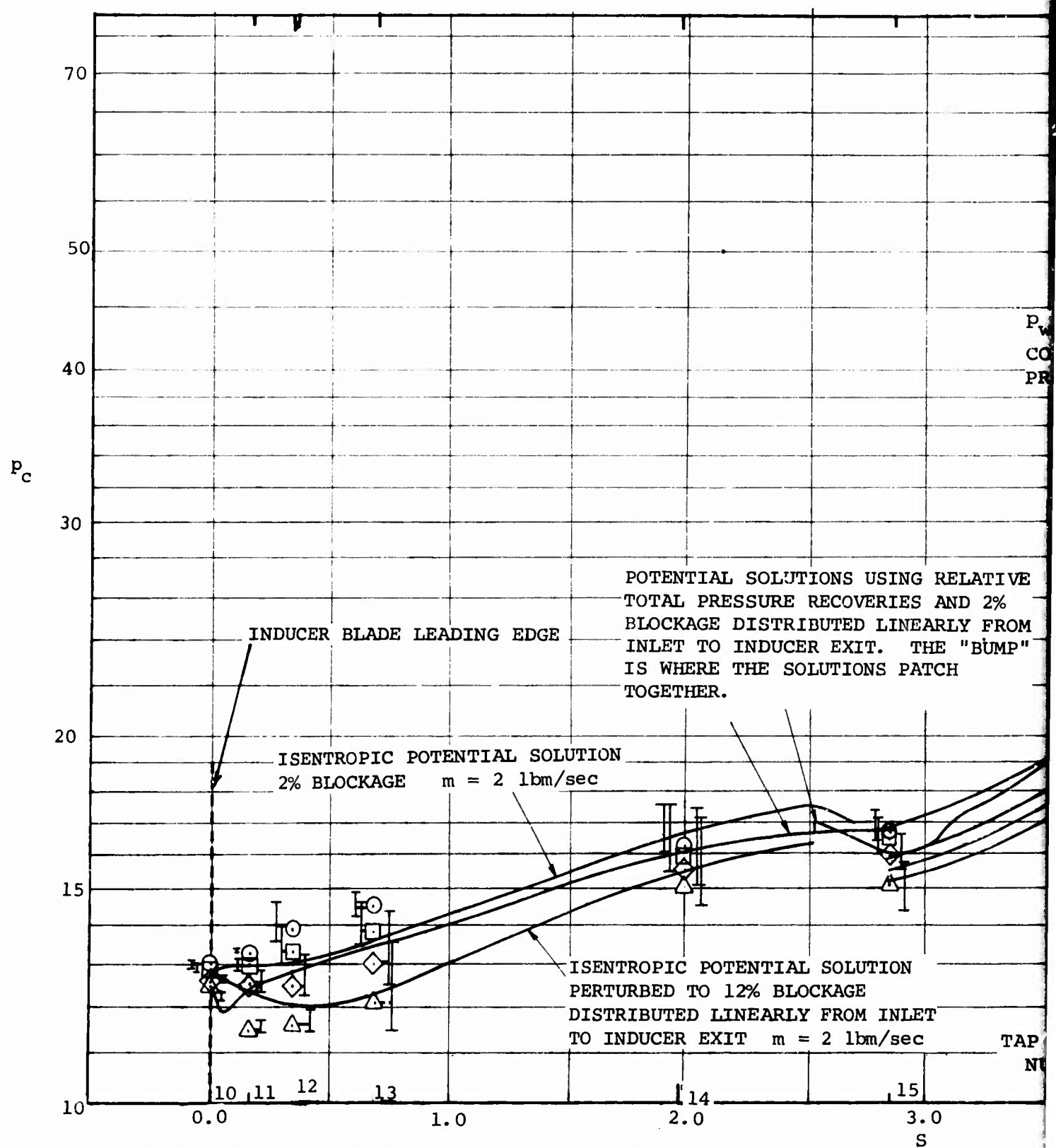
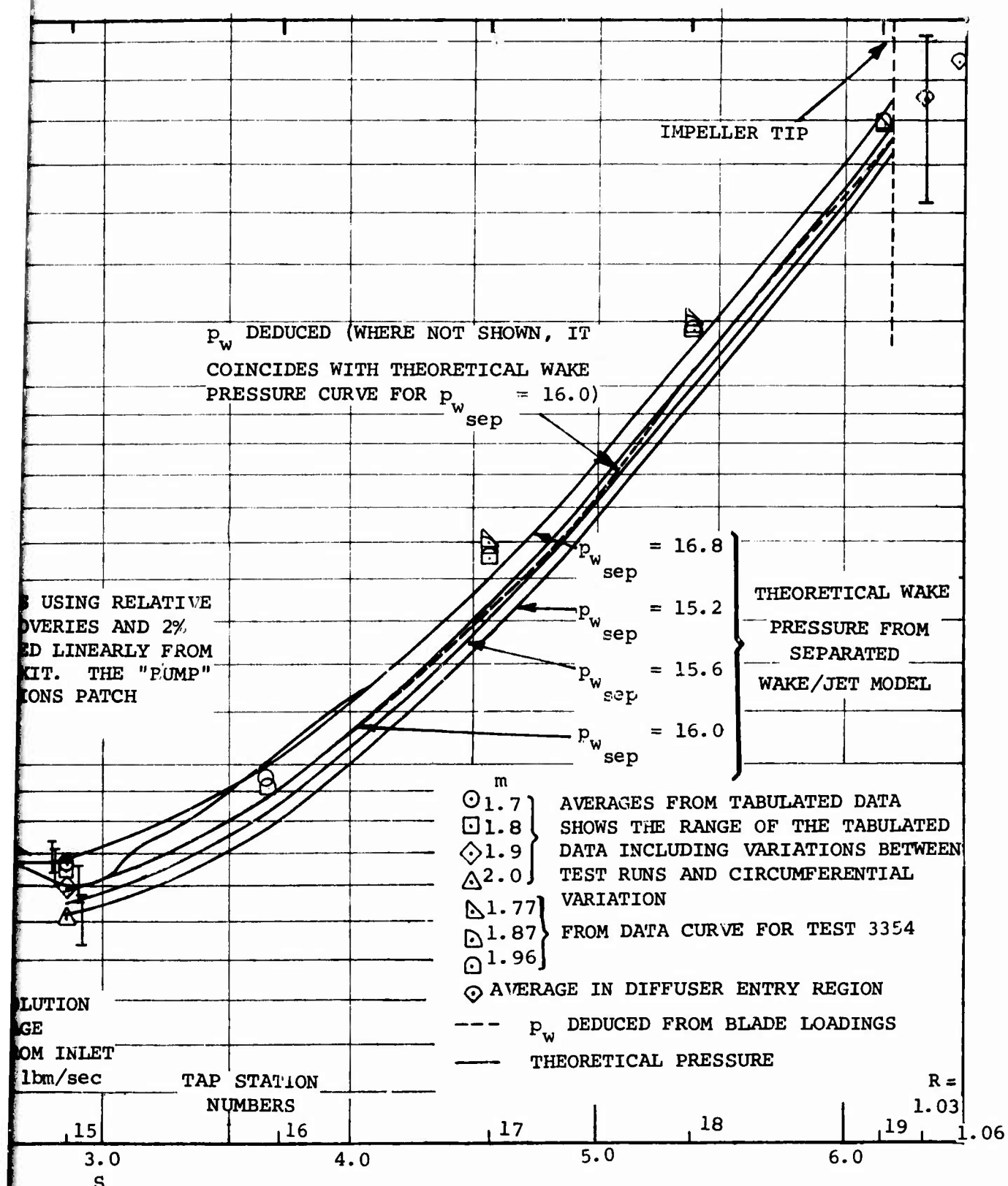


Figure 116. Impeller Cover Pressure Data, Results of Potential Solutions and Separated Impeller Theory.



B

characteristic is surprising, because the peak relative Mach number on the inducer tip should vary with flow rate. We have attenuated evidence of that in Figure 116, particularly at taps 11, 12, and 13. This observed behavior suggests that it is not diffusion from the peak Mach number on the inducer which governs the separation location, but rather the overall diffusion from the inducer inlet.

The circumferential variation of static pressure mentioned as a major source of uncertainty in Section 4.1 causes further uncertainty because the stationary tangential pressure pattern changes with flow and with diffuser design. Part of the data scatter indicated in Figure 116 is caused by these effects. A "mean" curve, faired through the points in Figure 117, was constructed similarly on plots made at each station on the cover. The uncertainty band is about  $\pm$  0.7 psi wide; this is a major uncertainty, as has been discussed in Section 4.1.

The only data available for the radial portion of the compressor is from Test 3354, Figures 60 - 62. No other data were presented by Welliver and Acurio. Presumably, considerably more data were taken on the cover but are no longer retrievable.

#### Impeller Diffusion

Figure 116 shows that a mass flow of 1.85 lbm/sec agrees well with the potential solutions in the inducer entry region. This mass flow appears to be fluid dynamically equivalent to Boeing's design predictions at a mass flow rate of 2 lbs/sec. The incidence on the inducer tip apparently was equal to the design value at a somewhat lower flow rate, perhaps because of greater inlet blockage than estimated by Boeing in design, but probably because of the flow distortion at inlet.

The potential solution used by Boeing takes no account of meridional shifts of the streamlines ahead of the impeller inlet. The data shown in Figures 71 and 82 demonstrate the effect. Blade blockage is higher at the hub than at the tip. Radial blockage variation causes the streamlines

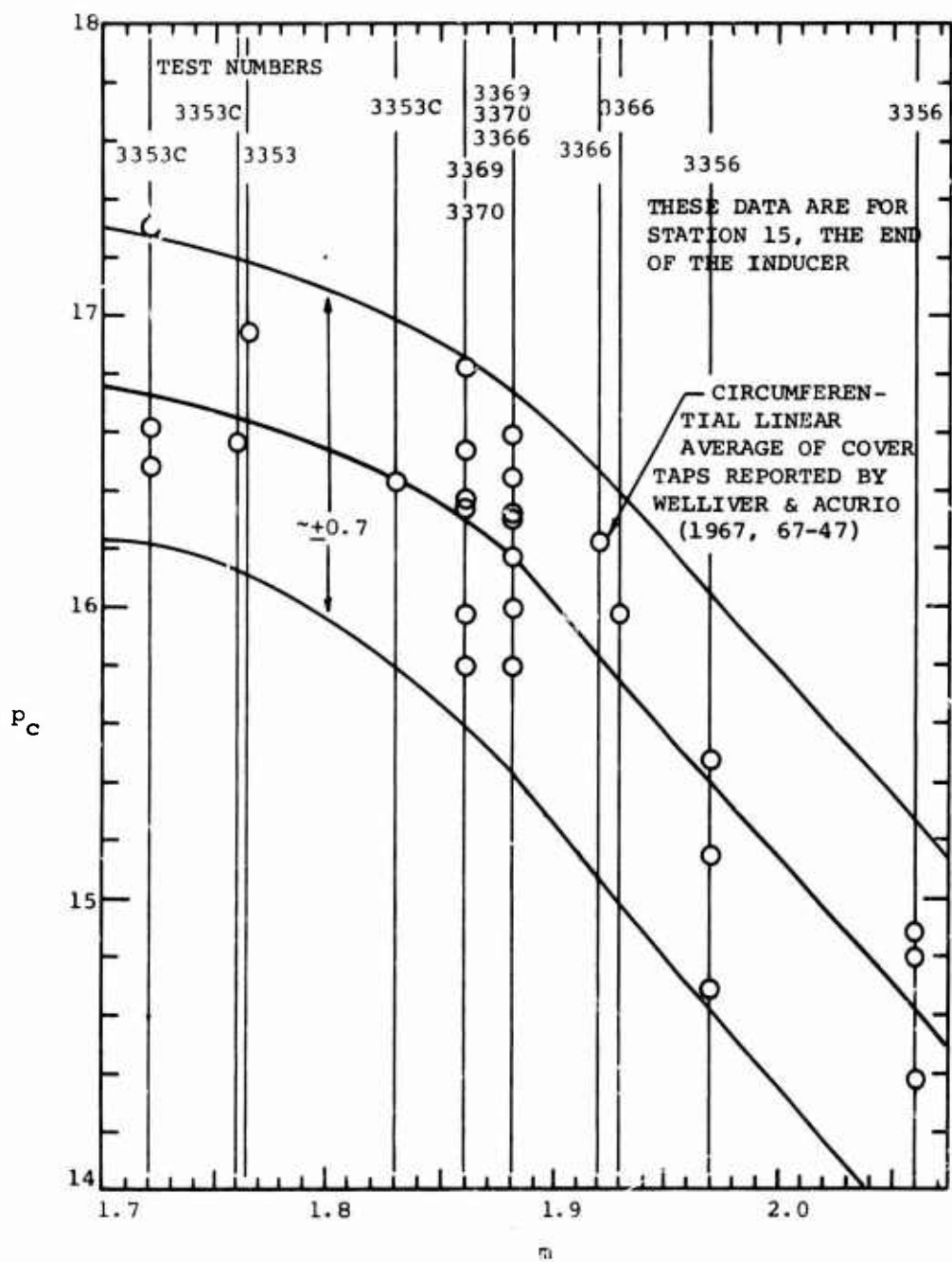


Figure 117. Cover Tap Data Showing Construction of Mean Curve.

to shift from hub toward the cover; the hub pressure is increased by the meridional turning. Also, the mass flow per unit area at the hub is reduced which forces up the mass flow per unit area at the tip, making the tip incidence correspond to a somewhat higher mass flow than the average value. Stanitz (1951) provides a theory for the meridional flow pattern caused by radial blockage variation.

In Section 5.4, by comparison of the separated impeller model and the cover data, we have concluded that the pressure at separation for  $m = 1.85$  is close to 16.0 psia. Figure 112 shows how the impeller diffusion achieved fits onto Dean's (1968) parametric study of pressure ratio 10,  $m \approx 2$  compressors. We note that there is very good agreement between the parametric study and the reduced RF-2 impeller data. (Note that the stage efficiency plotted is three points higher than that measured by Boeing, because Dean did not account completely for disc and cover friction.)

The RMS diffusion of the inducer works out to be 1.16; the diffusion from inducer tip average inlet velocity to the separation velocity is about 1.37. The local diffusion ratio on the blade surface must be quite a bit higher, perhaps as high as 1.8. The mean relative pressure recovery coefficient at the inducer tip is about 0.42.

In Section 7, we shall consider how to improve the Boeing-  
AVLABS compressor. One promising tactic is to raise the inducer tip pressure recovery coefficient to about 60%, which would yield an RMS diffusion ratio of about 1.4. If the diffuser pressure recovery coefficient\* remains at 72.5%, as measured by Boeing on their best diffusers, then a stage efficiency (corrected for cover and disc friction) of 77% would be won without reducing impeller tip backflow or improving the diffuser. Yet we expect that diffuser performance can be improved, which should lead to an overall diffuser pressure recovery coefficient as high as 80%. In that case, the stage efficiency (without disc or cover friction) would be about 83%, giving a predicted actual efficiency of around 80%. Reduction

\* From impeller tip to collector.

in backflow into the impeller could yield another two to four points.

It is important to realize that a major gain in stage efficiency can be achieved by a small improvement in the inducer pressure recovery alone.

#### Potential Solution in Inducer

There appear to be some anomalies in Welliver and Acurio's (1967, 67-47) comparison of their potential solutions for the inducer and the measured pressure distributions. In Figure 118 we have plotted Welliver and Acurio's curve and the newly calculated potential solution results from Winslow (1968) from the Boeing "pressure recovery factor" potential solution for the fifth streamtube, which is very close to the tip. Corrections to the tip would raise the plotted pressures only slightly. The "predicted" curve of Welliver and Acurio (1967, 67-47) is lower by about 3/4 psi, for unknown reasons.

The newly calculated result seems to agree with the measured pressure distributions much better than Welliver and Acurio's computation. In the analysis of Section 5, we have used only the potential results taken directly from the calculations made at Boeing especially for this program by Winslow (1968).

In Figure 116 are curves labeled "potential" solution. Two types of potential solutions are displayed: one labeled "isentropic" and the other labeled "pressure recovery factor". The difference between them is as follows:

Before the AVLabs program, Boeing investigated inducer design during their MERDC\* project. The deviation of potential solutions and the measured cover pressure distributions were accounted for by injecting a relative total pressure loss smeared over the entire flow (expressed

---

\*Details of this program are unknown to us. However Boeing used the results of this investigation to develop their inducer model which is described herein.

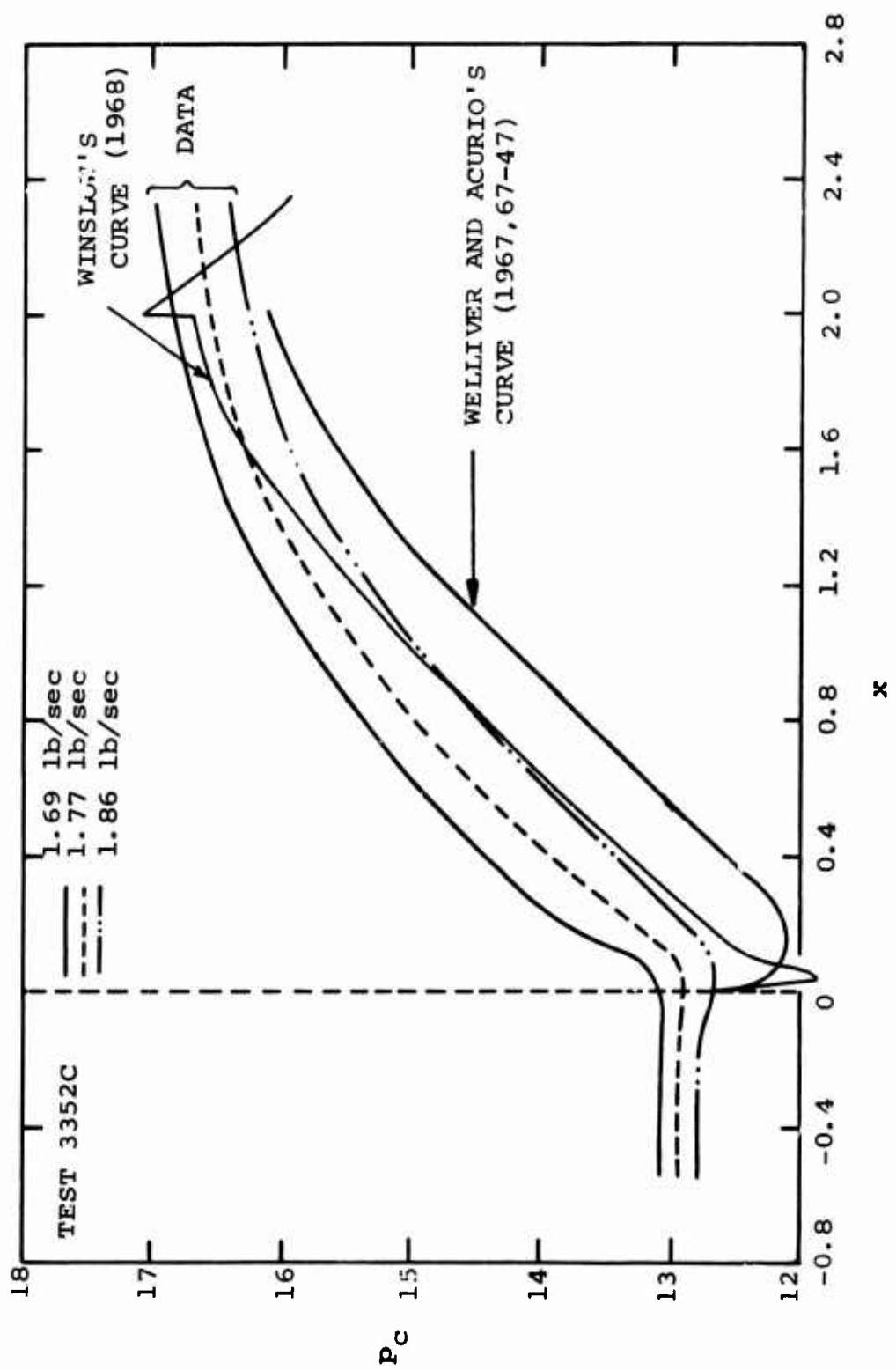


Figure 118. A Comparison of Cover Data and Potential Solutions by Welliver and Acurio (1967, 67-47) and by Winslow (1968).

in the form of a "pressure recovery factor"). This approach produced actually a "bugger" factor which fixes up the theoretical solution, rather than any sort of insight into the thermodynamics and fluid dynamics of the flow. For instance, if boundary layer blockage was misestimated in the potential solution, the correction by Boeing's approach would appear as an entropy increase.

The loss factors deduced from the MERDC inducers were used in the AVLabs program for Workhorse and RF-2 design calculations. The curve in Figure 116 marked "pressure recovery factor" potential solution is the result of this approach. The curve in Figure 116 for isentropic core flow is marked "isentropic" potential solution and is obtained with the pressure recovery factors set to unity.

A much more reasonable model of the actual fluid dynamics in the inducer is produced by assuming a reversible core flow. Indeed, we have shown in Section 5.4 that a reversible through-flow core can be assumed to exist all the way to the tip of the impeller.

Boundary layers grow on the suction, pressure, and hub surfaces of the impeller, and upon the cover. They produce a continuously increasing blockage which reduces the effective flow area of the passage. Perhaps deduction of blockage factors from the MERDC inducer work rather than fictitious loss factors would have been more enlightening.

The "isentropic" potential solution in Figure 116 was calculated by Boeing with a boundary layer blockage of 2% at the end of the inducer and zero at the beginning, with a linear distribution between. This blockage appears to be too small.

In order to reveal what blockage would close the gap between the isentropic potential solution and the measured RF-2 cover pressure, iterations were made at the fixed measuring stations in the inducer in order to deduce appropriate blockage corrections. The results are plotted in Figure 119; note that the additional blockage we have calculated is added to that assumed by Boeing for the isentropic potential solution.

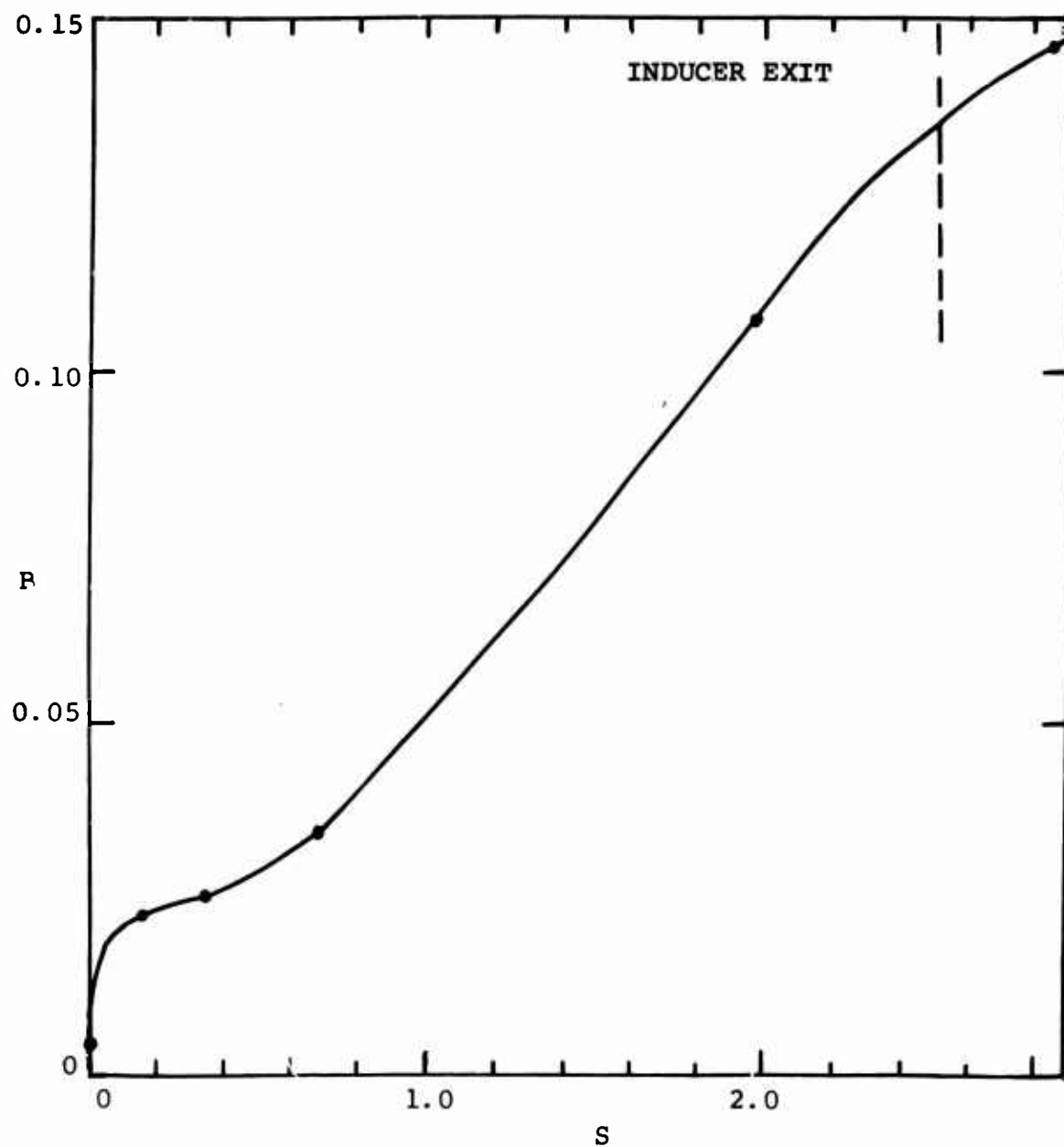


Figure 119. Aerodynamic Blockage in Inducer Required To Bring Isentropic Potential Solution (2% Blockage Already) Into Agreement With Measured Cover Pressure at Design Point (Potential Solution 2.0 lbm/sec; Data 2.0 lbm/sec).

We see that 13% blockage at the exit from the inducer appears to be more consistent with the data. This value cannot be checked by boundary layer calculations. Boundary layer predictions were made only at the inducer tip due to the lack of data on the actual pressure distributions elsewhere. However, if the displacement thickness of the boundary layers calculated at the tip of the inducer were applied uniformly all around the passage at exit, a blockage of 12% would result. This value is fairly consonant with the blockage derived by comparing the isentropic potential solution with the measured cover pressures (Figure 119).

The boundary layer calculations for the measured pressure distribution presented in Section 5.3 indicate that the boundary layer should not separate on the suction tip surface of the RF-2 inducer. Because the potential solution claims that the boundary layer situation is most adverse at the tip, we do not expect separation in any other location in the inducer. The prediction of separation beyond the inducer indicates that more relative diffusion could have been achieved.

Calculations of boundary layer behavior using the cover static pressure data shown in Figure 116 suggest separation at  $S = 3.4$ . Obviously then, a separation pressure higher than the 16.0 psi value measured and lower than the 17.5 psi value predicted from the isentropic inducer solution could have been achieved. Something on the order of 17.0 psi appears to be possible. An increase from the 16.0 measured to 17.0 will yield about three points improvement in stage efficiency (Figure 112).

This strong leverage arises from two sources: first, the impeller discharge mixing losses become smaller as more diffusion is won in the impeller; and second, the higher tip static pressure achieved reduces the diffusion demand in the diffuser and the impact of its inefficiencies on stage performance.

Figure 120 demonstrates how strongly changes in impeller pressure recovery affect the impeller tip pressure.\* For

---

\* See Appendix III for theory.

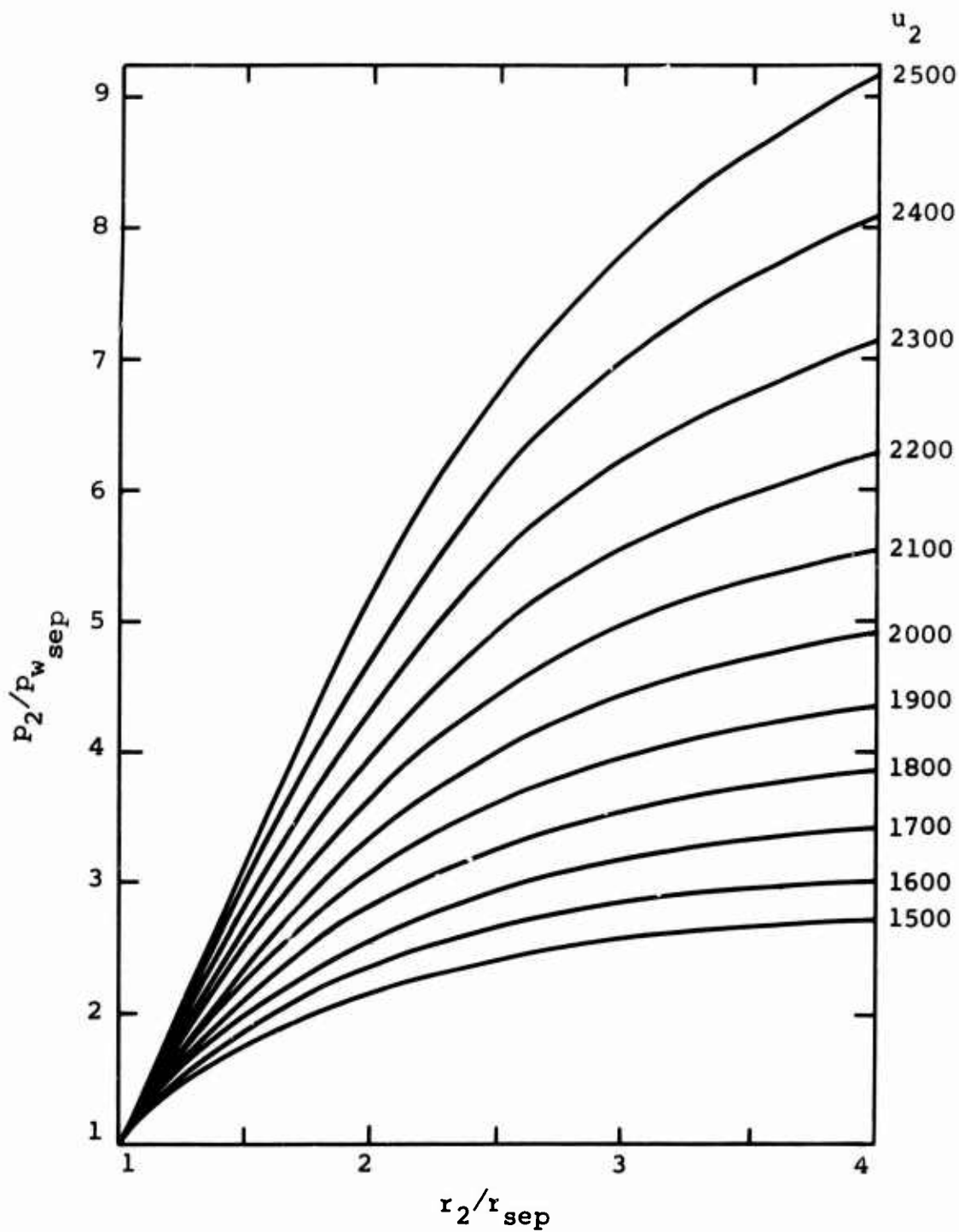


Figure 120. Dependence of Tip Pressure Upon Separation Pressure.

a series of different tip speeds and different radius ratios from impeller tip to separation radius, the ratio is plotted of static pressure at the tip to static pressure at separation. For RF-2 and Workhorse, the magnification factor is approximately 4; thus, a change of 1.8 psi at the separation point in the inducer amounts to a 7.35 psi change at the impeller tip -- one-half an atmosphere!

Such critical sensitivity demands good design analytical tools for optimized performance. A definitive research and advanced development effort is needed to provide working tools and proven inducer designs and design principles. See Section 8.1 for detailed suggestions.

In summary, it appears that Boeing could have won more inducer diffusion if more area ratio had been provided. The area ratio seems to be less than intended because Boeing underestimated blockage due to boundary layer growth in the inducer. Additional area ratio in the inducer could have been produced by altering either the cover or hub profiles or both.

The results also hint that boundary layer calculations coupled with potential flow solution applied in an iterative fashion should be competent to predict the pressure distribution and separation point in the inducer. But a definitive test of this method has been precluded by the absence of inducer separation in RF-2.

### 5.3 IMPELLER SEPARATION POINT PREDICTION MODEL

Separation occurs in the RF-2 impeller on the tip suction surface as asserted by Dean (1968), based on wake equilibrium arguments. However, Dean points out these arguments lead to an empirical inconsistency because the separation line tends to run off the front of the inducer. He concludes that there must be significant dynamic effects in the hub region along the separation line to cause it to run essentially normal to the relative flow streamlines as has been observed by boundary layer tracing techniques in research impellers. Figure 98 shows this schematically.

The Workhorse impeller separated in a contrary fashion on its hub because an excessive diffusion was designed into the machine there. These results, when contrasted, show that it is possible to design the impeller so that the assumption of tip suction surface separation initiation is not always valid. However, inducing early separation on the hub appears to have no virtues for achieving a maximum overall mean diffusion ratio in the inducer, so the practicality of designing for tip suction surface separation can be sustained. This is fortunate for practical measurements can be made only on the cover of high-speed impellers to indicate how much of the critical inducer diffusion has in fact been achieved.

As a safeguard during designing, boundary layer separation prediction calculations should be made across the inducer span from hub to tip.

Because the inducer recovery is so critical to stage performance, a strong research program in this area is recommended in Section 8.1.

The need for better methods of predicting separation is accentuated in high specific speed machines with their high inlet relative Mach numbers, because good diffusion in the inducer becomes, as inlet Mach number rises, more difficult to obtain and even more critical to stage performance, as pointed out by Dean (1968). Thus, an extraordinary effort must be made to achieve both improved diffusion and higher specific speed.

Below, a test of our separation prediction scheme incorporating potential flow calculations and boundary layer theory is attempted. The conclusions reached are "neutral", because the Boeing-AVLABS data offer only inappropriate or unchallenging cases, as will be explained.

### 5.3.1 Impeller Separation Predictions

Boundary layer calculations were made with the Englert (1951) method for the inducer using both the potential solution and the measured pressure distributions. In all cases, the relative Mach number along the suction tip streamline was the input.

The potential solution was made by Winslow (1968) for isentropic flow from the leading edge of the inducer to the streamline distance  $S = 2.69$ . The relative velocity was extrapolated to the tip radius from the fifth streamtube of the potential flow analysis. The required extrapolation is small; no corrections larger than 30 ft/sec were needed.

The starting conditions prescribed for the boundary layer calculations were:

$$H_i = 1.4 \quad \text{and} \quad \theta = 0 \quad \text{at } S = 0.137 \text{ in.}$$

The relative Mach number distribution used for this calculation is given in Figure 121 together with the boundary layer shape factors  $H$  and  $H_i$ , and the boundary layer thicknesses  $\theta$  and  $\delta^*$ , as a function of streamline distance along the blade tip suction surface.

### Measured Pressure Distribution

Section 5.2.3 shows that due to a larger distortion of axial velocity at the inducer inlet than was anticipated, the equivalent mass flow is 1.85. Figure 122 shows the relative Mach number as deduced from the cover static pressure at this mass flow rate. Three "overvelocity" distributions were assumed as shown in Figure 122. These had maximum "peak" Mach numbers of 1.0, 1.1, and 1.2. Some change in the calculated boundary layer results would occur, no doubt, with changes in the steepness of

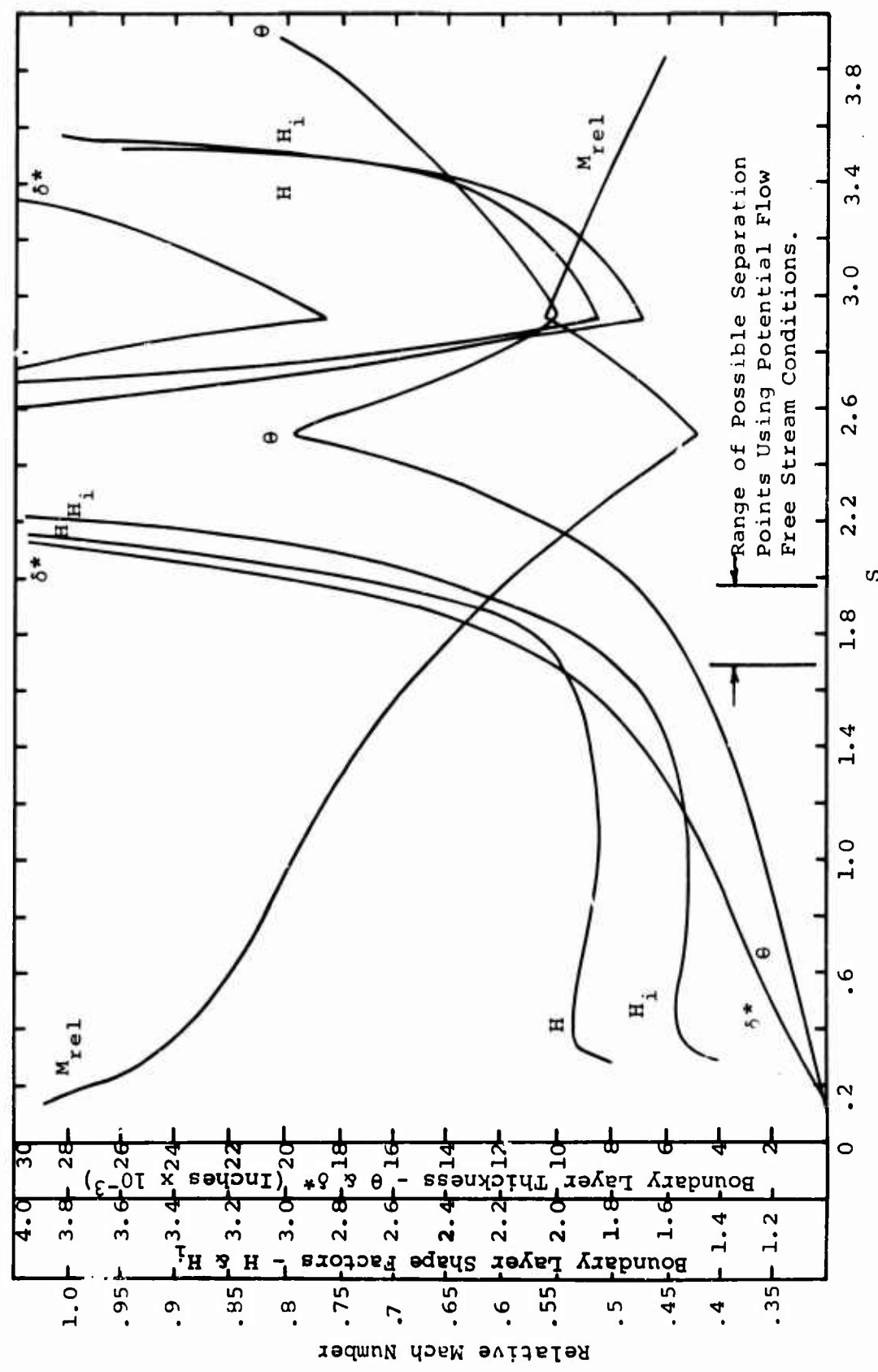


Figure 121. Boundary Layer Calculation with Potential Solution.

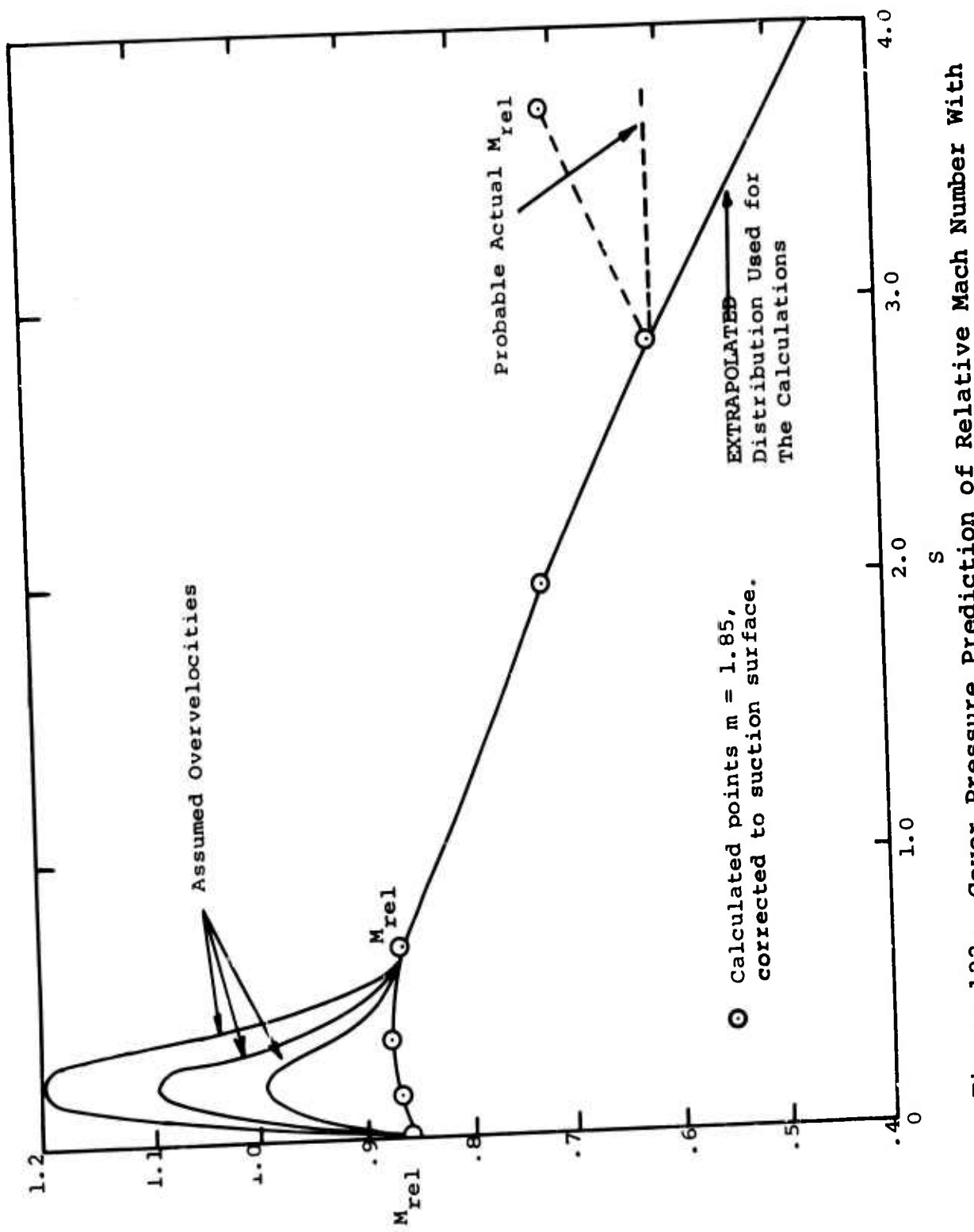


Figure 122. Cover Pressure Prediction of Relative Mach Number With Three Assumed Overvelocities.

the assumed leading edge deceleration, but they are expected to be secondary effects. The calculations have all assumed a turbulent boundary layer from the leading edge.

The results for the boundary layer calculations for the RF-2 inducer and the "measured" static pressures are shown in Figures 123, 124, and 125 for the  $M_{peak}$  = 1.0, 1.1, and 1.2 overvelocity cases respectively. These show the distribution of shape factors and boundary layer thickness with streamline distance.

We note in Figure 121, for the potential solution case, that the flow separates rather early in the inducer and achieves about 16.3 psi at the separation point.

For the measured pressure distributions, Figures 123, 124 and 125, the boundary layer does not separate before the bend to radial. It is also quite plain that the boundary layer will not negotiate the bend very far without stalling, although we do not know exactly where stalling occurs. We suspect that separation occurs near the entry to the bend where  $M_{rel}$  = 0.6. The reason for the indicated acceleration near the last static pressure tap on Figure 122 would then be that the tap is no longer representative of the mean pressure due to the separated wake width.

The calculations do indicate for the largest overvelocity case (Figure 125) that the boundary layer separates where the rapid deceleration on the blade leading edge occurs. However, the Englert method of calculation rapidly converges the boundary layer characteristics back to those typical of an unseparated boundary layer after the steep deceleration is eased. Physically, a slight separation in the inlet flow would be expected to reattach.

Since the measured pressure distributions have been "corrected" to the suction surface of the inducer blade in order to perform the boundary layer calculations, these calculations inherently embody the potential flow solution obtained for this impeller without accounting for boundary layer growth. No iteration has been attempted between the boundary layer calculations and the potential flow solution.

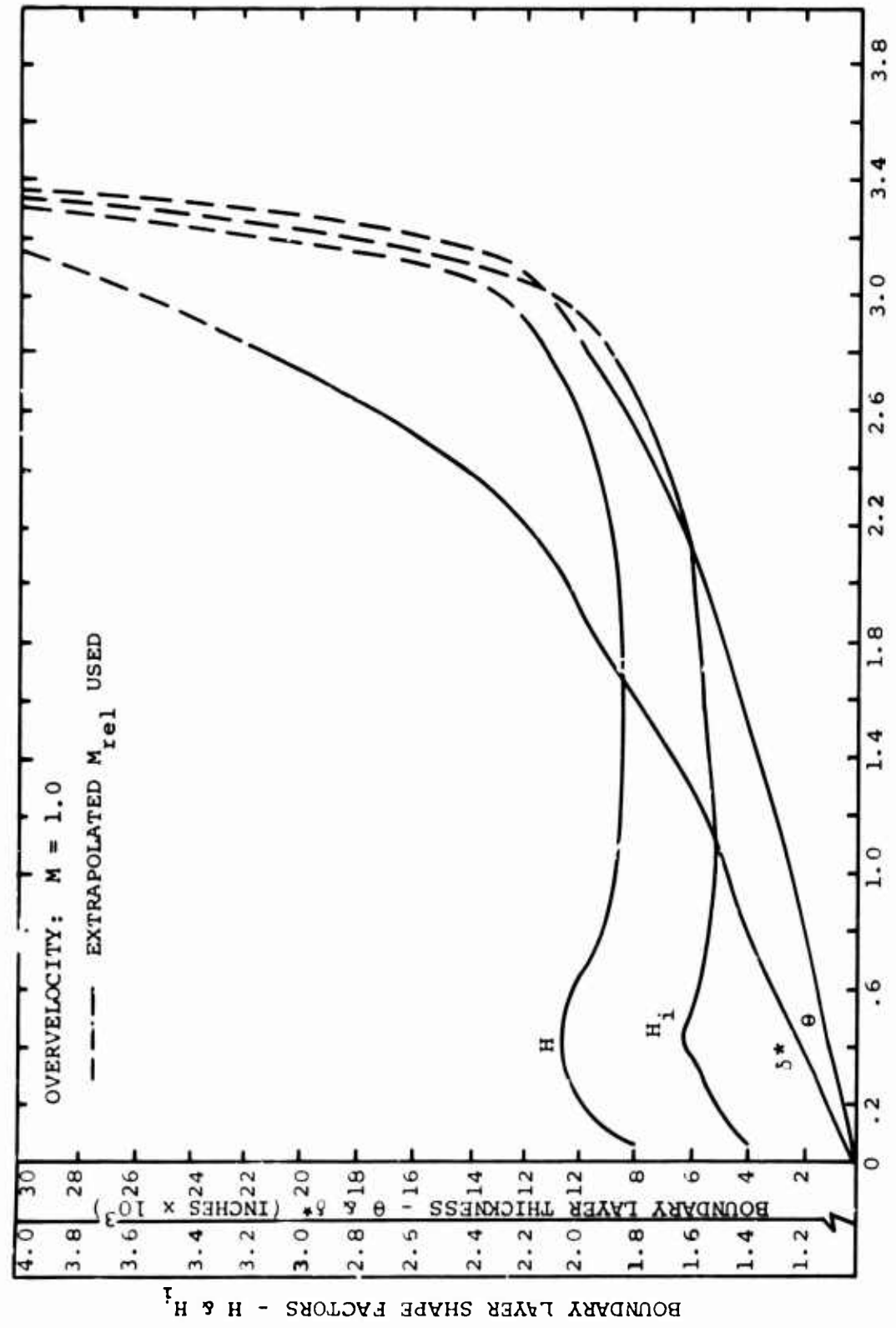


Figure 123. Boundary Layer Calculations Using Measured Pressure in the Inducer.

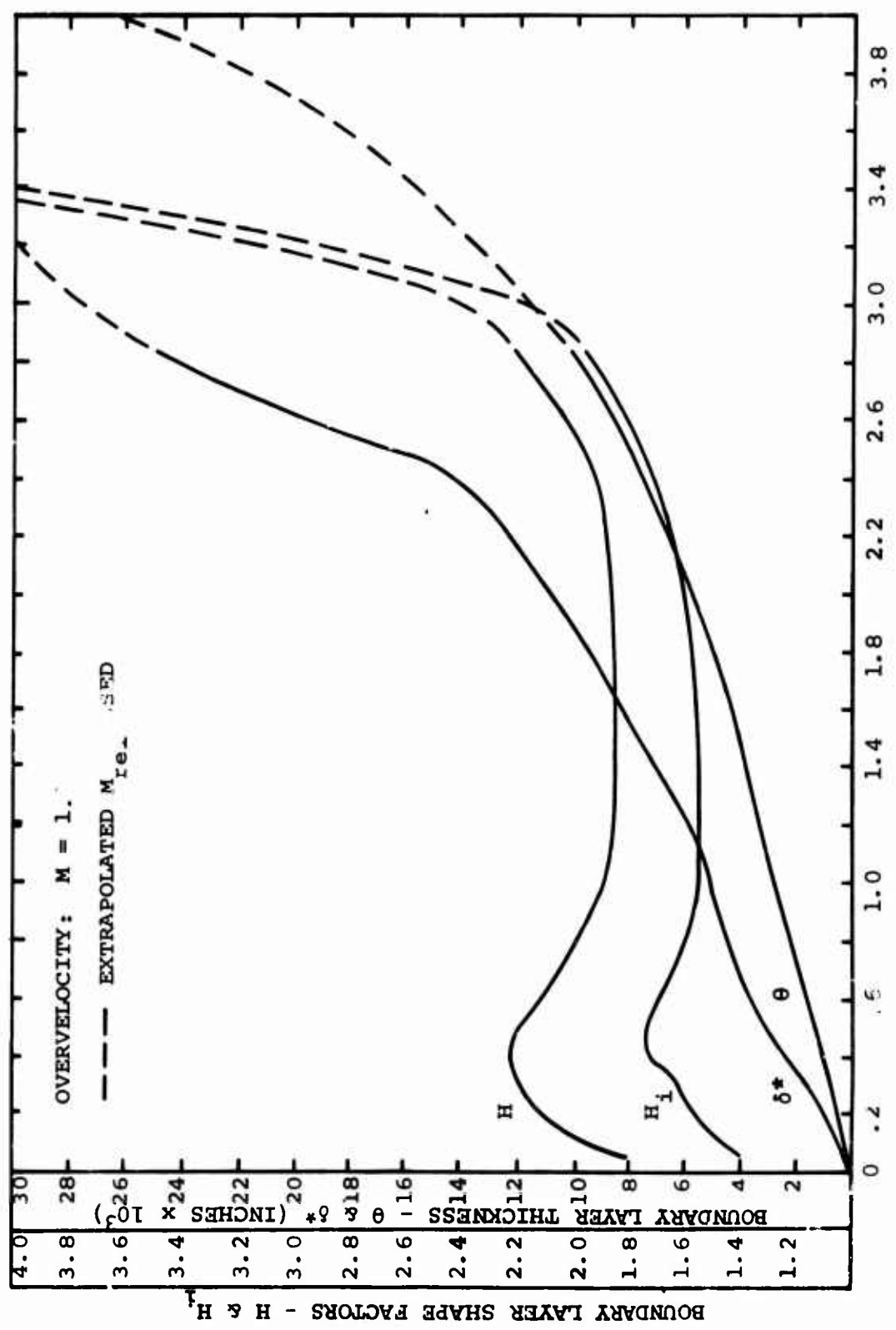


Figure 1.24. Boundary Layer Calculations Using Measured Pressure in the Inducer.

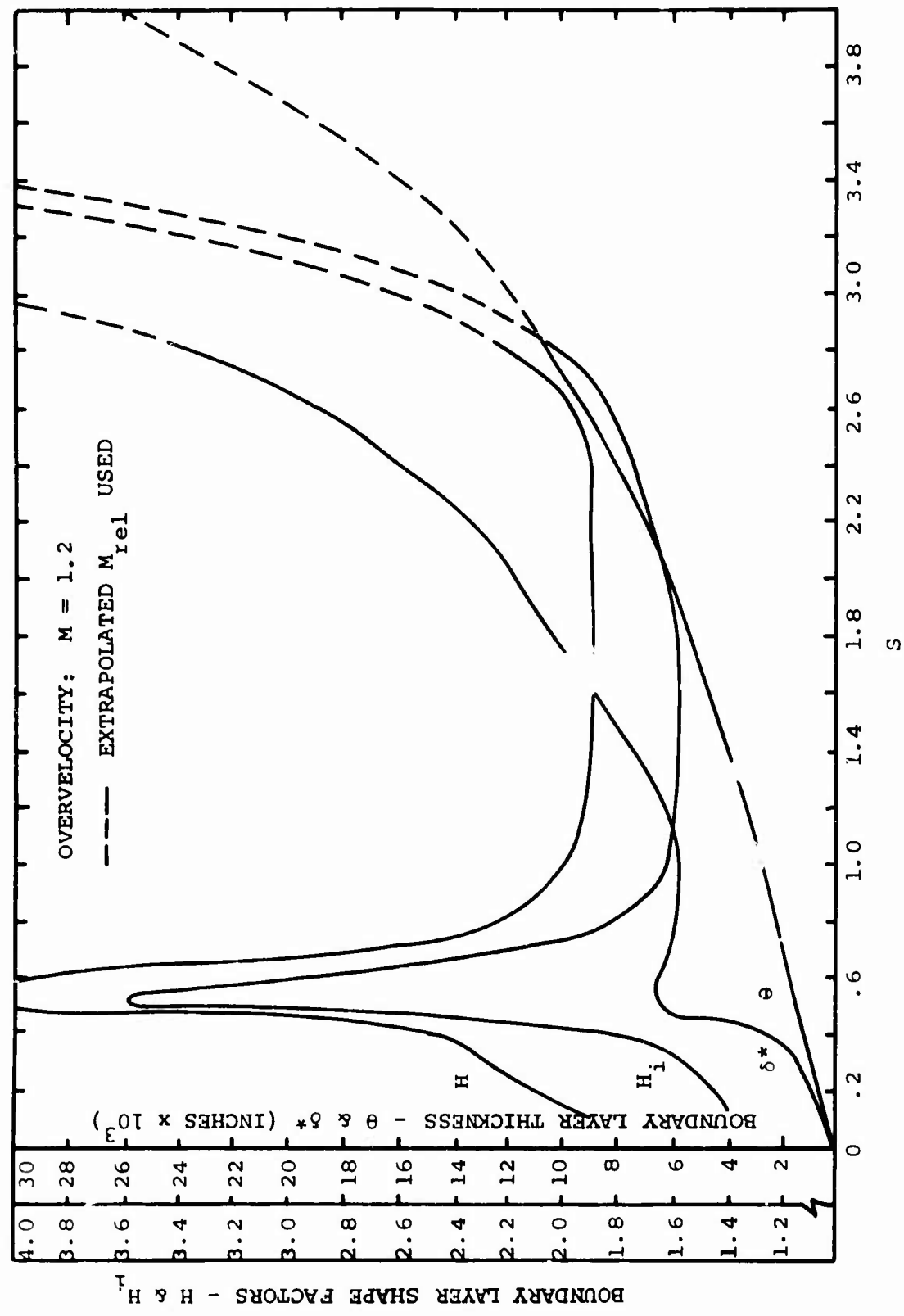


Figure 125. Boundary Layer Calculations Using Measured Pressure in the Inducer.

Since the Mach numbers are close to sonic, small changes in passage area can produce large changes in the actual pressure distribution. The potential flow solution should be corrected by iteration with the boundary layer solution, and this "corrected" potential solution should be used to alter further the inducer suction-surface "measured" pressure distribution used in the boundary layer calculations. Such has not been done here.

It is difficult to say from these boundary layer calculations whether the separation point can be predicted, because, for the measured pressure distribution, separation appeared to occur beyond the inducer. Boeing had an area ratio of 1.32 for their inducer. We suspect that area ratios near 2 are optimum. This will be discussed further in Section 6.

In summary, we find we cannot test these models critically against the data. A test is urgently needed so that accurate inducer design methods can be developed.

## 5.4 IMPELLER SEPARATED FLOW

Beyond the separation point in the impeller, our theoretical model structure is a simple essentially one-dimensional analysis.

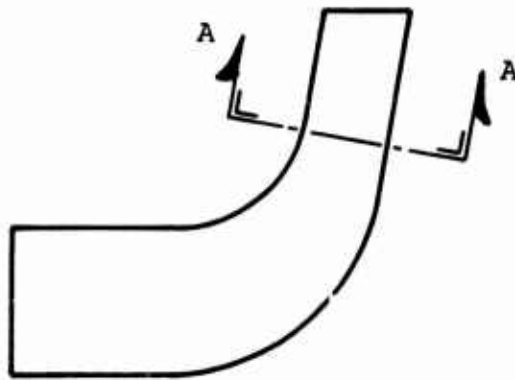
The basic assumptions are:

- (1) The wake fluid is quiescent (i.e.,  $W \approx 0$ ).
- (2) The through-flow jet is isentropic, having constant relative total pressure and total temperature (equal to the inlet absolute stagnation values in the absence of guide vanes).
- (3) The wake relative total temperature is constant and equal to the jet value (this assumption can be easily modified to account for the infusion into the wake of hotter fluid, from the cover boundary layers, for example, or to account for heat transfer from the metal surfaces).
- (4) The gas is perfect.
- (5) The location of the separation point can be specified, and the static pressure is known there.
- (6) There are no fluid shear stresses.

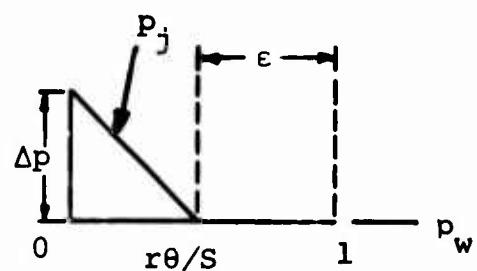
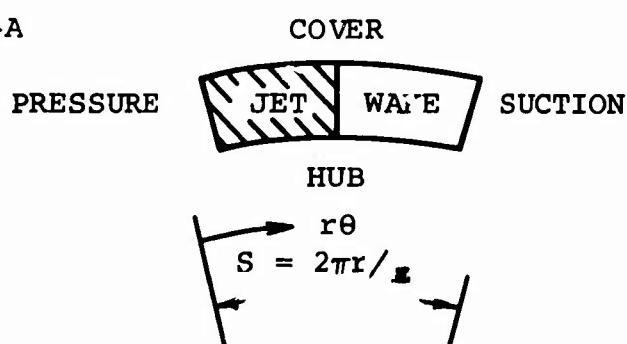
The theory is developed in detail in Appendix III. The development includes generation of the static pressure distribution for the wake region as well as analysis for calculating the characteristics of the through-flow jet. In order to do the latter, further assumptions are needed regarding the distribution of properties across the through flow. These will be considered in Section 5.6, where the flow pattern at the impeller tip is needed. Here we shall examine only whether the experimentally determined wake pressure distribution is in accord with the wake model for the separated part of the impeller.

### 5.4.1 Calculation of Wake Pressure

In the radial portion of the impeller, no potential solutions are available because the flow is separated. Instead, in order to convert cover data to wake pressure, the variation in static pressure across the separated jet was calculated from the model of Figure 126 by an iterative process using the output wake width from the separated flow calculation.



SECTION A-A



$$\begin{aligned}
 \text{ASSUMPTION: } p_c &= \epsilon p_w + (1-\epsilon)(p_w + \Delta p) \\
 &= p_w + (1-\epsilon) \Delta p
 \end{aligned}$$

Figure 126. Model for Jet Pressure Variation.

### Blade Loading Pressure Distribution

In order to test analytical models of impeller flow, the blade loading pressure distribution must be deduced from the time-average cover readings. To do this, the static pressure changes across the blade passage in the inducer were obtained from the Boeing potential solution, then applied to transform the measured mean value to the suction surface.

The slip factor variation along the jet was uncertain so two cases were calculated. The first assumed that the jet follows the blade and has a slip factor of 1. In the second case, the flow is allowed to begin slipping inside the impeller; at the impeller tip the observed mass-flow-average slip factor was matched.

For the first case, the application of the angular momentum relationships gives, for the pressure difference between the two blades,

$$\Delta p = \frac{2m\Omega}{bg_o Z}$$

For the second case, the radius ratio where slip begins was arbitrarily chosen to be 0.75, as recommended by Stanitz et al, from unseparated two-dimensional potential solutions for flow between the blading in the relative plane. The local slip factor was varied parabolically with radius ratio, starting with a slip factor of 1 at 0.75 and matching the actual tip slip factor at 1.0. Use of this procedure gives, for the pressure change across the jet,

$$\Delta p = \frac{2m\Omega}{bg_o Z} [1 - 16(1-\sigma) (r/r_2 - 0.75) (2r/r_2 - 0.75)]$$

In Section 6.6, a study is reported of impeller work input with the aim of deducing backflow and the most likely value of the slip factor for the through flow. There, it was concluded that the slip factor was probably on the order of 0.83 rather than the Boeing-reported value of 0.88 for RF-2. Using this slip factor in the equation above will

of course give a different change in static pressure across the jet near the tip. Therefore, calculations were made for slip factors of both 0.88 and 0.83 and are shown in Figure 127.

The corresponding variation in relative Mach number across the through-flow jet as a function of radius in the impeller and for the two different slip factors is shown in Figure 128.

#### 5.4.2 Results of Wake Pressure Comparison

The wake pressure calculated from the measured cover pressure and the blade loading schedule is compared to the theoretical wake pressure in Figure 116 for a series of assumed wake pressures at separation.

Excellent correspondence with the wake pressure data occurs for  $p_{sep} = 16.0$ . The measured and model curves are remarkably coincident. Note that the measured cover data does not agree nearly as well with the theoretical line, showing that correction to wake pressure is essential. For lightly separated cases, the wake pressure yielded from the separated impeller model is farther from the linear mean value between the blades than in heavily separated cases. Thus correction from cover data to wake is most important when  $\epsilon$  is small.

The relative Mach number corresponding to wake pressure and jet entropy should be, according to the model, the Mach number along the leading face of the through-flow jet. This Mach number was calculated for an (isentropic) jet from the measured wake pressure. On comparing the theory and data, we are in effect testing all of the assumptions:

$$\left. \begin{array}{l} p_w \text{ as given by separated model} \\ p_{T_{rel\ j}} = \text{constant} \\ T_{T_{rel\ j}} = \text{constant} \end{array} \right\} \text{isentropic jet flow}$$

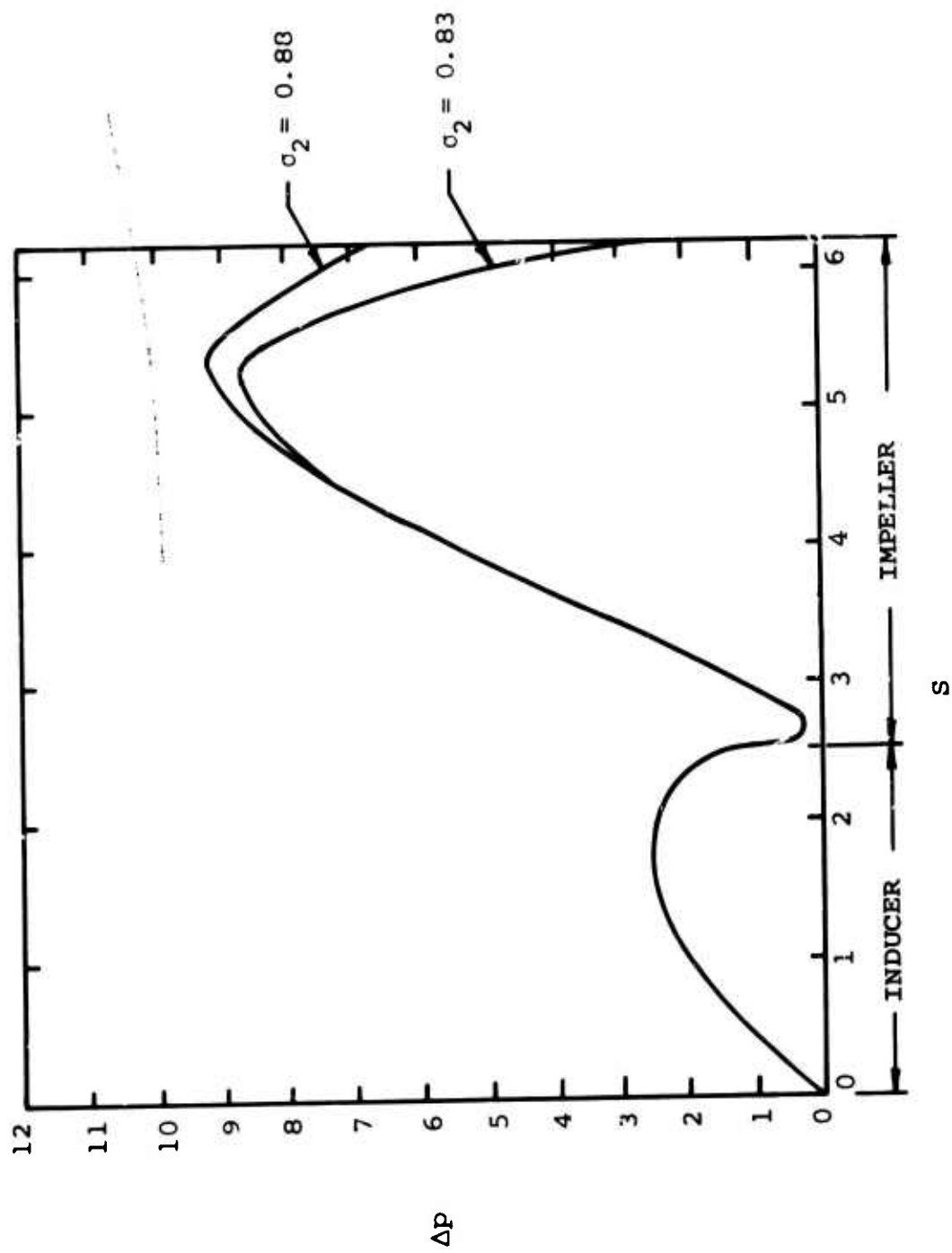


Figure 127. RF-2 Blade Loading at the Cover From the Potential Solution.

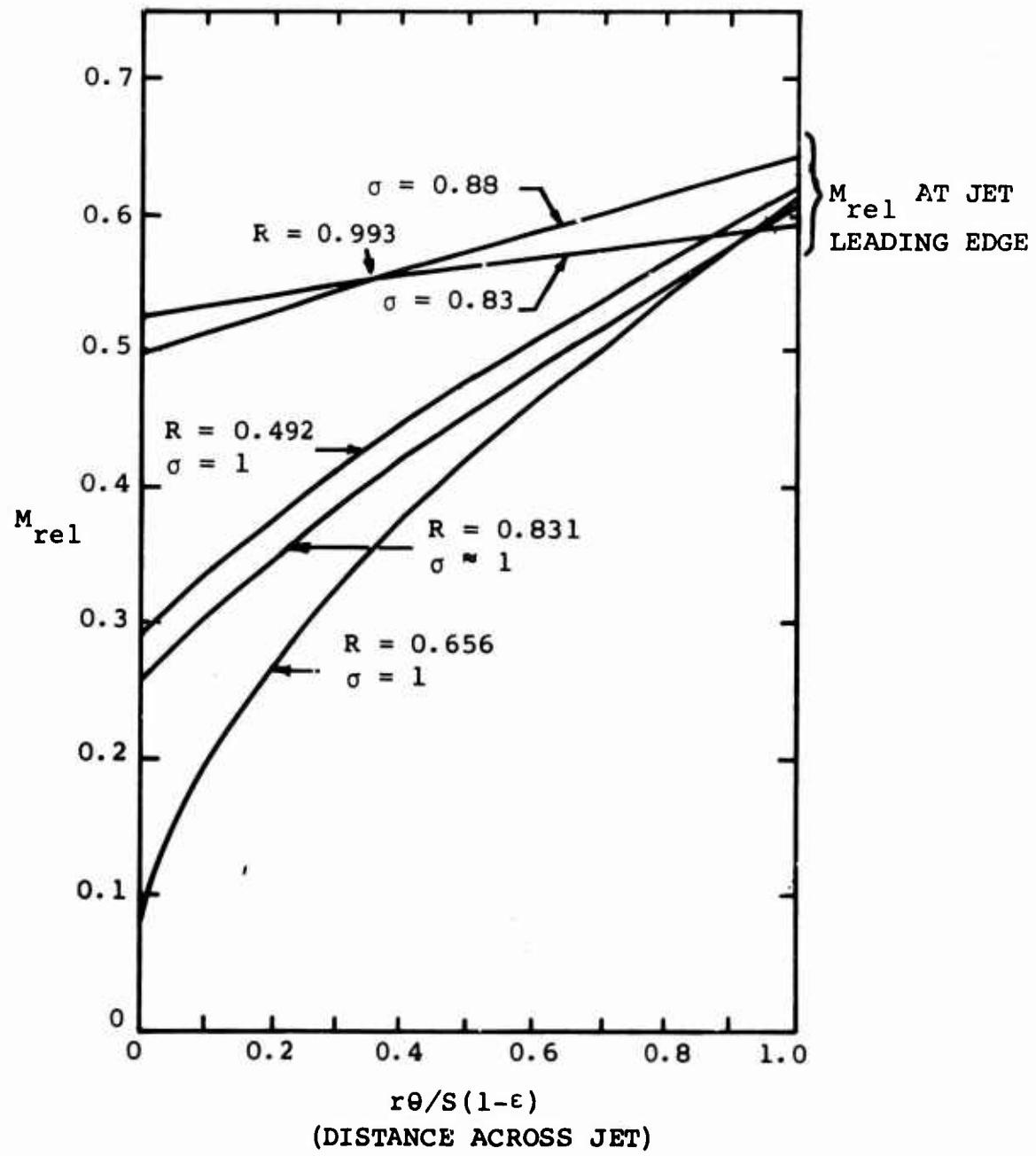


Figure 128. Calculated Relative Mach Number of Jet at Various Radii and With Various Tip Mean Slip Factor Assumptions -- Based on Measured Cover Pressure Data.

The agreement is excellent for the data of Figure 116 as is illustrated in Figure 128 where  $M_{\text{rel}}$  on the leading side of the jet is almost exactly constant with radius. This outcome is very encouraging although it could be fortuitous; the paucity of data precludes development of great confidence.

We are encouraged that the separated wake jet model without any mixing shear or losses engendered between the through-flow jet and the wake appears to be valid. Dean (1968) has explained this lack of mixing by the effect of Coriolis acceleration in damping mixing. If shear friction were allowed upon the jet/wake boundary, as one would expect in stationary flow, the jet would expand rapidly and the pressure distribution in the impeller would be considerably affected.

#### 5.4.3 Conclusions

The following conclusions are evident from the preceding analysis of the inducer and impeller:

- (1) The Creare separated flow model appears to be very accurate in its description of the fluid dynamics of a centrifugal impeller downstream of the separation point.
- (2) The great importance of diffusion in the inducer has been established and emphasized.
- (3) The accuracy of the model using  $\sigma_2 = 0.83$  in predicting wake pressure near the tip of the impeller leads to the conclusion that the flow at the tip of the impeller is more unloaded than would be deduced from the "measured" slip factor of 0.88. This analysis of the impeller flow, based on cover pressure distributions, supports the conclusion in Section 6.7 that the impeller slip factor is lower than the value Boeing reported. Further, this analysis supports the conclusions in Section 4.2 that the probes used at the tip of the impeller may not indicate fluid-dynamically and thermodynamically significant averages.
- (4) The static pressure at the separation point is

quite firmly established at 16.0 psia. Consequently, the mean tip diffusion in the inducer achieved a pressure rise of 3.3 psi or a mean tip diffusion ratio of about 1.37 ( $W_1$  unblocked/ $W_{sep}$  tip).

Dean (1968) asserts, from adopting axial compressor cascade performance, that a mean diffusion ratio of about 1.8 is the ultimate upper limit; thus, considerably more impeller diffusion should be obtainable. We expect that a gain of 4 to 5 points in stage efficiency can be won fairly readily from this source alone.

The mean RMS diffusion ratio (or approximately the mass flow average) is much lower than the 1.37 tip value; it is about 1.16, as shown in Figure 112. But it is the tip separating  $M_{rel}$  that is injected into the separated impeller theory, so tip diffusion ratio is most significant.

## 5.5 TESTS OF FLOW MODELS FOR IMPELLER SECONDARY EFFECTS

Within the impeller, there are several possible potent loss mechanisms which must be accounted if we are to define the impeller discharge flow with sufficient accuracy. This is important in order to calculate power input and to prepare needed data at the beginning of the impeller discharge mixing process. These loss mechanisms include:

- (1) Cover friction
- (2) Rear disc friction
- (3) Leakage over blades
- (4) Internal shear mixing and passage friction
- 5) Secondary flow

We shall discuss each of these individually and attempt to test whatever models exist for them.

### 5.5.1 Cover Friction

No well proven models for cover friction are known to us. Boeing used some sort of disc-friction model. From it they concluded that the loss by cover friction was "small". They estimated cover and disc friction to be 3 percent of the shaft work.

We have reexamined this issue in order to determine whether Boeing's estimates are satisfactory and whether adequate flow models exist for this prediction. To our knowledge, no one has written a definitive paper on the subject of friction torque on the cover of an unshrouded centrifugal impeller. There have been some theoretical attempts in the literature to do this, but we know of no public (or private) experimental investigations which confirm the hypotheses. This turns out to be an important deficiency in state of the art centrifugal compressor design technology.

The best approach we can adopt in view of the lack of specific information about impeller cover friction is to use smooth disc friction results (e.g. Daily and Nece, 1960). The literature was searched for applicable information from other fields. Only two sources were discovered: Mann and Marston (1961) and Pratt and Whitney

work on centrifugal shaft seals reported by Wood, Manfredi, and Cygnor (1964) and by Noell (1965). These results are used qualitatively to try to insure against large errors. In estimating cover friction, we included a 20% increase over the smooth disc in order to be conservative. Daily and Nece give the torque coefficient for one side of a smooth disc as

$$C_m \text{ Rey}^{1/5} = 0.038$$

$$\text{where } \text{Rey} = \frac{\rho_2 r_2^2 \Omega}{\mu_2} \approx 10^7$$

With a 20% increase,  $C_m = 0.00176$ . The impeller tip density is used because most of the friction shear occurs near the impeller tip.

The friction work per unit mass is given by:

$$w_x^{\text{cover}} = \frac{C_m \rho_2 \Omega^3 r_2^5}{2g_o m}$$

This amounts to 4.8 BTU/lb compared to a total work input of about 150. Therefore, the cover friction work is about 3.2% of the total or 3.6% of the aerodynamic work.

With about three more points lost due to friction on the rear of the impeller disc, smooth disc evidence would argue for a six point total loss, which is considerably higher than Welliver and Acurio's estimates and is not a "small" loss. Blades running over the cover should raise the friction loss above that for the same hub shape running in the same casing without any blades, although the decreased clearance may lower it somewhat. Mann and Marston investigated small partial-admission turbines, specifically the drag of the blading when turning out of the arc of admission. They conducted experiments varying blade length, radial tip clearance, and axial side clearance, all for constant impeller diameter and blade chord.

The friction was found to vary only slightly with clearance at constant blade aspect ratio. Above an aspect ratio of 0.7 (blade height/disc thickness), the torque coefficient ceased to change with aspect ratio for small clearance cases. Presumably this is due to the fact that most of the friction occurs near the tip. Extension of blades toward the hub ceases to change the friction, but the presence of blades does increase  $C_m$ , about 50%.

In order to eliminate data with massive radial circulation, only the very small radial clearance cases of Mann and Marston should be considered as applicable to the centrifugal compressor. Indeed, there is a serious question whether even these cases, with no through flow, represent in any way the drag of the bladed impeller on the centrifugal cover. We are of the opinion that there is some correspondence, so that Mann and Marston's data gives some indication for the centrifugal compressor.

From their data, we find a torque coefficient of 0.0039 for one side of the disc. This includes tip friction for a fairly thick wheel. To eliminate this effect, Mann and Marston calculated a correction factor based on the form of the friction work equation (variation with  $r^5$ ). Applying this correction, we get a torque coefficient of 0.0028. This number represents frictional drag with blades at low clearance excluding tip effects. Daily and Nece (1960) report 0.0029 for one side of a smooth disc with no tip friction operating at about blade depth clearance at a Reynolds number of  $10^7$ . This correspondence suggests that it is the depth of the impeller,  $b$ , and not the blade clearance which is the critical fluid dynamic dimension governing cover friction. Also, it should be emphasized that Mann and Marston discovered almost no variation of torque coefficient with axial clearance although values corresponding to a 0.020 inch clearance on RF-2 were investigated.

Further evidence can be drawn from the Pratt and Whitney work, although no directly equivalent case is included. The Pratt and Whitney investigators did install stationary "stagnator" vanes opposed to a smooth disc. The clearance was about 3% of the disc radius, in contrast to 0.4% at the tip of RF-2. Noell observed no increase in disc

friction with the addition of the stagnator vanes. However, the other side of the disc had spiral and circumferential vanes in the centrifugal seal. It is possible that the increase in friction on adding the stagnator vanes was so small, compared to the friction of the seal, that it was not observable.

#### 5.5.2 Rear Disc Friction

We have used Daily and Nece (1960) to calculate the friction torque on the rear of the impeller disc. Tip static density, based on the measured tip static pressure and a static temperature of 800° R, which is close to the static temperature of the fluid leaving the impeller, were employed. Since the shear coefficient increases as the fifth power of radius, most of the loss is generated near the tip of the impeller, and therefore the fluid properties there are the most significant.

The only serious question about the procedure we used is what temperature is appropriate. The fluid behind the impeller could become very hot, which would lower its density and the shear torque commensurately ( $C_m$  would be negligibly affected). Unfortunately, there were no measurements made by Welliver and Acurio which can yield a value for the temperature in the rear cavity near the impeller tip.

With this procedure and Daily and Nece's experimental results, we calculate that rear disc friction work is 3% of the total work input to RF-2.

Both cover and disc friction increase as  $r_2^2 u_2^3$ . Because the required work input determines  $\sigma_2 u_2^2$ , we cannot do much to reduce  $u_2$ , save to increase the slip factor. But by designing higher specific speed machines operating at higher shaft speeds, the tip radius can be reduced considerably. For example Morris and Keeny (1968) employed a six-inch diameter wheel in comparison to Boeing's 9.14 in. Therefore, Morris and Kenny's impeller would have suffered only 43% of the cover and disc friction loss attributable to the Boeing impeller. This would amount to an increase of 3.4 points in stage efficiency.

Probably neither Welliver and Acurio nor Morris and Kenny accounted for cover and disc friction adequately in reducing their data. Neither used a shaft torquemeter nor completely insulated their compressors. Therefore, 1% to 3% of the work input may have been lost by heat transfer through the casings and have not appeared as collector stagnation temperature.

It is interesting to speculate on how the sizable work input into the cavity between the impeller rear disc and the casing is dissipated. This will be treated in Section 6.5.

#### 5.5.3 Leakage Over Blades

Welliver and Acurio present an equation in 67-30 to estimate the losses due to leakage over the blades. The method was developed for radial inflow turbines and calculates a pressure loss for the blading based on orifice-like flow and other assumptions which were not explained.

Existing methods for estimating tip leakage depend on this sort of scheme, sometimes with the relative motion of the cover taken into account. Also, some private schemes employ experimental data from axial compressors and turbines. To our knowledge, no one has made a definitive experimental investigation of this matter for a centrifugal compressor, nor are there any adequate theories available, although a number of attempts have been made to develop such for axial compressors, turbines, and pumps. Further research is plainly needed here if we are to assess this source of loss properly and optimize it in design.

Welliver and Acurio report that leakage losses are "small". Our estimate is that between 10% and 20% of the through flow leaks over the tips of the blades. However, just what consequence this leakage has upon impeller efficiency is not so plain. We will discuss construction of better models in Section 6.5.

#### 5.5.4 Impeller Internal Shear Mixing and Passage Friction

Within the impeller, the through flow scrubs against the walls of the passage and the cover. Also, it scrubs

against "tired" fluid in the wake regions. The processes are very complex, involving three-dimensional, unsteady, and shearing flow in relative coordinates. There are no adequate theories available for predictions here, so we have nothing to test except some qualitative ideas in use by designers.

Often in designing, an impeller efficiency is arbitrarily assigned. This efficiency choice, supposedly derived from experience, is highly suspect. Only through detailed probing of the flow in three dimensions and time in the relative and absolute coordinates will we ever generate enough information to be able to understand the various loss processes, separate them adequately, and develop proper predictive flow models. Almost no research of this sort has ever been done, and that which is being done now is being closely held in the private sector. Plainly, open research is urgently demanded here.

Our experience indicates that it is very dangerous to arbitrarily assume an impeller efficiency or rely upon correlations of experimental data except in special cases. Those cases are mainly in the area of high-specific-speed machines which are slightly separated and of conservative design. Then one may begin to rely more heavily on impeller discharge tip probing for flow-significant information.

Our research has indicated strongly that there is usually a core of loss-free flow passing through the centrifugal impeller and virtually no mixing shear between jet and wake. Even in cases of heavy separation, this core flow persists. Around the core are boundary layers, and between the core and the cover/suction-surface is a wake region of low relative velocity. Rather than assume an impeller efficiency, our approach is to dump all the losses within the impeller into the wake region.

Only the cover friction will produce relative work and cause an increase in the wake's relative total temperature. If we can estimate the work input engendered by cover friction, we can then assign this power to be carried away by wake mass flux. However, if we are going to estimate the temperature rise caused by that, we have to know the mass

flow in the wake, and that is not an easy estimate to obtain.

After constructing the pattern of a loss-free through flow (or jet) and a lossy wake, we then use the impeller discharge mixing models of Section 5.7 to complete the calculation of impeller processes. With the mixed-out stagnation pressure  $p^*$  and temperature  $T^*$ , we can calculate the impeller's efficiency. So far, this approach seems to be valid and much more competent than those commonly used in the art, at least to our knowledge.

What does the Welliver and Acurio data have to say about the validity of our model for the internal flow? The answer is "Nothing", because there are no data available from the Boeing-AVLABS experiments which produce any resolution of impeller internal loss processes. We can put together the entire flow model and compare it to the reliable data, but there are so many unknowns when the entire model is assembled that one gets no definition of individual processes. All we can say is that the Boeing data do not refute any aspects of our proposed impeller internal flow model.

Actually, we can do more diagnosis than this, for as discussed in Section 5.4, the cover static pressure data can be used to test the impeller separated flow model. In that model is buried inherently the assumption that there are no significant friction forces acting upon the jet passing through the impeller. If there were significant shear mixing stress between the wake and the jet, the pressure distribution on the cover would be affected, for the wake fluid would be accelerated by the drag of the jet and there would no longer be a "centrifugal" distribution of pressure in the wake. As shown in Section 5.4, the agreement between the measured cover distribution, corrected to wake pressure, and the centrifugal theory is excellent. Therefore, we can conclude that Dean's (1968) hypothesis, based on visualization studies, that Coriolis acceleration almost completely damps the mixing between the wake and the jet is sustained.

We are less able to say anything definitive about passage friction, but then, because of the nature of the flow model,

we do not have to say anything. The passage friction in the impeller produces "tired" fluid, which contributes to the wake. Either it stays smeared around the through flow, or secondary flow carries it into the wake region; either way is the same as far as the impeller discharge mixing loss model is concerned. Therefore, passage friction contributes to the mass flow in the wake,  $m_w/m$  in our model. In so doing, it completely accounts for entropy flux generated by passage friction.

#### 5.5.5 Secondary Flow

"Secondary flow" is often looked upon as a universal specter to explain all the inadequacies of our analytical techniques. While the secondary flow phenomenon in centrifugal compressors has been only slightly explored by investigators such as Fowler (1968) and Senoo (1968), it has been explored heavily for axial compressors and turbines. Lakshminarayana and Horlock (1968) have made a definitive summary of secondary flow in axial turbomachinery. They show plainly that the kinetic energy flux associated with secondary flow is negligible. The main influence they identify is on the work input characteristics of the blading.

Dean (1954) and others have emphasized the importance of secondary flow to the details of blade stall. Dean showed that apparently slight modifications in secondary flow patterns (for instance, by allowing tip leakage over the blading) could make strong changes in the separation pattern, the lift distribution on the blading of an axial compressor cascade, and the losses. Taylor (1958) and Dean (1961) have emphasized that secondary flow has a very important bearing on the stability of stalling. In three-dimensional flow, separation bubbles often occur which cause little distress to the performance of the device. This is because the bubbles tend to be stable and quiescent. On the other hand, if the bubble tends to shed periodically, it can cause major losses. Sometimes large jumps in losses occur when the flow mode changes from one with a quiescent separation bubble to a shedding bubble. This is plainly seen in the drag of a cylinder or sphere.

We assert that the principal effect of secondary flow in the centrifugal impeller is upon the stability of the wake region. Visualization studies showed a number of years ago that there is a definite flow through the wake and that the wake is very quiescent in the cases studied. Why the wake does not shed from a centrifugal impeller passage\*, as it does, for instance, from a straight channel diffuser, was not plain at first. Then it was realized that the hub and cover boundary layers feed flow into the wake through the secondary flow mechanism and produce a stable separated pattern. As Kline (1959) explains, the stall bubbles shed from a straight-channel diffuser because of an imbalance between the rate at which fluid is carried away from the bubble by shear mixing and the rate at which it can return from the discharge by backflow. If backflow can satisfy the continuity balance, then the separation will be steady. If not, the bubble sheds periodically.

Because, as explained in Section 5.5, the shear mixing between the through flow and the wake is greatly suppressed by Coriolis forces, not much fluid is necessary to make up a continuity balance. Therefore the secondary flow is believed to have no difficulty in supplying enough fluid to the wake, thus stabilizing it.

This qualitative model was used by Welliver and Acurio. How good is it according to their data? Unfortunately, we cannot say, for the data is mute on this point. We can say that the wake did have a "centrifugal" pressure distribution as asserted by the model (basically from the assumption that the relative velocity in the wake is small).

The relative velocity generated by the three-dimensionally separated jet moving back into a two-dimensional pattern on the pressure surface of the blade with increasing radius could also be called secondary flow (see Figure 99). This secondary flow produces an important adjustment and reduces the impeller slip factor. We have no model for calculating how rapidly that adjustment occurs and therefore nothing to test with the data, which is mute on this subject anyway.

On the subject of impeller internal secondary flow, we can deduce little with the Boeing-AVLABS data.

---

\* Except near zero flow.      236

## 5.6 TEST OF IMPELLER DISCHARGE FLOW PATTERN MODEL

Welliver and Acurio (1967) use a discharge flow pattern model which is essentially a compressible version of the step wake-jet analysis of Johnston and Dean (1966). Tables of mixing loss, for zero flow in the wake, were prepared during the Boeing-AVLABS program; Welliver and Acurio offer graphical plots of these. Flow can be added into the wake with little difficulty; the relative velocity of the wake flow remains close to zero; the wake slip factor must be very close to 1.0. This modified model was employed at the very end of the Boeing-AVLABS program as discussed in Section 5.7.

Our purpose here is to determine whether this type of simple flow pattern for the impeller is authentic enough for our purposes, which are basically:

- (1) to calculate the slip factor and therefore the fluid dynamic work input of the rotor, and
- (2) to generate the input information for the impeller discharge mixing loss calculation of Section 5.7.

On the first score, the model is mute; in fact, it relies upon slip factor information developed from some other source before the discharge flow pattern can even be defined. As is discussed in Section 6.6, a much more elaborate theory for the impeller's separated flow must be in hand before there is any hope of calculating the mass-flow-average slip factor. The prospects of generating this far more complicated theory are dim today. Fundamentally involved is basic fluid dynamics theory which has not yet been developed; for instance, secondary flow in rotating coordinates, the influence of Coriolis accelerations on boundary layer growth, and the dynamics of separated flow in rotating coordinates.

Since Welliver and Acurio were forced to have recourse to other sources of slip factor information, let us examine how adequate these sources may be. A very common approach is to employ the potential-solution-based methods of Stanitz or Busemann; the various techniques have been surveyed by Wiesner (1967). To apply potential theory, which assumes that the flow follows the blading all the way to the tip of the impeller and fills the meridional plane passage, is

shear folly in light of the separated and highly distorted flow of the Boeing-AVLABS impellers.

Another approach might be to apply the potential theory, but only to the jet which fills part of the span between the blades. When this was done in Section 4.2, we found that the slip factors so determined were too high, indicating that the two-dimensional potential theory is not representative of the complex flow.

One of the principal causes for a large deviation from the classical theory is the fact that the separated jet is twisting around from the hub, where it was thrown by the cover separation, back onto the pressure surface of the blades as suggested in Figure 99. This motion causes secondary velocities of considerable magnitude. For instance, in the RF-2 impeller, the relative velocity of the through-flow jet is on the order of 850 ft/sec. It takes, therefore, about 200 microseconds for a fluid particle to pass through the radial part of the impeller. Assume that the mean distance jet particles must travel in order to go from the hub back onto the pressure surface is one-half the rms pitch between the blades, or 0.65 inch. This motion in 200 microseconds produces a backward relative tangential velocity of 270 ft/sec. If this were the only "slip", the slip factor would be 0.865; if this extra velocity were added to the classical potential theory "slip", the slip factor would be about 0.75. So we see that a three-dimensional adjustment of the separated flow pattern produces velocities which indeed have significant impact on impeller work input.

We cannot avoid the conclusion that the meridional separation (and indeed the  $r-\theta$  separation too) does seriously influence the impeller's work input characteristics. No classical potential-theory approach accounts for this effect. Since most centrifugal compressors are separated to some degree and since low-specific-speed machines are often heavily separated, doubt about the utility of the classical potential theory may be raised across the board.

Wiesner (1967) demonstrates considerable scatter of experimental data relative to the classical theories as, shown in Figure 129. We venture to suggest that this scatter is

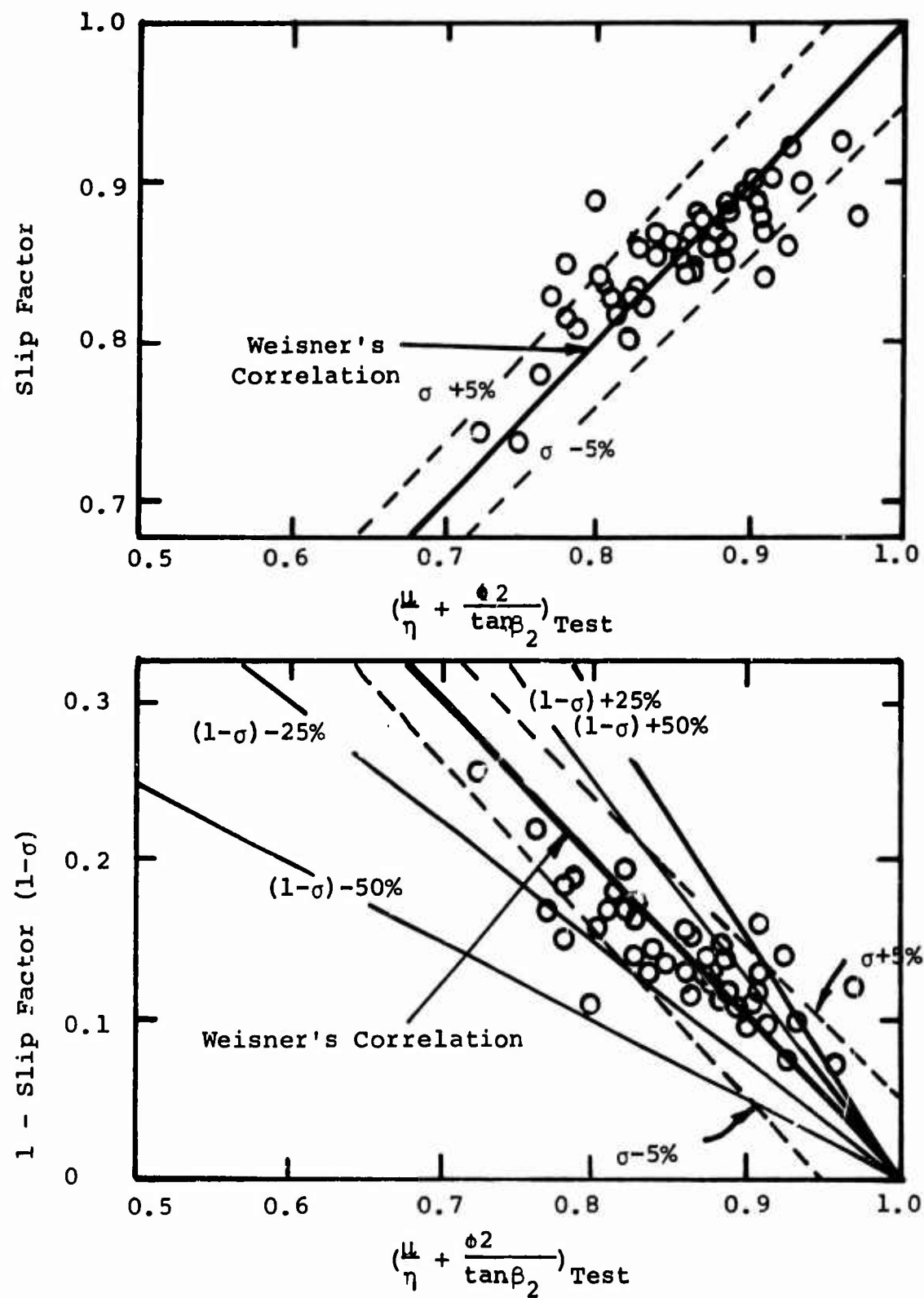


Figure 129. Wiesner's (1967) Slip Factor Correlation Showing Scatter of Slip and Deviation Data Versus Correlation Factor.

caused by separation. Because Wiesner makes no attempt to classify impellers by their separation characteristics, little sense can be made of the scatter of the empirical data he uses.

We conclude that recourse to conventional slip factor estimating methods will be seriously misleading for the Boeing-AVLABS type of impellers and any others which are significantly separated. Experience with this type of machine can give an empirical feeling for what kind of slip factors will be encountered in fact. However, when the designer moves into an entirely new area, like these high-pressure-ratio impellers, he has little security.

In order to reduce the risk involved and to achieve the highest possible slip factor, the use of splitters (e. g. Morris and Kenny, 1969) is recommended. The shorter the distance in the  $r-\theta$  plane between blades, the more quickly the meridionally separated flow adjusts back onto the pressure surface.

Morris and Kenny report slip factors between 0.90 and 0.92 for their H rotor, which had 64 blades in contrast to the Boeing-AVLABS impeller's 18. But even with so many blades, the slip factor fell well below the 0.97 predicted by Stanitz's theory. Morris and Kenny's slip factors are probably overestimated, for the same reasons that the Boeing-AVLABS slip factors came out too high. The Boeing reported values range from 0.88 (RF-2) to 0.93 (Workhorse), while the actual values in both cases are close to 0.83. Thus, the utility of using more blades at the impeller tip is not firmly established. Nevertheless, the simple fluid dynamic explanation provides good reason to try adding splitters.

Incidentally, the primary function of splitters is to raise the work input coefficient. Also, by splitting the separated flow into a series of smaller jets and wakes, the tendency for backflow from the diffuser is probably lowered too. This reduced backflow tendency is due to two sources. First, as the number of blades is increased, the surface area per unit volume of jet fluid is increased, and hence the jets more effectively energize the wake fluid. That is, mixing takes place in a shorter

distance and the long exposed diffuser vane surface has less fluid which it can push back into the impeller. Since the fluid must mix anyway, hastening the process by having smaller wakes and jets should not be detrimental. The dynamics of the mixing process are discussed in more detail in Sections 5.7.1 and 5.8.1.1.

The second reason to expect less backflow as the number of blades is increased lies in the expected transitory nature of the backflow. The pressure variations between jet and wake are smaller because the work input per blade is smaller. Also, the physical size of the low pressure wake is smaller. The low energy fluid pushed back by the diffuser vane has a smaller driving force (pressure difference) and also a smaller wake area which it must enter. The situation is similar to entering a revolving door. As the door revolves faster (i.e., more blades at a given rotative speed) it is harder to enter a compartment. If in addition one walks more slowly the problem is even more acute. Thus, raising the number of blades seems to have a desirable effect on the diffuser backflow.

Turning now to the input information needed for the impeller discharge mixing loss calculations of Section 5.7, what sort of success did the available models have there? Table IX shows a comparison of the full three-dimensional mixing loss calculation using the impeller discharge model employed as a test case in Section 4.2 and a two-dimensional representation employing the "true" mass-flow-averaged values from that pattern. Into the calculation were injected the mean static pressure, the mass-flow-averaged slip factor (presuming that we got an accurate value from some source), the mass flow, and the assumptions that the relative total pressure loss in the jet is zero and the wake mass flow fraction is 20%.

As shown in Table IX, the results from the full three-dimensional integration of the input distributions and the simple two-dimensional step-wake jet model are almost identical. The reason for this kind of concordance is that the impeller discharge mixing loss is primarily the loss of radial kinetic energy as the jets expand to fill the circumference. The radial velocity of the jet is primarily determined by the relative Mach number on the leading face of the jet, which is established by the tip

TABLE IX. TEST OF SIMPLE MIXING CALCULATION

Property	"True" Flow	Step* Wake-Jet Model
$\bar{p}_2$	66.5	66.5**
$\tilde{T}_{O_2}$	1106.1	1077.1
$\tilde{p}_{O_2}$	183.3	188.5
$\tilde{c}_{\theta_2}$	1703.5	1703.5**
$\bar{\tilde{c}}_r$	62.17	62.17**
e	-	.684
After Mixing		
$c_r^*$	281.5	269.4
$p^*$	70.35	71.3
$p_o^*$	171	177.5
$\tilde{p}_{O_2} - p_o^*$	12.3	11.0

\*Assumptions:  $\Delta p_{T_{rel_j}} = 0$ ;  $m_w/m = 0.20$

\*\*Input quantities to step jet-wake and mixing loss model.  
all other quantities calculated from this set.

static pressure, and by the relative tangential velocity of the jet, which is mainly determined by the slip factor.

So, given correct tip static pressure and slip factor for an impeller, we should be able to calculate the impeller discharge mixing loss by the simple step-wake model and with considerable accuracy. Of course, this brings up the question of how one obtains an accurate estimate of the slip factor for the three-dimensional flow pattern, as we have discussed above. Estimating the impeller tip static pressure is not so difficult, as explained in Section 5.4, provided that we can accurately calculate the diffusion ratio expected from the inducer.

Within these limitations, the input information to the impeller discharge mixing calculation offered by the simple step-wake jet model of Welliver and Acurio appears to be sufficiently adequate.

### 5.7 TEST OF IMPELLER DISCHARGE MIXING MODEL

Welliver and Acurio (1967, 67-47) indicated significant uncertainties in the prediction of the performance of RF-2 using existing loss models. A principal divergence between the data and theory is centered on the tip of the impeller and the impeller discharge mixing losses which occurred there. The indicated stagnation pressure at  $R = 1.03$  was as much as 30 psi below the value expected from the deduced impeller slip factor (0.88) and the application of the Johnston and Dean (1966) technique for predicting impeller discharge losses. The discrepancies observed for Workhorse and RF-2 are graphically displayed in Figures 95 and 96.

Despite the observed discrepancy, the impeller discharge mixing loss theory did predict the majority of the loss in stagnation pressure between impeller tip indicated values and the measurements in the diffuser throat. However, an important gap or "missing loss" remained. Welliver leaned toward explaining the "missing loss" by some powerful mixing process in the vaneless and semivaneless spaces which smeared the entropy born in the sidewall boundary layers across the core of the flow. This has been discussed in Section 5.8.1. Dean, on the other hand, could not find a suitable mechanism for this powerful mixing effect and tended instead to attribute the "missing loss" to clumsy application of the impeller discharge mixing loss theory, occasioned by a lack of sufficient knowledge about the distorted flow leaving the impeller tip.

Toward the very end of the Boeing-AVLABS program, Dean made a calculation using an impeller discharge mixing loss model improved from that of Johnston and Dean (1966) by adding a significant flow through the wake region. His calculation suggested that the jet-wake mixing loss was strongly increased, with only 20% of the through flow in the wake region; this increase was enough to explain the "missing loss". This result was not reported by Welliver and Acurio (1967, 67-47) but was reported by Schorr, Welliver, and Winslow (1969).

This was the situation at the end of the Boeing-AVLABS program. Under the current program, we have reexamined these issues because the "missing loss" is very significant

when measured in terms of stage efficiency. This re-examination and testing of the existing flow models has led to important conclusions. One of these is that the explanation previously offered by Dean (relying on adding flow in the wake) is erroneous. This is plainly shown in Figures 95 and 96. It may be seen that the impeller discharge mixing loss is not very sensitive to the mass fraction of flow in the wake for the cases studied.

There are actually four factors contending in this area:

- (1) What is the true value of mass-flow-average impeller discharge slip factor (after extracting the influence of backflow from the diffuser into the impeller)?
- (2) What are appropriate values for the parameters that must be entered into the impeller discharge mixing theory; namely, the mass flow fraction in the wake and the relative total pressure loss for the through flow?
- (3) Is the impeller discharge mixing loss theory competent?
- (4) What is the magnitude of core stagnation pressure loss from impeller tip to diffuser throat in excess of impeller discharge mixing loss?

On item (1), if the mass-flow-average slip factor is estimated too high (as we believe it is by about 5 points by Welliver and Acurio), then one calculates an excessive mass-flow-average stagnation pressure at the tip of the impeller unless a high  $\Delta p_{T_{rel,j}}$ , that is, a low impeller

efficiency (not including mixing losses), is estimated. The impeller loss model used by Welliver and Acurio and by us assumes that there is no internal impeller loss. All entropy flux increases are assumed to end up in the wake region. This entropy flux accumulated from all the loss sources in the wheel such as tip leakage, channel surface area friction, cover friction, mixing between jet and wake etc., becomes smeared across the entire flow during the discharge mixing process, which in turn engenders some more entropy increase. Into the mixing loss calculations we would insert  $\Delta p_{T_{rel,j}} = 0$ ; that is, a local jet core efficiency of 100%.

With this input, the Boeing-deduced slip factor of 0.88 for RF-2 yields a mass-flow-averaged stagnation pressure  $\bar{p}_o = 209$  psia. To the diffuser throat where the centerline stagnation pressure  $p_{o_4}^2 = 162$  psi was measured,

there would be a loss of 47 psi. As shown in Figure 96 for a  $\Delta p_T = 0$  (which is consistent with the efficiency  $_{rel}$ )

assumption), the maximum loss we could invoke at a mass fraction in the wake of 20% would be only 28 psi. Therefore, 19 psi remains to be accounted for by the other four factors above.

For Item (2), we do not have any definitive evidence. However, a number of different flow visualization studies made by various investigators, including Acosta and Osborne, reveal flow in the wake region. Our past studies using neutral-density bodies in the fluid proved this conclusively.

On the score of relative total pressure losses in the through-flow jet, we have even less evidence. However, as mentioned in Section 4.2, there is sufficient evidence to suggest that the jet often comes through the impeller with negligible relative total pressure loss in its core. The evidence from the RF-2 impeller discussed in Section 5.4 strongly asserts that this condition was realized by RF-2, so the available evidence suggests that the assumption of zero relative total pressure loss in the core of the through flow is probably authentic. This assumption is important, as can be seen in Figures 95 and 96 because a small change in relative pressure loss powerfully influences the mass-flow-average absolute stagnation pressure at the tip of the impeller. Incidentally, the relative stagnation pressure losses in the boundary layer surrounding the through-flow stream are not assigned to the jet. Rather, these boundary layers are regarded as part of the wake in the model.

For item (3) (competency of the mixing theory) we have, of course, no reliable evidence from this program. The uncertainties in the other factors preclude a definite test. The same is true for Item (4) (excess core losses to throat). In Section 5.7.1, it is suggested that strong

three-dimensional mixing effects, primarily engendered by the jet-wake mixing in the vaneless and semivaneless regions, could power the necessary mixing and could produce losses in the core flow as envisioned by Welliver.

The objective of this section is to attempt to sort out these various factors and to test the authenticity of the impeller discharge mixing model by using the Boeing-AVLABS data.

#### 5.7.1 Influence of the Unknown Factors

In Figure 130 we show for RF-2 the effect on  $p^*_o - p_{o4}$  of varying parameters  $m_w/m$ ,  $\Delta p_{T_{rel}}$ ,  $\sigma_2$ .

We note that the excess stagnation pressure loss above that predicted by the impeller discharge mixing loss theory varies strongly with slip factor. Because the mass-flow-averaged stagnation pressure at the tip of the impeller increases with slip factor, a larger loss is needed to reach the measured throat stagnation pressure.

In Figure 130, our best estimate for  $m_w/m$  and  $\Delta p_{T_{rel,j}}$  is

indicated. The arguments supporting these choices are made in Sections 5.6 and 6.5. Also shown is the Boeing-deduced slip factor of 0.88. On the basis of Boeing's deduction and our best-estimate curve, the excess stagnation pressure loss would be about 19 psi. This loss would have to be generated in the vaneless and semivaneless spaces by some violent mixing mechanism which distributed the entropy generated on the sidewall boundary layers across the core of the flow, as explained in Section 5.8.1

The questions are: Are these numbers reasonable? Can they be established from the data? After a thorough study of the data, we concluded that there is no concrete way to separate the impeller discharge mixing loss from core losses arising from the sidewalls of the vaneless and semi-vaneless spaces. The railroad track data for Workhorse show a rapid drop in indicated stagnation pressure near the tip of the wheel and then a quick transition to a more gradual decrease, see Figures 30 and 31. One might say that the portion of this distribution toward the throat was

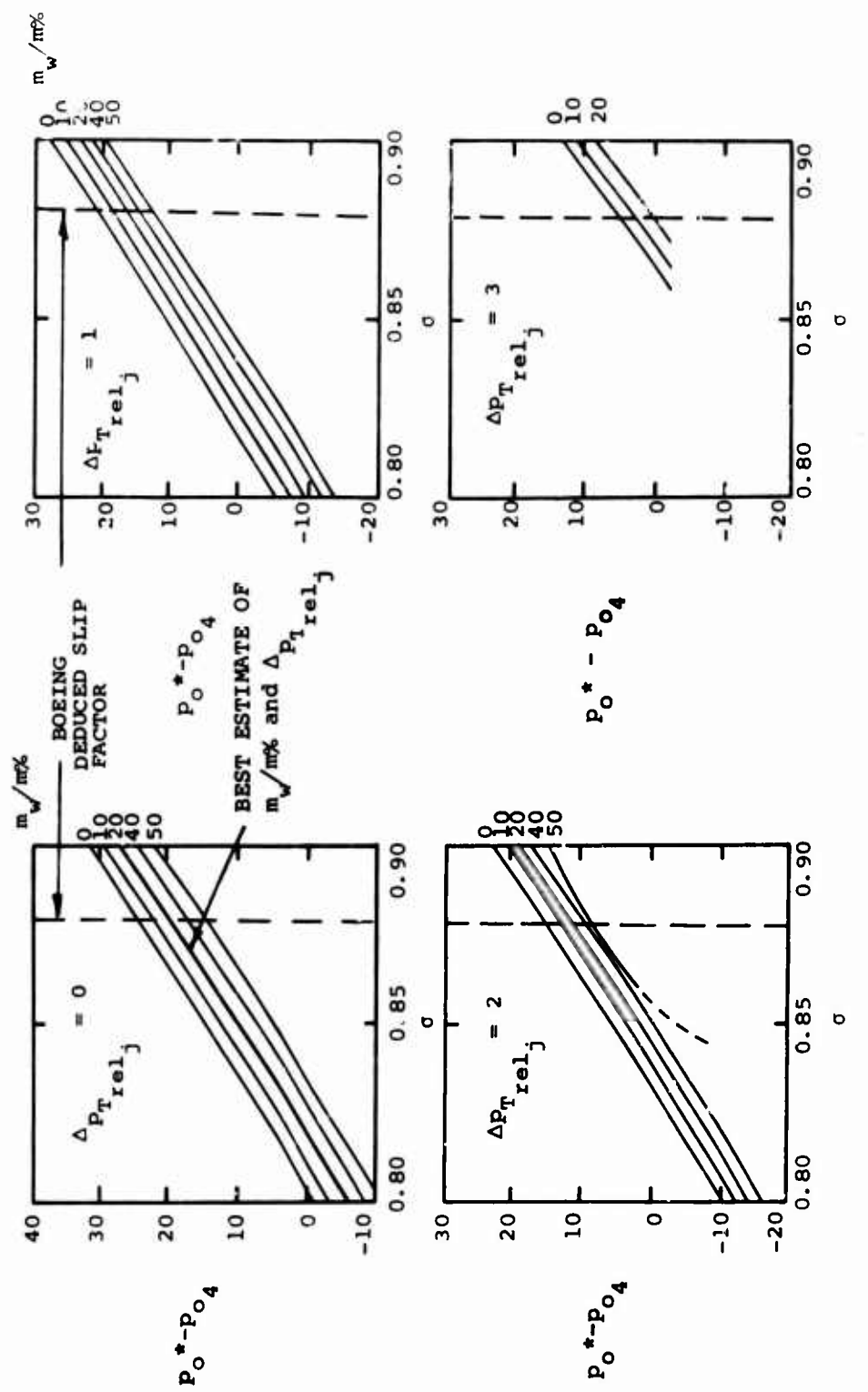


Figure 130. Vaneless and Semivaneless Space Loss in Excess of Impeller Discharge Mixing Loss,  
 $P_o^* - P_{o_4}$ .

due to sidewall entropy generation. However, there is good reason to suspect the validity of the railroad track data as explained in Section 4.3.1.

Welliver and Acurio state that the mixed-out radius ratio should be small according to Johnston and Dean (1966). Actually, that paper does not include calculated results pertaining to the Boeing-AVLABS cases.

Johnston and Dean present results for incompressible flow, shown in Figure 131, computer calculated from the Dean-Senoo theory. Only work input coefficients (slip factor for a radial machine without preswirl) up to  $\sigma_2 = 0.75$ , impeller tip swirl parameters  $\lambda_2 = (C_\theta/C_r)_2$  up to 7, and wake widths  $e_w$  up to 0.75 were included with zero wake flow ( $m_w/m = 0$ ). The Boeing-AVLABS cases had  $\sigma = 0.83 - 0.85$ ,  $\lambda \approx 8$ , and  $e \approx 0.75$  and, we estimate  $m_w/m \approx 0.20$ . Dean and Senoo showed that the mixing process goes out to much larger  $R^*$  when  $m_w/m \neq 0$ . Even if we ignore that effect, Figure 131 extrapolated in Figure 132 indicates a mixed-out radius ratio of  $R^* \approx 1.10$  for the Boeing-AVLABS cases. The vane leading edges of RF-2 were at  $R = 1.06$ ; the center of the diffuser channel entry was at  $R = 1.11$ . If the presence of the vanes does not hasten or delay mixing and if  $m_w/m \approx 0.20$  does not greatly alter the rate of mixing, Johnston and Dean (extrapolated linearly) would assert mixing to be complete at about the channel entry. We can improve a little on the linear extrapolation by noting that as the slip factor approaches unity, the mixed out radius,  $R^*$  must increase rapidly. An extrapolation based on this consideration is shown in Figure 132 and suggests that  $R^* \approx 1.25$ .

Boeing's impeller tip stagnation pressure probes for RF-2 and Workhorse show 175 psi indicated stagnation pressure at the tip of the impeller. For reasonable estimates of  $T_{Tre1}$  in the wake ( $520 - 820^\circ R$ ), the mass flow averaged stagnation pressure corresponding to this indicated stagnation pressure ranges from 150 psi to 183 psi, assuming  $m_w/m = 20\%$ . Thus, the measured stagnation pressure argues against any mysterious loss in the vaneless and semivaneless regions - there is not enough pressure available to lose.

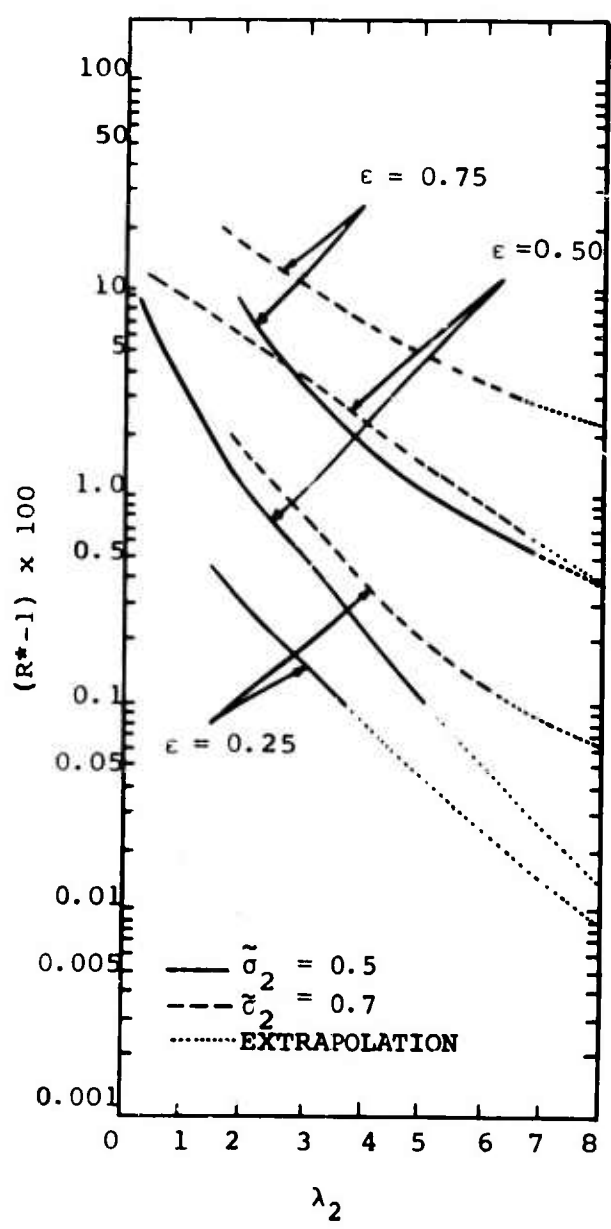


Figure 131. Mixed-Out Radius Ratio,  $R^*$ , Versus Impeller Tip Swirl Parameter  $\lambda_2 = (C_\theta / Cr_2)$  And Wake Width  $\epsilon_2$ .

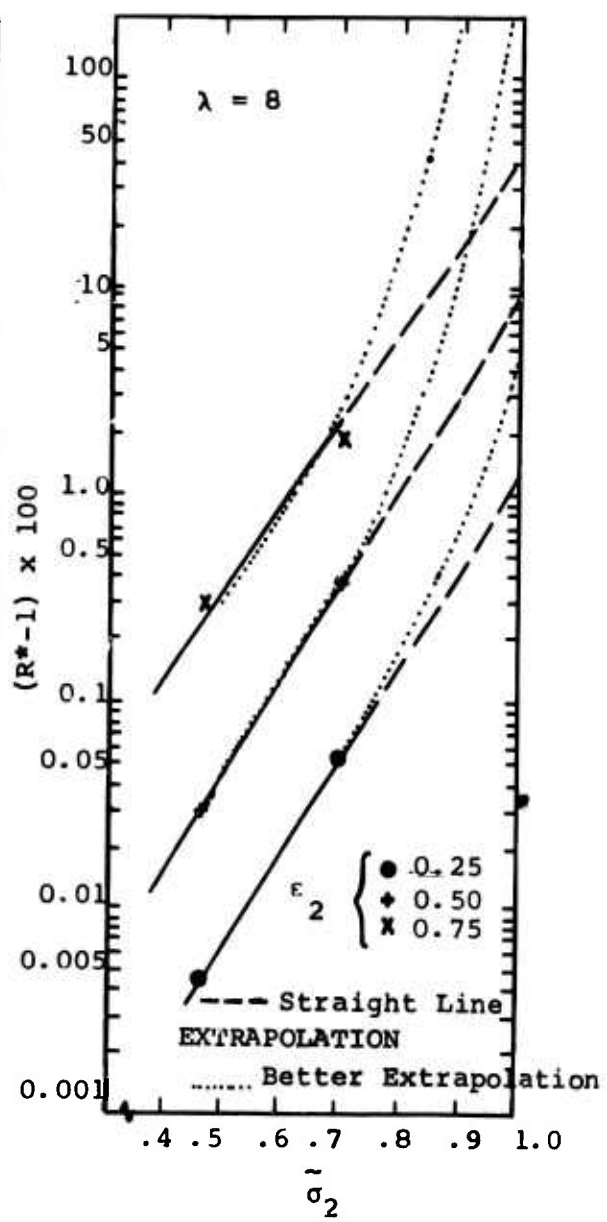


Figure 132. Impeller Discharge Mixing (Extrapolated From Figure 131).

The evidence from this examination of the data plus that in Section 6.7 strongly indicates that the impeller mass-flow-average slip factor is considerably lower than the Boeing-deduced value of 0.88. Rather a value of about 0.83 seems to be more in accordance with the data.

### 5.7.2 Test of The Mixing Loss Theory

In deducing the level of the sidewall stagnation pressure loss at the entry region of the diffuser in the last section, we tacitly assumed that the impeller discharge mixing loss theory was accurate. If this theory overestimates the loss, then proportionally more sidewall-induced stagnation pressure loss could be indicated.

There is no way now to unsnarl further these intertwined effects. All of the Boeing-AVLABS data does seem to hang together to support the mixing theory and the contention that there is no core flow stagnation pressure loss in the vaneless and semivaneless spaces. Substantiating evidence of this can be obtained from the diffuser throat data. The throat stagnation pressure distributions measured by nine point surveys for RF-2 (Figures 56, 57, 67, 68, 78, 79, 89, and 90) show that all of the midplane probes read the same core stagnation pressure within about  $\pm 2.5$  psi. In contrast, there is a large variation in the streamline length from the tip of the impeller to the probe location as shown in Figure 134. One would expect inherently that the longer the distance over which the boundary layer develops, the more thoroughly the entropy generated in the wall layers would be mixed across the core of the flow. So one would expect the stagnation pressure probe near the suction side of the passage to indicate a considerably lower stagnation pressure than the probe near the pressure side. This plainly did not happen in any of the tests.

This evidence suggests that there is no excess loss in the core of the flow caused by sidewall boundary layer friction and that a violent mixing process does not exist. Rather, it suggests that there is a core of potential flow from the end of the impeller discharge mixing process to the diffuser throat as hypothesized by Dean.

Referring again to Figure 130, these arguments suggest that  $p_o^* - p_{o_4}$  is approximately zero, and that all of the

loss in stagnation pressure from the tip of the impeller to the throat is due to impeller discharge mixing.

Despite the conclusion drawn above from a wide range of sources and empirical evidence, we recommend in Section 8 that this matter be directly investigated in a research program, for none of the data on which we have based the conclusion is definitive. Rather, in its aggregate, the evidence strongly suggests the conclusions reached, but the proof is not certain.

### 5.8 TEST OF THE FLOW MODELS FOR THE VANELESS AND SEMIVANELESS SPACE

The entry region of the diffuser determines in large measure the pressure recovery attained. While there is not much diffusion in the large expanse of the vaneless and semivaneless space (approximately 10% of the total diffuser pressure recovery for RF-2), the losses in the core of the flow and the growth of the boundary layers on the sidewalls and suction surface of the vanes set the stage for the eventual major recovery through the throat entry shock and the channel diffuser.

We shall demonstrate in Section 5.9 that the recovery of the subsonic channel diffuser (60% of the total diffuser pressure rise) depends mostly upon the magnitude of boundary layer blockage in the diffuser throat. This blockage accrues primarily from events in the broad expanse of the vaneless and semivaneless regions. We must have, as a consequence, a means for predicting boundary layer growth and core losses.

Welliver and Acurio (1967) have offered a model for the fluid dynamics of the diffuser which instructs how to compute the vital factors. This model, in the overall scene of centrifugal compressor performance, and the model for the diffusing inducer portion of the impeller are the two most vital to good compressor design. In this Section, we shall attempt to test the authenticity and the practicality of the Welliver and Acurio model for predicting diffuser throat blockage and center-line stagnation pressure.

### 5.8.1 Test of Flow Model for Predicting Diffuser Throat Blockage

The model evaluates throat blockage through the application of a two-dimensional turbulent boundary layer theory starting at the impeller tip. In the absence of any theoretical methods for calculating the entry flow field, such an approach must depend upon an empirical description of the entry pressure field. How successful that process may be inherently is open to real question. We shall not attempt to test that. Rather, we shall test the validity of using available boundary layer theory, presuming that the entry pressure distributions will be injected into the boundary layer calculations. Eventually a comparison of measured and calculated throat blockage will show success or failure.

The static pressure data available for these compressors in the vaneless and semivaneless spaces were used to calculate the throat blockage. This was done by:

- (1) Using the static pressure plots to determine free-flow streamline shapes.
- (2) Assuming a constant mid-depth total pressure in the vaneless space so that a Mach number distribution could be found for each streamline.
- (3) Applying two-dimensional boundary layer calculation techniques to the boundary layer growth up to the throat.
- (4) Assuming zero boundary layer thickness on the sidewalls at impeller tip.
- (5) From these calculations, evaluating the throat blockage.

These calculations were unsuccessful in predicting the throat blockage, although they provided some other useful information. The calculation procedure is explained below.

The static pressures at the wall taps were interpreted into isobaric plots: Figures 133 and 134. The preparation technique is described in Appendix IV. From these isobaric plots, Euler's 'n' equation

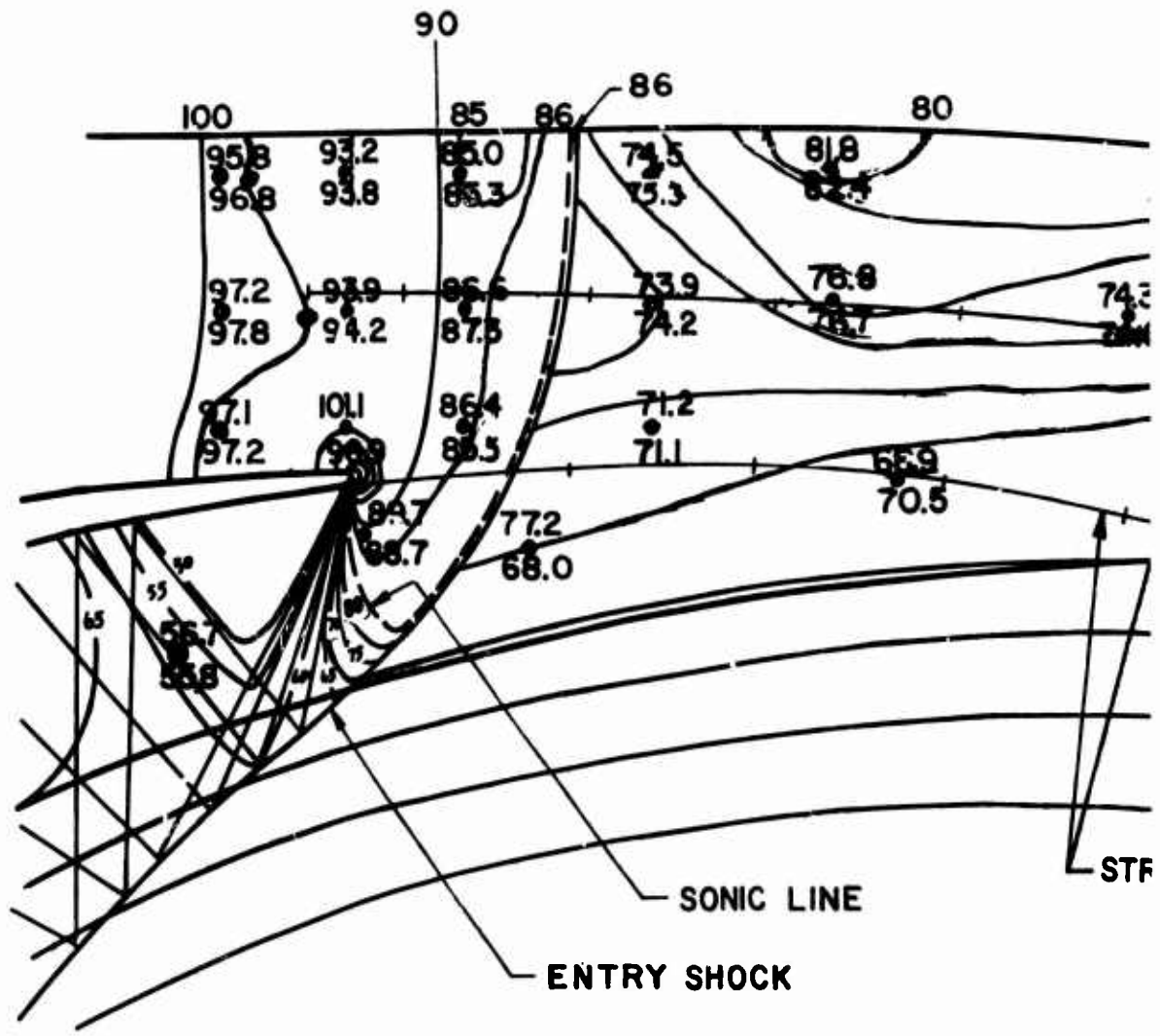
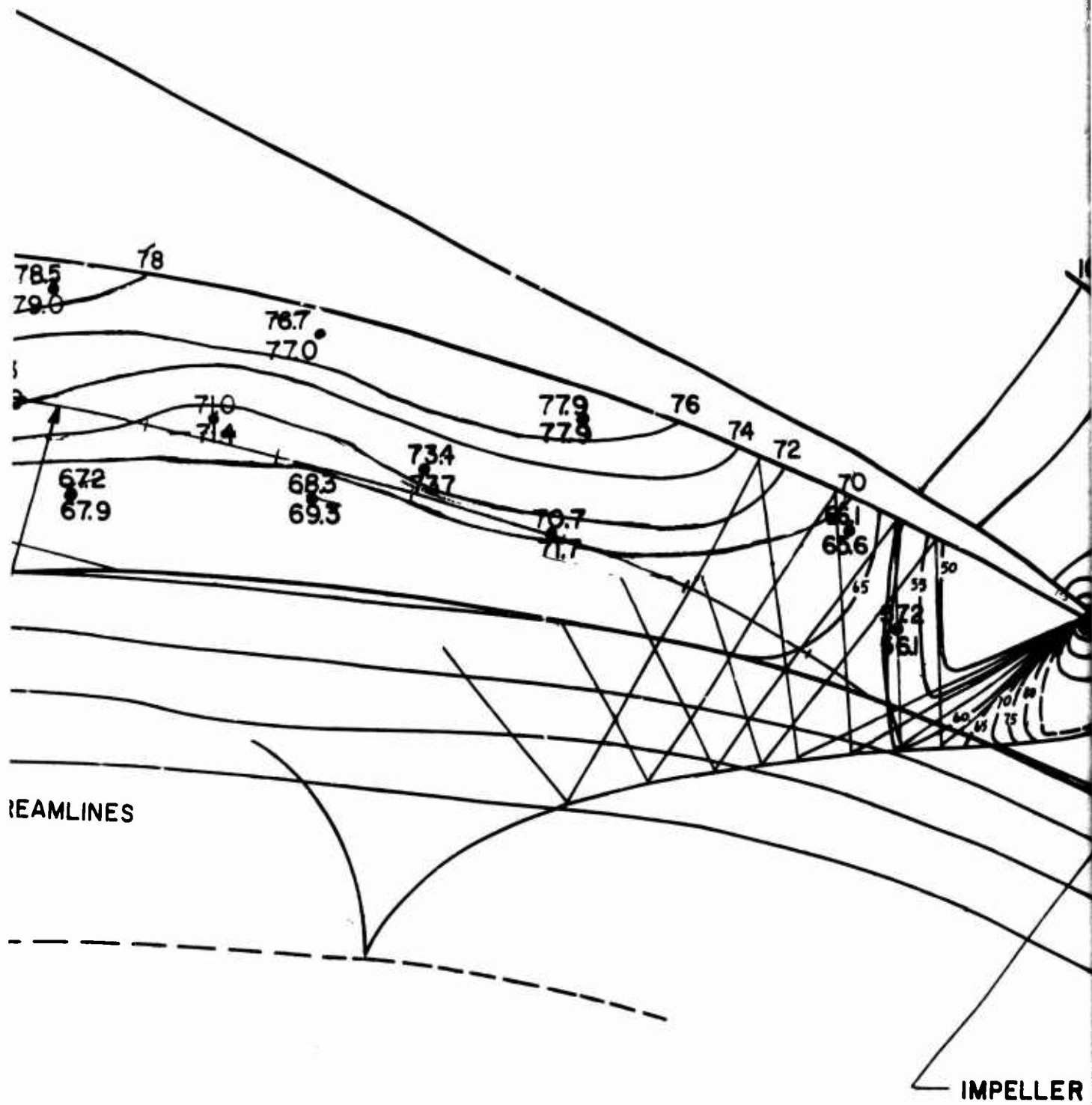
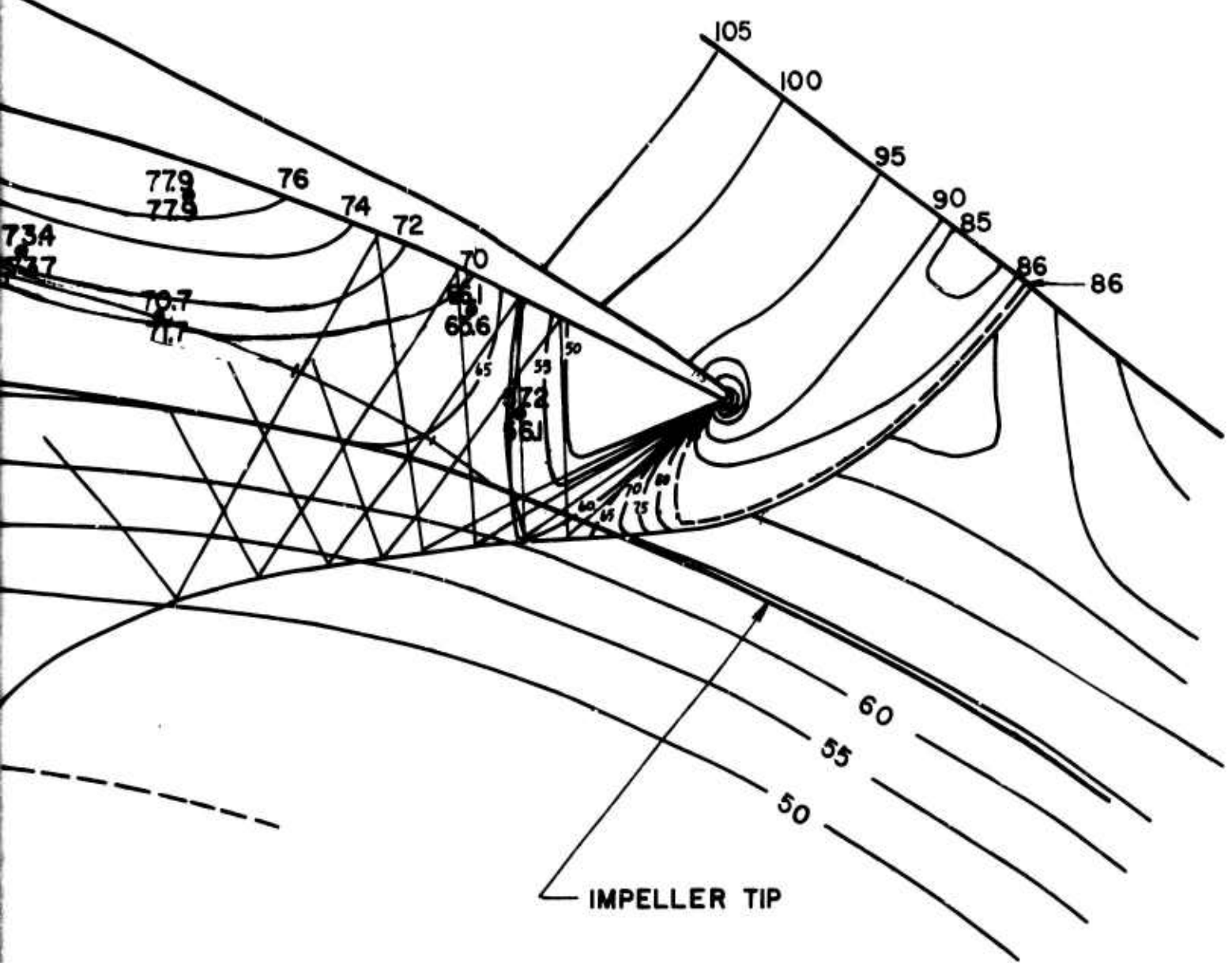


Figure 133. Isobaric Plot for Test 3366





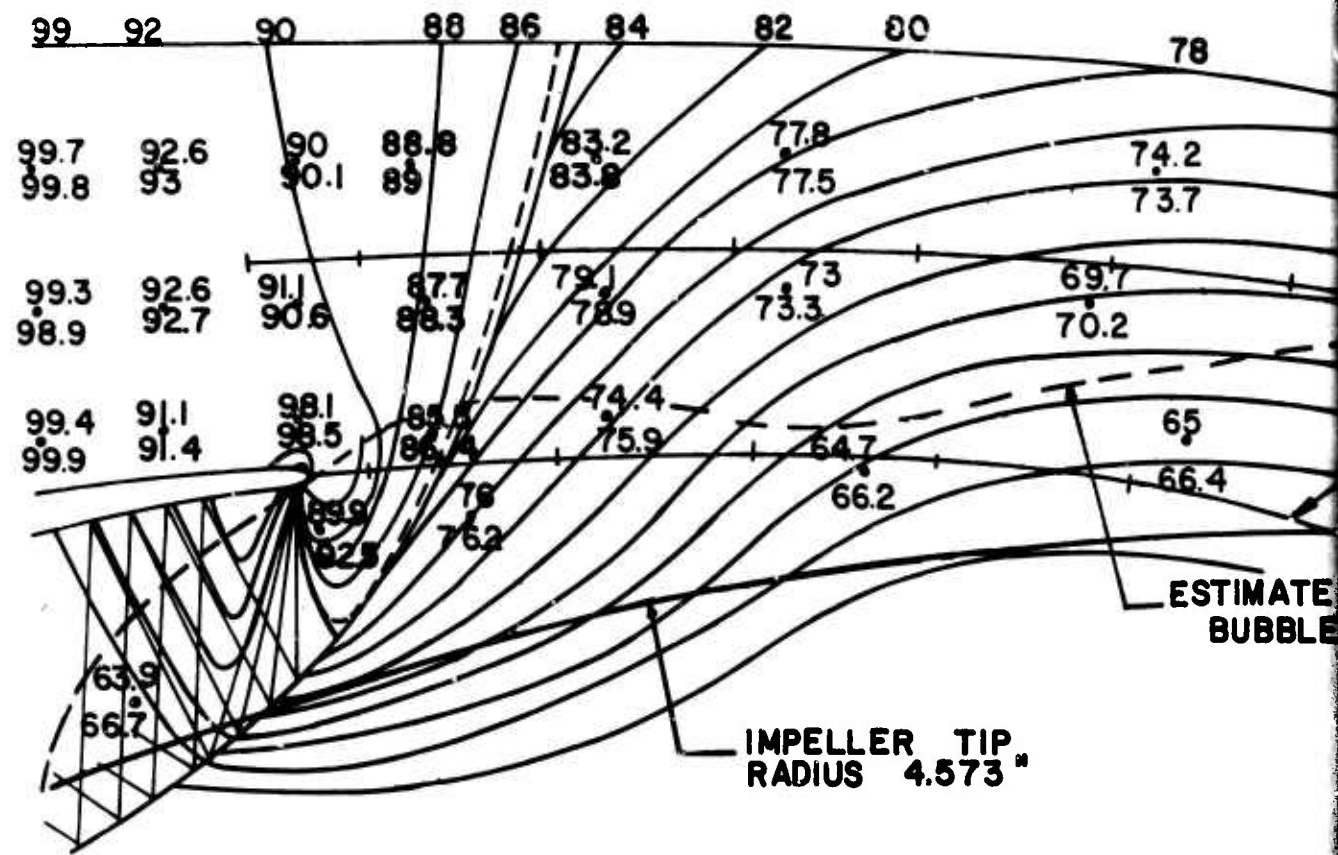
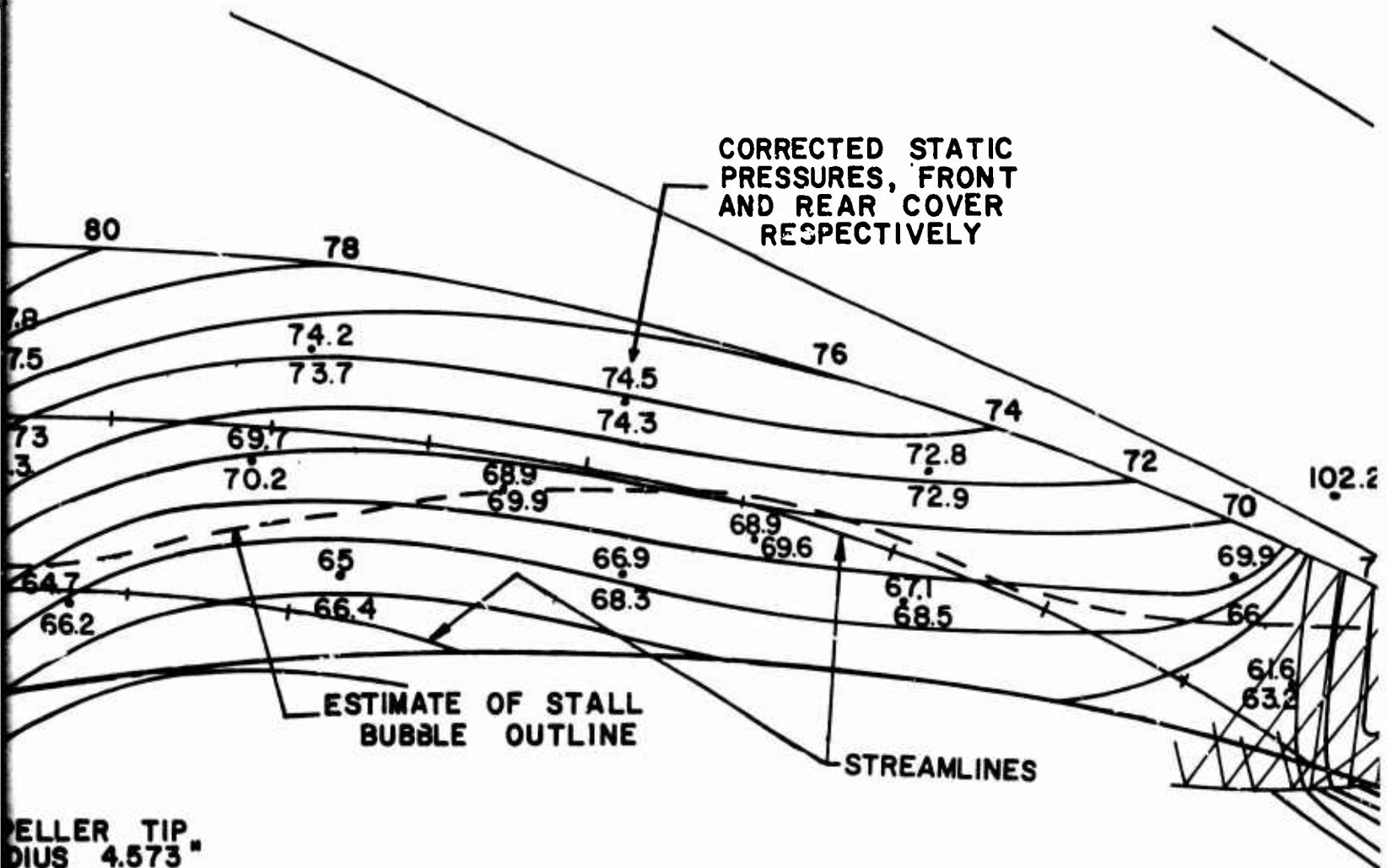
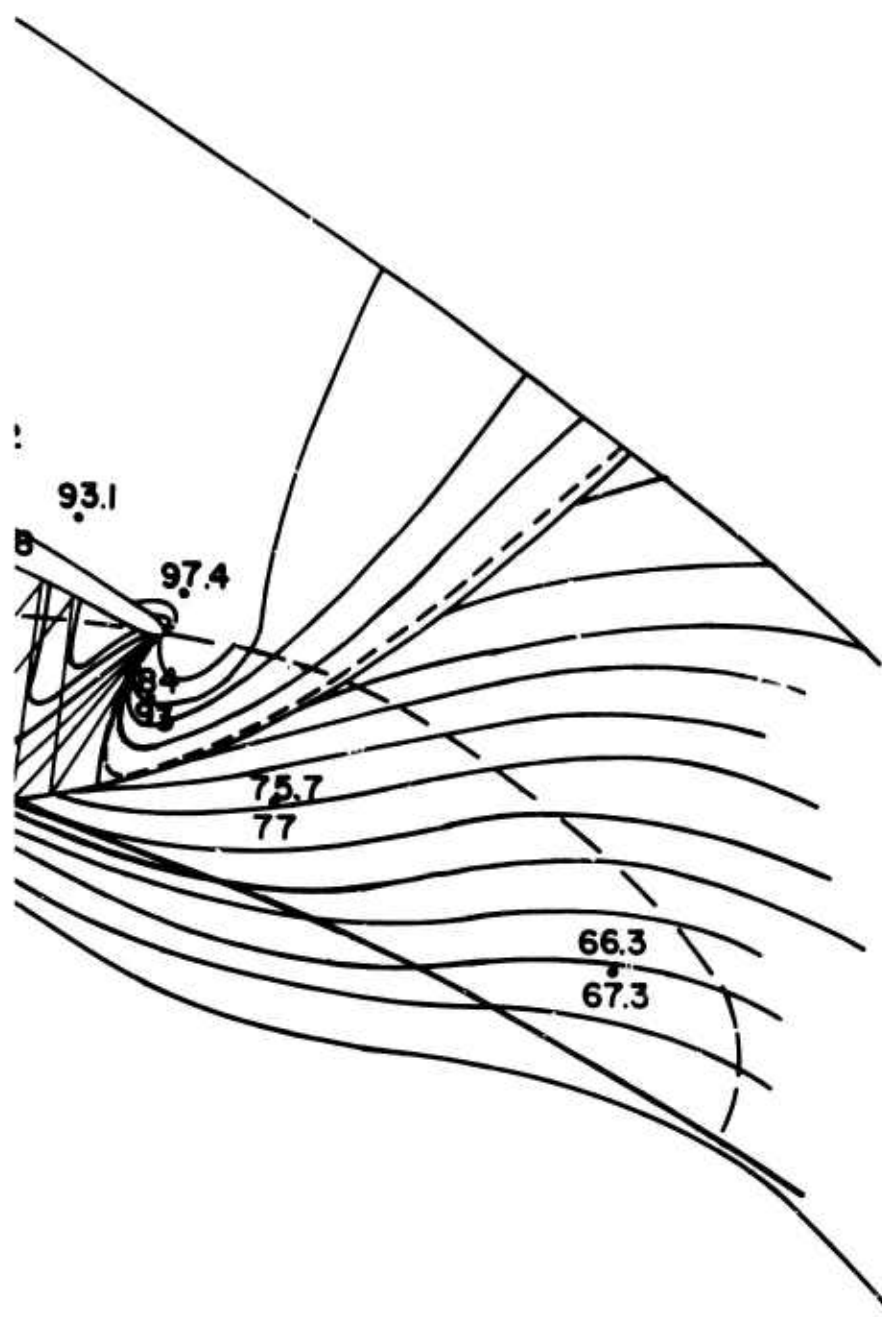


Figure 134. Isobaric Plot for Test 3369.



or Test 3369.



$$\frac{dp}{dn} = \frac{\rho C^2}{g_o R}$$

where  $\frac{dp}{dn}$  = pressure gradient normal to a streamline

$\rho$  = local density

C = local velocity

R = radius of curvature of streamline

has been used to determine streamline curvature in the vaneless space.

Streamlines were drawn from the diffuser throat to the impeller tip by assuming the flow was one-dimensional in the diffuser throat. This provided an initial direction (flow angle) for the streamlines. By extending the streamlines back through the vaneless space, the lines shown on Figures 133 and 134 were drawn.

The Mach number distribution in the vaneless space is deduced from the constant stagnation pressure assumption for the core flow. From this information (Mach number distribution and flow stagnation properties), boundary layer calculations were made using the Englert (1951) method. This method modifies Truckenbrodt's incompressible boundary layer equations with a Stewartson transformation to account for compressibility. This calculation procedure was further modified to take into account the divergence of the boundary layer in a polar flow field due to the change of "wetted perimeter" with changing radius. This theory does not attempt to account for secondary flow; that would require a three-dimensional boundary layer calculation that is now intractable.

The boundary layer growth was calculated along three streamlines: the streamline ending on the vane tip, the center streamline, and the suction surface streamline. These calculations for Tests 3354, 3366, and 3369 are shown in Figures 135, 136, and 137.

Throat blockage was calculated from the boundary layer

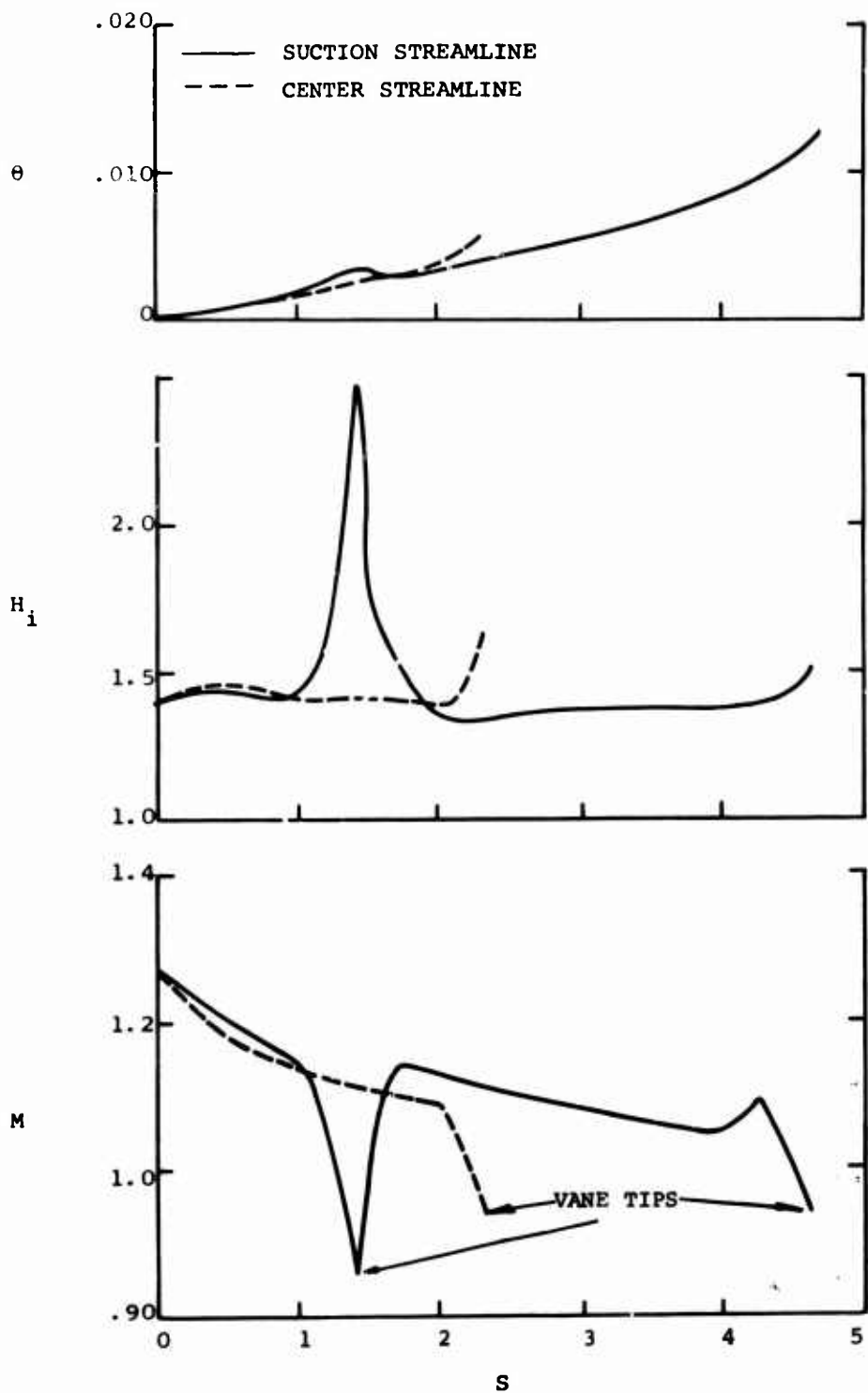


Figure 135. Boundary Layer Calculation for Test 3354,  
Line 7.

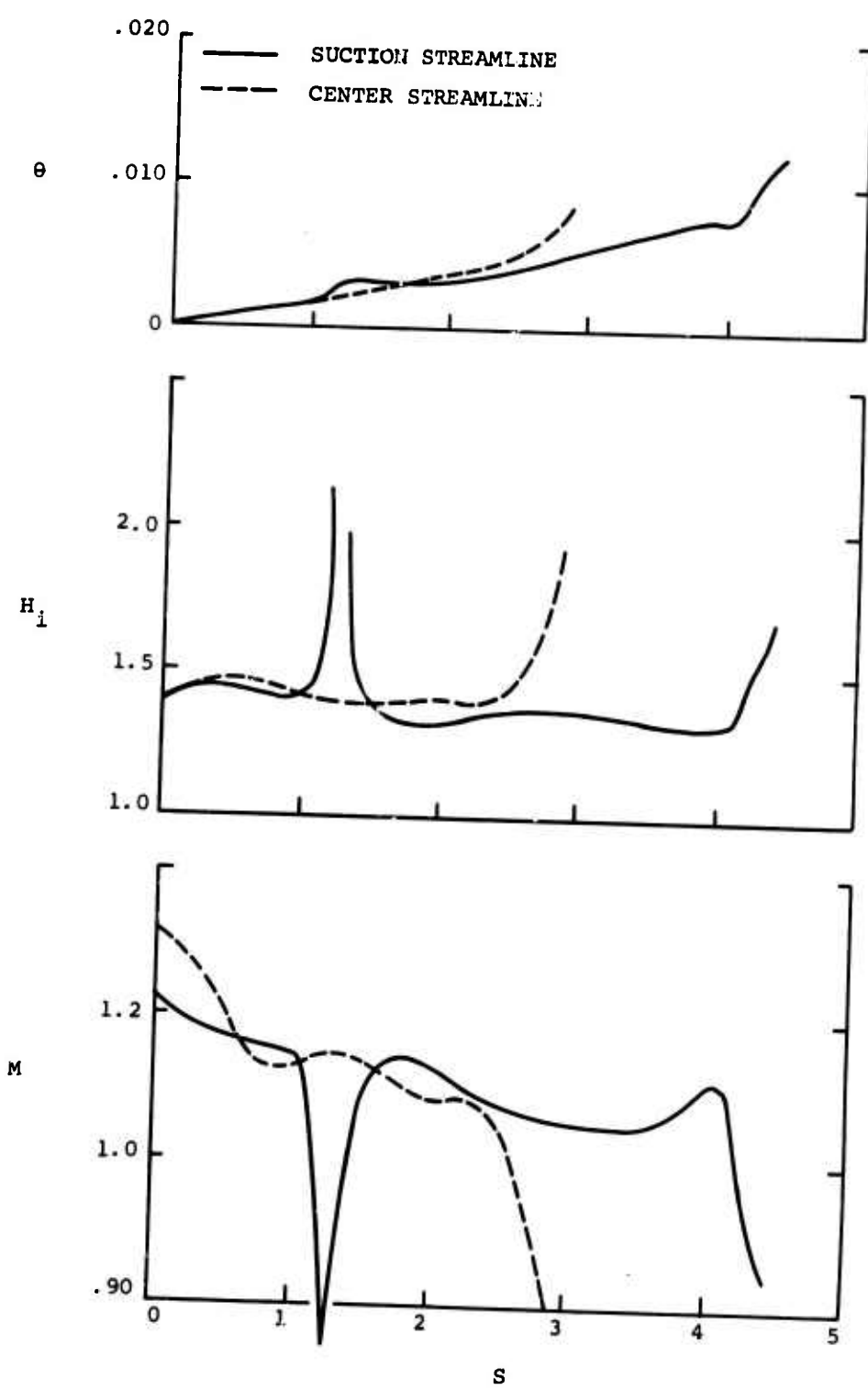


Figure 136. Boundary Layer Calculation for Test 3366,  
Line 5.

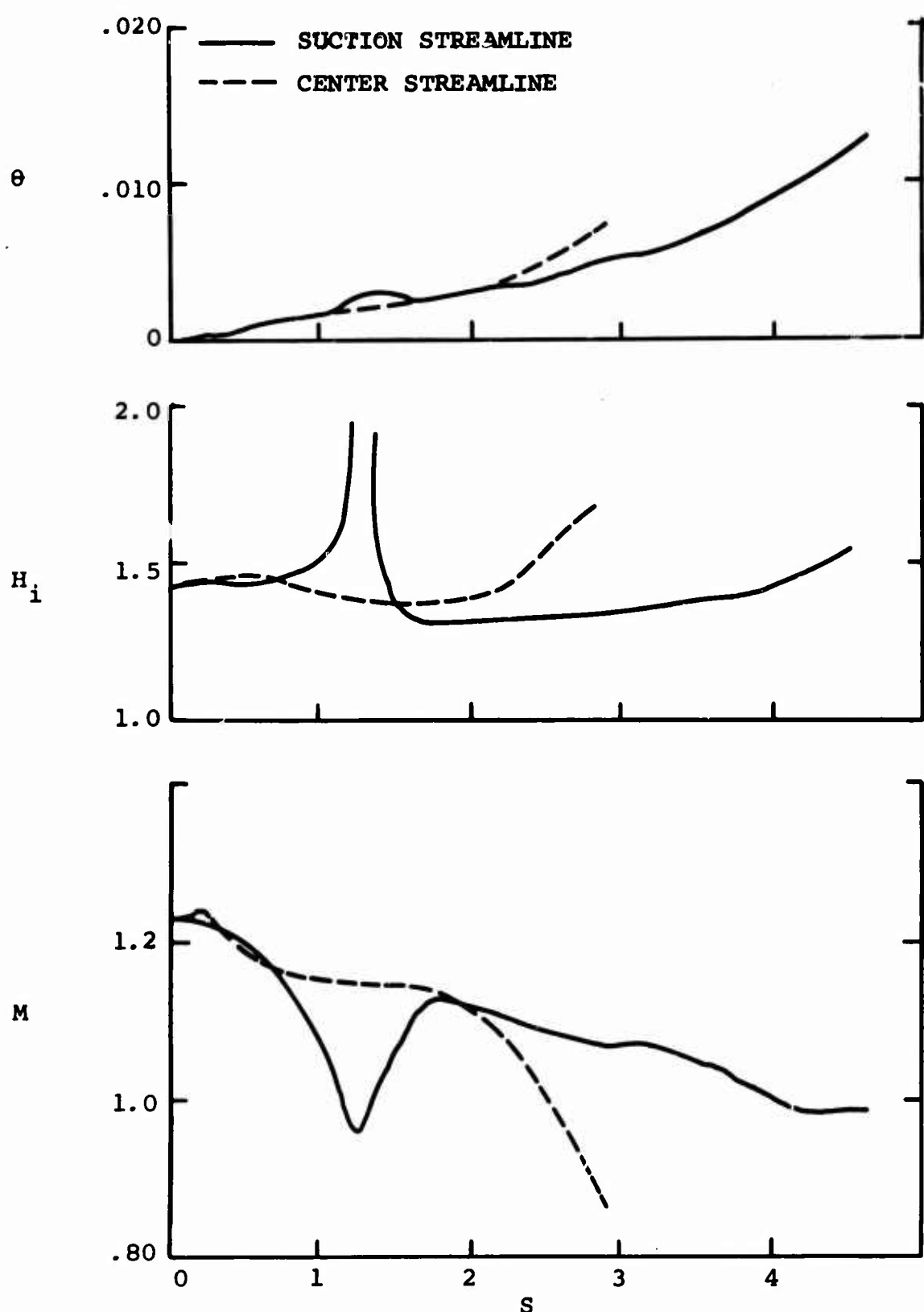


Figure 137. Boundary Layer Calculation for Test 3369,  
Line 5.

results by assuming a linear transverse variation of displacement thickness between calculated streamlines. The boundary layer thickness on the pressure surface is assumed to be zero since there is only a 0.125-inch length for boundary layer growth. (Also, the static pressures are not at all well defined over this distance, making calculations meaningless.) The resulting blockage has a particular shape due to the assumptions made in the calculation. A comparison of this boundary layer profile with that indicated by the total pressure measurements in the throat shows that they are quite different (see Figure 138).\*

The blockages calculated from boundary layer theory are about twice as large as those determined from the data.

Thus, two-dimensional boundary layer calculations appear to be inadequate for predicting throat blockage, even when the experimental static pressure distribution is employed.

#### 5.8.1.1 Possible Causes of Discrepancy

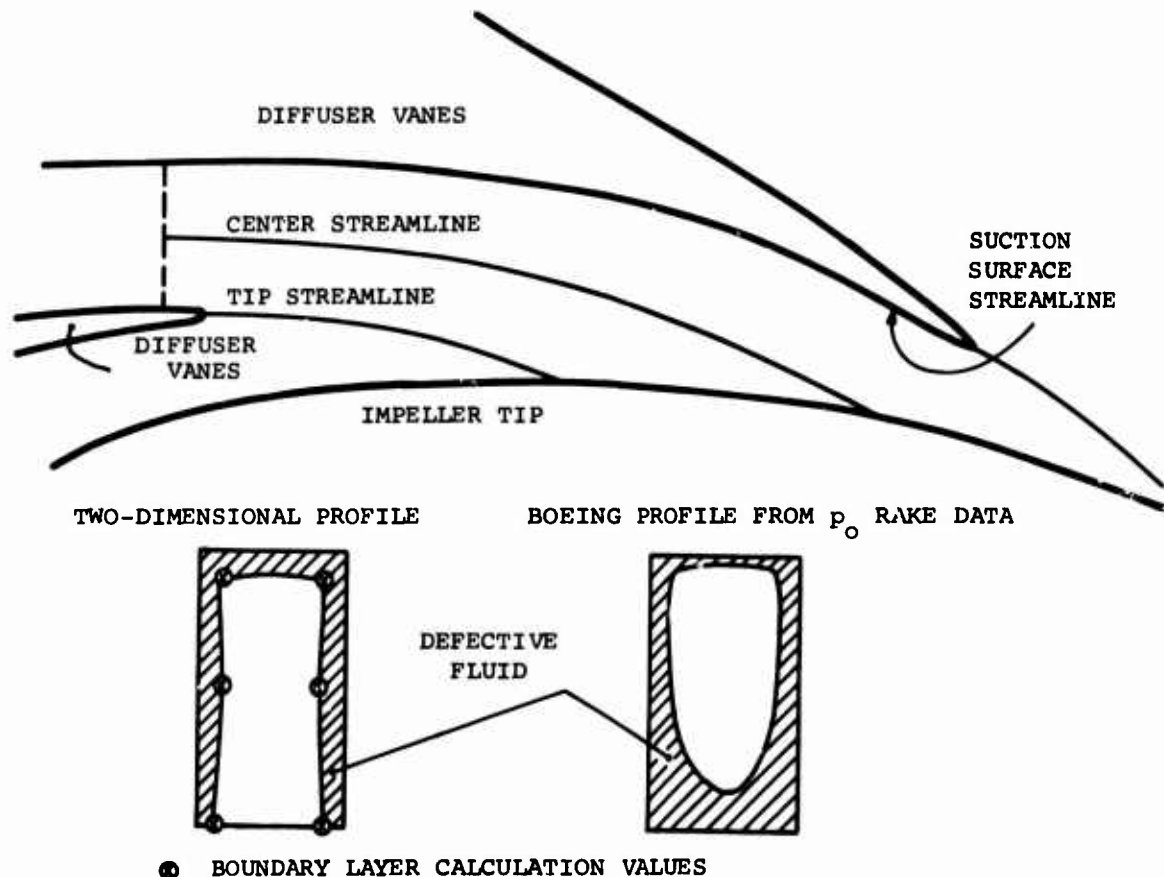
The causes of the major discrepancy between boundary layer calculations of throat blockage and measured values may be:

- (1) Secondary flow bleeding of the sidewall boundary layer back into the impeller for reenergizing and mixing with through flow.
- (2) Shock wave - boundary layer interaction in a very shallow passage.
- (3) Inapplicability of the two-dimensional boundary layer theory, particularly through shock (see Section 6.9).
- (4) A powerful process for mixing sidewall boundary layer into the core flow.
- (5) Inaccuracy of the boundary layer theory.
- (6) Erroneous measurement of throat blockage.

These sources of divergence will now be discussed separately.

---

\* The difference on the pressure surface may be due to wall interference effects on the probe.



Calculation Scheme	3354--7**	3366--5	3369--5
From Boundary Layer Calculation	0.2	0.23	0.27
Boeing Best Estimate	0.096	0.111	0.126
Method c Table X	0.096	0.111	0.126
Our Best Estimate Method b of Table X	0.095	0.119	0.128

\*\* Supercritical Case

Figure 138. Throat Blockage Comparison.

### Secondary Flow in the Vaneless and Semivaneless Space

Figures 33 and 34 show by means of oil streaks on the schlieren windows that there is some secondary flow on the sidewalls of the vaneless and semivaneless spaces. This is to be expected, of course, from the general curvature of the flow.

There are no oil streak photographs available at 50,000 rpm. Figures 33 and 34 suggest that relatively little backflow is occurring, but the same conclusion may not be justified at 50,000 rpm. Even a small amount of secondary flow can explain why the stagnation pressure profiles flatten significantly toward the suction surface. Further, as has been pointed out in Section 6.7, these oil streaks are some kind of time-average of a complex three-dimensional transitory flow pattern. They could, therefore, completely miss transient strong secondary flows out of the boundary layer.

We do not expect, however, that this explanation is valid over the great extent of boundary layer growth from the tip of the impeller to the diffuser throat entry, in spite of the fact that transient backflow near the impeller tip may be having a serious influence on impeller efficiency. It is obvious that this expectation cannot be proven with the existing state of three-dimensional boundary layer theory nor with the evidence on hand from the Boeing-AVLABS experiments, nor with any other evidence known to us.

### Shock Wave - Boundary Layer Interaction

The nature of the shock standing across the entry to the throat will be discussed at length in Section 5.8.2. This shock is always complex because of its interaction, in the shallow passage, with the relatively thick sidewall boundary layers. Near choke, the shock tends to spread out and repeat several times, indeed sometimes right through the throat into the diverging part of the channel.

We have applied the Englert boundary layer analysis through this shock; that is, along a pressure distribution made by drawing smooth curves through the measured data points. First, this is at best a poorly focused picture of the actual pressure distribution, but it is the best that can be done with the tap spacing used. Secondly, the Englert method actually collapses for pressure gradients as steep

as those encountered in these calculations through the shock region. So from this cause alone, we are not too confident of the Englert method predictions.

We have contemplated the application of our computerized shock wave - boundary layer interaction calculation techniques but have ruled out this approach because the shock in the shallow passage is so different from shocks on bodies in free-flow fields for which the theory was developed.

While various investigators, including Neumann and Lustwerk (1949) and Fejer, Heath, and Driftmyer (1964), have examined shocks in ducts with thick boundary layers, no one has yet made a detailed investigation nor developed any sort of theoretical methods for predicting the structure of the shocks and the nature of the boundary regions near the walls. The interaction in channels with thick boundary layers is known from the experiments to be very complicated.

#### Inapplicability of the Two-Dimensional Boundary Layer Theory

As suggested above, conventional two-dimensional boundary layer theory may not be appropriate to this case. The prime cause for concern is that the boundary layer is growing in a shallow passage without the well-defined free flow of a wing or other external boundary layer. Boundary layers in passages historically are hard to handle analytically. Their stability characteristics are different too (Kline, 1959). Very little useful theory, even for incompressible flow, is available today for this common, but analytically intractable, flow. At transonic speeds, all analytical methods fail.

This analytical difficulty is further amplified as the boundary layer thickens and approaches stall. A similar situation is found in the channel diffuser. There, boundary layer calculation techniques are reasonably successful when the boundary layer is fairly thin and the flow is not approaching stall. However, it is well known that when the boundary layers approach stall, which occurs with a diffuser of maximum pressure recovery, the analytical approach using boundary layer theory fails. The boundary layer penetrating

the centrifugal compressor's diffuser entry shock could be a related case.

#### Strong Boundary Layer Mixing Processes

A few general comments about boundary layer calculation methods will be made here. For turbulent flows, boundary layer calculations all use some empirical data. This is usually in the form of a shear-stress correlation. However, this data is largely external flow data. In particular, the separation criteria which are implicit in the empirical relationship between skin friction and boundary layer parameters and which were originally obtained from data on external flows may not be adequate for internal flows.

In internal flow when separation occurs, there is an immediate area-coupling effect caused by the bounding walls. It is possible to set up a quasi-stable separation whose overall behavior suggests unseparated flow. Such a boundary layer would be fully separated if it occurred in an external flow. This behavior of internal flow seems to be one of the reasons that no one has been able to theoretically predict diffuser performance using boundary layer methods.

As discussed in Section 5.7, there are some grounds upon which to suspect an unusually strong mixing process in the vaneless and semivaneless region, which causes unusually vigorous intermixing of the core and boundary layer fluid. Welliver has suggested secondary flow as a possibly responsible mechanism. However, we can find no evidence supporting this prospect. On the other hand, there are some other potent possibilities.

One of these suggested by Morris and Kenny (1969) is that vortices may be shed from the leading edges of the vanes into the semivaneless expanse. These vortices could be occasioned by the high angles of incidence of the sidewall boundary layer fluid onto the vanes. The leading edge could act like a vortex generator causing the roll-up of two counter-rotating vortices in the sidewall boundary layers. These vortices might, through a large expanse of the semivaneless region, produce strong mixing.

Despite the appeal of this suggestion, there is no evidence

we can discern in the pressure distributions, schlieren photographs, stagnation pressure distributions in the diffuser throat, or oil slick traces on the schlieren windows which suggests in any way the presence of such a vortex structure. One would expect the oil slick traces to show a separation line on the sidewalls associated with the vortices, as carbon-black traces do for axial compressor cascades operating at high incidence in the end wall boundary layers. The resolution is poor, however, and we cannot say for sure that such vortices do not exist - only that if they do, their effect is negligible as seen from the diffuser throat stagnation pressure profiles.

Another possibly powerful mechanism is the mixing between the wakes and the jets coming from the impeller. The kinetic pattern of mixing in the vaneless and semivaneless spaces and in the channel diffuser should look something like the sketch in Figure 139. Notice that the absolute flow in these spaces is a transitory pattern with moving regions of wake and jet fluid following successively. Shear-driving mixing is believed to occur rapidly between the jets and the wakes, although just how it occurs in a vaned diffuser is rather hard to appreciate after examining Figure 139. In the Dean and Senoo (1960) theory, for a vaneless diffuser, a relative velocity difference between jet and wake persists into the diffuser; shear mixing between these regions was attributed to that difference. However, with the boundary conditions imposed by the vanes of the vaned diffuser, it is hard to see how this pattern can persist for long. The boundary conditions imposed by the vanes should cause gross mixing between the jets and the wakes and indeed might evolve into the vortex structure suggested by Morris and Kenny (1969). Such a process in reality might be one of intense turbulence enhancement rather than the evolution of a well-defined vortex pattern, and thus, the oil streaks would not show it. Intense turbulence production could account for a substantial stagnation pressure loss as well as explain the thin boundary layer near the suction surface.

Another possible mechanism for the production of this turbulence is the three-dimensional interaction between the wakes and the jets. Because the wake fluid travels with a higher absolute velocity than the jet fluid, it

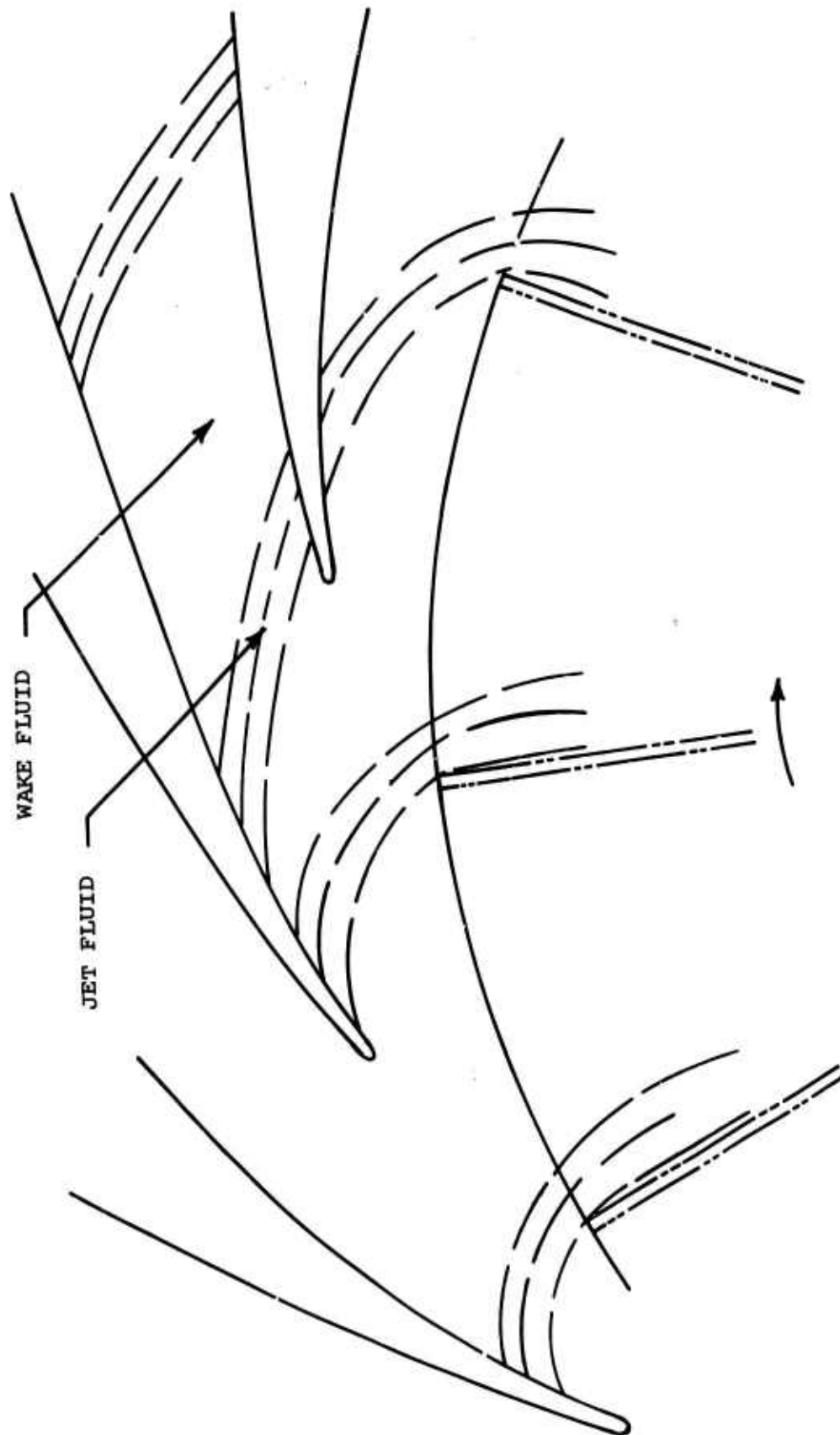


Figure 139. Schematic of Impeller Jet and Wake Moving Through the Diffuser.

should tend to overtake the jet fluid and drive right on through it. This is illustrated schematically in Figure 140. With the wake fluid overriding the jet fluid near the wall, as a warm front overrides a cold air mass, vortices and intense turbulence could be set up on the interface. A roll-up and mixing process on the interface may occur as suggested in Figure 141.

Boeing took a large number of schlieren photographs with the Workhorse stage of the diffuser entry flow. After a careful examination of all the photographs at speeds from 15,000 to 50,000 rpm, we have concluded that the turbulence level cannot be resolved from the extraneous factors (principally heat from the casing).

A vigorous mixing mechanism would be satisfying because it could explain the measured throat blockages falling far below those calculated from two-dimensional boundary layer theory and would lend support for a loss in core  $p_o$  between impeller and throat. However, none of the evidence we have seen supports such a mixing process (except possibly the railroad track data which seems to be a cross between static and stagnation pressure as has been mentioned). In aggregate, the evidence strongly asserts that there is no important mixing process at the impeller tip except that described by the Dean and Senoo theory.

#### Inaccuracy of the Boundary Layer Theory

There always exists the possibility that the Englert theory is not very competent under the conditions found in these compressors. Unfortunately, we have no really critical test of the accuracy of this theory even in supersonic external flow. However, we would not expect normally that the inaccuracy would be as large as indicated by comparison with the throat blockage data. On the other hand, this expectation could be faulty when the boundary layer approaches the verge of separation in a shallow passage and through a shock.

#### Erroneous Measurement of Throat Blockage

There always exists the outside possibility that the Boeing measurements made to define throat blockage are seriously in error. However, this possibility is not expected to be

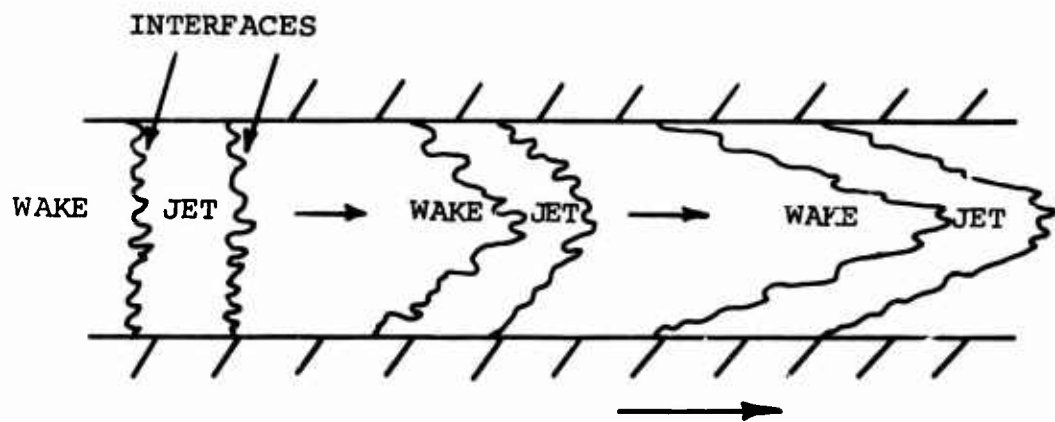


Figure 140. Penetration of Wake Fluid Into Jet Fluid -- Schematic of Changing Interface Form.

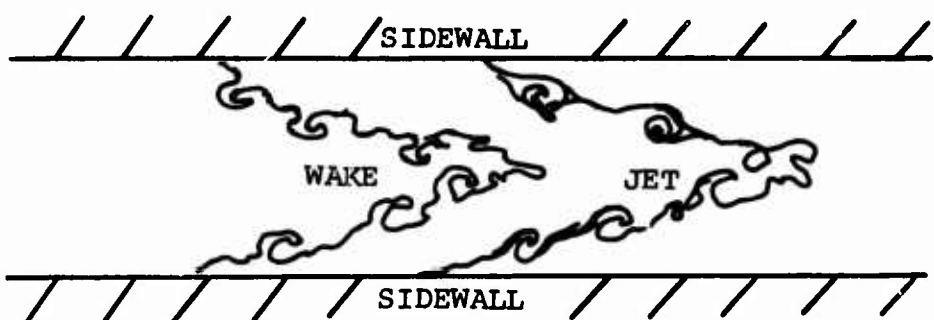


Figure 141. Schematic of Vortex Roll-Up on Interfaces Between Jet and Wake.

great, particularly with the good correspondence between the channel diffuser performance and the laboratory simple diffuser tests of Runstadler (1969) reviewed in Section 5.9. If the blockage were truly as high as the two-dimensional boundary layer theory predicts, then the stagnation pressure profiles should show a substantial stalled region. Therefore, we reject any compulsion to explain the throat blockage prediction discrepancy as major measurement errors.

### Conclusion

In conclusion, it would appear that of the six possibilities offered above, Numbers (1), (2), and (3) are most likely. In other words, we expect that the two-dimensional boundary layer theory is not very good for this prediction because of significant (in terms of boundary layer thickness) secondary flow, the thick boundary layers in the shallow passage, and the complex shock-boundary layer interaction.

#### 5.8.1.2 Summary

The use of two-dimensional turbulent boundary layer theory to calculate throat blockage has failed its test against the data. This is indeed an unfortunate outcome for, as pointed out in the introduction to this section, prediction of throat blockage is the most critical prediction in estimating diffuser performance. Consequently, we do not have available a crucial tool needed for optimization. All is not completely hopeless, however, for it is still reasonable to predict trends with the boundary layer theory as major geometrical changes are made. We shall do just this in Section 7.4 when attempting to optimize diffuser design. We will rely upon the assumption that the boundary layer theory can indicate direction of changes, and even magnitude of changes, despite the fact that it yields misleading absolute values.

### 5.8.2 DIFFUSER ENTRY MODEL

Welliver and Acurio (1967, 67-30) offered a model for the flow at the entry to the channel diffusers of a centrifugal stage. This model pivots the entry flow patterns upon the Mach number and blockage in the diffuser throat. An entry shock forms ahead of the channel entry with a strength appropriate to the throat Mach number as determined by mass flow rate, blockage, stagnation temperature, and pressure.

Boundary layer blockage occurs in the throat, which reduces the effective area from the geometrical area. The blockage was considered to be caused by boundary layer growth in the vaneless and semivaneless region, enhanced somewhat by the entry shock.

In a "zone of rapid adjustment", juxtaposed to the entry shock, the flow converts from a swirling pattern to a one-dimensional pattern and locally adjusts its Mach number to suit the one-dimensional normal entry shock. Ahead of the shock, the fluid stagnation pressure and temperature were considered to be constant in the core of the flow. These values are impeller discharge mixed-out values ( $p^*$  and  $T^*$ ). The boundary layers growing on the walls were ignored except as contributors to the channel throat blockage.

As the mass flow rate was reduced toward surge, the throat Mach number dropped, thus requiring a stronger entry shock which caused a further thickening in the boundary layer and more blockage in the diffuser throat. Thus as the flow rate reduced, the throat blockage increased. As blockage increased, the static pressure recovery coefficient of the diffuser decreased, just as portrayed by the laboratory diffuser data.

This model was applied by Welliver and Acurio to the Workhorse data with apparent success. Good correlation was evidenced of throat blockage versus channel diffuser static pressure recovery coefficient. Figure 142 shows this correlation. Although the scatter at first appears to be small, this conclusion is wrong. The arrows show the maximum range of  $C_p$  observed by Runstadler (1969) for all tests at aspect ratio 0.25 with diffuser double angles less than 14°. Further, blockage factors below about 0.85 are not possible unless the diffuser entry flow is separated.

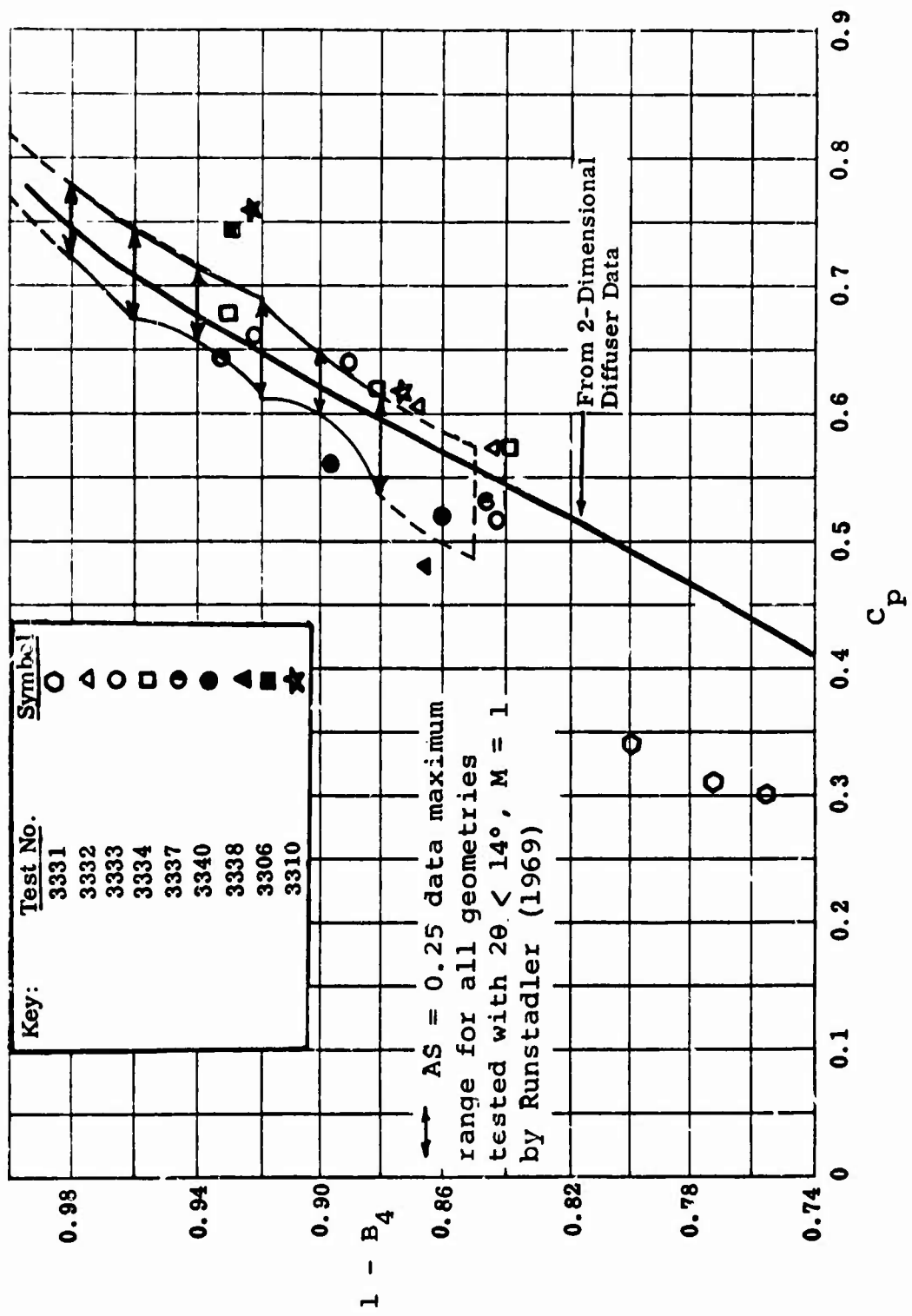


Figure 142. Comparison of Pressure Recovery for Compressor Channel with Two-Dimensional Diffuser Data-Workhorse.

Only 4 out of 19 points from the compressor data fall within the maximum possible limits of the correlation.

A similar situation was found when diffuser throat blockage was plotted versus Mach number ahead of the entry shock.

The comparison of model and data made in Welliver and Acurio (1967, 67-30) was accomplished entirely by using the measured wall static pressures "upstream"  $p_x$  and "downstream"  $p_y$  of the entry shock to establish: the shock strength, the Mach numbers before and after the shock, the throat center-line stagnation pressure, and the throat blockage. For Workhorse, independent observers had little difficulty in most cases in agreeing on what were appropriate values of  $p_x$  and  $p_y$  to be taken from the data. The entry shock was fairly strong in most cases, enabling ready identification of its termini.

When this so-called " $p_x - p_y$ " data reduction suggested that the diffuser throat center-line stagnation pressure varied quite erratically with mass flow, in a "shotgun" pattern as indicated in Figure 143, Boeing abandoned this data analysis.

Welliver and Acurio believed that the relatively constant stagnation pressure characteristic of the impeller indicated by the railroad track probe was the valid observation, but the railroad track was sufficiently suspect in itself that no firm conclusions could be drawn from Workhorse.

A more critical test of the diffuser entry flow model was planned with the RF-2 stage. In order to shed light on the validity of the model, extensive stagnation pressure surveys were planned for the RF-2 in the diffuser throat. These were carried out in Tests 3352C, 3354, 3366, and 3369. Profiles of stagnation pressure in the throat were obtained (Figures in Section 3), which indicated that there was a core of constant stagnation pressure in the center of the diffuser throat. More important, the probing showed that the center-line stagnation pressure was constant with mass flow. This data confirmed Welliver and Acurio's suspicion as to the truth regarding the stagnation pressure characteristic of the Workhorse impeller.

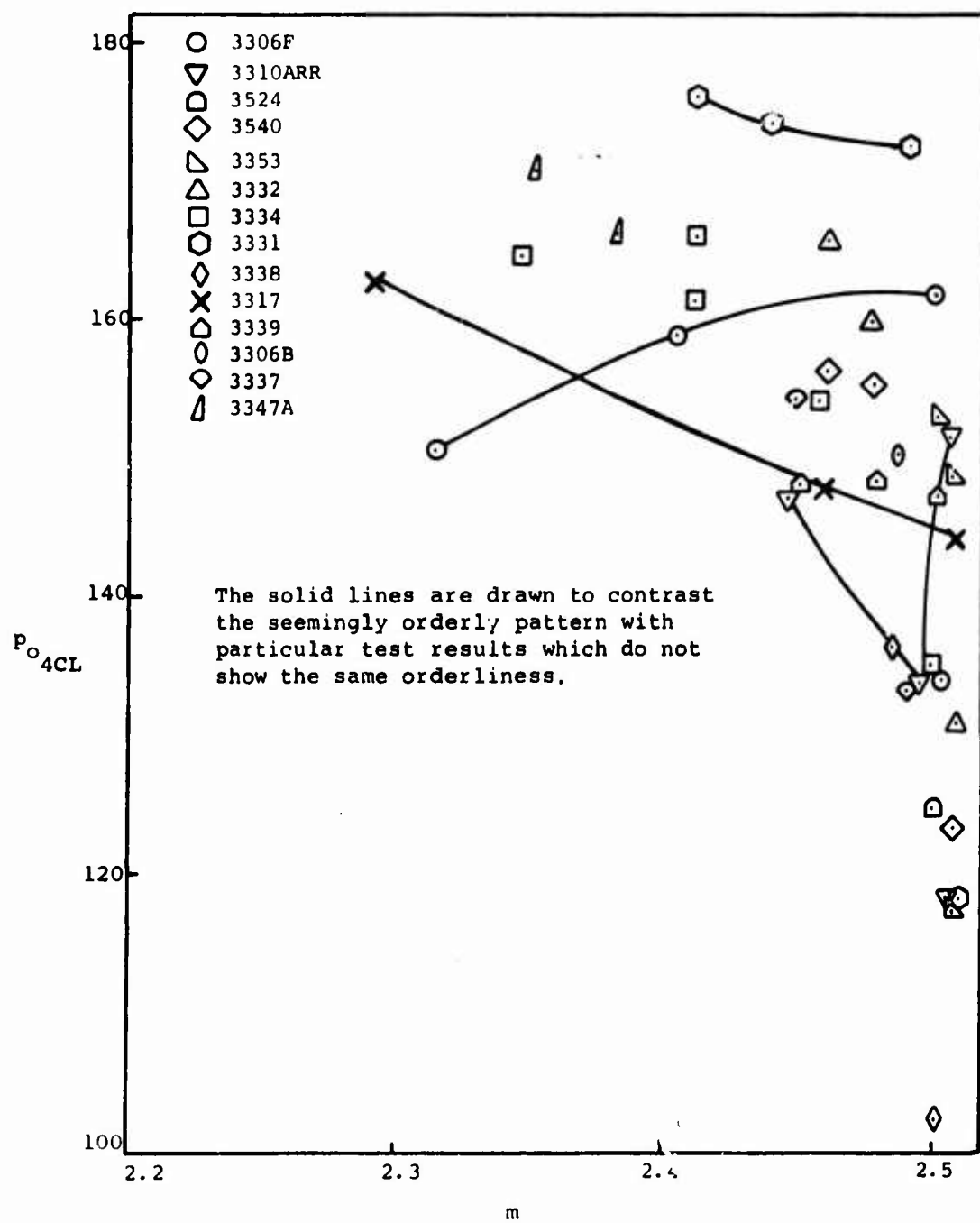


Figure 143. Diffuser Throat Center-Line Stagnation Pressure Deducing by  $p_x - p_y$  Method - Workhorse.

We have reduced the RF-2 diffuser data in as many reasonable ways as we could, to try to find out which set of measurements would give consistent and meaningful results. A similar analysis of Workhorse data was not made because measured throat stagnation pressure was not available. Some of these data reduction procedures were used by Welliver and Acurio; some are new. All but two show major inconsistencies and one of the others shows a minor but nevertheless significant inconsistency. Because of the importance of the diffuser, each of these methods will be described along with reasons for its acceptance or abandonment.

Method (a): Uses static pressure ahead of the shock,  $p_x$ , and the throat stagnation pressure,  $p_y = p_{o_4CL}$ .

Method (b): Uses static pressure at the channel entry, as  $p_y$ , and the throat stagnation pressure,  $p_y = p_{o_4CL}$ .

Method (c): Uses static pressure at the first tap after the diffuser divergence (0.035" from divergence) as  $p_y$ , and the throat stagnation pressure  $p_y = p_{o_4CL}$ . This is the method finally adopted by Welliver and Acurio.

Method (d): Uses static pressure ahead of the shock,  $p_x$ , and static pressure behind the diffuser divergence (0.035" from divergence) as  $p_y$ .

For all of these methods, the normal shock relations and the collector temperature were used to calculate other properties of interest. None of the methods was particularly impressive, but Method (b) was better than the rest.

#### Method (a)

"Method a" uses the static pressure upstream of the shock,  $p_x$ , instead of the "throat" static pressure because the

pressure in the throat varies rapidly with distance, making it quite uncertain as to which value truly represents  $p_y$ . In contrast, because  $p_x$  seems to vary slowly with stream-line distance, as may be seen in Figure 144, 145, 146, and 147, perhaps a much more accurate reduction of the data could be achieved using  $p_x$ .

Table X compares the various data reduction methods. From the trend of events for "Method a", we note that the throat entry shock appears to weaken or remain constant as the mass flow decreases, which is a great violation of the flow model proposed.

The most damaging evidence against "Method a" is the peculiar behavior  $p_y = f(m)$  and the comparison between the predicted  $p_y$  and the measured pressure distributions through the throat. This is shown in Figures 144, 145, 146, and 147. We find that the entry shock in certain cases appears to extend far back into the diffuser in a way we would not suspect from the schlieren photographs. If  $p_y$  is forced to be realized in the throat, then there is a wide discrepancy between the values predicted by "Method a" and those measured in the throat.

#### Method (b)

"Method b" chooses  $p_y$  taken to be the static pressure at the entry plane of the channel diffuser in the plane of the stagnation pressure measuring probes. We note in Figures 144, 145, 146, and 147 that this particular pressure tap seems to have some virtues, for while other neighboring taps yield quite wildly varying pressures, the pressure at the entry plane seems to stay very near the Mach 1 critical pressure. Certainly we would expect that somewhere in the throat at choke the pressure should stay near the critical value despite variation of the diffuser back pressure. Of course, this method will fail if the diffuser becomes greatly supercritical, but that is not the case for the RF-2 diffusers (in marked contrast to Workhorse, where a shock was often observed halfway into the diffuser). As long as the diffuser is not greatly supercritical, we suspect that throat entry static pressure measurement is the most meaningful one. This suspicion is heightened by

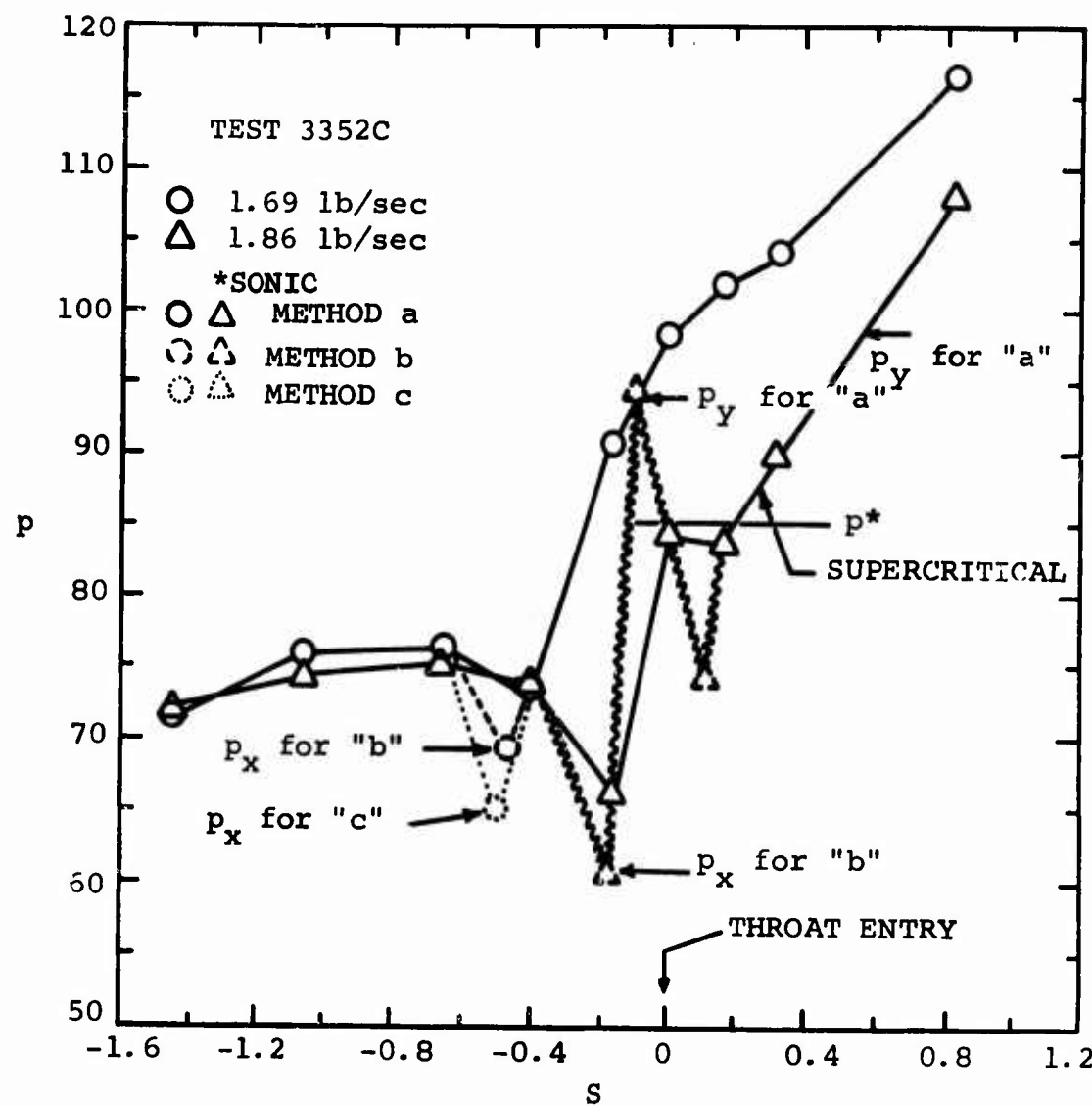
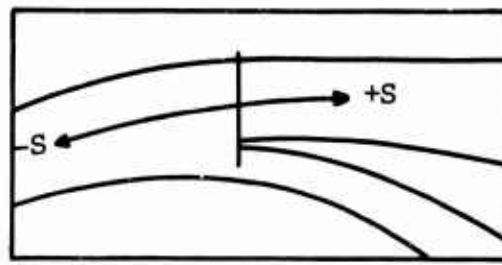


Figure 144. Static-Pressure Variation in Diffuser.  
RF-2

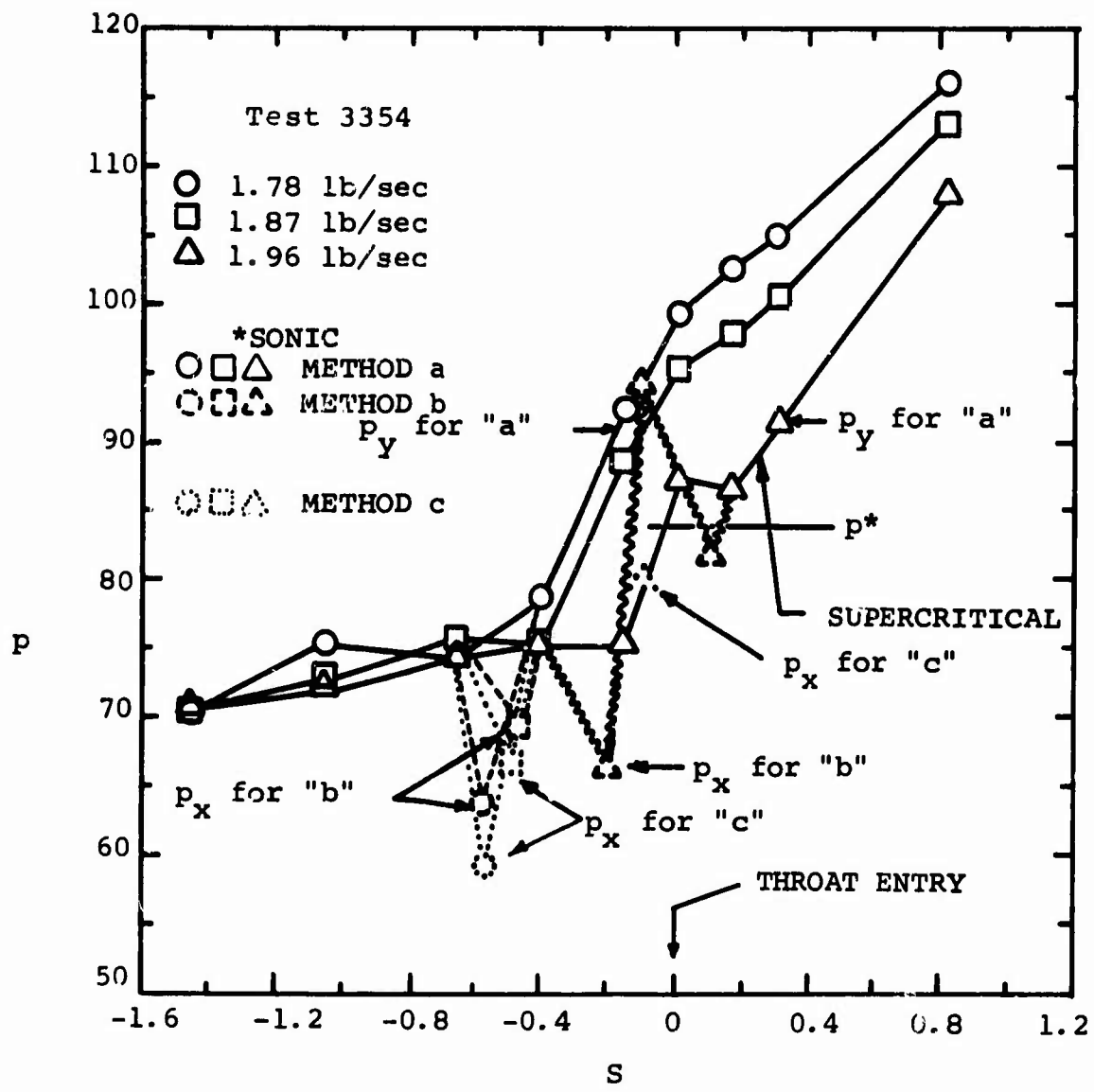


Figure 145. Static-Pressure Variation in Diffuser.  
RF-2

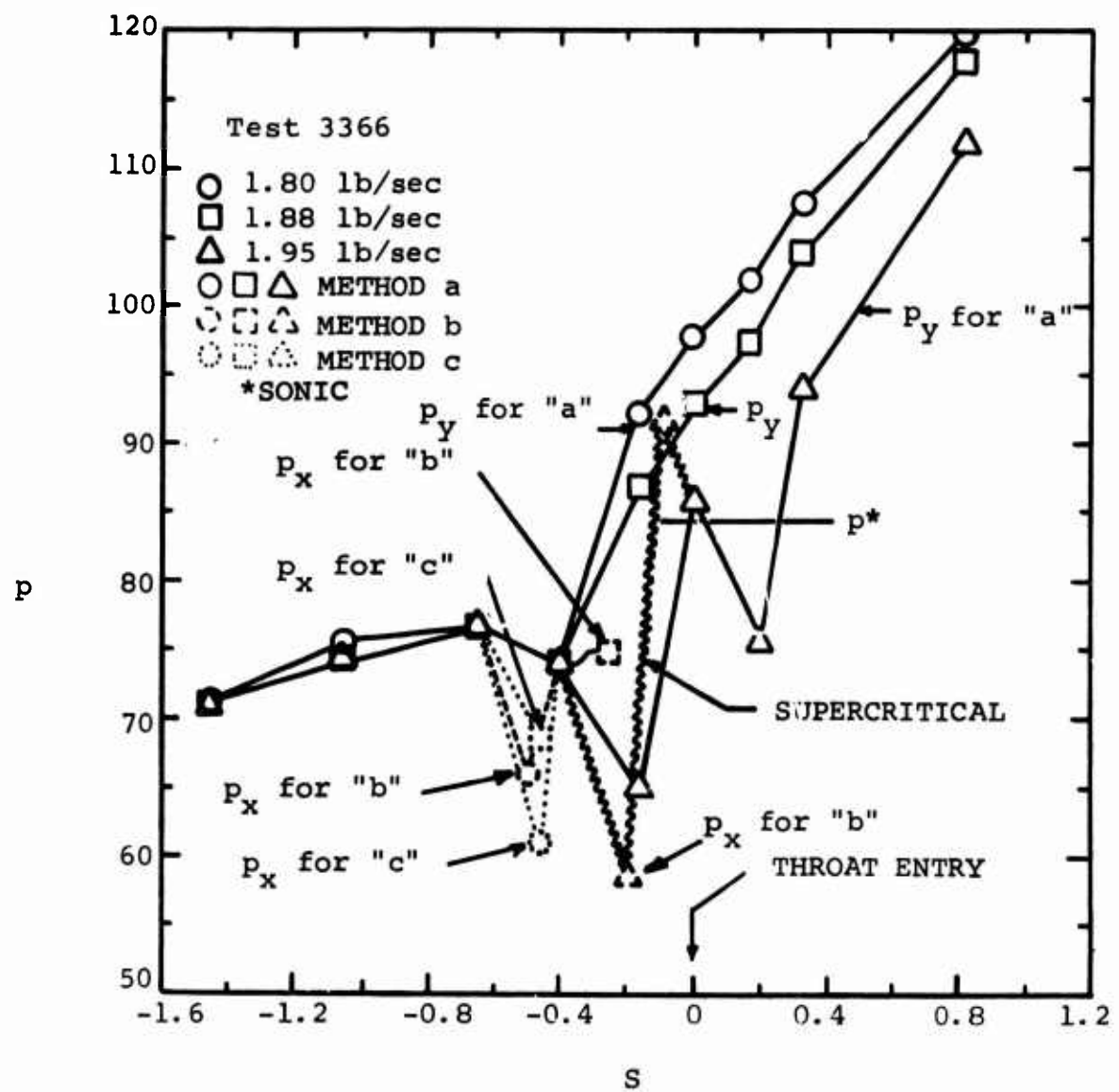


Figure 146. Static-Pressure Variation in Diffuser.  
RF-2

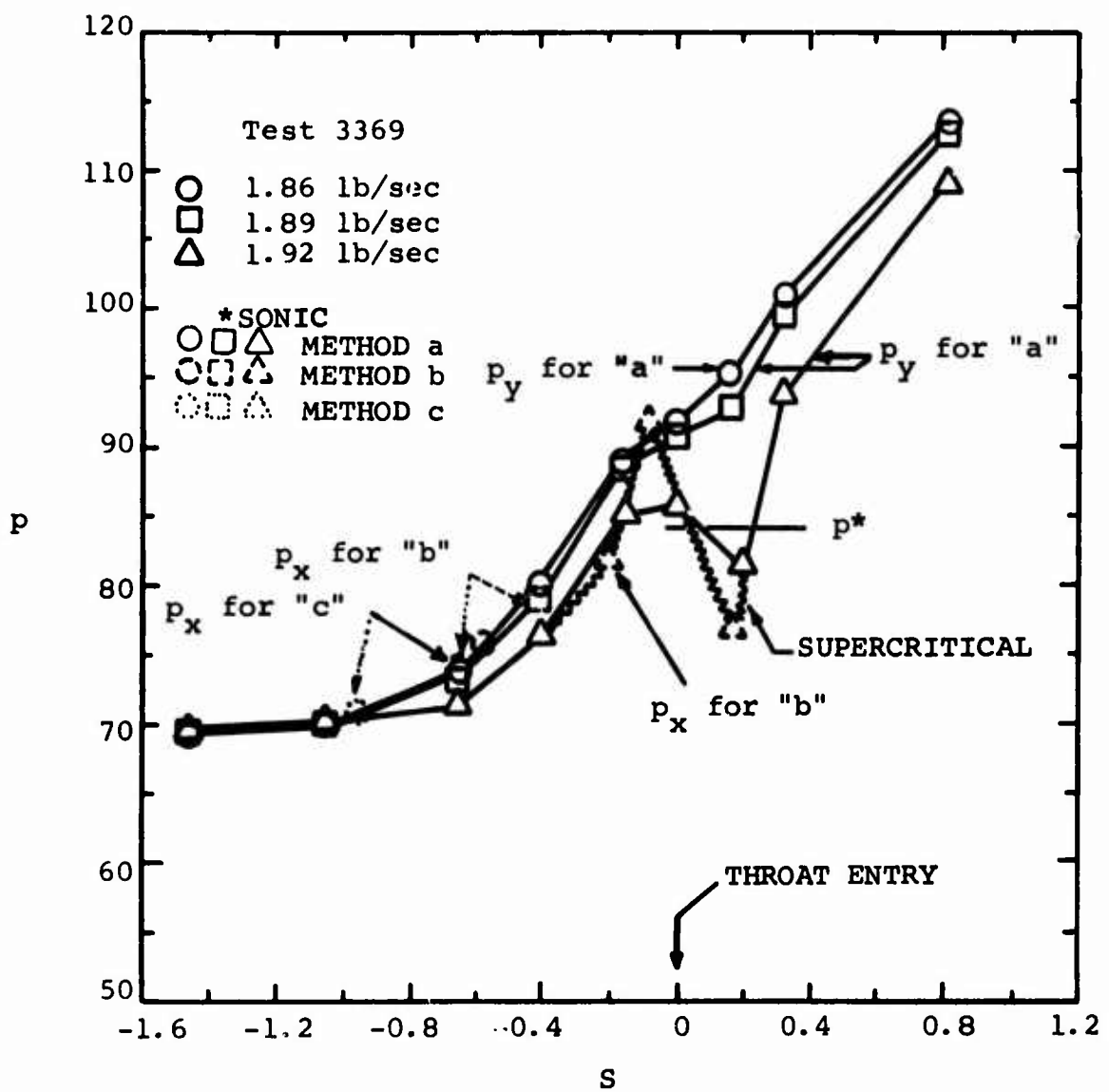


Figure 147. Static-Pressure Variation in Diffuser.  
RF-2

TABLE X. COMPARISON OF DIFFUSER DATA REDUCTION SCHEMES

Test	Diffuser	m	$T_{O_{coll}}$	$P_{coll}$	$A_4$	$b_4$	$w_4$	$2\theta$	
3353D*	V1-3	1.66	1157	135		0.813	0.183	0.450	10
(3352C)		1.75	1152	133					
		1.83	1150	128					
Choke		1.825							
(3353D)									
Choke		1.885							
(3352C)									
3354A	V1-4	1.77	1152	134	+	0.869	0.183	0.477	10
		1.87	1149	132	+				
		1.94	1149	130	+				
Choke		1.977							
(3354)									
3366C	V2	1.80	1156	136	++	0.865	0.203	0.427	10
		1.87	1150	134	++				
		1.92	1148	133	++				
Choke		1.96							
(3366)									
3369	V2-2	1.83	1136	133		0.862	0.158	0.541	10
		1.86	1134	133					
		1.91	1133	131					
Choke		1.926							

\*One rake in diffuser throat for  $p_{O_4}$ , corresponds otherwise to 3352C.

\*\*(a)  
(b)  
(c)

L	L/W	$P_{O_4}$	$P_x^{**}$			$P_y^{**}$			$M_x$				
			a	b	c	a	b	c	$P^{**}$	a	b	c	
5.85	13.0	160	75.5	68.4	75.5	93.5	99.5	102.0	84.5	1.097	1.180	1.097	0.
		160	71.3	73.2	71.3	97.1	95.5	95.5	84.5	1.145	1.124	1.143	0.
		161	67.5	82.6	****	02.2	88.0	84.0	84.5	1.195	1.028	****	0.
5.85	12.2	156	73.7	63.6	73.7	91.1	99.5	102.5	82.4	1.096	1.219	1.096	0.
		157	75.4	69.7	75.4	90.1	95.5	97.5	82.9	1.083	1.148	1.082	0.
		158	75.5	78.8	75.5	91.5	88.5	87.0	83.4	1.087	1.052	1.087	0.
5.85	13.7	157	73.5	66.6	73.5	92.2	98.0	102.0	82.9	1.104	1.185	1.103	0.
		158	74.1	73.8	74.1	92.7	93.0	97.0	83.4	1.103	1.106	1.102	0.
		160	72.5	81.0	****	96.1	88.5	76.0	84.5	1.131	1.039	****	0.
5.85	10.8	158	68.5	74.3	68.5	97.5	92.5	95.0	83.4	1.168	1.100	1.164	0.
		158	69.5	74.9	69.5	96.6	92.0	93.0	83.4	1.156	1.094	1.153	0.
		160	71.3	82.6	71.3	97.1	87.0	87.0	84.5	1.145	1.023	1.143	0.

1)  $p_y$  calculated from  $p_x$  measured

\*\*\*At speed of sound

2)  $p_y = p_4$  measured,  $p_x$  calculated

\*\*\*\*Supercritical (shock

3)  $p_y = p$  throat exit taps ( $x = 0.170"$ ),  $p_x$  calculated

in channel diffuser)

$M_x$	$M_y$			$B_4$			$C_p$			
	b	c	a	b	c	a	b	c	a	b
1.180	1.097	0.914	0.855	0.831	0.176	0.166	0.160	0.624	0.587	0.569
1.124	1.143	0.878	0.894	0.894	0.128	0.130	0.130	0.571	0.581	0.581
1.028	****	0.845	0.973	1.01	0.086	0.106	0.106	0.448	0.548	0.571
1.219	1.096	0.914	0.830	1.013	0.159	0.142	0.133	0.661	0.611	0.589
1.148	1.082	0.925	0.876	0.801	0.120	0.112	0.108	0.624	0.593	0.580
1.052	1.087	0.922	0.952	0.856	0.092	0.095	0.096	0.579	0.597	0.606
1.185	1.103	0.908	0.851	0.812	0.144	0.133	0.122	0.676	0.644	0.618
1.106	1.102	0.910	0.907	0.867	0.120	0.119	0.111	0.632	0.631	0.607
1.039	****	0.888	0.963	1.091	0.104	0.113	0.108	0.578	0.622	0.643
1.100	1.164	0.863	0.912	0.887	0.132	0.140	0.136	0.587	0.618	0.603
1.094	1.153	0.871	0.917	0.907	0.120	0.128	0.126	0.593	0.621	0.615
1.023	1.143	0.878	0.978	0.978	0.109	0.128	0.121	0.539	0.603	0.603

of sound  
tical (shock  
l diffuser)

+ from 3354 data  
++ from 3366 data

C

further developments with "Method b".

In "Method b",  $p_4$  is combined with  $p_{o4CL}$  to give  $M_4$ , which is taken equal to  $M_y$  after the entry shock. Then the normal shock tables are used to obtain  $M_x$  and  $p_y/p_x$ . This gives the shock entry conditions. The values of  $p_x$  derived are plotted in Figures 144, 145, 146, and 147.

#### Method (c)

"Method c" uses the throat "discharge" static pressure as  $p_y$  (which is actually 0.035" downstream of the geometrical exit of the throat) and the throat entry center-line measured stagnation pressure  $p_{o4CL}$  as the stagnation pressure.

Then the upstream static pressure  $p_x$  along with the Mach number  $M_x$  was deduced and the blockage calculated. A small variation of blockage with flow and an extreme range of  $M_x$  from 1.0 to about 1.33\* result. There is very little evidence anymore of blockage shooting up rapidly as  $M_x$  rises above about 1.2 as would be expected from shock wave - boundary layer interaction theory. The values of  $M_x$  predicted in some cases are very high; they imply much lower values of  $p_x$  than observed.

The results produced by "Method c" (used in the Boeing-AVLAES work) tend to blast somewhat the validity of the diffuser entry flow model. In themselves, they are unsatisfactory for low shock-entry pressures are predicted far below the measured data (although not demonstrated by Boeing in their report). Further, the shock entry Mach number seems to become very high without much effect upon the boundary layer, at least as evidenced by throat blockage.

---

\* The highest values of  $M_x$  are not tabulated in Table X because they correspond to supercritical cases.

### Method (d)

"Method d" takes  $p_x$  ahead of the shock and  $p_y$  0.035" downstream of the diffuser geometrical throat. Very little analysis was attempted with Method (d) because it predicts a wild variation of  $p_{o,4CL}$  with mass flow; this variation was not observed for any of the data.

We have excluded Methods (a) and (d) because they produce somewhat odd results. This behavior may be due to the fact that the thick boundary layers tend to blur the pressure changes which occur in the free stream. The shock wave boundary layer interaction may be such that the boundary layers "diffuse" the pressure gradients. Schlichting (1960) describes this behavior. Shapiro (1953) reports pressure distributions through a multiple shock in a straight duct. Although the shock pattern clearly repeats as shown by schlieren photographs, the wall static pressure does not show any evidence of this behavior. Thus, although we can understand qualitatively why Methods (a) and (d) fail, we can do nothing to improve them. The shock boundary layer theory today cannot even predict what happens in a straight duct.

We note in Table X that both "Method b" and Method c" give the same type of trends, blockages, Mach numbers, and so forth, although "Method c" gives a very low value of  $p_x$  near choke (not shown in the table for supercritical cases which are denoted by the symbol \*\*).

There is one disturbing factor from both of these methods, however, compared to the general assertions of the diffuser entry model. The model shows that the entry shock weakens to the point of dying away when the flow chokes in the diffuser throat. The throat Mach number is then 1, and a normal entry shock must be of vanishing strength when  $M_y$  goes to 1.0. Yet, a glance at the static pressure distribution for Figures 144, 145, 146, and 147 convinces us that this is not at all so. On approach to choking,  $p_x$  drops rapidly. This is not at all what we expected. Rather,  $p_x$  should rise to  $p^*$  (sonic). We get a hint as to

what is going on from the schlieren photographs. Figure 32 shows schlieren results for 4 flow rates; Line 2 is near (but not at) surge, Line 7 is at choke. The most significant part of the shock structure is the detached entry shock. As the flow rate increases, this shock progresses toward the diffuser. The schlieren photographs suggest (and the static pressure distributions tend to confirm) that the shock becomes stronger as the mass flow increases.

A more significant clue to what is happening is the expansion region under the vane tip. Near surge we would expect a high incidence on the vane tip. As the flow increases, we would expect it to go away. But the photographs show that it returns again. The only logical explanation seems to be that the entry shock turns the flow and spills it over the vane tip as choke approaches.

The events in the diffuser throat are also interesting. The shock on the pressure surface suggests that the flow turns quickly there to become one-dimensional. The shock in the diffuser for Line 5 and to the right of the picture for Line 7 shows that these diffusers are operating in the significantly supercritical regime, while the overall pressure recovery shows no sudden drop (see overall pressure ratio data plotted in Figure 37).

### Conclusions

These results and observations are incorporated into an improved diffuser entry model in Section 6.9. From the data itself, we conclude:

- (1) The static pressure measured at the wall may not (and probably does not) resolve the details of the mainstream flow.
- (2) Method (b), using  $p_{o_y}$  and  $p_y$  measured at the entry to the short straight channel ahead of the diffuser divergence, gives the most reasonable data reduction if the diffuser is not highly supercritical.

- (3) The entry shock approaches the diffuser and increases in strength as the flow increases from surge to choke.
- (4) The diffuser entry model proposed by Welliver and Acurio does not appear to be valid except qualitatively.

## 5.9 COMPARISON OF CREARE-AVLABS CHANNEL DIFFUSER DATA WITH BOEING-AVLABS DIFFUSER DATA

The flow model offered by Welliver and Acurio breaks the compressor's diffuser into several discrete elements; one is the channel diffuser from throat entry to collector. The flow model asserts that this element behaves very much like a geometrically similar, straight-channel simple diffuser fed with a flow of equal throat center-line Mach and Reynolds numbers and with equal throat flow blockage. Here we will attempt to test this assumption with a careful comparison of channel diffuser performance from the Boeing-AVLABS compressors and Creare-AVLABS laboratory straight-channel diffuser data.

### 5.9.1 Uncertainty

The Creare-AVLABS data were obtained at aspect ratios of 0.25, 1.0, and 5.0, while the Boeing-AVLABS data were for various aspect ratios between 0.289 to 0.476. There is no obvious way to make continuous curves between the Creare-AVLABS aspect ratios, so results for aspect ratios of 0.25 and 1.0 will be included.

An analysis of the uncertainty interval for the Creare-AVLABS data made for essentially the Boeing conditions gives the uncertainties in Table XI. Uncertainties in the Boeing-AVLABS data are given in Section 4.3.

### 5.9.2 Data Reduction

Static pressure recovery and blockage are defined as follows:

$$c_p = \left\{ \begin{array}{ll} \frac{p_{coll} - p_4}{p_{o_4} - p_4} & \text{for } M_4 < 1 \\ \frac{p_{coll} - .528p_{o_4}}{p_{o_4} (1-.528)} & \text{for } M_4 = 1, \text{ (supercritical} \\ & \text{flow with} \\ & \text{shock in} \\ & \text{channel diffu-} \\ & \text{ser}) \end{array} \right.$$

TABLE XI. UNCERTAINTY IN CREARE-AVLABS DATA

	High Blockage	Moderate Blockage
$\frac{\Delta p_o}{p_o}_{CL}$	$\pm 0.36\%$	$\pm 0.36\%$
$\frac{\Delta A}{A}$	$\pm 0.86\%$	$\pm 0.86\%$
$\frac{\Delta T}{T_o}$	$\pm 0.28\%$	$\pm 0.28\%$
$\frac{\Delta m}{m}$	$\pm 0.66\%$	$\pm 0.64\%$
$\frac{\Delta C_p}{C_p}$	$\pm 1.5\%$	$\pm 1.3\%$
$\frac{\Delta B}{B}$	$\pm 9.4\%$	$\pm 15\%$

NOTE: AS = 0.25, L/W = 12, 2θ = 12, Mach Number = 1.0

$$B_4 = 1 - \frac{m}{m_{\text{theor}}}$$

where:

$m_{\text{theor}}$  = theoretical mass flow based on  $p_4$ ,  $p_{o4}$ ,  $T_{\text{coll}}$  and geometrical throat area  $A_4$

Since the conventions for evaluating diffuser performance are not standardized yet, some explanation of the above definitions is in order. The collector pressure has been used to evaluate the pressure recovery coefficient in order to maintain consistency with Welliver and Acurio (1967) and the Creare-AVLABS data.

What "throat" static pressure to employ is not plain. First, it is not plain because no tap was provided at the Boeing diffuser throat exit. Secondly, it is not plain because the throat exit pressure will not correspond exactly to the actual minimum pressure before diffusion commences (in subcritical cases). Runstadler (1969) shows that a deviation of about 0.3 point of recovery exists. All of the Creare-AVLABS data including that used here for comparison employed the actual minimum pressure at the start of diffusion for calculating  $C_p$ ,  $M$ , and  $B$ . For this comparison we have used the static pressure at the plane of the stagnation pressure probes. This tap is 0.125 inch ahead of the actual throat. Thus the method used for comparing diffuser performance is "Method b" of Section 5.8.2. If a Fanno process were assumed in this short throat, pressure drops of as much as 3 psi, but usually on the order of 1 psi, would be expected. The uncertainty analysis assumes no contribution from this source.

If the Mach number corresponding to this minimum pressure equals 1, the flow is critical. Recovery data in the supercritical region are displayed against the Mach number ahead of the shock  $M_x$  in the diverging channel.

The throat center-line stagnation pressure is assumed to be the pressure measured by the probe centered in the throat.

The mass flow is that recorded by Boeing's flowmeter divided by the number of channels. The theoretical mass flow  $m_{\text{theor}}$  is calculated from Fleigner's formula, e.g.,

$$\frac{m\sqrt{T_0}}{p_0 A^*} = 0.532$$

using center-line properties and the throat's geometrical area.  $A^*$  is then calculated from the throat Mach number.

All input data may be found in Section 3. Table X shows the results of the diffuser data reduction. In that table, a comparison is made with results by the data reduction scheme ("Method c", Section 5.8.2) used by Welliver and Acurio (the reduced data are not their numbers, but only very small differences were found). Theoretical mass flow has been calculated using the ratio of specific heats for air; at the approximate throat static temperature of 1,000° R,  $k = 1.38$ . This produces a small but significant difference in the theoretical mass flow from assuming  $k = 1.4$ .

### 5.9.3 Comparison

The data, including uncertainties, from both sources are compared in Figures 148, 149, and 150.

The data from the Boeing-AVLABS compressors and the Creare-AVLABS diffusers correlate quite well, considering that the maximum deviation is only 3 points in recovery for the shortest distance between a data point and Creare-AVLABS curves (an appropriate measure of deviation in view of the approximately equal uncertainties in  $B$  and  $C_p$  for the Boeing data). For all but one point, the deviation is 2 points of recovery or less. While 2 points of channel diffuser recovery amount to about 0.4 point in stage efficiency, the uncertainty in design from adopting the simple diffuser data is far smaller than ever before attained or from using any other approach.

While the two sets of data correlate fairly well, there appears to be a trend in the Boeing-AVLABS data which is

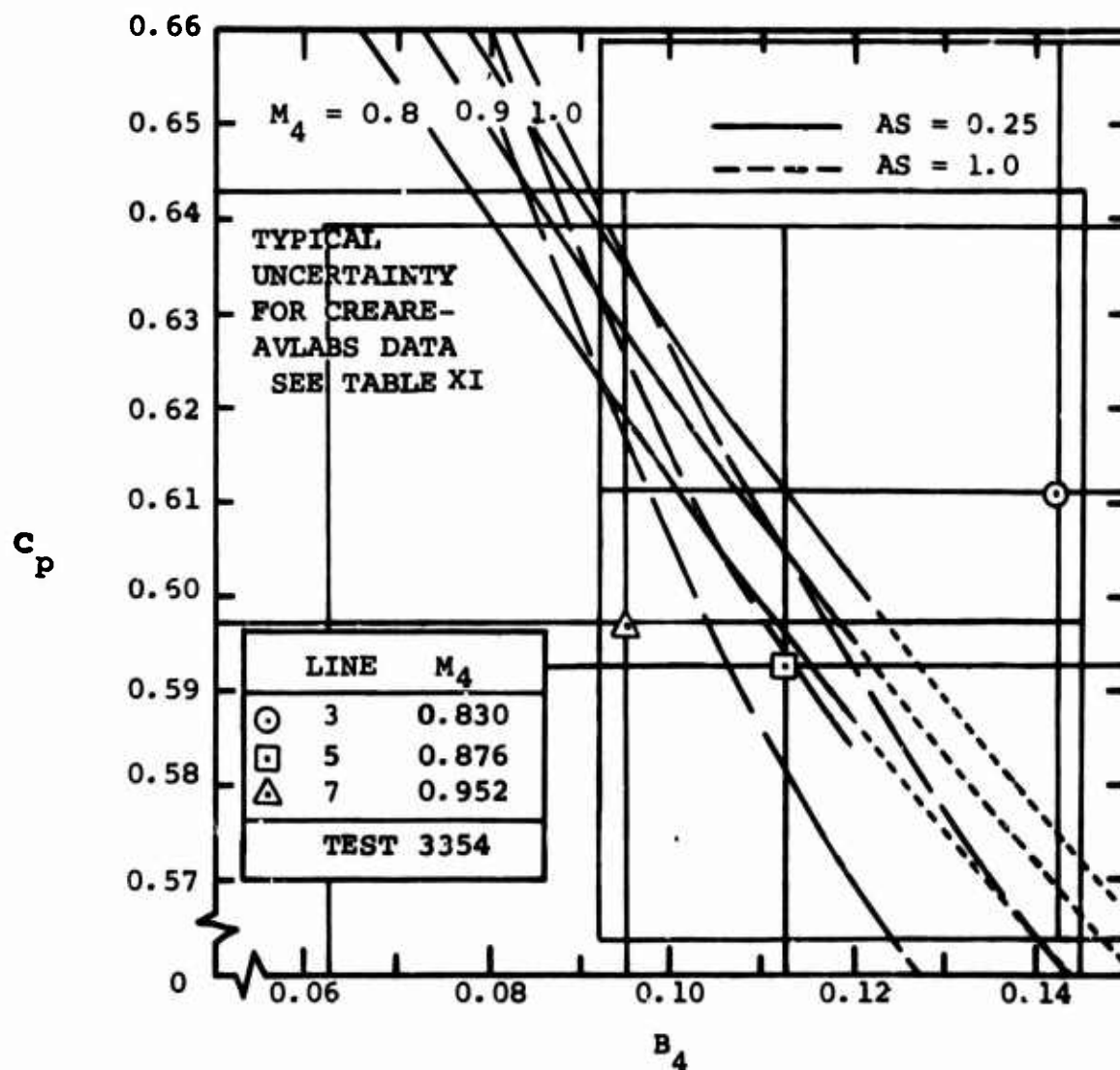
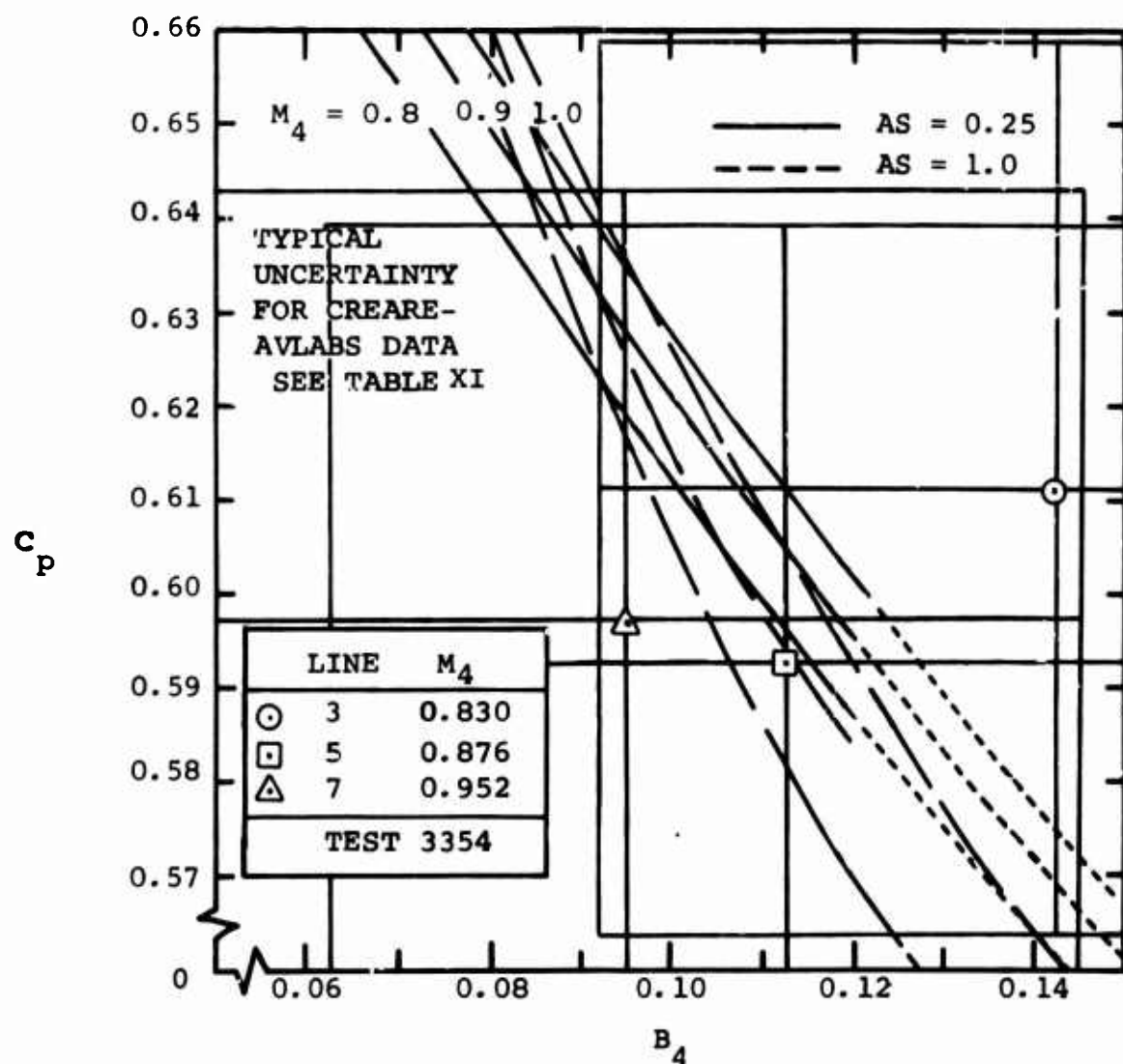
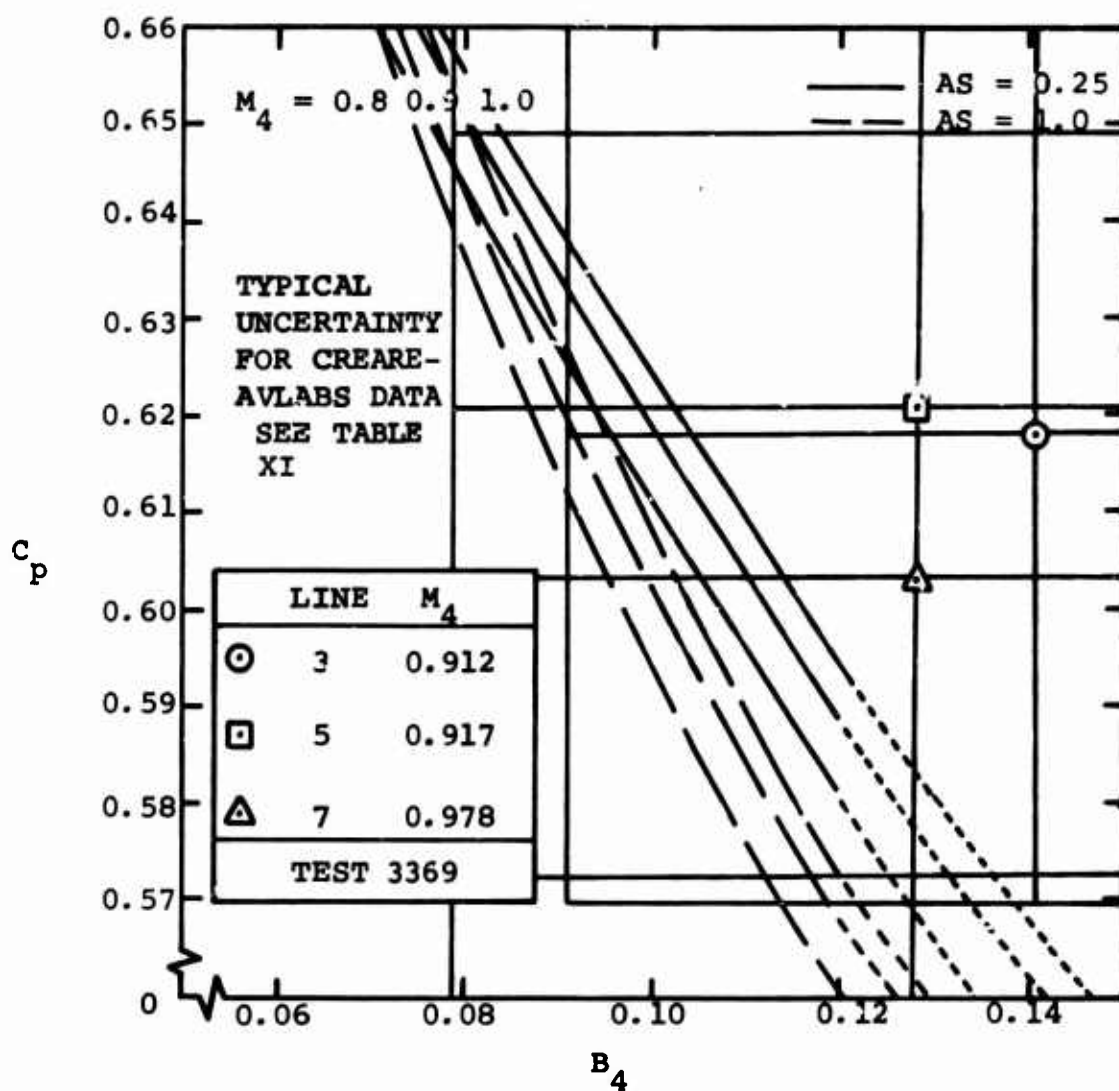


Figure 148. Comparison of Boeing-AVLabs Channel Diffuser Data From Compressors With Creare-AVLabs Straight Channel Diffuser Data. Pressure Recovery  $C_p$  Versus Throat Blockage  $B_4$  and Mach Number  $M_4$ .



NOTE: THE LARGE BOXES INDICATE DATA UNCERTAINTY RANGE.

Figure 148. Comparison of Boeing-AVLabs Channel Diffuser Data From Compressors With Creare-AVLabs Straight Channel Diffuser Data. Pressure Recovery  $C_p$  Versus Throat Blockage  $B_4$  and Mach Number  $M_4$ .



NOTE: THE LARGE BOXES INDICATE DATA UNCERTAINTY RANGE.

Figure 150. Comparison of Boeing-AVLabs Channel Diffuser Data From Compressors With Creare-AVLabs Straight Channel Diffuser Data. Pressure Recovery  $C_p$  Versus Throat Blockage  $B_4$  and Mach Number  $M_4$ .

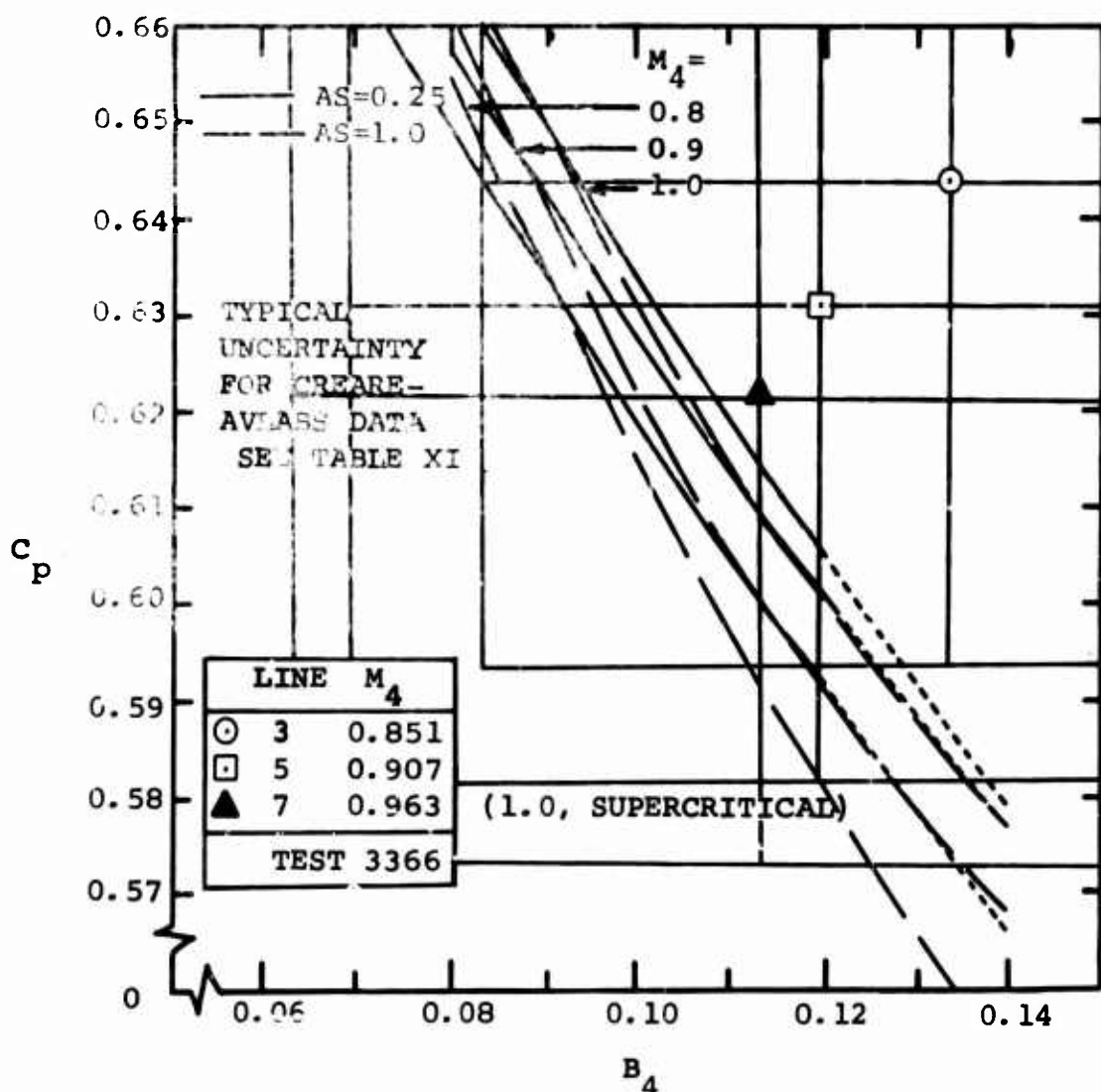
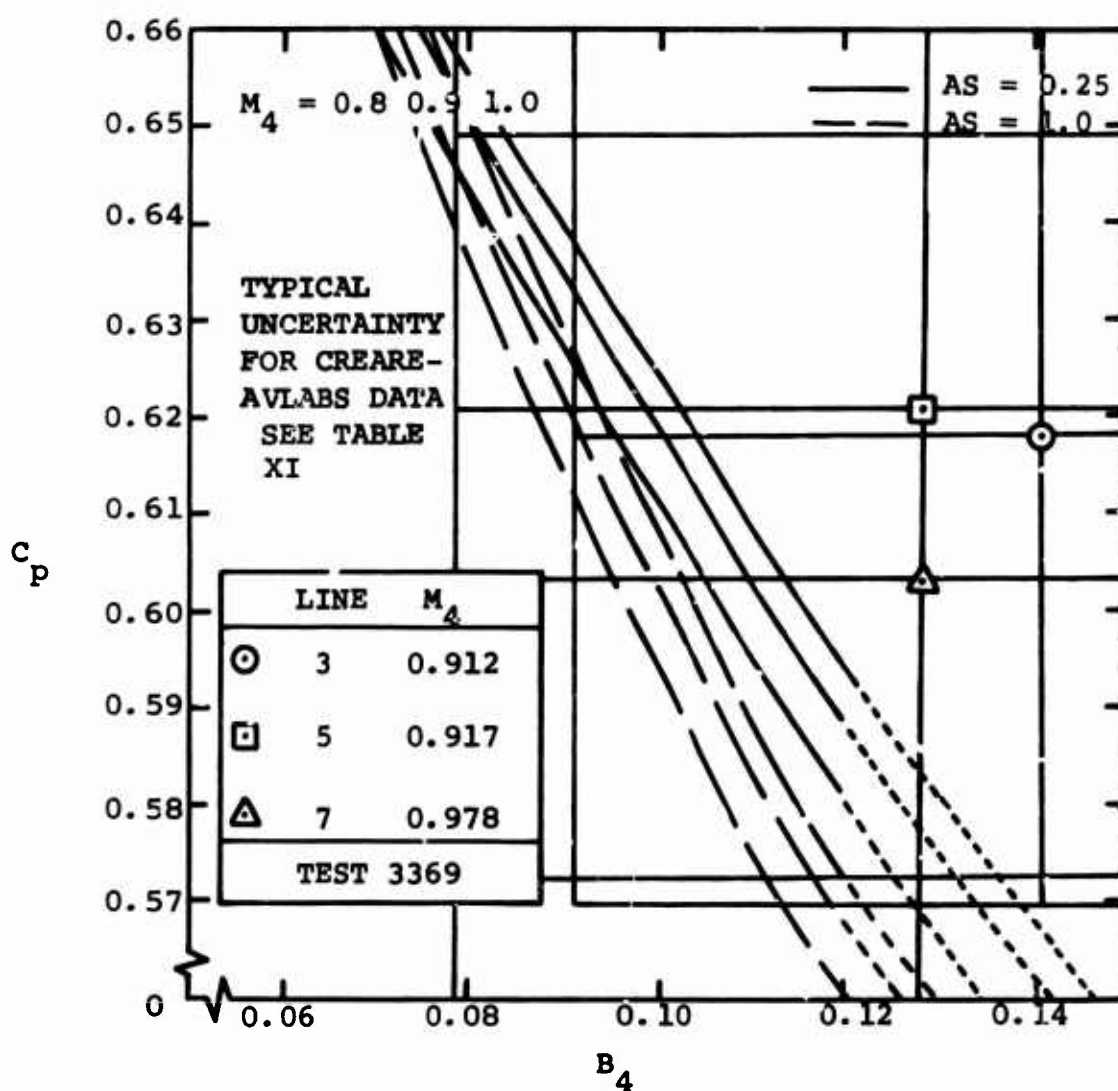


Figure 149. Comparison of Boeing-AVLabs Channel Diffuser Data From Compressors With Creare-AVLabs Straight Channel Diffuser Data. Pressure Recovery  $C_p$  Versus Throat Blockage  $B_4$  and Mach Number  $M_4$ .



NOTE: THE LARGE BOXES INDICATE DATA UNCERTAINTY RANGE.

Figure 150. Comparison of Boeing-AVLABS Channel Diffuser Data From Compressors With Creare-AVLABS Straight Channel Diffuser Data. Pressure Recovery  $C_p$  Versus Throat Blockage  $B_4$  and Mach Number  $M_4$ .

contrary to the Creare-AVLABS diffuser data. The latter indicate that performance should continue to rise to Mach 1 for this range of aspect ratios and that, for a fixed geometry, the blockage should decrease as the throat Mach number goes up, according to the Welliver and Acurio diffuser entry model. This blockage decrease is observed in the Boeing data, but the corresponding increase in  $C_p$  is not observed. Tests 3352, 3354, and 3366 show a decrease in performance with increasing throat Mach number; Test 3369 shows a mixed trend. Most of the other data reduced by Boeing show a decrease in  $C_p$  as Mach number,  $M_4$ , increases.

Additional Creare-AVLABS investigations of three-dimensional profile distributions at the inlet to the diffuser are reported by Runstadler (1969). Only slight influences were noted from nonuniform blockage distribution around the throat. Other three-dimensional variations were not studied experimentally.

Perhaps the most creditable explanation for the difference in Mach number trends is suggested by the evidence reviewed in Section 5.8.2. The entry shock Mach number seems to increase toward choke. Diffuser blockage is proportional to boundary layer displacement thickness,  $\delta^*$ . However, diffuser performance is probably more dependent on the momentum defect,  $\theta$ . These parameters are related by the shape factor,  $H = \delta^*/\theta$ . Only a few attempts have been made to correlate diffuser data on the basis of  $\theta$ , chiefly because of the difficulty of measuring  $\theta$  experimentally. In an external flow, shocks tend to raise  $\delta^*$  faster than  $\theta$ . However internal flow is strongly affected by continuity. For instance, in Test 3366,  $M$  ranges from 0.851 to 0.963 (Method b, Table IX). This Mach number change amounts to a flow rate change of about 2%, while the measured change in flow rate is about 7%. This situation dictates about 5% less blockage. Thus the blockage and hence  $\delta^*$  decreases with mass flow while the entry shock is getting stronger, in complete disagreement with present shock wave boundary layer interaction theory. We hypothesize that  $\theta$  must increase due to the larger pressure rise associated with the stronger shock, and thus, the performance degenerates even though the blockage is smaller.

The mixed results from Test 3369 tend to add additional support to this hypothesis because the entry shock for this diffuser system was much softer than for all other tests.

Runstadler (1969) made a series of special tests with a normal shock in the straight duct ahead of the diffuser. He found that pressure recovery was constant for the same inlet length for a high blockage,  $2\theta = 10^\circ$ ,  $L/W = 12$ ,  $AS = 0.25$  diffuser. However, the shock was about 2 inches upstream of the throat, allowing the flow ample time to readjust to its normal profile. With Workhorse diffusers having longer throats, further light could have been thrown on this matter except for the fact that this data lacks reliable  $p_o$  measurements in the throat.

This explanation is, of course, only tentative because the data uncertainty levels in Figures 148, 149, and 150 are too high to be sure that the  $C_p$ , blockage, and Mach number trends actually exist.

#### 5.9.4 Summary of Tests of Channel Diffuser Models

Our attempt to test the Welliver and Acurio hypothesis that the channel diffuser section of a centrifugal compressor's diffuser can be simulated accurately with laboratory simple diffuser data has been frustrated partially by uncertainty in both sets of diffuser data, particularly in the set from the compressor. However, agreement was obtained within about + 3, - 0 points of recovery.

Different Mach number trends appear through the uncertainty haze. These have been tentatively assigned primarily to Mach number trends of the entry shock.

Despite the imperfect agreement, the Welliver and Acurio channel diffuser model is well vindicated by the evidence. There appears to be little doubt that their model is useful and a more accurate design tool than any other known approach.

The opportunity to dissect the complex diffuser flow into simpler pieces is a major advance in understanding and

optimizing the compressor's diffusing element. Because about 60% of the diffuser pressure recovery occurs in the subsonic channel diffuser and because it is a complex device whose performance and optimization depends on six variables ( $B$ ,  $AS$ ,  $2\theta$ ,  $L/W$ ,  $M$ ,  $Rey$ ), and because no purely theoretical approach has ever been successful for optimum-recovery channel diffusers, the successful recourse to the now extensive data for transonic channel diffusers is a most welcome improvement in design tools.

## 5.10 SUMMARY ASSESSMENT OF ADEQUACY OF EXISTING MODELS

As we review the discussions of this section concerning the adequacy of the various flow models available, the view below is somewhat bleak.

In the critical diffusing portion of the impeller, available design tools are fundamentally weak in predicting the peak velocity on the inducer from which the flow must diffuse. Until more detailed evidence is available and analytical methods are considerably improved, the designer must rely upon good judgement, estimates from other fields such as wing theory, axial compressor semiempirical technology, and to a certain extent upon boundary layer calculations. His objective is to achieve the maximum diffusion possible in the inducer; we have shown how critical that is to stage performance. No doubt the developer must turn to empirical testing, which, however, must be done in a very thoughtful way with a clear view of objectives; otherwise, it is very easy to get lost among all the variables.

For predicting the separation point in the impeller, we are basically hampered by the same causes. It is important to know what the pressure and radius are at the separation point. Our review of the models against the data suggests that if we can make reliable calculation of the diffusion obtained, that the potential theory for the flow in the impeller ahead of the separation point does give good measure of where the separation point is, providing blockage calculations can be improved. We believe that Welliver and Acurio seriously underestimate the blockage due to boundary layer growth in their inducer. We have suggested that two-dimensional boundary layer calculations should rectify this situation, provided that the overvelocity in the inducer vane leading edge can be calculated with some accuracy.

Beyond the separation point, the models seem to work very well to the tip of the impeller. At least for RF-2, which was a heavily separated impeller, the pressure in the wake closely follows the theory. Experience with less separated impellers indicates concordance too. We did find that it is very important in reducing the data to make a correction from the mean pressure between the blades to the pressure in the wake region if a good fit with the data is to be obtained.

The models available for calculating the impeller tip flow pattern cannot be tested by the Boeing-AVLABS data so we have no idea from this source how excellent or poor they may be.

The model for the impeller discharge mixing loss similarly cannot be tested by the data within a considerable range of uncertainty because there are several parameters which must be estimated. Due to the considerable errors produced by impeller tip probes in dissecting the flow pattern there, we cannot rely upon that information. For less heavily separated impellers, it may be possible to do more, but then the mixing losses are smaller and more difficult to check with the data. All in all, we have been able to define a number of these parameters, but the range left is still too great to say definitively that the impeller discharge mixing theory as used here is adequate.

In the entry to the diffuser, we are left with a completely unsatisfactory situation regarding prediction of the growth of the boundary layer from the impeller tip to the diffuser throat. In the model used, the two-dimensional boundary layer theory has not been successful. We find that the Welliver and Acurio model (which we helped to devise) is universally erroneous at flows near choke and surge. This is shown by the fact that the mass-flow-averaged stagnation pressure at the tip of the impeller, deduced by the use of the model, varies strongly with mass flow, while impeller tip data and diffuser throat stagnation pressure data show that it is almost invariant. While we do not trust the stagnation pressure probes at the tip of the impeller, there is sufficient other evidence about impeller behavior and sufficient reliance can be placed upon our knowledge of the fundamental physics of this situation within the impeller, that the variation of impeller discharge stagnation pressure with mass flow which comes from blind application of the Welliver and Acurio model is not believable.

For the straight-channel diffuser, the Welliver and Acurio proposition that straight-channel laboratory diffuser data can be used is a good one. At least, it is capable of predicting channel diffuser pressure recovery within about 2 points. However, the Boeing-AVLABS data seem to show

better straight-channel diffuser performance, especially near choke, than the laboratory experiments would indicate. Therefore, predictions for the Welliver and Acurio hypothesis will be conservative. We will further discuss in Section 6.9 reasons for the observed enhancement of diffuser recovery.

We have not specifically considered choke and surge models. Welliver and Acurio proposed that when the diffuser throat entry shock Mach number approach 1.2, the shock would separate the sidewall boundary layers, causing the blockage in the diffuser throat to rise rapidly and making the parallel diffuser array unstable. The data refute this proposition, but do not provide a clear recommendation of exactly what conditions will set off surge.

While available flow models for design are not always very good at numbers, they do seem to explain the flow physics. One may be optimistic that the centrifugal compressor fraternity can be on its way toward developing adequate and accurate designing tools from these models.

## 6.0 DEVELOPMENT OF NEW FLOW MODELS

One of the principal objectives of this program is the improvement of available fluid dynamic design tools for high pressure ratio centrifugal compressors in order that better optimization can lead to substantially improved performance. In Section 5, we pointed out in detail the inadequacies of the existing models used by Welliver and Acurio. When it is realized that those models were in a number of ways considerably advanced over those routinely used in the art, perhaps it is inappropriate to try to improve them further. But this is essential, for we can see now that the better performance desired will come only through better design tools.

The high pressure ratio centrifugal compressor will not for many years enjoy the extensive empirical development that lower pressure ratio machines have had. So if we are to have greatly improved performance quickly, it must come from a better understanding followed by a much more competent fluid dynamic design.

It is the purpose of this Section to examine the various flow models and ask:

- (1) Are they worth improving?
- (2) Is there fundamental knowledge available upon which to found improvements without recourse to new research?
- (3) Is data available now with which to test the new models?

In general, we have found in the critical area where the models are really weak that the basic scientific foundations are inadequate to make major improvements. Further, little definitive data is available to test the models.

## 6.1 INDUCER FLOW

The objective of any inducer flow model is to enable the design of inducer blading to swallow the flow between choke and surge points of the compressor and to achieve as high a mean flow diffusion in the inducer as possible before the flow separates in the impeller. In order to meet these inducer requirements, we will need to understand how to calculate the boundary layer and the potential flow around the inducer blades.

The nature of the flow around the leading edge of the inducer blade depends upon:

- (1) The blade shape.
- (2) The blade blockage.
- (3) The approach relative Mach number upstream of the inducer blades and the flow incidence.
- (4) The Reynolds number.

A proper model for the inducer should include these effects in a quantitative fashion and relate them to the problem of predicting the boundary layer growth and its interaction with the potential flow that allows us to predict the amount of diffusion in the inducer.

The region of inlet flow governed by the inducer extends well upstream from the leading edge. Therefore, it is very important to include flow distortion and turbulence caused by upstream elements such as inlet plenums, blading, ducting, and the boundary layers thereon. If not properly related to inducer design, the presence of upstream distortions can have serious consequences on the performance of the compressor stage.

Other secondary factors have some influence on the inducer flow and the ultimate diffusion obtained. These are tip leakage, three-dimensional boundary layer behavior, and unsteadiness. For the present, these effects must largely remain untreated. This is because they cannot be easily evaluated with present theory to permit a rational quantitative inclusion of their importance.

Qualitatively, tip leakage should be important for, as shown by Dean (1954), it tends to blow the suction surface

boundary layer and reduce its tendency to separate.

Three-dimensional boundary layer behavior may impede adequate prediction of separation. This is particularly true on the suction surface at the hub, where local piling up of tired fluid by secondary motions may greatly thicken the boundary layer. At high Mach numbers where a very small percentage change in flow area can have pronounced effect upon the diffusion obtained in the flow, boundary layer accumulation may also have serious consequences for the overall potential flow behavior.

Also separation in the inducer is likely to be quite three-dimensional and perhaps unsteady. Steady two-dimensional calculations of boundary layer separation may be only loosely related to the actual three-dimensional unsteady behavior. For instance, separation may be less disastrous than in two-dimensional cases, as pointed out by Taylor (1958).

We expect that these phenomena will eventually be understood and their importance to the inducer flow will be included in proper models. However, they must now be considered secondary in analyzing the inducer flow process.

As pressure ratio and efficiency of centrifugal compressors continually increase, two inlet regimes of the inducer will be of critical importance. These are when the approach relative Mach number is in the supercritical regime but subsonic and where the approach relative Mach number is supersonic.

In the supercritical regime, extended regions of supersonic flow may occur on both the suction and pressure surfaces; these will be terminated by local normal shocks. Depending upon the turning and thickness schedule of the inducer blading, several situations can occur to produce regions of subsonic and supersonic flow mixed together with isentropic acceleration and deceleration and then compression through shocks.

One case is typified by the situation in which the flow on the suction or pressure surface undergoes an acceleration through a supersonic region, which is then terminated by a single shock wave. After the shock, the flow remains

subsonic as it is diffused by the inducer turning to axial. A second case exists when the turning is delayed and the blade thickness schedule is such as to cause the flow to first accelerate through a supersonic region terminated by a shock wave, then undergo a second acceleration to supersonic flow, and finally undergo a second compression through a shock to subsonic flow.

When the approach relative Mach number is greater than unity and the inducer is operating entirely in the supersonic relative Mach number range, methods have been fairly well developed for the analysis of the inlet flow. These techniques were surveyed by Erwin (1960); they have been developed largely for the analysis of supersonic axial compressors, but these may be readily adopted for the design of the centrifugal inducer.

Behind the terminating shocks in the supersonic case, analytical difficulties are encountered in analyzing the inducer flow.

In the axial compressor, the blade is terminated at the shock location because the boundary layer separates always when  $M_x > 1.25$ . But in the usual centrifugal inducer the blading continues -- stalled, no doubt. In Section 7, we propose and analyze an uncommon inducer designed to avoid the shock stalling problem. The severe pressure rise through the shocks usually separates the boundary layers so that there will be a series of repeating shocks of the type often encountered in straight channels. In spite of the investigations of repeating normal shocks in channels, such as those of Neumann and Lustwerk (1951) and Fejer, Heath, and Driftmeyer (1964), the shock in the channel with heavy boundary layer growth has largely defied analysis.

The remainder of this discussion will be limited to approach relative Mach numbers less than 1.0. The supersonic regime is considered in more detail in Section 7.1.

Because of the variation in wheel speed from hub to tip, the approach relative Mach number on a single inducer will vary considerably over the span of the blading. As approach relative Mach numbers are increased into the supercritical flow regime (and also the supersonic flow regime), one can expect severe radial matching problems. Two-

dimensional arguments on the behavior of flow at a given inducer radius may be valid for the purely two-dimensional flow situation, but it can be expected that matching the flow well over the span of the blading will present grave difficulties. Of particular importance will be the matching of the pressure conditions along the span of the blading at any given axial position. As the blade flow regime changes along the leading edge from supersonic to supercritical to high subsonic, it can be expected that the potential flow in these various regions will interact in unexpected ways. These interactions, which are beyond the scope of "radial equilibrium" solutions, will cause alterations in the flow behavior from that postulated based on local two-dimensional flow and the approach relative Mach number at a given span location.

The extent to which such perturbations are important is not now known. They are ignored in axial rotor design. Efforts to discover the importance of such effects must eventually be undertaken as recommended in Section 8. For the present, we postulate an improvement in the inducer design system based upon two-dimensional flow arguments at any given span location and the use of information which has been gained from isolated airfoil supercritical flow behavior and shock boundary layer interaction processes.

In the general case of transonic supercritical flow, no well-developed analytical techniques are available for predicting fluid dynamic behavior. This is even true for the isolated aircraft wing. In spite of the extensive research efforts over the last 20 years to understand transonic wing behavior, no general analytical techniques have yet been perfected.

However, a large body of semiempirical information related to transonic flow behavior on wings has been collected. In an attempt to improve the leading edge inducer flow models, we postulate that the information contained in the transonic wing theory can be applied to the inducer blading.

Much of the isolated wing technology is based upon parameters related to the airfoil chord. It is difficult to relate this technology to the centrifugal inducer because of the effectively infinite chord of the inducer blade. Also in the case of the isolated airfoil, the trailing edge condition

powerfully influences the flow over the wing. The inducer flow obviously has different downstream pressure conditions imposed by the flow through the impeller. Much of the transonic wing theory has been developed by relating the downstream conditions to the location of shocks and the extent of imbedded supersonic flow. In adopting this transonic wing information to the inducer design problem, one must continually be aware of the extent to which transonic flow information has already been extrapolated in relating it to the boundary layer flow in the inducer.

The most important reservation about adopting transonic airfoil data, however, is the order of magnitude difference in Reynolds number.

We shall first review the known information about the transonic flow behavior around airfoils, emphasizing that which can be applied to inducer design. A method will then be suggested to use this information as a means to extend our design capabilities.

#### 6.1.1 Transonic Airfoil Theory

When local supersonic flow exists on the airfoil surface, the flow regime is called "supercritical". If the maximum local Mach number on the surface exceeds about 1.10 an abrupt pressure rise to subsonic conditions occurs through a shock. This flow pattern is illustrated in Figure 151 together with the associated pressure distribution on the suction surface.

The flow can be discussed conveniently in three portions:

- (1) The subsonic and supersonic region upstream of the shock wave.
- (2) The shock wave itself.
- (3) The subsonic flow downstream of the shock wave.

Further increase in the free-stream Mach number causes a

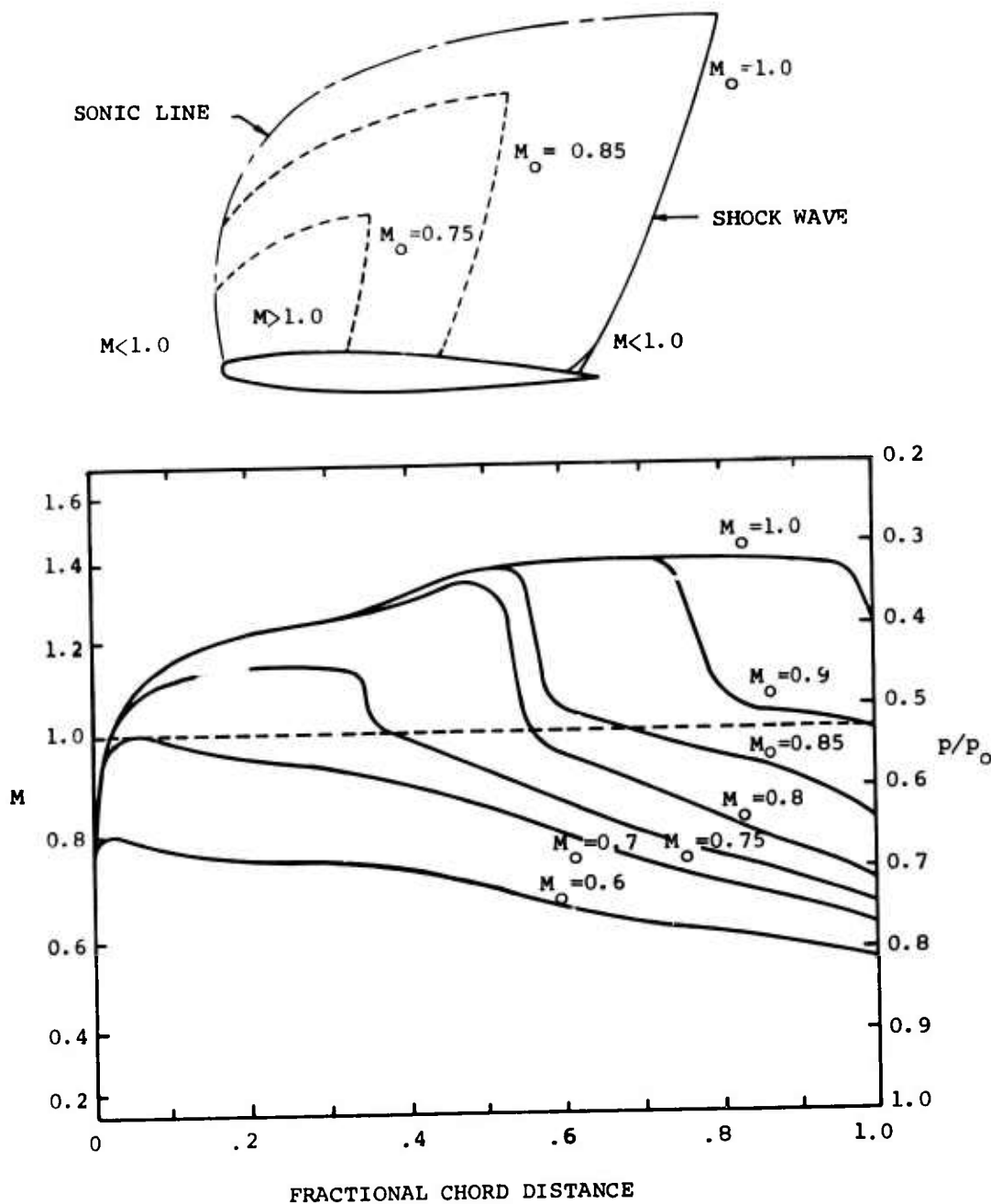


Figure 151. Development of the Flow Past an Airfoil as the Stream Mach Number Increases to Unity.

downstream movement of the shock wave and an enlargement of the supersonic region. However, only small changes occur in the local pressure ahead of the shock when the free-stream Mach number is close to unity. This phenomenon has become known as the "Mach number freeze".

The "Mach number freeze" concept states that the pressure distribution on the airfoil upstream of the shock for high supercritical values of approach Mach number is essentially the same as that found when the free stream Mach number is unity (i.e., what is called the "sonic range" pressure distribution).

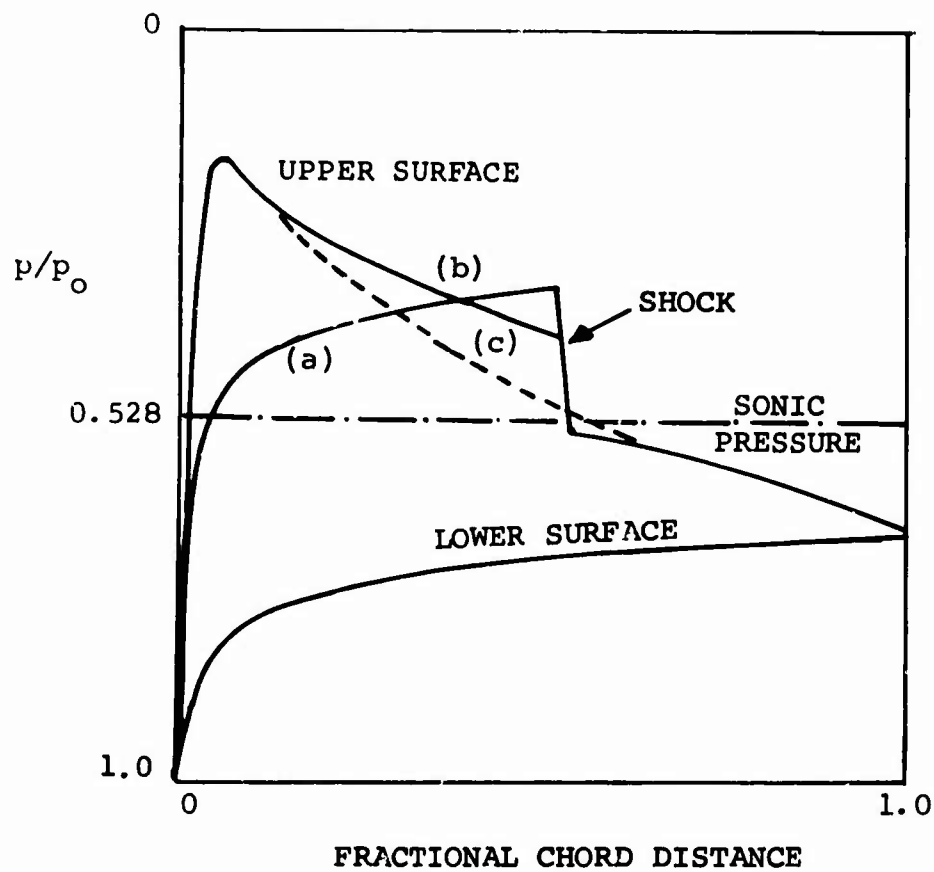
Pressure distributions obtained experimentally for a wide range of airfoil shapes have been observed to fall under two main categories illustrated in Figure 152:

- (1) Those for which there is a monotonic reduction in pressure from the stagnation point, through the sonic pressure to a shock wave.
- (2) Those for which there is a rapid reduction in pressure to supersonic values near the leading edge, followed by a general rise in pressure toward a shock wave.

The second type of pressure distribution has become known as "peaky", since it contains high-velocity (i.e., low pressure) peaks. The type of pressure distribution achieved for an airfoil depends upon the airfoil geometry, the angle of incidence, and the free-stream Mach number.

It has been found that pressure distributions of the "peaky" type bring about significant improvements in our ability to prevent boundary layer separation.

For the "peaky" type of pressure distribution, the mechanism responsible for the improved separation performance is a consequence of the details of the nose shape. Low pressures associated with expansion waves in the start of the supersonic region immediately downstream of the stagnation point leave the surface and reflect from the sonic line as compression waves. This is illustrated in Figure 153. The compression waves from the sonic line are re-reflected at the airfoil surface as like kind. These compression waves



- (a) "Nonpeaky"
- (b) "Peaky" (partial isentropic compression)
- (c) Ideal "peaky" (with completely isentropic compression)

Figure 152. Surface Pressure Classifications for Supercritical Approach Mach Numbers.

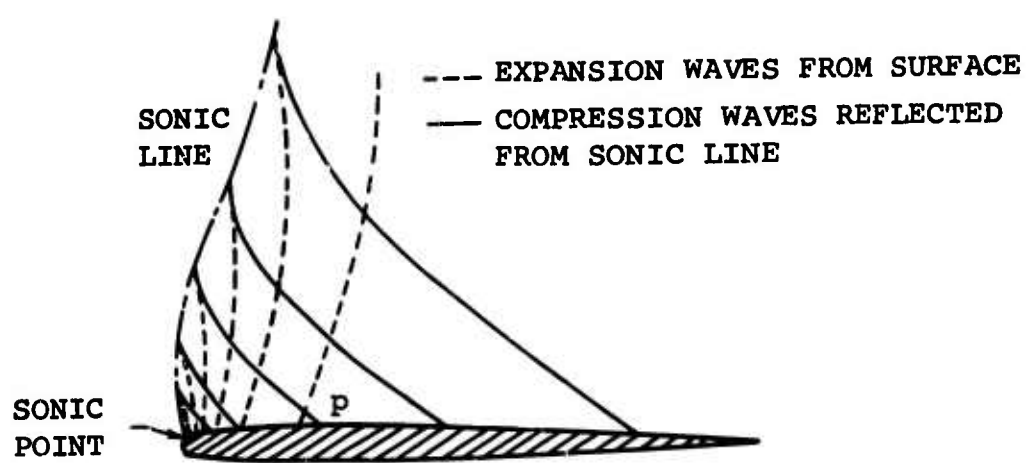


Figure 153. Schematic Representation of Expansion and Compression Waves Within Supersonic Region on "Peaky"- Type Airfoils.

striking the surface cause isentropic compression in the supersonic region, leading to a reduction in the Mach number at the end of the supersonic region and hence a reduction in the strength of the shock wave. This case is an interesting anomaly wherein it pays to accelerate in order to diffuse better.

Airfoils have been empirically developed which closely approach having a true isentropic compression in the supersonic imbedded region for a range of incidence angles and free-stream Mach numbers. Through a great deal of empirical effort, it has been found that the essential feature of "peaky" airfoils is the rapid change of curvature from a high value at the leading edge to a low value further back. The high rate of curvature immediately after the stagnation point produces a rapid expansion to high, supersonic velocities; the sudden transition to low curvature stops this expansion and determines the "peak" pressure height. Surface shape from then on must be matched to the incoming compression waves in order to produce the optimum pressure distribution.

One characteristic of many transonic airfoils is a "roof top" pressure distribution. A "roof top" is shown in Figure 154. The "roof top" distribution has an almost constant pressure over most of the airfoil chord; this is responsible for a rapid motion of the location of the normal shock on the airfoil surface in the downstream direction with slight increases in Mach number.

The "roof top" characteristic is important to a peculiar feature of transonic airfoils. Most information on transonic wing behavior has been obtained from wind tunnel investigations. At transonic speed wind tunnel wall interference effects are of major importance. Slotted wind tunnel walls have been devised to make the airfoil appear as if it existed in "free air" conditions. Recent work (Graham, 1966) has shown, as wall interference effects were increased in wind tunnel tests, that the location of shocks on "peaky" airfoils was substantially altered.

Near the leading edge, where the pressure distribution is peaked, the pressure distribution was frozen (i.e., changes in the wall configuration did not affect pressure distribution

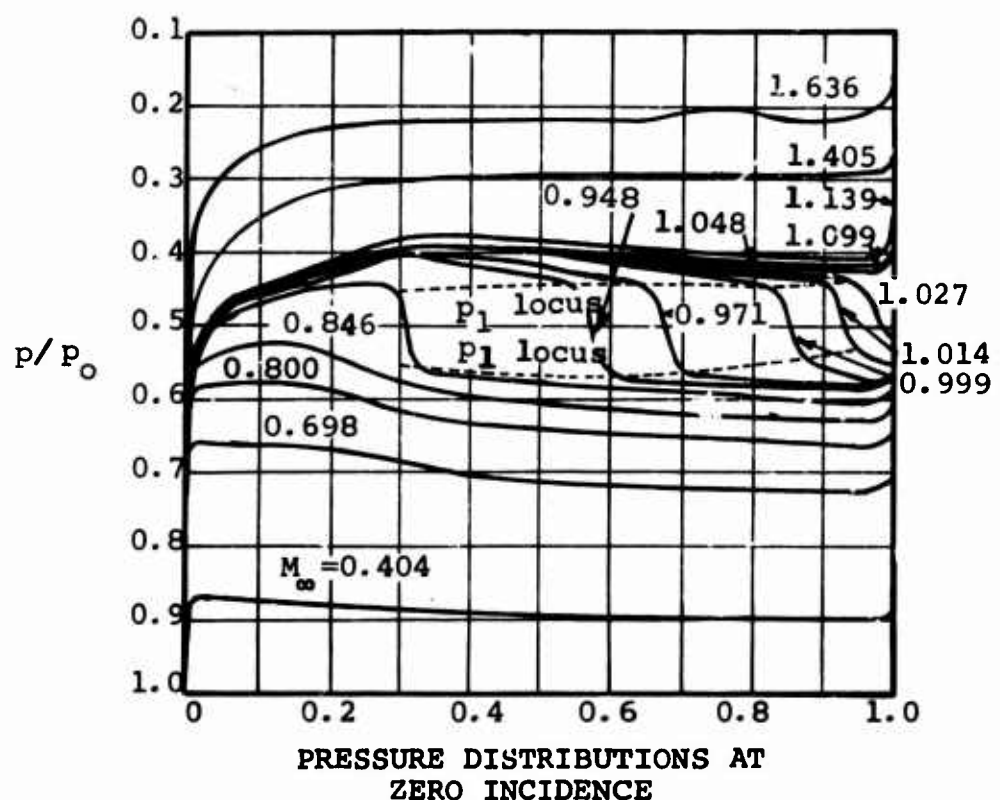


**Figure 154.** "Roof Top" Pressure Distribution in the Supersonic Region on an Airfoil at Supercritical Approach Mach Numbers.  
Airfoil: NPL 491.

for the same airfoil at the same Mach number and same incidence). Further back, however, there was a marked effect associated with the movement of the shock from a region very near the leading edge to the rear portion of the airfoil.

The importance of this observation to the inducer design is that the pressure distribution on and near the leading edge of an inducer blade can be expected to be the same as that found on an isolated airfoil of similar nose geometry. Furthermore, the distribution downstream may be expected to be altered in a manner similar to that produced in the wind tunnel investigations where wall interference effects have been increased. For example, in the case of the inducer suction surface, the flow downstream of the blade leading edge region comes under the influence of the pressure surface of the adjacent blade. This may be considered analogous to the wind tunnel interference in the wind tunnel tests. The important fact here for use in modeling the inducer flow is that the altered pressure distribution up to the location of the shock still assumes the form of the "sonic range" pressure distribution even when wall interference effects are present.

In the inducer supercritical flow regime, the pressure distribution from the stagnation point of the inducer blade through the supersonic region up to the location of a shock should closely follow the pressure distribution for a free-stream Mach number of unity. This approximation improves as the relative Mach number approaches unity.

So far, the only parameter which has been proposed to correlate both "peaky" and "nonpeaky" airfoils is the K parameter (see Pearcey, 1969) discussed by Welliver and Acurio (1967).

In general, it has been found from experimental data that transonic airfoils having a large K parameter produce incidence/free-stream Mach number plots which have only small or no regions of unseparated flow at high subsonic Mach numbers. Airfoils with small values of K, however, have significantly larger regions of unseparated flow.

Typical examples of the change in the separated flow regime behavior of the airfoils from which only the nose shape was varied are shown in Figure 155.

An important effect that must be taken into account in applying airfoil data to the centrifugal compressor inducer is the magnitude of the length Reynolds numbers present in each case. At approach relative Mach numbers of 0.9 and higher, a boundary layer undergoes transition from laminar to turbulent flow on a flat plate at about 1/2 inch behind the leading edge. The actual point of transition will be affected by many phenomena, such as surface roughness, free stream flow unsteadiness, and magnitude of surface pressure gradient on the inducer blade. On a transonic wing, the flow can be expected to undergo transition only a very short distance downstream from the stagnation point. In comparison, a considerable fraction of the inducer blade, perhaps even up to the "throat" of the inducer passage, if not carefully designed, may be comprised of a laminar boundary layer on the blade suction surface.

Since the laminar boundary layer can withstand only a very small pressure rise before it separates, the transonic flow on the inducer blade deserves special consideration.

If the shock terminating the supersonic imbedded region falls upon the nose surface of the blade before the laminar boundary layer becomes turbulent, it is extremely likely that the laminar layer will separate. Depending upon the shape of the inducer passage downstream of the inducer leading edge, the laminar boundary layer may undergo transition and reattach immediately as a turbulent boundary layer, it may remain as a laminar separation for an appreciable distance before undergoing transition and reattachment, or it may never reattach. Because the flow in this region will be close to sonic conditions, very small changes in flow area can cause a large change in the amount of relative diffusion obtained. Thus great care must be maintained in the design of the inducer blading to avoid extended laminar separation effects.

Pearcey (1961) recommends that the analysis of Sinnott and Osborne (1961) be used to correlate:

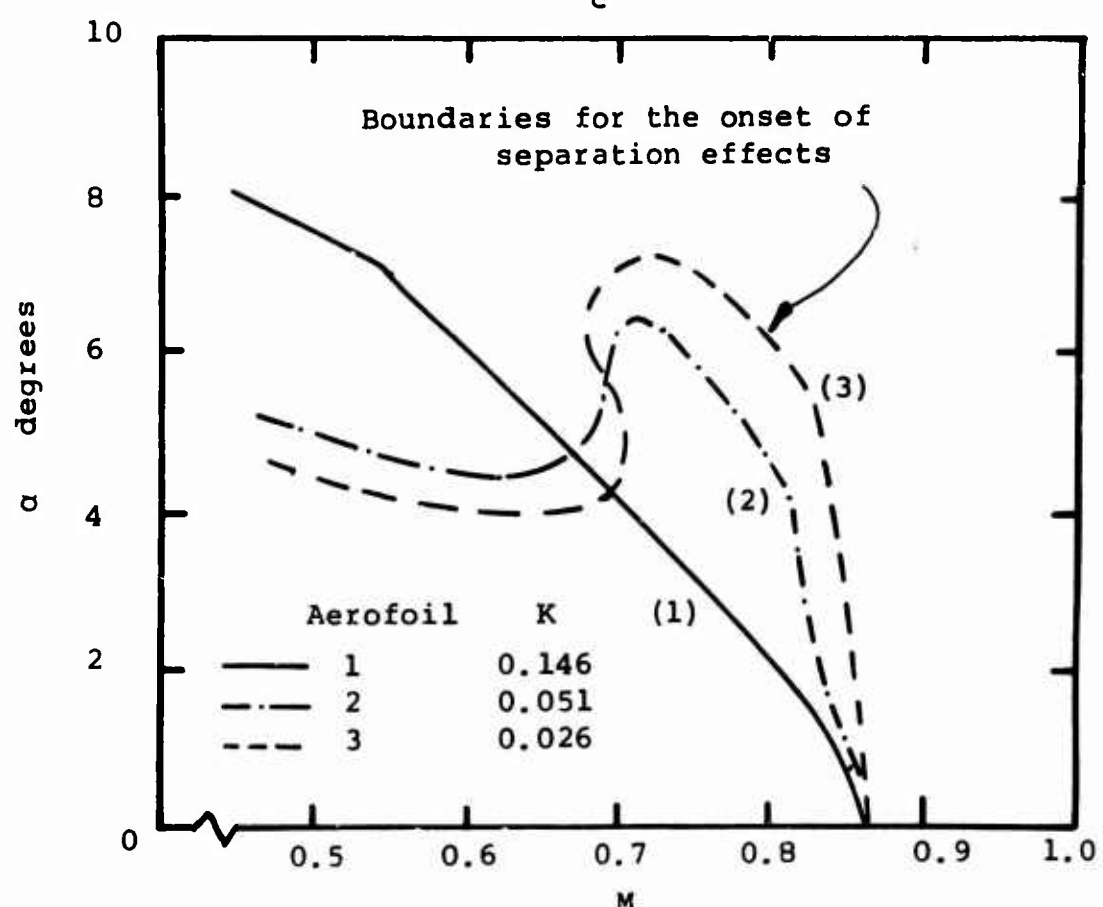
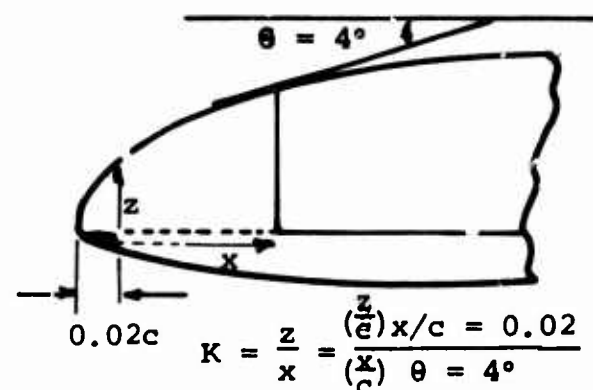


Figure 155. Change in "Separation Effects" Boundary With Alteration in Leading Edge Radius and Parameter K.

- (1) The location of the shock terminating the supersonic imbedded region of flow.
- (2) The pressure rise  $\Delta p = p_x - p_{SR}$  that occurs across the shock and is imposed upon the boundary layer.

For the transonic airfoil of the "peaky" type, Sinnott has shown that the pressure immediately upstream of the shock,  $p_x$ ,  $p_0$ , correlates with the quantities

$$\frac{(p_x - p_{SR})}{p_0} = f[(M_\infty - M_*)/(1 - M_*)]$$

where

$M_\infty$  = free stream approach Mach number

$M_*$  = the free stream Mach number for which the local sonic speed is first reached at the airfoil surface as calculated for shock-free flow.

$p_{SR}$  = pressure (distribution) for shock-free flow at Mach number  $M_*$

Shock-free flow is defined as the pressure distribution obtained with the Glauert compressibility rule applied to the airfoil shape using the incompressible pressure distributions.

The Glauert pressure correction rule can be applied to the measured pressure distributions at low Mach numbers to derive the pressure distribution at the approach Mach number  $M_\infty$  under consideration:

$$\left( \frac{p - p_\infty}{p_0 - p_\infty} \right)_{M_\infty} = \frac{1}{\sqrt{1 - M_\infty^2}} \left( \frac{p - p_\infty}{p_0 - p_\infty} \right)_{M_\infty \rightarrow 0}$$

where  $p_\infty$  = Static pressure at approach Mach number,  $M_\infty$

Glauert's rule says that the local pressure at any point on the inducer vane for the subsonic approach Mach number under consideration is equal to

$$1/\sqrt{1 - M_\infty^2}$$

times the same pressure (nondimensionalized) for the incompressible flow situation.

A plot of Sinnott's correlation is shown in Figure 156.

Sinnott presents evidence that shock interactions on transonic airfoils do not produce a pressure rise through the shock at the location of the shock equal to the pressure rise evaluated from one-dimensional shock relations. Evidence indicates that it is some distance downstream of the shock location before the subsonic pressure distribution produces a downstream pressure equivalent to that evaluated for a normal shock at the given upstream shock pressure. A sketch of this situation is given in Figure 157.

For transonic airfoils there is excellent experimental confirmation that the pressure distribution sufficiently far downstream of the shock interaction region closely approximates that obtained by calculating the "shock-free" pressure distribution obtained for the same airfoil geometry at the same approach Mach number using the Glauert compressibility rule. Thus in Figure 157, the dashed distribution labeled "shock-free" is the subsonic downstream pressure distribution experimentally found to occur.

From a large collection of experimental data, Sinnott found that the shock pressure ratio evaluated in terms of the "shock-free" distribution  $p_{y_G}/p_x$  when plotted as a function of the shock pressure ratio  $p_x/p_o$  produced a fairly good correlation, as shown in Figure 158 that was independent of the details of the airfoil section shape or other flow characteristics.

From this combination of experimental data, Sinnott determined that the pressure distributions for a wide range of transonic airfoil configurations could be approximated using the following procedure.

- (1) For the given transonic profile and angle of incidence, the sonic range pressure distribution  $p_{SR}/p_o$  was evaluated as a function of chord distance.

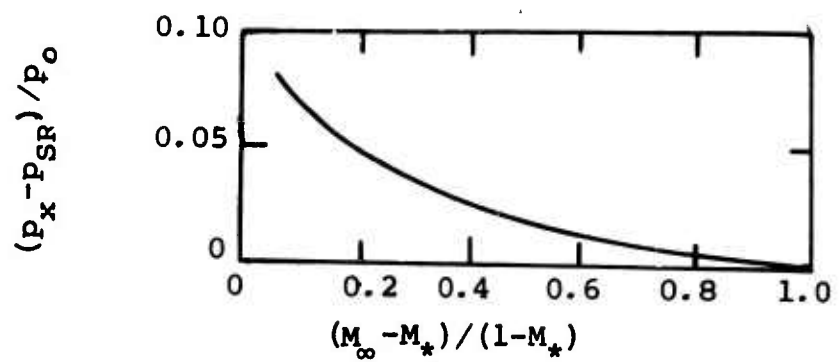
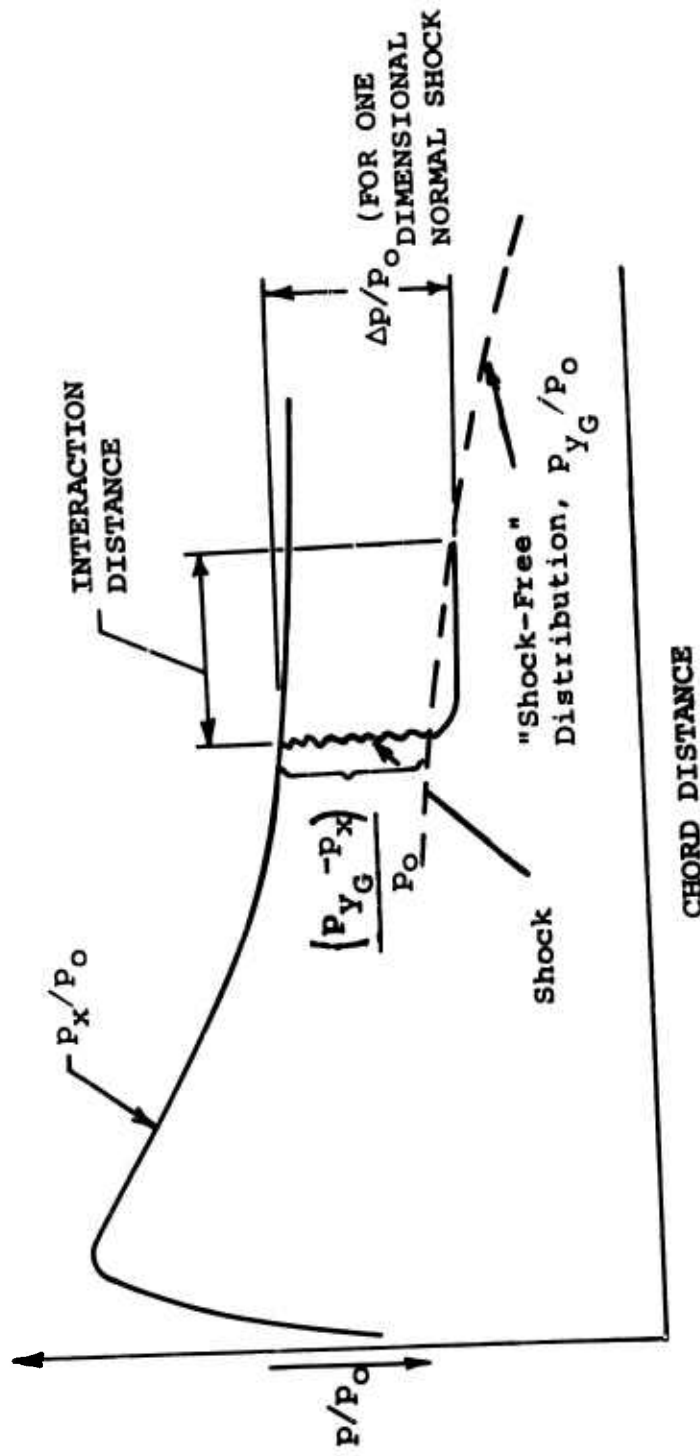
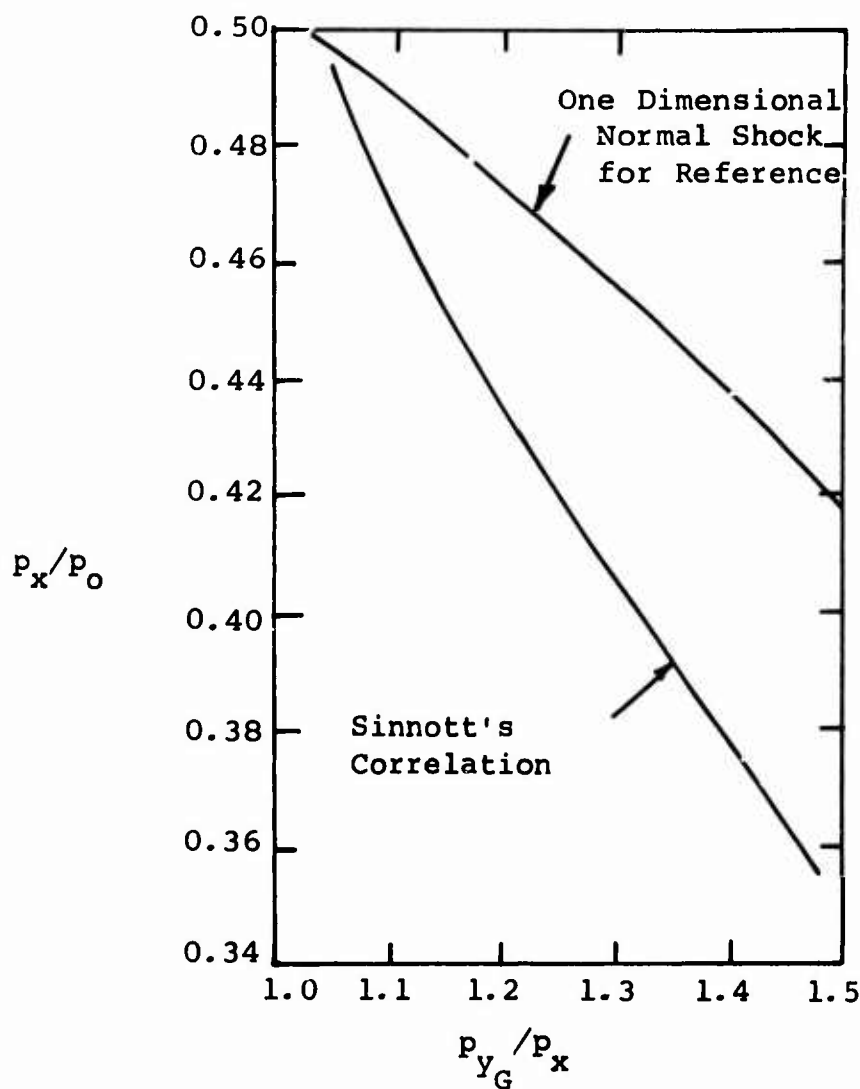


Figure 156. Transonic Airfoil Correlation by Sinnott and Osborne (1961).



1. Locus of  $P_x/P_o$  obtained from sonic range pressure distribution.
2. Locus of  $P_{Y_G}/P_o$  obtained from use of Glauert's compressibility correction to "incompressible" flow solution.

Figure 157. Shock Location and Evaluation of Static Pressure Distribution on Transonic Airfoil.



See Figure 157 for Definitions of Symbols

Figure 158. Empirical Shock Pressure Ratio Relation Derived by Sinnott and Osborne (1961).

- (2) Using the relationship shown in Figure 156  $(p_x - p_{SR})/p_o$  vs.  $(M - M_*)/(1 - M_*)$ , the locus of possible upstream static pressure distributions  $p_x/p_o$  could be evaluated as a function of chord length since  $M_\infty$ ,  $M_*$ ,  $p_o$ , and  $p_{SR}$  were already known.
- (3) Using the Glauert compressibility relation, the subsonic downstream pressure distribution  $p_{y_G}/p_o$  could be evaluated for the given geometry and approach relative Mach number.
- (4) Using Figure 158, i.e.,  $p_{y_G}/p_x$  vs.  $p_x/p_o$ , the pressure difference  $\Delta p = p_{y_G} - p_x$  could be evaluated.
- (5) The shock location along the chord could be evaluated by finding the chord position for which the difference between the  $p_x/p_o$  locus and the  $p_{y_G}/p_o$  locus produced the evaluated  $\Delta p$  found in step (4).
- (6) The combination of steps (1) through (5) permitted the evaluation of the upstream pressure distribution, shock location, and downstream pressure distribution as a function of airfoil chord position.

#### 6.1.2 Adaptation of Transonic Airfoil Theory to Inducer Flow

We propose that an adaptation of the Sinnott shock location and shock pressure rise correlation information can be combined with the information relating the effects of wall tunnel interference on "peaky" profile pressure distributions to assist in modeling the centrifugal inducer suction surface blade pressure distribution needed to obtain good diffusion in the centrifugal inducer. Using this information, the following general procedures are recommended to specify inducer blade shapes operating in the supercritical flow regime.

### (1) Relative Mach Number

The subsonic inducer should be designed to give the lowest possible inlet relative Mach number consistent with the other compressor design requirements.\*

### (2) Diffusion

The inducer passage geometry, the blade turning schedule, and thickness schedule downstream of the inducer inlet region should be designed using three-dimensional, potential, compressible, meridional, and blade-to-blade flow solutions.

### (3) Incidence

The blading should be designed to maintain a low value of incidence (approximately  $+1^\circ$ ) to the camber line at the nose based upon the upstream unblocked axial velocity. This rule insures that the inducer blade geometry will be operating near optimum conditions as far as maintenance of a separation-free suction surface can be obtained.

The potential flow solution should account for the effects of blade blockage along the span of the inducer blade and resulting meridional streamline shifts and variable angle of incidence along the inducer blade span.

It is recommended that iteration of the potential solution and blade design be made. Also, the inducer blading should not be restricted to purely radial elements if alterations in the blading are required to maintain low angles of incidence along the entire span.

It may be desirable to actually design the inducer blading with a zero or negative angle of incidence based upon the upstream unblocked axial velocity. A negative angle of incidence will relieve the usual overvelocity on the suction blade surface and greatly help to prevent separation there.

Evidence for this can be found from the work of Kramer

---

\* See Section 7.1 for alternative tactic of purposely designing supersonic inducers.

(1956) in which compressible, subsonic relaxation solutions around the inducer leading edge for a centrifugal compressor were obtained. Kramer's results for two angles of incidence, a positive and a negative value respectively, are shown in Figures 159 and 160. The velocity contours are shown; the general reduction in overvelocity along the suction surface around the nose region with negative incidence can be seen on these figures. Although Kramer's results are for an almost purely radial inducer, in which the potential flow was turned meridionally just prior to entering the inducer, the qualitative effects observed in these solutions will be identical for an axial inducer.

Even though there will be little blade loading or even negative loading near the leading edge with such a design, this may be desirable in order to reduce the acceleration and rapid deceleration of the laminar boundary layer on the blade suction surface until it has a chance to undergo transition.

At the same time, adverse effects can be expected to occur in the pressure surface boundary layer. However even if the pressure surface separates, it must reattach immediately and should be able to negotiate the inducer diffusion downstream of the leading edge without hindrance.

The angle of incidence cannot be made too negative, as separation on the pressure surface will then begin to affect the potential flow distribution. However, such an effect would be felt far down upon the suction surface side of the blading because of the large stagger of inducer blades.

There is not much specific evidence that can shed much light on the performance of centrifugal impellers with pronounced negative angle of incidence at design. The fact that impeller efficiency is rather invariant with decreasing flow in vaneless diffuser stages is heartening. The available evidence argues for at least a slightly negative angle of incidence onto the blading; further research study of this important matter is needed.

#### 4) Inducer Leading Edge Shape

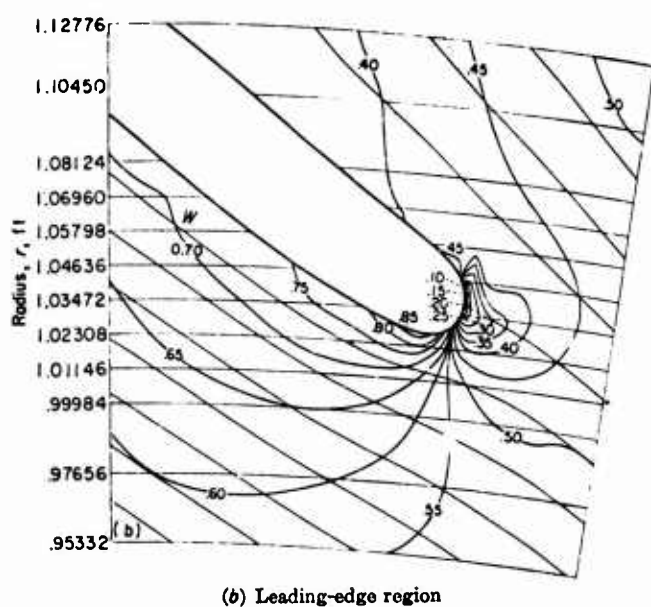


**Figure 159. Velocity Contours Around Centrifugal Compressor Inducer Leading Edge. Positive Incidence.**

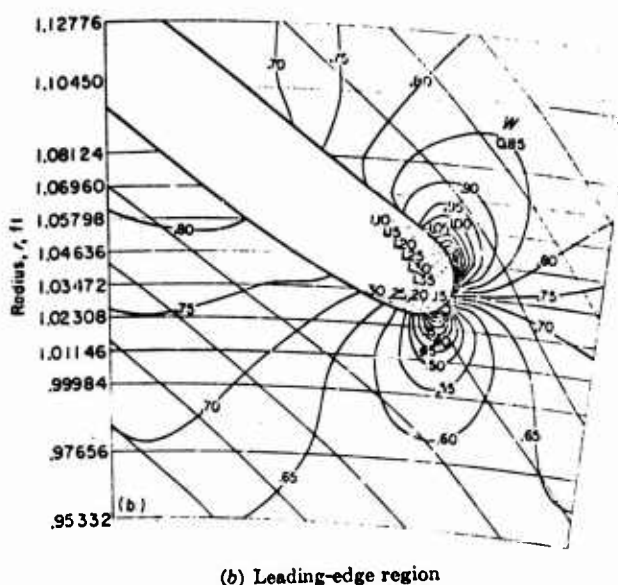


**Figure 160.** Velocity Contours Around Centrifugal Compressor Inducer Leading Edge.  
Negative Incidence.

An inducer leading edge geometry should be specified that can be expected to produce a "peaky" pressure distribution behavior over the inducer blade suction surface. From the evidence presented on transonic airfoils, such a profile should have a large curvature on the leading edge changing to a low curvature further along the profile. Such a shape should lead to the rapid attainment of a peak velocity in the supersonic regime followed by a gradual isentropic compression (i.e. the "roof-top" pressure distribution).

#### 5) Boundary Layer Predictions

The pressure distribution over the blade surface can be found by applying transonic wing methods to predict the pressure distribution from the leading edge through the inducer passage at each radial location. With this pressure distribution the boundary layer calculations can be made ahead of the shock location by using appropriate boundary layer techniques.

#### 6) Shock Pressure Rise

One of the main difficulties is in predicting the pressure rise through the terminating shock and the behavior of the boundary layer through the shock/boundary layer interaction process. There is very little evidence to recommend what should be done here. The only method that treats the normal shock/boundary layer interaction at these Mach numbers is Gadd's (1961). He provides a model for the boundary layer behavior. Experimental validation is insufficient, however. Until better information is obtained we are forced to use such a model or something similar to it to describe the shock-boundary layer interaction process.

#### 7) Shock Separation

If the shock/boundary layer interaction calculation shows that the boundary layer separates, then a redesigned downstream inducer passage shape, an altered nose geometry, or a higher negative incidence or lower relative Mach number should be selected, and the above procedures should be repeated until a suitable diffusion ratio is obtained for the inducer passage.

### 6.1.3 Comments

The above procedure should be repeated at a number of radial positions along the span of the blade to determine with sufficient accuracy the separation behavior of the inducer and the diffusion over the inducer blade span. We recommend using the tip separation velocity input to the calculations for the separated impeller. This is justified in Sections 5.3 and 6.3. However, it is possible to overload the inducer near the hub, occasioning early separation there and ruining tip diffusion. Apparently, Workhorse suffered this fate; see Section 5.2.

The above approach to modeling the inducer flow is postulated upon assuming that a significant amount of transonic isolated airfoil information can be applied to the supercritical inducer flow problem. Not until greatly improved methods for calculating the potential flow under high subsonic/transonic conditions are perfected will much improvement in analytical ability be obtainable. Since such is not expected in the immediate future, the above is the best that can be applied to the inducer now. Research on better methods and to confirm the specific recommendations here is urgently needed. If impeller diffusion is spoiled by a poor inducer (and this seems to happen too often), good stage performance is beyond reach.

### 6.1.4 Conclusions

In summary, the important points that appear qualitatively well founded are the following:

At high transonic relative Mach numbers, supercritical flow over the pressure and suction surfaces near the leading edge can be expected. It is important to design the inducer blading to minimize these effects and in particular to minimize the impact of terminating shocks on the blade surface boundary layers. Because the blade Reynolds numbers are low, it is of particular importance to treat the boundary layers gently until transition Reynolds numbers are reached. For this reason, it is desirable to design inducers with long passages before turning to axial, in order to delay deceleration in the inducer passage until the suction surface boundary layer undergoes transition,

to use a minimum number of blades to minimize blockage,  
and to design for some negative incidence.

One should pay particular attention to the details of the leading-edge profile shape so as to avoid severe super-critical transonic flow effects which may separate the flow permanently and destroy impeller diffusion.

## 6.2 INDUCER PRESSURE DISTRIBUTION

Behind the leading edge of the inducer (covered in Section 6.1), the existing model uses the potential solution for the impeller by assuming that the flow follows the camber line of the blading, and by assuming blockage factors and core relative stagnation pressure losses to account for boundary layer growth.

As was pointed out in Section 5.2, this approach seems to be adequate except for the assumption of blockage and recovery factors. Rather, one should use two-dimensional boundary layer calculations, provided that the inducer leading-edge velocity distribution can be estimated with sufficient accuracy.

There is no point here in setting up any specific means for using two-dimensional boundary layer calculations, for that is rather straightforward from axial compressor technology. We recommend that the blading in the axial portion of the inducer be treated two-dimensionally (the boundary layer theory would not be expected to work in the part of the impeller with significant radial velocities because of the Coriolis effect). The meridional stream surfaces of the potential solution about the blades are regarded as a two-dimensional flow surface. The boundary layer grows along the blades under the calculated pressure distribution. The core of the flow between the blades is considered to be loss free. This should be a very accurate assumption until inducer entry Mach numbers reach into the supersonic range over 1.2, where shock losses begin to be significant. We will treat the supersonic inducer as a special case in Section 7 when considering redesign. Iteration is required to account for boundary layer blockage in the potential solution's continuity equation.

The use of diffusion factors on the blade surfaces is not recommended. These have been developed from the axial compressor technology and are based upon correlations of cascades of certain profiles. We would not expect the diffusion factor to have meaning in the inducer of the centrifugal compressor which does not have a Kutta condition imposed. Rather, normal two-dimensional boundary layer separation criteria should be used.

For the choice of a turbulent boundary layer theory, refer to the careful evaluation organized during 1968 by Kline et al at Stanford. The report of this conference has not yet been published; it is expected momentarily.

Of course, detailed boundary layer calculations cannot be used for the inducer unless the velocity distributions are available for the blading at all radii. The normal potential flow solutions usually give five or seven stream surfaces, which should be entirely adequate.

We cannot test this approach adequately with the Boeing-AVLABS data. In Section 5.2 we did show with the limited RF-2 data that conventional boundary layer calculations plus the potential solution gave reasonable agreement with the measured cover static pressure distribution. However, this is a very limited test because of the paucity of data. The Workhorse impeller was not useful for this purpose because the calculations indicated very early hub separation.

A careful investigation of inducers and tests of the flow models available for them should be made, as recommended in Section 8.

### 6.3 IMPELLER SEPARATION

Welliver and Acurio located the impeller separation point largely by assuming an overall diffusion ratio for the inducer of RF-2 and by using limiting diffusion factors for Workhorse. We have already discussed in the previous Section the inadequacy of axial compressor diffusion factors for centrifugal inducers.

The assumption of an overall diffusion ratio is largely a guess. Given a great deal of empirical data which can be correlated against inducer geometry, inlet relative Mach number, etc., one might develop a fairly good empirical appreciation for the location of separation. Without such information, and to our knowledge sufficiently extensive collections are not available, it is necessary to predict separation by more detailed, but less certain, means.

Out of the use of the two-dimensional turbulent boundary layer recommended in the previous Section, one will get predictions of separation points. Care must be exercised with the boundary layer theory used that it does not blow up for the steep gradients or other factors characteristic of inducer distributions. For instance, the Englert (1951) method we employ collapses for steep velocity distributions typical of the variations near the leading edge of the inducer vanes.

If separation is predicted on the tip suction surface streamline, then as discussed by Dean (1968), the separation line should be drawn normal to the meridional streamlines over the suction surface of the blade. Empirical evidence shows that this is approximately correct. This trajectory violates the assumption of zero relative velocity in the separated wake; that condition requires that the relative Mach number be constant along the separation line of the suction surface, which soon drives the separation line off the leading edge of the inducer blades.

If separation first occurs at the hub, then matters are not so plain. Again, zero relative velocity in the wake would require constant relative Mach number along the separation line. If this line is drawn out toward the tip,

it will tend to lean heavily backward into the impeller. Probably the separation line will tend to fall around the bend to radial. The boundary layer is expected to separate in the bend due to the additional stress on it.

If the separation line, when extended upon the suction surface from the hub on a constant relative Mach number contour of the potential solution falls downstream of the separation point predicted for the tip streamline, then we would recommend joining the two with a near straight line. There is no satisfactory experimental evidence supporting this view, but it appears to be reasonable.

Two-dimensional turbulent boundary layer literature should be referenced for analytical separation criteria. Usually, the solution goes to pieces so quickly near the separation point that there is little uncertainty as to where separation occurs, no matter which one of several reasonable criteria for separation is employed.

For the centrifugal inducer, we expect the same level of success with separation prediction methods that has been achieved with the axial compressor. By careful application of potential and boundary layer theories, Schlichting (1959), Mellor (1959), and others have shown that the two-dimensional axial compressor cascade pressure distribution can be predicted up to the critical Mach number. Above that level, no one appears to have constructed accurate analytical methods for the axial compressor.

The subsonic methods fail near the ends of the blades in the casing boundary layers; similar difficulties might be expected for the centrifugal compressor. However, the cover and hub boundary layers in the inducer tend to be thinner than they are on the casing of axial compressors after the first few blade rows. The inducer is more typical of the first rotor of a fan; for that, the end-wall boundary layer problem tends to ameliorate.

In summary, the prediction of separation and boundary layer growth in the inducer is confounded largely by the complex transonic or supersonic flow in the inducer entry region. The development of better models for that has been discussed

in Section 6.1. Providing that problem can be resolved adequately, there should be no difficulty in continuing the solutions back into the inducer, using the methods recommended here.

#### 6.4 IMPELLER SEPARATED FLOW AND DISCHARGE PATTERN

As we have shown in Section 5.4, the simple wake-jet model for the separated flow in the impeller is entirely adequate for predicting the pressure distribution from the separation point to the tip of the impeller. This is a very important accomplishment because the static pressure at the tip of the impeller so critically determines many of the fluid dynamic effects from there on.

On the other hand, we have shown that the simple model is mute or even dumb when it comes to predicting the mass-flow-average slip factor of the through flow out of the impeller. This prediction is a critical one, for the slip factor tells us how effectively we have used the inevitable loss processes associated with a high-speed impeller. Therefore, a theory for the separated three-dimensional flow within the impeller is essential. The theory must recognize the three-dimensional nature of the separation occasioned by the meridional bend to radial and the blade-to-blade separation.

In this program we commenced the development of such a theory, but after reviewing the small amount of experimental data available on this matter, we decided that the development of a realistic theory was beyond the scope of this program and could not be tested with the data available in the Boeing-AVLABS program. Therefore, we recommend in Section 8 that a research program be initiated which will provide an adequate theory for the slip factor of a separated impeller.

We have already shown in Section 5.7 that the impeller discharge mixing predictions are not significantly affected by the three-dimensional nature of the impeller discharge distortion pattern. This is because the mixing loss is primarily the excess kinetic energy of the separated jet which is governed mostly by static pressure and the slip factor at the impeller tip. Scrambling up the flow pattern in a three-dimensional way (and probably also in time) has only a minor secondary effect on the predicted losses. Consequently, there is no need, from this source, for the separated impeller theory to yield a three-dimensional distortion pattern for the impeller tip.

In developing a theory for the separated three-dimensional flow within the impeller, in order to generate accurate slip factor predictions, it will be important to recognize the distributed flow pattern in the  $x-\theta$  plane of the through-flow and wake. Detailed experimental investigations have shown a complex pattern with significantly high relative tangential velocities, as explained in Section 5.6. In order to calculate these velocities with sufficient accuracy for the slip factor prediction, it appears that a field-type solution will be needed.

Given a lot of good detailed experimental data, one might be able to develop a simpler theory, if undetermined constants could be established empirically; that is, analogous to the simply structured impeller discharge mixing theory, it may be possible to develop a separated impeller flow pattern theory which uses more gross patterns such as a solid body spin about the jet axis, mindful of the Stodola slip factor model.

## 6.5 IMPROVED MODELS FOR SECONDARY EFFECTS

The principal secondary effects in the impeller were those discussed in Section 5.5:

- cover friction
- rear disc friction
- leakage over blades
- internal shear mixing and passage friction
- secondary flow

### 6.5.1 Cover Friction Losses and Influence on Internal Flow

We find it impossible at this time to improve upon the methods used in Section 5.5 for estimating cover friction. The drag of the cover must have some influence on the secondary flow patterns within the impeller. This is not believed to be very significant, but we have no satisfactory way of even estimating it.

In Section 8.2 a program of research is advised in which cover friction torque would be directly measured as a function of important impeller parameters.

### 6.5.2 Rear Disc Friction

The same conclusion may be drawn as above for the friction on the rear of the impeller disc. The best methods available are similar to those of Daily and Nee (1960). However, we find some serious objection to these and feel that a more direct investigation is needed.

One of the paradoxes of the high-tip-speed centrifugal compressor is how the energy dissipated in the cavity between the impeller rear casing is rejected to the environment. Heat transfer calculations through the rear casing indicate that it is very difficult to transmit more than about 1% of the work input of RF-2 without invoking very high temperatures. The same is true of heat transfer through the disc. Since we estimate that about 3% of the total work input is dissipated in this space, there must be some other way for this energy to escape. To our knowledge, no one has made careful measurements of temperature distributions in the disc and casing in order to determine where this energy goes.

We suspect that a third potent transfer mechanism involves flow between diffuser and rear cavity driven by the strong pressure variation around the tip of the impeller shown in Figure 93. The rear cavity should be at a pressure which is approximately a linear average of the varying pressure around the impeller tip. Therefore, pressure differences at the peak of the patterns in Figure 93 as high as 25 psi will cause flow to squirt into the rear cavity. This ingested fluid must be expelled in the low-pressure areas of the impeller tip. As it departs, it could carry away a sizable amount of the energy dissipated in the rear cavity by friction. In other words, the ingested flow is presumed to mix with the flow in the cavity and to be expelled much hotter than it came in.

The proposed pattern is not pure fantasy, for it is known to occur in water turbines with aerated shrouds and discs. In the high pressure regions of the stator vanes, water tends to flow into the cavities, while in the low pressure regions water and air tend to flow out. This is a principal mechanism for air loss on such machines. In fact, we can see no plausible way to argue that there is no recirculation between the diffuser and rear cavity. The pressure differences can be sustained only by accelerating fluid in and out of the rear cavity.

What are the consequences of this process? Certainly there should be some impact on the performance of the diffuser and impeller. Where flow is ingested into the rear cavity, there is a beneficial boundary layer suction effect and, since this comes in a region of high pressure where the hub wall boundary layer would tend to stall, it may be beneficial. But, where the flow is expelled from the rear cavity, flux normal to the wall could occur that should tend to separate the boundary layer. However, because this occurs in the regions of low pressure found under the leading edge of the suction surface, the separation may be only local and may cause minor damage. On the other hand, the hot fluid being mixed into the flow there will behave differently as it diffuses toward the throat entry, leading to more distorted channel entry flow.

No doubt these effects are transitory, due to the rotating pressure field of the impeller. Low response measurements possibly miss them entirely. A direct research investigation is warranted to understand this problem better. If the expelled flow produces a harmful effect, bleeding fluid from the rear cavity to atmosphere might be beneficial. Bleed also would provide general boundary layer suction of the hub sidewall which would tend to reduce blockage in the diffuser throat and might win back enough performance to compensate.

The bleed flow would carry away energy from the rear cavity, keeping it cool. However, the temperature there should be kept as high as the materials will tolerate in order to reduce the gas density and therefore the friction power.

#### 6.5.3 Impeller Blade Tip Leakage

We have made calculations of leakage over the tip of the impeller, including the effect of the moving cover wall, which suggest that the leakage flow could be anywhere from 10% to 30% of the mass flow through the impeller. This analysis is relatively crude; it assumes an orifice-like flow driven by the average blade pressure loading at the particular radius. While this model can be made more elegant, there is no justification for doing so because serious doubts arise as to what the real forces are that act at the tip of the blade.

Previous compressor experience suggests that the leakage over the tips of the vanes may be smaller than indicated by our simplistic calculation. Indeed, this may be why lower speed impellers seem to have about the same performance whether they are shrouded or not. Since the cover friction as estimated in Section 5.5 is close to that which would be expected upon a smooth disc, the friction power from windage on the outside of the shroud should be about equal to that on the cover of the unshrouded impeller. This common observation in commercial process compressors, which cannot be proven to our knowledge by any direct experimental evidence, suggests that tip leakage does not add much loss to an unshrouded wheel for the magnitudes of clearances which are regularly employed.

There may be private or even public evidence available which shows the efficiency of the stage as a function of the clearance between the impeller and the cover. We are not aware of any reliable data of this sort; if it does exist, it could shed a great deal of light upon this question. The amount of leakage and the loss engendered should depend upon the degree of separation in the impeller and on how skewed the flow is through the impeller. So evidence on the effect of tip clearance from one type of machine may be completely inapplicable to another type.

At this time with all these uncertainties, it does not seem wise to attempt a more exact theory accounting for tip leakage. Plainly, specific research is needed in this area, and that is recommended in Section 8.2.

#### 6.5.4 Internal Shear and Passage Friction

On the basis of our model which assigns all of the "tired" fluid within the impeller to the wake, there is a general need to estimate how much wake fluid is generated within the impeller in order to evaluate  $m_w/m$ . Part of the generating process involves scrubbing relative kinetic energy out of the flow against the walls of the passage and on the boundary between the jet and the wake. Calculating the shear forces acting on the flow does not produce much useful information.

A more sensible approach would be to use boundary layer theory to calculate the growth of displacement thickness on the wall within the impeller. Perhaps conventional jet mixing theory could be employed for the jet-wake boundary, if a shear coefficient could be estimated. But, for both of these approaches, there is serious question as to whether conventional stationary boundary layer theory is applicable in rotating space.

Johnston (1968) has studied the behavior of the laminar boundary layer in the rotating system of the centrifugal compressor and concluded that it should grow about as expected in stationary coordinates (using, of course, the changes in relative velocity to indicate the effective pressure gradient).

The turbulent boundary layer of concern here has not, to our knowledge, been similarly studied. We expect that Coriolis forces influence boundary layer turbulence considerably. Halleen and Johnston (1967) found significant differences in the turbulence structure caused by rotation, although the results are for much different conditions and quantitative comparison was not attempted.

Likewise, as we have discussed before, the mixing between the wakes and the jets is shown by visualization studies to be strongly suppressed. Thus, one is not at all confident as to what type of shear coefficient should be invoked. If a coefficient of the usual magnitude for jet mixing in stationary coordinates is used, then the kinematics of the flow in the impeller completely disagree with what is observed in visualization studies and the pressure distribution in the wake region diverges from the centrifugal gradient of the quiescent wake.

With these difficulties, it seems that little more can be done now to more accurately model the frictional processes within the centrifugal impeller. Only through detailed research investigations of the phenomena could one hope to gain enough understanding to write a better theory than we have now. Fortunately, the penalties for our poor capability are not great. The "tired" fluid becomes part of the wake in our model, so only the magnitude of  $m_w/m$  is affected, and the loss is not very sensitive to  $m_w/m$ .

#### 6.5.5 Secondary Flow

The fact that the mass flow in the wake region has some effect upon the impeller discharge mixing losses as shown in Figures 95 and 96 (although it is not a powerful influence) means that better tools for predicting the secondary flow into the wake would be useful. However, chances of constructing such tools for the complex flows encountered are not great.

Kramer (1954) has set up the basic equations for secondary flows in rotating coordinates. Naturally, he does not include the complexities of the three-dimensional and separated flow pattern or the influence of tip leakage,

backflow, and other disturbances. We are of the opinion that the available secondary flow theories are rather impotent for this problem. That opinion is bolstered mightily by the general debility today in calculating three-dimensional turbulent boundary layers. As yet no useful theory has emerged, although the approach of Herring and Mellor (1968) offers some promise of filling this historic gap. However, we would have little confidence even in using the methods of Herring and Mellor to try to predict the secondary flow in an unshrouded centrifugal impeller.

So for the moment, our estimates of mass flow through the wake must be at best "guesstimates". Direct experimental investigation of the subject recommended in Section 8.2 should produce empirical information and give us more confidence as to what sort of mass flow fractions occur in the wake and how these vary with various impeller parameters. Until that research is accomplished, we must continue to "guesstimate"; fortunately, overall performance is not critically dependent upon the number adopted for  $m_w/m$ .

#### 6.5.6 Summary

For cover friction effects, there seems to be no alternative to conducting experiments, for the flow is so complicated that the construction of improved flow models must be guided by better empirical understanding. After studying this matter, we feel it would be fallacious to attempt to construct anything better than what now exists, as discussed in Section 5.5.

On the rear disc friction, the existing empirical data of Daily and Nece (1960), for example, are probably adequate, although we must know more about the gas temperature generated within the closed cavity. To know that, we have to understand better how fluid moves in and out of the rear cavity, as has been discussed in Section 6.5.2.

Probably an adequate theoretical prediction means could be put together if we had a satisfactory way of predicting the pressure distribution around the tip of the impeller. We do not have that, as explained in Section 6.8, and it

does not appear that an adequate theory can be developed short of solving the traditional problem of supersonic-transonic two-dimensional flow with boundary layer. We have worked quite extensively on this matter; it proves even more than expected to be a major analytical problem. When we remember that this problem has not been solved for aircraft wings or axial compressor blading, we can appreciate the difficulty. Therefore, we do not expect that a good analytical approach to the rear cavity ventilation problem will be made for a long time. Rather, empirical data should be sought whenever a diffuser impeller combination is tested.

From the point of view of the diffuser sidewall boundary layers and their health and separating tendencies, it is also very important to know how this interchange with the rear cavity affects the boundary layer, as discussed in Section 6.7.

On blade tip leakage, the losses do not appear to be very severe from this source for the usual clearance magnitude, although this is not plain. Fluid that leaks over the tip of the blade will contribute to the flow in the wake in part, although some of it no doubt slips by on the cover and flows again through the next vane tip.

The difficulty with predicting tip leakage well lies with predicting the pressure distribution on the blading, particularly in the radial portion of the impeller, where the flow is likely to be separated from the cover and the through-flow jet is undergoing a twisting motion back onto the pressure surface of the blading. Since we have no means for predicting the three-dimensional separated flow pattern in the impeller, we at the present time have no means for making better models to predict the leakage over the tips of the blades. The conventional models which assume a uniform loading on the blades from cover to hub are not capable of providing anything more than a qualitative appraisal of tip leakage.

The prediction of secondary flow in the centrifugal impeller is hampered by the general problem of predicting the behavior of three-dimensional turbulent boundary layers. Since this problem has not been solved even for

simple geometries like two-dimensional flow or axisymmetric flow, it is fantasy to expect that it can be solved for the complicated shape of the impeller passage with the flow separated and probably transient. Secondary flow will also interact with tip leakage over the blades in the fashion that has been explored by Dean (1954); this has an important influence on the effect that the secondary flow produces. We need a better model for secondary flow in centrifugal impellers primarily in order to calculate the mass flow through the wake region with its parameter to inject into the impeller discharge mixing model. However, as shown in Figure 95, this parameter does not strongly affect the loss prediction over fairly wide ranges. In other words, we assume a usual value of 20%; changing down to 10% or up to 30% will not greatly influence the loss prediction.

Before attempting to develop a theory for the secondary flow within the centrifugal channel, it would be wise to secure experimental data on what kind of flow patterns actually exit from impellers. This will give some feeling for the gross amount of flow in the wake and jet; this information is far more useful now than elegant secondary flow theory, which stumbles when trying to predict simple, overall characteristics of the flow. Therefore, we recommend in Section 8 that a research program which includes extensive probing of impeller discharges with high response instrumentation be conducted to get a better feeling for distribution of slip and mass flow per unit area over the discharge pattern. Until that has been done, it would be unwise to attempt a secondary flow theory.

In summary, the utility of trying to build better internal flow models for the centrifugal compressor is not encouraging at this time. More research is needed on the critical matters, particularly an accurate means for predicting slip factor.

## 6.6 IMPELLER DISCHARGE MIXING

Welliver and Acurio (1967) used a very simple model for calculating impeller discharge mixing recommended by Johnston and Dean (1966). This model assumes a step wake-jet pattern with zero flow in the wake. It was extended by making it apply to compressible flow, but in no other way.

During this program, we have generalized the impeller discharge mixing theory to accept any kind of three-dimensional distortion pattern for all of the flow properties. The same basic assumptions of sudden expansion are still in the theory because those have withstood the test of time since it was first shown that the detailed two-dimensional mixing theory of Dean and Senoo could be approximated by a sudden expansion process over the usual range of centrifugal compressor designs. (This matter is discussed by Johnston and Dean.)

The new and extended impeller discharge mixing theory is contained in Appendix II. Not only have we extended it to arbitrary distortion patterns, but we have removed an analytical anomaly contained in the original theory. This is discussed in Appendix II; it involves the fact that if the Johnston and Dean analysis is applied to a given flow pattern, but with different orientation of the coordinates relative to the blading, different mixed out states result. This is because in the integrals for momentum flux, cosine and sine terms appear which resolve the fluxes through the control surfaces into a given fixed direction in Newtonian space. Because the distortion patterns are not linear, the integrals will be different depending upon the orientation of the arbitrary fixed direction to the distortion pattern.

We can think of this in another way by imagining a series of solutions carried out with the impeller in progressively different positions relative to the coordinate system. Then we find that there is a periodically varying set of mixed-out properties changing at blade-passing frequency. This result plainly violates the spirit of the analysis which assumes an axisymmetric mixed-out state.

In order to rectify this analytical anomaly, we have time averaged the mixed-out state; on so doing, the sine and cosine terms disappear from the integrals. The final calculated result is steady in time and uniform in space, which is a more satisfying outcome. The new theory is also simpler than the old one, and the flux integrals have a more direct physical significance.

For the sort of distortion patterns encountered with the Boeing-AVLABS impellers, the corrections by the new theory in predicted mixed-out properties are small. Therefore, we would not seriously alter the mixing calculations of Welliver and Acurio.

Another useful development for impeller discharge mixing would be a more complete field-type analysis of the Dean and Senoo type. With that, we would predict the variation of properties with radius and the mixed-out radius ratio. This theory should be written recognizing the boundary conditions of the vanes; thus it would become a terribly complicated analysis. A theory of this sort with a dissipative field-type solution of basically unsteady flow at transonic speeds is intractable today.

In summary, the improvements we have made under this program in the impeller discharge mixing theory are valuable in quantity, but they do not change the analysis in kind. We have shown, however, that the inclusion of flow in the wake and the concern for the relative total pressure of the jet are important. While calculated output is not very sensitive to wake flow, low response instrumentation is sensitive to it. The relative jet loss makes a big difference; we have too little evidence on which to base its choice. As a consequence, a research program is recommended in Section 8 which includes detailed probing of the impeller tip region with high-response instrumentation. This probing will provide more information about the proper kind of parameters to enter into the impeller discharge mixing theory.

We reemphasize that the impeller discharge mixing theory of Dean and Senoo, and Johnston and Dean, which is widely used, has never been adequately tested to our knowledge.

The testing of this is a very difficult task; some of the reasons for that have been discussed herein and by Dean (1968). In Section 8 we recommend a critical study of this important analytical tool. Because the impeller discharge mixing losses are large, for low specific speed machines of the sort encountered in the Boeing-AVLABS program, it is essential that an accurate loss theory be available.

## 6.7 IMPELLER - DIFFUSER INTERACTION

Existing flow models, covered in Section 5, are silent on the influence of the diffuser upon the impeller flow. The Boeing-AVLABS experience produced little evidence on this subject, although there was from time to time an indication that modification of the diffuser affected impeller work input and perhaps efficiency. Most of this evidence is so slight that it does not emerge distinctly from the data uncertainty. However, there is one case which is plain: Tests 3369 and 3370 of RF-2.

For these, the depth of the impeller was reduced from 0.180 in. to 0.135 in., giving, with clearance included, values for  $b_2$  about 0.195 in. and 0.150 in. respectively. The change made a 23% reduction in impeller discharge flow area. Concomitantly, the diffuser depth was reduced from the normal value of 0.180 in. to 0.158 in. In the RF-2 test series, there is one test (3366) which had a wider diffuser (0.202) for the usual impeller discharge depth of 0.195.

While the change between the original configuration and Test 3369-70 is not great, it was large enough to make a significant change in the data. The significant change was in the temperature rise or overall work input. The work input decreased 3%, and the stage efficiency rose 3 points, from 70.5 to 73.5% (total to static). (Compare Figures 80 and 91.)

We shall now consider the changes in the fluid dynamics which should have occurred on reduction of the impeller tip depth. First, impeller tip static pressure would be expected not to change; indeed it did not, as may be seen in Figure 161 through the data scatter.

The wake fraction at the tip of the impeller should decrease considerably, so we would expect a noticeable reduction in the impeller discharge mixing loss. The only data to check this are the indicated stagnation pressure profiles in the diffuser throat. The impeller tip profiles are unreliable for deducing even trends because of the changed flow pattern. Nevertheless, the trend shown by Figures 83 and 84 compared to 72 and 73 seems to be in the right direction.

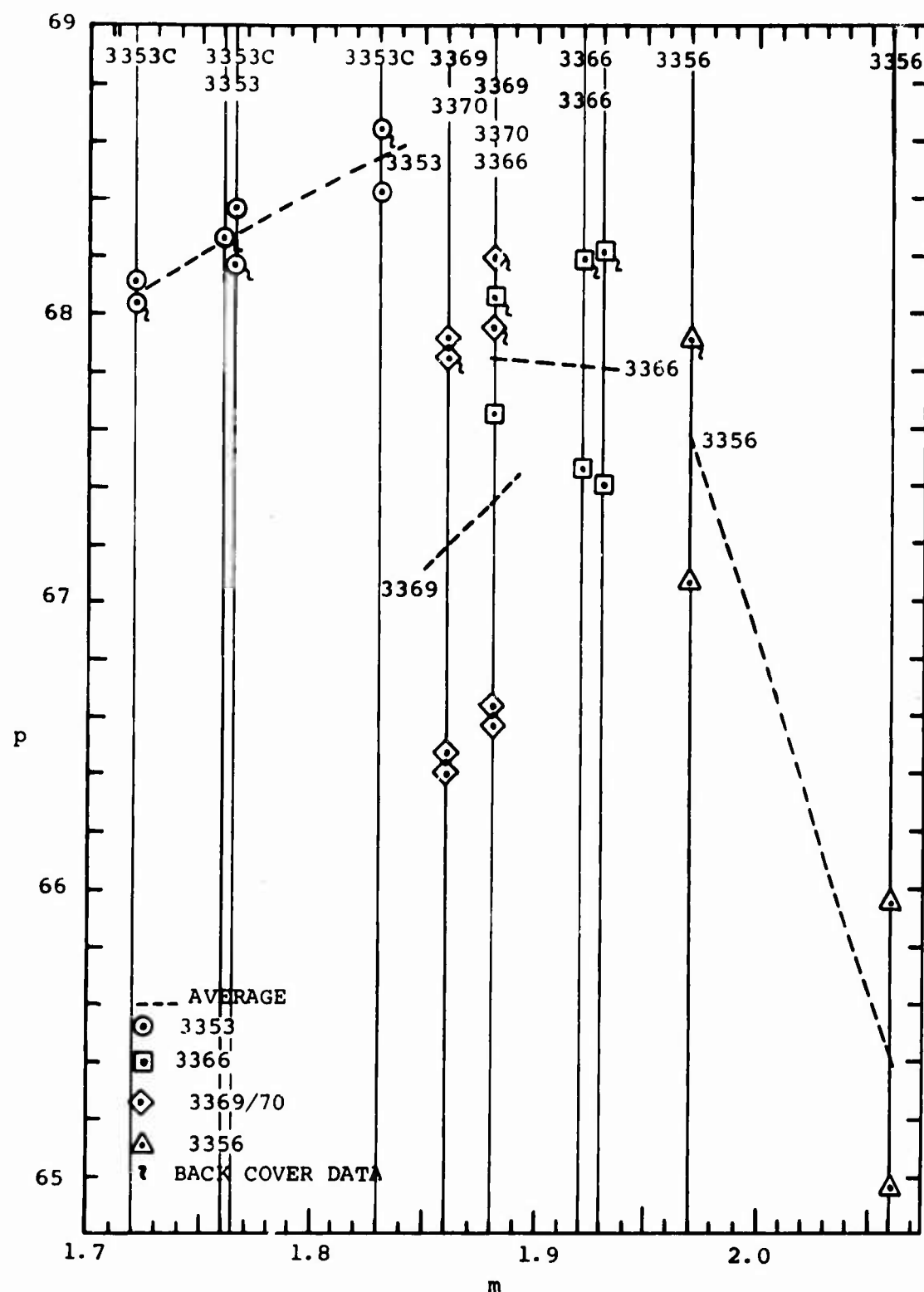


Figure 161. Static Pressures at  $R = 1.03$ .  
RF-2

If the mixing losses are reduced, one would expect to see a rise in diffuser throat stagnation pressure. The evidence in Figures 78-79 and 89-90 is contrary. The center line and hub stagnation pressures were higher for the wider diffuser in Test 3366. On the cover side, the pressure did not change. Just what these alterations mean, if anything, is hard to deduce. We expected, however, to see a general rise in the diffuser throat pressure distribution for 3369-70 compared to 3366. This was not observed experimentally.

The reduction in temperature rise is explained by the fluid dynamic argument that backflow into the impeller has been considerably reduced with the reduction in tip width. As explained below, the impeller shaft work is composed of three parts:

- (1) Fluid dynamic work done on the through flow.
- (2) Work done against cover and disc friction forces.
- (3) Work done to repump fluid flowing back from the diffuser.

Of these, the friction work (2) would not be expected to change significantly with impeller depth. The through-flow work would change if the mass-flow-averaged slip factor changed, and that might happen. Formerly, we were of the opinion that the more separated an impeller became and the shallower the through-flow stream on the driving face of the blade, the more the through flow would conform to the blade shape and the higher the slip factor should become. This hypothesis explains the general upward trend of TRF and slip factor with reducing flow observed in the Boeing-AVLABS program and by many other investigators; e. g., Sakai et al (1967). Now various research studies show that the jet is spread across the hub with a relatively low slip factor. Nevertheless, as the depth of the impeller is reduced, one would expect the jet to get deeper and therefore the guidance produced by the blading to decrease and the slip factor with it. So some of the reduction in the temperature rise can be explained this way, but not the commensurate increase in stage efficiency.

As the impeller tip depth reduces so does the extent of the wake region. One would expect reduced tendency for backflow from the diffuser sidewalls. This is explained at greater length below.

#### 6.7.1 Nature of Diffuser Backflow Into Impeller

If backflow of sidewall boundary layer significantly increases impeller work input, then this is an important phenomenon which must be controlled. While there might be significant mass flow backward, this does not necessarily indicate a significant increase in impeller work input if the change of tangential velocity of the backflow from entering to exiting from the impeller is very small. Unfortunately, without a thoroughly detailed model, it is impossible to separate the magnitude of the back mass flow from the magnitude of the tangential velocity change. However, we can estimate roughly the geometry of the backflow and reduce approximately the added backflow work input to the impeller. Before we do this, however, it is worthwhile to discuss the backflow fluid dynamics in some detail.

#### Fluid Dynamics

Backflow from the diffuser into the impeller occurs when:

- (1) The impeller is heavily separated, particularly when one side of the meridional passage (usually the cover) tends to be separated almost from blade to blade at the impeller tip.
- (2) The impeller discharge flow angle is close to tangential.
- (3) There are significant disturbances around the impeller discharge region (normally produced by the diffuser).

All of these factors affect backflow.

Sometimes evidence of backflow can be seen in compressors by means of oil and dirt streaks on the diffuser sidewalls. It has been shown by Stalker (1955) that these markings are indications of the "limiting streamlines" on the flow-bounding walls. Of course, when the flow is unsteady or

the wall markings are not frozen at the beginning of shutdown, the pattern will be some sort of an average of a number of different flow states. (Normally in a compressor which runs under fairly constant conditions, the pattern that is left on the wall tends to be the running one, dried there during operation.)

It is perhaps unnecessary to emphasize that these wall markings do not represent the streamline pattern of the through flow outside the wall boundary layers. As limiting streamlines, they show the limit at the wall of the flow angle distribution through the boundary layer. The local wall shear stress vector is tangent to the streaks, as has been explained by Maskell (1955). This entire subject has been surveyed by Dean in Chapter 11 of the McGraw-Hill Handbook of Fluid Dynamics.

The radial pressure gradient in the diffuser entry region turns the mainflow, but overturns the boundary layers which have tried to negotiate more of a pressure hill than their momentum allows. This produces backflow which is clearly shown by Figures 162 and 163 from Faulders (1954). Figures 33 and 34 from the Workhorse studies also show this pattern. Figure 163 emphasizes the fact that diffuser flow is not uniform around the tip of the impeller.

While it is impossible today to calculate in detail the three-dimensional turbulent boundary layer flow expected in a given pressure field, we can estimate the limiting streamline pattern from the measured pressure fields of Figures 133 and 134. Plainly, one would expect sidewall boundary layer backflow in the high-pressure regions observed near the entry shock. This is not observed in Figures 33 and 34 because there is no entry shock at these low rotative speeds. Of course, the general radial pressure gradient caused by the swirl of the main flow will tend to drive the boundary layer backward, as has been examined in detail by investigators of vaneless diffusers such as Gardow (1958), but the general tendency is greatly enhanced in the local pressure highs caused by the diffuser vanes.

As an observer on the impeller travels around, he will notice  $Z_d$  localities where backflow is occurring as he



Figure 162. Limiting Wall Streamline Traces From Faulder's (1954) Diffuser.



Figure 163. Limiting Wall Streamline Traces From Faulder's (1954) Diffuser.

passes the diffuser vanes. The diffuser backflow is therefore unsteady in rotor space. Further, we would not expect much backflow in the presence of the strong jet flow leaving the impeller. Rather, one would expect backflow in the wake region lying against the suction surface and over the cover.

When the impeller wake region passes through the high-pressure regions under the vanes, then backflow should occur. But, when the through-flow jet passes through these same high-pressure regions, the backflow probably terminates. So we conclude that the backflow is unsteady in stator space too. It is then a doubly unsteady phenomenon, but with a regular pattern. This characteristic is probably responsible for the fact that backflow is rarely measured near the tip of centrifugal impellers. Also, it would only be expected close to the walls in the thin sidewall boundary layers and therefore might not be revealed by normal probing in production-size machines. Only wall traces are likely to show its presence, and in view of the unsteady situation of the backflow, even wall traces may average out to a pattern indicating no backflow.

In the usual situation where impeller separation is much more severe on the cover side than on the hub, one would expect more backflow on the cover side. This does not mean that backflow will not occur on the hub sidewall too, but it should not be as severe. Occasionally, as with the Workhorse impeller, the hub separates heavily too. This may cause a thick boundary layer on the hub, after reattachment in the bend to radial, and enhance hub-side backflow from the diffuser.

Boundary layer leaving the impeller on the hub moves at wheel speed at the wall. This fluid loses tangential velocity rapidly when it glides onto the stationary diffuser sidewall. With diminishing swirl, the boundary layer fluid has less ability to withstand the radial pressure gradient in the diffuser established by the core of the flow. When the sidewall fluid slips back into the impeller, it will be moving tangentially with less velocity than tip speed. Therefore, in the relative coordinate system, the backflow might appear as sketched in Figure 164. We would expect the backflow not to penetrate the impeller very deeply; it

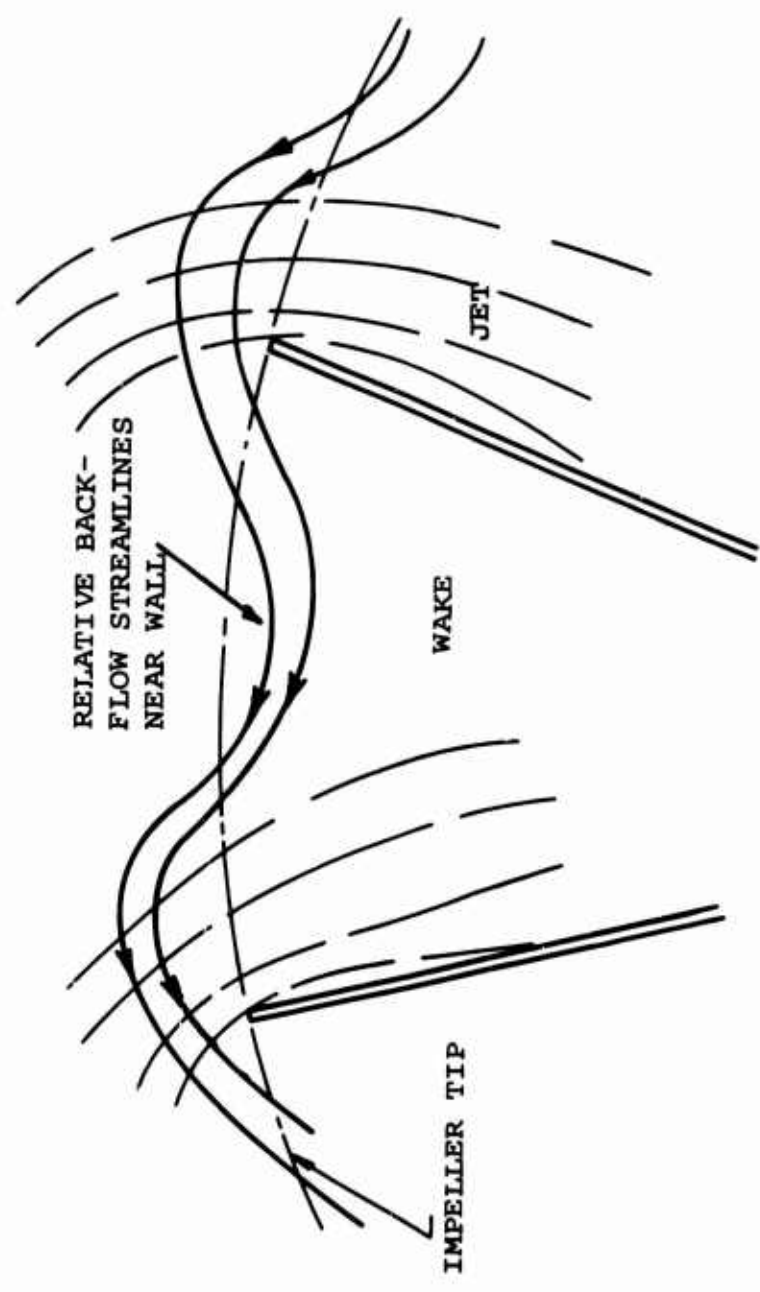


Figure 164. Schematic of Backflow Pattern in Rotor Space.

will be ejected, with an increase in angular momentum, perhaps as illustrated in Figure 164.

On the cover side, the wall limit fluid velocity is zero. However, the blades turn steadily over the cover and should "scrape" the boundary layer therefrom. The situation is analogous to that at the tip of axial machines. Measurements made by Dean et al (1954) are shown in Figure 165. They indicate that the interaction between the moving cover and the leakage over the blades should cause the roll-up of a vortex in the passage between the blades. The flow visualization photographs of Senoo (1968) also indicate this kind of roll-up. How the cover side backflow entangles with the three-dimensional flow configuration leaving the impeller is hard to visualize. Again, we would not expect the backflow to penetrate very deeply into the impeller due to its small radial in-velocity.

It must be remembered that the sketch in Figure 164 is only intended to be faintly representative of what must be a very complex three-dimensional and unsteady flow.

#### 6.7.2 Estimate of Backflow Work Input

The total shaft work which must be delivered to the impeller per unit mass of fluid is given by

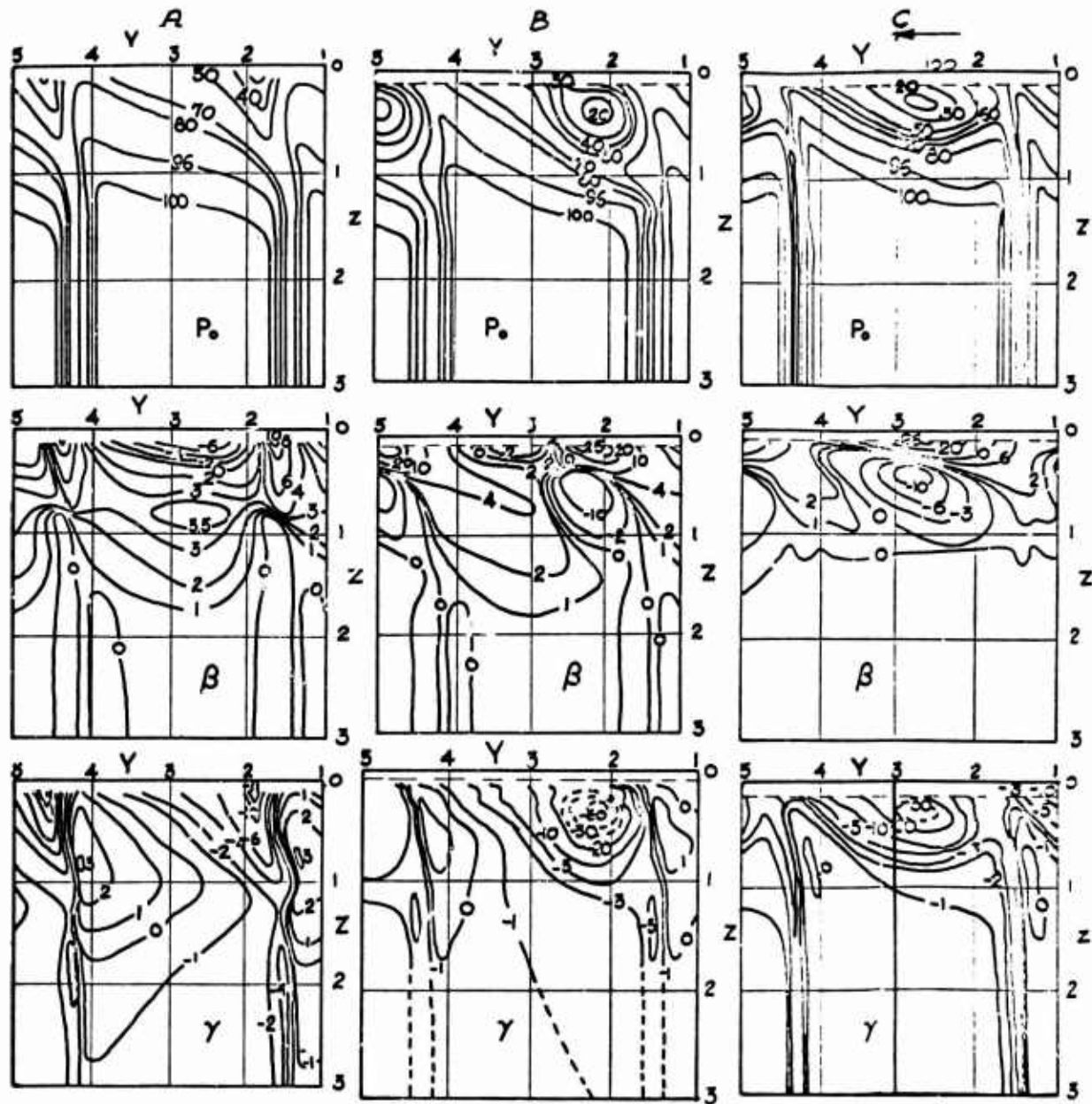
$$W_x = W_{x_{fl}} + W_{x_f} + W_{x_{bf}}$$

where  $W_{x_{fl}}$  is the fluid dynamic work given by

$$W_{x_{fl}} = \frac{\Omega}{g_o} [r_2 c_{\theta_2} - (r_i c_{\theta_i})]$$

$W_{x_f}$  is the friction work, principally cover and disc.

$W_{x_{bf}}$  is the additional work done on the recirculating fluid.



STRAIGHT BLADES  
 NO END CLEARANCE  
 STATIONARY WALL  
 BLADE CHORD 2.8  
 PITCH 2.8  
 LENGTH 16  
 TURNING ANGLE  $26^\circ$  INLET ANGLE  $40^\circ$

STRAIGHT BLADES  
 4.5% CHORD END CLEARANCE  
 STATIONARY WALL

STRAIGHT BLADES  
 4.5% CHORD END CLEARANCE  
 MOVING WALL  $C_x/u = 0.87$

$\beta$  = UNDERTURNING ANGLE  
 $\gamma$  = SPANWISE DEVIATION ANGLE  
 (+TOWARD END OF BLADE)

Figure 165. Interaction of Tip Leakage and Blade (Wall) Motion in an Axial Cascade.

We define the work input coefficient

$$\psi = g \omega_x / u_2^2$$

and write

$$\psi = \psi_{fl} + \psi_{bf} + \psi_f = \frac{J_c p (T_{o_{coll}} - T_{o_i})}{u_2^2 / g_o}$$

assuming that heat transfer is nil.

Using the definition of impeller efficiency applied only to the through flow we can write

$$\psi_{fl} = \frac{(p_{o_2} / p_{o_i})^{k-1} - 1}{\pi M_i^2 (k-1) \eta_{i_{fl}}} = \sigma_2 \text{ (for no preswirl)}$$

where  $\eta_{i_{fl}}$  = efficiency of pumping the through flow.  
Computationally we usually replace  $p_{o_i}$  with  $p_{T_{rel}}$  and adjust  $p_{T_{rel}}$  to agree with the entropy implied by  $\eta_{i_{fl}}$ .

The two are entirely equivalent  $p_{T_{rel}}$  is merely easier to use.

$p_{o_2}$  = not including backflow (separation of the flow at the discharge of the impeller into two streams is pragmatically difficult)

For the Workhorse and RF-2 impellers, the friction work is about 6% of the total work. These estimates are probably accurate to only  $\pm 1$  point. With them, we may write

$$\psi_f \approx 0.06 (\pm 0.01) \psi$$

or since  $\psi_{fl}$  is about 85% of  $\psi$ ,

$$\psi_f \approx 0.07 (\pm 0.012) \psi_{f1}$$

This gives, finally

$$\psi = 1.07 (\pm 0.012) \psi_{f1} + \psi_{bf}$$

$\psi_{f1}$  may now be calculated if we have a way of estimating the efficiency of  $\eta_{i_{f1}}$ . This is hard to do accurately; as

discussed in Section 5.6, the losses in the core of the through-flow jet appear to be close to zero. However, the wake region convects as much as 20% of the flow and has suffered a relative total pressure loss.

The indications are that the through flow is pumped at quite high efficiency, if cover friction, backflow, and exit mixing loss are discounted. But to be least prejudiced, we must allow a range of efficiency in the calculation. Below, we shall permit the through-flow pumping efficiency to range from 100% to 90%.

#### Through-Flow Work Input

It is impossible with the data on hand from the Boeing-AVLABS work to identify the backflow directly. Instead, we must meld the data and theory.

The impeller discharge mixing loss theory (Appendix II) gives the relationship between the mass flow average impeller discharge stagnation pressure and the value after mixing as a function of primarily the impeller tip static pressure,  $p_2$ , the wake mass fraction,  $m_w/m$ , and the mass-flow-average relative total pressure loss of the through-flow jet,  $\Delta p_{T_{rel,j}}$ . Calculated results made in an attempt

to predict the measured diffuser throat stagnation pressures have been presented in Figure 130. Following the arguments of Section 5.6, we shall set the "mixed out" stagnation pressure,  $p_o^*$  equal to the measured diffuser throat centerline pressure,  $p_{o4}$ . The static pressure is fixed

at 64 psia measured for RF-2.

The comparison of data and theory in Section 5.4 indicated that  $\Delta p_{T_{rel,j}} \approx 0$ . Our calculations and some experimental

results suggest  $m_w/m \approx 0.20$ . When these values are injected into Figure 130, the resulting mass flow average slip factor (same as work input coefficient of the through flow for no preswirl) is about 0.83-0.84. Even if  $\Delta p_{T_{rel,j}}$

rose to 2 psi (3.6 psi represents a complete loss of relative kinetic energy) and  $m_w/m$  were changed to 0.30, the slip factor still comes out below 0.85. Boeing's deduction from the data was 0.88. The reasons for this difference have already been explained to be due to the unreliability of low resolution impeller tip probes for heavily separated impellers.

Based on these calculations, we estimate that the through-flow slip factor for the RF-2 impeller is on the order of  $0.84 \pm 0.02$ . Remember that this number has been calculated on the foundation of the simple step-wake two-dimensional impeller discharge mixing theory. However, more sophisticated discharge flow models and mixing theories do not produce significantly different answers. What is being lost primarily is the excess radial kinetic energy due to the flow's not filling the impeller at discharge. Whether the pattern leaving the impeller is two-dimensional or highly three-dimensional, it is the mass-flow-averaged radial kinetic energy before and after mixing which is important.

Once the slip factor for the through flow has been deduced, we are then in a position to calculate the work input coefficient of the backflow from the measured total work input  $\psi$  (from  $T_{coll} - T_{O_i}$ ) = 0.968. As mentioned previously,

it is impossible to separate the magnitude of the backflow from the change in tangential velocity it encounters on reentering and being expelled again from the wheel. Our best estimate of the magnitude of the backflow work is that it has a work input coefficient of  $0.07 \pm (0.02)$ . This is a large effect; if the backflow were eliminated completely,

impeller efficiency would rise an amount approximately equal to  $\psi_{bf}$ , that is, 7-8 points. When the impeller tip depth  $b_2$  was reduced for Test 3369-70, the work input dropped 3 points, indicating that 1/3 to 1/2 of the backflow was eliminated. A further reduction in  $b_2$  might have gotten it all and yielded another 3-5 points in efficiency.

#### Summary

These studies of backflow phenomena have led to the conclusion that backflow is a significant cause of inefficiency in the RF-2 and Workhorse stages. The fluid dynamics discussion has shown qualitatively the factors which influence the magnitude of backflow. Unfortunately, the examination in Section 6.8 has convinced us that the construction of an adequate theory for the three-dimensional boundary layer in the entry region of the diffusers is certainly well beyond the scope of this program and would be an extensive and uncertain task today. However, it is also plain that backflow must be controlled if high stage efficiencies are to be had. The tendency of high-pressure-ratio centrifugal stages to have large impeller exit flow angles and thick boundary layers relative to meridional depth enhances backflow phenomena. In other words, this type of machine is inherently prone to this disease. In redesign, basic means must be found to change the character of the flow. Considerations in Section 7 suggest that this can be done by some radical approaches.

## 6.8 DIFFUSER ENTRY FLOW

We shall discuss the critical fluid dynamics between impeller tip and diffuser throat. We shall also need to consider interaction of this region with the impeller flow field.

The discussion of fluid mechanics in Section 5.8.2 reviewed the flow models proposed by Boeing-AVLABS. This section describes the flow physics and attempts to improve the flow models.

### 6.8.1 General Description of Flow

The sidewall and suction surface boundary layers play a vital role in molding the diffuser entry flow pattern. The interaction between the "free" flow and the boundary layers is strong; this interaction is unusually important because the displacement thickness of the boundary layers is significant relative to the depth of the passage. In addition, there are intense local interactions produced by shocks; the response of the boundary layer to these shocks generates a significant disturbance in the shallow passage. On top of these major features, there is a host of secondary influences which combine to make this flow problem extremely complex.

However, there are aspects of the flow which would be present even in the absence of boundary layers. First we shall consider the flow field in the absence of sidewall influences, and then we shall attempt to add the boundary layer.

#### 6.8.1.1 Flow in Absence of Sidewall Effects

For the supersonic flow typical of these stages, the velocity pattern to be expected in the diffuser entry region is not apparent even for isentropic flow. However, this situation is not unique to the supersonic case, even in subsonic flow the velocity patterns measured and calculated by relaxation methods do not agree with one's first impressions. The observer tends to be deluded by his knowledge of rectilinear flow, which is not always enlightening for a polar flow pattern.

We have found no easy way to estimate the velocity field of the diffuser entry region; rather, experimental data first and then relaxation solutions have taught the nature of this field.

Figure 166 shows isobaric contours measured in the Workhorse diffusers; very similar patterns for RF-2 are found in Figures 133 and 134. The common feature of these patterns is the small diffusion which occurs from the impeller tip to the near vicinity of the channel diffuser entry, and the isobars are almost parallel to the streamlines of the flow. We have no simple explanation to offer for this behavior; it seems to be characteristic of a high stagger cascade because the same general pattern has been theoretically calculated for a wide range of diffuser geometries. Apparently, the great exposure of the semivaneless region under the suction surface of the vanes to the relatively axisymmetric pattern of the impeller flow field prevents much pressure rise from occurring in this region. A radial gradient is observed which corresponds well to the curvature of the streamlines as dictated by the suction surface.

As Figure 166 demonstrates, the flow in the channel is nearly one-dimensional. So, the entry shock must stand nearly normal across the streamlines. Otherwise, the static pressure and Mach number after the shock would not be uniform. Reacceleration must occur near the vane suction surface just ahead of the shock, as is observed in fact and may be noted in Figure 166. This same feature may be seen in many of the pressure distributions of Section 3. This is a rather unusual situation, for it means that the approaching supersonic flow ahead of the shock is aware of the shock downstream. Supposedly in supersonic flow, no upstream adjustment can occur.

A possible explanation could involve the sidewall boundary layers with pressure signals fed through their subsonic portions to influence the supersonic flow upstream. This may happen. However, we are of the opinion that, even if this diffuser were infinitely deep, there would still be this adjustment from a swirling flow to a channel flow just ahead of the shock in what has been called, in the Boeing-AVLABS work, the "zone of rapid adjustment".

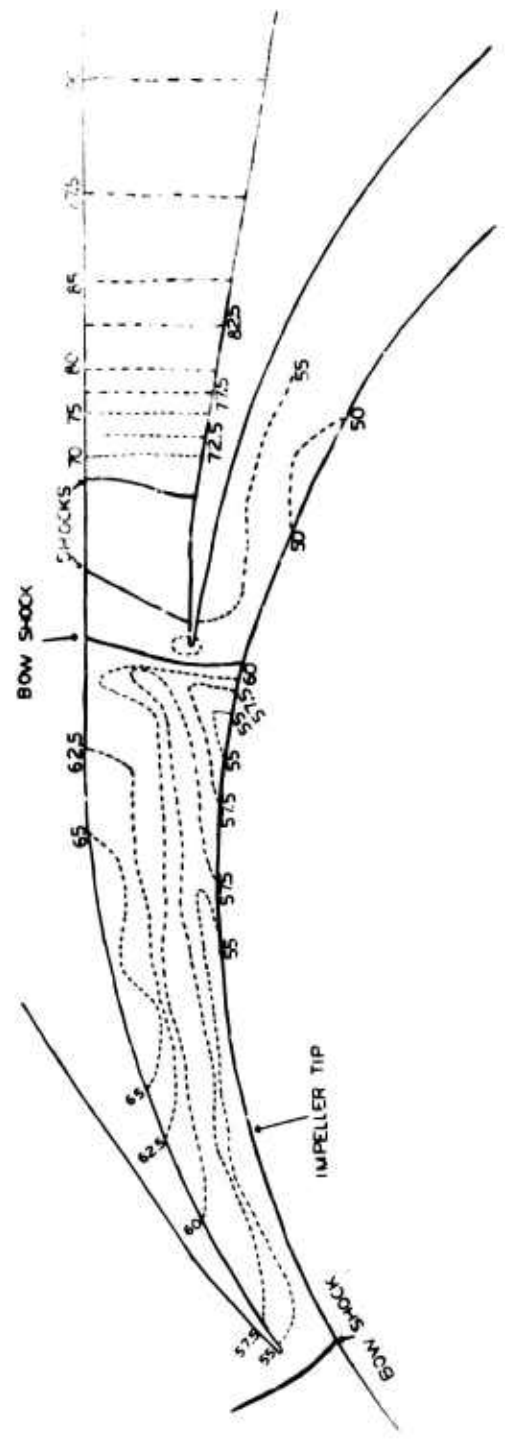


Figure 166. Isobarics Measured in Workhorse Diffuser (Numbers on Contours are p).

We must remember, however, that pressure signals can be transmitted in the supersonic two-dimensional flow across the streamlines. Therefore, one region of the flow can influence another within the Mach cone of a disturbance. In this polar flow field, this can account for information being transmitted "upstream". Somehow compression or expansion wavelets are generated, propagated, and perhaps reflected from the circumferential sonic line inside the impeller to accumulate ahead of the throat entry shock and adjust its Mach number to an appropriate value for the channel throat area, mass flow, and stagnation conditions.

It is not at all plain how this complex interaction occurs, although it seems to be reasonable physically. The conditions downstream of the entry shock could propagate across the streamlines toward the center of the impeller and there generate some sort of wave pattern, perhaps by reflecting from the sonic line, which is sketched in Figure 134, to reflect back into the region ahead of the shock. Not until competent mathematical solutions for these flows are available will such questions be answerable in detail.

The channel entry shock resembles a detached bow wave ahead of a propulsion engine inlet. If the throat Mach number is subsonic, as it was in all of the Boeing-AVLabs designs, then the bow shock must be detached or, in the limit and under only one particular set of conditions, attached to the vane leading edge. In general, there will be a strong adjustment of the flow behind the entry shock as the subsonic streamline pattern develops to provide the required flow through the diffuser throat. In some cases, the flow should "spill" around the vane leading edge as suggested in Figures 133 and 134. In other cases the captured area will exceed the throat area. Boeing-AVLabs observed large changes of sign and magnitude in the pressure gradient across the stagnation point streamline near the vane leading edge. These changes are caused by the subsonic streamline pattern adjusting to satisfy continuity.

The diversion of a subsonic flow around the vane leading edge causes a disturbance in the supersonic streamline pattern near the suction surface leading edge. In numerous cases, a low-pressure region is found under the vane leading edge,

followed by a compression ramp, as is obvious in Figures 133 and 134. In many of the schlieren photographs, an optical density ramp is seen within one throat width on the lower side of the vane leading portion. This is plainly seen in Figure 32. At first glance, it is hard to explain this compression ramp in the supersonic flow. Because the impeller disc blocked the view, the schlieren was unable to trace the entry bow shock and the compression ramp far enough into the flow field to identify the full wave structure.

We have reconstructed the flow field as shown in Figures 133 and 134. The compression ramp is identified to be generated by Prandtl-Meyer wavelet expansion from the vane tip, reflected from the trailing portion of the entry shock.

A careful study of the sequential photographs taken by Boeing-AVLABS at different impeller positions shows that this compression ramp sometimes disappears, although we have been unable to correlate that with impeller position. We would expect this particular wave structure to be sensitive to impeller position because the jet-wake pattern disturbs it. The rest of the shock pattern is not. We have not worked out a detailed hypothetical picture of the transient wave behavior as the impeller turns under the diffuser.

The pressure field of the vanes near the vane leading edge is a principal perturbation to the circumferential pressure distribution around the tip of the impeller (and down into the inducer too); see Figures 133 and 93. Normally there is a high-pressure region just ahead of the bow shock, followed by a considerable pressure depression under the suction surface of the vane. Rather large excursions were observed by Boeing-AVLABS for the RF-2, as may be seen in Figure 93. Peak-to-peak excursions of 25 psi were observed; a 1.0-psi variation was not uncommon. These values represent 50% and 20%, respectively, of the total impeller static pressure rise. Because impeller tip pressure has such a strong influence on the relative flow pattern in both velocity and direction, we can anticipate a significant disturbance of the relative flow caused by the impeller turning through the pressure field of the diffuser vanes.

Ahead of and below the vane leading edges, there is a sonic line extending downward toward the impeller tip; see Figures 133 and 134. Across this line, the flow accelerates from subsonic behind the shock to supersonic again. The sonic line also extends above the vane tip, across the channel, all the way to the far wall.

Further details are observed around the nose of the vanes which may contain important information. Unfortunately, there is not sufficient static pressure data or corresponding schlieren photographs in these regions so that we can be certain of a detailed diagnosis. In any event, the shock pattern under the diffuser vane on the suction surface may not be of much consequence. Even if it is of consequence, we do not know how to handle it quantitatively.

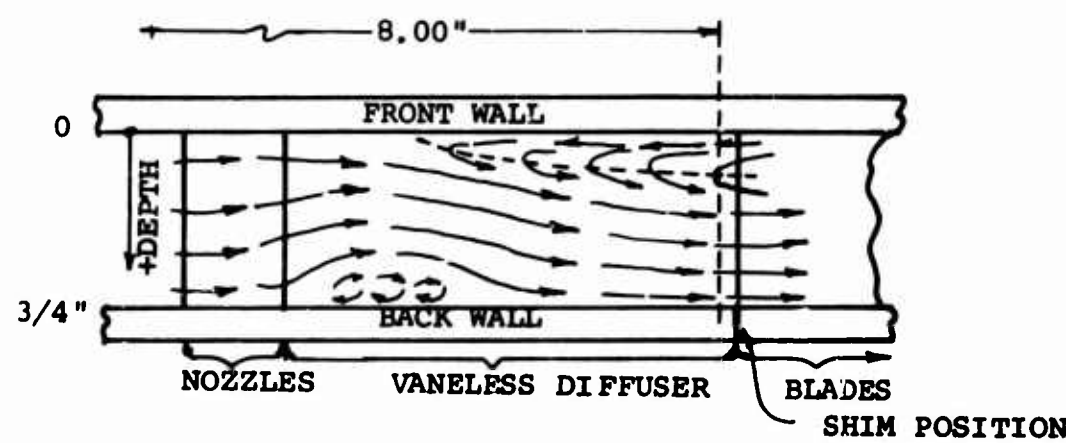
#### 6.8.1.2 Sidewall Boundary Layer Effects

Skewed boundary layers sweep out of the impeller and onto the diffuser sidewalls. As these boundary layers travel outward, the tired fluid near the walls must negotiate the same pressure "hill" that the main flow is climbing. But the tired fluid near the wall has much less radial momentum and so soon loses that. Then the limiting streamlines become tangential on the wall, and the three-dimensional flow separates as observed in Faulders' (1954) diffuser inlet by Johnston (1954), Figure 167.

An outline of a cover-wall static bubble, estimated from pressure differences between cover and hub walls, is sketched in Figure 134.

This sidewall separation may have little consequence if it does not accumulate into a large pool of stagnant fluid and if the tangential limiting streamlines do not continue to turn and dive back into the impeller.

As explained below, no competent theories are available, nor can they be soon generated, for calculating the three-dimensional sidewall boundary layer flow in the diffuser entry region. And very little experimental data is available except for some studies showing oil streak patterns. Some of these show gross backflow (see Figures 162 and 163) while others show only slight evidence, as



DEDUCED RADIAL FLOW PATTERN IN  
THE VANELESS DIFFUSER ASYMMETRICAL CASE

**Figure 167.** Diffuser Sidewall Separation Measured by Johnston (1954) in Faulder's (1954) Vaned Diffuser.

does Figure 33 from the Boeing-AVLABS work. Already, we have discussed the uncertain meaning these traces made in unsteady flow (Section 6.7).

In Section 6.7, we estimated from the experimental data that about 7% of the RF-2 impeller torque was due to boundary layer backflow. Guessing at the change of angular momentum of the backflow, when traversing the impeller, as 70% of the tip speed, then back mass flow must be about 10% of the through flow. Part of this backflow seems to drain out of the wall boundary layers on their run from the impeller tip to the diffuser throat, because two-dimensional boundary layer calculations predict about twice the throat blockage measured (see Section 5.8.1). On the order of 10% of the through flow must be drained out of the boundary layers in order to explain the measured blockage. Perhaps this is where the backflow comes from thus making the boundary layer calculations and measurement in agreement.

Note that in all the data, no significant disturbances appear along the vane suction surface where one might expect, from first-order considerations, to encounter separation. However, when it is realized that there is very little diffusion along this surface, except near the leading edge due to the supersonic compression ramp discussed above, then it is not surprising that the boundary layer appears to be placid on this surface. Also, dynamic stability considerations indicate that separation on the concave surface is difficult because boundary layer fluid there is unstable and tends to be mixed rapidly into the through flow and because a separation bubble on that surface cannot steadily sustain the surrounding centrifugal pressure field caused by the general curvature of the flow. Thus, if separation did occur on the suction surface, one would expect it to be highly transient. Nevertheless, the schlieren photographs, taken with 1-microsecond exposures, do not show any such transient separation. Our studies indicate that the shape of the suction surface in the semivaneless region is of little consequence.

### 6.8.1.3 Shock Wave - Sidewall Boundary Layer Interaction

Welliver and Acurio (1967, 67-30) propose a model for the diffuser which importantly involves the channel entry shock/sidewall boundary layer interaction. It was speculated that when the strength of this shock reached a Mach number of around 1.2, it separated the sidewall boundary layer and greatly increased the channel throat blockage. The consequence was that the diffuser should suffer a drastic reduction in pressure recovery. Further, this occasion was speculated to cause a positively sloped pressure recovery versus mass flow characteristic of the diffuser which was claimed to be unstable and the cause of surge (refer to Section 6.9.3 for further discussion of surge).

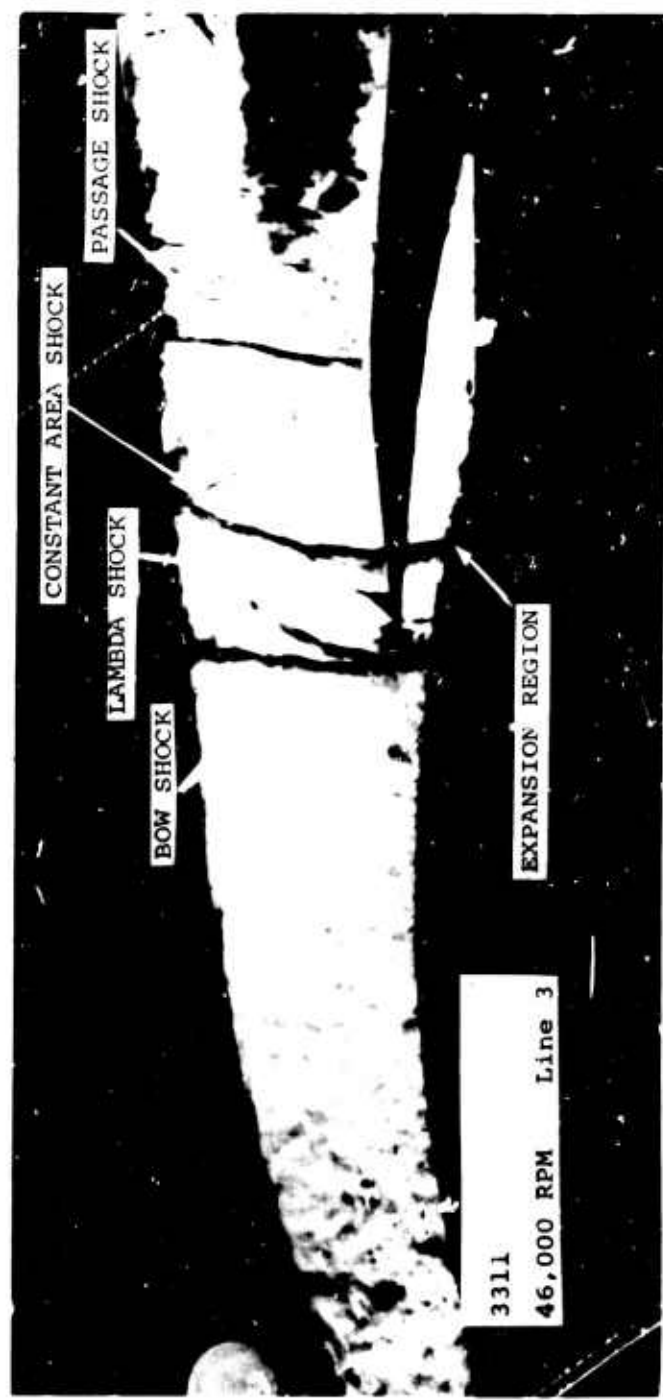
There is a normal shock in the constant area section ahead of the diffuser for Workhorse. The features of this shock structure are labeled in Figure 168, although substantially the same details may be seen in Figure 32. One possible explanation of this pattern is that the bow shock repeats through the diffuser passage in a manner similar to the repeating shocks observed in straight ducts with thick boundary layers. While there are striking similarities between the two cases, we think it more likely that transition and/or local separation of the laminar boundary layer on the vane tip causes the normal shock in the constant area section. The displacement thickness of the boundary layer decreases when the laminar to turbulent transition occurs, thus making the flow see a converging-diverging nozzle.

The above phenomenon does not seem to occur for RF-2, presumably because the constant area section is too short to cause transition. The laminar boundary layer in RF-2 must undergo transition soon, however, because it does not affect diffuser performance.

### 6.8.2 The Development of a Boundary Layer Analysis for The Diffuser Entry

Blockage is the single variable which primarily determines channel diffuser recovery, and the throat blockage is more determined by the velocity ratio from impeller to throat than by anything else. As a consequence, as the outflow

Figure 168. Diffuser Entry Shock Pattern.



tangential velocity from the impeller is raised, with rising work input, the boundary layer displacement thickness in the diffuser throat will increase because the throat Mach number must remain close to 1.0. Eventually there will be a work input which requires such a high velocity at the tip of the impeller that the boundary layer cannot negotiate all the way to the diffuser throat without separating. This limit is expected to keep efficient single-stage centrifugal compression below pressure ratios of 15:1 - 20:1.

The diffuser schedule from impeller tip to diffuser throat is of considerable importance. Adopting the most favorable diffusion strategy will change the throat displacement thickness by more than 50% compared to the worst strategy. For blockages on the order of 8 - 12% normally encountered, this 50% change will result in about 6 points change in diffuser recovery and 2 points in stage efficiency. However, our subsonic studies have convinced us that only a radical geometry change can change the diffusion schedules presently encountered.

Also, the throat blockage in contradistinction to the displacement thickness can be changed by changing the hydraulic radius of the passage. If very shallow throats are employed, blockage will soar for a given displacement thickness. Likewise, if very narrow throats are employed in a diffuser of many vanes with much excess suction surface area imposed, blockage will again soar. These tendencies are investigated in Section 6.9. There is an optimum throat aspect ratio, for a given displacement thickness and throat area, which minimizes throat blockage.

But yet we have no way to calculate the blockage expected in a given case. The rather marked insensitivity of the displacement thickness to geometrical alteration for the RF-2 and Workhorse seems fortunate; it could mean that experience can effectively replace theory. However, all of the geometry changes were rather minor for these machines.

The situation regarding the diffuser inlet sidewall and suction surface boundary layers might be tractable under these circumstances if it were not for our need also to be

able to estimate sidewall boundary layer backflow into the diffuser. That can vary by large amounts and is always significant when it occurs. In Section 6.7, we have deduced that backflow in the RF-2 impeller was responsible for as much as 7 points of lost stage efficiency. By decreasing the impeller tip width 25%, a 3-point increase in efficiency was won. No doubt a competent sidewall boundary layer theory is a must for the designer's tool kit if he is to keep backflow under control during optimization.

Consequently, we have considered means to generate a competent diffuser entry boundary layer theory. Unfortunately this need runs straight into a disability of modern fluid dynamics; that is, the general three-dimensional turbulent boundary layer is as yet unpredictable. Even for relatively simple, axisymmetric, or two-dimensional main flows, adequate boundary layer technique is not available.

In the axial compressor, whose fluid dynamic technology is far more advanced than the centrifugal's, the boundary layers on casing and hub cannot today be predicted adequately. Since stalling and deviations from two-dimensional cascade behavior occur most strongly near the casings, this gap in axial compressor theory is seriously hampering the improvements in that machine. But, in the axial, with its many blades and frequent transition from rotating to stationary blade rows, the situation is theoretically much simpler than for the centrifugal machine, which has few blades and far thicker boundary layers relative to the passage depth. So the prospects of generating an adequate sidewall boundary layer theory for the centrifugal are very dim now.

Nevertheless, we commissioned Professor George Mellor of Princeton University, who is currently working on the axial casing boundary layer theory, to assess the prospects of generating an adequate three-dimensional turbulent boundary layer method for the entrance region of the centrifugal diffuser. His report is included here:

"I have been asked to comment on the prospects for a theory capable of providing information on loss of efficiency and

flow blockage due to casing boundary layers. Fortunately, my remarks are conditioned by an extended research study I have undertaken as a consultant for Pratt and Whitney Aircraft applied to axial compressor casing boundary layers. Unfortunately, this work will not be released for general publication until September 1969. Nevertheless, some remarks can be made without violating Pratt and Whitney's proprietary rights.

"The equations of motion applicable to centrifugal compressor casings are:

$$\frac{\partial}{\partial x}(\rho r u) + \frac{\partial}{\partial y}(\rho r v) + \frac{1}{r} \frac{\partial}{\partial \theta}(\rho r w) = 0$$

where  $r = r(x, y)$  and

$$\frac{\partial}{\partial x}(\rho r u^2) + \frac{\partial}{\partial y}(\rho r v u) + \frac{1}{r} \frac{\partial}{\partial \theta}(\rho r w u) - \rho(w^2 + 2\Omega r w - \Omega^2 r^2) \sin \phi$$

$$= -r \frac{\partial p}{\partial x} + \frac{\partial}{\partial x}(r \tau_{xx}) + \frac{\partial}{\partial y}(r \tau_{yx}) + \frac{1}{r} \frac{\partial}{\partial \theta}(r \tau_{\theta x})$$

$$\frac{\partial}{\partial x}(\rho r u v) + \frac{\partial}{\partial y}(\rho r v^2) + \frac{1}{r} \frac{\partial}{\partial \theta}(\rho r w v) - \rho(w^2 + 2\Omega r w - \Omega^2 r^2) \sin \phi$$

$$= -r \frac{\partial p}{\partial y} + \frac{\partial}{\partial x}(r \tau_{xy}) + \frac{\partial}{\partial y}(r \tau_{yy}) + \frac{1}{r} \frac{\partial}{\partial \theta}(r \tau_{\theta y})$$

$$\frac{\partial}{\partial x}(\rho r u w) + \frac{\partial}{\partial y}(\rho r v w) + \frac{1}{r} \frac{\partial}{\partial \theta}(\rho r w^2) + \rho(wv + 2\Omega r v) \cos \phi$$

$$+ \rho(wu + 2\Omega r u) \sin \phi = - \frac{\partial}{\partial \theta} + \frac{\partial}{\partial x}(r \tau_{x\theta}) + \frac{\partial}{\partial y}(r \tau_{y\theta})$$

$$+ \frac{1}{r} \frac{\partial}{\partial \theta}(r \tau_{\theta\theta})$$

where:

x, y are coordinates parallel and normal to the casing wall and  $\theta$  is the circumferential coordinate. u, v, and w are the respective velocity components. r is the radial coordinate and  $\phi$  is the wall angle measured with respect to the axial direction.  $\tau_{xx}$ ,  $\tau_{yx}$ , etc., are combined viscous and turbulent Reynolds number stress components.  $\Omega$  is the rotational velocity of an impeller; in the diffuser section  $\Omega = 0$ . (A meridional projection of this coordinate system is shown in Figure 169).

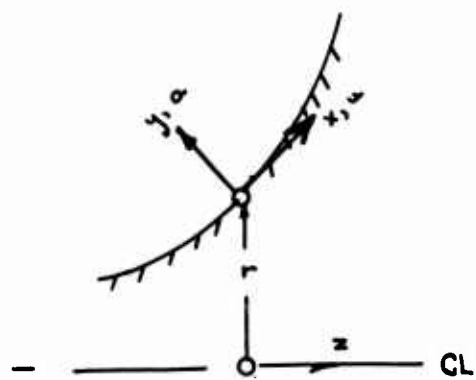


Figure 169. Coordinate System.

"Terms representing meridional curvature effects ( $R^{-1} = \partial\phi/\partial x$ ) have already been neglected. Note that such terms cannot be neglected in a mainstream potential flow calculation, but it is a valid simplification for the boundary layer region.

"The equations as they stand are, at present, completely intractable. However, they can be simplified by gap averaging; i.e., integrating the equation from one blade to another. Further 'boundary layer type' simplifications are then possible so that the resulting equations are:

$$\frac{1}{r} \frac{\partial}{\partial x} (\bar{\rho} \bar{u} \bar{u}) + \frac{\partial}{\partial y} (\bar{\rho} \bar{v}) = 0$$

$$\begin{aligned}
 \bar{\rho} u \frac{\partial \bar{u}}{\partial x} + \bar{\rho} v \frac{\partial \bar{u}}{\partial y} - \frac{\bar{\rho}}{r} (\bar{w}^2 + \bar{w}'^2 + 2\Omega \bar{r} \bar{w} + \Omega^2 \bar{r}^2) \sin \phi \\
 = \frac{\partial f_x}{\partial x} - \frac{\partial \bar{p}}{\partial x} + \frac{\partial}{\partial y} (\bar{\tau}_{yx} - \bar{\rho} u' v') \\
 \bar{\rho} u \frac{\partial \bar{w}}{\partial x} + \bar{\rho} v \frac{\partial \bar{w}}{\partial y} + \frac{\bar{\rho}}{r} (\bar{w} \bar{u} + \bar{w}' \bar{u}' + 2\Omega \bar{r} \bar{u}) \sin \phi \\
 = \frac{\partial f_\theta}{\partial x} + \frac{\partial}{\partial y} (\bar{\tau}_{y\theta} - \bar{\rho} w' v') \\
 0 = \frac{\partial \bar{p}}{\partial y}
 \end{aligned}$$

"The overbars represent gap-averaged quantities. Stress-like terms such as  $w'^2$  and  $u'v'$  result from circumferential distortion and blade force terms such as  $\partial f_x / \partial x$  appear as a result of the gap averaging process.

"These equations can be solved with reasonable assumptions concerning  $\tau_{yx}$ ,  $\tau_{y\theta}$ ,  $u'v'$ ,  $w'v'$ ,  $w'^2$ ,  $w'v'$  and  $\partial f_x / \partial x$ ,  $\partial f_\theta / \partial x$ . For the near future, a practical ploy is to cast the equations in the form of simple integral equations in which case further empirical information relevant to boundary layer profile shapes is required.

"In the case of axial compressors we are now convinced that the integral equations together with a rational procedure to match boundary layer and main stream calculations and a procedure to jump from a rotating to a stationary coordinate system will provide a powerful new approach to compressor performance prediction. In fact, in hindsight, there does not appear to be any alternative since these equations represent relatively exact constraints on possible flow situations, and on any analytical model constructed to predict the flow. (In the case of axial compressor flows we observe that casing stall can be predicted; such predictions depend quantitatively but not qualitatively on the specific empirical assumptions.) Viewed another way the equations represent an opportunity to correlate the results of experimental observation in a rational way.

"The geometry of axial compressors does permit certain simplifications (e.g.  $\phi \approx 0$ ) not available to centrifugal compressors. Nevertheless, it is my strong conviction that, if significant further progress is to be made in our ability to predict centrifugal compressor performance, the approach outlined above cannot be bypassed. The question is not whether the theory will be useful, the question is how useful it will be. This question can only be answered by a relatively long range research program directed by the need to provide specific information required by the integral equations of motion."

In effect, Mellor advises that the generation of a complete, detailed, three-dimensional turbulent boundary layer theory which will competently handle the diffuser entry region is beyond present accomplishments. He recommends a quasi-axisymmetric approach which will recognize:

- (1) The skewed boundary layer leaving the impeller
- (2) The pressure fields of the vanes, by "smearing out" these influences into tangential averages.

This approach, he estimates, is in itself a large task well beyond the scope of the present program. But the work must be done eventually for, as Mellor says, "The question is not whether the theory will be useful, the question is how useful it will be."

We expect that Mellor's kind of theory will be useful for predicting the boundary layer blockage at the channel diffuser throat. Mellor does not consider in the discussion above the influence of shocks impinging upon the boundary layer. However, he could handle these in some sort of a quasi-two-dimensional way to impose in a mathematically tractable fashion the pressure forces that the shock imposes on the boundary layer.

The quasi-two-dimensional approach of Mellor probably would give a fair measure of the total boundary layer backflow into the impeller and of the propensity for this catastrophic pattern. Yet, Mellor's approach would not be intended to

produce an indication of the local strength of the backflow. Nevertheless, we expect that the quasi-two-dimensional result would be of great importance in design and perhaps adequate except for deciding how to configure the leading portion of the vanes. Probably Mellor's approach would not give sufficient information for setting the angle of the vane leading edge to minimize its impact on the boundary layer flow. Mellor's approach probably would not give an evaluation of the swallow-tail upstream extensions of the diffuser vane proposed in the past by Dallenbach and Van Le (1960), and more recently used by Morris and Kenny (1968) with their "pipe" diffuser.

As a result of this advice from Mellor and even more pessimistic advice from Johnston (1968), we have not attempted within the scope of this program to attack the improvement of the sidewall boundary layer theory.

#### 6.8.3 Qualitative Design Rules

While we do not have available a competent theory for the entry region of the diffuser, certain qualitative rules are obvious from the basic physics and experience available. Here we shall discuss these in preparation for using them in the parametric studies for redesign in Section 7.

##### Secondary Flow

The secondary flow of the sidewall boundary layers has two important consequences:

- (1) It may lead to backflow into the impeller.
- (2) It may significantly alter the boundary layer blockage in the diffuser throat.

However, when we consider these two consequences together, we are faced with the possibility of a "tit-for-tat" situation. In other words, moves that tend to reduce the backflow into the impeller may increase the blockage of the boundary layer in the diffuser throat. It is not at all plain whether a given reduction in backflow will lead to a gain in stage efficiency, a loss, or a null. We believe that the occurrence of backflow into the impeller has far more serious consequences than if the same amount

of "tired" fluid were passed through the diffuser throat. In effect, the impeller reenergizes tired sidewall boundary layer fluid when it flows backwards and thereby permits that fluid to pass through the diffuser throat with vigor. The impeller is in effect a boundary layer energizer.

There are other ways to energize this fluid if it can be caused to mix with the main flow, but that leads to increases in entropy also. The forward swallow-tail extensions of the pipe diffuser of Morris and Kenny (1968) are claimed to act as boundary layer fences while they roll up vortices and cause mixing of the sidewall boundary layer. Morris and Kenny assert that this is a positive benefit, and one would anticipate from other fluid devices that it may be. This approach has the virtue that it can give the tired boundary layer fluid radial momentum, which is what is needed to carry it out in the diffuser.

When the boundary layer slips back into the impeller, it is primarily given tangential momentum which helps the fluid to balance the radial pressure field imposed by the main flow. In fact, if the boundary layer fluid leaves the impeller with a higher slip factor than the main flow, it will dynamically tend to move outward rather than flow backward.

We see that the energizing mechanism of the passive mixing devices compared to the impeller are basically different and, while they both discourage backflow, they probably have different trends.

From an overview, we expect that it pays to avoid boundary layer backflow into the impeller.

#### Impeller Distortion at Discharge

Other than the inevitable mixing loss which must occur at the tip of the impeller when the flow is separated, three-dimensional distortion of the impeller discharge does not appear to be significant except as it affects the sidewall boundary layers. There is no evidence we can discern in the Boeing-AVLABS experience to suggest that the skewed flow coming from the impeller into the diffuser causes any

significant disturbance at the vane leading edges. One might expect that the skewed flow, which causes high incidence near the walls, might lead to adverse separation. While it might cause separation on the suction surface of the vane near the leading edge, this does not appear to be significant, although it may cause some minor losses.

The vane does not stall on the suction tip at high incidence and separate all the way back to the throat, as one might expect for a conventional airfoil. High incidence of the flow in the boundary layer is probably the cause of the lambda shock on the pressure surface of the vane in the throat as seen in the Boeing-AVLABS schlieren pictures. But this shock does not seem to have any primary influence on diffuser behavior because, as we have shown in Section 5.9, diffuser performance seems to agree, within the data uncertainty, with the laboratory straight-channel diffuser empirical results.

On the other hand, in the Boeing-AVLABS tests, bleed holes near the pressure side of the diffuser throat apparently improved the pressure recovery coefficient by several points. The results reported by Runstadler (1969) do not sustain the Boeing-AVLABS bleeding tests because he found no particular benefit from bleeding the boundary layer on one side of the diffuser passage at constant blockage. The Boeing-AVLABS bleeding probably did reduce the blockage and thereby may have produced the gains measured. (The overall gain, excluding the bleed loss, is not greater than 2 points. Including the lost bleed flow, a net loss of about 1 point was recorded.)

The critical aspect of impeller three-dimensional distortion at discharge is that a very thick separated region may exist on the cover side over most of the pitch between the impeller vanes. Thus there can be little radial momentum discharged from the impeller on the cover side, which means that backflow is very likely there. Johnston (1968) has suggested that rotating stall may occur on one wall of the diffuser (the cover wall) because the swirl angle of the flow there is so large. One can envision a flow pattern with rotating stall on one wall and unstalled flow on the other. Certainly this kind of behavior would not enhance diffusion nor impeller performance.

As a general rule, it is important to avoid extensive separation on the cover or the hub side and to keep the impeller separation as two-dimensional as possible in the  $r-\theta$  plane. This can be accomplished generally by minimizing the degree of separation at the impeller tip and by minimizing the sharpness of the meridional bend to radial in the impeller. The more sharply the impeller passage is turned, the greater the tendency for the separated jet to splash against the hub of the impeller. A theory is needed which will give guidelines for the penalty to be paid for meridional curvature. However, this penalty cannot be assessed directly, for it is so intimately tied up with the boundary layer behavior in the diffuser entry region. Qualitatively we can say that the meridional distortion should be minimized, but that is about all that can now be stated.

In order to minimize the general separation at the impeller tip, the tip depth should be made as small as possible, and the maximum diffusion ratio should be achieved in the impeller. High diffusion ratio, as discussed in Section 5.3, has a double benefit, for it raises the impeller tip static pressure and reduces impeller discharge mixing. It also tends to a much lesser degree, to minimize meridional distortion.

The limits to which the tip depth can be reduced below diffuser depth depends upon how successfully the rapid transition between impeller and diffuser can be carried out in the vaneless and semivaneless space. This subject will be considered further in Section 7.3.

#### Magnitude of Diffuser Vane Disturbance

There is no question that disturbance of the impeller tip region flow by the diffuser vanes should be minimized. In the past, there has been a tendency to use far fewer diffuser vanes than impeller vanes, which means that each diffuser channel is receiving the separated flow from several impeller passages. The situation is not probably as most view it, but more along the lines as shown schematically in Figure 139.

It is important to recognize that the boundaries between the wakes and jets coming from the impeller tend to lie more or less normal to the streamlines of the absolute flow. This means that the diffuser receives a pulsating flow. Some diffuser investigators feel this may actually enhance diffuser behavior by producing another mixing mechanism which can help to energize the diffuser wall boundary layers.

By using a large ratio of impeller vane number to diffuser vane number, the layers traveling through the diffuser tend to be thin compared to the depth and the width of the diffuser passage. However, we know of no evidence that proves this to be an advantage.

Rather, a better strategy would seem to be to minimize the extent of the diffuser vane pressure loading disturbance by making the vanes as small as possible. Therefore, within the limits of blockage and aspect ratio considerations, we recommend that the diffuser have many vanes. The implications of this recommendation will be seen in Section 7.4.

#### Choice of Diffuser Throat Area

One of the most critical choices in the design of a centrifugal stage is the diffuser throat area. There is an optimum choice of throat Mach number or pressure which will give the best combination of throat blockage, diffuser entry Mach number, pressure recovery through the entry shock, and channel diffuser recovery. Just how to strike the best balance is not entirely plain.

The extensive diffuser data now available from Runstadler (1969) in conjunction with the entry region flow model, discussed in Sections 6.8.1 and 6.8.2, enlighten the choice of throat Mach number. However, in the absence of a sidewall boundary layer theory and a means for predicting the shock pattern ahead of the entry, our tools are weak. Obviously, the throat Mach number cannot be chosen too low at the design point for there will be no range to surge under the presumption that surge occurs when  $M_x$  approaches 1.2, that is, when  $M_x$  is about 0.84. If the design throat Mach number is made 0.9,  $A/A^*$  changes by only 3% between

design and surge. A more significant change from surge to design is the typical reduction in blockage from about 0.15 to 0.10, which gives an added 6% flow increase. If we combine the two, it would not be hard to secure 8% to 10% flow range from surge to design.

From the design point to choke the  $A/A^*$  increases only about 1%, but there should be a further reduction of 0.02 to 0.04 in blockage, giving from 3% to 5% range from design point to choke. And beyond the critical point where the throat Mach number reaches unity, experience shows that another 2% to 3% increase in flow will occur, presumably due to thinning of the boundary layers in the throat by an influence of the back pressure reduction through the subsonic boundary layer from the diffuser into the throat. So, one may expect a range from surge to choke of 13 to 18%. This sort of range was actually achieved in a number of the Boeing-AVLABS stages. It would appear that a throat Mach number choice around 0.9 (with blockage taken into account) would be of the right order, although the final choice needs to be studied more carefully.

#### Shape of Vanes

The shape of the suction surface of the vanes does not appear to be of any great moment. The throat of the diffuser should be made short to avoid frictional losses and acceleration. The wedge angle of the vane probably should be kept small, although there is no direct evidence of the penalty paid for a thick wedge. Obviously a blunt leading edge symmetrically positioned will lead to a supersonic expansion around the nose of the vane onto the pressure side, which could cause a terminating shock and disturb the boundary layer significantly, as it does in an inducer. Therefore, the pressure surface of the vane should be aligned with the design flow at the channel entry (which is not predictable by any straightforward scheme). Any adverse flow adjustment due to blade thickness should be taken on the suction side where the supersonic overexpansion and recompression perhaps due to a shock, is not of any considerable moment because of the long distance for the boundary layer to recover before entering the next throat. Because there may be considerable curvature of the stagnation point streamline ahead of the vane leading

edge, the vane should be contoured to accommodate this incoming flow. We know of no successful means for predicting this detail, see Figure 170.

The vanes should be shaped in such a way as to tend to attach the entry shock to the leading edge of the vanes at the stage design point. However, it is not plain how to go about this task successfully. Probably there exists a vane shape which does not require flow spillage. This should permit the shock to closely approach the vanes. More work is in order in this region close to the leading edge of the vanes.

#### Throat Blockage and Diffuser Entry

The more critical aspect of the flow relative to diffuser performance is the inlet blockage at the channel diffuser throat. Every attempt should be taken to minimize this blockage. In Section 7, parametric studies will be made using existing models in an attempt to discover what sort of a vane arrangement is optimum from this point of view. Obviously, reducing the length of the wall over which the boundary layer must run from the tip of the impeller to the diffuser throat is a move in the right direction. On the other hand, putting the vanes too close to the impeller tends to increase their pressure disturbance upon the impeller flow and may tend to enhance backflow rather than reduce it. This depends in large measure on how close the boundary layer is to separating when it leaves the impeller. The low angle from the impeller should be minimized so as to reduce the length of run relative to diffuser throat. This also tends to reduce the tendency for backflow because the limiting streamlines are dragged more radial by the more radially directed main flow. Also, the flow near the wall tends to start into the diffuser further from the tangential direction, which delays separation and backflow.

#### 6.8.4 Practical Prediction of Blockage

While Mellor's approach may be tactically optimum, we will not have its results anytime soon. In the meantime, what can the designer do to predict throat blockage?

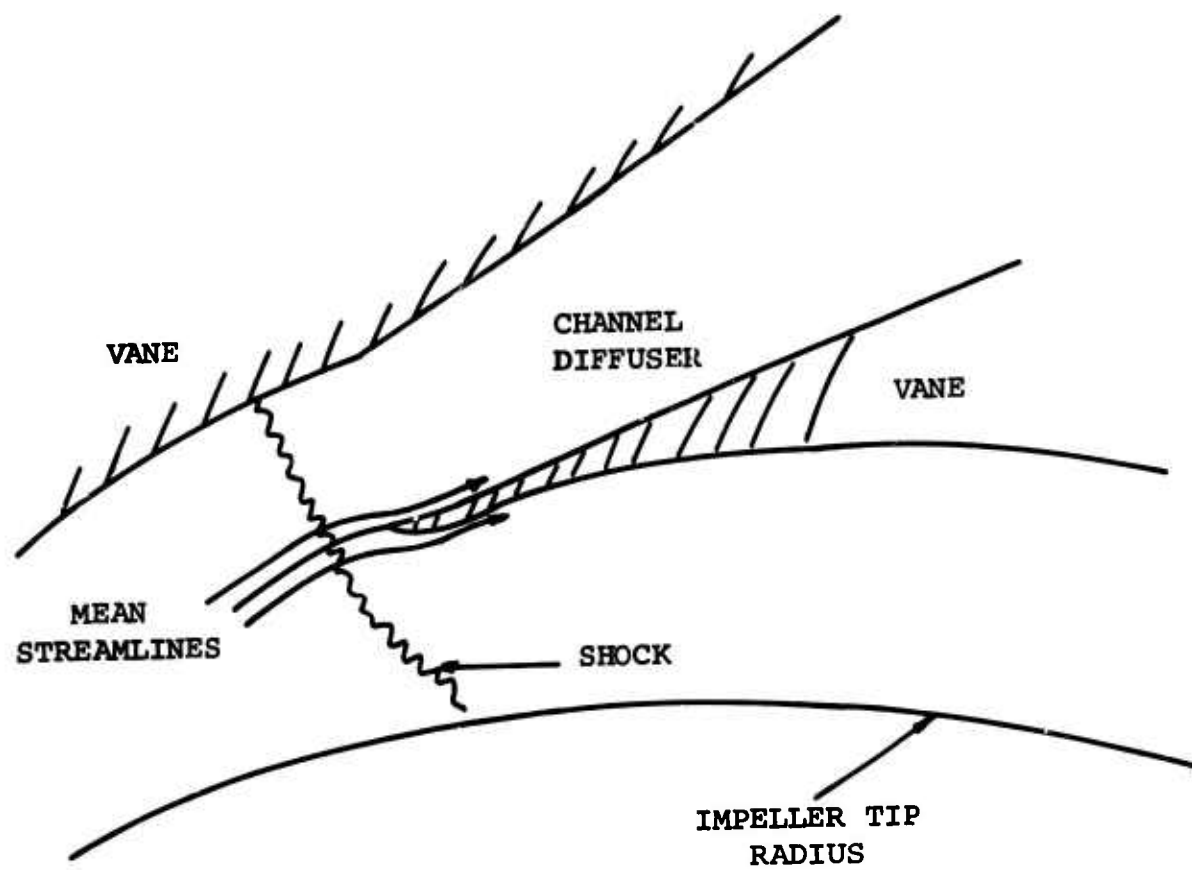


Figure 170. Vane Leading Edge Shape Concept to Accommodate Streamline Orientation.

The entry shock confounds the boundary layer analysis more than anything else. Is there a way to circumnavigate it?

In Section 5.8.1, two-dimensional turbulent boundary layer theory failed to predict adequately the blockage measured in the Boeing-AVLABS diffuser throats. The predicted blockage was from 30% to 80% greater than that measured.

On seeking a clue for the failure of the boundary layer theory, we note that diffuser throat blockage did not vary near surge nearly as greatly as had been expected by Welliver and Acurio from their Workhorse results (1967, 67-30). They hypothesized that blockage would soar as  $M_x$  of the entry shock approached 1.2. We can see some increase, but nothing that would be called "soaring". Does this suggest, perhaps, that the shock has far less influence on the boundary layer than formerly expected? Its influence appears to be even softer when we remember that the throat Mach number is decreasing toward surge so that the overall diffusion ratio from the impeller tip is generally increasing. This increase will increase the blockage, even in the absence of a shock.

Even though the entry shock is positioned ahead of the throat so that there is the possibility of flow spilling around the vane tip, the nearness of the shock to the channel entry and the shallow channel may make it behave similar to a shock in a constant area duct.

The work of Neumann and Lustwerk (1949) has demonstrated that the complex repeating shock systems found in constant area ducts generate an overall pressure rise closely corresponding to an abrupt, one-dimensional normal shock. Neumann and Lustwerk rationalize the unexpected results by postulating that wall shear stresses are negligible compared with pressure forces acting on the flow. Shapiro (1954) suggests that the shear stress at the wall may be zero because the shock system effectively separates the boundary layer from the wall.

In an attempt to explain the blockage anomaly, let us presume that the wall friction forces in the shock system are negligible, and that simple one-dimensional normal shock relations apply to the core flow outside of the boundary layer. Then across the shock,

$$\rho_x C_x = \rho_y C_y$$

from continuity. For the entire flow in the passage, the continuity relation must be

$$\rho_x C_x^{(A-\delta_x^*)} = \rho_y C_y^{(A-\delta_y^*)}$$

where  $\delta^*$  here represents the area blocked by boundary layer.

Hence, the assumption of a normal shock pressure rise imposes the condition that the displacement thickness of the boundary layer does not substantially change through the shock system. Because the simple normal shock model of the channel entry shock system, even when repeating, does work fairly well, we can extract the conclusion that the shock does not substantially affect the boundary layer displacement thickness. Therefore, if techniques can be developed for predicting the displacement thickness immediately ahead of the shock system, throat blockage will be known.

In Table XII, the boundary layer blockage calculated at the entry to the shock system by application of the Englert method to the measured pressure distribution in the RF-2 diffusers is presented and compared to the measured and calculated throat blockage. Certainly the calculated blockage ahead of the throat is closer to the measured value in the throat than the output of boundary layer calculations which passed right on through the shock to the throat. However, the blockages predicted ahead of the shock are not close enough to the measured values to give the designer confidence in using boundary layer calculations only up to the shock.

Before abandoning analysis and guessing at throat blockage, we must remember that the displacement thickness in the throat is primarily a function of the diffusion ratio from the impeller tip to throat Mach number and the length of the path over which the boundary layer grows. Also, we should remember that the entry shock strength will be mostly established by the throat Mach number picked by the designer. We have as a consequence the opportunity to

TABLE XII. DIFFUSER BLOCKAGE COMPARISON

Blockage Calculation Method	3354 Line 7	Test Number 3366 Line 5	Test Number 3369 Line 5
Data (Method 'b' in Table X)	0.095	0.119	0.128
Englert Method Ahead of Shock	0.123	0.118	0.157
Englert Method Extra- polated as Straight Line Through Shock Region	0.166	0.158	0.235
Englert Method at Diffuser Throat	0.201	0.234	0.271

extrapolate measured data, such as that taken in the Boeing-AVLABS program, using simple boundary layer ideas, from one diffuser to another. As long as the diffusion ratio remains unchanged (which it does for a given pressure ratio) and as long as we have blockage data for a stage of that pressure ratio, we should be able to calculate fairly accurately what throat blockage to expect as we vary diffuser geometry.

It is remarkable that, through all the Boeing-AVLABS experience with the wide range of diffuser types, all operating at roughly the same diffusion ratio from impeller tip to throat, the blockage observed varied only from 0.09 to 0.16. Some of this apparent range is occasioned no doubt by scatter in the data and through uncertainty introduced by the data reduction system. It would not be far wrong to say that all the Boeing-AVLABS diffusers had throat blockages of about 0.12. In Figure 171 the sensitivity of the diffuser may be appreciated. For aspect ratios near 1.0, uncertainty range in  $C_p$  is about  $\pm 0.07$  for the overall blockage range of the Boeing-AVLABS data of  $\pm 0.04$ . This  $C_p$  range amounts to a  $\pm 2$ -point variation in stage efficiency.

With a bit more empirical data on a given type of diffuser, the designer should be able to reduce his blockage estimation uncertainty to  $\pm 0.02$  or  $\pm 0.04$  in  $C_p$  and  $\pm 1.2$  points of stage efficiency.

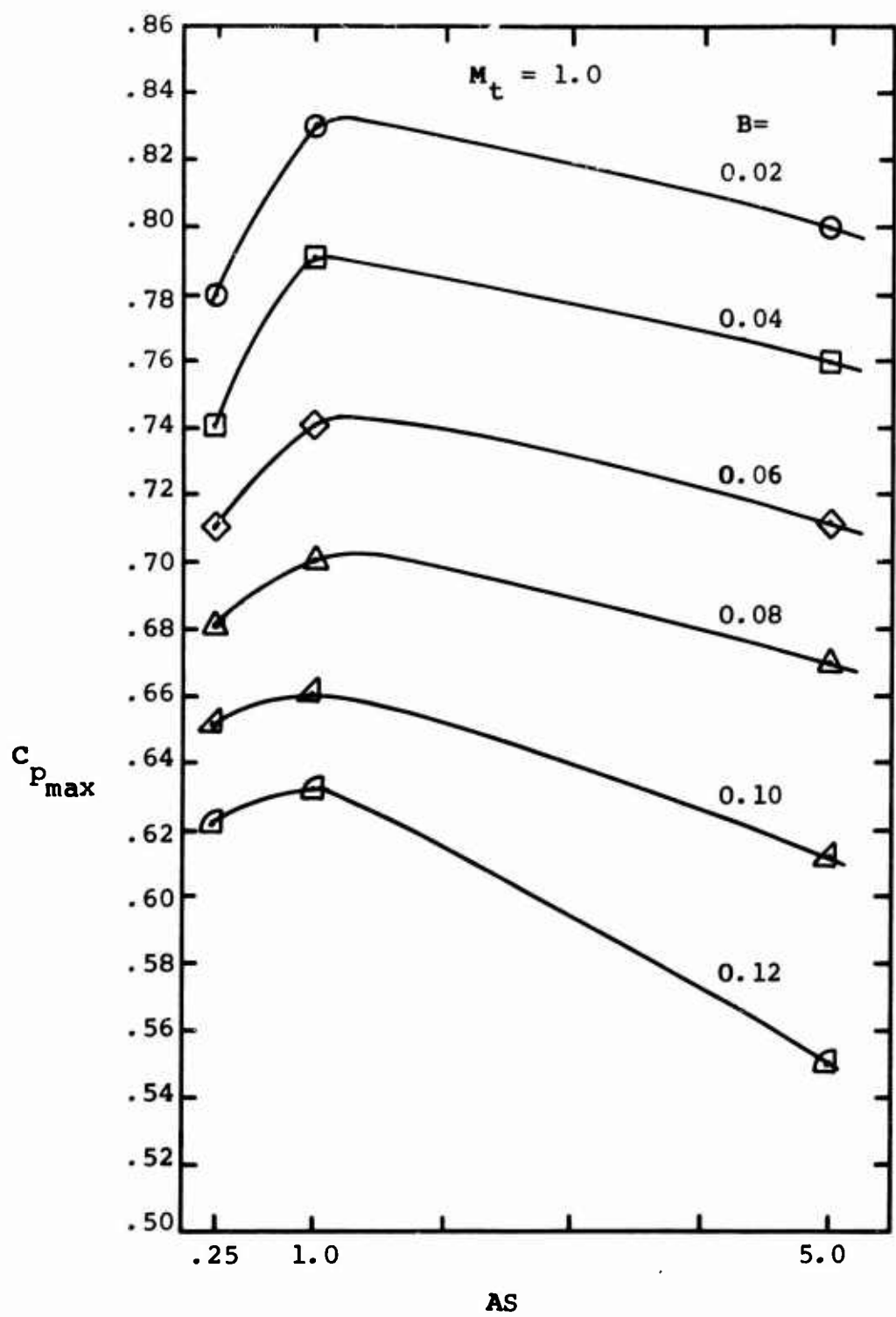


Figure 171. Variation of Channel Diffuser Recovery With  $B_4$  and  $AS_4$  (Runstadler 1969).

## 6.9 DIFFUSER DESIGN METHODS

### 6.9.1 Diffuser Passage Design

In conjunction with the design of the diffuser entry, the channel diffuser pressure recovery must be optimized. The vaned diffuser may take one of two forms illustrated in Figure 172, the cascade or vane-island. These types are distinguished primarily by the thin trailing edges of the cascade and thick trailing edges of the vane-island.

Although the cascade diffuser by the use of multiple rows may have some advantages in overall recovery, it is far less well understood and more difficult to optimize than the vane-island. Not only does the cascade have more variables to specify optimally, but its channel geometry is constrained by the number of vanes. The noncritical trailing edge thickness of the vane-island decouples the diffuser divergence angle from the number of passages and so presents the designer with an easier task.

Runstadler (1969) has presented a large collection of data on pressure recovery performance of straight channel rectangular diffusers over a range of geometries, inlet Mach numbers, and inlet blockages. While sufficient data are still lacking on the details of diffuser performance as a function of throat aspect ratio, this information supplies the designer with the necessary tools to appreciate the optimization trade-offs needed for the channel diffuser design.

#### Inlet and Geometric Variables

To a first approximation, the diffuser pressure recovery is a function of the diffuser geometry, inlet Mach number, and inlet throat blockage. Of these parameters, inlet Mach number is the weakest. This fact, coupled with the need to design the diffuser for close to choked flow at the throat, largely relegates the Mach number to secondary importance as a design parameter.

The geometric variables are diffuser aspect ratio,  $AS = b/W$ , the total divergence angle  $2\theta$ , and the diffuser center line length to width ratio,  $L/W$ . Diffuser area ratio is another

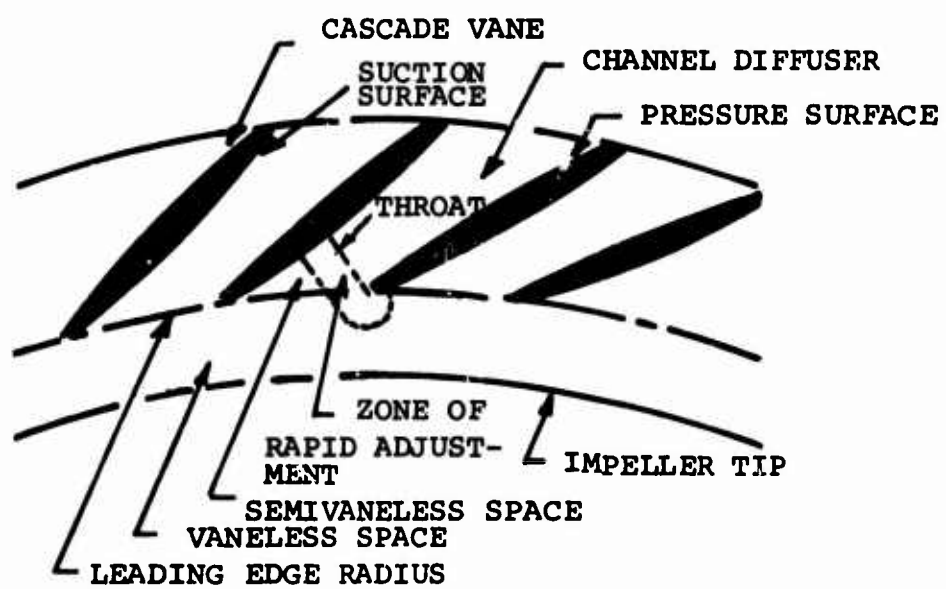
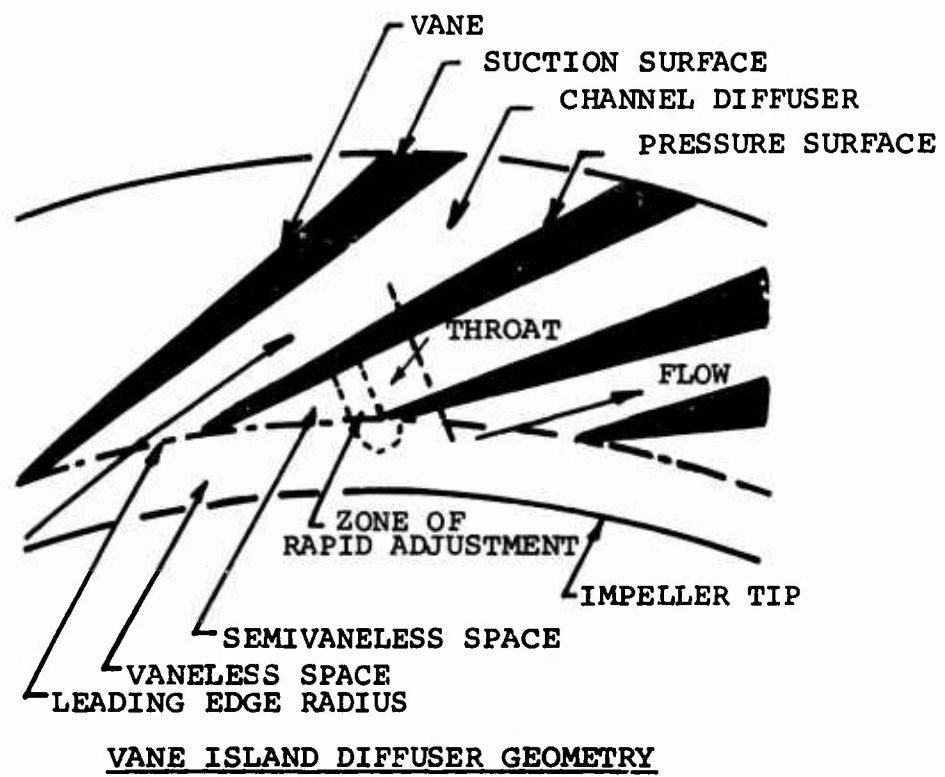


Figure 172. Cascade and Vane-Island Diffusers.

geometric parameter often used, but this is related to the preceding geometric variables by the equation

$$\text{Area Ratio} = AR = 1 + 2(L/W) \tan (\theta)$$

Of all the inlet variables, throat blockage is by far the most important. Every effort must be made to reduce the throat blockage to as low a value as possible. The selection of the design flow rate and the design of the inlet flow region will determine the growth of the diffuser boundary layers on the sidewalls, pressure, and suction surface and hence the blockage at the inlet throat. The selection of the diffuser throat area has a major effect upon the boundary layer displacement thickness in the diffuser throat by setting the overall diffusion required between the impeller tip and throat. However, even after selection of the diffuser throat Mach number which gives flow area, some opportunity remains to optimize the diffuser design.

For example,  $\theta$  and  $L/W$  should be optimized. Sometimes however, space limitations prevent  $L/W$  from being set at the best value, although that was not the case in the Boeing-AVLABS work. The diffuser performance maps (see Runstadler, 1969) must be consulted to obtain the optimum diffuser recovery. Examples of such performance maps, showing pressure recovery contours as a function of geometry and the inlet variables, Mach number, and blockage are given in Figures 173, 174, and 175 for  $M = 1.0$ ,  $B = 0.10$ , and  $AS = 0.25, 1.0$  and  $5.0$  respectively.

#### Blockage Versus Throat Aspect Ratio

Assuming a uniform displacement thickness on the sidewalls and diffuser suction surface at the throat, the relationship between throat blockage and diffuser throat width, aspect ratio, and inlet displacement thickness is

$$B = \frac{2\delta^*}{\sqrt{A_4 AS}} \left[ 1 + \frac{AS}{2} - \delta^* \sqrt{\frac{AS}{A_4}} \right]$$

$A_S = 0.25$   
 $M = 1.0$   
 $B = 0.10$   
 Rey. No. = 588,000

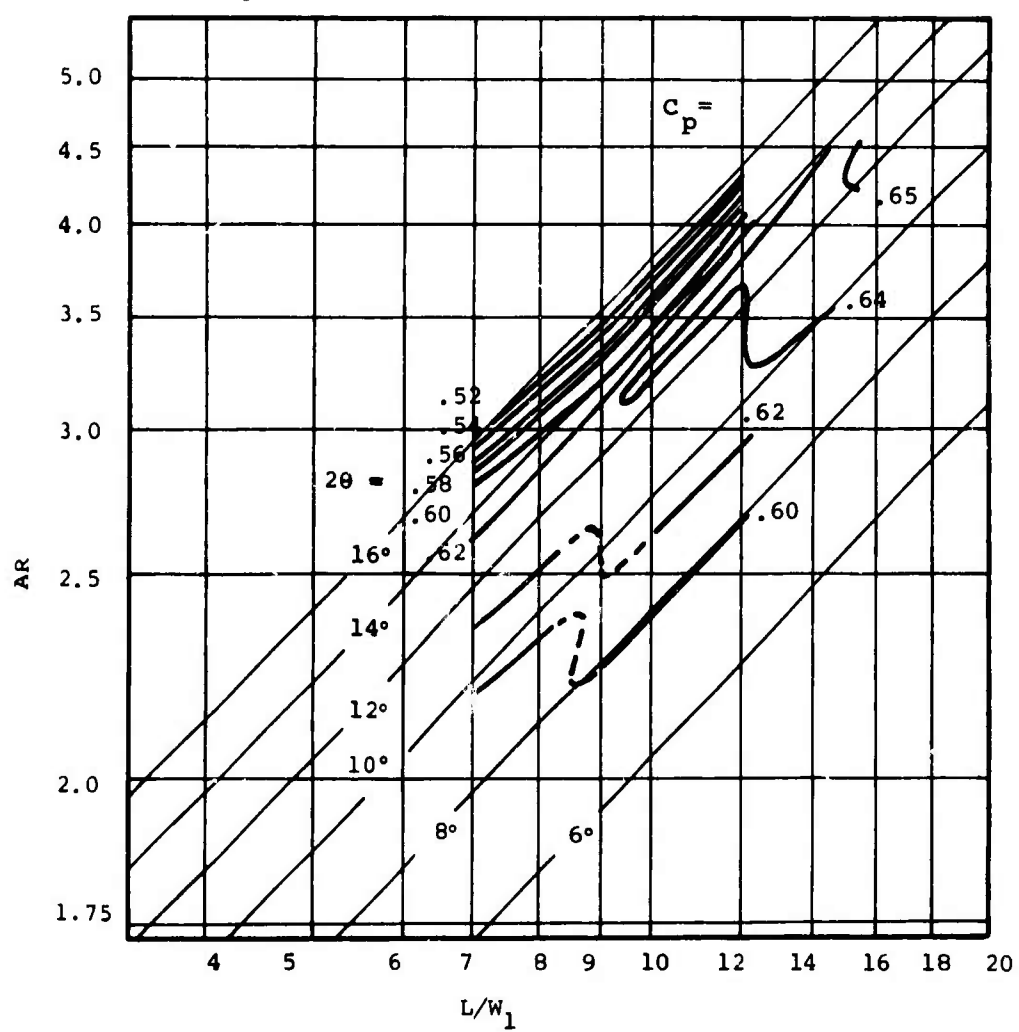


Figure 173. Straight-Channel Diffuser Performance  
(Runstadler 1969).

$A_S = 1.0$   
 $M = 1.0$   
 $B = 0.10$   
Rey. No. = 965,000

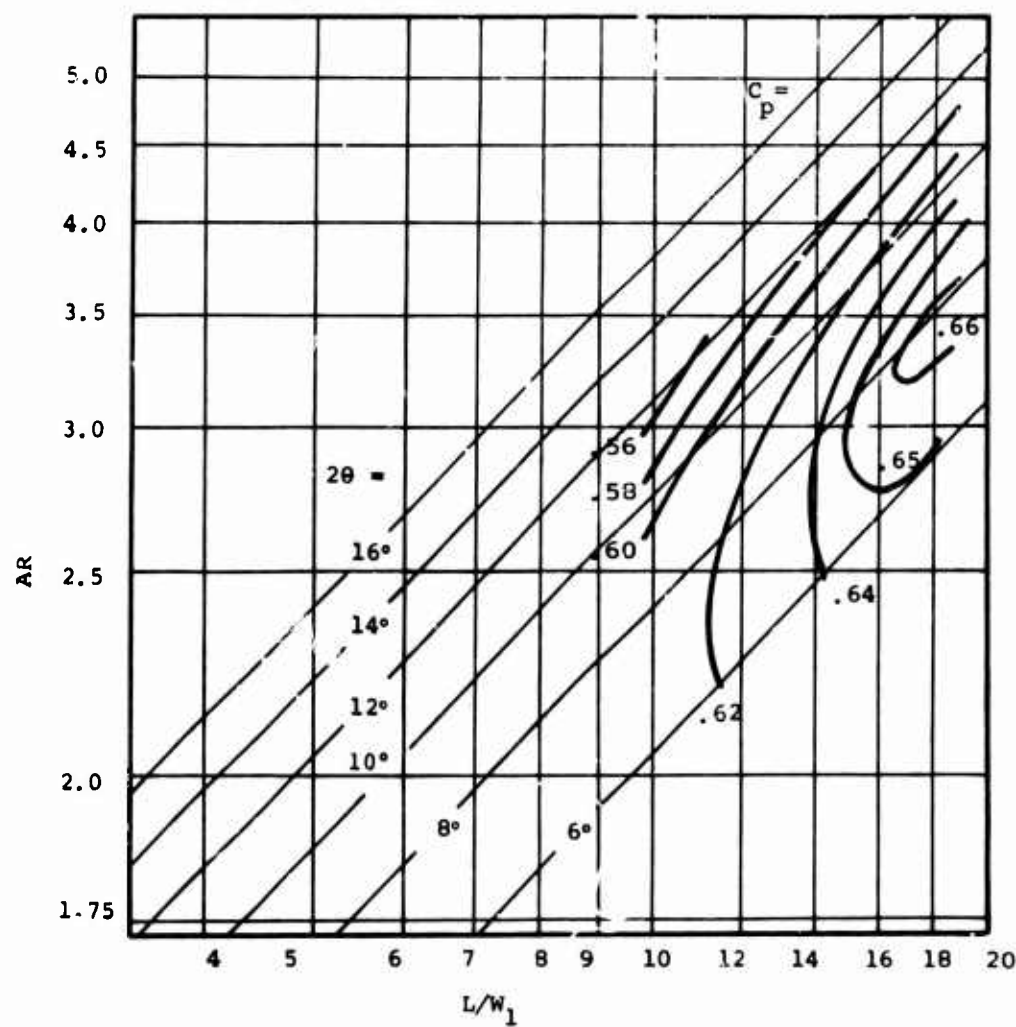


Figure 174. Straight-Channel Diffuser Performance  
(Runstadler 1959).

$AS = 5.0$   
 $M = 1.0$   
 $B = 0.10$   
Rey. No. = 740,000

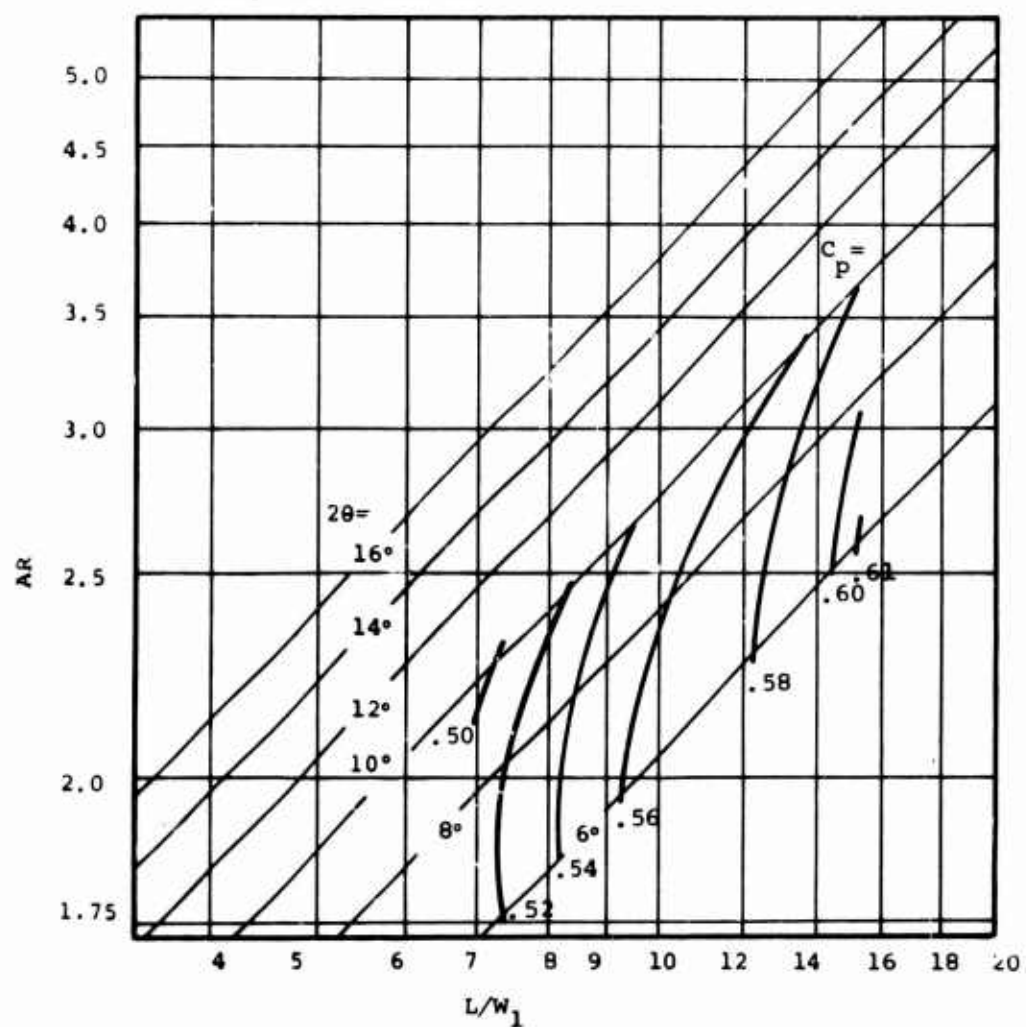


Figure 175. Straight-Channel Diffuser Performance  
(Runstadler 1969).

$$B = \frac{2\delta^*}{A} \left( \frac{b}{2} + \frac{A}{b} \right)$$

This expression is plotted in Figure 176 giving representative values for the RF-2 impeller. For a given displacement thickness  $\delta^*$  and throat area A, the minimum blockage occurs when the diffuser aspect ratio is 2.0.

A plot of diffuser pressure recovery as a function of aspect ratio showing the maximum pressure recovery available for a prescribed inlet Mach number of unity and constant blockage is shown in Figure 177 from Runstadler (1969).

Plainly, the aspect ratio at the diffuser throat is a powerful variable, as may be seen by examining Figure 177. While insufficient data are available to define precisely the influence of aspect ratio (see Runstadler, 1969), it appears that aspect ratios near 1.0 are probably optimum. Aspect ratios as low as 0.25 as used in Test 3369 for RF-2 in the Boeing-AVLABS program are too small, and a penalty is paid.

Thus, from a cursory examination, aspect ratio = 1.0 is an optimum design because such a design will have:

- (1) A low inlet blockage for given throat area and inlet  $\delta^*$ .
- (2) The highest pressure recovery performance for a given blockage.

However, limitations on the embodiment of the diffuser design in practice may force the design away from this "optimum", as trade-offs in performance with the rest of the compressor stage are required.

#### Cascade Diffuser Design

For the thin-blade cascade diffuser, the design may be forced away from the optimum design because the diffuser divergence angle is intimately tied to the number of diffuser vanes. (The diffuser divergence angle is approximately  $360^\circ$  divided by the number of diffuser vanes.)

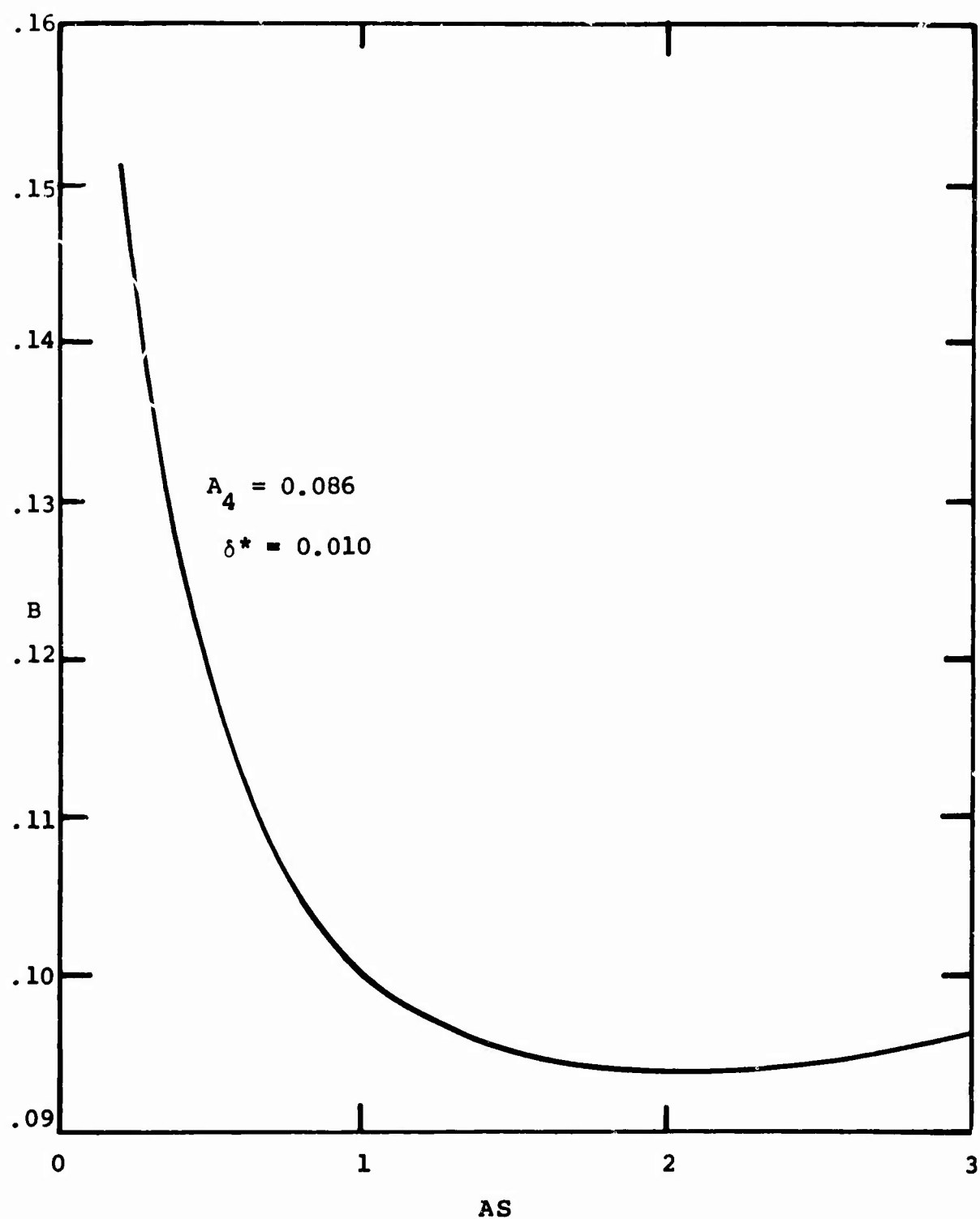


Figure 176. Variation of Blockage With Diffuser Throat Depth for Constant  $A_4$  and  $\delta^*$ .

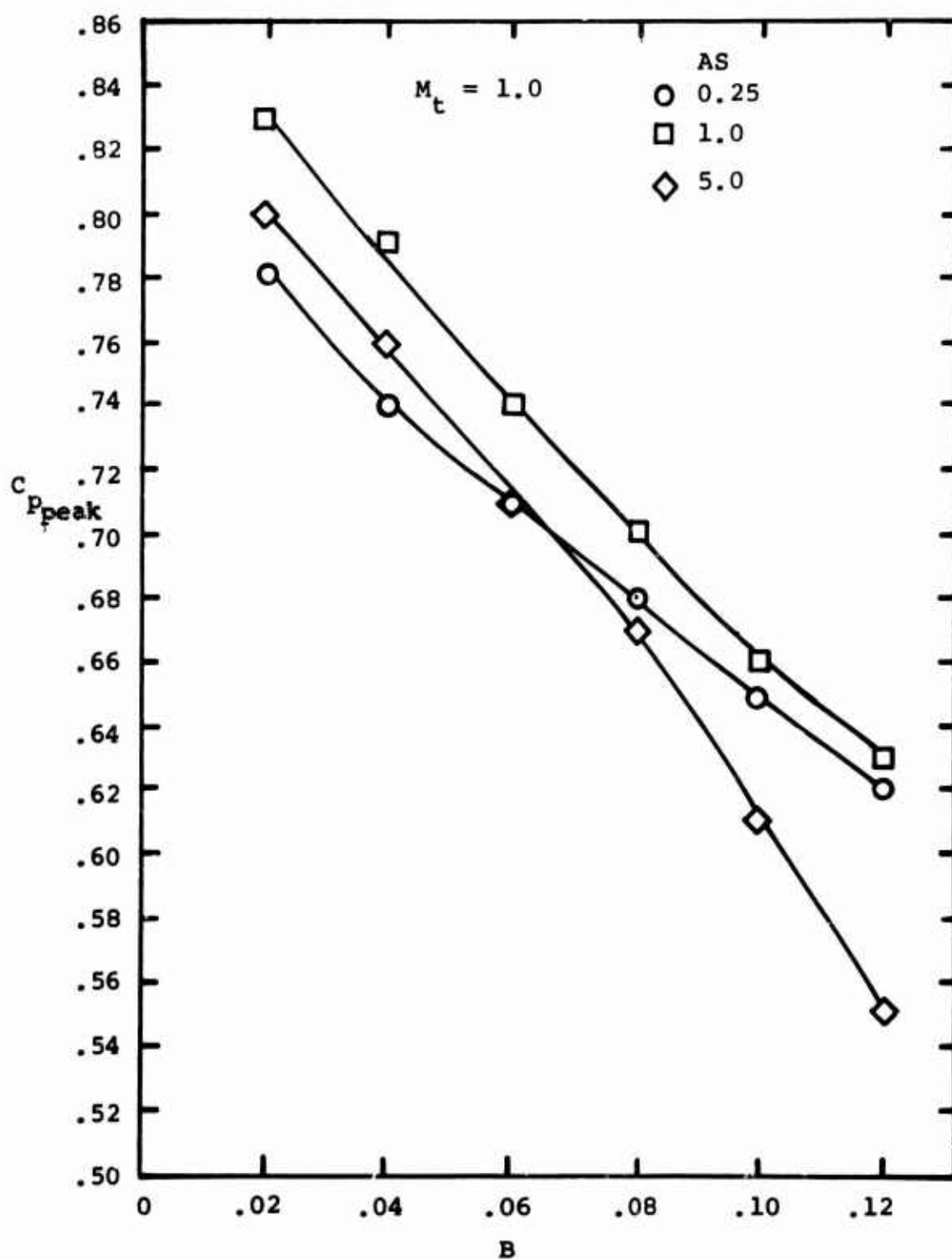


Figure 177. Variation of Maximum Recovery With Blockage.

For prescribed A and  $\delta^*$ , the throat blockage B will still be a function of AS as previously given except AS will now be a function of vane tip radius and setting angle,

$$AS = \frac{A_4}{\left[ 2\pi r_3 \left( \frac{\pi}{2} - \alpha_2 + \frac{\pi}{z} \right) \right]^2}$$

where thin vanes and large z have been assumed.

Thus the geometry is prescribed for the cascade diffuser once the vane leading edge radius, the number of vanes, and the impeller discharge flow angle are defined.

As the number of vanes increases, the throat width decreases, and the aspect ratio of the diffuser goes up. Unfortunately, along with this trend, the diffuser divergence angle  $2\theta$  increases, the throat width increases, and the aspect ratio goes down.

Although more detailed information on the behavior of pressure recovery with aspect ratio at values slightly less than and greater than unity are needed, the maps in Figures 173, 174, and 175 show the trends of the performance data with variation in AS,  $2\theta$ , and L/W. Referring to these maps, we see that the changes in diffuser parameters that arise from altering cascade geometry in general follow the shifts in location of the optimum or maximum peak recovery on these maps. At low aspect ratios, the higher recovery values occur at high divergence angles; while at large aspect ratios, the high recoveries occur at reduced divergence angles. For example, at aspect ratio = 0.25, maximum recovery occurs around  $12^\circ$ ; while at aspect ratio 5.0, maximum recovery occurs at about  $2\theta = 6^\circ$ .

While the trends are right, sometimes the values are not. There will be some geometries for which a good cascade diffuser cannot be specified. This problem is attacked (and solved) in Section 7. The cascade diffuser requires a very careful design optimization which can be carried out only with the type of information obtained by Runstadler (1969).

### Vane-Island Diffuser Design

The vane-island diffuser is freed from some of the constraints imposed upon the cascade. Now one is free, within broad limits, to choose independently the divergence angle, length to width ratio, and diffuser aspect ratio.

The same relations hold as before between blockage, displacement thickness at the throat, throat width, area and depth. It is desirable to keep the throat location close to the impeller tip in order to reduce the run of boundary layer between tip and throat and thus keep  $\delta^*$  as small as possible.

An important difference between the vane-island design and the cascade design is that the vane-island design does not allow multiple blade row diffusion because of the blunt trailing edges of the vane islands. The effect of this option is discussed further in Section 7 relative to redesign of the RF-2 stage.

#### 6.9.2 Secondary Effects

Although to a first-order approximation, the inlet parameters of Mach number and blockage are the most important to diffuser performance, other (secondary) effects also affect diffuser performance. Primary among the secondary effects are the inlet throat Reynolds number and turbulence level.

The data analysis comparing the RF-2 channel diffuser performance with the laboratory diffuser channel performance of Runstadler (1969) presented in Section 5.9 indicated that slightly higher pressure recovery in the centrifugal diffuser than was measured for the laboratory diffuser was obtained. Probably the primary cause of this increase was the high level of free-stream turbulence impressed upon the inlet flow by the impeller discharge jet-wake mixing process. This periodic jet-wake flow passing through the diffuser (see Figure 139) has the effect of imposing upon the boundary layers a high-frequency fluctuating flow that should appear to the boundary layers as free-stream turbulence. In the Boeing-AVLABS RF-2

impeller, the frequency due to the passing of jet-wake flow would be around 15,000 cycles per second. Such an increased free-stream turbulence level should effectively improve diffuser performance by promoting momentum exchange between the core flow and the boundary layers.

Runstadler's data on channel diffuser performance also showed, depending upon where the diffuser lay on the performance maps, that pressure recovery was a function of the throat Reynolds number. For diffuser geometries that are below the ridge of diffuser optima (see Runstadler, 1969) there was very little difference between pressure recovery performance over the 3:1 range in inlet Reynolds number (based upon inlet hydraulic diameter) in the range of Reynolds numbers applicable to the high performance, high-pressure-ratio centrifugal compressor diffusers discussed in this report. As it is desirable to design diffusers with divergence angles slightly below those corresponding to the ridge of optimum performance (in order to avoid the inherently unstable diffuser performance that occurs at larger angles), there should only be a small difference between diffuser designs which span a range of Reynolds numbers. The throat Reynolds number should be made as large as possible but this requirement may have to be compromised by other considerations. Depending upon the location of the diffuser geometry, a few points improvement in pressure recovery might be obtained by using the largest possible throat hydraulic diameter.

Runstadler's (1969) work has also shown that rounding the corners of the diffuser throat is of no particular help. Apparently, the detailed shape of the diverging sidewalls near the throat is not greatly significant. Having the diffuser diverge on one side or symmetrically does not appear to be of primary importance based on the Boeing-AVLABS work. There is some evidence that double divergence diffusers, which diverge in two planes, have inherent advantages over two-dimensional diffusers, but this certainly is not well proven. It must be remembered that in a practical machine the diffuser can diverge in the meridional plane entirely or partially. During development, the divergence usually is restricted to the r-θ plane for convenience. However, we emphasize that this may not lead to optimum diffusers.

Obviously as the diffuser is optimized, the optimum throat area must be maintained. Failure to observe this stricture is very common in much experimental work reported in the literature. For instance, vanes are often rotated (e. g., see Rodgers 1968), causing the area to change with everything else. Such a procedure is very poor, for it tends to confuse the optimization of the diffuser by mismatching the diffuser to the impeller.

#### 6.9.3 Surge Prediction Model

When designing a centrifugal stage, it is essential that accurate models be available for predicting the surge line and choking flow. The latter is considered in the next Section.

Welliver and Acurio (1967) hypothesized that stage surge is rooted in the diffuser. This opinion is strongly supported by the fact that the surge point of the stage, with an invariant impeller geometry, moved greatly as the diffuser geometry was altered. They also found that seemingly trivial disturbances in the diffuser could cause large changes in range. For instance, the condition of the caulking compound filling the small gap between the schlieren windows and diffuser sidewalls definitely had a major influence. Unfortunately, Welliver and Acurio did not dwell on these matters in their report, but their original data show strong effects without question.

It is also well known in the centrifugal compressor art that a given impeller configuration coupled with a vaneless diffuser of proper design will be stable over a much broader range than a vaned diffuser. And, with a properly sized vaneless diffuser, the impeller can work at low flow with high inducer incidence without destabilizing the stage.

No doubt it is possible to produce rotating stall in the impeller, but this does not usually seem to set the stage into surging. Nevertheless this common observation may be based on experience with impellers having poor internal diffusion ratios. Future experience may show that high diffusion impellers tend to destabilize the stage when operated at high inlet incidence. However, we know of no conclusive evidence which makes this outcome a certainty.

We hold little doubt that diffuser instability is most often the cause of surge. Therefore, we agree with Welliver and Acurio that the surge line location must be fixed with the diffuser and that an accurate model for doing so is essential in the designer's kit of tools.

As already shown in Section 5.8.2 the diffuser entry region flow model championed by Welliver and Acurio (with our support) is too vague for sufficiently accurate identification of the surge point. A correlation of blockage versus shock entry Mach number shows that the surging  $M_x$  lies between 1.15 and 1.25, but this latitude is too broad for competent design predictions.

Our desire here is to sharpen the surge predictions. In order to do that, we must examine more deeply the phenomena which govern diffuser stability. Unfortunately, too little data can be extracted from the Boeing-AVLABS set for better empirical guidance. What is needed is careful measurement of channel diffuser recovery as a function of mass flow. Because stability was not specifically explored in depth during the Boeing-AVLABS program, testing points were spread too far apart; particularly they did not creep up close enough to the surge line.

If critical stability experiments had been made, we expect that they would have shown the channel diffuser pressure recovery coefficient varying with mass flow as illustrated in Figure 178. In Figure 179 is plotted the data available from Table X, which does show similar trends.

The Welliver and Acurio diffuser flow model incorporated the sort of diffuser behavior portrayed in Figure 178. Below the mass flow for peak recovery, increasing blockage in the diffuser throat, caused by the strengthening entry shock with reducing flow, was hypothesized to degenerate channel diffuser recovery and cause the positively sloped portion of the  $C_p$  versus  $m$  curve.

Runstadler (1969) showed that diffuser recovery degenerates rapidly with increasing blockage. This trend is hypothesized to explain the low mass flow, positively sloped portion of the diffuser characteristic in Figure 178.

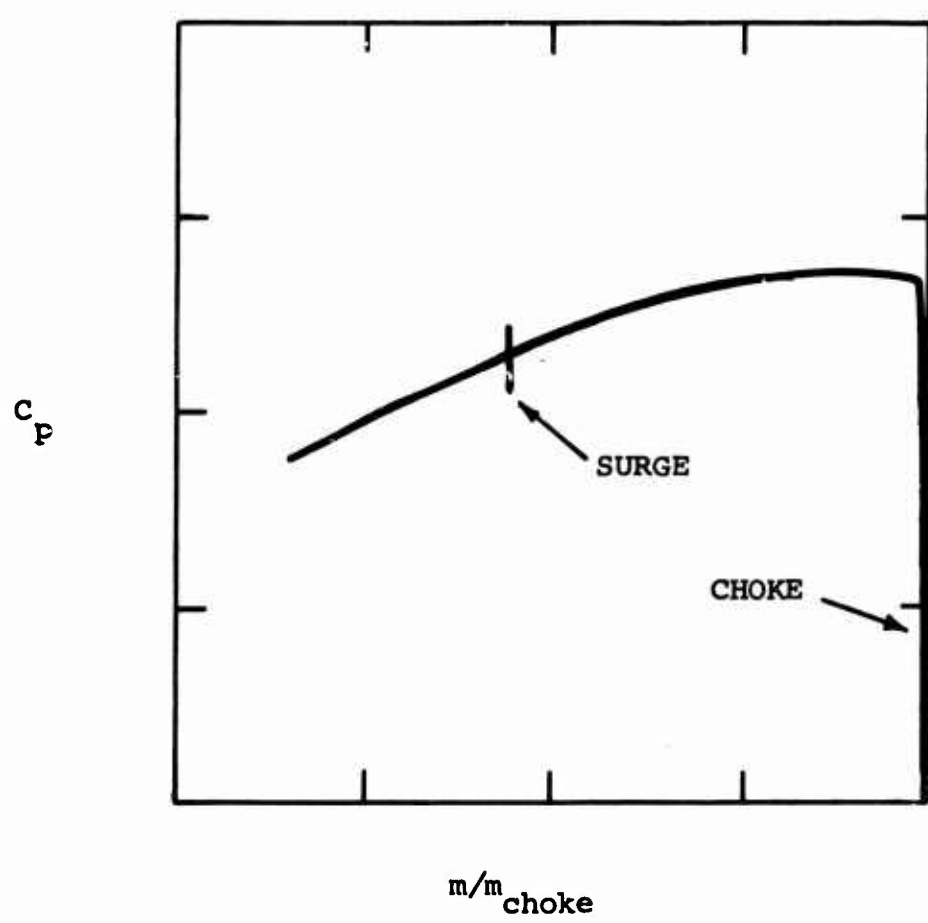


Figure 178. Schematic of Channel Diffuser Recovery Characteristic.

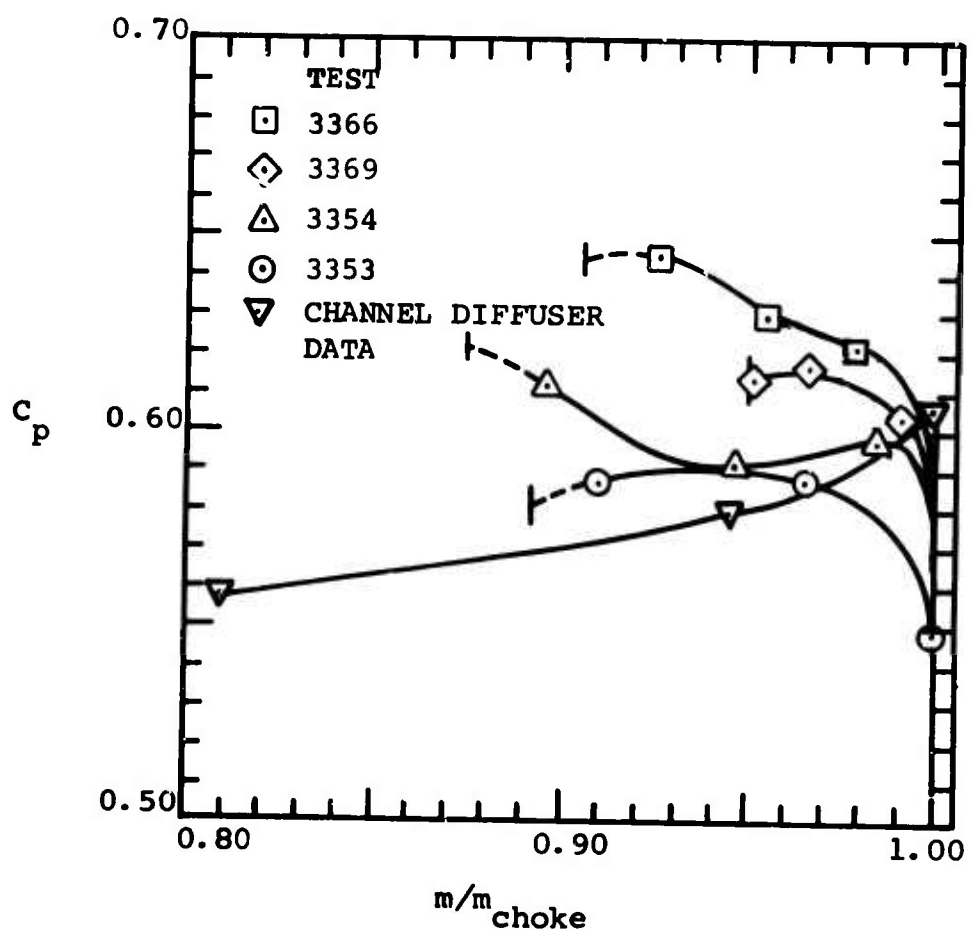


Figure 179. Channel Diffuser Pressure Recovery Versus Mass Flow.

At the high mass flow end near choking, the negative slope of  $C_p$  versus  $m$  is explained by the degeneration of recovery due to the increasing strength of the shock standing in the diverging portion of the channel diffuser.

In order to expand the flow model concept further, we shall here examine qualitatively reasons why the diffuser is believed to become unstable.

The basic physical fact of diffuser stability is that a number of diffusing channels are running in parallel. They take flow from the tip of the impeller and deliver it into a common collector. Whether the parallel array is stable depends on whether an individual diffuser, when disturbed, can still match the pressure rise produced by its neighbors. If the damaged channel fails in this attempt, it cannot match the collector pressure; thus flow through it would be expected to reverse. This breakdown is expected to cause rotating stall even as it does in axial cascades and compressors.

A stable diffuser array must have negatively sloped characteristics. Should the flow rate through one of the channels decrease momentarily, the pressure rise across the channel must remain constant if the array is to be stable. With reduced flow through the channel throat, the denominator of the pressure recovery coefficient,  $C_p$ , decreases. Therefore, if the pressure rise across the channel in the numerator of  $C_p$  is to stay constant, the pressure recovery coefficient itself must increase.

If the diffuser has a positive characteristic, then when the flow momentarily decreases, the pressure recovery coefficient through the channel will decrease and the pressure rise across the channel must fall. That is disastrous, for then this channel cannot match its neighbors. The flow through it will further decrease; probably it will eventually halt or even reverse.

So we expect then that the stage will not surge when the channel diffusers are operating on the negatively sloped portion of their characteristics.

We note in Figure 179 that some of the stages did operate stably (at least as far as the test operator was concerned) with positive slopes. It appears from this evidence, and other similar data, that the diffusers can operate slightly unstably without setting the stage into surge. Probably this is because the dissipative processes at work in the flow provide some damping, which can stabilize a slightly positive diffuser characteristic. Or it may be that the diffuser can suffer mild rotating stall on the positive part of its characteristic, without the transient disturbances becoming large enough to set the entire compressor system into oscillation.

For surge to occur, there must be a sufficiently strong driving oscillation as well as a responsive system. Often, turbomachinery is observed to run at flows just above surge in an unsteady fashion, which we believe signals that mild rotating stall is occurring, but it is too mild to overwhelm the system damping and set the machine into massive oscillation.

The mechanism of rotating stall and the transient flow patterns associated with it for the vaned diffuser of the centrifugal compressor are expected to be much like those well known for the axial compressor. That is, when one of the parallel passages suffers a flow decrease for any reason, the approaching flow diverges around this passage, causing disturbances in the two neighbor passages. One of these will be disturbed unfavorably compared to the other, causing it to become unstable and letting the stall propagate.

We expect in the centrifugal vaned diffuser that the spilling of flow out of the zone of rapid adjustment ahead of the perturbed channel causes high incidence on the vane leading edge, which stalls or at least significantly disturbs the suction surface leading into the next channel in the direction of impeller rotation. Therefore, the stall should progress in the direction of wheel rotation but at a much lower rotating frequency. To our knowledge, no definitive research investigations have been made of this matter, nor of centrifugal diffuser stability in general.

While the mechanisms proposed above seem entirely reasonable and consistent with known behavior of similar arrays of parallel diffusing passages in axial compressors and in cascades, the stability model does not offer us the quantitative information needed to predict surge. Plainly, the first thing we must be able to do is to predict the sort of channel diffuser characteristic shown in Figures 178 and 179. Laboratory diffuser studies do not appear to be any help in this matter as Figure 179 shows. Plainly, the flow adjustment and entry shock regions determine diffuser entry conditions and hence pressure recovery. As we have explained previously, the generation of a competent and general flow model for the diffuser entry region is well beyond the state-of-the-art today. Sufficient scientific understanding does not exist, particularly of the interaction of shock and the sidewall boundary layers in shallow channels, to build a theoretical model.

The problem of the stability of internal flows is a basic one which has not yet been resolved satisfactorily for any configuration. Kline (1959) emphasizes that the stability of internal flows is different from that of external flows, and he calls for research emphasis on this ubiquitous and critical problem. There has been, as far as we know, very little response.

We find ourselves, as a consequence of these deliberations and assessments, unable to produce a better diffuser-surge analytical model than that proposed by Welliver and Acurio. However, the existing model, despite its quantitative inadequacies, does form a credible skeleton to define critical experiments. We shall recommend in Section 8 that research aimed along these lines be carried forward in order that range and surge locations can be predicted and optimized along with the other features of the stage.

#### 6.9.4 Choke Prediction

No acceptable methods are available for predicting the choke point of the diffuser. Usually a 1% to 3% increase in flow rate occurs beyond the point where the core flow Mach number in the throat of the channel diffuser first

reaches the sonic value as given by the one-dimensional, isentropic, static-to-stagnation pressure ratio. This increase appears to be the result of disturbances fed back upstream through the "choked" throat in the subsonic portions of the boundary layers. These disturbances appear to thin the boundary layers sufficiently to provide the observed increase in flow to the ultimate choke point. Basic work on the three-dimensional aspects of the choked diffuser throat flow must someday be made to resolve the true throat flow behavior. The work of Bernstein, Heiser and Hevenor (1967) on mixed entropy nozzle flow should be a good starting point.

At present, our best procedure is to calculate the core flow "choke" point and to allow the 1% to 3% increase in mass flow rate to ultimate choke.

## 7.0 STAGE REDESIGN

The ultimate goal of this program is to make design recommendations for a pressure ratio of 10, 2 lbm/sec, 80% total-to-static efficiency centrifugal compressor stage. Insofar as possible these design recommendations were to be concrete and built upon a foundation of basic fluid dynamics that demonstrates the utility of fluid dynamic models.

We have been unable to effect completely on paper a concrete and detailed stage redesign. While the guidelines toward improved performance are straightforward, as elucidated below, the fluid dynamic prediction models are yet too weak to bypass empirical development. Actually, a substantial amount of development is required before stages with ultimate performance can be defined. However, the 80% target here still falls about 8 points below the ultimate performance envisioned by Dean (1968). So we have good expectations that the target can be achieved without extensive research or development. In Section 8, we lay out a research program with priorities indicated relative to the immediate target and to the ultimate achievement.

The design recommendations below should be regarded as guidelines. In order to appreciate them and make good use of them, what is known of the fluid dynamics must be absorbed from earlier chapters of this report.

We cannot pretend that these recommendations are infallible or perfectly optimized against one another. The insight into the fluid mechanics developed by Welliver and Acurio and furthered here goes far beyond the usual design knowledge for centrifugal compressors. We expect the recommendations below to have a certain validity that will point the route toward major improvements in performance with more certainty than exists now in the art.

### 7.1 INDUCER AND IMPELLER GEOMETRY TO SEPARATION

The importance of achieving maximum relative diffusion in the inducer has been thoroughly discussed in Section 5.2. Figure 112 clearly illustrates the potential gain for the Boeing-AVLABS stages of achieving a higher inducer diffusion ratio and consequently a lower relative Mach number at the impeller separation point. With an inducer tip relative Mach number on the order of 0.84, an increase of the tip mean diffusion ratio from the 1.37 achieved by Boeing to about 1.66 is estimated to give the stage the target efficiency of 80%, without any other changes. This requires a pressure recovery coefficient of 0.59 at the inducer tip. Based on axial compressor rotor performance, such recovery should be obtainable.

In order to make still further improvements in performance, we shall recommend other major design changes.

Because impeller discharge mixing losses are a major source of inefficiency, it is highly desirable to reduce the degree of separation at the impeller tip. Roughly, the loss of the radial "component" of kinetic energy is what is important to the mixing loss. This kinetic energy loss is dependent on the relative Mach number at separation and also on the wake fraction. Because the lower limit of relative Mach number for the separated jet is set by the attainable diffusion in the inducer, the Boeing-AVLABS impeller tip discharge area must be reduced in order to achieve a smaller wake fraction. For the RF-2 impeller, a reduction of the tip depth to about 0.10 inch (including clearance) would be required. If the diffuser is made the same depth, as is common practice, this results in a very shallow diffuser with a very low aspect ratio, on the order of 0.25, and increased blockage.

In order to keep the diffuser throat aspect ratio closer to the peak performance value of around 1.0 indicated by Runstadler (1969), and to minimize throat blockage, the diffuser depth should be on the order of 0.20. This criterion is in conflict with that above. Unless another way is found to resolve this dilemma, a reduction in impeller discharge mixing loss by the above procedure would lead to a commensurate decrease in diffuser recovery

and nothing much would be gained. Fortunately, there are several ways to attack this problem, some old and some new.

One proven method for reducing the impeller discharge area while at the same time maintaining satisfactory diffuser depth is to reduce the impeller diameter. Because the tip speed must be kept approximately constant, this requires a substantial increase in shaft angular velocity. Morris and Kenny (1968) arguing from the analysis of Balje (1960) also recommend this move on the basis of specific speed considerations. Figure 180 indicates that a specific speed,  $N_s$ , of 130 should give maximum performance.

Balje's curve in Figure 180 is overly pessimistic for low specific speed machines. For instance, the Boeing-AVLABS RF-2 stage impeller had a specific speed of 43, while Morris and Kenny's "H" rotor was designed at 70. According to Balje's curve, the RF-2 should have had 10 points lower performance than Morris and Kenny's "H" rotor. In fact, it produced three points better total-to-static stage efficiency. Obviously, Balje's correlation is not the entire answer. We find, however, on making detailed studies of stage design using the flow models offered herein, a considerable performance improvement resulting from raising the specific speed of the Boeing-AVLABS impellers closer to 100 as recommended by Morris and Kenny.

Unfortunately, when this is done, the inducer tip Mach number tends to rise greatly, as shown in Figure 181 taken from Morris and Kenny (1968). If the specific speed of the Boeing-AVLABS RF-2 design were simply raised to a value of 70 at pressure ratio 10, an inducer tip Mach number of about 1.1 would result. This high value can be expected to ruin the impeller's tip diffusion ratio and badly hurt impeller efficiency by increasing the discharge mixing losses as a consequence of the higher relative Mach number at separation. The penalty is a double one, for not only will the shocking phenomena on the leading portion of the inducer strengthen, and degenerate the internal diffusion, but also the higher relative Mach number at the leading edge requires greater diffusion in order to achieve the chosen low relative Mach number at separation. The influence of raising the inducer tip

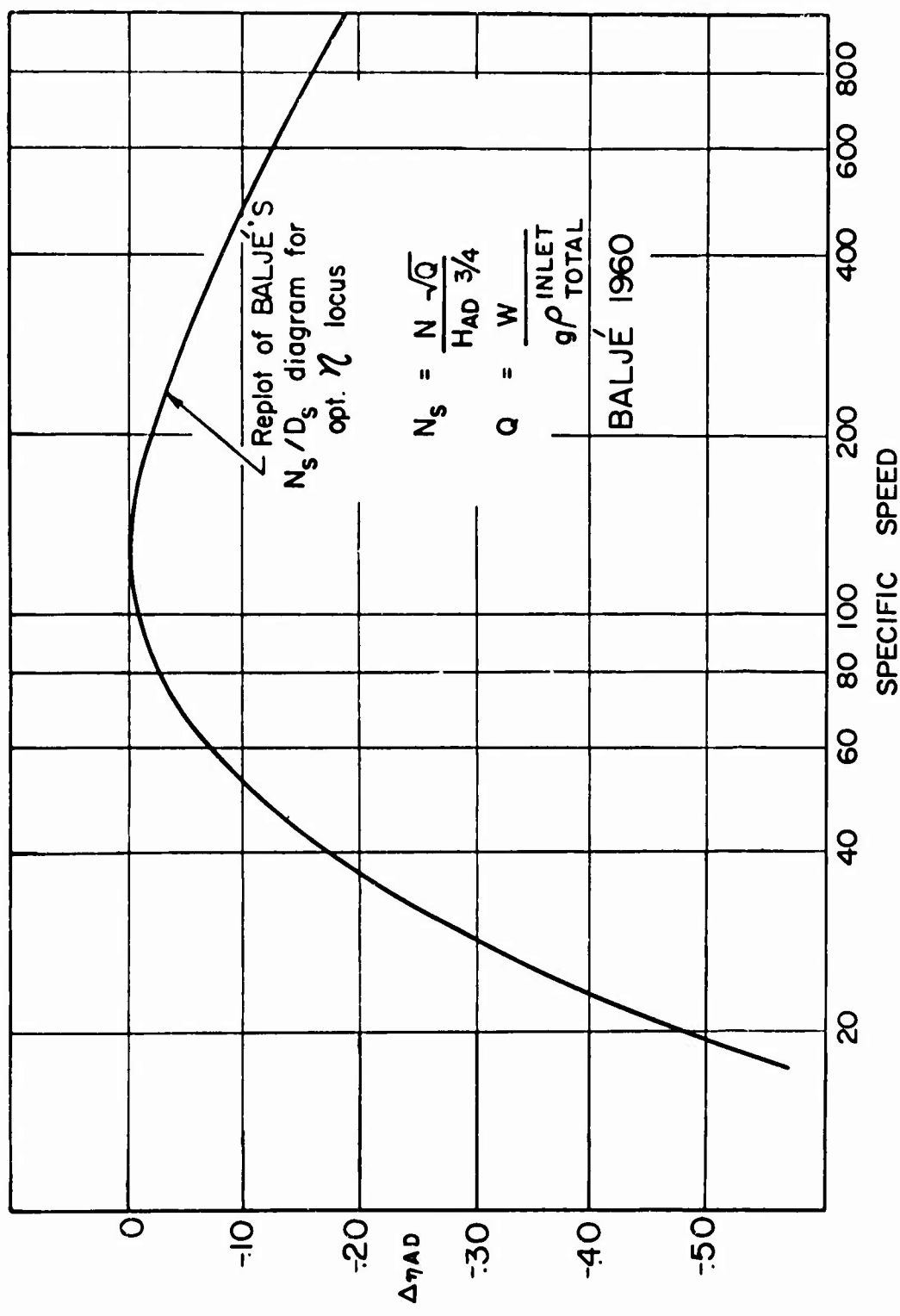


Figure 180. Balje's Correlation of Efficiency Versus Specific Speed.

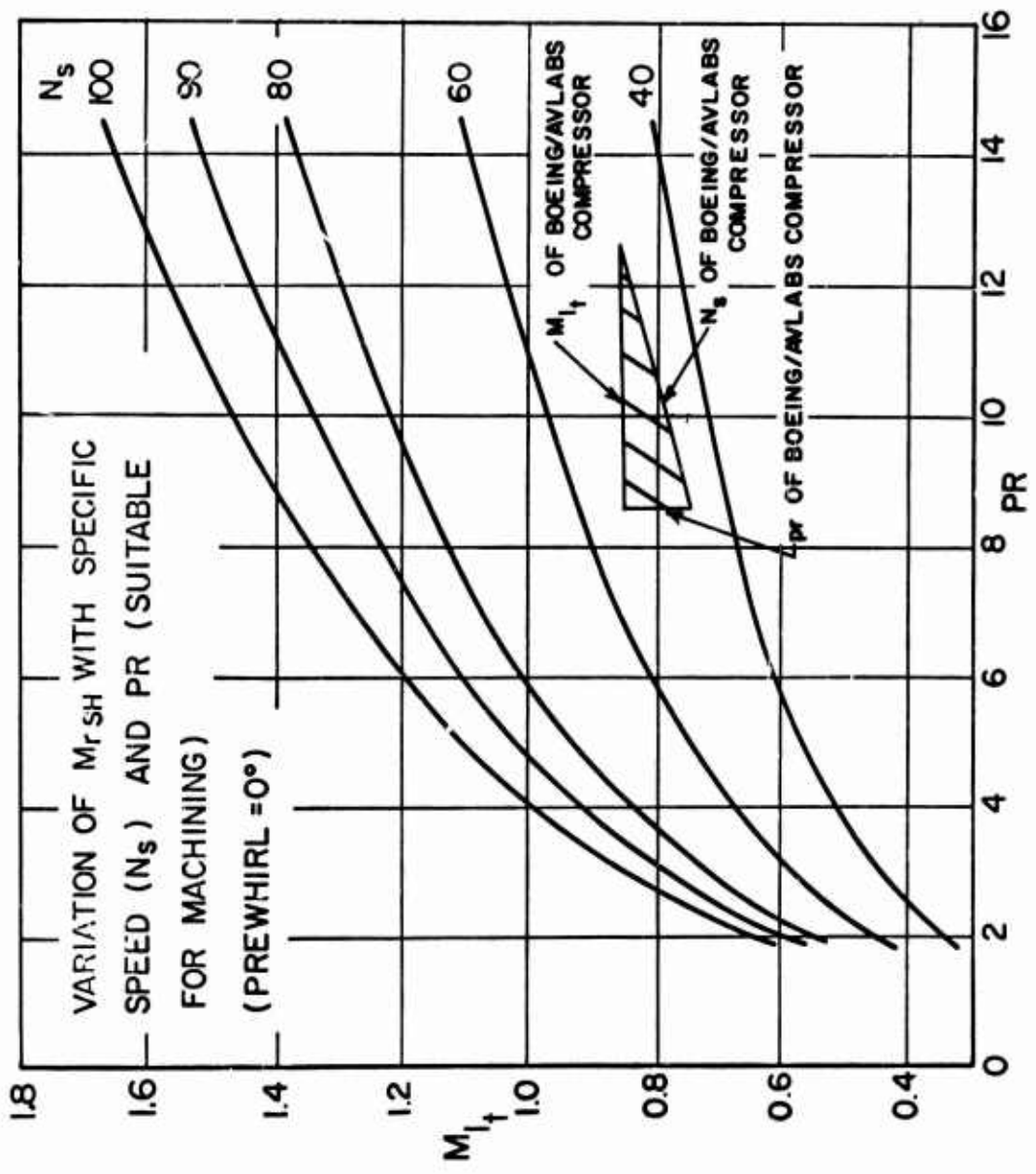


Figure 181. Variation of Inducer Tip Relative Mach Number With Specific Speed and Pressure Ratio.

relative Mach number on overall stage performance is illustrated in Figure 182.

Morris and Kenny resorted to inlet forward preswirl of 25° at the inducer tip in order to lower inducer tip Mach number to about 0.9. Forward preswirl requires more tangential velocity at the tip of the impeller and therefore a somewhat higher tip speed. However, Figure 183 shows that the increase in cover and disc friction loss occasioned are not at all severe for the Morris and Kenny rotor, which had inherently only about 40% of the friction losses of the Boeing RF-2 impeller due to its smaller tip diameter (6 in. in comparison to 9.14 in. for RF-2). We estimate that the Morris and Kenny rotor would suffer only about 2.6 points loss in efficiency due to friction in the impeller in contrast to the 6 points estimated for the Boeing RF-2.

Morris and Kenny's inducer tip relative Mach number of 0.9 is relatively high when attempting to limit the strength of suction surface shocks on the inducer and to enhance maximum diffusion. Perhaps this explains why their stage did not achieve considerably better performance than the Boeing stages in spite of its much more favorable impeller discharge and diffuser geometry occasioned by a much higher specific speed. Their diffuser apparently is slightly better than the Boeing vane-island diffusers, as one would expect from the arguments above. Their pipe diffuser performance is shown in Figure 184.

Unfortunately, Morris and Kenny do not offer any tip static pressure data so we cannot diagnose the reasons why their stage fell considerably short of our expectations for it. However, their impeller potential solution indicates early separation and inadequate internal diffusion.

#### Tandem Inducer

The virtues of raising the specific speed are so beneficial that we recommend redesign at a specific speed of about 70. But rather than struggle to correct the inherent disadvantages occasioned by the increase in inducer tip relative Mach number through the use of preswirl, the concept of using a transonic rotor ahead of

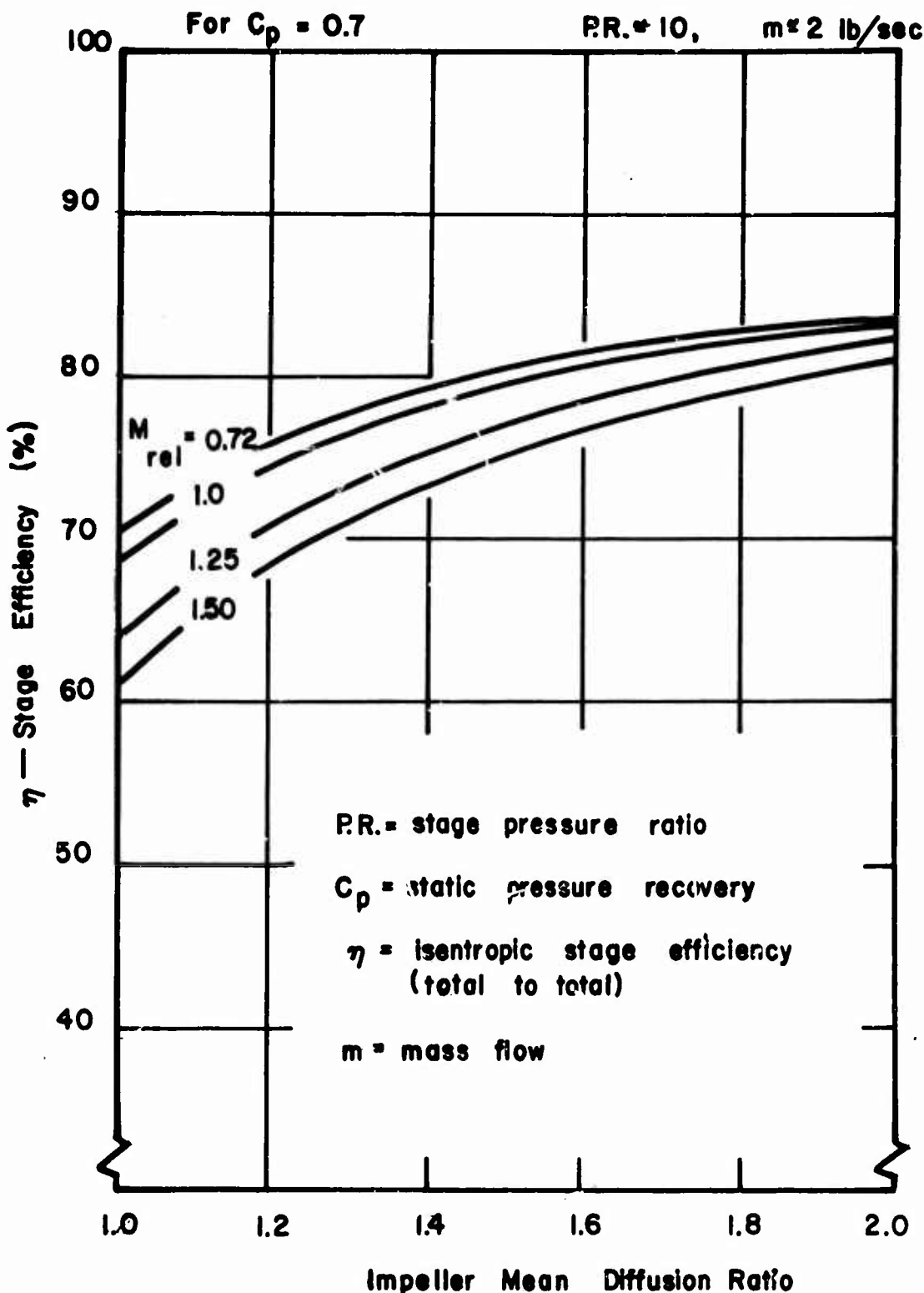


Figure 182. The Influence of Inducer Tip Mach Number on Stage Efficiency (Single-Row Inducers).

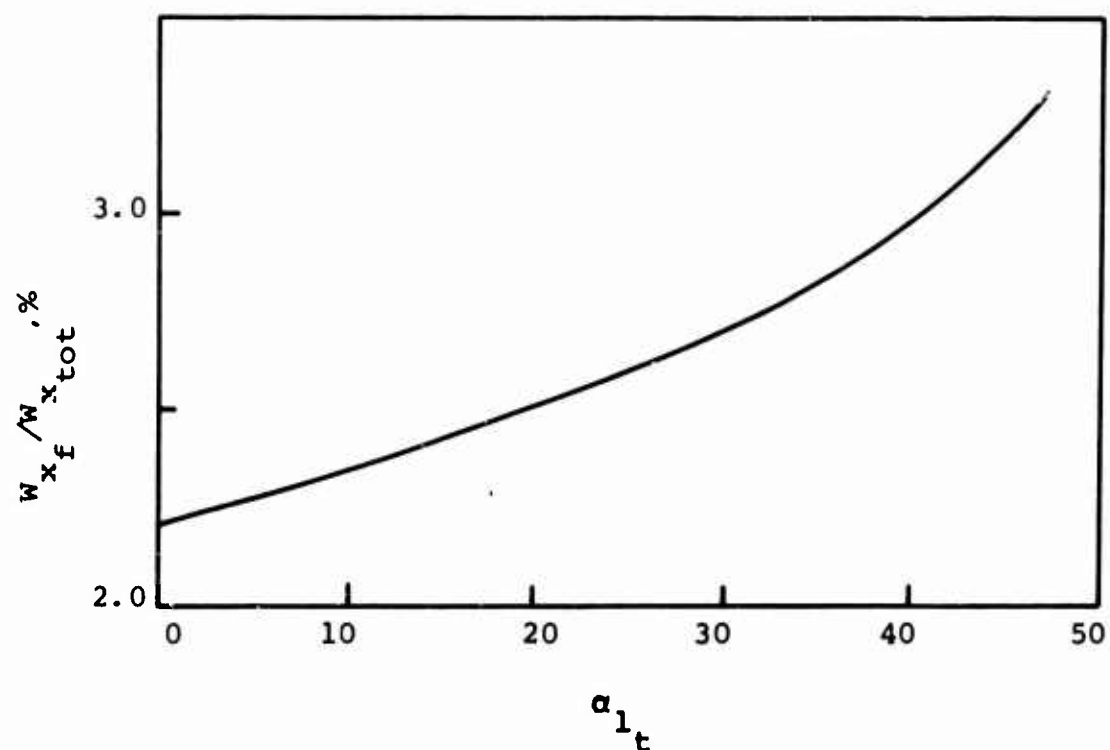


Figure 183. Variation of Impeller Friction Work With Inlet Preswirl Angle (for Morris and Kenny's Impeller).

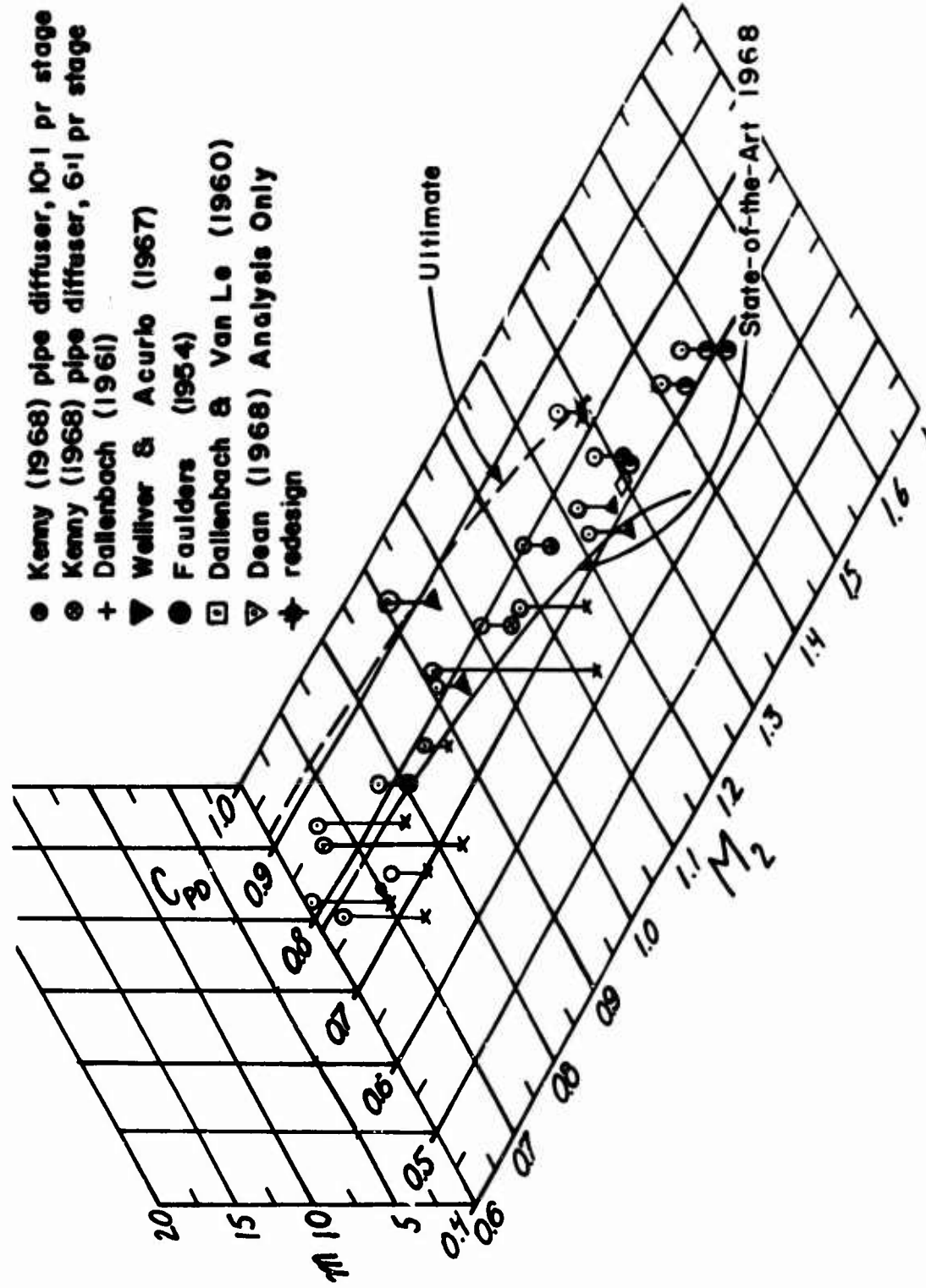


Figure 164. State-of-the-Art Centrifugal Compressor Diffuser Performance and Projected Ultimate (from Dean 1968).

the subsonic inducer has been explored. This scheme, which amounts to a tandem inducer as shown in Figure 185 appears to be very promising.

The basic idea is to accept the high inducer tip Mach number indicated by Figure 182 but to take advantage of the high Mach number with a transonic rotor. This rotor must be separate from the subsonic inducer in order to shed the shock-separated boundary layer from the blades into the passages between the subsonic inducer vanes.

If the transonic vanes and subsonic vanes were made continuous, no further recovery would occur in the subsonic diffuser because the boundary layers would already be separated from the suction surface by the entry shock. However, if the two rows are made separate as illustrated in Figure 185, the work of Wolfe and Johnston (1968) and others suggest that recovery of the subsonic inducer will be largely unimpaired. A further and substantial advantage for the transonic inducer arises from the substantial pressure ratio which can be achieved across it.

Remember that the Boeing RF-2 inducer achieved a separation pressure of 16.0 psia. We see in Table XIII that the transonic inducer by itself should yield a discharge static pressure of 16.72 psia and a relative Mach number of 0.84 which happens to be exactly that found at the inducer tip of the RF-2. So already before entry to the subsonic inducer, more pressure rise has been achieved; still more is available from the subsonic inducer.

Assuming a mean tip diffusion ratio of 1.5, which is less than the ultimate we believe can be achieved with development, the static pressure at the separation point in the subsonic inducer is calculated to be 21.9 psia in contrast to 16.0 in the RF-2. However, because of the larger ratio of separation radius to tip radius (Tables XIV and XV), a smaller separated centrifugal pressure ratio occurs for this new impeller than for the RF-2. The tip pressure is calculated to be 57.9 psia in contrast to the RF-2's measured value of 64.0, but the jet relative Mach number is 0.52 in contrast to 0.60 for RF-2. This reduction of jet relative Mach number and the decrease in tip area leads to a reduction in discharge mixing loss from 3.7 points to 1.1 points.

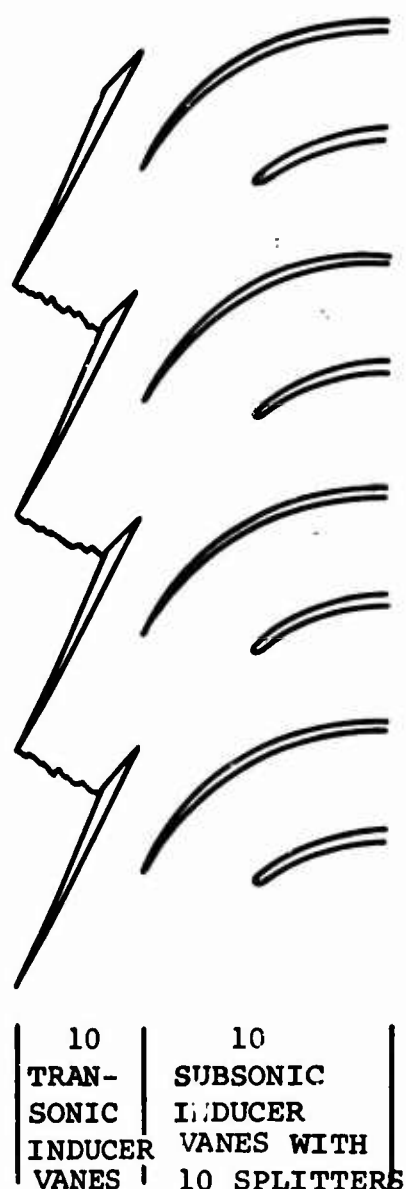


Figure 185. Tandem Inducer Concept.

TABLE XIII. TRANSONIC INDUCER

	$P_o$	$T_o$	$M_x$	$C_x$	$C_\theta$	$w$	$M_{rel}$
Tip Inlet	14.7	520	.652	700	0	1287.8	1.2
Tip Exit	20.07	569.5	.458	521.8	275.2	958.9	.842
Hub Inlet	14.7	520	.652	700	0	934.2	.871
Hub Exit	19.46	563.4	.517	579.6	409	622.8	.556
	$r$	$u$	$\beta$	$p$	$T$	$pr$	$\eta$
Tip Inlet	1.769	1080.9	-57.1	11.05	479.2	-	-
Tip Exit	1.769	1080.9	-57.1	16.72	540.5	1.365	.955
Hub Inlet	1.013	618.7	-41.5	11.05	479.2	-	-
Hub Exit	1.043	637	-21.5	14.85	519.6	1.324	.95

The tandem inducer design requires that the leading edge of the subsonic inducer depart from a radial line. While this raises problems with stressing and vibration, the advantages are so great that it seems worthwhile to conquer the mechanical problems.

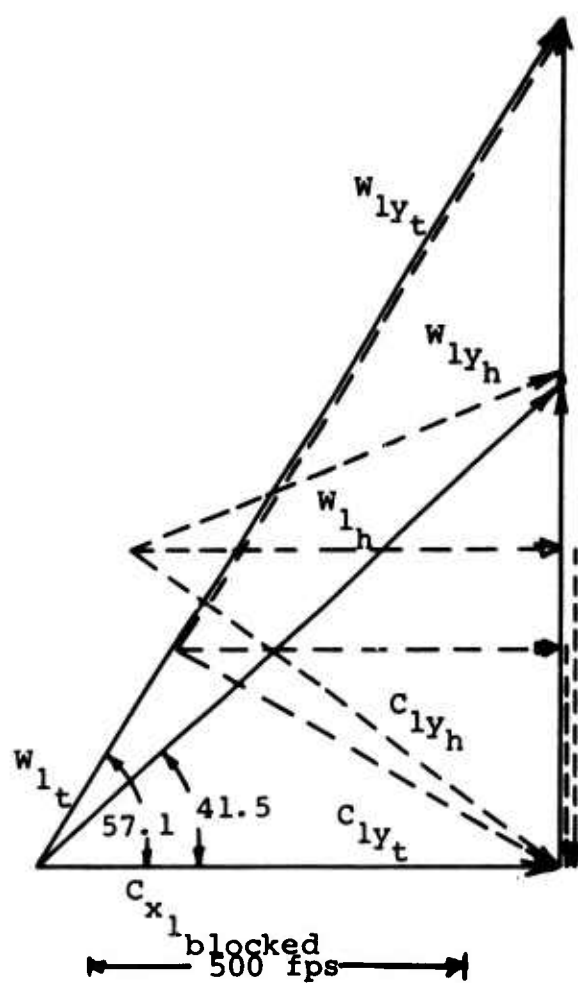
#### Transonic Inducer

The transonic inducer has been given a preliminary design treatment mainly to insure that it is feasible. This rotor is similar to transonic axial compressor rotors and has been designed using the same principles.

At the tip of the transonic inducer, the blades are essentially flat and produce only a few degrees of turning. The work input and diffusion is achieved by a normal shock as shown in Figure 185. The maximum tip relative Mach number is limited by diffusion limits at the hub. A hub mean velocity ratio of 1.5 was chosen. When designing this rotor in detail, conventional transonic axial design methods should be employed incorporating NASA diffusion factors.

While this design study is only preliminary, the proposed transonic inducer appears to be conservative in light of modern transonic axial practice. The vector diagram is shown in Figure 186 and the inducer thermodynamics are summarized in Table XIII. Losses have been included, actually, it may not be essential to include losses within our aim of achieving a maximum pressure rise in the inducer. On the other hand, the wake mixing losses from the transonic inducer will be injected into the core flow through the subsonic inducer and should be recognized as a loss of jet relative total pressure. These losses are included, but they are not of any substantial consequence.

One consequence of using a transonic inducer is that the impeller will operate close to choked at the design point. This means that the stage will have the short range typical of a transonic axial. While this move eliminates one range advantage of the simple centrifugal compressor, the short



("y" INDICATES STATION AT TRANSONIC  
INDUCER EXIT)

Figure 186. Transonic Inducer Vector Diagram.

range is not believed to be insurmountable in light of the wide usage of transonic axials for small gas turbine service. Starting the supersonic tip flow should be no problem. If wider range is essential, adjustable inlet guide vanes ahead of the inducer may be employed.

The addition of the transonic inducer does not substantially increase cover friction loss relative to the total friction loss of the impeller, because of the low tip speed in the inducer and the fact that cover friction losses increase as tip speed cubed times the radius squared. A meridional plan of the transonic inducer is shown in Figure 187.

#### Subsonic Inducer

The characteristics of the subsonic inducer are summarized in Table XIV. Relative Mach numbers entering the blade tip are conventional and similar to those of the Boeing RF-2. The tip relative flow angle is larger, thus increasing blade blockage somewhat. However, the increased stagnation pressure contributed by the transonic inducer substantially eases any blockage problems. Nevertheless, we are of the opinion that fewer subsonic inducer vanes than used in RF-2 should be employed; ten are shown in Figure 185. In order to reduce loading on the subsonic inducer and enhance diffusion, 10 splitters are recommended as shown in Figure 185.

No detailed design of the subsonic inducer has been carried out here. The methods recommended in Sections 5 and 6 should be employed. Without a question empirical development, guided by the flow models, will be necessary.

We recommend that the transonic and subsonic inducers be developed together; a workhorse impeller should be installed behind the subsonic inducer during development. The objective is to achieve maximum static pressure at the separation point while engendering minimum relative total pressure losses in the core flow. The use of internal probes and pressure taps is strongly recommended. In order to enhance their use, development with a gas of low sonic velocity is highly desirable. (Appropriate modifications in area schedules are necessary in order to guarantee the same Mach number schedules.) Another advantage of using a

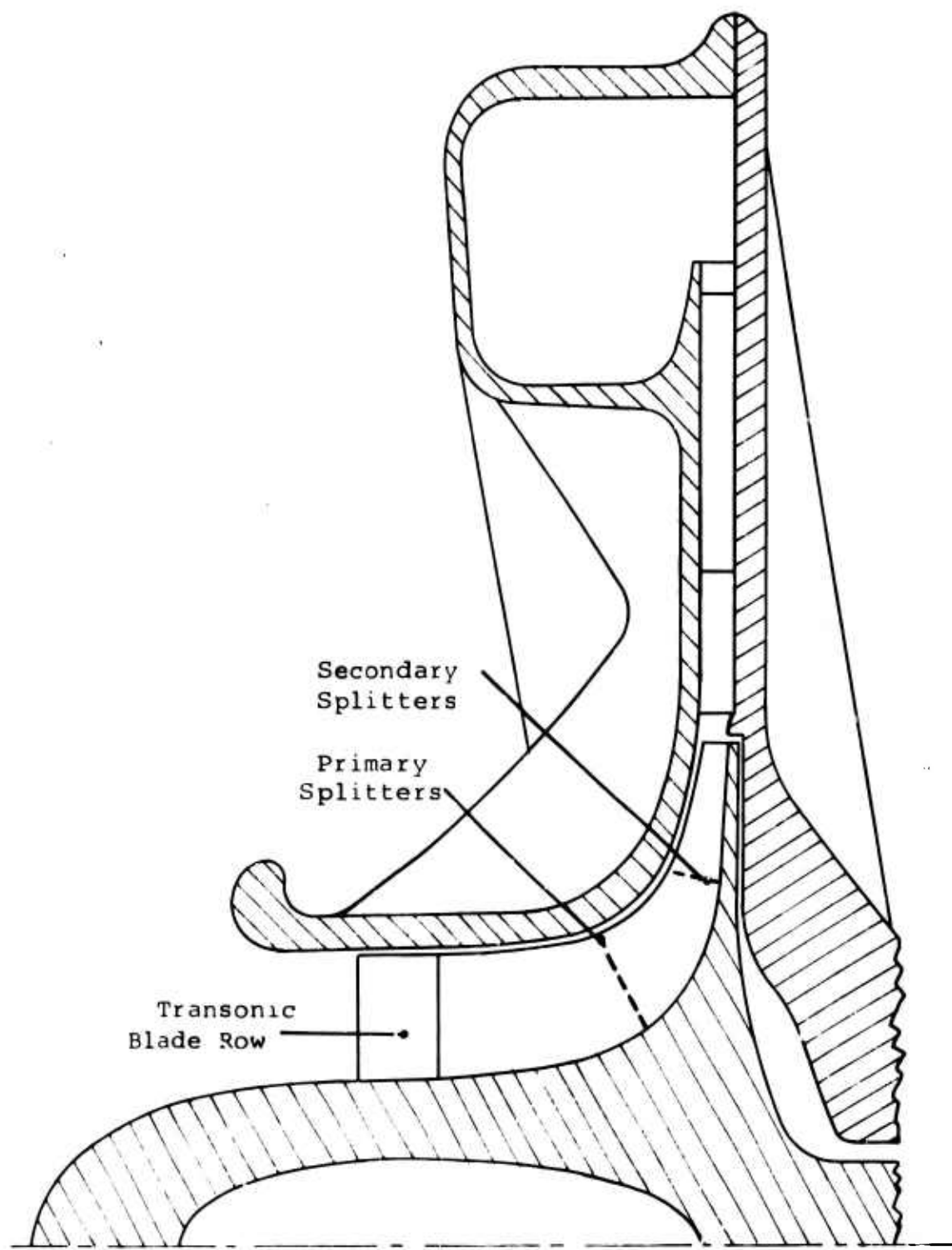


Figure 187. Meridional Plan of Redesigned Stage.

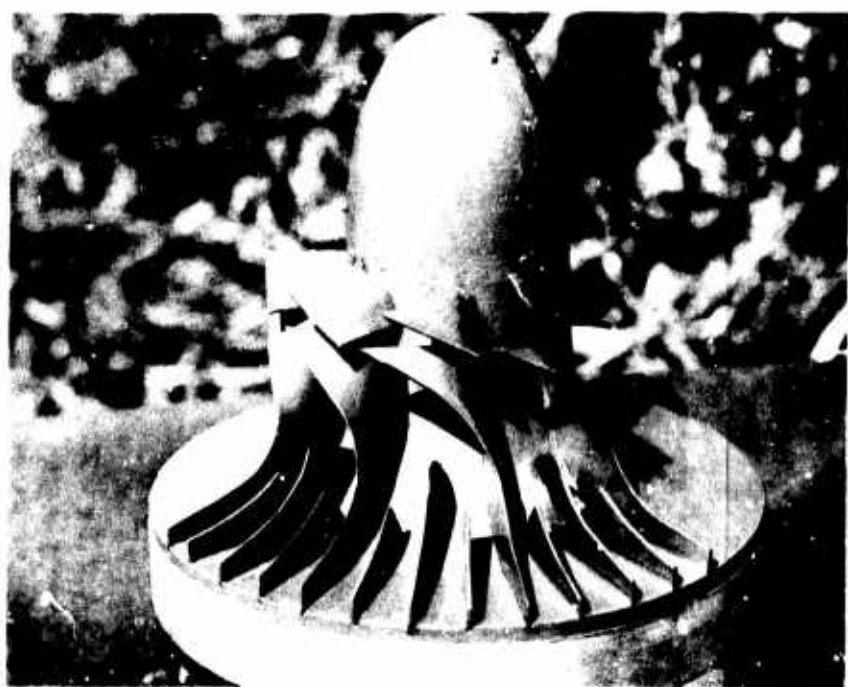


TABLE XIV. SUBSONIC INDUCER

	$P_o$	$T_o$	$P$	$T$	$r$	$W$	$M_{rel}$	$\beta$	DR
Inlet Tip	20.07	569.5	16.72	540.5	1.769	959.9	.842	-57.1	-
Inlet Hub	19.46	563.4	14.85	519.6	1.043	622.8	.556	-21.5	-
Tip Sepa- ration	26.4*	617.23*	21.9	583.2	1.769	639.7	.523	0	1.5

\* RELATIVE STAGNATION PROPERTIES

low-sonic-velocity gas is that easily modified construction materials may be used for the vanes because the inducer tip speed would only be about 560 fps.

## 7.2 IMPELLER GEOMETRY AFTER SEPARATION

The radius of curvature of the bend-to-radial in the meridional plane is important, as has been stressed in Section 6.6. The sharper the bend, the more the through flow tends to separate from the cover, run along the hub wall, and enhance the possibility of backflow into the impeller on the cover wall.

There is little hope of keeping the flow attached at the cover, especially on the cover suction surface, because the flow is separated from the suction surface at the end of the subsonic inducer and presumably ahead of the bend-to-radial. Sometimes it may be possible to continue the flow unseparated around the bend-to-radial although in our experience this rarely happens. The principal difficulty in an attempt to negotiate the bend unseparated is that the flow models and prediction tools available are extremely weak, as has been emphasized in Sections 5 and 6. Morris and Kenny (1968) make an interesting suggestion of a design tool utilizing "equivalent pipe bends". However, they provide no empirical justification whatsoever, so, in our opinion, the validity of their method must be suspected. If they had offered tip static pressure data for their impeller, it would have been possible to determine whether the flow in their impeller did indeed successfully negotiate the bend to radial. Static pressure distributions on the cover would be even more helpful for this diagnosis. Since their impeller did not achieve its expected potential, compared to the much lower specific speed Boeing impellers, we suspect that their impeller's internal diffusion is at fault. This expectation casts a shadow of doubt over the utility of their "equivalent pipe bend" design method.

Lacking an adequate method now, all we can recommend here is that the radius of curvature of the bend-to-radial be kept at a maximum. The passage also should be kept as shallow as possible in the meridional plane. Further development of design tools recommended in Section 6 for analyzing the behavior of the separated flow in the impeller and the effect of its dynamics upon the slip factor would be greatly appreciated at this point in the design procedure.

In order to elevate the impeller slip factor so that the tip speed and cover and rear disc friction losses may be minimized, additional splitter blades are recommended near the tip of the impeller. Morris and Kenny (1968) use 64 blades on their "H" rotor. In contrast, the Boeing RF-2 had only 18 blades. Morris and Kenny report slip factors on the order of 0.92 in contrast to our estimates for the Boeing RF-2 impeller of 0.83. Morris and Kenny's slip factor determinations may be high, as were Boeing's; we have not been able to scrutinize their slip data critically because sufficient detail is not available.

The leading edge of the second set of 20 splitters should lie somewhere in the meridional bend-to-radial or just beyond. These splitters must be carefully designed not to disturb the flow heavily. However, because the flow is expected to be separated before the leading edge of this last set of splitters, their design is not highly critical. Visualization studies show that the insertion of splitters does not alter the pattern of the separated flow in the impeller, the through flow jet relative Mach number, nor the tip static pressure. They may beneficially affect the work input by substantially raising the slip factor of the through-flow jet. As argued in Section 5.6, the smaller the tangential distance that the jet on the hub must move back onto the vane pressure surface, the smaller the relative slip at the tip due to the secondary adjustment motion. Further, if the discharge jets are subdivided more finely, they are thinner and will hug the blade direction more closely with less outflow deviation.

With this double splitter arrangement and 10 subsonic inducer vanes, there would be 40 vanes at the tip of the impeller. The blockage occasioned by these vanes is of no consequence so long as the wake area fraction is greater. The vanes merely fill up part of the wake region. The splitters do increase the passage surface area and wall friction, but this is a very minor effect. Clearance leakage will increase; the effect of this increase is unknown.

If helpful in design, and within stress limitations, the blades may be thickened in certain regions to reduce the cross-sectional area of the passage. Actually, once separation occurs, this move will do little more than fill up part of the wake region with metal.

We have tacitly assumed during this program that impellers with this high rotative speed must have radial blades for stress reasons. We are not familiar with the current capabilities of materials for this type of service. However, if an impeller with backward leaning blades could be built, it should be given first consideration. Significantly better performance can be expected from backward leaning blades despite the increased tip speed if such impellers can be constructed; we have assumed that they cannot be built.

The redesigned impeller geometry is given in Table XV and is shown in Figure 187 along with a photograph of a plaster/lead model.

TABLE XV. IMPELLER CHARACTERISTICS

N	m	$N_s$	$r_{it}$	$r_{ih}$	$r_2$	$b_2$	$l^*$	$u_2$
70,000	2	61	1.769	1.013	3.078	0.160	2.35	1880

\*Axial Length, approximately.

### 7.3 IMPELLER TIP - DIFFUSER ENTRY

The meridional geometry of the new impeller is shown in Figure 187. The design is by no means final, as should be obvious from this discussion.

### 7.3.1 Impeller Discharge Mixing Losses

The tip depth,  $b_2$ , has been chosen, in light of the relative Mach number expected at separation, in order to force the wake fraction at impeller tip below 0.50.

The impeller tip properties before and after mixing are shown in Tables XVI and XVII. The mixing loss (mass-flow-averaged stagnation pressure ratio) is calculated to be 0.975. This causes a 1.1 point reduction in stage efficiency.

Because the through flow much more greatly fills the discharge area of this new impeller, in contrast to the Boeing RF-2 design, we expect that backflow from the diffuser will be reduced substantially. This reduction should be further enhanced by the less severe bend-to-radial.

When Welliver and Acurio reduced the tip depth of the RF-2 from 0.195 to 0.150, they won a 3-point reduction in impeller work input and a 3 point improvement in stage efficiency as has been discussed in Section 6.7. The further reduction in impeller tip discharge area for this new design should cut the backflow loss even further. We anticipate that another 3 points could well be won from the total of 8 points estimated for backflow work in RF-2.

Modifying the impeller specific speed, enhancing better impeller internal diffusion, and reducing the impeller tip discharge area are predicted to yield the increases shown in Table XVI.

TABLE XVI. INCREASE IN STAGE EFFICIENCY DUE TO  
IMPELLER IMPROVEMENTS (Compared to RF-2)

<u>Source of Gain</u>	<u>Gain in Stage Efficiency, Points</u>
Impeller Discharge Mixing	2.5
Reduction in Backflow	3.0*
Cover and Disc Friction	3.4
Total Gain	8.9

\* Compared to best RF-2 impeller, 3369/70

TABLE XVII. IMPELLER TIP PROPERTIES

$m = 2.0$	$N = 70,000$	$T_{o_i} = 520$
$p_{o_i} = 14.7$	$k = 1.336$	$u_2 = 1880$
		$m_w/m = 0.20$
BEFORE MIXING		AFTER MIXING
$r_2 = 3.078$	$\Delta p_T_{rel} = 0.208$	$r^* = 3.078$
$b_2 = 0.160$		$b^* = 0.160$
$p_2 = 57.9$		$p^* = 60.6$
$\tilde{p}_{o_2} = 168.8$		$\tilde{p}_o^* = 165.2$
$\tilde{T}_{o_2} = 1068.4$		$T^* = 804$
$T_{o_{j2}} = 1045.7$		$T_o^* = 1068.4$
$T_{o_{w2}} = 1159.1$		$C_r^* = 457$
$C_{r_{j2}} = 685.2$		$C_\theta^* = 1729.6$
$C_{\theta_{j2}} = 1692$		$\tilde{p}_{o_2} - p_o^* = 3.6$
$C_{\theta_{w2}} = 1880$		$p^* - p_2 = 2.7$
$\sigma = 0.92$		$M^* = 1.29$
$\overline{\rho C_r} = 93.09$		
$M_{rel_{j2}} = 0.523$		
$\varepsilon_2 = 0.464$		

The stage efficiency should rise from the best RF-2 value of 73.5 to as much as 82.0% from these impeller refinements alone.

### 7.3.2 Diffuser Entry Region

A further major advantage of reducing the impeller discharge area, and thus increasing the bulk mean radial velocity, is that the swirl parameter into the diffuser is reduced from about 7.8 (RF-2) to 3.78. This means that the average flow angle to radial is reduced from  $82.7^\circ$  to  $75.0^\circ$ . The smaller absolute discharge flow angle of the new impeller has a principal virtue in reducing the length of the streamline from impeller tip to diffuser throat. Therefore, the distance is decreased over which the side-wall boundary layers grow to generate undesirable blockage in the diffuser throat.

On designing a centrifugal stage, a compromise usually must be struck between the optimum depth of the impeller and the optimum depth of the diffuser. Johnston and Dean (1966) elucidate the reasons for the compromise and show that it is particularly demanding for low specific speed machines. The designer desires to reduce the impeller depth in order to decrease wake fraction and impeller discharge mixing. On the other hand, he usually wishes to increase the diffuser depth in order to provide a more favorable throat aspect ratio and to reduce blockage. (This objective is not always valid as pointed out in Section 6.9.) As long as equal diffuser and impeller depths are adopted, a compromise must be made.

With the Boeing-AVLABS RF-2 impeller, the apparent optimum design wake fraction was about 0.75. (This choice may not be optimum and should be scrutinized very carefully if that particular stage geometry were to be refined.)

The higher specific speed redesigned stage offered here is less compromised by this problem. The smaller tip diameter tends to cause an increase in tip depth. Further, the reduction in diffuser throat radius decreases the width of the diffuser throats and therefore increases their aspect ratio naturally. Despite these improvements, it is wise to examine the constant-depth design rule, for, if it can be

overthrown, a new optimization freedom is won.

A study has been made of the potential gain from rapidly expanding the meridional depth of the diffuser entry from impeller tip to vane leading edges as shown in Figure 188.

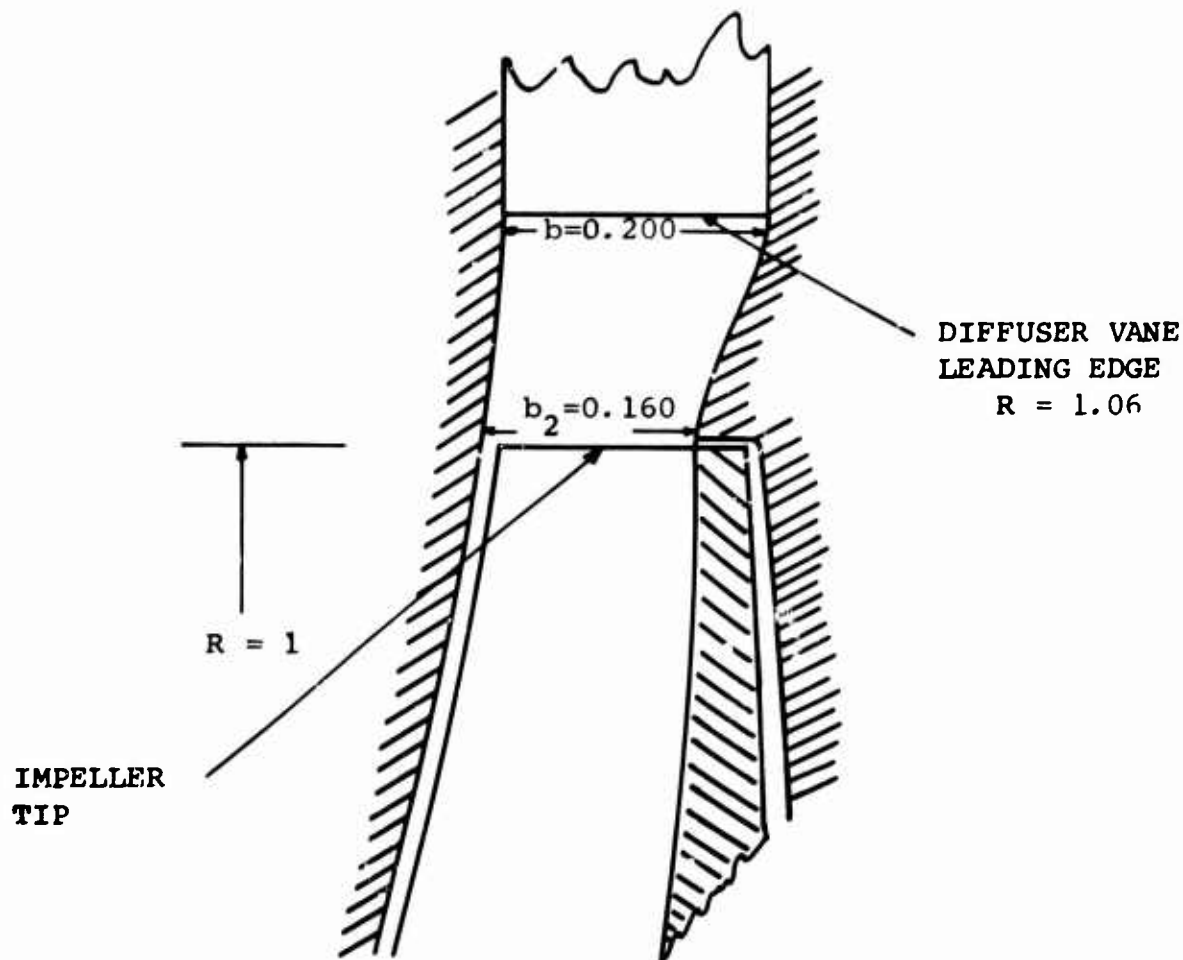


Figure 188. Diffuser Entry Axial Expansion.

On first glance, the expansion of the meridional depth looks atrocious. One would expect the flow on the hub wall to separate because of its relatively sharp curvature. On second thought, though, it is realized that the fluid-

dynamically significant view is along the flow streamlines. This view is shown in Figure 189 transformed from Figure 188. Now the hub wall curvature looks rather mild.

In order to examine this prospect more critically, we have made a two-dimensional turbulent boundary layer calculation for a set of conditions fitting the RF-2. Three cases were analyzed:

Case	$b_2$	b at R = 1.06
I	0.090	0.090
II	0.180	0.180
III	0.060	0.180

Case II approximately represents the original RF-2 design. Case I is for a reduced depth version of RF-2 with sufficient reduction to cut the discharge mixing losses and backflow substantially and with equal diffuser and impeller depths. Case III represents a 3:1 meridional depth expansion.

The analysis was carried out for a compressible free vortex flow, without wall friction but including boundary layer blockage, from  $R = 1.0$  to  $1.06$  at the vane leading edge radius. The changes in the streamline directions of the free flow are shown in Figure 190. We also note in Figure 190 the much shorter run of the flow from the impeller tip to the vane leading edges, which will reduce boundary layer displacement growth.

Because meridional depth expansion affects the diffusion in the vaneless space somewhat, the boundary layer growth on the sidewalls was studied in order to determine the impact of the added diffusion. Actually, the addition is not great, for the meridional expansion only affects the radial velocity component which contributes only between 1% and 4% of the total fluid kinetic energy. Therefore, great expansions in meridional depth hardly change the velocity ratio across the vaneless space for cases with high impeller discharge swirl.

For the cases shown in Figure 191, results of the two-dimensional boundary layer calculations are presented in

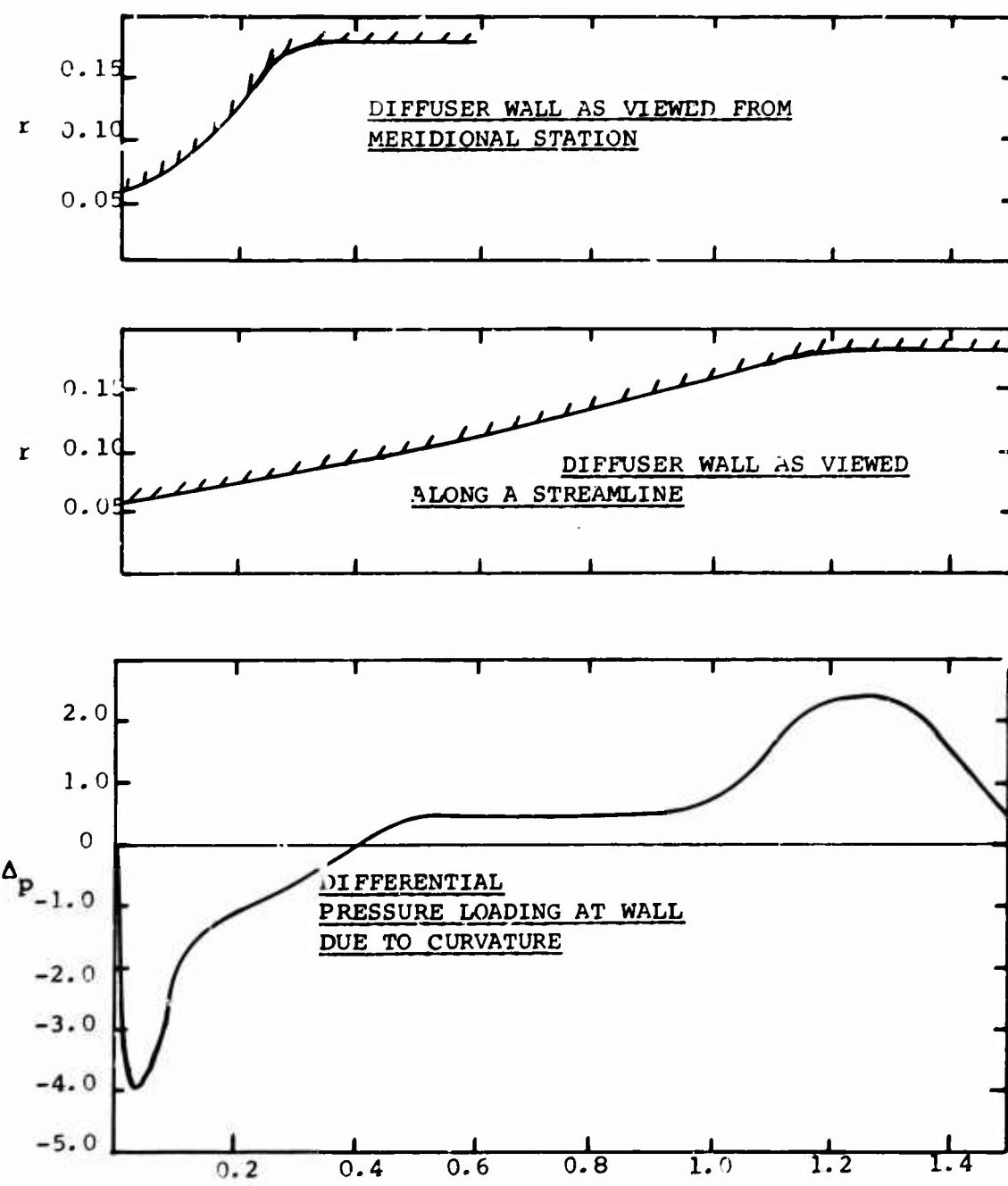


Figure 189. Comparison of Meridional and Streamline-Wise Views of Depth Expansion and Perturbation of Hub Wall Static Pressure Due to Wall Curvature

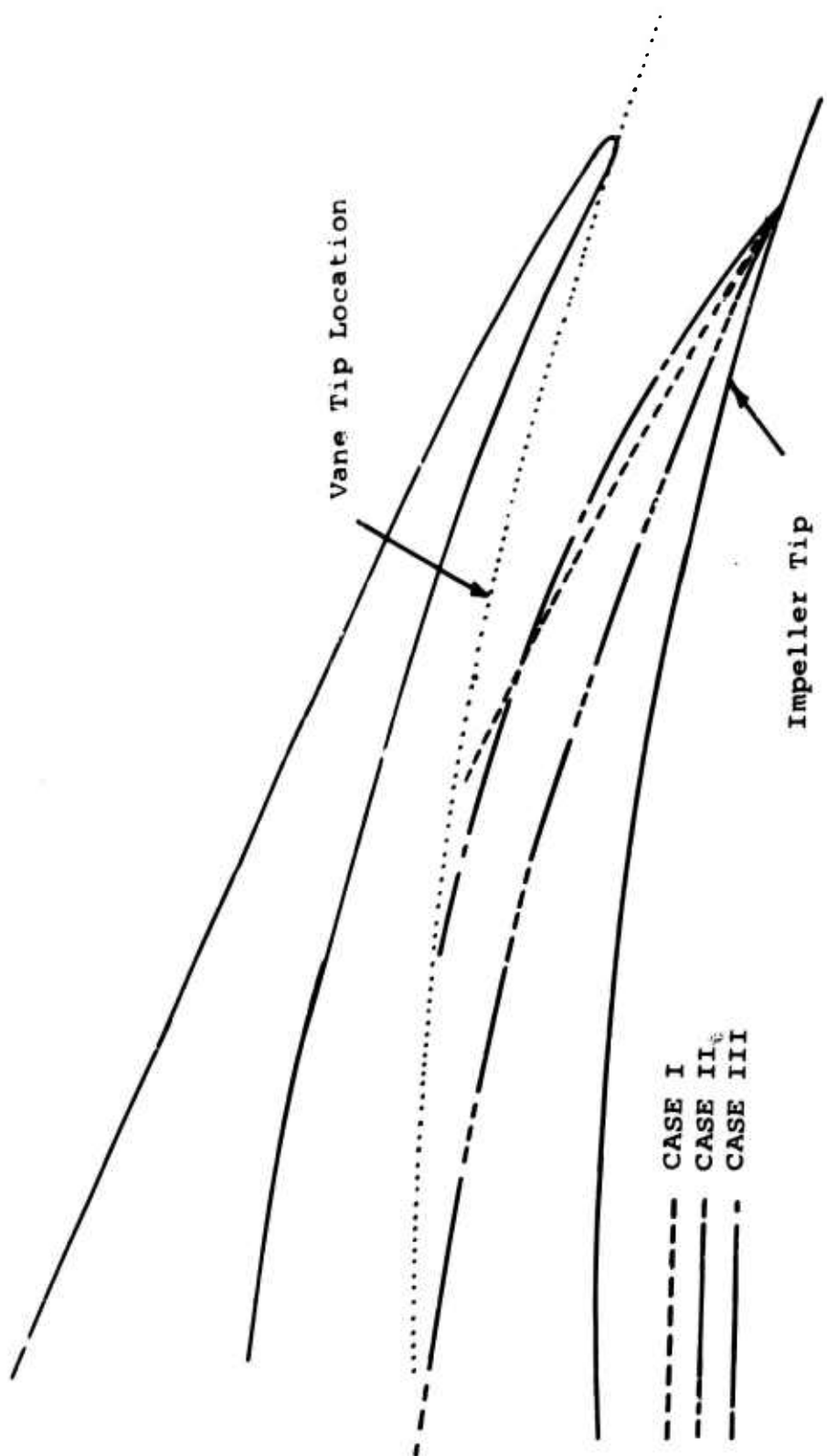


Figure 190. Streamline Trajectory Changes Due to Diffuser Entry  
Axial Expansion.

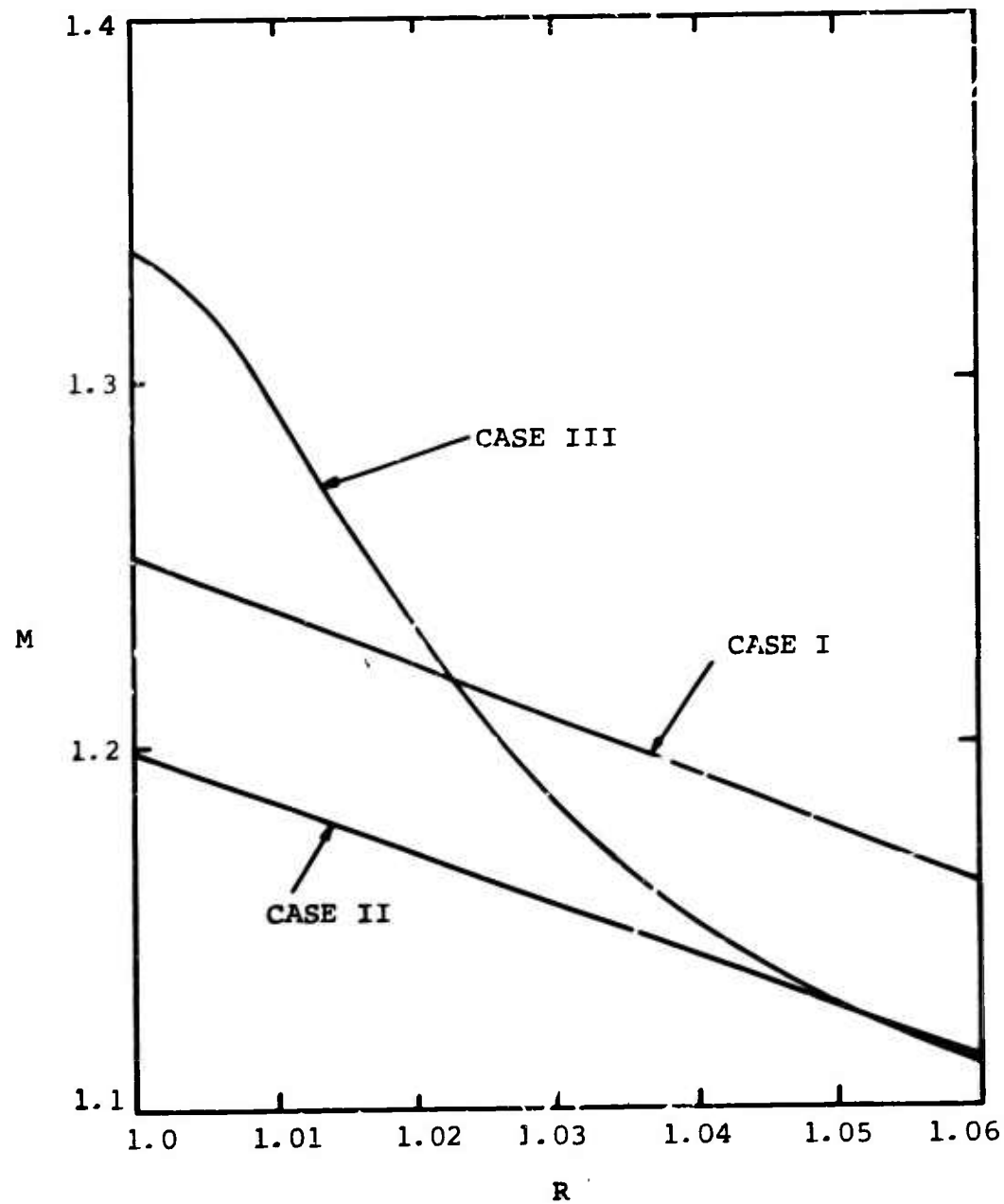


Figure 191. Mach Number Schedule of Various Axial Expansions.

Figures 192 and 193. We note that the 3:1 meridional expansion in Case III hardly affects the displacement thickness of the boundary layer at the diffuser vane leading edges. From that point on, the diffusion proceeds as before; thus, the change in displacement thickness at the throat entry should be minor.

Before one enthusiastically accepts the prospect of making a rapid meridional expansion at the entry to the diffuser, it would be wise to determine whether the local pressure perturbations on the curved hub and the curvature of the wall can seriously affect the boundary layer growth or separation tendencies. As far as the wall curvature is concerned, radius of curvature is nowhere smaller than 25 times the displacement thickness of the boundary layer. According to Schlichting (1960), this ratio should have no effect upon the growth of the boundary layer due to normal acceleration forces. The wall pressure perturbations were calculated for the most extreme 3:1 expansion case, Case III. The perturbation versus the streamline distance is plotted in Figure 189. Next, the vaneless free vortex pressure distribution of Case III without regard for wall curvature was perturbed and the boundary layer calculations were repeated. In Figure 194 the two boundary layer histories are compared. We note that the pressure perturbation occasioned by wall curvature only slightly affects the boundary layer behavior and nowhere suggests separation.

As a result of this study, we are confident that a rapid expansion of the meridional depth of the diffuser entry can be invoked if desired. Even a 3:1 expansion in a radius ratio of  $R = 1.06$  appears to affect the boundary layer only slightly. With this freedom, we can now search for optimum diffuser depth.

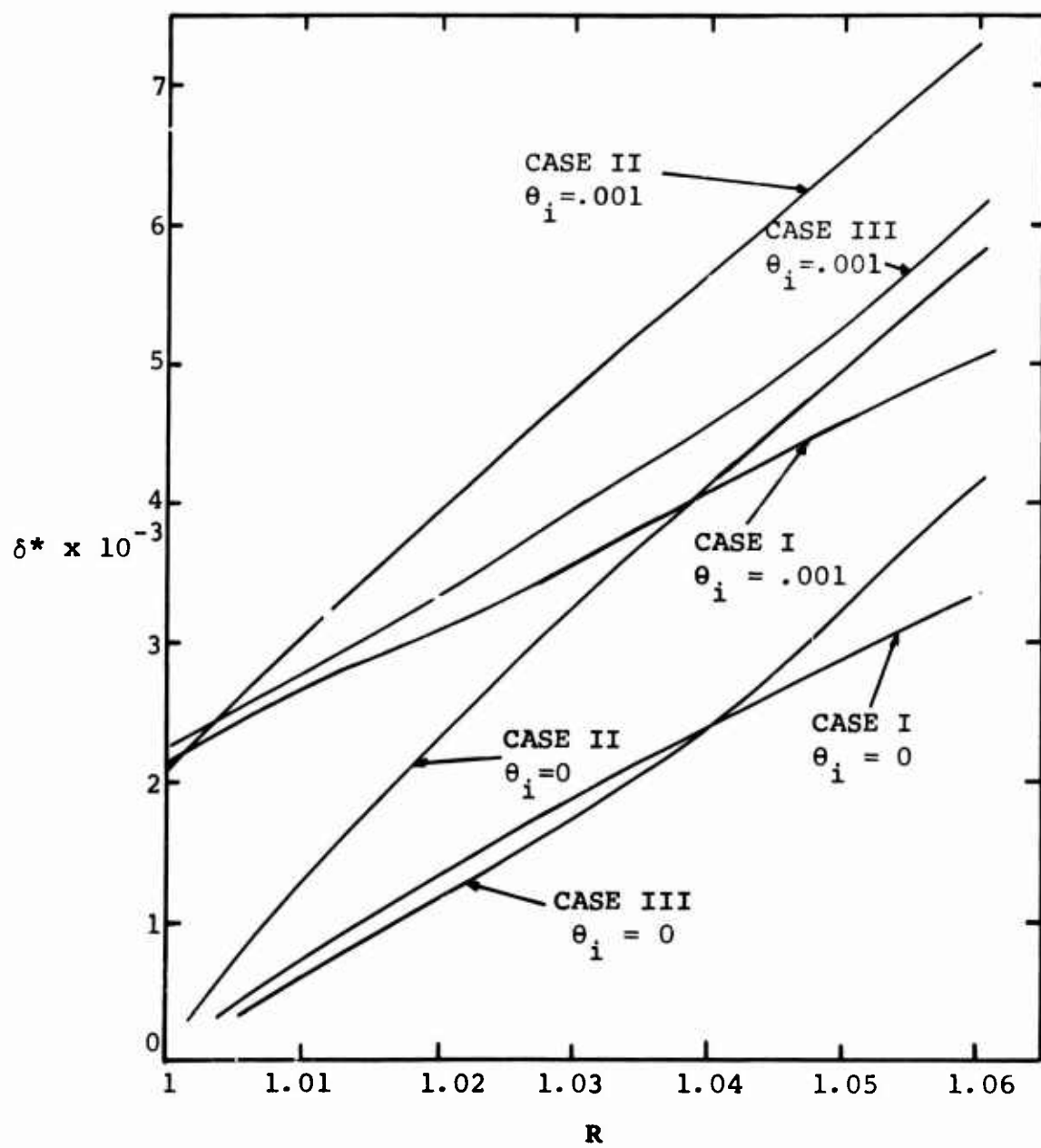


Figure 192. Sidewall Boundary Layer Displacement Thickness Growth for Various Axial Expansions ( $\theta_i$  = initial momentum thickness assumed at  $R = 1$ ).

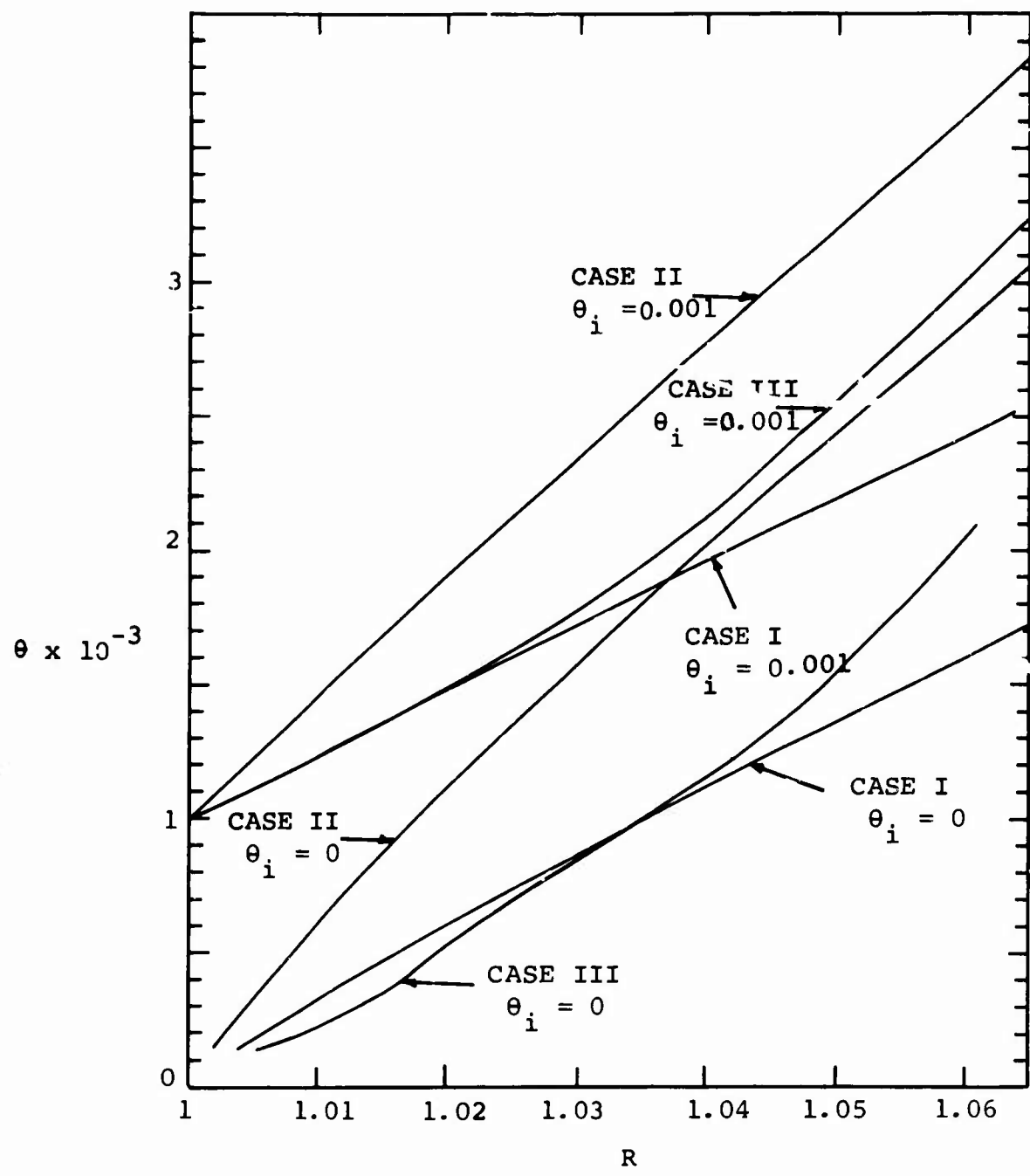


Figure 193. Sidewall Boundary Layer Momentum Thickness Growth for Various Axial Expansions ( $\theta_i$  = initial value assumed at  $R = 1$ ).

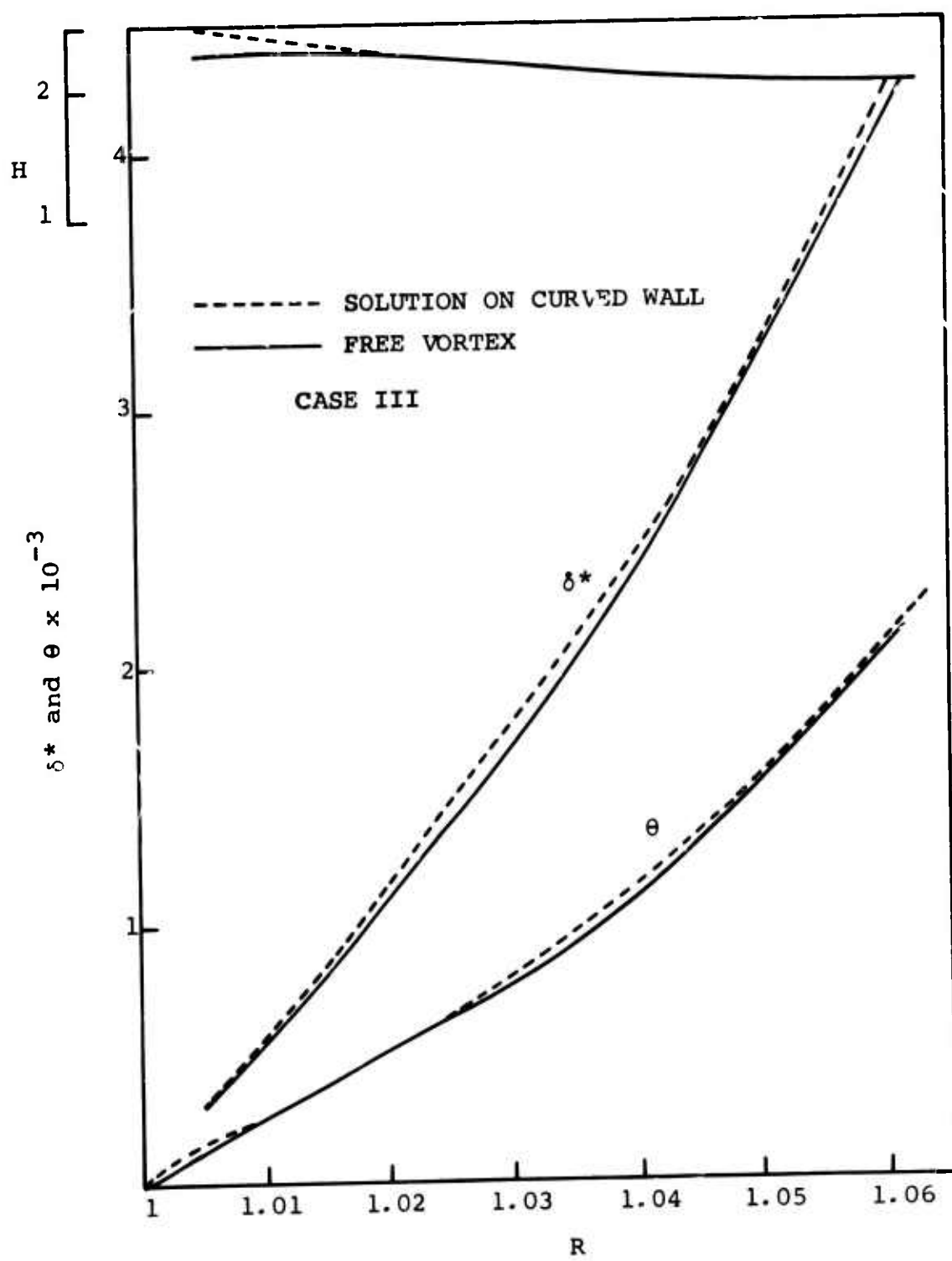


Figure 194. Boundary Layer Growth on Curved and Straight Sidewall.

#### 7.4 VANE DIFFUSER GEOMETRY

Because channel diffuser throat blockage is so critical to overall stage performance, every means should be adopted to reduce blockage. The blockage arises from boundary layer growth on the sidewalls and vane suction surface as enhanced by the pressure rise from impeller tip to throat entry.

In Sections 5.8 and 6.8, we have explored in depth the analytical tools available for predicting throat blockage. Unfortunately, tests of the tools were at worst pessimistic and at best inconclusive. Nevertheless, we expect that trends predicted from these flow models, principally using two-dimensional boundary layer calculations on the sidewalls, are significant and can be used to point the way toward optimization.

In order to reduce the sidewall extent from impeller tip to diffuser throat to a minimum, the design would tend toward an infinite number of diffuser vanes with leading edges at  $R = 1.0$ . Without considering the problems of noise and vibration, let us examine the optimum number and placement of the vanes.

Obviously, if a large number of diffuser vanes are employed, a great deal of excess suction surface area is placed in the semivaneless space. This surface will grow boundary layer and cause throat blockage. But, in the limit, with an infinite number of vanes, the length of the suction surface is zero and this objection disappears.

Because we shall recommend using a double-row cascade diffuser, it is essential that the first-row vanes have thin trailing edges. Further, in order to eliminate the disastrous secondary flow which polluted Faulders' (1954) vaned diffuser, the centerline of the cascade passages should be made straight. This has a further great advantage in that it minimizes excessive diffusion on the convex wall.

As pointed out by Dean (1968), designers of vaned diffusers have often fallen into the trap of expecting to reduce the stress on the vane surface boundary layers by curving the passage. Sometimes, as did Faulders (1954), transformaticns

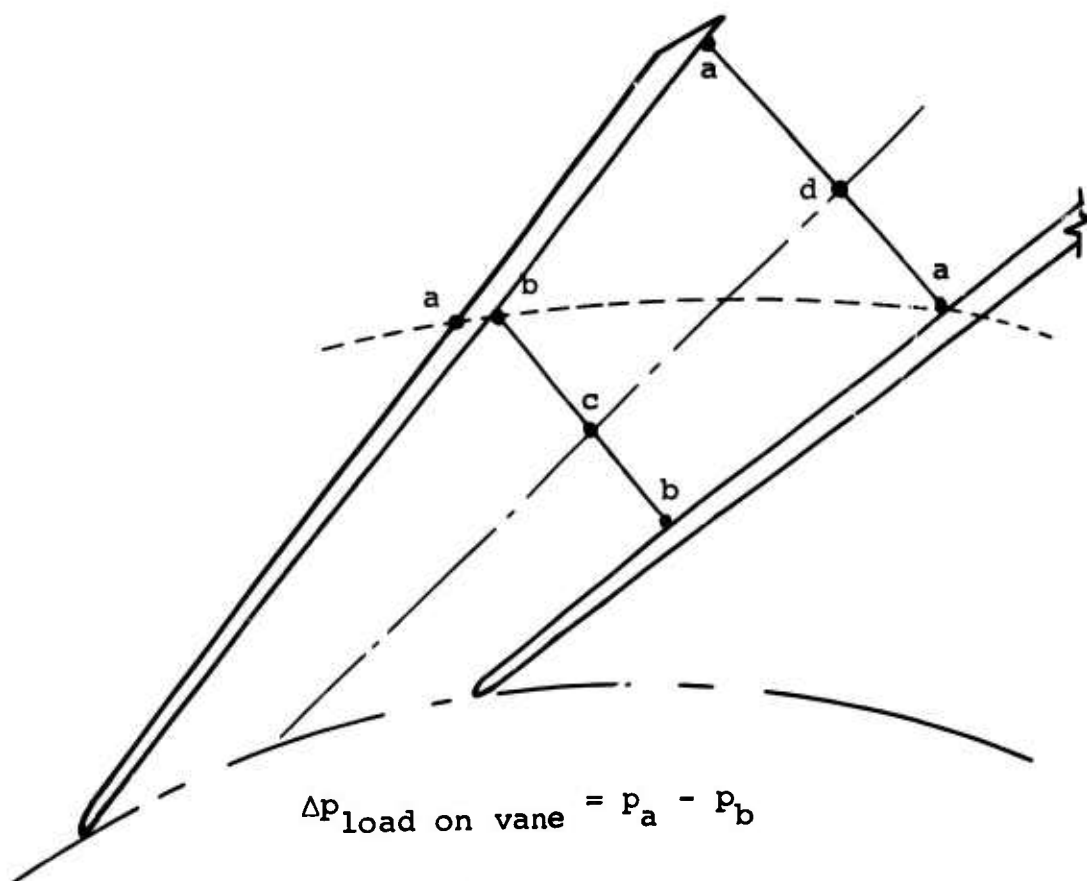
are made from axial compressor cascades. Curved passages result in the polar coordinates which turn gently away from the log spiral undisturbed flow to reproduce the rectilinear cascade turning.

We assert that this is an erroneous view of the basic fluid-dynamic situation. This is easily seen by considering a straight channel passage between the cascade diffuser vanes. The pressure distribution on both walls of the channel from throat to discharge is identical and just about identical to that down the center line. If this passage were curved, the boundary layer situation on one wall would be improved, but it would be harmed on the other, which would tend to separate more readily. Once one of the walls separates, the diffuser has achieved all the recovery it will, even if the other wall remains attached.

Another reason that designers curve the cascade blades is to limit the turning they produce. This limitation is taken from axial compressor ideas where turning is essential in order to increase the flow area and achieve diffusion. However, in the radial geometry this is entirely unnecessary, since the change of radius produces an area increase even when the passage does not turn.

The conventional wisdom would say that these flat blades are greatly overloaded and turn too much. Indeed, if they were transformed back into axial coordinates, they would. But in the polar plane, the turning is accomplished in a subtle way which does not affect boundary layer growth in the passage.

The pressure loading on the vanes which causes the turning torque can be seen by looking at two sides of a vane at the same radius. Then a normal to the streamlines can be drawn across the passage, as shown in Figure 195, to find the equal pressure point on the other wall. We see then that there is a large pressure difference across the blade which is not produced, however, by apparent turning of the flow. On the other hand, when the changes of tangential velocity along the straight center line are considered, it is realized that the flow really is being turned quite a lot.



$$p_a = p_d$$

$$p_b = p_c$$

$$\text{So } \Delta p_{\text{load}} = -\Delta p_{cd}$$

Figure 195. Pressure Loading in Straight-Channel Cascade Diffuser.

Figure 195 shows how the blade pressure loading is generated by diffusion in the channel rather than by cambering the blade. This same argument applies to vane-island straight-channel diffusers and is recognized in the art.

In order to employ the straight channel cascade with thin trailing edges, the divergence angle is locked to the number of vanes. For a vane-island diffuser, channel divergence angle and vane number are decoupled within limits because of the arbitrarily thick vane trailing edges. But the use of an effective second row is defeated by the very thick vane wakes.

Here we shall not further consider the vane-island design (except as a backup), although it may prove to be a fairly close competitor to the cascade type. A cursory comparative examination indicates that for this stage an optimum vane-island channel might achieve a recovery of 0.68 (not including diffusion ahead of the throat) and 0.73 overall from impeller tip to collector. In contrast, the two row cascade peaks at about 0.75 from throat to collector and about 0.83 overall.

The increase of 6 points in overall diffusion is worth about 2 points of stage efficiency gain. On the other hand, we can be quite certain of the vane-island recovery prediction based on the extensive Boeing-AVLABS experience and Runstadler's (1969) data. For the two-row cascade, no reliable test data exists, so considerable uncertainty over performance and even the basic flow processes clouds the predictions of superior performance.

#### 7.4.1 Optimization of the Cascade Diffuser

Because we believe that the two-row cascade will eventually show a rewarding improvement in performance over the vane-island type, we shall adopt it in this redesign. However, recourse can always be made to the proven vane-island design without suffering efficiency reduction of more than two points.

Here we shall discuss the optimization of the cascade diffuser, concentrating our attention on the first row, where the bulk of the diffusion is achieved. Under the impediment of

substantial blockage entering the second row, due to the diffusion processes in the first, even an optimized second row will produce no more than the 0.3 to 0.4 pressure recovery coefficient of a fully stalled diffuser. But even that small recovery is rewarding. About 27 psi of dynamic pressure is discharged from the first row; the second row recovery will be 8 - 9 psi, which corresponds to about 2 points of stage efficiency.

Optimization of the vaned diffuser is a very tricky business. There are a large number of variables involved with complex nonlinear interrelations among them, as has been amply demonstrated by Runstadler (1969) and discussed in Section 6.9. Without Runstadler's data, optimization attempts would be futile. As much as 6 points of recovery could easily be missed, dragging stage efficiency about 2 points below optimum.

The principal variables involved are:

Given:

$M_4$  throat Mach number: chosen at the design point to provide sufficient margin;  $M_4 = 0.9$  should be near optimum, but this choice requires further refinement in design and development

$A_4(1-B_4)$  throat effective flow area: specified by mass flow, throat stagnation properties, and throat Mach number

$p_{o_4}$ ,  $T_{o_4}$  throat stagnation conditions

To Be Chosen:

$w_4$  throat width

$b_4$  throat depth (or throat aspect ratio, AS =  $b/w$ )

$2\theta$  channel divergence angle

$L/W$

$R_3$  vane leading-edge radius ratio

Vane Form

$Z_d$  the number of vanes: follows from the choice of divergence angle

$Rey_4$  follows from geometry,  $M_4$ ,  $T_{o_4}$  and  $p_{o_4}$

Of secondary importance is the schedule of diffusion in the vaneless and semivaneless spaces and the entry shock. The boundary layer blockage in the throat will be largely determined by the overall velocity ratio from impeller tip to throat and by the length of the walls over which the boundary layer grows.

The output:

$B_4$  throat blockage

$A_4$  geometrical area

$C_{p_1}$  channel pressure recovery coefficient (the 1 indicates the first row)

We have made a preliminary study of the optimization of this cascade diffuser using Runstadler's (1969) data. The principal objective of this study was to lend certainty now to the achievement in later development of a specified pressure recovery coefficient. It has served this purpose. We are convinced that a first-row pressure recovery of 0.65 can be attained without extreme difficulty or resort to "tricks". In contrast, Boeing-AVLABS achieved 0.645 at their highest point; 0.60-0.63 was realized frequently. See Table X. The consistent tendency of the Boeing-AVLABS channel diffusers to best Runstadler's (1969) data by 2 - 3 points (Figures 148, 149, and 150) is comforting insurance.

As has been pointed out in Section 6.9, there is a large displacement of the hills of high recovery between the aspect ratio 0.25 and 1.0 data of Runstadler. Yet the hills are about the same elevation. Compare the maps in Figures 173 and 174.

It is recommended for stability purposes that diffuser design be placed on the low-angle side of the pressure hill. On the high-angle side, the diffuser is on the verge of stalling over the steep cliff. Figures 173 and 174 show for an aspect ratio of 0.25 that a diffuser

$L/W \approx 7$  and  $2\theta \approx 12^\circ$  is optimum. While for an aspect ratio of 1.0 diffuser,  $L/W \approx 16$  and  $2\theta \approx 6^\circ$  is optimum. Both diffusers give about the same pressure recovery coefficient of 0.65.

The aspect ratio 1.0 diffuser, because of its small divergence angle, requires a large number of (thin trailing edge) vanes, about 60 as a matter of fact. This high number will create excessive throat blockage, on the order of 0.20, which, as can be appreciated in Figure 196 greatly reduces available pressure recovery. The AS = 1.0 route is unsuccessful.

Instead, let us attempt to turn to a low-aspect-ratio diffuser which would have about 30 vanes at the optimum point. The blockage is about 0.10, and recoveries of 0.65 could be achieved as illustrated in Figure 171. This result is encouraging, but can we design a diffuser with such a low aspect ratio? In order to get a passage of aspect ratio 0.25, the distance between the vane tips would have to be on the order of about 2.4 inch, requiring about 8 vanes with leading edges at  $R = 1.06$ . This is grossly incompatible with the divergence-angle constraint of 30 vanes. The throat width could be increased without decreasing the vane number substantially by a large increase in vane leading edge radius ratio, but this will substantially increase blockage and degenerate performance. So we find ourselves blocked in an attempt to design an efficient thin-trailing-edge cascade diffuser with a throat aspect ratio around 0.25.

We have explored the middle ground between aspect ratio 0.25 and 1.0 without much success. It is very hard to drive the throat aspect ratio low enough. When it moves toward 1.0, the vanes' suction surface area increases so much, for the optimum recovery design, that blockage becomes excessive.

Before reaching any final conclusion on this matter, the multidimension diffuser performance space should be explored in conjunction with the restrictions of geometry and the dictates of inlet sidewall and suction surface boundary layer growth. In lieu of deeper exploration, we are quite confident that the 0.65 target pressure recovery for the

first row will not be realized from the simple designs above.

In order to break the vicious circle, we have split up the diverging channel between the vanes into smaller divergence angle passages (Figure 196). If the splitters start at the throat or just behind it, extra throat blockage is not generated because the splitters have no long suction surfaces sticking down into the semivaneless space. The recommended design is shown in Figure 196. This is predicted to produce the performance shown in Table XVIII. The relationship of this design to the state of the art is shown in Figure 184.

Preliminary optimization of the diffuser indicates a throat depth of 0.160. Therefore, it happens that the impeller tip depth and diffuser throat depth are equal; the meridional expansion discussed in Section 7.3.2 is unnecessary. However, on further optimization, this fortuitous correspondence may not persist and recourse to meridional expansion or contraction may be indicated.

#### 7.4.2 Deswirl

At the end of the second cascade row, the flow contains residual swirl. If necessary, a third-row set of deswirl vanes, operating fully stalled, can be emplaced. The same effect is often achieved by turning the flow to axial through a set of elbows.

These deswirl devices should not harm diffuser performance even though they operate fully separated. As long as they are properly designed not to block and accelerate the flow again, their losses are merely a part of the wasted kinetic energy in the outflow from the end of the diffuser vanes.

Probably it is impossible to design this third row to achieve any further pressure rise, although if the channels are made long enough after turning, a small amount of sudden expansion mixing rise might be won. Probably the increased size, weight, and cost do not warrant this attempt, for only 2 to 3 psi would be gained at most, amounting to a 0.5-point increase of stage efficiency.

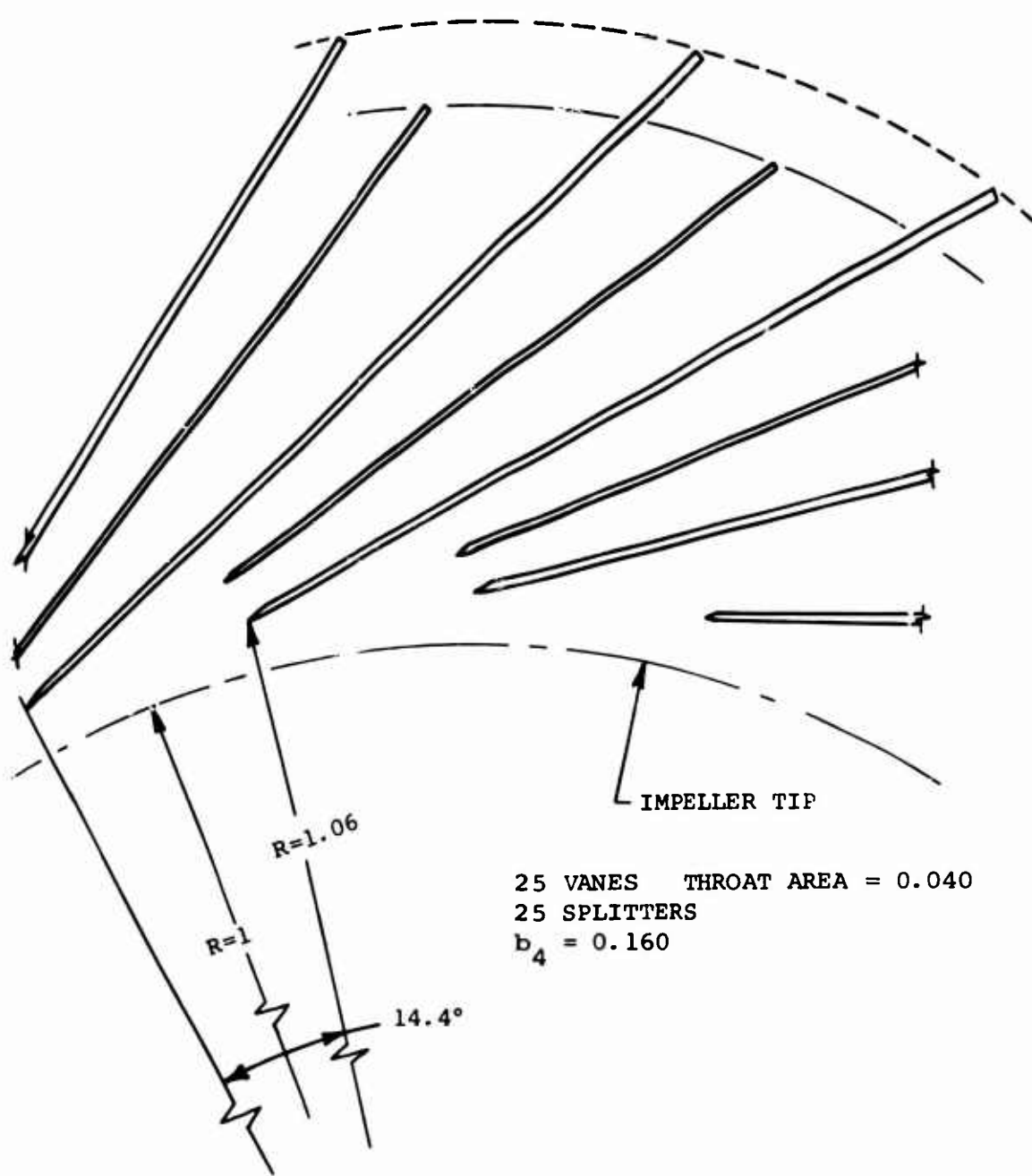


Figure 196. Cascade Diffuser, First-Row Vanes.

TABLE XVIII. TWO-ROW CASCADE DIFFUSER PARAMETERS

	First Row	Second Row	Overall
$p_{o_4}$ <sub>CL</sub>	165	$p_{o_5}$ <sub>CL</sub>	165
$T_{o_4}$	1080	$p_5$ <sub>CL</sub>	141.5
$M_4$ <sub>CL</sub>	0.90	$p_{coll}$	148.6
$B_4$	0.12	$c_{p_2}$	0.3
$p_5$	141.5		
$p_{o_5}$ <sub>CL</sub>	165		
$c_{p_1}$	0.65		
$Rey_4$	$1.97 \times 10^5$		
$AS$	1.28		
$2\theta$	7°		
L/W	16		

## 7.5 STAGE CHARACTERISTICS

Design point stage characteristics are summarized in Table XIX.

The range of this stage would be expected to be shorter than the Boeing-AVLABS RF-2 and somewhat longer than that of a transonic axial compressor operating at the inducer inlet tip Mach number of 1.20. A better range prediction must await much more detailed performance analysis; we anticipate that less uncertainty about range can be won through more analysis before resorting to experimental confirmation.

The choking flow is expected to be about 3% higher than design point mass flow or about  $m = 2.06$ . Two-thirds of the range from design to choke flow is predicted to occur by boundary layer adjustment in the diffuser throat after critical (sonic) throat conditions are reached.

Note that the overall total-to-static stage efficiency is predicted to be 84%. No doubt this prediction is optimistic, although it is based upon our best judgement of reasonable values for losses throughout the stage and extensive use of the flow models, including computer calculations, for prediction. On the other hand, this stage has not been designed with sufficient attention to detail. The design effort is certainly preliminary. But, we are unable to foresee pitfalls where disappointment awaits.

The principal reasons for the large efficiency gain (10 points) over the state of the art are:

- (1) Use of the transonic inducer for efficient diffusion without separating the boundary layer in the subsonic inducer.
- (2) Careful subsonic inducer design and development in order to achieve a mean tip diffusion ratio of 1.5 in contrast to Boeing's achievement of 1.37.
- (3) Increase of mass-flow-averaged slip factor from about 0.83 to 0.92 principally through the use of 40 impeller blades at the tip, in contrast to Boeing's 18, and the much smaller tip wake fraction.

TABLE XIX STAGE CHARACTERISTICS

Impeller Geometry	$r_{i_t}$	1.769
	$r_{i_h}$	013
	$r_2$	3.078
	$b_2$	0.160
	$Z_{inducer}$	10
	$Z_2$	40 (10 full, 10 secondary splitters, 20 tertiary splitters)
Diffuser Geometry	$R_{le}$	1.06
	$A_4$	0.04
	$Z_{d_1}$	50 (25 full vanes; 25 splitters)
	$2\theta$	7
	$L/W$	16
	$AS_4$	1.28
Aerothermo States	$Z_{d_2}$	50
	$p_{o_i}$	14.7
	$T_{o_i}$	520
	$\infty$	2.0
	N	70,000
	$M_{rel_{lt}}$	1.20

TABLE XIX - Continued

Aerothermo States	$M_{rel,1h}$	0.871
	$u_2$	1,880
	$\tilde{\sigma}_2$	0.92
	$p_2$	57.9
	$\tilde{p}_{o_2}$	168.8
	$T_{o_2}$	1,068.4
	$N_s$	61
	$\epsilon_2$	0.46
	$m_w/m$	0.20
	$\Delta p_{T_{rel}}$	0.208
	$M^*$	1.29
	$p_o^*$	165.2
	$\eta_i^*$	89.0
	$p_{o_4 CL}$	165.2
	$p_4$	97.7
	$M_4$	0.90
	$B_4$	0.12
	$Rey_4$	$1.97 \times 10^5$
	$c_{p_1}$	0.65
	$c_{p_2}$	0.30

TABLE XIX - Continued

Aerothermo States	$p_{coll}$	148.7
	$c_p$ overall	0.83
	$pr$	10.1
	$\eta$	84.5 inlet total to collector static, isentropic

- (4) Substantial reduction of the impeller discharge mixing loss, principally through reduction of the wake fraction occasioned by decreasing the impeller tip discharge area as a consequence of raising the specific speed from 43 to 61.
- (5) Increase in overall diffuser static pressure recovery coefficient from 0.73 to 0.83 principally by using a second diffuser row (despite its low expected recovery coefficient of 0.3).
- (6) Reduction of cover and disc friction losses from about 6 points to about 2.6 points, principally through the increase in specific speed.

While the predicted stage efficiency seems optimistically high, we feel that the prediction methods are well founded and not overoptimistic. However, we have injected into this redesign several rather unproven design concepts; principally the tandem inducer and the double-row cascade diffuser. Further, we have insisted upon impeller internal diffusion beyond the state of the art.

#### DESIGN UNCERTAINTY

Obviously, any new design which relies upon new flow elements and substantial improvements in old ones is risky. Yet to achieve a 6-to-7-point gain in total-to-static stage efficiency is a challenge which demands risk.

After this extensive study, we are of the strong opinion that the target efficiency and pressure ratio at a 2 lbm/sec flow rate is achievable today by using good basic fluid dynamics, physically valid design tools, and intelligent empirical development. It does not appear that the attainment of the current goal should require a great struggle.

We certainly are of the opinion that the stage efficiency from this redesign study of 84.5% is on the high side and indeed may be very close to the ultimate limit. But fortunately, it gives a safety margin of 4.5 points above the current target. This band will be employed to guarantee the target. For instance, the double-row cascade diffuser may prove to hide an adder in its thickets. Then recourse can be made to the well-proven vane-island design which, with

the extensive data of Runstadler now available, should easily achieve good enough recovery so that the decrease in stage efficiency from the change should be no more than 2 points.

As has been explained repeatedly in Sections 5 and 6, much uncertainty lies within the impeller, particularly involving secondary effects in the separated portion. As shown in Table XX we have assigned 2.6 points of lost efficiency to cover and disc friction; about these, we are fairly confident. We have assigned 2.4 more points for leakage and other contingencies, not including impeller discharge mixing; here we are not as certain. We are quite certain about the estimated 1 point for impeller discharge mixing loss.

All in all, the total loss inflation above our predictions should not be greater than 3 points. With this added to the potential decrease of 2 points occasioned by adoption of a vane-island diffuser, the maximum degeneration of our efficiency prediction should not be more than 5 points. Therein lies our confidence in reaching the target efficiency.

TABLE XX. SUMMARY OF LOSSES (DECREASE OF STAGE EFFICIENCY IN POINTS)

Only losses appropriate to flow model calculations are shown.\*

Inducer	
Transonic	0.8
Subsonic*	<u>0</u>
	0.8
Impeller	
Cover and Disc Friction	2.6
Blade Clearance	2.4
Miscellaneous	1.0
Discharge Mixing	1.1
Backflow	<u>2.0</u>
	<u>9.1</u>
Total Impeller	9.9
Diffuser	
Entry	0*
Cascade Rows 1 and 2 (equivalent to $C_p$ <sub>overall</sub> = 0.83) 5.6	
Total Diffuser	<u>5.6</u>
Total Loss	<u>15.5</u>
Stage Efficiency	84.5

\*Entropy generated in impeller partially contributes to discharge mixing loss; irreversibility in diffuser sidewall boundary layer contributes to throat blockage and decreases  $C_p$ ; etc.

## 8.0 RESEARCH NEEDED

The previous discussions of what is known of the fluid dynamics within the centrifugal stage and the critical examination of available analytical tools argue that more research is urgently needed to improve performance and predictability. Here we summarize the needs and make some expansive comments. No attempt is made to develop detailed instructions for a research program.

## 8.1 INDUCER

### 8.1.1 The Subsonic Inducer

The significance of inducer leading-edge supersonic flow and shocking coupled with boundary layer transition and separation should be investigated. First, a set of inducers with different suction surface shock Mach numbers, but with only this difference, should be carefully compared by testing. This investigation will validate or disprove Welliver and Acurio's concern, which we have subscribed to herein, for the leading-edge region.

If performance sensitivity is sustained by tests, then greatly improved leading-edge design tools should be devised. Section 6.1 emphasizes how difficult the fluid dynamics of this region are and the general paucity of good design methods for transonic airfoils, even for aircraft. A clever research program is vital to making effective progress here without expenditure of great sums of money. The gains will be applicable to axial compressors too and, if the investigators are very fortunate, might even aid aircraft wing design.

The teachings of transonic airfoil theory have already been employed by Welliver and Acurio to improve inducers, but a more sophisticated approach is needed to achieve optimum performance. Analyses must be generated both for the potential flow outside the boundary layer and for the boundary layer itself.

Boundary layer techniques such as those developed by Herring and Mellor (1968) are probably adequate to significantly improve our capabilities to predict inducer flow if proper shock-boundary layer interaction methods can be developed.

However, the analytical techniques for the potential flow field are not sufficiently developed and probably will not be for some time to come. A complete transonic flow analysis for the flow around the inducer blading, including subsonic and supersonic imbedded regions terminated by normal shocks is badly lacking. It would appear that modern computational methods and techniques are now available

to construct such theories, and indeed people are working on this problem. However, it will be some time before such computational methods become generally available and can be applied to the inducer problem.

In lieu of potential flow calculation methods, the analysis of the inducer will have to rely upon the type of empirical information that has been gained for transonic airfoils and was discussed in Section 6.1.

For the subsonic inducer, research studies are needed (1) to obtain a better understanding of the real flow phenomena and (2) to develop and test simple flow models sufficient for design.

#### Water Table Studies

It is most probable that a substantial gain in information can be obtained most easily from modeling inducer cascades in water table studies. The objective of such studies would be to obtain preliminary information about the transonic flow over the leading edge of the inducers and of the shock systems developed in the "channels" downstream of the leading edges. Such studies and observations would provide most useful starting points for further analysis and development of inducer shapes. Through water table studies, a large number of blade shapes could be empirically analyzed quickly and with a minimum expenditure.

#### Air Cascade Tests

Because water table studies cannot simulate properly boundary layer phenomena, and in order to obtain a detailed examination of the boundary layer's behavior (its interaction with shocks and separation characteristics), air cascade experiments are also needed. Such cascade studies, if properly conducted, should provide valuable information on the details of inducer flow as related to boundary layer separation characteristics. The cascade pressure rise would be correlated to that predicted by conventional theory. Such studies should also employ optical observations to

examine the transonic flow behavior together with hot wire and pressure instrumentation to study the details of the flow and shock waves/boundary layer interactions. Static pressure distributions around the blading would be very revealing. Overall pressure recovery, separation characteristics and losses as functions of incidence should be obtained. These cascade tests should cover the Mach number range from about 0.5 to 1.5.

#### 8.1.2 Separation Prediction and Control

Continuing diffusion after the leading edge region is vital in order to win the rewards of high inducer diffusion ratios. No adequate analyses or empirical information is available for the condition of a boundary layer passing through a leading-edge shock. Certainly as a minimum, a research program should confirm the usefulness of available tools for analyzing the boundary layer and the influence of impinging shocks. But we expect that the development of high-performance inducers must resort, out of necessity, to substantial empirical development of actual designs. This development should be heavily guided by basic flow principles and analysis. Detailed probing and use of some high-response instrumentation must be incorporated. Internal static pressure taps within the inducer would be highly desirable, for it is almost impossible to deduce hub flow conditions from a station on the cover. In order to facilitate internal probing and geometrical modification, the use of a low-sonic-speed gas is recommended for the early stages of development.

#### 8.1.3 Transonic Inducer

A detailed design study using well established axial compressor technology should be made in conjunction with an overall stage design effort. The transonic element should be tested alone and succeeded by the subsonic element.

#### 8.1.4 Coupling Between Transonic and Subsonic Inducers

We have good reasons to believe that the transonic inducer will not substantially influence the performance of the subsonic row by reason of the wakes passing through the latter. However, the interactions between the two-blade rows should

be investigated empirically in cascade and rotating rigs.

#### 8.1.5 Inducer Exploratory Development

A series of candidate inducer designs should be constructed, tested, and developed. It is most important to prove conclusively what internal diffusion ratio is attainable at various levels of impeller tip relative Mach number. For this testing, a workhorse impeller should be used behind the inducer. Sufficient experimental data must be taken from the rig to demonstrate without question the level of overall diffusion attained and its impact upon stage performance. The influence of the inducer design upon performance of the succeeding impeller should not be ignored.

For the inducer alone, a persistent research effort should be sustained until the designer of high performance centrifugal stages can find assured guidance from proven inducers with good diffusion ratios.

## 8.2 IMPELLER

The fluid dynamics of the separated impeller is one of the two least-known territories in the centrifugal stage. Fortunately, this ignorance is not predicted to be of momentous concern, for the unappraisable internal phenomena are not believed to cause substantial losses. The behavior of the separated flow does, however, powerfully influence the flow pattern at the tip of the impeller, particularly the through-flow slip factor. We have identified the latter as one of the principal reasons why Boeing's stage fell below expectations for pressure ratio and efficiency.

The prime need now from an impeller research program is the development of a relatively simple and easy-to-use model for the three-dimensional gyration of the separated jet within the impeller, particularly as it is influenced by meridional bend separation. This model must give adequate predictions of slip factor, for that is its principal reason for being.

The analytical results should be confirmed by a set of tests, which do not have to be carried out at high pressure ratios and tip speeds. In these tests, the severity of the meridional bend should be increased, with all other things constant and the slip factor of the impeller determined. The theory should be critically evaluated as to its success in showing the measured effects. Then, splitter vanes should be placed in the impeller, as recommended herein and as used by Morris and Kenny (1968), to prove that a large number of blades raises the slip factor for even a thoroughly separated impeller. The hypothesis that splitter vanes raise the slip factor without increasing losses should be carefully evaluated.

A direct experiment is demanded in order to evaluate cover and disc friction prediction models. Particularly the cover friction evaluation is uncertain because of the influence of the blades passing over the cover. We recommend that a test setup be built where the cover is mounted on a torque balance for direct measurement of friction torque. We have briefly studied this prospect and believe it to be relatively easy to effect, particularly on low-speed

machines. There is no need to simulate the tip speeds, pressure ratios, and Mach numbers of the high-speed, high-pressure-ratio compressors. Results at much lower speeds will be entirely valid after proper (known) extrapolations to high speed.

The influence of leakage over the impeller vanes should be explored explicitly. This can be done by systematically increasing the gap. The impact upon the fluid dynamics should be measured by detailed impeller tip probing with high-response instruments and through extensive cover taps. Again, results at low to medium speed should be sufficient.

The probability of generating a secondary flow model for the separated centrifugal which will allow authentic predictions of flow into the wake region is so slight today that we do not recommend a research program here. Further, it does not appear to be very important to understand these flow patterns in detail, particularly if a good and simple slip prediction method can be developed as recommended above. We expect that the predilection of some research investigators to look at all the detailed secondary flows in the impeller will prove, in the end, as fruitless as the extensive studies of secondary flows in axial compressors. While it is good to know what is going on, and eventually to prove from this knowledge that the secondary flows are not of great consequence, in the end less precise models have proven to be adequate for design. In the case of the axial compressor, it is most intriguing to speculate on the reason why, in light of the great depth to which secondary flow and boundary layer problems have been explored, no valid design tool is available for predicting the critical casing boundary layers and the controlling stall limits they impose upon the blades.

For the centrifugal compressor, we believe that best progress will be made by starting from the simplest possible flow models, and then elaborate them only where absolutely necessary to design for good performance.

We have asserted with some vigor that internal mixing processes within the centrifugal compressors are strongly damped by Coriolis effects. While visualization data from centrifugal impellers have strongly supported this

assertion, a direct confirmation would be welcome. We recommend that the mixing of jets and of wakes be studied in rotating coordinates through a program analogous to the extensive work in stationary coordinates.

While we have not attempted to drive effective relative diffusion into the radial portion of the wheel, because of the uncertain influence of Coriolis acceleration, separation criteria for turbulent boundary layers in rotating coordinates should be developed. An approach similar to that of Lieblein (1959) should be expeditious. He shows that the stalling characteristics of 6500 series axial cascade blades can be correlated against the diffusion (velocity) ratio on the blade surface.

We recommend that Lieblein's approach and experimental technique be employed on rotating blades. In the experiments, a systematic variation of the Rossby number ( $W/u$ ) would be made and used to correlate the separating diffusion ratio. For negative Rossby numbers (on the driving side of a radial vane), the separating diffusion ratio can be expected to increase, perhaps very greatly. Dean (1968) offers evidence from visualization studies that this is so. For positive Rossby number (on the trailing face of the radial vane) the separating diffusion ratio is expected to be greatly diminished as the Rossby number increases. For infinite Rossby number, Lieblein's separating diffusion ratio of about 2 should be observed. This basic study as well as that of mixing in rotating coordinates, will have important implications in fields other than the centrifugal compressor.

The existing impeller discharge mixing theory appears to be authentic; however, as demonstrated in Section 5, no direct experimental confirmation has ever been reported. This should be done for the flow conditions of high-speed impellers. The experimental task is not easy; high-response instruments and detailed three-dimensional probing are essential.

The high frequencies encountered in air compressors encourage use of low-sonic-speed gas in order to ease instrumentation problems. The tests should deliver data on the mixed-out radius  $R^*$  and on the characteristics of the mixed-out state,

particularly blockage and turbulence level. The mixing process should be studied in an authentic supersonic flow with and without diffuser vanes. The existing theory must be the starting point for the experiments and must be used, at least initially, to unify the data.

### 8.3 IMPELLER TIP/DIFFUSER ENTRY

The most important region of basic fluid dynamic ignorance in the centrifugal stage surrounds the impeller tip and diffuser entry, discussed at length in Sections 5 and 6. No reliable means are available for predicting the blockage at the diffuser throat, which is the most important variable governing diffuser performance. Further, no methods are known that can yield a good estimate of the backflow into the impeller, which can cause substantial efficiency loss. Further, the influence of the pressure fields over the diffuser vanes is known to penetrate deeply into the impeller and may affect its diffusion capabilities. No satisfactory means are available now to predict this interaction. For instance, use of a large number of small diffuser vanes may be beneficial because of their less extensive pressure fields, and therefore, expected smaller impact upon impeller processes. But we have no analyses to assess their virtues.

The greatest research need now of the high-performance centrifugal compressor is a thorough exploration of the impeller tip/diffuser entry region, with the objective of generating appropriate design tools. While the Boeing-AVLABS program contributed monumentally to our understanding of this region, a more basic and detailed general investigation is required. We recommend that a program of detailed probing, schlieren and perhaps interferometric visualization and the use of high-response instrumentation be initiated. It is absolutely critical that this investigation be guided by the best knowledge available of the many flow phenomena involved.

We hold little hope that a completely general theory will be developed within decades. This is because this flow region involves some of the most difficult fluid dynamics known and in an especially intractable fashion because of the shallow passages, thick boundary layers, and shock wave/boundary layer interactions. While attempts to further the general theory always should be included in any research programs, more expeditious today is an attempt to make substantial improvements on the kind of flow model offered by Welliver and Acurio.

Using the flow models available now, we have redesigned the Boeing-AVLABS compressor along lines which should minimize backflow. Further, we have used trends predicted by boundary layer theory to extrapolate the Boeing-AVLABS blockage data to the new design. We are quite certain these moves are significant and will lead to major gains in performance. But if ultimate performance is to be won, we are also sure that the missing tools must be provided to the designer. We still believe that the ultimate performance for this type of compressor lies about 8 points above the AVLabs target as shown in Figure 197.

In the research program for the diffuser entry, further exploration should be made of flow details around the channel entry and vane leading edges in order to provide the grist needed for a better surge prediction model. Welliver and Acurio were of the opinion that the conventional wisdom's attention to flow incidence on the diffuser vanes, as dictated by the flow angle out of the impeller, is fallacious. Rather, they attributed surge, and we support this view, to the influence of growing blockage on the channel diffuser performance. However, these hypotheses need to be critically confirmed.

Also from the entry program, validation or disproof should be effected of our hypothesis that the entropy generated on the sidewall and suction surface in the boundary layers does not penetrate rapidly into the core of the flow so that the diffuser throat center-line stagnation pressure is equal to the mixed-out stagnation pressure from the impeller. This matter can be explored by stagnation pressure probes, although high-response probes must be employed in a critical experiment. Fortunately, miniature solid-state, high-frequency-response stagnation probes have recently become available; they appear to be quite attractive for this task. Such instruments will also be vital to understanding the onset of surge.

In studying surge in the research program, our hypothesis that the characteristics of the channel diffusers are responsible for stability should be critically tested. This can be done by determining the characteristics of a series of different diffusers and correlating these with the onset of surge.

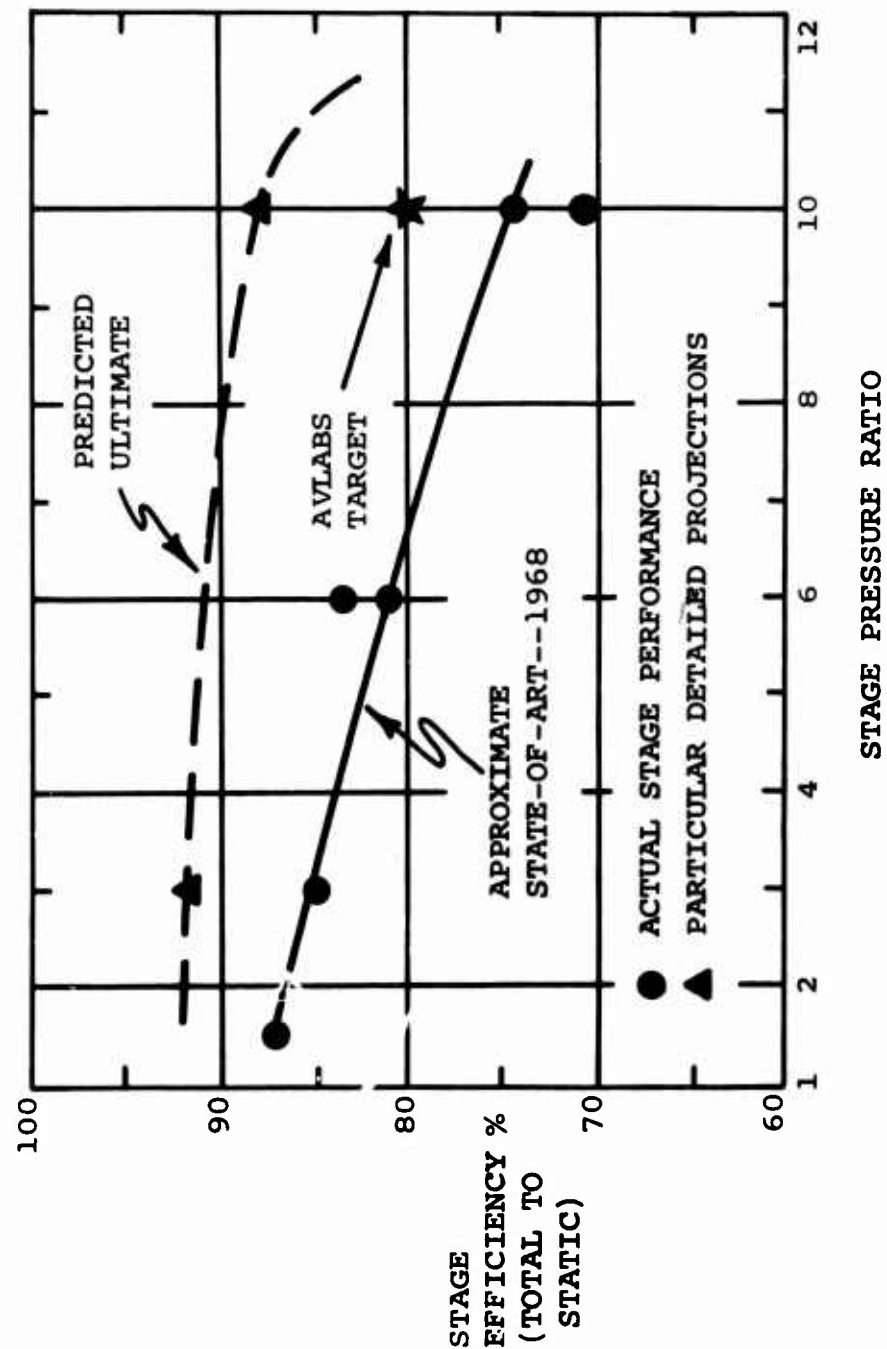


**Figure 197. State-of-the-Art Centrifugal Compressor Performance and Predicted Ultimate (from Dean 1968).**

When studying the entry region, it would be interesting, although we are not sure it is vital, to observe the interaction of the diffuser entry shock with the impeller. Perhaps this shock has an important influence on the slip factor of the impeller and backflow into it. We recommend that a transparent disc be used on the impeller through which the schlieren or interferometer can stare. A transparent disc can be run on a high-pressure-ratio, high-Mach-number machine operating in a low-sonic-speed gas.

The backflow pattern should be measured in order to ascertain the nature of backflow and how it depends upon the flow pattern leaving the impeller and the geometry of the diffuser. First, the expected existence of transient backflow should be proven. Then some quantitative data should be generated on the extent of backflow and how it depends on other variables.

Water-table studies of the diffuser entry region may be useful to give early indications of the entry shock pattern and detailed flow around the vane leading edge. Welliver and Acurio's water table results do compare quite well with their schlieren data.

#### 8.4 DIFFUSER

For the channel diffuser of the vane-island type, a monumental advance was made by the Boeing-AVLABS program when it was shown that diffusers in actual stages could be replicated by simple laboratory diffusers. The extensive data collected during the Creare-AVLABS diffuser program reported by Runstadler (1969) has greatly enabled the tricky optimization of the diffuser. Unfortunately, without a means for predicting blockage accurately, application of this new diffuser information is hampered.

We are of the opinion that no further research needs to be done at this time to advance the knowledge of the simple straight-channel diffuser in the centrifugal stage except to study the influence of flow turbulence. Beneficial improvement in recovery over Runstadler's levels appeared to be caused by the high turbulence resulting from discharge mixing. If mixing is suppressed, will diffuser recovery suffer?

If multirow cascade diffusers are advantageous, as we suspect they are, then research is needed on the interaction between the first and second rows. Even more important immediately is the confirmation that such a diffuser has inherently a substantially higher recovery than the optimum vane-island type. The stability of the double row diffuser needs investigation too.

For cascade type diffusers, we have recommended straight passages. This imposes certain implications on vane shapes which need to be studied further analytically and experimentally.

We recommend strongly that an exploratory development program be initiated to search for optimum centrifugal diffusers along the lines discussed herein.

### 8.5 INSTRUMENTATION

In Section 4.2, we have explored in depth the meaning of low-response probe indications from the tip of an impeller. The inherent errors of the conventional probing means are quite significant; common methods of treating the data occasion seriously-misleading indicated values which are not representative of aerothermodynamically-significant quantities.

A research and exploratory development program is needed to improve the instrumentation available for small, high-pressure-ratio, high-speed centrifugal compressor development. New types of high-response instruments should be evaluated and better means developed to make acceptable probes live in the compressor environment. A new standard of much greater experimental sophistication is needed for the small, high-performance centrifugal compressors. The same argument can be made, incidentally, for the small axial compressor.

Hot wire and hot film instruments are attractive for this duty, although they often do not provide sufficient life in this rugged service. Miniature solid-state stagnation pressure probes and wall static transducers appear very promising and potentially offer good life.

## 8.6 MISCELLANEOUS

Of course, there are many other important factors governing the successful performance of the centrifugal compressor which we have not dwelled upon in this study. Such matters as noise generation, vibration, fatigue, and stressing are all candidates for research of varying intensity.

The noise problem is assuming greater importance; very little is known about the noise-generating characteristics of small, high-pressure-ratio centrifugal compressors. A research program to map out the extent, severity, and nature of the problem would be worthwhile.

No doubt the small centrifugal compressor designer will have to incorporate noise as a significant design criterion some time in the future just as his brother designing large axial compressors must do today. To prepare for this day, the significant noise sources in the centrifugal compressor should be identified. For instance, it may be desirable to locate the diffuser vanes as close to the impeller tip as possible in order to enhance performance, but this may cause severe noise. As far as we know, no one has any adequate way of evaluating this compromise today.

## 9.0 CONCLUSIONS

The prime objective of this program was to identify fluid dynamic means for making major improvements in the efficiency of the high-pressure-ratio, small centrifugal compressors under development by AVLabs. The study was based principally upon the extensive data available from the Boeing-AVLabs program as reported by Welliver and Acurio (1967). The program's objectives were to test available means for predicting the fluid dynamics of the compressor, to develop better means where possible, to redesign the stage, and to make research recommendations. The goal was to provide well-validated guidelines for the next stage of exploratory development in order to insure that the target performance would be reached.

The results of this program are very encouraging. We believe that the causes for the Boeing-AVLabs stages falling well below the target performance have been established. Unfortunately, enough data of the right kind are not available to prove our causal identification beyond question. But the confluence of evidence from various sectors of the Boeing-AVLabs data in combination with extensive evidence from other realms makes the identification quite positive.

Some of the flow models offered by Welliver and Acurio have stood up well against our critical testing, while others have failed in part or whole. Some improvement in the models has been made under this program, but usually where the Welliver and Acurio models faltered, we have found that the basic fluid-dynamic foundations needed to improve the models is too weak for much advance. In order to rectify this situation, we have laid out a research program in brief.

The Boeing-AVLabs stage has been extensively redesigned herein, although the design studies are of a preliminary nature only. Nevertheless, we assert that the trends predicted by this preliminary design are indeed significant. Further, the performance margin predicted above the AVLabs target is substantial, leaving considerable room for slippages.

The major calculated performance gains principally arise from almost doubling the specific speed of the impeller,

with a consequent increase in shaft speed to 70,000 rpm. Also, inclusion of a new kind of inducer, which is based upon transonic axial compressor technology, promises superior impeller internal diffusion.

At the tip of the impeller, we see the consequences of raising the specific speed as a deep cut in impeller discharge mixing losses. Also, the tendency for backflow from the diffuser should be greatly damped.

Finally, a major potential contribution arises from recourse to a two-row cascade diffuser. Not much can be done to reduce the throat blockage in the first row from that found by Boeing, but the first row can now be optimized based on the extensive AVLabs straight-channel diffuser data which have just become available. This optimization promises to yield a few points of improvement in diffuser recovery at most; at least, it should prevent degeneration of diffuser recovery by the more stringent design conditions of a cascade with thin trailing edges. But most important to the improvement of diffuser performance is the inclusion of a second row. Although it is expected to have rather poor recovery, it adds significantly to the overall performance of the diffuser and to the stage.

The results of the redesign studies for a mass flow of 2 lb/sec and pressure ratio 10 are a high limit prediction of 85% total to static stage efficiency and a minimum expectation of 80%. The 85% efficiency level was predicted from the most probable estimates we could make. Therefore, it is not intentionally an optimistic figure. The resulting latitude to the AVLabs target is very comforting and provides much assurance, in our opinion, that the AVLabs targets can be met fairly readily in the next round of exploratory development.

## 10.0 RECOMMENDATIONS

As a result of this study, we offer the following recommendations:

1. Proceed to exploratory development of a new stage aimed at the AVLabs target. The program should incorporate in its initial phases simplified exploration of the major improvements in component performance which are essential in order to win the large gain in efficiency needed.

We recommend that a low-sonic-speed gas be used in the first stage of development because of its small temperature rise and the low impeller speed which facilitates instrumentation and modification. The avoidance of the high temperature rise of an air machine will greatly simplify the work. Means are known for properly scaling a low-sonic-speed impeller to give credible replication of air performance. However, it would be wise to prove performance gains by direct comparison with a known stage running in the low-sonic-speed gas. For instance, the Boeing-AVLabs RF-2 (transformed as appropriate for the gas type) could be tested to serve as a base point against which to compare the performance of a new stage. By this means, possible distortion occasioned by the use of the different gas can be largely eliminated from the appraisal of potential gains in performance by design changes.

2. A research program should be initiated along the lines recommended in Section 8. The program will help to insure a continuing effort by the compressor fraternity toward improving the basic design tools in areas where they are overly weak. The stimulation provided by an open research program should do a great deal to counter the euphoria, even complacency, which unfortunately tends to pervade design departments, especially the more successful ones. Often this sense of well being is rudely shattered during an excursion into new territory. That happened in fact on the Boeing-AVLabs expedition. An ongoing research program aimed at the basic ignorances does much to counter this ubiquitous human tendency.

Lay especial research emphasis on three areas:

- a. Development of high tip relative Mach number inducers with good diffusion ratios.
  - b. Development of adequate basic fluid dynamic understanding and appropriate design tools for the impeller tip/diffuser entry region, with special concentration on the prediction of throat blockage and impeller backflow.
  - c. Exploration of the multirow cascade diffuser in order to determine the potential gain it may offer.
3. Once it is plain that the current AVLabs target of 80% stage efficiency will be won, raise the target to 85%. Also, the target pressure ratio should be raised to 13, perhaps even 15. We hazard to predict that this level can be achieved within four to six years, if a vigorous research and exploratory development program is continued.

## 11.0 LITERATURE CITED

Acosta, A. J. and Osborne, W.; CINEMATOGRAPHIC STUDIES OF FLOW IN PUMPS; Available from Professor A. J. Acosta, Mechanical Engineering Department, California Institute of Technology.

Balje, O. E.; A STUDY ON DESIGN CRITERIA AND MATCHING OF TURBOMACHINES, PART B - COMPRESSOR AND PUMP PERFORMANCE AND MATCHING OF TURBO COMPONENTS; ASME Paper No. 60-WA/231, 1960.

Bernstein, A., Heiser, W. H. and Hevenor, C.; COMPOUND-COMPRESSIBLE NOZZLE FLOW; ASME Paper No. 67--APM-L, 1968.

Daily, J. W. and Nece, R. E.; CHAMBER DIMENSION EFFECTS ON INDUCED FLOW AND FRICTIONAL RESISTANCE OF ENCLOSED ROTATING DISKS; Transactions ASME, Journal of Basic Engineering, Series D, Vol. 82, 1960, Pages 217-232.

Dallenbach, F. and Van Le, N.; SUPERSONIC DIFFUSER FOR RADIAL AND MIXED FLOW COMPRESSORS; Transactions ASME, Journal of Basic Engineering, December 1960, Pages 973-979.

Dean, R. C., Jr., et al; AERODYNAMIC MEASUREMENTS; MIT Press 1953. Out of Print.

Dean, R. C., Jr.; SECONDARY FLOW IN AXIAL COMPRESSORS; MIT Gas Turbine Laboratory, May 1954.

Dean, R. C., Jr. and Senoo, Y.; ROTATING WAKES IN VANELESS DIFFUSERS; Transactions ASME, Journal of Basic Engineering, September 1960, Pages 563-570.

Dean, R. C., Jr.; SEPARATION AND STALL; Chapter 11 in Handbook of Fluid Dynamics, McGraw-Hill, 1961.

Dean, R. C., Jr.; ON THE UNRESOLVED FLUID DYNAMICS OF THE CENTRIFUGAL COMPRESSOR; Presented at the ASME Gas Turbine Conference, March 1968; Creare Technical Note TN-68.

Delio, G. J., Schwent, G. V. and Cesaro, R. S.; TRANSIENT BEHAVIOR OF LUMPED-CONSTANT SYSTEMS FOR SENSING GAS PRESSURE; NACA TN 1988, 1949.

Dussourd, J. L.; COMPARISON OF ANALYTICAL AND EXPERIMENTAL BLADE LOADINGS OF A CENTRIFUGAL IMPELLER; Proceedings Symposium on Measurement in Unsteady Flow, ASME, 1962.

Englert, G. W.; ESTIMATION OF COMPRESSIBLE BOUNDARY LAYER GROWTH OVER INSULATED SURFACES WITH PRESSURE GRADIENT; NACA Technical Note 4022, June 1951.

Erwin, John R.; EXPERIMENTAL TECHNIQUES; Section D of Aerodynamics of Turbines and Compressors, W. R. Hawthorne, Editor, Pages 167-266, Princeton University Press, 1964.

Faulders, C. R.; AN AERODYNAMIC INVESTIGATION OF VANCED DIFFUSERS FOR CENTRIFUGAL COMPRESSORS; MIT Gas Turbine Laboratory, January 1954.

Fejer, A. E., Heath, G. L., and Driftmyer, R. T.; AN INVESTIGATION OF CONSTANT AREA SUPERSONIC FLOW DIFFUSION; Aerospace Research Laboratories AR1 64-81, May 1964.

Fowler, H. S.; THE DISTRIBUTION AND STABILITY OF FLOW IN A ROTATING CHANNEL; ASME Paper No. 68--GT-1, Presented at ASME Gas Turbine Conference, 1968.

Gadd, G. E.; INTERACTIONS BETWEEN NORMAL SHOCK WAVES AND TURBULENT BOUNDARY LAYERS; Aeronautical Research Council R & M 3262, 1961.

Gardow, E. B.; THE THREE-DIMENSIONAL TURBULENT BOUNDARY LAYER IN A FREE VORTEX DIFFUSER; MIT Gas Turbine Laboratory Report No. 42, January 1958.

Graham, W. J.; FLOW ABOUT A FAMILY OF SIMPLE, BLUNT AND SHARP LEADING-EDGES TWO-DIMENSIONAL AIRFOILS AT TRANSONIC AND LOW SUPERSONIC SPEEDS; NPL Aero Report 11-89, ARC 27 838, February 1966.

Halleen, R. M. and Johnston, J. P. THE INFLUENCE OF ROTATION ON FLOW IN A LONG RECTANGULAR CHANNEL - AN EXPERIMENTAL STUDY; Department of Mechanical Engineering, Stamford University, 1967.

Herring, H. J. and Mellor, G. L.; A METHOD OF CALCULATING COMPRESSIBLE TURBULENT BOUNDARY LAYERS; NASA CR-1144, September 1968.

Hubbard, P. G.; INTERPRETATION OF DATA AND RESPONSE OF PROBES IN UNSTEADY FLOW; Proceedings of Symposium on Measurement in Unsteady Flow, ASME, 1962.

Jansen, W.; STEADY FLUID FLOW IN A RADIAL VANELESS DIFFUSER; Transactions ASME, Journal of Basic Engineering, Series D, Volume 86, 1964, Pages 607-619.

Johnson, R. C.; AVERAGING OF PERIODIC PRESSURE FLUCTUATIONS BY A TOTAL-PRESSURE PROBE; NACA TN 3568, 1955.

Johnston, J. P.; EXPERIMENTAL DATA ON THREE-DIMENSIONAL FLOW IN A CENTRIFUGAL COMPRESSOR DIFFUSER; MIT Gas Turbine Laboratory, December 1954.

Johnston, J. P. and Dean, R. C., Jr.; LOSSES IN VANELESS DIFFUSER OF CENTRIFUGAL COMPRESSORS AND PUMPS; Transactions ASME, Journal of Engineering for Power, Vol. 88, No. 1, January 1966.

Johnston, J. P.; PRIVATE COMMUNICATION; Stanford University, 1968.

Kline, S. J.; ON THE NATURE OF STALL; Transactions ASME, Journal of Basic Engineering, September 1959.

Kline, S. J. and McClintock, F. A.; DESCRIBING UNCERTAINTIES IN SINGLE SAMPLE EXPERIMENTS; Stanford University, Mechanical Engineering Department, January 1953.

Kramer, J. J. and Stanitz, J. D.; A NOTE ON SECONDARY FLOW IN ROTATING RADIAL CHANNELS; NACA Report 1179, 1954.

Kramer, J. J.; ANALYSIS OF INCOMPRESSIBLE, NONVISCOUS BLADE-TO-BLADE FLOW IN ROTATING BLADE ROWS; Transactions ASME, February 1958, Pages 263-275.

Ladenburg, R. W.; PHYSICAL MEASUREMENT IN GAS DYNAMICS AND COMBUSTION; Princeton University Press, Princeton, New Jersey, Pages 309-321.

Lakshminarayana, B. and Horlock, J. H.; REVIEW: SECONDARY FLOWS AND LOSSES IN CASCADES AND AXIAL-FLOW TURBOMACHINES; International Journal Mechanical Sciences, Pergamon Press, Ltd., Vol. 5, 1963, Pages 287-307.

Lieblein, S.; LOSS AND STALL ANALYSIS OF COMPRESSOR CASCADES; Transactions ASME, Journal of Basic Engineering, Series D, Vol. 81, No. 3, September 1959.

Mann, R. W. and Marston, C. H.; FRICTION DRAG ON BLADED DISCS IN HOUSING (AS A FUNCTION OF REYNOLDS NUMBER, AXIAL AND RADIAL CLEARANCE AND BLADE ASPECT RATIO AND SOLIDITY); Transactions ASME, Journal of Basic Engineering, December 1961, Pages 719-723.

Maskell, E. C.; FLOW SEPARATION IN THREE DIMENSIONS; Royal Aircraft Establishment, Farnborough, Report Aero 2565, November 1955.

Mellor, G. L.; AN ANALYSIS OF AXIAL COMPRESSOR CASCADE AERODYNAMICS; Transactions ASME, Journal of Basic Engineering, September 1959, Pages 362-386. (Parts I and II.)

Moffat, R. J. and Dean, R. C., Jr.; WAKE INTERACTION EFFECTS AND PERFORMANCE CHARACTERISTICS OF STAGNATION TYPE THERMO-COUPLES; Appendix VII, Vol. II, AVLabs Report 67-30, August 1967 (Welliver & Acurio).

Morris, R. E. and Kenny, D. P.; HIGH PRESSURE RATIO CENTRIFUGAL COMPRESSORS FOR SMALL GAS TURBINE ENGINES; Presented at the AGARD Propulsion and Energetics Panel on Helicopter Propulsion Systems, Ottawa, June 1968. (Document available from United Aircraft of Canada, Limited.)

Neumann, E. P. and Lustwerk, F.; SUPERSONIC DIFFUSERS FOR WIND TUNNELS; Journal Applied Mechanics, Vol. 16, No. 2, 1949, Page 195.

Noell, G. L.; WATER TESTS OF HIGH SPEED CENTRIFUGAL SHAFT SEALS, Pratt & Whitney Aircraft, Canel Division, Report TIM-914, June 1965.

Pearcey, H. H.; SHOCK-INDUCED SEPARATION AND ITS PREVENTION BY DESIGN AND BOUNDARY LAYER CONTROL; In Vol. 2 of Boundary Layer and Flow Control by G. V. Lachmann, Pergamon Press, 1961, Pages 1166-1344.

Rayle, R. E.; AN INVESTIGATION OF THE INFLUENCE OF ORIFICE GEOMETRY ON STATIC PRESSURE MEASUREMENTS; MIT S.M. Thesis, Department of Mechanical Engineering, 1949.

Rodgers, C.; VARIABLE GEOMETRY GAS TURBINE RADIAL COMPRESSORS; ASME Paper No. 68-GT-63, Presented at Gas Turbine Conference, Washington, D. C., March 17-21, 1968.

Rodgers, C.; PRIVATE COMMUNICATION; March 3, 1969.

Runstadler, P. W., Jr.; PRESSURE RECOVERY PERFORMANCE OF STRAIGHT CHANNEL, SINGLE PLANE DIVERGENCE DIFFUSERS AT HIGH MACH NUMBERS; U. S. Army Aviation Materiel Laboratories, Fort Eustis, Virginia, to be published, 1969.

Sakai, T., Watanabe, I., Fujie, K., and Takayanagi, I.; ON THE SLIP FACTOR OF CENTRIFUGAL AND MIXED-FLOW IMPELLERS; ASME Paper 67-WA/GT-10, 1967.

Schlichting, H.; APPLICATION OF BOUNDARY-LAYER THEORY IN TURBOMACHINERY; Transactions ASME, Journal of Basic Engineering, December 1959, Pages 543-551.

Schlichting, H.; BOUNDARY LAYER THEORY; McGraw-Hill Book Company, Inc., 1960.

Schorr, P. G., Welliver, A. D. and Winslow, L. J.; DESIGN AND DEVELOPMENT OF SMALL, HIGH-PRESSURE RATIO, SINGLE-STAGE CENTRIFUGAL COMPRESSOR; The Boeing Company, Seattle, Washington, March 11, 1969.

Senoo, Y., Yamaguchi, M. and Nishi, M.; A PHOTOGRAPHIC STUDY OF THE THREE-DIMENSIONAL FLOW IN A RADIAL COMPRESSOR; ASME Paper No. 68-GT-2, 1968.

Shapiro, A. H.; THE DYNAMICS AND THERMODYNAMICS OF COMPRESSIBLE FLUID FLOW; Volume II, The Ronald Press Company, New York, Pages 1153-1156, 1953.

Shaw, R.; THE INFLUENCE OF HOLE DIMENSIONS ON STATIC PRESSURE MEASUREMENTS; Department of Mechanical Engineering, Liverpool, July 1959.

Sinnott, C. S. and Osborne, J.; REVIEW AND EXTENSION OF TRANSONIC AEROFOIL THEORY; Ministry of Aviation, Aeronautical Research Council R & M No. 3156, 1961, Her Majesty's Stationery Office, London.

Stalker, R. J.; A STUDY OF THE CHINA-FILM TECHNIQUE FOR FLOW INDICATION; Aeronautical Research Laboratories, Victoria, Australia, October 1955.

Stanitz, J. D.; APPROXIMATE DESIGN METHODS FOR HIGH SOLIDITY BLADE ELEMENTS IN COMPRESSORS AND TURBINES; NACA TN 2408, July 1951.

Stanitz, J.D. and Prian, V.D.; A RAPID APPROXIMATE METHOD FOR DETERMINING VELOCITY DISTRIBUTION ON IMPELLER BLADES OF CENTRIFUGAL COMPRESSORS; NACA TN2421, July 1951.

Stein, P. K.; THE MEASUREMENT OF HIGH FREQUENCY PRESSURE FLUCTUATIONS BETWEEN IMPELLER BLADES IN AN OPERATING GAS TURBINE COMPRESSOR; Soc. for Exp. Stress Analysis, October 1960.

Taylor, E. S.; THE SKEWED BOUNDARY LAYER; ASME Paper 58-A-113, December 1958.

Welliver, A. D. and Acurio, J.; ELEMENT DESIGN AND DEVELOPMENT OF SMALL CENTRIFUGAL COMPRESSORS; USAAVLABS Technical Report 67-30, Vol. I & II, U.S. Army Aviation Materiel Laboratories, Fort Eustis, Virginia, August 1967, AD 384923-Vol.I, AD 384924-Vol. II.

Welliver, A. D. and Acurio, J.; DESIGN AND DEVELOPMENT OF SMALL, SINGLE-STAGE CENTRIFUGAL COMPRESSOR; USAAVLABS Technical Report 67-47, U. S. Army Aviation Materiel Laboratories, Fort Eustis, Virginia, September 1967, AD 385595.

Wiesner, F. J.; A REVIEW OF SLIP FACTORS FOR CENTRIFUGAL IMPELLERS; Trans. ASME, Journal of Engineering for Power, Series A, Vol. 89, No. 4, October 1967, Page 558.

Winslow, L. J.; PRIVATE COMMUNICATION; Commercial Airplane Division, The Boeing Company, November 1968.

Wolf, S. and Johnston, J. P.; EFFECTS OF NON-UNIFORM INLET VELOCITY PROFILES ON FLOW REGIMES AND PERFORMANCE IN TWO-DIMENSIONAL DIFFUSERS; ASME Paper No. 68-WA/FE-25, presented at the Winter Annual Meeting, December 1968.

Wong, R. Y. and Stewart, W. L.; CORRELATION OF TURBINE BLADE ELEMENT LOSSES BASED ON WAKE MOMENTUM THICKNESS WITH DIFFUSION PARAMETER FOR A SERIES OF SUBSONIC TURBINE BLADES IN TWO-DIMENSIONAL CASCADE AND FOR FOUR TRANSONIC TURBINE ROTORS; NACA RM #55D08, 1955.

Wood, George P. and Gooderum, Paul B.; A FACTOR AFFECTING TRANSONIC LEADING-EDGE SEPARATION; Technical Note 3404, National Advisory Committee for Aeronautics, October 1956.

Wood, G. M. Manfredi, D. V. and Cygnor, J. E.; CENTRIFUGAL TYPES OF DYNAMIC SHAFT SEALS; ASME Paper 63-WA/167, 1963.

## APPENDIX I

### YAW PROBE - ERROR CAUSED BY VELOCITY GRADIENT

#### SUMMARY

Calculated error for yaw probes at  $R = 1.03$ , PF-2 impeller,  
 $= 0.134^\circ$ .

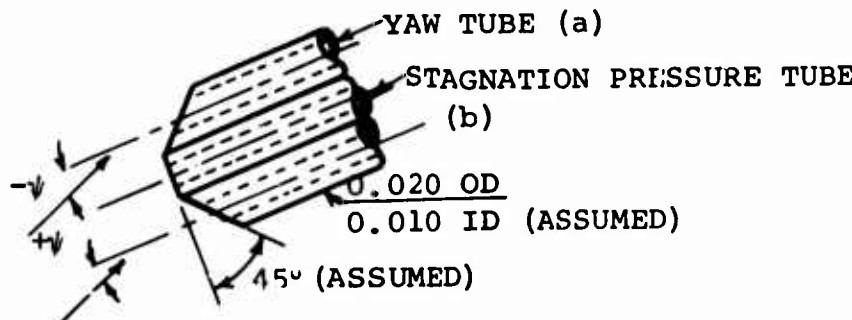


Figure 198. Yaw Probe Geometry.

According to Dean et al (1953), the variation of pressure with incidence angle,  $\psi$ , for a yaw tube cut off at a  $45^\circ$  angle is given as:

$\frac{\hat{p} - p}{p_o - p}$	$\psi$	$\frac{\Delta p^*}{p_o - p}$
.85	+10	.13
.72	0	0
.55	-10	-.17

\*  $\Delta p$  is indicated pressure difference between yaw tubes

We can write:

$$\hat{p} = p + f(\psi)(p_o - p)$$

where:  $f(\psi) \approx 0.72 + 0.015\psi$  ( $\psi$  in degrees)

(See equation in Figure 105)

at null,  $\hat{p}_a = \hat{p}_b$ , or

$$p_a + (0.72 + 0.015\psi)(p_{o_a} - p_a) = p_b + (0.72 - 0.015\psi)(p_{o_b} - p_b)$$

$$p_b - p_a + 0.72(p_{o_b} - p_{o_a}) - 0.72(p_b - p_a)$$

$$- 0.015\psi [(p_{o_b} - p_b) + (p_{o_a} - p_a)] = 0$$

$$0.28(p_b - p_a) + 0.72(p_{o_b} - p_{o_a})$$

$$- 0.015\psi [(p_{o_b} - p_b) + (p_{o_a} - p_a)] = 0$$

Assume:

$$p_{o_b} = p_{o_a}, (p_{o_b} - p_b) \approx (p_{o_a} - p_a)$$

So:

$$0.28 \left( \frac{dp}{dr} dr \right) + 0 - 0.015\psi [2(p_o - p)] = 0$$

$$\frac{0.28}{0.03} \frac{\frac{dp}{dr} dr}{p_o - p} = \psi$$

For RF-2:

$$\frac{dp}{dr} \approx \frac{18}{1/2} = 36 \text{ psi/in.}, p_o - p \approx 100$$

$$\frac{dp}{dr} dr = 36(0.04)$$

Therefore:

$$\psi = \frac{0.28}{0.03} \frac{36}{100} (0.04) = 0.134^\circ$$

## APPENDIX II

### IMPELLER DISCHARGE MIXING -- SUDDEN EXPANSION ANALYSIS

#### SUMMARY

The sudden expansion analysis (SEA) of Johnston and Dean (1966) for evaluating the losses due to a distorted flow at the tip of a centrifugal impeller has been generalized to include distortion in the meridional ( $x$ ) direction as well as in the tangential ( $\theta$ ) direction.

#### ASSUMPTIONS

- (1) The flow is steady relative to the impeller and is the same in each blade passage.
- (2) The mixing process produces a uniform final state and occurs quickly enough so that  $\Delta r$  of control volume is zero.
- (3) Shear stresses on the faces of the control volume may be neglected. (Notice that the wall shear stresses produce zero force anyway because the control volume has zero  $r-\theta$  surface area.)
- (4) The flow has negligible axial velocity, i.e.,  $C_x = 0$ .
- (5) The flow is an adiabatic process.
- (6) The gas is perfect and has constant specific heats.

The coordinate system is shown in Figure 19?

The coordinate system may be redefined to apply to mixed flow compressors with no change in the form of the equations.

#### ANALYSIS

Using the assumptions, we write:

a. Continuity Equation:

$$\int_{x=0}^{b^*} \int_{\theta=0}^{2\pi} \rho_2 C_{r_2} r_2 d\theta dx = \rho^* C_r^* 2\pi r_2 b^* \quad (1)$$

b. Energy Equation:

$$\int_{x=0}^{b^*} \int_{\theta=0}^{2\pi} T_{o_2} (\rho_2 c_{r_2} r_2 d\theta dx) = T_o^* \rho^* c_r^* 2\pi r_2 b^* \quad (2)$$

c. Angular Momentum:

$$\int_{x=0}^{b^*} \int_{\theta=0}^{2\pi} c_{\theta_2} (\rho_2 c_{r_2} r_2 d\theta dx) = c_{\theta}^* \rho^* c_r^* 2\pi r_2 b^* \quad (3)$$

d. State:

$$p = \rho RT \quad (4)$$

$$T_o = T + \frac{c^2}{2g_o J c_p} \quad (5)$$

e. Momentum:

The other equations have been written for the total impeller discharge flow because they are easier to handle in that form. However, the momentum equation presents a problem, since writing it in a fixed direction in Newtonian space (as demanded by Newton's laws) for the total circumference of the impeller ~~does~~ results in a trivial "zero equals zero" result. ~~So~~ we use the control volume shown in Figure 199, write the momentum equation in the fixed direction OMN and integrate over a period of time which is large compared to ~~the~~. This time integration insures that the fluid state mixed out is steady. If the mixing analysis is applied at an instant in time, as it may be, different mixed out states result for different orientations of the impeller blades relative to the fixed direction OMN. This unsteady outcome is inconsistent with the assumptions of a steady, axisymmetric mixed out state.

The momentum equation becomes, after time averaging:

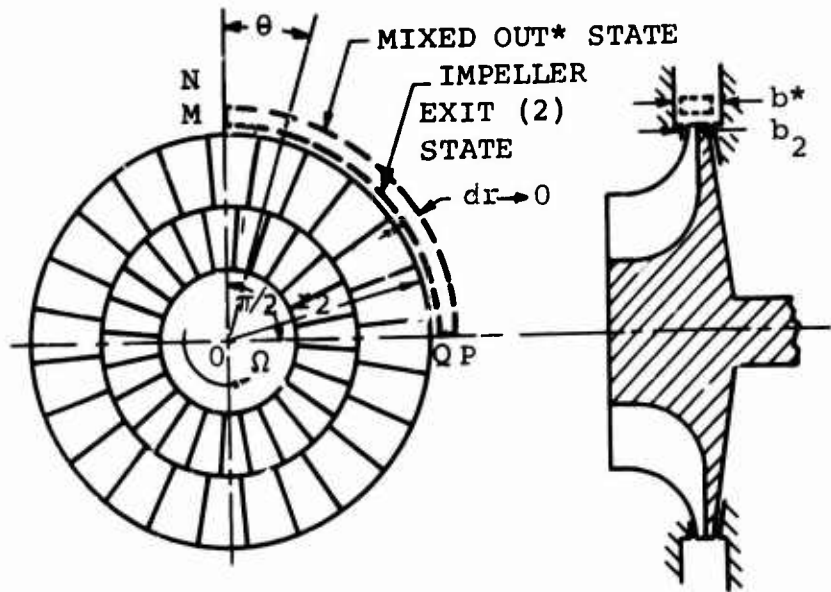


Figure 199. Control Volume Geometry.

$$\begin{aligned}
 & \frac{1}{T} \int_{t=0}^T \int_{x=0}^{b^*} \int_{\theta=0}^{\frac{\pi}{2}} p_2 r_2 \cos \theta d\theta dx dt + \frac{1}{T} \int_{t=0}^T \int_{x=0}^{b^*} \int_{\theta=0}^{\frac{\pi}{2}} \rho_2 c_{r_2}^2 r_2 \cos \theta d\theta dx dt \\
 & + \frac{1}{T} \int_{t=0}^T \int_{x=0}^{b^*} \int_{\theta=0}^{\frac{\pi}{2}} \rho_2 c_{r_2} c_{\theta_2} r_2 \sin \theta d\theta dx dt - p^*(r_2 + dr) b^* \\
 & - \rho^* c_r^* (r_2 + dr) b^* + \rho^* c_r^* c_\theta^* (r_2 + dr) b^* \\
 & + \frac{dr}{T} \int_{t=0}^T \frac{p_2 + p^*}{2} dt = 0 \tag{6}
 \end{aligned}$$

Since  $dr \rightarrow 0$  the last term disappears. The triple integrals can be simplified by noting that integrating over  $T$  means time averaging the integrals and that this time integration is the same as integrating in space once around the tip of the impeller since the impeller speed is constant.

For instance:

$$\frac{1}{T} \int_0^T \left[ \int_0^b \int_0^{2\pi} p_2 r_2 \cos \theta d\theta dx \right] dt = \frac{1}{2\pi} \int_0^{2\pi} \left[ \int_0^b \int_0^2 p_2 r_2 \cos \theta d\theta dx \right] d\phi$$

where  $\phi$  is an angular coordinate. In the integral on the right,  $\phi$  and  $\theta$  are independent. Thus, if we reverse the order of integration, we can move  $\cos \theta$  across the integral sign. But

$$\int_0^b \int_0^{2\pi} p_2 r_2 d\phi dx = \bar{p}_2 (2\pi b^* r_2)$$

where  $\bar{p}_2$  is a constant. Thus,

$$\begin{aligned} \frac{1}{T} \int_0^T \int_0^b \int_0^{2\pi} p_2 r_2 \cos \theta d\theta dx dt &= \frac{1}{2\pi} \bar{p}_2 2\pi b^* r_2 \int_0^{\frac{\pi}{2}} \cos \theta d\theta \\ &= \frac{1}{2\pi} \int_0^b \int_0^{2\pi} p_2 r_2 d\phi dx \end{aligned}$$

Using the same argument for the other triple integrals, Equation (6) becomes (upon simplification using Equation (3))

$$\frac{1}{b^*} \frac{1}{2\pi} \int_0^{b^*} \int_0^{2\pi} p_2 d\theta dx + \frac{1}{b^*} \frac{1}{2\pi} \int_0^{b^*} \int_0^{2\pi} p_2 c_{r_2}^2 d\theta dx - p^* - p^* c_r^{*2} = 0 \quad (7)$$

where  $\theta$  is used for the spatial integration holder instead of  $\phi$ .

For convenience, define

$$i_1 = \frac{1}{b} * \frac{1}{2\pi} \int_0^b \int_0^{2\pi} \rho_2 c_{r_2} d\theta dx \quad (8)$$

$$i_2 = \frac{1}{b} * \frac{1}{2\pi} \int_0^b \int_0^{2\pi} p_2 d\theta dx \quad (9)$$

$$i_3 = \frac{1}{b} * \frac{1}{2\pi} \int_0^b \int_0^{2\pi} \rho_2 c_{r_2}^2 d\theta dx \quad (10)$$

$$i_4 = \frac{1}{b} * \frac{1}{2\pi} \int_0^b \int_0^{2\pi} \rho_2 c_{r_2} c_{\theta_2} d\theta dx \quad (11)$$

$$i_5 = \frac{1}{b} * \frac{1}{2\pi} \int_0^b \int_0^{2\pi} \rho_2 c_{r_2} T_{o_2} d\theta dx \quad (12)$$

$$i_6 = \frac{1}{b} * \frac{1}{2\pi} \int_0^b \int_0^{2\pi} \rho_2 c_{r_2} p_{o_2} d\theta dx \quad (13)$$

The equations to solve then become

$$T_o^* = \frac{i_5}{i_1} \quad (14)$$

$$c_{\theta}^* = \frac{i_4}{i_1} \quad (15)$$

$$\rho c_r^* = i_1 \quad (16)$$

$$(p^* - i_2) 144 + \frac{\rho c_r^{*2}}{g_o} - \frac{i_3}{g_o} = 0 \quad (17)$$

where appropriate constants have been inserted to account for the units used in this report (psi, lbm/ft<sup>3</sup>, ft/sec, etc.). Inserting Equations (4), (5), (14), (15), and (16) into Equation (17) and solving for  $c_r^*$ , we get

$$c_r^* = \frac{k}{k+1} \left\{ \frac{i_3}{i_1} + 144 g_o \frac{i_2}{i_1} \right. \\ \left. \pm \left[ \left( \frac{i_3}{i_1} + 144 g_o \frac{i_2}{i_1} \right)^2 + \left( \frac{2k+2}{k} \right) \left| c_{\theta}^{*2} \frac{k-1}{2k} - (g_o R T_o^*) \right| \right]^{1/2} \right\} \quad (18)$$

Application of the second law of thermodynamics permits a choice between the roots. The lower has always been the acceptable one in our experience. The higher root is a solution to the equations of motion, but it is not physically possible because the fluid's entropy would decrease through the mixing process.

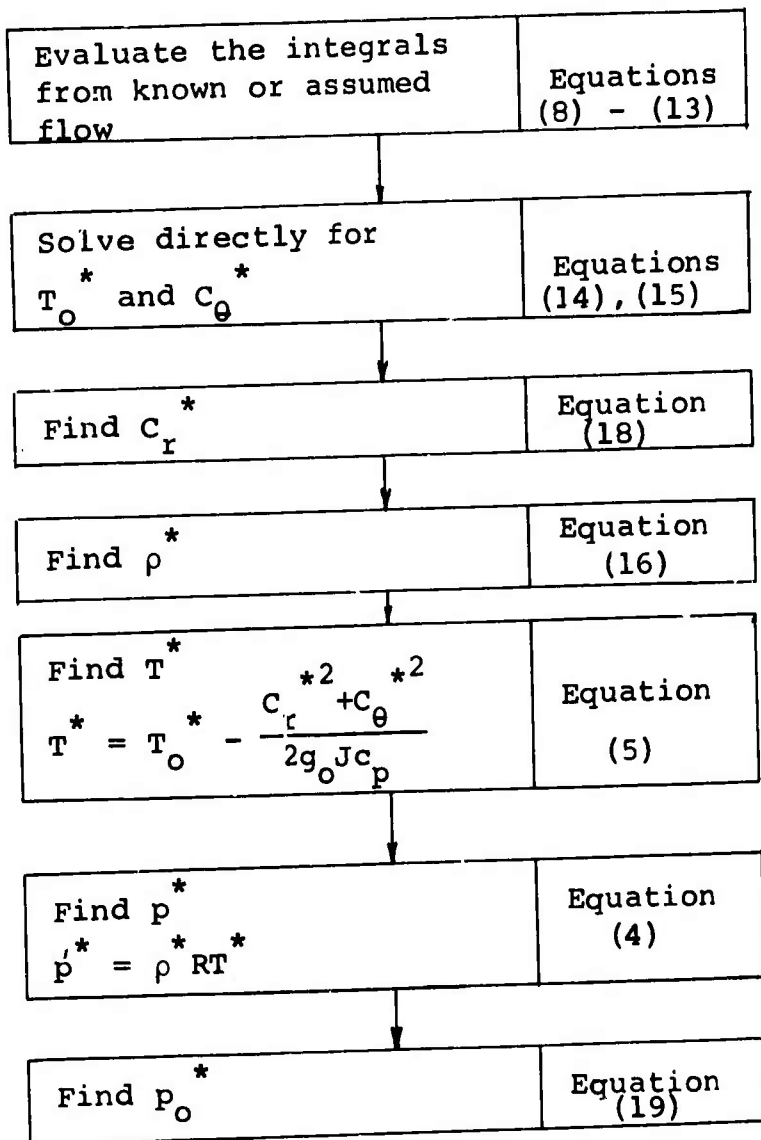
The other mixed out properties can be calculated from Equations (4) and (5) and

$$\frac{p}{p_o} = \left( \frac{T}{T_o} \right)^{\frac{k}{k-1}} \quad (19)$$

In summary, once the impeller exit flow integrals (Equations (8)-(13)) are known, it becomes a relatively simple matter to calculate the mixing loss,  $\tilde{p}_{o_2} - p_o^* = i_6 - p_o^*$ .

### COMPUTATION FLOW CHART

The preparation of a computer program for this analysis is so simple that only a flow chart is needed here:



### Simple Case

If we assume incompressible flow and a square jet of width  $(1-e)$ , we deduce immediately from (7),

$$p^* - \bar{p}_2 = \frac{\rho^* C_r^{*2}}{144g_o} \left( \frac{e}{1-e} \right)$$

and from Bernoulli's equation,

$$p_{o_2} - p_o^* = \frac{1}{288g_o} \frac{\rho * C_r^*^2}{1-e} - \frac{e}{1-e}$$

These simple equations provide a "feel" for the sudden expansion loss, but should not be used for calculation except for incompressible flow and a square jet since a reasonably exact solution is available. Note that the  $p_o$  loss for  $e = 0.75$  is six times as large as for  $e = 0.5$ .

APPENDIX III  
IMPELLER INTERNAL SEPARATED FLOW MODEL

SUMMARY

The equations for separated compressible flow in a centrifugal impeller are developed for the case of an isentropic through flow. The flow in the quiescent region (wake) is analyzed for two cases: one with an adiabatic wake; the other with heat transfer rate proportional to radius.

INTRODUCTION

There are several conventional calculation methods for the flow within a centrifugal impeller. The most common is the potential solution where the fluid is assumed to be inviscid and the entropy is assumed to be constant along meridional streamlines or varied at an arbitrary rate deduced from empirical data. Blockage factors are often employed; sometimes these are deduced from centrifugal impeller test data. Occasionally the potential solution is iterated with boundary layer calculations to account for wall and cover friction and boundary layer blockage.

When impellers are tested in detail, however, it is usually found that the observed flow properties deviate appreciably from the calculated pattern. Probing with fixed hot wires and high-response pressure transducers as well as internal pressure measurements and flow visualization studies has offered an explanation of what is happening. The impeller internal flow has been observed often to separate into a high velocity "jet" or through flow, generally on the pressure surface of the vanes, and a low-velocity "wake" region toward the suction side. Visualization studies indicate very little mixing at the jet-wake interface which has been attributed by Dean (1968) to be the influence of the Coriolis forces in the relative flow.

The impeller separated flow model has been built to account for these experimental observations and therefore to allow more realistic design predictions to be made.

### FLOW MODEL

This flow model for a separated impeller is summarized as follows:

- (1) The flow pattern essentially obeys the potential solution up to the point of separation.
- (2) After separation, there are two regions: a "jet" and a "wake" separated by a shearless interface.
- (3) The jet does not diffuse after separation.
- (4) The pressure in the wake region is determined by centrifugal acceleration requirements.
- (5) The pattern may be two- or three-dimensional and the flow compressible.

An internal relative total pressure loss may be applied to the jet; however, experimental data indicates only very small losses in the jet for the cases studied in detail. All entropy generated within the impeller, due to passage and cover wall friction, tip leakage, and any other source, is assumed to accumulate in the wake. On mixing outside the impeller tip this entropy is redistributed into the total flow, with an added loss due to the discharge mixing process. This mixing process is analyzed in Appendix II.

### ASSUMPTIONS

- (1) The flow in the jet is isentropic.
- (2) The relative flow is steady.
- (3) There is no relative work (except by cover friction).
- (4) There is no mixing or shear between jet and wake within the impeller.
- (5) The static pressure at the separation point and the location of the separation point are known.
- (6) There is no significant curvature of the streamlines at the separation point.
- (7) The fluid is a perfect gas with constant specific heats.
- (8) The relative velocity in the wake is negligible (although the mass flow through the wake may be finite).

We will calculate the flow in the jet first, then we will calculate the flow in the wake, and finally we will integrate the two analyses.

## JET

From the definition of  $T_{T_{rel}}$  and  $T_{O_{rel}}$

$$T_{T_{rel}} = T + \frac{W^2 - U^2}{2g_o J c_p} \quad (20)$$

$$T_{O_{rel}} = T + \frac{W^2}{2g_o J c_p} \quad (21)$$

It follows that

$$T_{O_{rel}} = T_{T_{rel}} + \frac{U^2}{2g_o J c_p} \quad (22)$$

Also,

$$T_{T_{rel_1}} = T_{O_i} + \frac{2UC_{\theta_1}}{2g_o J c_p}$$

where  $2UC_{\theta_1}$  is due to preswirl.

Define  $V^2 = \frac{U^2}{2g_o J c_p T_{T_{rel}}}$  as a convenient velocity ratio.

Then from Equation (22),

$$\frac{T_{O_{rel}}}{T_{T_{rel}}} = 1 + V^2 \quad (23)$$

From the isentropic flow assumption

$$\frac{P_{O_{rel}}}{P_{T_{rel}}} = \left( \frac{T_{O_{rel}}}{T_{T_{rel}}} \right)^{\frac{k}{k-1}} = (1 + V^2)^{\frac{k}{k-1}} \quad (24)$$

For no preswirl and isentropic flow

$$p_{T_{rel}} = p_{o_i}$$

For no preswirl and no relative work

$$T_{T_{rel}} = T_{o_i}$$

Including preswirl

$$T_{T_{rel}} = T_{o_i} + \frac{2UC_\theta}{2g_J C_p}$$

$$p_{T_{rel}} = p_{o_i} \left( \frac{T_{T_{rel}}}{T_{o_i}} \right)^{\frac{k}{k-1}} - \text{IGV losses}$$

It is also useful to define  $M_{rel}$  for the relative flow as

$$M_{rel}^2 = \frac{2}{k-1} \left[ \frac{T_{o_{rel}}}{T} - 1 \right]$$

Similarly, the usual relationships are valid for relating

$$T, T_{o_{rel}}, p, p_{o_{rel}}, M_{rel}, \text{ and } w_{rel}.$$

Thus, the state of fluid in the jet is completely described if  $p_{T_{rel}}$ ,  $T_{T_{rel}}$ ,  $v$ , and any of  $T$ ,  $p$ ,  $M_{rel}$ , or  $w_{rel}$  are known.

#### WAKE

A force balance of an element of fluid in the wake gives

$$\frac{dp}{dr} = \frac{\rho}{g_o} r \Omega^2 \quad (25)$$

From the first law of thermodynamics written in relative coordinates,

$$dQ - dw_{rel} = Jc_p dT_{T_{rel}} = Jc_p dT_{T_{rel}} - d \left( \frac{r^2 \Omega^2}{2g_o} \right)$$

where

$dQ$  = heat transferred per unit mass of fluid.

Since  $dw_{rel} = 0$  and  $T = T_{T_{rel}}$  in the wake,

$$\frac{dQ}{dr} = c_p \frac{dT}{dr} - \frac{d \left( \frac{r^2 \Omega^2}{2g_o J} \right)}{dr} \quad (26)$$

Solving and inserting the initial conditions

$$T = T_{T_{rel}} + \frac{r^2 \Omega^2}{2g_o J c_p} + \int_{r_s}^r \frac{1}{J c_p} \frac{dQ}{dr} dr \quad (27)$$

We now examine two cases for which solutions may be readily obtained.

$$\text{Case 1: } \frac{dQ}{dr} = 0$$

Using Equations (25), (27) and  $p = \rho RT$ , we get

$$\frac{dp}{dr} = \frac{\rho r \Omega^2}{g_o R \left( T_{T_{rel}} + \frac{r^2 \Omega^2}{2g_o J c_p} \right)} \quad (28)$$

Remembering that  $J c_p = \frac{k}{k-1} R$ , and integrating, we get

$$p_w = K_1 (1+v^2)^{\frac{k}{k-1}}$$

To eliminate the integration constant,  $K_1$ , take the ratio of

$$\frac{p_w}{p_{ws}} = \left[ \frac{1+v^2}{1+v_s^2} \right]^{\frac{k}{k-1}} \quad (29)$$

Case 2: Let:  $\frac{1}{Jc_p} \frac{dQ}{dr} = 2K_2 r$

Then

$$T = T_{T_{rel}} + \frac{r^2 \Omega^2}{2g_o Jc_p} + K_2 (r^2 - r_s^2)$$

and Equation (28) becomes

$$\frac{dp}{dr} = \frac{p}{g_o R} \frac{r\Omega^2}{\left[ T_{T_{rel}} + r^2 \left( \frac{\Omega^2}{2g_o Jc_p} + K_2 \right) - K_2 r_s^2 \right]}$$

which integrates to

$$p = K_1 \left[ T_{T_{rel}} + \frac{r^2 \Omega^2}{2g_o Jc_p} + K_2 (r^2 - r_s^2) \right] \left[ \frac{k}{k-1} \left( \frac{\Omega^2}{\Omega^2 + K_2 2g_o Jc_p} \right) \right]$$

Let  $\pi_Q = \frac{K_2 (2g_o Jc_p)}{\Omega^2}$ . Then using  $\pi_Q$  and dividing by  $p_{ws}$

to eliminate  $K_1$ , we get

$$\frac{p_w}{p_{ws}} = \left[ \frac{1+v^2 + \pi_Q (v^2 - v_s^2)}{1 + v_s^2} \right] \left[ \frac{k}{k-1} \left( \frac{1}{1+\pi_Q} \right) \right] \quad (30)$$

Figure 200 shows a comparison of Equations (29) and (30) using values typical of the RF-2 impeller.

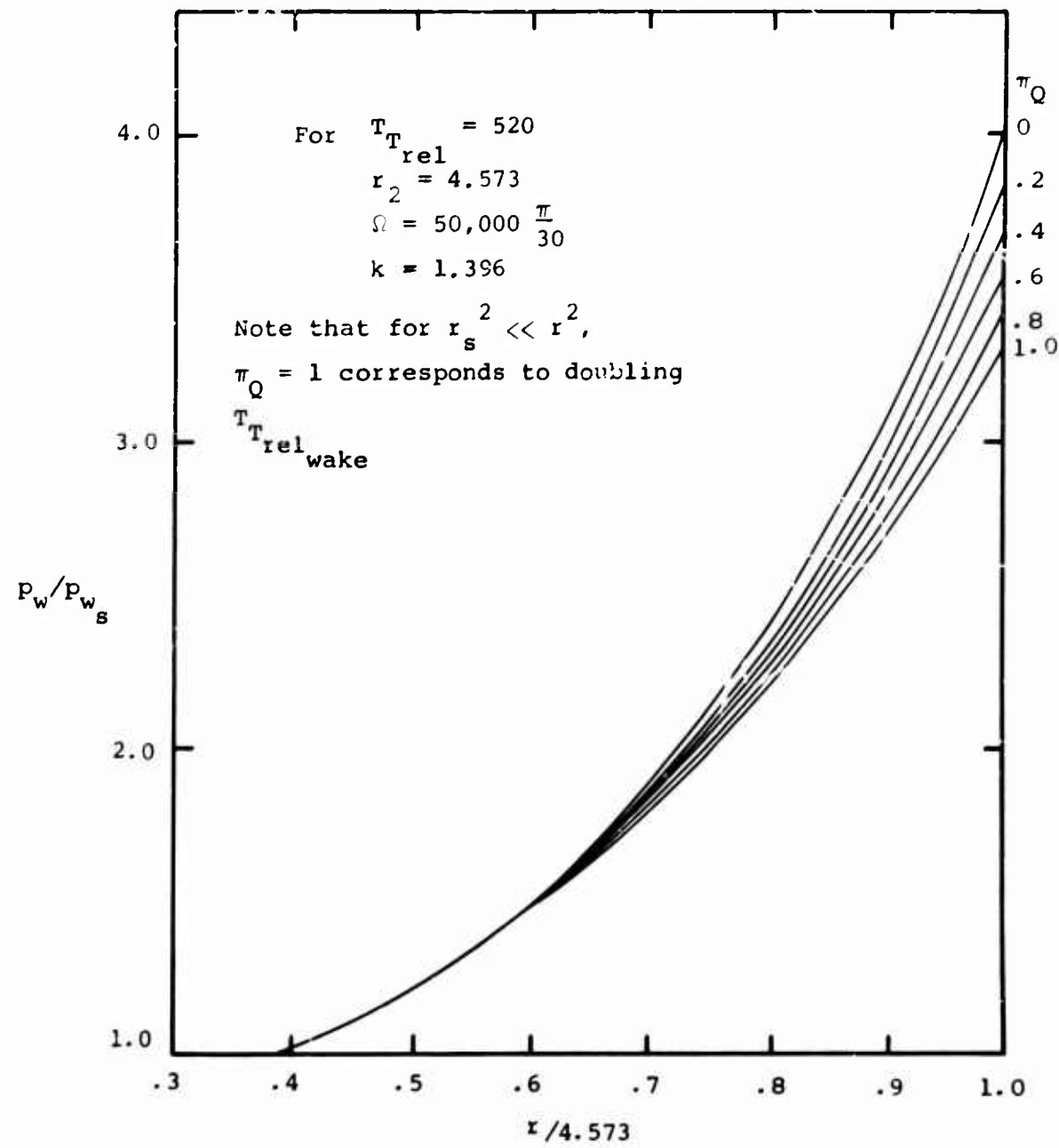


Figure 200. Wake Static Pressure Ratio Versus Radius.

It is useful to have the connection between  $p_{w_s}$  and  $M_{rel_s}$ . From Figure 201,  $p_{w_s} = p_{j_s}$ .

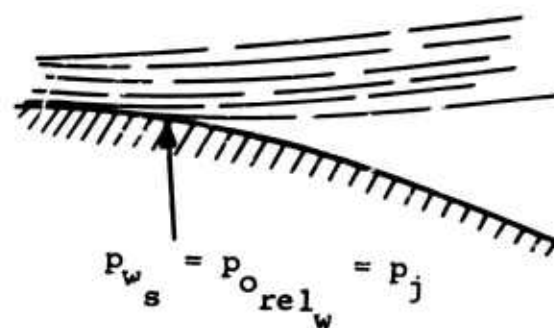


Figure 201. Pressures at Separation.

$$\text{But } p_{j_s} = \frac{p_{o_{rel_j_s}}}{\left(1 + \frac{k-1}{2} M_{rel_s}^2\right)^{\frac{k}{k-1}}}$$

Then

$$p_{w_s} = \left[ \frac{p_{j_s}}{p_{o_{rel_j_s}}} \right] \left[ \frac{p_{o_{rel_j_s}}}{p_{T_{rel}}} \right] p_{T_{rel}}$$

or

$$\frac{p_{w_s}}{p_{T_{rel}}} = \left[ \frac{1 + v_s^2}{1 + \frac{k-1}{2} M_{rel_s}^2} \right]^{\frac{k}{k-1}} \quad (31)$$

From this equation, the importance of  $M_{rel_s}$  on  $p_{w_s}$  can be seen. Also, from Equations (23), (24), (29), (31), and the

isentropic relations, since on the boundary of the jet,  
 $p_j = p_W$ ; then

$$\frac{p_W}{p_{W_s}} \frac{p_{W_s}}{p_{T_{rel}}} \frac{p_{T_{rel}}}{p_{o_{rel}}} \frac{p_{o_{rel}}}{p_j} = 1 = \left[ \frac{1 + \frac{k-1}{2} M_{rel}^2}{1 + \frac{k-1}{2} M_{rel_s}^2} \right]^{\frac{k}{k-1}}$$

or the relative Mach number on the boundary of the jet is constant.

#### COMBINATION OF JET AND WAKE RESULTS

There are many ways to proceed from here. The impeller separated flow equations are complete to this point, but in order to apply them to a specific impeller to determine, for instance, the relative sizes of the jet and wake regions or the average static pressure on the cover, some more information is needed. This additional information is the variation of static pressure in the jet, the heat transfer rate into the wake, and the mass flow in the wake. The general case cannot be solved in closed form; in fact, even the simplest case is most easily solved by iteration, as follows.

#### Simple Case

Assume no heat transfer and that the blade loading is  $\Delta p_b$  known. (Section 5.4 describes one method of calculating this.) Further, assume a linear variation of static pressure from the pressure surface to the edge of the jet. Then

$$p_j = p_W + \Delta p_b \left[ 1 - \frac{e}{\frac{2\pi}{z}(1-e)} \right]$$

This is indicated in Figure 126.

Now we can use the continuity equation to find the wake width  $\epsilon$ . This equation in its relevant form is:

$$(1-\epsilon) \overline{\rho_j w_j} 2\pi c b = m \left[ 1 - \frac{m_w}{m} \right] \quad (32)$$

and  $\overline{\rho_j w_j}$  can be found by integrating:

$$\overline{\rho_j w_j} = M_{rel,j} \sqrt{\frac{k g_o}{R T_{rel,j}}} p_{T_{rel,j}} \left[ \frac{1+v^2}{1 + \frac{k-1}{2} M_{rel,j}^2} \right]^{\frac{k+1}{2(k-1)}}$$

where  $M_{rel,j}$  is given by:

$$M_{rel,j} = \left[ \frac{2}{k-1} \left[ \frac{p_{T_{rel,j}}^{(1+v^2)^{\frac{k}{k-1}}}}{p_w + \Delta p_b \left[ 1 - \frac{\theta}{2\pi} (1-\epsilon) \right]} \right]^{\frac{k-1}{k}} - 1 \right]^{1/2}$$

Since  $\epsilon$  is needed to find  $\overline{\rho_j w_j}$ , which is needed in Equation (32) to find  $\epsilon$ , some iteration is required, but convergence is usually very rapid.

#### APPENDIX IV PREPARATION OF DIFFUSER ISOBARIC PLOTS

Isobaric plots were constructed from the static pressure data for Tests 3366 and 3369 in order to provide input for boundary layer calculations. These plots were made in considerable detail -- certainly more than the pressure data warrants -- because the static pressure taps are spread out too thinly for computational purposes. Information from the Workhorse schlieren photographs and stagnation pressure traverses was included subjectively. This detailed interpretation was necessary in order to obtain essential flow pattern information.

Generally, the isobaric plots indicate that the flow in the vaneless space of this machine is complex and three-dimensional. Figures 133 and 134 show two isobaric plots (Tests 3366, Line 5, and 3369, Line 5) which are typical of the others.

Figure 134 shows a large area which is thought to encompass a stall bubble on one wall. The existence of this separated region has been deduced from the following evidence:

- 1) The difference in static pressure between front and back covers indicates curvature in the meridional plane. The locus of large differences between these pressures should indicate the separation line. Of course, to define the exact extent of the separation region much more static pressure data are required. However, we can estimate the fraction of fluid in this region by calculating the meridional curvature of the stream from Euler's "n" equation. We then estimate the distance for which this curvature applies, and calculate:

$$\Delta h = \left( \frac{\Delta s}{R} \right) \left( \frac{\Delta s}{2} \right)$$

where:

$$\frac{1}{R} = \text{curvature} = \frac{dp/\rho c^2}{dn} g_0 \quad \text{from Euler's equation}$$

$\Delta h$  = height of separated fluid

$\Delta s$  = distance over which the curvature,  $\frac{1}{R}$ , acts

$\frac{dp}{dn}$  = pressure gradient normal to the flow (this acts from front cover to back cover)

$\rho$  = density

C = fluid velocity

This calculation yields 4% of the area blocked by separated fluid under the vane tip for the case shown in Figure 134. This is a very approximate calculation since the velocity, C, and  $\Delta s$  both have to be estimated.

2) Sidewall boundary layer calculations predict separation near the throat entry. However, this prediction is subject to the severe reservations of Section 5.8.1.

3) The impeller tip instrumentation hints at separation and backflow. Other evidence strengthens this to a positive conclusion; Section 6.8 agrees with our interpretation here of the meridional static pressure variations.

The isobaric plots now appear to be very significant to the interpretation of the diffuser data. But their preparation involves a fair amount of induction (which must always be questioned); a complete explanation of their preparation is now given.

#### TECHNIQUE

1) First, lines of constant pressure were sketched by linearly interpolating among the static pressure data. (The static pressures are the numbers written on Figures 133 and 134. The numbers above and below the taps are respectively the cover and hub measurements.)

2) This first approximation is refined by using the facts that:

- a. Isobaric lines do not cross each other.
- b. Isobaric lines do not end in the middle of a flow field.
- c. The pressure assumes all of the intermediate

values between two data points in the space between the taps at least once.

Isobaric lines can cross or end in a flow field only where there is an infinite pressure gradient. No real fluid is capable of supporting such a pressure gradient, although shocks almost approach this condition. Therefore, all the isobaric lines must end on solid surfaces, on themselves, or on shocks.

The third fact seems trivial at first glance, but it is very important in practice. It says simply that all pressure contours for pressures between the values measured at two taps must pass between the two taps at least once.

3) If the flow follows the blade surface there are certain relationships between the normal pressure gradient and the streamwise pressure gradient. From the known radius of curvature of the vane and the measured streamwise pressure gradient along the wall, we can write a relationship for the (vector) pressure gradient at the wall. We use this pressure gradient to determine the angle of intersection of isobars with the wall from the condition that the pressure gradient,  $\text{grad}(p)$ , is perpendicular to an isobaric.

4) It has been assumed that the shock system in the RF-2 diffusers is rather soft. The static pressure data (e.g., Figures 133 and 134) show a "smooth" rise in static pressure along the streamlines approaching the throat. In contrast, the static pressure data for the Workhorse seemed to show sharper discontinuities at these flow rates. Near choking, the RF-2 diffusers have a sharper shock system which is similar to that of the Workhorse diffusers.

The most uncertain region of the isobars is the portion under the vane tip. The structure of the complex shock patterns in this region is developed in Section 5.8.1. Figure 133 presents a graphic reconstruction of the inferred pattern. The uncertainty level is high, unfortunately, because only three wall taps were provided in this interesting region of maximum interference between diffuser vanes

and impeller. The schlieren photographs are a vital guide, without which we would be at a loss to restructure the flow, but they are mostly occluded by the impeller in the region under the vane leading edge. Despite these problems, the shock pattern was injected into the isobarics of Figures 133 and 134.

## APPENDIX V

### SAMPLE UNCERTAINTY CALCULATION FOR WELLIVER AND ACURIO CHANNEL DIFFUSER DATA

#### GENERAL

$$\frac{\Delta U}{U} = \left\{ \sum_{i=1}^n \left( \frac{\partial \ln U}{\partial \ln X_i} \frac{\Delta X_i}{X_i} \right)^2 \right\}^{1/2}$$

where

$U = f(X_i)$  is the derived quantity  
 $X_i$  = the individual measurements taken

The relationship shown relates the uncertainty in the derived quantity to the uncertainties in the measurements

$\left( \frac{\Delta X_i}{X_i} \right)$  weighed by appropriate influence coefficients  $\left( \frac{\partial \ln U}{\partial \ln X_i} \right)$ .

This uncertainty can be derived from assuming a normal distribution for each  $X_i$  and linearizing the equation for  $U$ .

While this seems somewhat restrictive, Kline and McClintock (1953) showed that the above equation was pretty good for some other (quite different) distributions.

#### PRESSURE RECOVERY UNCERTAINTY

From the definition of  $C_p$

$$C_p = \frac{p_{coll} - p_4}{p_{O_4} - p_4}$$

We get

$$\left( \frac{\Delta C_p}{C_p} \right)^2 = \left( \frac{p_{coll}}{p_{coll} - p_4} \frac{\Delta p_{coll}}{p_{coll}} \right)^2 + \left[ \left( \frac{p_4}{p_{coll} - p_4} - \frac{p_4}{p_{O_4} - p_4} \right) \frac{\Delta p_4}{p_4} \right]^2$$

$$+ \left( \frac{p_{o_4}}{p_{o_4} - p_4} \frac{\Delta p_{o_4}}{p_{o_4}} \right)^2$$

### BLOCKAGE UNCERTAINTY

$$B_4 = 1 - \frac{m}{m_{theor}}$$

$$\frac{\Delta B_4}{B_4} = \frac{m}{m_{theor}} \frac{1}{B_4} \left[ \left( \frac{\Delta m}{m} \right)^2 + \left( \frac{\Delta m_{theor}}{m_{theor}} \right)^2 \right]^{1/2}$$

### MASS FLOW THEORETICAL UNCERTAINTY

$$m_{theor} = A_4 (\rho C)_{4_{C_L}} = \frac{p_4}{R T_4} A_4 M_4 \sqrt{\frac{kg_o}{RT_4}}$$

$$= p_4 A M_4 \sqrt{\frac{kg_o}{RT_4}} \sqrt{\frac{T_{o_4}}{T_4}}$$

The uncertainty expression is rather long so it is represented by

$$\frac{\Delta m_{theor}}{m_{theor}} = \left[ \sum \left( \frac{\partial \ln m_{theor}}{\partial \ln x_i} \frac{\Delta x_i}{x_i} \right)^2 \right]^{1/2}$$

where the influence coefficients are given by

$$\frac{\partial \ln m_{theor}}{\partial \ln A} = 1$$

$$\frac{\partial \ln m_{theor}}{\partial \ln T_{o_4}} = -\frac{1}{2}$$

$$\frac{\partial \ln m_{\text{theor}}}{\partial \ln \text{constants}} = 0 \text{ (assumed that the constants are not uncertain)}$$

$$\frac{\partial \ln m_{\text{theor}}}{\partial \ln p_{c_4}} = \frac{k-1}{2k} \left( 1 + \frac{1}{1 - \left( \frac{p}{p_o} \right)^{\frac{k-1}{k}}} \right)$$

$$\frac{\partial \ln m_{\text{theor}}}{\partial \ln p_4} = 1 - \left[ \frac{p_4}{2} \frac{\frac{k-1}{k} \left( \frac{p_o}{p} \right)^{\frac{1}{k}} \frac{p_o}{p}}{\left( \frac{p_o}{p} \right)^{\frac{k-1}{k}} - 1} \right] - \frac{k-1}{2k}$$

### UNCERTAINTY EVALUATION

For Test 3354, Line 7:

$$p_4 = 87.1 \pm 3 \quad \frac{\Delta p_4}{p_4} = 0.034$$

$$p_{o_4} = 158 \pm 5 \quad \frac{\Delta p_{o_4}}{p_{o_4}} = 0.032$$

$$A_4 = .0608$$

$$T_{o_4} = 1148 \pm 10 \quad \frac{\Delta A_4}{A} = 0.0126$$

$$m_4 = 1.96$$

$$p_{coll} = 128 \pm 0.5$$

$$\frac{\Delta T_{o_4}}{T_{o_4}} = 0.009$$

$$\frac{\Delta m}{m} = 0.01$$

$$\frac{\Delta p_{coll}}{p_{coll}} = 0.004$$

### THEORETICAL MASS FLOW

After evaluating the influence coefficients, we have

$$\begin{aligned} \left( \frac{\Delta m_{theor}}{m_{theor}} \right)^2 &= \left( \frac{\Delta A_4}{A_4} \right)^2 + \left( \frac{1}{2} \frac{\Delta T_{o_4}}{T_{o_4}} \right)^2 + \left( .057 \frac{\Delta p_4}{p_4} \right)^2 + \left( 1.04 \frac{\Delta p_{o_4}}{p_{o_4}} \right)^2 \\ &= (1.26^2 + 0.45 + 0.19^2 + 3.33^2) \times 10^{-4} \\ &= 12.9 \times 10^{-4} \end{aligned}$$

Therefore

$$\frac{\Delta m_{theor}}{m_{theor}} = 3.6\%$$

$$m_{theor} = 2.143$$

PRESSURE RECOVERY

$$\left(\frac{\Delta C_p}{C_p}\right)^2 = \left(\frac{p_{coll}}{p_{coll} - p_4} \frac{\Delta p_{coll}}{p_{coll}}\right)^2 + \left[\left(\frac{p_4}{p_{coll} - p_4} - \frac{p_4}{p_{o_4} - p_4}\right) \frac{\Delta p_4}{p_4}\right]^2$$

$$+ \left(\frac{p_{o_4}}{p_{o_4} - p_4} \frac{\Delta p_{o_4}}{p_{o_4}}\right)^2 = [3.1(.004)]^2 + [.9(.034)]^2$$

$$+ [2.23(.032)]^2 = 1.56 + 9.35 + 50.5 = 61.4 \times 10^{-4}$$

$$\frac{\Delta C_p}{C_p} = 7.8\%$$

BLOCKAGE

$$\frac{\Delta B_4}{B_4} = \frac{m}{m_{theor}} - \frac{1}{B_4} \left[ \left( \frac{\Delta m}{m} \right)^2 + \left( \frac{\Delta m_{theor}}{m_{theor}} \right)^2 \right]^{1/2}$$

$$= \frac{1.96}{2.143} \frac{1}{.086} [(.01)^2 + (.036)^2]^{1/2}$$

$$\frac{\Delta B_4}{B_4} = 40\%$$

APPENDIX VI  
DATA REDUCTIONS FOR SECTION 4.3

DATA REDUCTION METHOD No. 1

Assume a tip blockage factor  $BF_2 = 0.8$ . Adopt the following "instrument indicated" values.

$$\bar{p}_2 = 67.25$$

$$\tilde{p}_{o_2} = 196$$

and let

$$\tilde{T}_{o_2} = \bar{T}_{o_2} = T_{coll} = \tilde{T}_{o_2} \quad ("true" \text{ value, Table VI} = 1106.1)$$

From mass flow and tip area:

$$\overline{\rho C_r} = m / 2\pi r_2 b_2 = 62.17$$

Then:

$$T_2 = T_{o_2} \left( \frac{p_2}{p_{o_2}} \right)^{\frac{k-1}{k}} = 816^\circ R$$

$$c_2 = \left[ (T_{o_2} - T_2) 2g_o J c_p \right]^{1/2} = 1874$$

$$\rho_2 = .223$$

$$c_{r_2} = \frac{\overline{\rho C_r}}{\rho (BF_2)} = 349$$

$$c_{\theta_2} = \left[ c_2^2 - c_{r_2}^2 \right]^{1/2} = 1842$$

(Note that Euler's Equation would give  $c_{\theta_2} = 1772$  from  $\Delta T_o$ )

After mixing,

$$C_{\theta}^* = 1842$$

$$T_o = 1106.1$$

$$C_r^* = 278$$

$$p^* = 68.2$$

$p_o^*$  = 196 (-) (mixing loss too small  
to get reliable number,  
would be .55 psi for  
incomp. flow)

Changing  $C_{\theta_2}$  to 1772 would have had little effect on the  
loss although  $p_{o_2}$  would have been lower.

#### DATA REDUCTION METHOD No. 2

Assume the axial  $p_{o_2}$  and  $T_{o_2}$  profiles are correct except  
that the  $T_{o_2}$  profile has to be lowered to match  $T_{coll}$  when  
mass flow averaged. Take from "instrument indicated" data,  
Table VI.

$$\bar{p}_2 = 67.25$$

$C_{\theta}$  was calculated from the work input; i.e.,

$$2U_2 C_{\theta_2} = (\tilde{T}_{o_2} - T_{o_i}) 2g_o \bar{x}_p$$

Doing this leads to the following axial distributions:

x/b	$\hat{T}_o$	$\hat{C}_{\theta}$	$\hat{\rho}C_r$
.25	1136	1863.7	120.5
.5	1112	1791.1	125
.75	1076	1682	140.5

Mass flow averaging these distributions, we get

$\tilde{T}_o = 1106.4$  (we tried to match 1106.1; this seems to be close enough)

$$\tilde{C}_\theta = 1772$$

$$\tilde{p}_o = 195.4$$

Note that  $\bar{\rho}C_r = 128.7$ , about twice the actual value. Assume that this computational error is caused by taking the difference of large numbers, and use the measured mass flow rate,  $\bar{\rho}C_r = m/2\pi r_2 b_2 = 62.17$ . In doing this, we are overspecifying the problem, of course.

Applying the stepped jet wake model to the tip state so defined gives:

$$T_{o_{rel2}} = T_{o_i} + \frac{U_2^2}{2g_o x_p} = 850^\circ R$$

$$p_{o_{relj}} = \tilde{p}_{o_2} \left( \frac{T_{o_{rel2}}}{T_{o_2}} \right)^{\frac{k}{k-1}} = 77$$

(Note that now the jet is not isentropic from inlet)

$$M_{relj} = .445 \text{ (from } \hat{p}_2 \text{)}$$

$$w_{\theta_{j_2}} = 228$$

$$T_{j_2} = 818$$

$$w_{j_2} = .445 \sqrt{kg_o RT} = 625$$

$$w_{r_{j_2}} = \left[ w_{j_2}^2 - w_{\theta_{j_2}}^2 \right]^{1/2} = 582$$

$$\rho_{j_2} = 0.222$$

$$(1-e) \rho_{j_2} w_{r_{j_2}} = \overline{\rho c_r}$$

$$\text{for } \overline{\rho c_r} = 62.17, \quad 1 - e = 0.481, \quad e = 0.519$$

After mixing:

$$c_r^* = 265$$

$$c_\theta^* = 1772$$

$$p^* = 71.57$$

$$T_o^* = 1106.4$$

$$\rho^* = 0.230$$

$$p_o^* = 193.2 \text{ psia}$$

#### DATA REDUCTION METHOD No. 3

Assume that the following instrument values are true:

$$\bar{p}_2 = 67.25$$

$$\tilde{T}_{o_2} = T_{coll} = 1106.1$$

$$\overline{\rho c_r} = m/2\pi r_2 b_2 = 62.17$$

Assuming  $m_w/m = 0$  (no mass flow in the wake) and applying the step jet wake flow model to the measured conditions, we calculate

$$\tilde{p}_{O_2} = 211.4$$

$$\tilde{c}_{\theta_2} = 1778$$

$$e = 0.632$$

$$c_{r_{j_2}} = 838.8$$

(See Appendix III for the basic equations.) The specifying assumptions are:

- (1) No flow in the wake
- (2) Isentropic through flow from inlet
- (3) Constant static pressure at impeller tip

And after mixing:

$$c_r^* = 261.9$$

$$c_\theta^* = 1778$$

$$T_o^* = 1106.1$$

$$p^* = 73.7$$

$$p_o^* = 195$$

#### DATA REDUCTION METHOD No. 4

Use the same procedure as for Method No. 3 except assume  $m_w/m = 0.2$  (20% of the flow in the wake)

$$T_{T_{rel_w_2}} = 520 \text{ (no heat transfer to the wake)}$$

From the step jet wake model, we get

$$T_{o,j_2} = 1088.1$$

$$T_{o,w_2} = 1178$$

$$\tilde{T}_o = 1106.1$$

$$\tilde{p}_o = 202.8$$

$$c_{r,j_2} = 725$$

$$c_{r,w_2} = 83.1$$

$$\tilde{c}_\theta = 1782$$

After mixing

$$c_r^* = 269.4$$

$$c_\theta^* = 1782$$

$$T_o^* = 1106.1$$

$$p_o^* = 190.1$$

$$p^* = 71.6$$

DATA REDUCTION METHOD No. 5a

This data reduction is identical to Method 3 but uses the "true" slip factor (aerodynamic work input) instead of the collector temperature ( $m_w/m = 0$ ).

DATA REDUCTION METHOD No. 5b

This data reduction is identical to Method 4 but uses the "true" slip factor instead of the collector temperature ( $m_w/m = 0.20$ ).

APPENDIX VII  
DEFINITION OF  $p_{T_{\text{rel}}}$

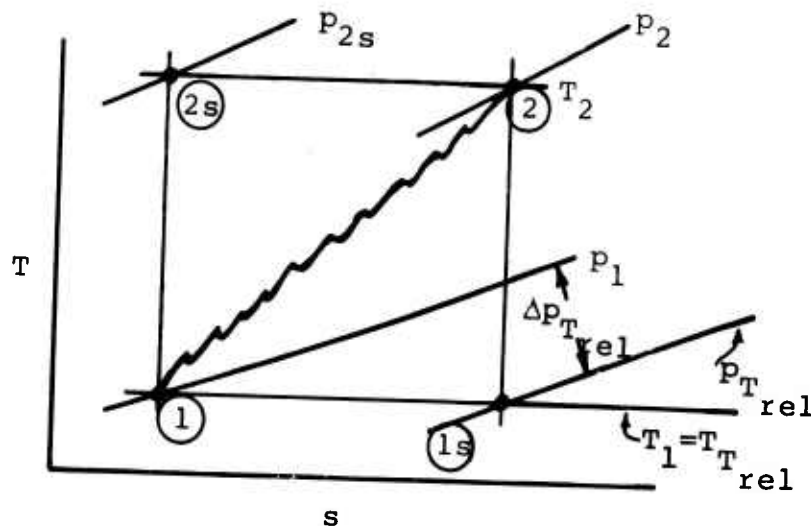


**Figure 202.** T-s Diagram for an Arbitrary Process Between Stagnation States 1 and 2.

$\Delta p_{T_{\text{rel}}}$  defines  $p_{T_{\text{rel}}} = p_1 - \Delta p_{T_{\text{rel}}}$  so that  $p_{T_{\text{rel}}}$  is at the same entropy as the final state (2).

This means:

$$\frac{p_{2s}}{p_1} = \left( \frac{T_2}{T_{T_{\text{rel}}}} \right)^{k/k-1} = \frac{p_2}{p_{T_{\text{rel}}}}$$

Then

$$p_{T_{\text{rel}}} = p_1 \frac{p_2}{p_{2s}}$$

Along the  $T_{T_{\text{rel}}}$  line,

$$T_{T_{rel}} = c_p \frac{dT_{T_{rel}}}{T_{rel}} - \frac{dp}{\rho} = - \frac{dp}{\rho}$$

$$\frac{ds}{R} = - \frac{dp}{\rho R T_{T_{rel}}} = - \frac{dp}{P}$$

Integrating,

$$-\ln \frac{p_{T_{rel}}}{p_1} = \frac{\Delta s}{R}$$

$$\frac{p_{T_{rel}}}{p_1} - 1 = e^{\frac{-\Delta s}{R}} - 1$$

$$\Delta p_{T_{rel}} = p_1 (1 - e^{\frac{-\Delta s}{R}})$$

Unclassified

Security Classification

**DOCUMENT CONTROL DATA - R & D**

(Security classification of title, body of abstract and indexing annotation must be entered when the overall report is classified)

1. ORIGINATING ACTIVITY (Corporation author)		2a. REPORT SECURITY CLASSIFICATION Unclassified	
Creare Incorporated Hanover, New Hampshire		2b. GROUP	
3. REPORT TITLE <b>FLUID MECHANICS ANALYSIS OF HIGH-PRESSURE-RATIO CENTRIFUGAL COMPRESSOR DATA</b>			
4. DESCRIPTIVE NOTES (Type of report and inclusive dates) Final Report			
5. AUTHOR(S) (First name, middle initial, last name) Robert C. Dean, Jr.      Peter W. Runstadler, Jr. David D. Wright			
6. REPORT DATE February 1970		7a. TOTAL NO. OF PAGES 565	7b. NO. OF REFS 65
8a. CONTRACT OR GRANT NO. DAAJ02-68-C-0073 <i>1/6/68</i>		8c. ORIGINATOR'S REPORT NUMBER(S) USA AVLabs Technical Report 69-76	
8b. PROJECT NO. Task 1G162203D14413		9b. OTHER REPORT NO(S) (Any other numbers that may be assigned this report)	
10. DISTRIBUTION STATEMENT This document is subject to special export controls, and each transmittal to foreign governments or foreign nationals may be made only with prior approval of US Army Aviation Materiel Laboratories, Fort Eustis, Virginia 23604.			
11. SUPPLEMENTARY NOTES		12. SPONSORING MILITARY ACTIVITY US Army Aviation Materiel Laboratories Fort Eustis, Virginia	
13. ABSTRACT The results of a review and distillation of the fluid dynamic information gained during the Boeing-AVLabs program to develop superior high-pressure-ratio compressors for small gas turbine service are reported. The objectives were to critically test the design flow models proposed by Welliver and Acurio (1967) of Boeing, to improve these models where feasible, and then to redesign the compressor with concrete guidelines for reaching the U.S. Army Aviation Materiel Laboratories (USA AVLabs) target of pressure ratio 10 and 80% total to static stage efficiency at 2 lbm/sec flow.  This report presents an extensive review of the Boeing data and a testing of the Boeing flow models. The models are improved to a certain extent. Basic weaknesses in the scientific foundations are delineated. A research program to strengthen the foundations is presented in brief.  The redesign effort produced very encouraging results. By raising the specific speed by adopting a tandem row transonic inducer, and by using an improved diffuser, a stage efficiency between 80% and 85% is predicted with confidence.  The results of this study are expected to enable the attainment of the USA AVLabs target without great difficulty in the next round of exploratory development.			

DD FORM 1 NOV 68 1473 REPLACES DD FORM 1473, 1 JAN 64, WHICH IS  
OBSOLETE FOR ARMY USE.

Unclassified

Security Classification

Unclassified

Security Classification

14. KEY WORDS	LINK A		LINK B		LINK C	
	ROLE	WT	ROLE	WT	ROLE	WT
Centrifugal Compressor High-Pressure-Ratio Compressor Fluid Mechanics Small Gas Turbine						

Unclassified

Security Classification

1219-70